United States
Environmental Protection
Agency

Industrial Environmental Research
Laboratory
Research Triangle Park NC 27711

EPA-600/9-80-039c
September 1980

Research and Development

EPA

Second Symposium on the Transfer and Utilization of Particulate Control Technology

Volume III. Particulate Control Devices

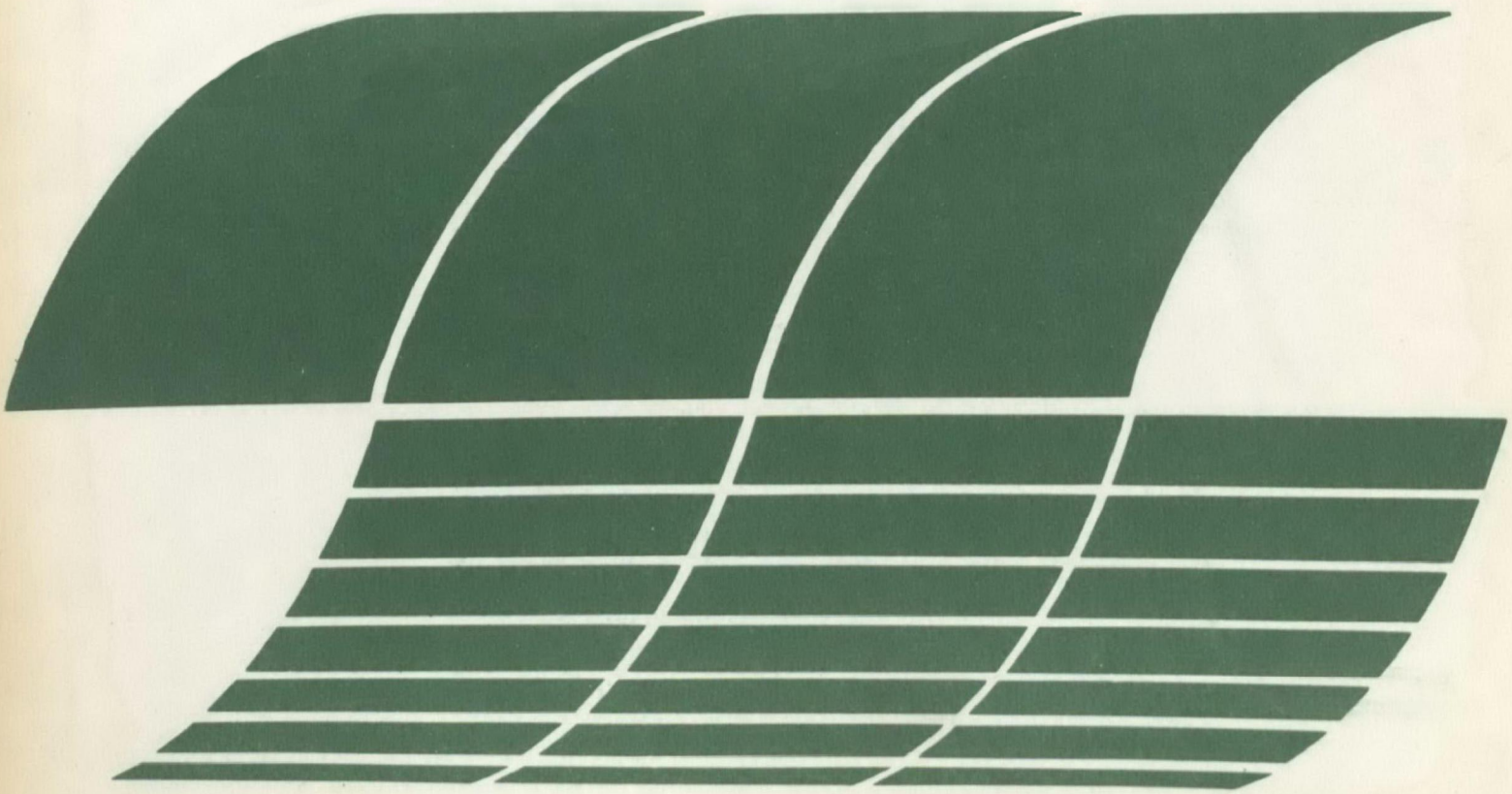

RESEARCH REPORTING SERIES

Research reports of the Office of Research and Development, U.S. Environmental Protection Agency, have been grouped into nine series. These nine broad categories were established to facilitate further development and application of environmental technology. Elimination of traditional grouping was consciously planned to foster technology transfer and a maximum interface in related fields. The nine series are:

1. Environmental Health Effects Research
2. Environmental Protection Technology
3. Ecological Research
4. Environmental Monitoring
5. Socioeconomic Environmental Studies
6. Scientific and Technical Assessment Reports (STAR)
7. Interagency Energy-Environment Research and Development
8. "Special" Reports
9. Miscellaneous Reports

This document is available to the public through the National Technical Information Service, Springfield, Virginia 22161.

EPA-600/9-80-039c
September 1980

SECOND SYMPOSIUM ON THE TRANSFER AND UTILIZATION OF PARTICULATE CONTROL TECHNOLOGY VOLUME III. PARTICULATE CONTROL DEVICES

by

F.P. Venditti, J.A. Armstrong, and Michael Durham

Denver Research Institute
P.O. Box 10127
Denver, Colorado 80210

Grant Number: R805725

Project Officer

Dennis C. Drehmel
Office of Energy, Minerals, and Industry
Industrial Environmental Research Laboratory
Research Triangle Park, NC 27711

INDUSTRIAL ENVIRONMENTAL RESEARCH LABORATORY
OFFICE OF RESEARCH AND DEVELOPMENT
U.S. ENVIRONMENTAL PROTECTION AGENCY
RESEARCH TRIANGLE PARK, NC 27711

DISCLAIMER

This report has been reviewed by the Industrial Environmental Research Laboratory-Research Triangle Park, North Carolina, Office of Research and Development, U.S. Environmental Protection Agency, and approved for publication. Approval does not signify that the contents necessarily reflect the views and policies of the U.S. Environmental Protection Agency, nor does mention of trade names or commercial products constitute endorsement or recommendation for use.

ABSTRACT

The papers in these four volumes of Proceedings were presented at the Second Symposium on the Transfer and Utilization of Particulate Control Technology held in Denver, Colorado during 23 July through 27 July 1979, sponsored by the Particulate Technology Branch of the Industrial Environmental Research Laboratory of the Environmental Protection Agency and hosted by the Denver Research Institute of the University of Denver.

The purpose of the symposium was to bring together researchers, manufacturers, users, government agencies, educators and students to discuss new technology and to provide an effective means for the transfer of this technology out of the laboratories and into the hands of the users.

The three major categories of control technologies - electrostatic precipitators, scrubbers, and fabric filters - were the major concern of the symposium. These technologies were discussed from the perspectives of economics; new technical advancements in science and engineering; and applications. Several papers dealt with combinations of devices and technologies, leading to a concept of using a systems approach to particulate control rather than device control. Additional topic areas included novel control devices, high temperature/high pressure applications, fugitive emissions, and measurement techniques.

These proceedings are divided into four volumes, each volume containing a set of related session topics to provide easy access to a unified technology area.

CONTENTS

	Page
VOLUME I CONTENTS	vi
VOLUME II CONTENTS	ix
VOLUME IV CONTENTS	xii

Section A - Scrubbers

	Page
FLUX FORCE/CONDENSATION SCRUBBER DEMONSTRATION PLANT IN THE IRON AND STEEL INDUSTRY R. Chmielewski, S. Bhutra, S. Calvert, D.L. Harmon, J.H. Abbott	1
COLLECTION CHARACTERISTICS OF A DOUBLE STAGE SCRUBBER TO ELIMINATE THE PAINT MIST FROM A SPRAY BOOTH T. Isoda and T. Azuma	16
APPLICATION OF SLIPSTREAMED AIR POLLUTION CONTROL DEVICES ON WASTE-AS-FUEL PROCESSES F.D. Hall, J.M. Bruck, D.N. Albrinck and R.A. Olexsey	25
EVALUATION OF THE CEILCOTE IONIZING WET SCRUBBER D.S. Ensor and D.L. Harmon	39
DEMONSTRATION OF A HIGH FIELD ELECTROSTATICALLY ENHANCED VENTURI SCRUBBER ON A MAGNESIUM FURNACE FUME EMISSION M.T. Kearns and D.L. Harmon	61
DROPLET REMOVAL EFFICIENCY AND SPECIFIC CARRYOVER FOR LIQUID ENTRAINMENT SEPARATORS J.H. Gavin and F.W. Hoffman	81
AN EVALUATION OF GRID ROD FAILURE IN A MOBILE BED SCRUBBER J.S. Kinsey and S. Rohde	95
OPERATION AND MAINTENANCE OF A PARTICULATE SCRUBBER SYSTEM'S ANCILLARY COMPONENTS P.A. Czuchra	104
LOWERING OPERATING COSTS WHILE INCREASING THROUGHPUT AND EFFICIENCY OF REACTORS AND SCRUBBERS R.P. Tennyson, S.F. Roe, Jr. and R.H. Lace, Sr.	117
OPTIMIZING VENTURI SCRUBBER PERFORMANCE THROUGH MODELING D.W. Cooper	127
THE IMPACT OF HUMIDIFICATION CHAMBER PHYSICS ON WET GAS CLEANUP SYSTEMS D.P. Bloomfield, M.L. Finson, G.A. Simons and K.L. Wray	145

Page

IMPROVING THE EFFICIENCY OF FREE-JET SCRUBBERS 162
D.A. Mitchell

Section B - Fabric Filters

HIGH VELOCITY FIBROUS FILTRATION 171
M.J. Ellenbecker, J.M. Price, D. Leith and M.W. First

THE EFFECT OF DUST RETENTION ON PRESSURE DROP IN A HIGH VELOCITY PULSE-JET FABRIC FILTER 190
M.J. Ellenbecker and D. Leith

ROLE OF FILTER STRUCTURE AND ELECTROSTATICS IN DUST CAKE FORMATION 209
G.E.R. Lamb and P.A. Costanza

PRESSURE DROP IN ELECTROSTATIC FABRIC FILTRATION 222
T. Ariman and D.J. Helfritch

EXPERIMENTAL ADVANCES ON FABRIC FILTRATION TECHNOLOGY IN JAPAN - EFFECTS OF CORONA PRECHARGER AND RELATIVE HUMIDITY ON FILTER PERFORMANCE 237
K. Iinoya and Y. Mori

BAGHOUSE OPERATING EXPERIENCE ON A NO. 6 OIL-FIRED BOILER 251
D.W. Rolschau

NEW FABRIC FILTER CONCEPT PROVEN MORE FLEXIBLE IN DESIGN, EASIER TO MAINTAIN, AND UNSURPASSED FILTRATION 260
B. Carlsson and R.J. Labbe

EPRI'S FABRIC FILTER TEST MODULE PROGRAM: A REVIEW AND PROGRESS REPORT 270
R.C. Carr and J. Ebrey

Section C - Granular Beds

ELECTROSTATIC ENHANCEMENT OF MOVING-BED GRANULAR FILTRATION 289
D.S. Grace, J.L. Guillory and F.M. Placer

ELECTRICAL AUGMENTATION OF GRANULAR BED FILTERS 309
S.A. Self, R.H. Cross and R.H. Eustis

Page

THEORETICAL AND EXPERIMENTAL FILTRATION EFFICIENCIES IN ELECTROSTATICALLY AUGMENTED GRANULAR BEDS 344
G.A. Kallio, P.W. Dietz and C. Gutfinger

AEROSOL FILTRATION BY A CONCURRENT MOVING GRANULAR BED: DESIGN AND PERFORMANCE 363
T.W. Kalinowski and D. Leith

DEEP BED PARTICULATE FILTRATION USING THE PURITREAT (TM) PROCESS 382
L.C. Hardison

Section D - Novel Devices

PILOT-SCALE FIELD TESTS OF HIGH GRADIENT MAGNETIC FILTRATION. 404
C.H. Gooding and C.A. Pareja

EXPERIENCES WITH CONTROL SYSTEMS USING A UNIQUE PATENTED STRUCTURE 416
G.C. Pedersen

ELECTROSTATIC EFFECTS IN VORTICAL FLOWS 429
P.W. Dietz

CONDENSATIONAL ENLARGEMENT AS A SUPPLEMENT TO PARTICLE CONTROL TECHNOLOGIES 439
J.T. Brown, Jr.

Section E - Specific Applications

WELDING FUME AND HEAT RECOVERY - THE PROBLEM, THE SOLUTION, THE BENEFITS 448
R.C. Larson

PARTICULATE REMOVAL CONSIDERATIONS IN SOLVENT EMISSION CONTROL INSTALLATIONS 472
E.A. Brackbill and P.W. Kalika

ARSENIC EMISSIONS AND CONTROL TECHNOLOGY - GOLD ROASTING OPERATIONS 484
J.O. Burckle, G.H. Marchant and R.L. Meek

CONTROL OF SALT LADEN PARTICULATE EMISSIONS FROM HOGGED FUEL BOILERS 508
M.F. Szabo, R.W. Gerstle and L. Sims

AUTHOR INDEX 526

VOLUME I

CONTROL OF EMISSIONS FROM COAL FIRED BOILERS

Section A - Electrostatic Precipitators

COST AND PERFORMANCE OF PARTICULATE CONTROL DEVICES FOR LOW-SULFUR WESTERN COALS 1
R.A. Chapman, D.P. Clements, L.E. Sparks and J.H. Abbott

CRITERIA FOR DESIGNING ELECTROSTATIC PRECIPITATORS . . . 15
K. Darby

EVALUATION OF THE GEORGE NEAL ELECTROSTATIC PRECIPITATOR 35
R.C. Carr

EPA MOBILE ESP HOT-SIDE PERFORMANCE EVALUATION 56
S.P. Schliesser, S. Malani, C.L. Stanley and L. E. Sparks

PRECIPITATOR UPGRADING AND FUEL CONTROL PROGRAM FOR PARTICULATE COMPLIANCE AT PENNSYLVANIA POWER & LIGHT COMPANY 80
J.T. Guiffre

MODIFICATION OF EXISTING PRECIPITATORS TO RESPOND TO FUEL CHANGES AND CURRENT EMISSION REGULATIONS. 100
D.S. Kelly and R.D. Frame

PERFORMANCE OF ELECTROSTATIC PRECIPITATORS WITH LOAD VARIATION. 117
W.T. Langan, G. Gogola and E.A. Samuel

FLY ASH CONDITIONING BY CO-PRECIPITATION WITH SODIUM CARBONATE 132
J.P. Gooch, R.E. Bickelhaupt and L.E. Sparks

PREDICTING FLY ASH RESISTIVITY - AN EVALUATION 154
R.E. Bickelhaupt and L.E. Sparks

SO_3 CONDITIONING FOR IMPROVED ELECTROSTATIC PRECIPITATOR PERFORMANCE OPERATING ON LOW SULFUR COAL 170
J.J. Ferrigan, III and J. Roehr

DOES SULPHUR IN COAL DOMINATE FLYASH COLLECTION IN ELECTROSTATIC PRECIPITATORS? 184
E.C. Potter and C.A.J. Paulson

ANALYSIS OF THERMAL DECOMPOSITION PRODUCTS OF FLUE GAS CONDITIONING AGENTS 202
R.B. Spafford, H.K. Dillon, E.B. Dismukes and L.E. Sparks

Page

BIOTOXICITY OF FLY ASH PARTICULATE 224
A.R. Kolber, T.J. Wolff, J. Abbott and L. E. Sparks

Section B - Fabric Filters

FABRIC FILTERS VERSUS ELECTROSTATIC PRECIPITATORS . . . 243
E.W. Stenby, R.W. Scheck, S.D. Severson, F.A. Horney and D.P. Teixeira

DESIGN AND CONSTRUCTION OF BAGHOUSES FOR SHAWNEE STEAM PLANT 263
J.A. Hudson, L.A. Thaxton, H.D. Ferguson, Jr., and N. Clay

OPERATING CHARACTERISTICS OF A FABRIC FILTER ON A PEAKING/CYCLING BOILER WITHOUT AUXILIARY PREHEAT OR REHEAT 297
W. Smit and K. Spitzer

OBJECTIVES AND STATUS OF FABRIC FILTER PERFORMANCE STUDY 317
K.L. Ladd, R. Chambers, S. Kunka and D. Harmon

START-UP AND INITIAL OPERATIONAL EXPERIENCE ON A 400,000 ACFM BAGHOUSE ON CITY OF COLORADO SPRINGS' MARTIN DRAKE UNIT NO. 6 342
R.L. Ostop and J.M. Urich, Jr.

DESIGN, OPERATION, AND PERFORMANCE TESTING OF THE CAMEO NO. 1 UNIT FABRIC FILTER 351
H.G. Brines

EXPERIENCE AT COORS WITH FABRIC FILTERS - FIRING PULVERIZED WESTERN COAL 359
G.L. Pearson

FABRIC FILTER EXPERIENCE AT WAYNESBORO 372
W.R. Marcotte

A NEW TECHNIQUE FOR DRY REMOVAL OF SO_2. 390
C.C. Shale and G.W. Stewart

SPRAY DRYER/BAGHOUSE SYSTEM FOR PARTICULATE AND SULFUR DIOXIDE CONTROL, EFFECTS OF DEW POINT, COAL AND PLANT OPERATING CONDITIONS 410
W.R. Lane

SELECTION, PREPARATION AND DISPOSAL OF SODIUM COMPOUNDS FOR DRY SO_x SCRUBBERS 425
D.A. Furlong, R.L. Ostop and D.C. Drehmel

VOLUME I CONTENTS (Cont.)

Page

HIGH VELOCITY FABRIC FILTRATION FOR CONTROL OF COAL-FIRED BOILERS 432
J.C. Mycock, R.A. Gibson and J.M. Foster

EPA MOBILE FABRIC FILTER - PILOT INVESTIGATION OF HARRINGTON STATION PRESSURE DROP DIFFICULTIES 453
W.O. Lipscomb, S.P. Schliesser and V.S. Malani

PASSIVE ELECTROSTATIC EFFECTS IN FABRIC FILTRATION . . . 476
R.P. Donovan, J.H. Turner and J.H. Abbott

A WORKING MODEL FOR COAL FLY ASH FILTRATION. 494
R. Dennis and H.A. Klemm

Section C - Scrubbers

PARTICULATE REMOVAL AND OPACITY USING A WET VENTURI SCRUBBER - THE MINNESOTA POWER AND LIGHT EXPERIENCE . . 513
D. Nixon and C. Johnson

PERFORMANCE OF ENVIRONMENTALLY APPROVED NLA SCRUBBER FOR SO_2 529
J.A. Bacchetti

DESIGN GUIDELINES FOR AN OPTIMUM SCRUBBER SYSTEM. . . . 538
M.B. Ranade, E.R. Kashdan and D.L. Harmon

TESTS ON UW ELECTROSTATIC SCRUBBER FOR PARTICULATE AND SULFUR DIOXIDE COLLECTION 561
M.J. Pilat

EPA MOBILE VENTURI SCRUBBER PERFORMANCE 570
S. Malani, S.P. Schliesser and W.O. Lipscomb

THE RESULTS OF A TWO-STAGE SCRUBBER/CHARGED PARTICULATE SEPARATOR PILOT PROGRAM 591
J.R. Martin, K.W. Malki and N. Graves

AUTHOR INDEX 616

VOLUME II

ELECTROSTATIC PRECIPITATORS

Section A - Fundamentals

Page

COLLECTION EFFICIENCY OF ELECTROSTATIC PRECIPITATORS BY NUMERICAL SIMULATION 1
E.A. Samuel

THE EFFECTS OF CORONA ELECTRODE GEOMETRY ON THE OPERATIONAL CHARACTERISTICS OF AN ESP 31
G. Rinard, D. Rugg, W. Patten and L.E. Sparks

THEORETICAL METHODS FOR PREDICTING ELECTRICAL CONDITIONS IN WIRE-PLATE ELECTROSTATIC PRECIPITATORS 45
R.B. Mosley, J.R. McDonald and L.E. Sparks

LATERAL PROPAGATION OF BACK DISCHARGE 65
S. Masuda and S. Obata

THEORETICAL MODELS OF BACK CORONA AND LABORATORY OBSERVATIONS 74
D.W. VanOsdell, P.A. Lawless and L.E. Sparks

CHARGE MEASUREMENTS ON INDIVIDUAL PARTICLES EXITING LABORATORY PRECIPITATORS 93
J.R. McDonald, M.H. Anderson, R.B. Mosley and L.E. Sparks

OPTIMIZATION OF COLLECTION EFFICIENCY BY VARYING PLATE SPACING WITHIN AN ELECTROSTATIC PRECIPITATOR 114
E.J. Eschbach and D.E. Stock

INTERACTION BETWEEN ELECTROSTATICS AND FLUID DYNAMICS IN ELECTROSTATIC PRECIPITATORS 125
S. Bernstein and C.T. Crowe

PARTICLE TRANSPORT IN ELECTROSTATIC PRECIPITATORS . . . 146
G. Leonard, M. Mitchner and S.A. Self

Section B - Operation and Maintenance

THE "HUMAN ELEMENT" - A PROBLEM IN OPERATING PRECIPITATORS 168
W.J. Buchanan

ELECTROSTATIC PRECIPITATORS - ELECTRICAL PROBLEMS AND SOLUTIONS 173
R.K. Raymond

VOLUME II CONTENTS (Cont.)

Page

ELECTRODE CLEANING SYSTEMS: OPTIMIZING RAPPING ENERGY AND RAPPING CONTROL 189
M. Neundorfer

COMPOSITION OF PARTICULATES--SOME EFFECTS ON PRECIPITATOR OPERATION 208
J.D. Roehr

INCREASING PRECIPITATOR RELIABILITY BY PROPER LOGGING AND INTERPRETATION OF OPERATIONAL PARAMETERS - AN OPERATORS GUIDE 219
P.P. Bibbo and P. Aa

ELECTROSTATIC PRECIPITATORS - START-UP, LOW LOAD, CYCLING, AND MAINTENANCE CONSIDERATIONS 242
F.A. Wybenga and R.J. Batyko

ELECTROSTATIC PRECIPITATOR EMISSION AND OPACITY PERFORMANCE CONTROL THRU RAPPER STRATEGY 256
W.T. Langan, J.H. Oscarson and S. Hassett

RAPPING SYSTEMS FOR COLLECTING SURFACES IN AN ELECTROSTATIC PRECIPITATOR 279
H.L. Engelbrecht

LOW POWER ELECTROSTATIC PRECIPITATION - A LOGICAL SOLUTION TO COLLECTION PROBLEMS EXPERIENCED WITH HIGH RESISTIVITY PARTICULATE 296
J.H. Umberger

Section B - Advanced Design

HIGH INTENSITY IONIZER TECHNOLOGY APPLIED TO RETROFIT ELECTROSTATIC PRECIPITATORS 314
C.M. Chang and A.I. Rimensberger

BOXER-CHARGER - A NOVEL CHARGING DEVICE FOR HIGH RESISTIVITY DUSTS 334
S. Masuda and H. Nakatani

PRECIPITATOR ENERGIZATION UTILIZING AN ENERGY CONSERVING PULSE GENERATOR 352
H.H. Petersen and P. Lausen

PRECHARGER COLLECTION SYSTEM - DESIGN FROM THE LABORATORY THROUGH FIELD DEMONSTRATION 369
M. Nunn, D. Pontius, J.H. Abbott and L.E. Sparks

VOLUME II CONTENTS (Cont.)

Page

TOWARDS A MICROSCOPIC THEORY OF ELECTROSTATIC PRECIPITATION 374
C.G. Noll and T. Yamamoto

ION CURRENT DENSITIES PRODUCED BY ENERGETIC ELECTRONS IN ELECTROSTATIC PRECIPITATOR GEOMETRIES 391
W.C. Finney, L.C. Thanh and R.H. Davis

EXPERIMENTAL STUDIES IN THE ELECTROSTATIC PRECIPITATION OF HIGH-RESISTIVITY PARTICULATE 399
J.C. Modla, R.H. Leiby, T.W. Lugar, and K.E. Wolpert

PILOT PLANT TESTS OF AN ESP PRECEDED BY THE EPA-SoRI PRECHARGER 417
L.E. Sparks, G.H. Ramsey, B.E. Daniel and J.H. Abbott

Section C - Industrial Applications

PILOT PLANT/FULL SCALE EP SYSTEM DESIGN AND PERFORMANCE ON BOF APPLICATION 427
D. Ruth and D. Shilton

THE SELECTION AND OPERATION OF A NEW PRECIPITATOR SYSTEM ON AN EXISTING BASIC OXYGEN FURNACE 441
D. Ruth and D. Shilton

CONTROL OF FINE PARTICLE EMISSIONS WITH WET ELECTROSTATIC PRECIPITATION 452
S.A. Jaasund

TUBULAR ELECTROSTATIC PRECIPITATORS OF TWO STAGE DESIGN 469
H. Surati, M.R. Beltran and I. Raigorodsky

PRESENT STATUS OF WIDE-SPACING TYPE PRECIPITATOR IN JAPAN 483
S. Masuda

LOW FREQUENCY SONIC CLEANING APPLIED TO ELECTROSTATIC PRECIPITATORS 502
S.B. Smith and J.A. Schwartz

AUTHOR INDEX 514

VOLUME IV

SPECIAL APPLICATIONS FOR AIR POLLUTION MEASUREMENT AND CONTROL

Section A - High Temperature High Pressure Applications

Page

FUNDAMENTAL PARTICLE COLLECTION AT HIGH TEMPERATURE AND PRESSURE 1
R. Parker, S. Calvert, D.C. Drehmel and J.H. Abbott

PARTICULATE COLLECTION IN A HIGH TEMPERATURE CYCLONE . . 14
K.C. Tsao, C.O. Jen and K.T. Yung

EVALUATION OF A CYCLONIC TYPE DUST COLLECTOR FOR HIGH TEMPERATURE HIGH PRESSURE PARTICULATE CONTROL 30
M. Ernst, R.C. Hoke, V.J. Siminski, J.D. McCain, R. Parker and D.C. Drehmel

CERAMIC FILTER TESTS AT THE EPA/EXXON PFBC MINIPLANT . . 42
M. Ernst and M.A. Shackleton

HOT GAS CLEAN-UP BY GLASS ENTRAINMENT OF COMBUSTION BY-PRODUCTS 64
W. Fedarko, A. Gatti and L.R. McCreight

THE A.P.T. PxP DRY SCRUBBER FOR HIGH TEMPERATURE AND PRESSURE PARTICULATE CONTROL 84
R.G. Patterson, S. Calvert and M. Taheri

GAS CLEANING UNDER EXTREME CONDITIONS OF TEMPERATURE AND PRESSURE 98
E. Weber, K. Hübner, H.G. Pape and R. Schulz

PROGRESS ON ELECTROSTATIC PRECIPITATORS FOR USE AT HIGH TEMPERATURE AND HIGH PRESSURE 126
G. Rinard, D. Rugg, R. Gyepes and J. Armstrong

REDUCTION OF PARTICULATE CARRYOVER FROM A PRESSURIZED FLUIDIZED BED 136
R.W. Patch

COMPARATIVE ECONOMIC ANALYSIS OF SELECTED PARTICULATE CONTROL SYSTEMS FOR ADVANCED COMBINED CYCLE POWER PLANTS 154
J.R. Bush, F.L. Blum and P.L. Feldman

CONCLUSIONS FROM EPA'S HIGH TEMPERATURE/HIGH PRESSURE CONTROL PROGRAM 170
D.C. Drehmel and J.H. Abbott

VOLUME IV CONTENTS (Cont.)

Section B - Fugitive Emissions

Page

WATER SPRAY CONTROL OF FUGITIVE PARTICULATES: ENERGY AND UTILITY REQUIREMENTS 182
D.P. Daugherty, D.W. Coy and D.C. Drehmel

THE CONTROL OF DUST USING CHARGED WATER FOGS 201
S.A. Hoenig

SPRAY CHARGING AND TRAPPING SCRUBBER FOR FUGITIVE PARTICLE EMISSION CONTROL 217
S. Yung, S. Calvert, and D.C. Drehmel

CONTROL OF WINDBLOWN DUST FROM STORAGE PILES 240
C. Cowherd, Jr.

THE CONTRIBUTION OF OPEN SOURCES TO AMBIENT TSP LEVELS 252
J.S. Evans and D.W. Cooper

FUTURE AREAS OF INVESTIGATION REGARDING THE PROBLEM OF URBAN ROAD DUST 274
E.T. Brookman and D.C. Drehmel

STATUS OF CONNECTICUT'S CONTROL PROGRAM FOR TRANSPORTATION-RELATED PARTICULATE EMISSIONS 291
J.H. Gastler and H.L. Chamberlain

NEW CONCEPTS FOR CONTROL OF FUGITIVE PARTICLE EMISSIONS FROM UNPAVED ROADS 312
T.R. Blackwood and D.C. Drehmel

DEVELOPMENT OF A SAMPLING TRAIN FOR THE ASSESSMENT OF PARTICULATE FUGITIVE EMISSIONS 321
R.L. Severance and H.J. Kolnsberg

SECONDARY NEGATIVE ELECTRON BOMBARDMENT FOR PARTICULATE CONTROL 333
W.E. Stock

Section C - Measurement and Analysis

HIGH TEMPERATURE AND HIGH PRESSURE SAMPLING DEVICE USED FOR PARTICULATE CHARACTERIZATION OF A FLUIDIZED BED COAL GASIFICATION PROCESS 338
S.P. Tendulkar, J. Pavel and P. Cherish

ON-STREAM MEASUREMENT OF PARTICULATE SIZE AND LOADING 351
E.S. VanValkenburg

VOLUME IV CONTENTS (Cont.)

Page

ANALYSIS OF SAMPLING REQUIREMENTS FOR CYCLONE OUTLETS 368
M.D. Durham and D.A. Lundgren

ELECTROSTATIC EFFECTS ON SAMPLING THROUGH UNGROUNDED PROBES 387
W.B. Giles and P.W. Dietz

OPTICAL PARTICULATE SIZE MEASUREMENTS USING A SMALL-ANGLE NEAR-FORWARD SCATTERING TECHNIQUE 396
J.C.F. Wang

IN-STACK PLUME OPACITY FROM ELECTROSTATIC PRECIPITATOR SCRUBBER SYSTEMS 411
L.E. Sparks, G.H. Ramsey and B.E. Daniel

TI-59 PROGRAMMABLE CALCULATOR PROGRAMS FOR IN-STACK OPACITY 424
S.J. Cowen, D.S. Ensor and L.E. Sparks

UTILIZATION OF THE OMEGA-1 LIDAR IN EPA ENFORCEMENT MONITORING 443
A.W. Dybdahl and F.S. Mills

EFFECTS OF PARTICLE-CONTROL DEVICES ON ATMOSPHERIC EMISSIONS OF MINOR AND TRACE ELEMENTS FROM COAL COMBUSTION 454
J.M. Ondov and A.H. Biermann

A SOURCE IDENTIFICATION TECHNIQUE FOR AMBIENT AIR PARTICULATE 486
E.J. Fasiska, P.B. Janocko and D.A. Crawford

PARTICLE SIZE MEASUREMENTS OF AUTOMOTIVE DIESEL EMISSIONS 496
J.D. McCain, and D. Drehmel

CONTROL STRATEGIES FOR PARTICULATE EMISSIONS FROM VEHICULAR DIESEL EXHAUST 508
M.G. Faulkner, J.P. Gooch, J.R. McDonald, J.H. Abbott and D.C. Drehmel

AN EVALUATION OF THE CYTOTOXICITY AND MUTAGENICITY OF ENVIRONMENTAL PARTICULATES IN THE CHO/HGPRT SYSTEM . . 524
N.E. Garrett, G.M. Chescheir, III, N.A. Custer, J.D. Shelburne, Catherine R. De Vries, J.L. Huisingh and M.D. Waters

AUTHOR INDEX 536

FLUX FORCE/CONDENSATION SCRUBBER DEMONSTRATION PLANT IN THE IRON AND STEEL INDUSTRY

by

Richard Chmielewski, Sudarshan Bhutra, and Seymour Calvert

Air Pollution Technology, Inc.
San Diego, California 92117

and

Dale L. Harmon and James A. Abbott

Industrial Environmental Research Laboratory
U.S. Environmental Protection Agency
Research Triangle Park, North Carolina 27711

ABSTRACT

A flux force/condensation scrubber was designed, built, and operated by Air Pollution Technology, Inc. to control the particulate emissions from an iron and steel melting cupola. The cupola had a production rate of approximately 14,000 kg/hr (15 tons/hr). The entire exhaust gas flow of 8.5 kg/s (14,000 dscfm) was cleaned in the scrubber system. The major components included an afterburner, spray saturator, condenser, scrubber, and fan. A cooling tower was used to reject heat from the system and a parallel plate settler was used to separate solids from the circulation water.

Flux force/condensation scrubbing technology has been extensively developed by A.P.T. under EPA sponsorship. The flux forces of thermophoresis and diffusiophoresis and the condensation of water vapor on the particles are used to improve the collection efficiency for fine particles and reduce the energy requirements.

Performance data were obtained by sampling for particulates at several locations. Several operating conditions were tested and experimental results were compared with theoretical predictions of particle collection. The performance of the flux force/condensation scrubbing system was evaluated and compared to high energy gas atomized scrubbing.

FLUX FORCE/CONDENSATION SCRUBBER DEMONSTRATION PLANT IN THE IRON AND STEEL INDUSTRY

INTRODUCTION

This paper describes a flux force/condensation (F/C) scrubber for controlling emissions from an iron melting cupola. The air pollution control system has been designed, built, and operated by Air Pollution Technology, Inc. under contract by the EPA. The objectives of this project are to verify the design, performance, and economics of F/C scrubbing.

F/C scrubbing uses the flux forces of diffusiophoresis and thermophoresis to improve fine particle collection. Condensation of water vapor on the particles and the subsequent increase in mass is the third mechanism which improves performance.

This demonstration program is the most recent in a number of EPA contracts to develop F/C scrubbing as a means of improving the fine particle collection in wet scrubbers. Earlier work involved laboratory and pilot-scale projects to verify the technical feasibility and develop design data and methods for F/C scrubbing. This paper presents the results to date of a second demonstration plant which is operating on the total emissions from an iron melting cupola. An earlier demonstration F/C system was designed and operated to control the emissions from a secondary metal recovery furnace.

DESCRIPTION OF SOURCE

The melting furnace is a No. 9, water-cooled cupola whose inside diameter at the melting zone is approximately 180 cm. The melting capacity of the cupola is 14,000 kg/hr (15 tons/hr). Figure 1 shows the process flow diagram for the system. The raw materials for the cupola include approximately 16,000 kg/hr scrap, 2,750 kg/hr coke and 500 kg/hr limestone. The combustion air is supplied at a rate of 3.4 DNm^3/s (7,700 dscfm).

The uncontrolled emission factor for an iron melting cupola is 8.5 g particulate per kg of metal charged. For the cupola at rated capacity this corresponds to 136 kg particulate/hr. The emission limit is 14.4 kg/hr for this application where the process weight is 19×10^3 kg/hr. The maximum allowable system penetration is 0.106.

Figure 2 shows the measured particle size distribution for the emissions from the cupola. These size data were obtained using University of Washington cascade impactors. The mass median particle diameter is about 0.9 μmA. The measurements were made at the inlet to the condenser vessel.

PERFORMANCE REQUIREMENTS

The pressure drop required to achieve a penetration of 0.10 for a high energy gas atomized scrubber is predicted to be approximately 100 cm W.C. This calculation was performed using the particle size distribution shown in Figure 2. The existing air pollution control system at the foundry was capable of providing a scrubber pressure drop in excess of 100 cm W.C.

The F/C scrubber system is designed to minimize the total scrubber system pressure drop and thereby reduce power requirements. Collection of fine particulate using flux forces and growth due to condensation reduce the pressure drop required by the scrubber system.

Figure 3 shows the predicted "grown" particle size distribution leaving the condenser. The grown particle size distribution will depend upon the condensation ratio achieved and the particle number concentration. The condensation ratio is defined as the mass of water condensed per unit mass of dry gas. The particle number concentration is not measured directly by the cascade impactor, however it can be calculated using the particle mass size distribution and the mass concentration. Calculated number concentrations range from 10^8 to 10^9 particles/cm^3.

The predicted scrubber pressure drop required to obtain the desired penetration of 0.10 based on the grown size distribution shown in Figure 3 is 40 cm. W.C. An additional 13 cm W.C. is required for the condenser pressure drop. The total pressure drop required of the F/C scrubber system for this case is 53 cm W.C. versus 100 cm W.C. for a high energy gas atomized scrubber. This pressure drop saving would translate to a 40 percent reduction in fan power requirement.

PROCESS DESCRIPTION

The exhaust gases from the cupola bed are mixed with additional combustion air which enters through the charging door. The gases then enter an afterburner tank which ensures complete combustion of any carbon monoxide produced. The combustion gases leave the afterburner at a maximum temperature of about 1,100°C. The exhaust gas is then cooled in the saturator by water sprays and passes into the condenser at the saturation temperature of about 75°C. Approximately 3.6 g/s of water is evaporated in the saturation process.

The saturated exhaust gases are cooled in the condenser by contacting with cold water. It is in the condenser that the F/C effects are applied. Water vapor is condensed and temperature and concentration gradients established driving the flux forces.

The cooled gases pass into a gas atomized scrubber where the grown particles are collected before passing through the exhaust fan and out the stack.

The heat rejection loop of the system involves a pump to circulate the hot water from the condenser through a cooling tower where the heat is rejected to the atmosphere.

EQUIPMENT DESIGN

Table 1 summarizes the specifications for the major pieces of equipment.

Saturator

The function of the saturator is to cool the hot exhaust gases from the afterburner to the adiabatic saturation temperature. The design chosen was a horizontal tank with high pressure water sprays. Mass transfer calculations were performed on the evaporation process to ensure sufficient residence time for evaporation. The physical layout of the plant dictated that a horizontal vessel be used. The material of construction is 316 stainless steel. City water is supplied to the internal spray nozzles using a high pressure centrifugal pump. The head developed by the saturator pump is 15 atm. The high pressure results in small spray drops which evaporate more effectively than large drops. The co-current spray pattern minimizes gas pressure drop across the saturator.

Condenser

The condenser is a key component of the F/C system. Water vapor is condensed and temperature and concentration gradients established in this part of the system. The design chosen was a counter-current packed bed using 1.25 m of Intalox packing having a nominal dimension of 5 cm. The cooling water is distributed through a trough system across the top of the packing. The gases pass from the saturator into the condenser. Flow straighteners are used to direct the gas flow upward into the condenser. Liquid drains from the bottom of the condenser into a sump tank adjacent to the condenser. The material used for the condenser is 316 stainless steel.

Scrubber

The scrubber used to collect the grown particles is a gas atomized scrubber having a variable area throat. The throat area can be adjusted using a hydraulic cylinder from the instrument trailer or by manual adjustment of the throat blades. The scrubber design incorporates an integral liquid sump and entrainment separator.

The scrubber entrainment separator is a tubebank separator made of 304 stainless steel tubes. The rest of the scrubber is made of 316 stainless steel.

Cooling Tower

The function of the cooling tower is to reject the heat which is given off by the exhaust gases as they are cooled in the condenser. Hot water from the condenser is drained into a sump. The water is pumped from the sump to a commercial-packaged cooling tower. The cooling tower is a standard design incorporating countercurrent air and water flows. The air flow is provided by a set of three centrifugal fans in a forced draft configuration.

Water Treatment

The water treatment for the F/C system involves two processes. Control of water pH is required because of formation of sulfurous acid by absorption of sulfur dioxide from sulfur present in the coke. The pH of the water is maintained above 6 by addition of soda ash.

The solids collected in the system amount to approximately 1,000 kg/day. Particulate matter collects in the bottom of the afterburner tank and in the bottom of the condenser. This material is removed manually from the afterburner and pumped from the condenser using an air operated diaphragm pump.

Suspended solids are removed from the water system by use of a parallel plate gravity settler. A side stream of 1.5 L/S is passed through the settler where solids are separated from the water. A flocculent aid is used to improve solids separation in the settler.

EQUIPMENT LAYOUT

The equipment layout is shown in Figure 4. The space available at the site limited the equipment layout, requiring an innovative design to ensure adequate access for testing and maintenance. The saturator runs north-south with the center line approximately 2 m above grade.

The condenser vessel and scrubber are located on a concrete pad just north of the existing water sump which is used in the new system. The existing exhaust fan is being used and remains in its original location. The ducting system has been designed with sampling requirements in mind.

The cooling tower is located on a platform above the condenser. This design feature allows gravity flow of cooling water from the cooling tower to the condenser eliminating one pump.

Figure 5 shows an alternate design with the scrubber in the forced draft mode. This configuration will be tested in a later portion of the test phase.

TEST METHODS

The performance tests are being made using standard stack sampling techniques. EPA Method 5 tests are made at the inlet to the condenser and at the outlet of the scrubber to determine total mass efficiency of the F/C system. Cascade impactor tests are also made at various locations to obtain size penetration data.

A detailed test plan has been established which will yield performance data at various operating conditions. The primary variable which will be investigated is the condensation ratio achieved by varying the cooling liquid flow rate and the scrubber pressure drop.

Performance Data

The tests have recently started and to date we have obtained performance data on the collection efficiency in the condenser. The main mechanisms for particle collection in the condenser are by inertial impaction and by the combined effects of thermophoresis and diffusiophoresis. Figures 6, 7, and 8 show the experimental penetrations and the predicted penetrations for three different condensation ratios. Log-probability coordinates have been used to facilitate the presentation of the data.

In each case the experimental penetration is lower than the predicted penetrations. This is reasonable in view of the fact that the collection prediction did not include that occurring in other parts of the system. Testing is now under way to obtain data on the total system performance.

SUMMARY

A demonstration F/C scrubber system has been designed, built, and is in operation on the emissions from an iron melting cupola. The system has the potential of reducing the power requirements for control of particulate emissions compared to high energy gas atomized scrubbers which are in use on this type of source.

Results of tests on the performance of the condenser show that the experimental penetration is better than predicted. Testing is now in progress to determine the optimum performance of the F/C scrubber system.

TABLE 1. SUMMARY OF EQUIPMENT DESIGN DETAILS

Component	Description	Size	Construction Materials
Saturator	Horizontal Spray Tower - APT Design	1.5 mϕ x 10.5 m	316 Stainless Steel
Condenser	Counter Current Packed Tower - APT Design	2.75 mϕ x 6 m	316 Stainless Steel with Stainless Packing
Scrubber	Gas Atomized Scrubber - APT Design	2 mϕ x 2 m	316 Stainless Steel
Exhaust Fan	Centrifugal Radial Blade - Westinghouse	Wheel Dia.1.6 m	Carbon Steel
Cooling Tower	Baltimore Air Coil VST 400	3.7 m x 2.7 m x 5.5 m	Epoxy Coated Galvanized
Saturator Pump	Allis Chalmers Two-Stage Centrifugal	54 ℓ/s @ 15 atm	Carbon Steel
Cooling Tower Pump	Peabody - Vertical Turbine	754 ℓ/s @ 2 atm	Cast Iron
Scrubber Pump	Carver Single-Stage Centrifugal	254 ℓ/s @ 1 atm	Cast Iron
Settler	Parkson-Lamella	Settling Area 12 m^2	Carbon Steel Shell PVC Plates
Ducting	--	0.8 mϕ & 0.9 mϕ	FRP
Piping	--	5 cm, 10 cm, 20 cm	FRP

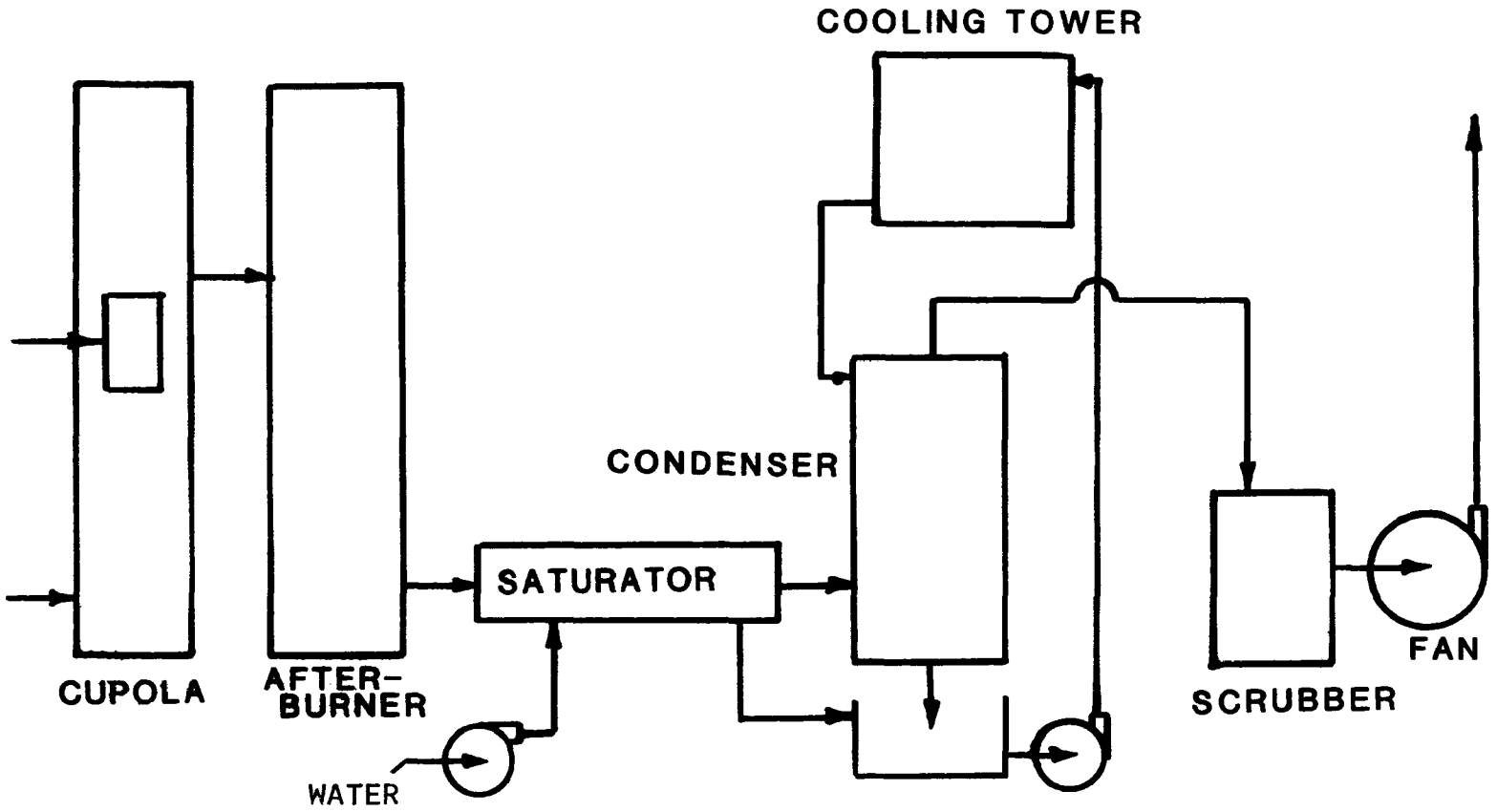

Figure 1. F/C demonstration system flow diagram.

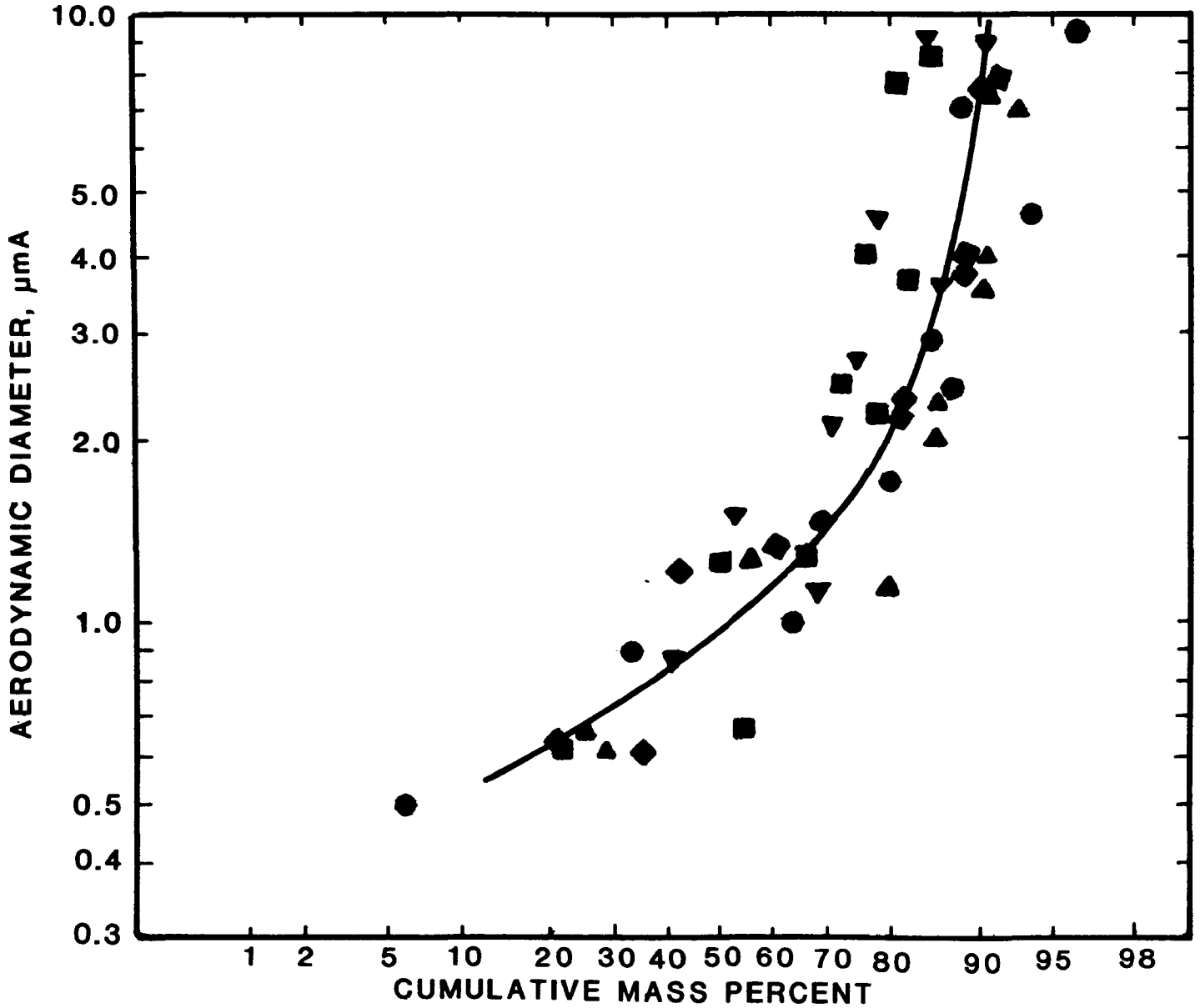

Figure 2. Particle size distribution at condenser inlet.

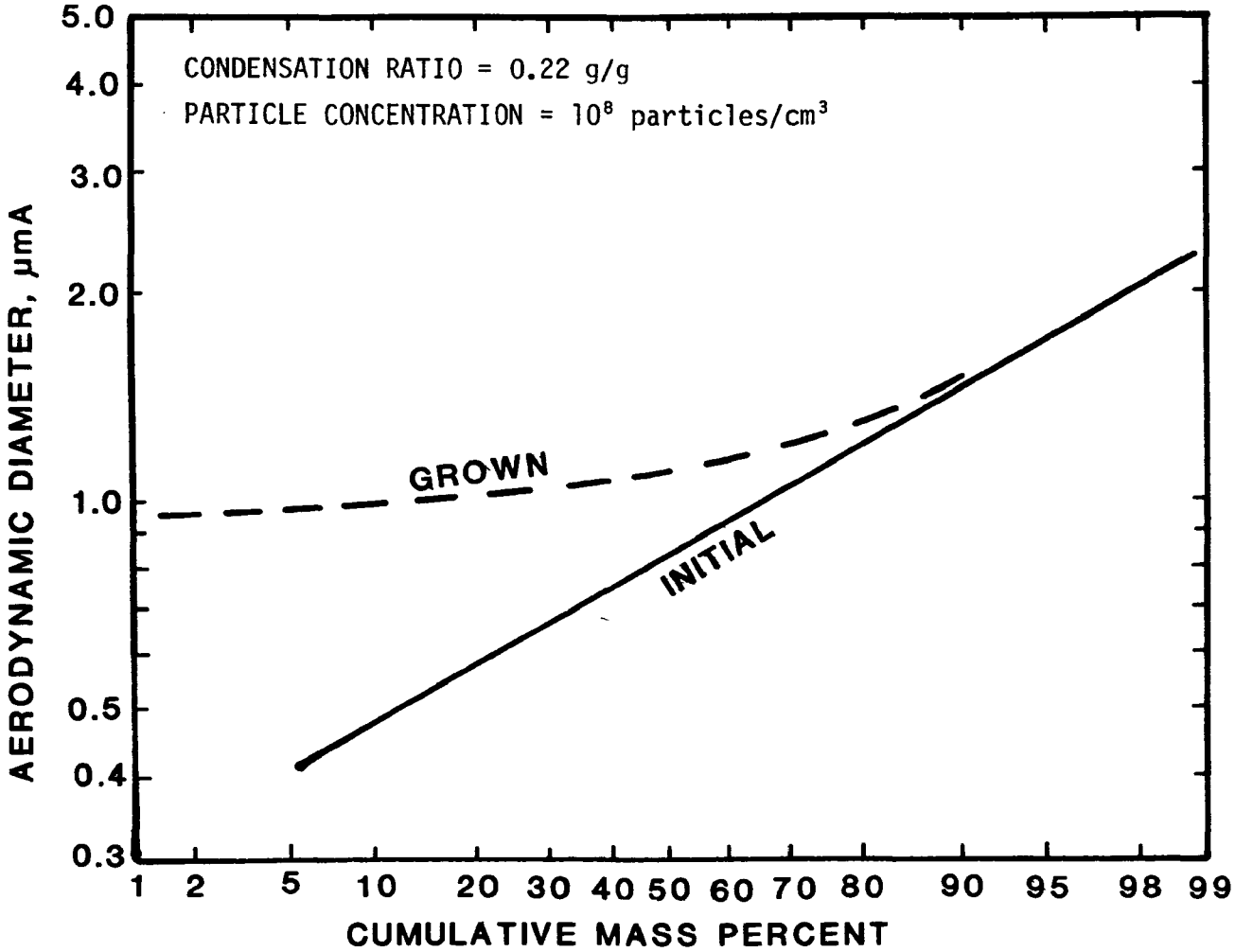

Figure 3. Predicted grown particle size distribution at condenser outlet.

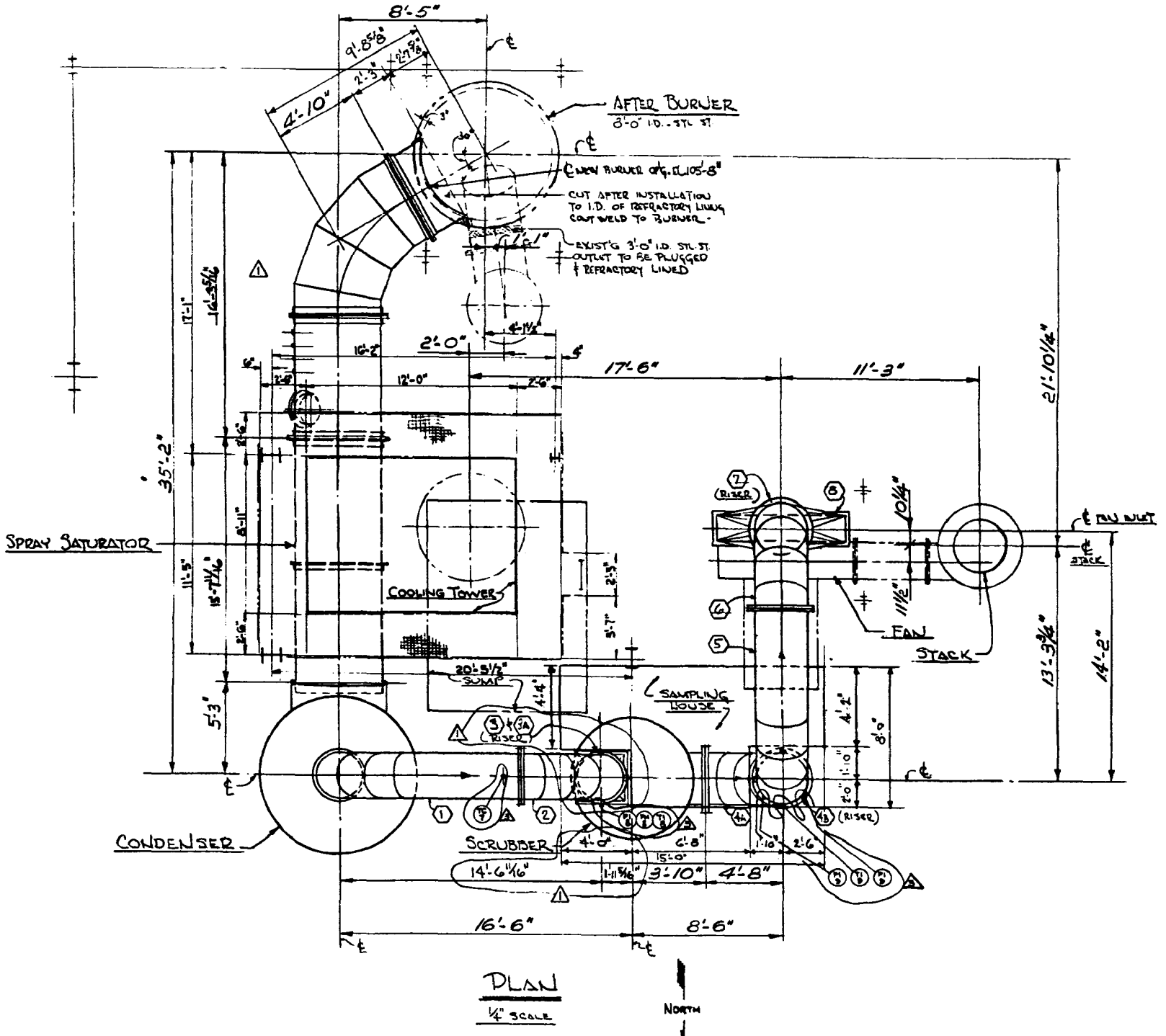

Figure 4. F/C plant induced draft.

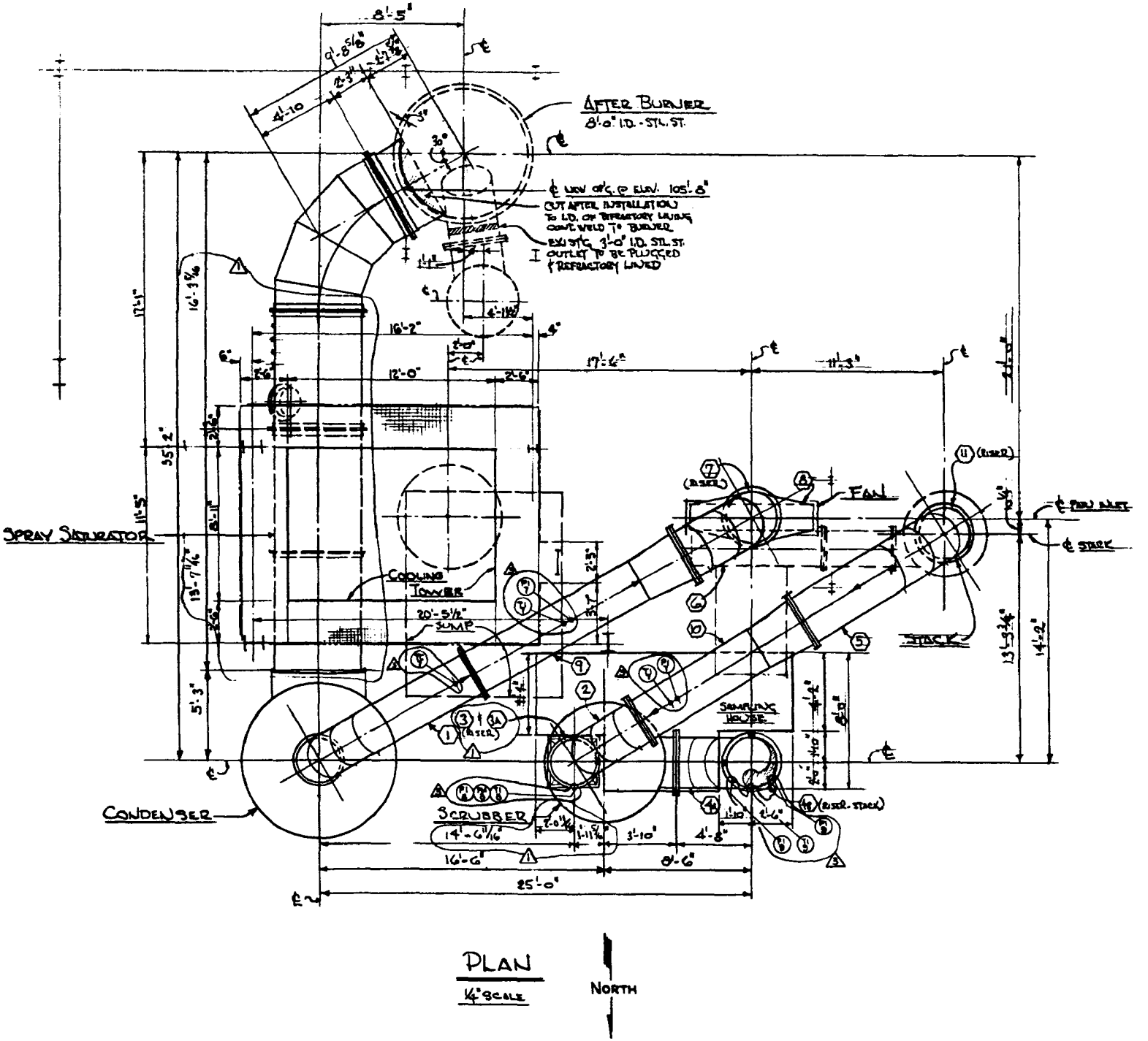

Figure 5. F/C plant forced draft.

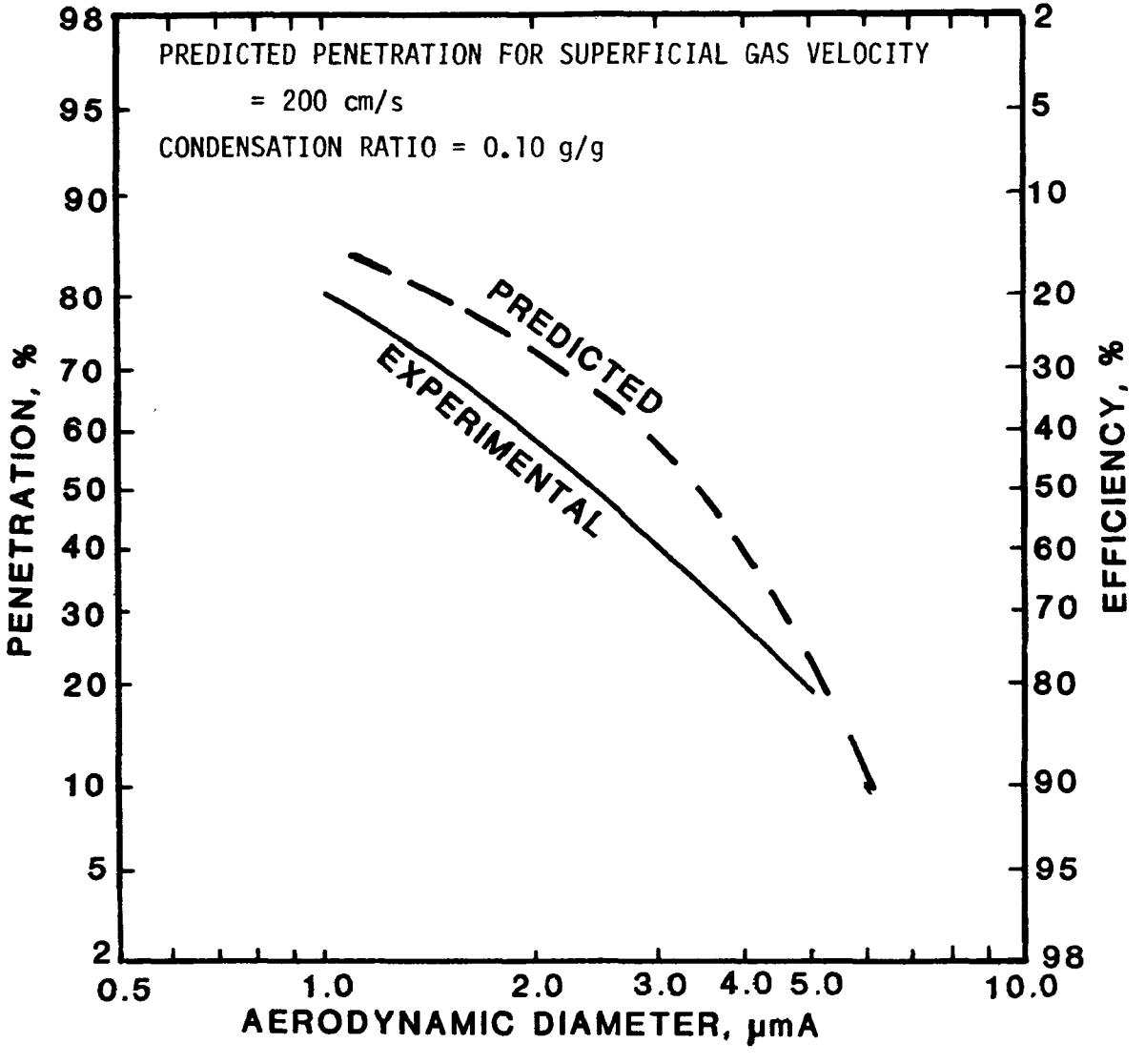

Figure 6. Predicted and experimental penetration for condenser.

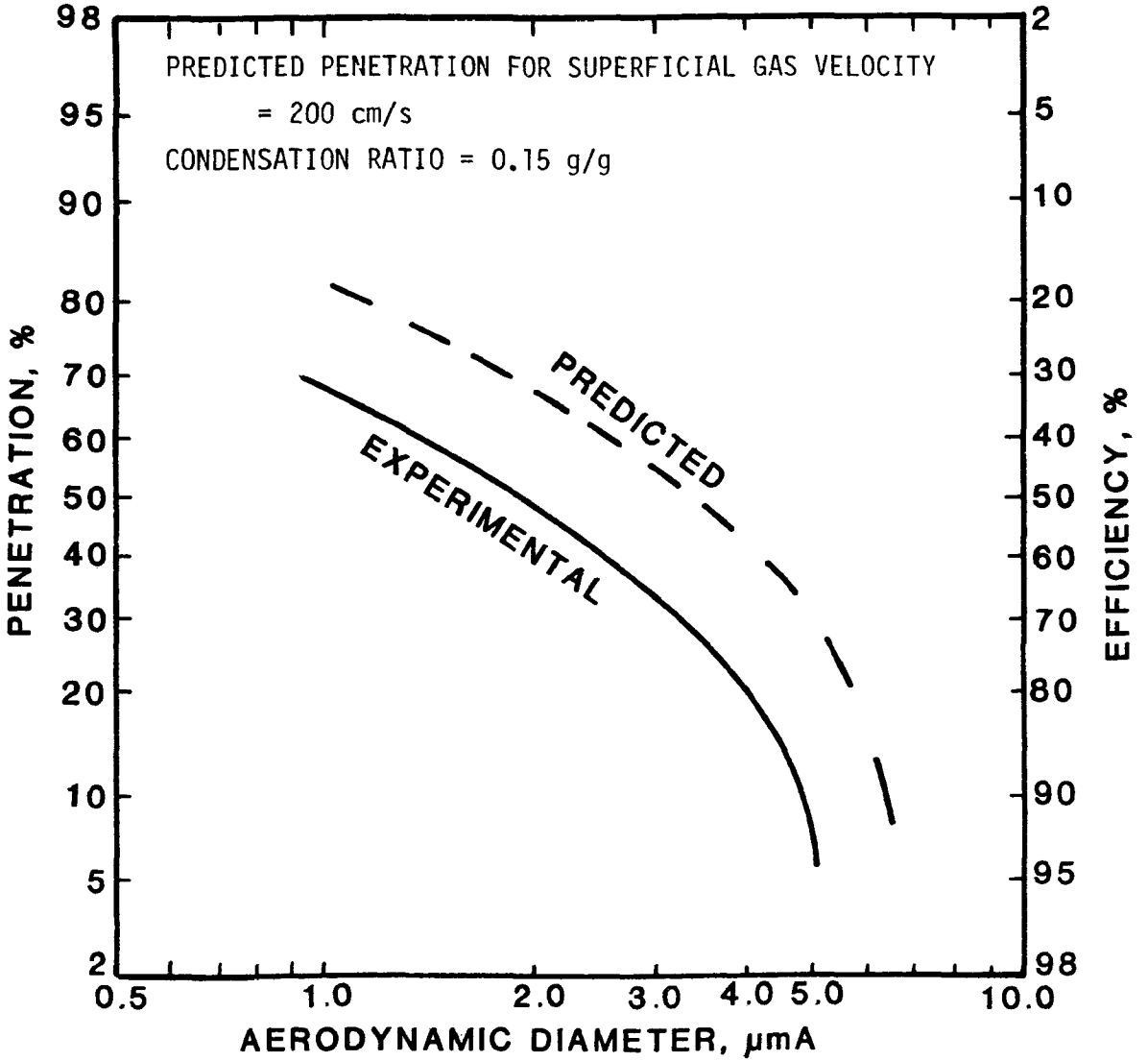

Figure 7. Predicted and experimental penetration for condenser.

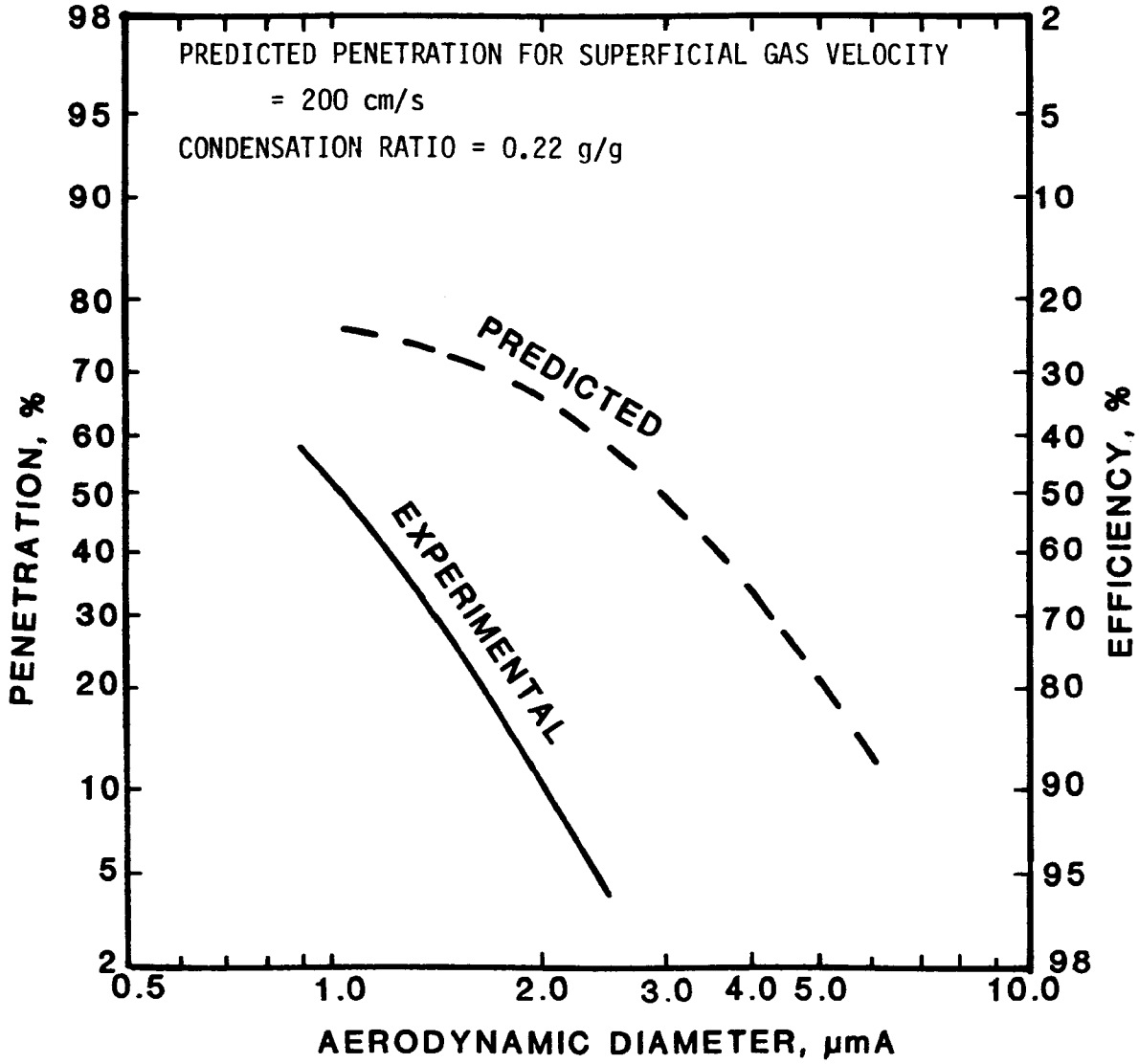

Figure 8. Predicted and experimental penetration for condenser.

COLLECTION CHARACTERISTICS OF A DOUBLE STAGE SCRUBBER TO ELIMINATE THE PAINT MIST FROM A SPRAY BOOTH

By:

Toru Isoda and Tadahiro Azuma
Osaka Prefectural Industrial Research Institute
Enokojima, Nishi-ku, Osaka City 550, Japan

ABSTRACT

A 4.5 m^3/min laboratory paint spray booth was built adopting a double-stage scrubber with heavy oil as the scrubbing liquid. The relationship between the collection efficiency E and the pressure drop ΔP was studied using a cylindrical paper tilter and a Digital Dust Counter. Experimental results indicated that the collection efficiency in this system is in accordance with the collection efficiency equation based on the theory of inertial impaction. With water used as the scrubbing liquid, the factor K is about 0.5 for single-stage scrubbing, while it is 0.6 for double-stage scrubbing.

At a pressure drop of 60 mm of H_2O, heavy oil used as the scrubbing liquid gained about 2.0 % more in collection efficiency than water. The zigzag baffler equipped for removing heavy oil mist was also effective for the paint mist collector, and 99.1 % of E was gained at a pressure drop of 135 mm H_2O.

INTRODUCTION

A high performance scrubber is urgently required in order to eliminate paint mist particles that result from treatment of solvent gas which is emitted from a spray booth by a catalytic combustor. An experimental study of the collection characteristics of paint mist particles is carried out using a new type double-stage scrubber which is equipped with a zigzag baffler. The test is carried out using both water and heavy oil as the scrubbing liquids. This paper presents the experimental results of the relationship between the collection efficiency, pressure drop and fractional efficiency.

EXPERIMENTAL APPARATUS

Figure 1 is a schematic diagram of the experimental scrubber system, which includes a zigzag baffler, a paint spray system, a recorder for the gas flow rate and the pressure drop, an apparatus with a cylindrical paper filter for the measurement of the particle concentration, and a cascade impactor for the measurement of the particle size distribution.

The zigzag baffler has the function of separating the oil mist generated from the scrubber section. Table 1 shows the operating condition in this experiment, and Table 2 presents the property of the paint that was used in this study.

The paint particle concentration in the both the outlet and the inlet of the scrubber was measured on the basis of the paint in its solid form because of its volatility.

EXPERIMENTAL RESULTS

Given in Figure 2 are the relations hips between the counting rate of the Digital Dust Counter and the weight concentration of the solid paint particles. Figure 3 shows the particle size distribution of the solid in spray paint particles.

Collection Characteristics of the Double-Stage Scrubbing Apparatus and the Value of K in the Equation: $Pt = \exp(-K\sqrt{\psi}\,L)$

Shown in Figure 4 is a comparison of the collection characteristics against the solid paint particles on both single and the double-stage scrubbing. The collection efficiency for a venturi scrubber is given approximately by,

$$Pt = \exp(-K\sqrt{\psi}\,L) \qquad (1)$$

where, Pt = penetration

ψ = dimensionless parameter for collection by inertial impaction

L = liquid to gas ratio

K = factor

The dimensionless inertial parameter ψ is expressed as,

$$\psi = \frac{\rho_p d_p^2 u_o}{18 \mu_g \delta} \qquad (2)$$

where, ρ_p = particle density

d_p = particle diameter

u_o = velocity of the aerosol stream

μ_g = gas viscosity

δ = dro-let diameter

In a previous report, the factor K was reported as being from about 0.7 to 1.5[1][2] in a venturi scrubber. The collection performance of the scrubber, a kind of "self-induced spray wet collector" as is the one in this study, is also approximately in agreement with the value given by eq.(1). In this case the liquid to gas ratio L and the droplet diameter δ in eq. (1), (2) is given by the equation[3][4] as follows.

$$Ps = 0.1023\ ug^2 L \qquad (3)$$

$$\delta = \frac{4980}{V_r} + 28.8\ L^{1.5} \qquad (4)$$

where, V_r = gas velocity relative to the liqud. Futhermore, in each case of single and double-stage scrubbing, the factor K is about 0.5 and 0.6 respectively under the operating condition which ranges between 65 to 90 mmH_2O with a pressure drop ΔP.

Effects of the Heavy Oil as a Scrubbing Liquid on Collection Characteristics

Figure 5 gives the collection characteristics of the double-stage scrubbing unit which utilized water and heavy oil as scrubbing liquids. The heavy oil exerts an influence on the ability to collect paint particles to some extent under the operating condition of a low pressure drop. It appears that an increase in collection efficiency is attributed to the property of the paint particle which is hydrophobic.

Zigzag Baffler for Collection of the Paint and Oil Mist Particles

Shown in Figure 6 is the comparison of the collection characteristics of the paint particles between the double-stage scrubber equipped with a zigzag baffler and the scrubber alone. It can be seen that the zigzag baffler effectively acts as the collector of the paint particles which are agglomerated by the oil mist particles generated from the scrubbing section. Figure 7 gives the relationships between a pressure drop ΔP and oil mist generation in the scrubber. Given in Figure 8 is the collection efficiency of the zigzag baffler for the paint particles on various oil mist generations. The collection efficiency of the paint particles increases as the oil mist

generation is increased. Therefore, it appears that the oil film formed on the surface of the battle plates and the agglomarations of the fine paint particles affects the collection efficiency of the paint particles. Given in Figure 9 is the collection efficiency of the oil mist particles due to the zigzag baffler.

Fractional Efficiency

Figure 10 gives the fractional efficiency of the paint particles. The measurement of the fractional efficiency could not be carried out under a range of particle size which is below 1-2μm because of the agglomeration of the particles which occurred in the area of the scrubber, zigzag baffler, and the ducts.

REFERENCE

1. Johnstone, H.F., R.B. Feild, and M.C. Tassler "Gas absorption and aerosol collection in a venturi atomizer" Ind. Eng. Chem. 46, 160, August 1954

2 Morishima, N., "Presumption of Scrubber Performance" Performance of Dust Collector, ed. by Iinoya, K., Ind. Tech. Center Press (1976)p.146

3. Calvert, S. "Source Control by Liquid Scrubbing", Air Pollution III, 2nd, ed. by Stern, A. C., Acad. Press (1968) p.475

4. Nukiyama, S., and Tanasawa, Y., "Study of Liquid Atomization" Trans. Soc. Mech. Engrs. (Japan), 5, No.18, 68-136, February (1939)

Table 1. Operating condition

Gas flow rate(m^3/min)	4.5
Scrubbing liquid—7 l	Water, Heavy oil
Scrubber, pressure drop(mmH_2O)	60, 75, 90
Zigzag baffler, pressure drop(mmH_2O)	45
Paint spray pressure(kg/cm^2)	1.5, 3.5
Scrubbing liquid circulation(l/min)	20

Table 2. Property of paint

Specific gravity	1.05
Solid in paint	472.3 g/l

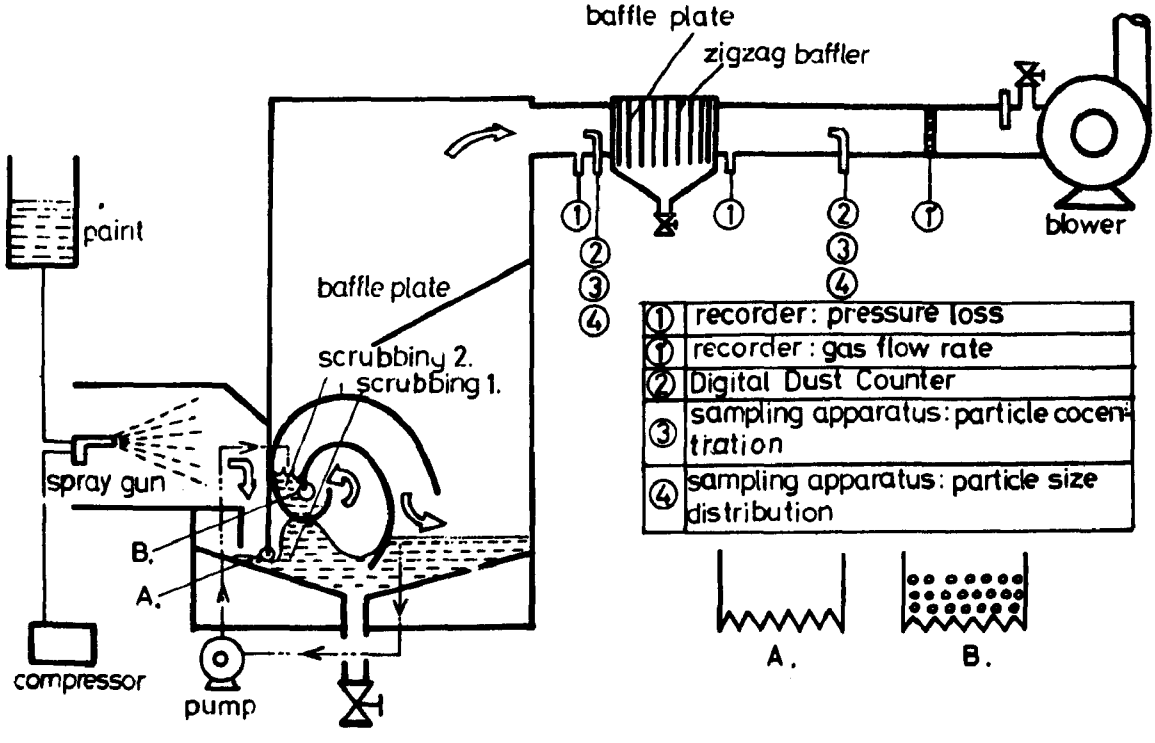

Figure 1. Schematic of the experimental apparatus

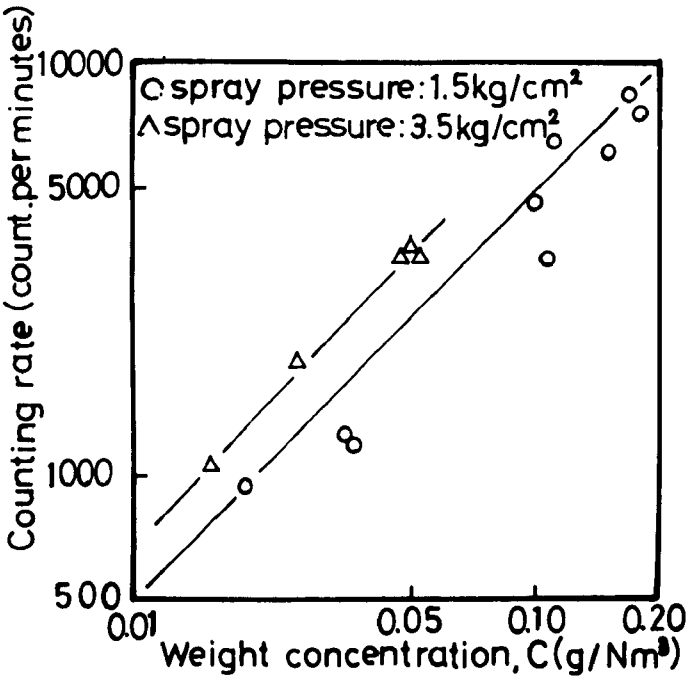

Figure 2. Counting rate vs. weight concentration of solid paint particles

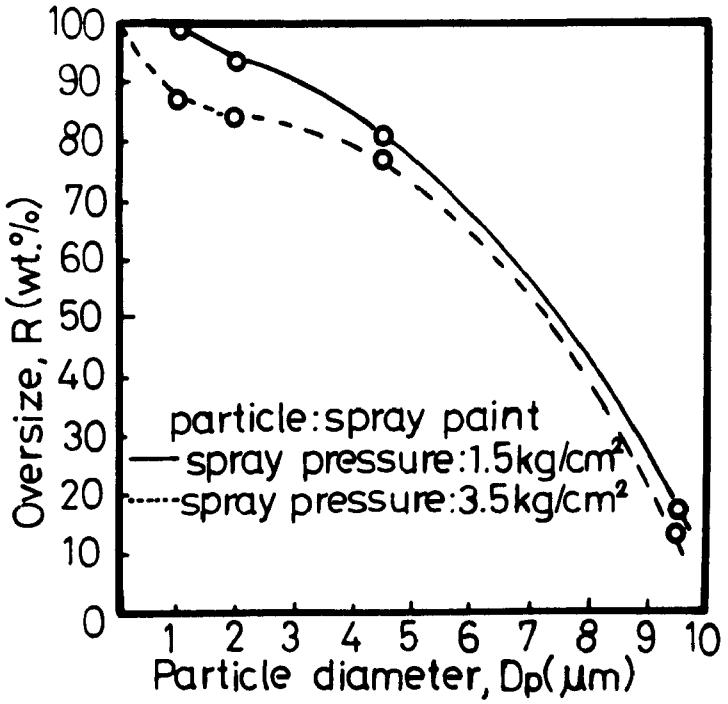

Figure 3. Particle size distribution of solids in paint

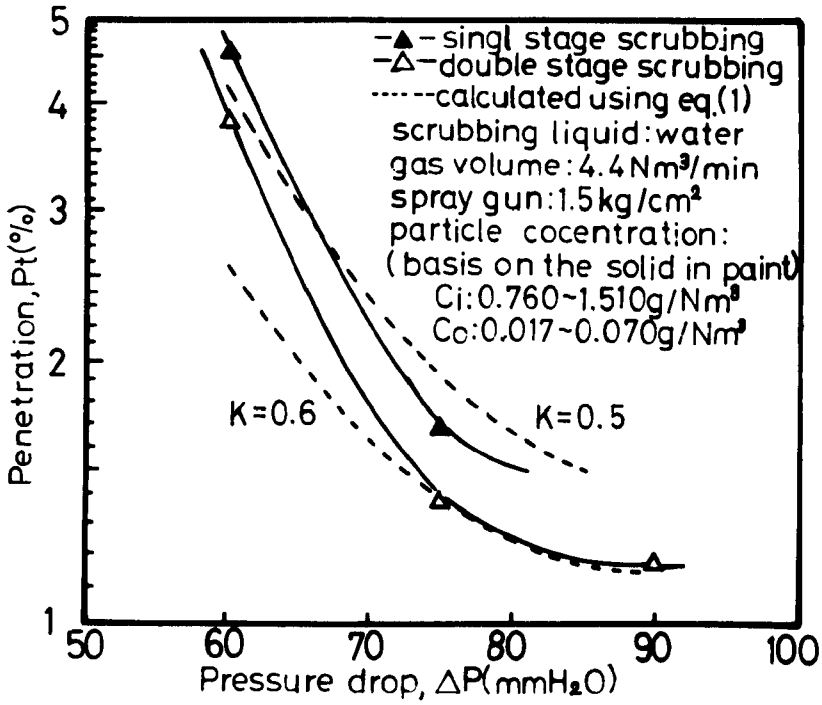

Figure 4. Collection characteristics of single and double-stage scrubbing

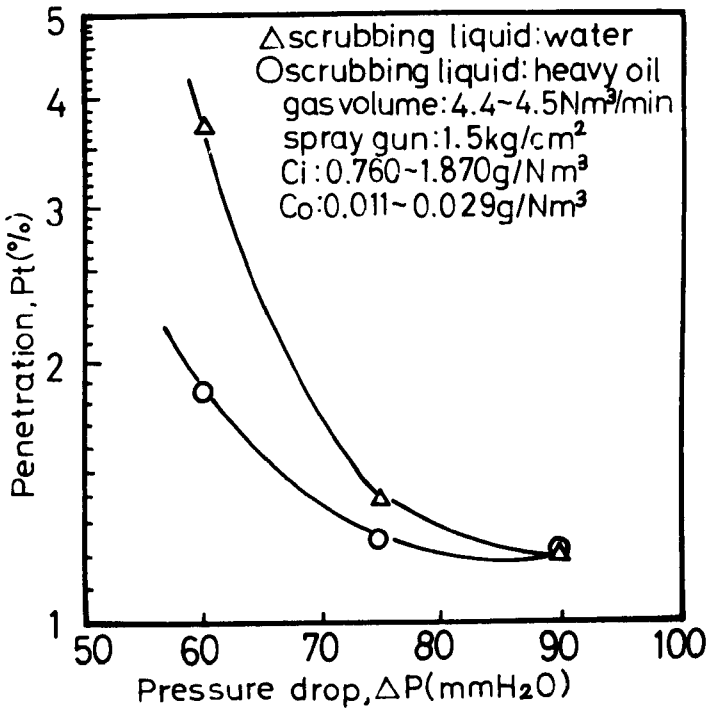

Figure 5. Collection characteristics of water and heavy oil as scrubbing liquids

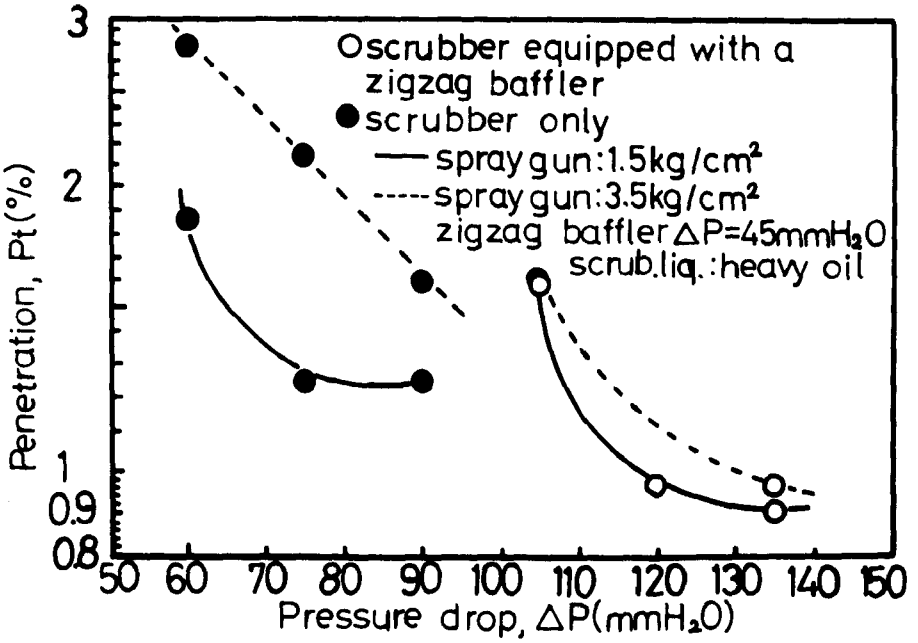

Figure 6. Collection characteristics of a double-stage scrubber with a zigzag baffler

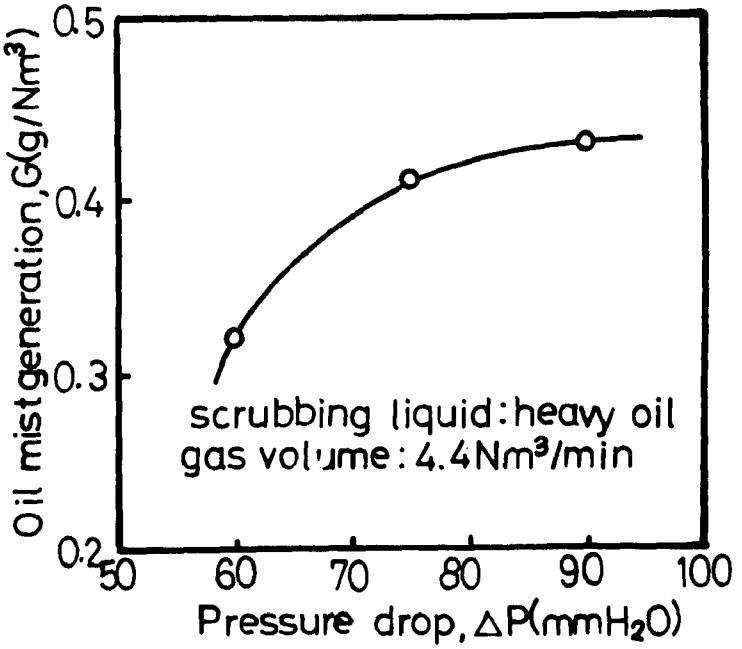

Figure 7. Relations between ΔP and oil mist generation in the scrubber section

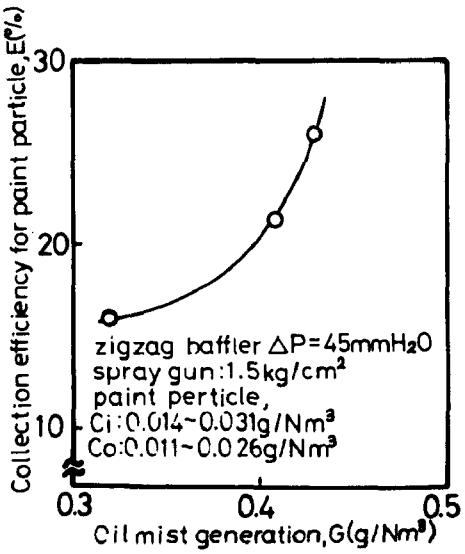

Figure 8. Effect of the zigzag baffler in removing paint particles on various oil mist generations

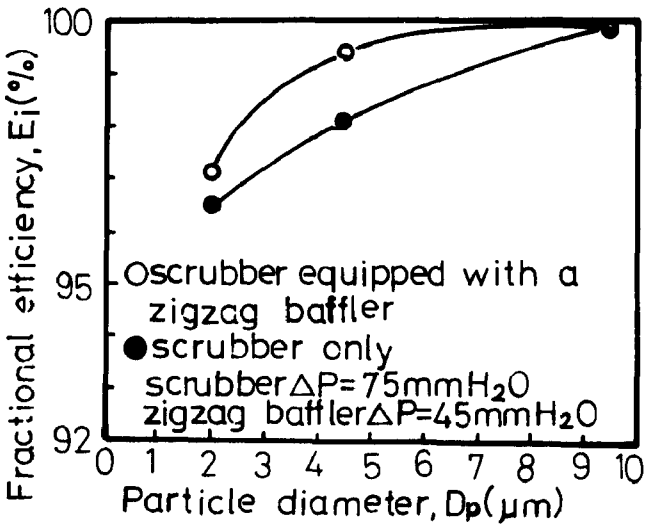

Figure 10. Fractional efficiency of paint particles

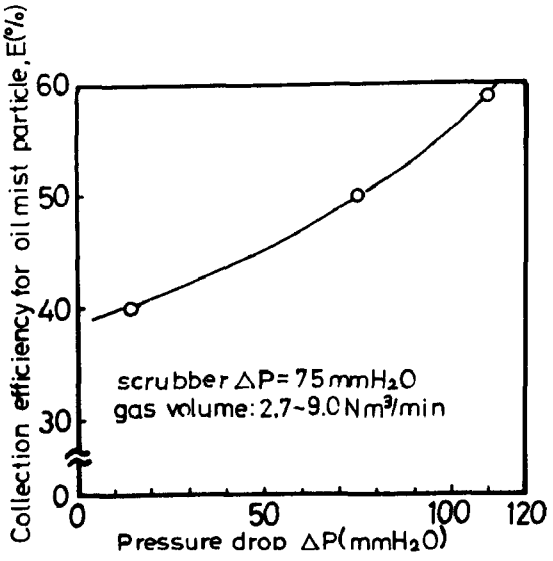

Figure 9. Collection efficiency of oil mist particles by a zigzag baffler

APPLICATION OF SLIPSTREAMED AIR POLLUTION CONTROL DEVICES ON WASTE-AS-FUEL PROCESSES

By:

Fred D. Hall
John M. Bruck
Diane N. Albrinck

PEDCo Environmental, Inc.
Cincinnati, Ohio

Robert A. Olexsey
U.S. Environmental Protection Agency
Cincinnati, Ohio

The recovery of energy from the combustion of municipal solid wastes is becoming an attractive alternative as landfill space becomes scarce and the availability of fossil fuels decreases. Particulate emissions from "waste-as-fuel" processes, however, may differ significantly in chemical and physical properties from particulate emissions produced by firing only coal. Such differences can affect the design and operation of air pollution control equipment. Presented in this paper are the results of a 2-month test program at Ames, Iowa, with a mobile electrostatic precipitator (ESP) and a mobile scrubber supplied by the U.S. Environmental Protection Agency (EPA), Industrial Environmental Research Laboratory (IERL), Research Triangle Park. PEDCo Environmental, Inc., and Acurex Corporation jointly conducted the test program to examine the effect of burning refuse-derived fuel (RDF) on particulate and heavy metal control efficiencies. The mobile ESP was used only as a primary control device, whereas the mobile scrubber was tested both upstream and downstream of the existing full-scale ESP. This paper also presents a status report on a PEDCo test program with a pilot fabric filter at Ames.

APPLICATION OF SLIPSTREAMED AIR POLLUTION CONTROL DEVICES ON WASTE-AS-FUEL PROCESSES

INTRODUCTION

PEDCo is currently engaged under an EPA contract in testing and evaluating prototype air pollution control devices on various waste-as-fuel processes for the control of potentially harmful air emissions. As part of the contract, a sampling and analysis program was conducted at the RDF and coal cofiring facility in Ames, Iowa. This program involved evaluating the pollutant removal efficiency of a mobile ESP and a mobile scrubber from IERL by slipstreaming flue gas from the suspension fired boiler. The objective of the program was to determine the pollutant removal efficiencies of each device for variable boiler loads, RDF inputs, and device operating parameters. Installation and testing of the mobile devices took place in October and November 1978.

TEST PROGRAM

The PEDCo study depended on procuring small-scale air pollution control devices and on slipstreaming and testing appropriate waste-as-fuel facilities to generate necessary data.

Early in the project, several waste-as-fuel facilities were visited as candidate sites for this program. The Ames, Iowa, site was chosen because of the cooperation of the management, availability of data from previous studies and evaluations, high reliability of the preprocessing and utility operations, and limited facility modifications required.

The execution of a program of this type relies heavily on the cooperation of plant management. The administrative, operating, and maintenance staff of the Ames Municipal Electric System provided EPA, PEDCo, and Acurex with invaluable assistance throughout the program.

This test program was jointly conducted by Acurex, under contract to the IERL Fine Particulate Control Branch, and PEDCo, under contract to the IERL Fuels Technology Branch. Acurex was responsible for operating the mobile devices and measuring particulate loading and sizing at the inlet and outlet streams of each device. PEDCo was responsible for interacting with the Ames Municipal Electric System and performing more complex sampling and analytical tasks, involving characterization of fuels and of the inlet and outlet streams of each device.

The project objective was to characterize the specific pollutant removal efficiencies of each control device for different boiler loads, RDF inputs,

and operating parameters. It has been assumed that any full-scale application of these control devices to a coal- and RDF-fired boiler must operate with varying flue gas temperatures and compositions. A plan was developed to monitor and measure these two factors, but not to modify or control them.

Ames Boiler 7 was used for the test program. The unit, which was installed in 1968, burns pulverized coal with a tangential firing mechanism. The specifications of Boiler 7 are given by Hall et al. (1978) as follows:

Manufacturer	Combustion Engineering
Heat input	460 GJ/h (436 x 10^6 Btu/h)
Steam output	160 Mg/h at 491½C and 5860 kPa (360,000 lb/h at 900½F and 850 psi)
Furnace pressure	Balanced draft
Coal firing equipment	2 pulverizers; 8 nontilting tangential burners
Dust collection equipment	American ESP

PEDCo characterized emissions by simultaneously measuring total particulates, halogens, selected trace metals, and elemental composition of particulates at the inlet and outlet of each device. The operating parameters that were varied during testing of the mobile scrubber included pressure drop, actual gas flow rate, and scrubber liquor flow rate. The gas flow rate was increased as the scrubber liquor flow rate was decreased in such a manner that the liquid-to-gas ratio remained relatively constant. The operating parameters that were varied during testing of the mobile ESP included the number of energized fields, specific collection area (SCA), and actual gas flow rate.

Figure 1 shows the slipstream and sampling locations for the test program. Both mobile control devices were slipstreamed into the emission effluent stream upstream of the existing ESP. The mobile scrubber was also operated as a secondary device and tested downstream of the plant ESP. Samples were taken at the inlet and outlet of each mobile control device while boiler conditions, fuel composition, and control device operating conditions were monitored.

The PEDCo sampling and analysis program is outlined in Table 1. A Method 5 source sampling train (SST) was used simultaneously at the inlet and outlet of each device. Total particulates were determined from the front half of the SST. Halogens and trace elements were determined from the front and back halves of the SST and from specified grab samples of coal and RDF. Elemental analyses were conducted on the particulate catch of Acurex samples that correlated to PEDCo runs.

Discrete grab samples of coal, RDF, ESP ash, and scrubber liquor were collected at the time of emission testing. Coal samples were taken before the pulverizer, processed refuse samples were collected at the Atlas storage bin

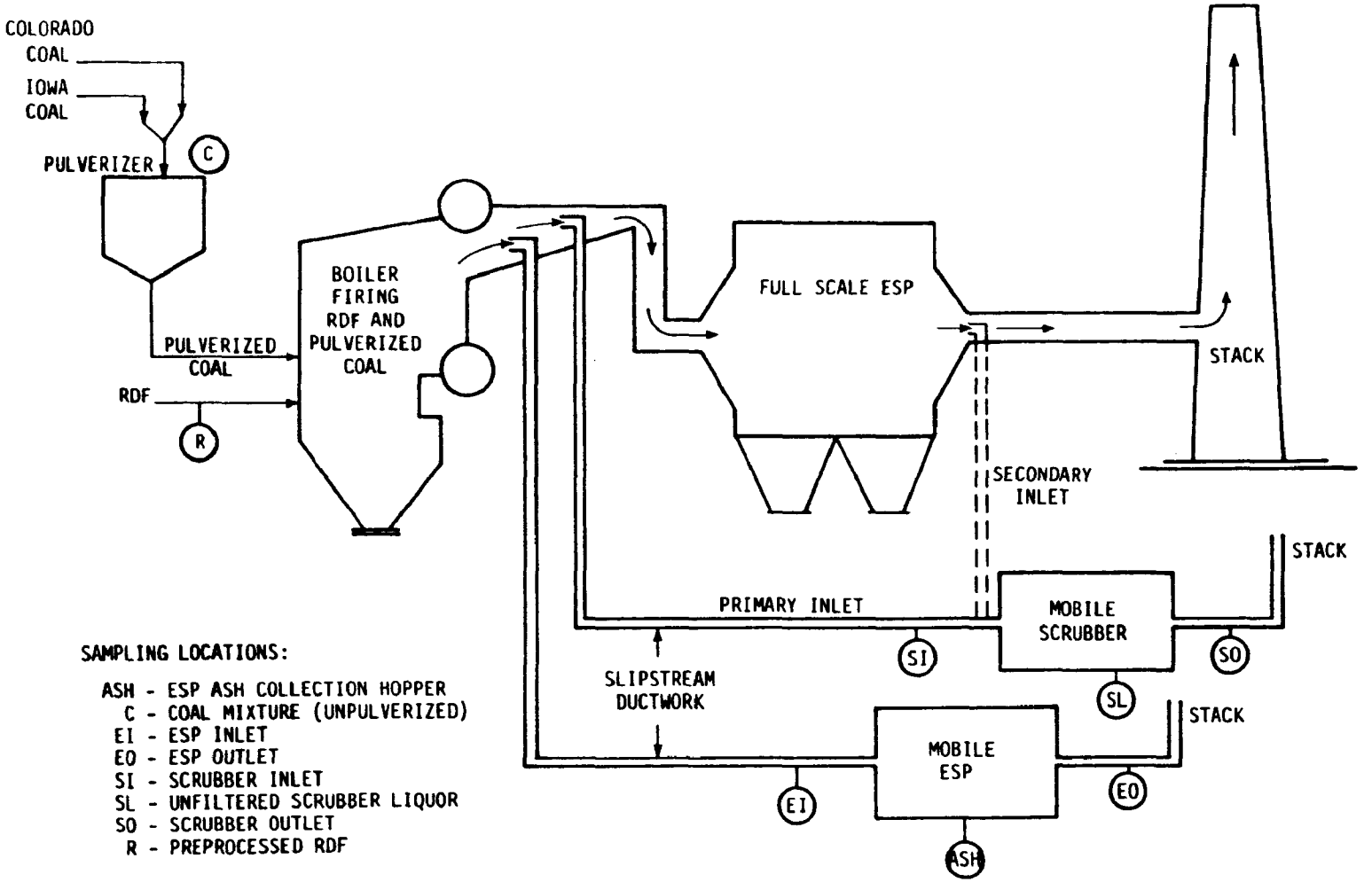

Figure 1. Schematic of the waste-as-fuel test site, at Ames, Iowa.

Table 1. SAMPLING AND ANALYSIS PROGRAM FOR THE COFIRING FACILITY AT AMES, IOWA

Sample stream	Collection technique	Chemical species and other items determined	Analysis method	Sampling and analysis responsibility
Air				
Inlet/outlet	Grab	O_2	Fryrite	PEDCo/Acurex
		CO_2	Fryrite	PEDCo/Acurex
	SST	Total particulates	EPA Method 5	PEDCo/Acurex
		Pb, Sb, Cd, Fe, Cu	AAS	PEDCo
		Cl	[a]	PEDCo
		Br	[a]	PEDCo
		F	EPA Method 13B	PEDCo
		Inorganic elements	SSMS	PEDCo/Acurex/Brehm
		SO_2	EPA Method 6	Acurex
		Particle size distribution	Cascade impactor	Acurex
Solid				
Coal/RDF	Grab/composite	Density[b]	Gravimetric	PEDCo
		Pb, Sb, Cd, Fe, Cu	AAS	PEDCo
		Cl	[a]	PEDCo
		Br	[a]	PEDCo
		F	EPA Method 13B	PEDCo
		Inorganic elements	SSMS	PEDCo/Brehm
		Fuel characterization	Ultimate and proximate	PEDCo
ESP ash	Grab[c]			PEDCo/Acurex
Liquid				
Scrubber liquor	Grab[d]			PEDCo

[a] Specific ion probe/titration with $AgNO_3$ or $Hg(NO_3)_2$.

[b] Only RDF was measured.

[c] Stored for future reference.

[d] Sent to Montgomery Engineering.

before the fuel entered the pneumatic feed to the boiler. The ESP particulate catch was collected from the mobile ESP daily, and samples of unfiltered scrubber liquor were collected at the time of emission testing. The temperature and pH of scrubber liquor were measured immediately after sampling and recorded. Ultimate and proximate analyses were performed on ground and homogenized coal and RDF.

TEST RESULTS

Test results are based mainly on analyses of PEDCo samples. Acurex, however, supplied the Method 5 samples analyzed by spark source mass spectrometry (SSMS) for particulate elemental composition and provided size distribution data. The Acurex samples were taken at the same time as PEDCo samples to allow comparison of analytical data.

Table 2 presents average fuel analyses for coal and RDF at Ames. The samples analyzed were composites of coal and RDF taken daily during the test program. On a dry basis, the ash content of RDF (14.83 percent) is higher than the ash content of coal (11.06 percent), whereas the sulfur content of RDF (0.38 percent sulfur) is significantly lower than the sulfur content of coal (3.13 percent). Heating values for RDF and coal as received are 15,450 kJ/kg (6,644 Btu/lb) and 23,680 kJ/kg (10,180 Btu/lb).

Figure 2 shows the particulate size distribution at the control device inlet for each test condition. Each distribution value is an average for several runs. Given the uncertainty of particulate sizing techniques, the distribution when RDF and coal are fired does not appear appreciably different from the distribution when only coal is fired. As expected, significantly fewer particulates less than 1 μm in diameter were found at the inlet of the scrubber when used as a secondary device; submicron particulates accounted for less than 5 percent by weight of the total particulate matter at the scrubber inlet in the former case, but more than 10 percent in the latter case.

Figures 3, 4, and 5 show the particulate removal efficiencies of the control devices as measured during the test program. The scrubber operated at pressure drops of 25.4 and 76.2 cm (10 and 30 in.) H_2O. The pressure drop was increased by increasing the gas flow rate through the scrubber and adjusting the scrubber liquor flow rate to maintain a constant liquid-to-gas ratio of about 2.1 liters/standard m^3 (15 gal/1000 scf). The efficiency of the scrubber was consistently above 99 percent when used as a primary device, but considerably less (72 to 97 percent) when used as a secondary device. The efficiency of the ESP ranged from 94 to 98 percent. Neither scrubber nor ESP particulate removal efficiencies appreciably changed as the portion of heat input supplied by RDF increased.

Table 3 shows the differences in elemental composition between coal and RDF fuel samples, and Table 4 shows the differences in elemental composition between uncontrolled emissions from burning coal plus RDF and uncontrolled emissions from burning only coal. The fuels were analyzed from composite samples from each test. The factors for uncontrolled emissions were determined from measured data and engineering judgement. The elements not shown in Table

Table 2. AVERAGE FUEL ANALYSES
(values in percent except as shown)

	Coal	RDF[a]
Fuel as received		
Proximate analysis		
Water	16.13	13.25
Ash	9.27	12.78
Volatile matter	36.54	61.36
Fixed carbon[b]	38.06	12.62
Heating value, kJ/kg	23,680	15,450
(Btu/lb)	(10,180)	(6,644)
Dry fuel		
Ultimate analysis		
Ash	11.06	14.83
Carbon	73.53	50.31
Hydrogen	1.38	3.97
Oxygen	9.72	30.10
Sulfur	3.13	.38
Nitrogen	1.17	.14
Heating value, kJ/kg	28,210	17,800
(Btu/lb)	(12,130)	(7,654)

[a] Average of grab samples from Atlas storage bin.

[b] By difference.

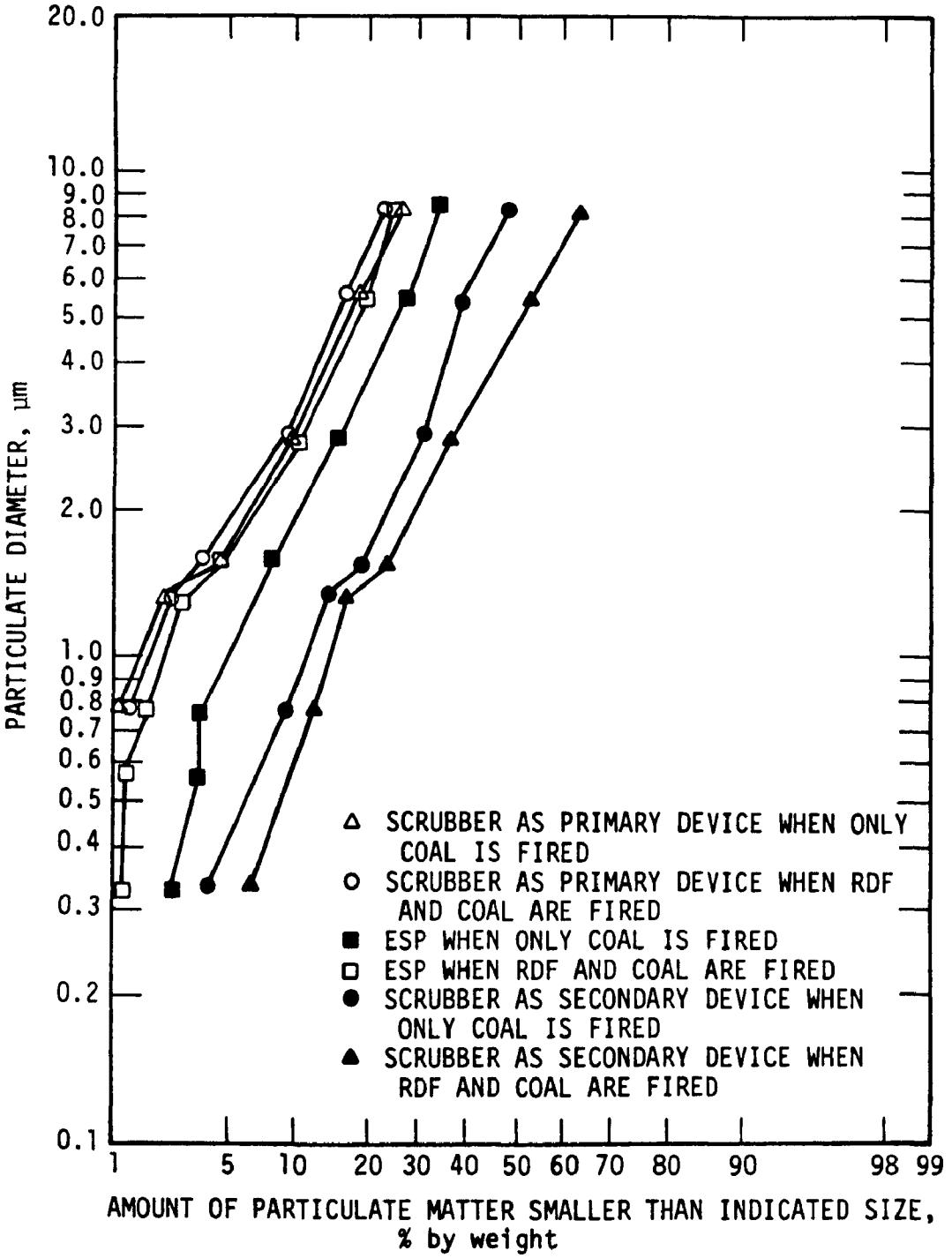

Figure 2. Particulate size distribution at control device inlets.

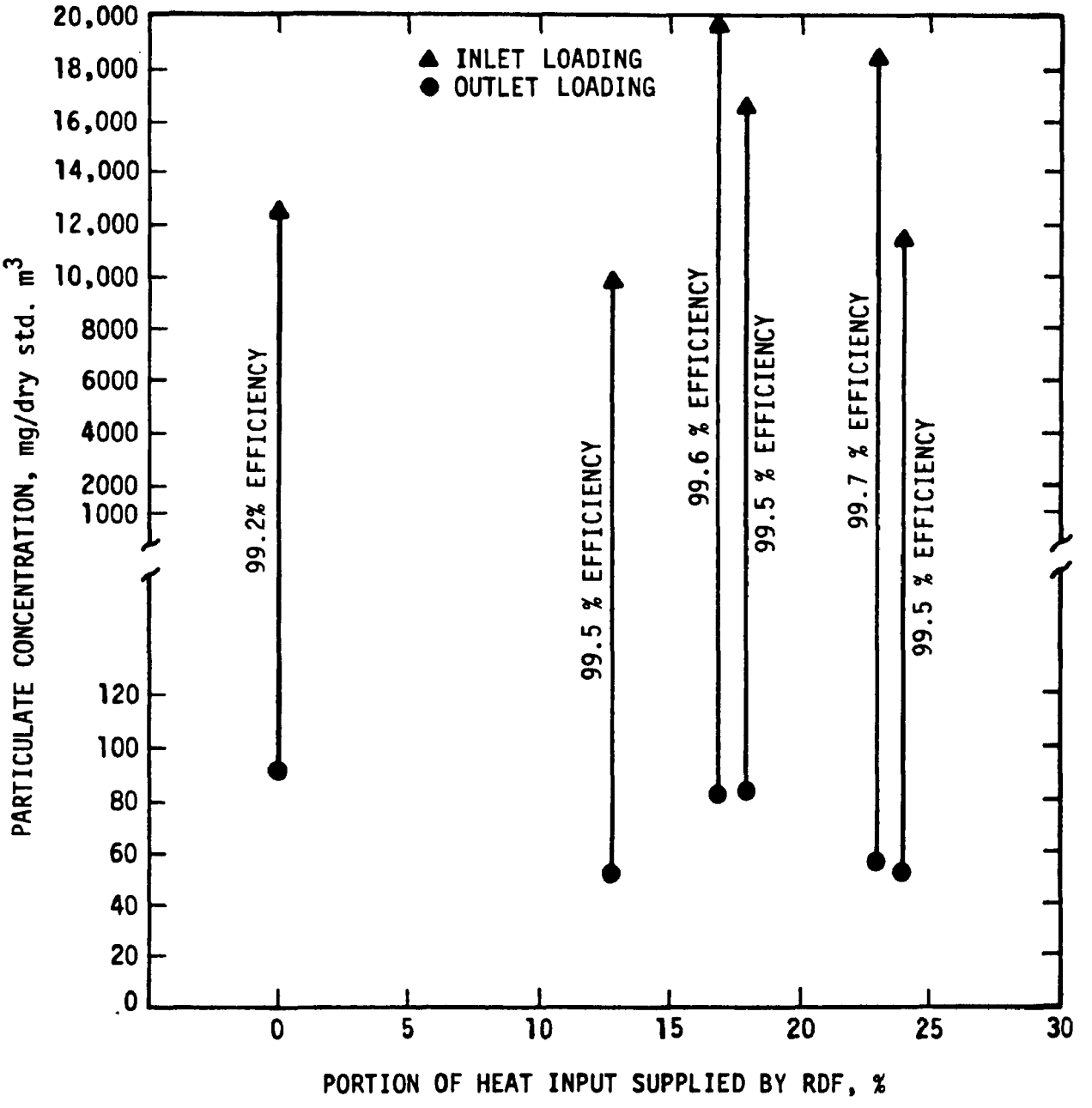

Figure 3. Efficiency of mobile scrubber as a primary device.

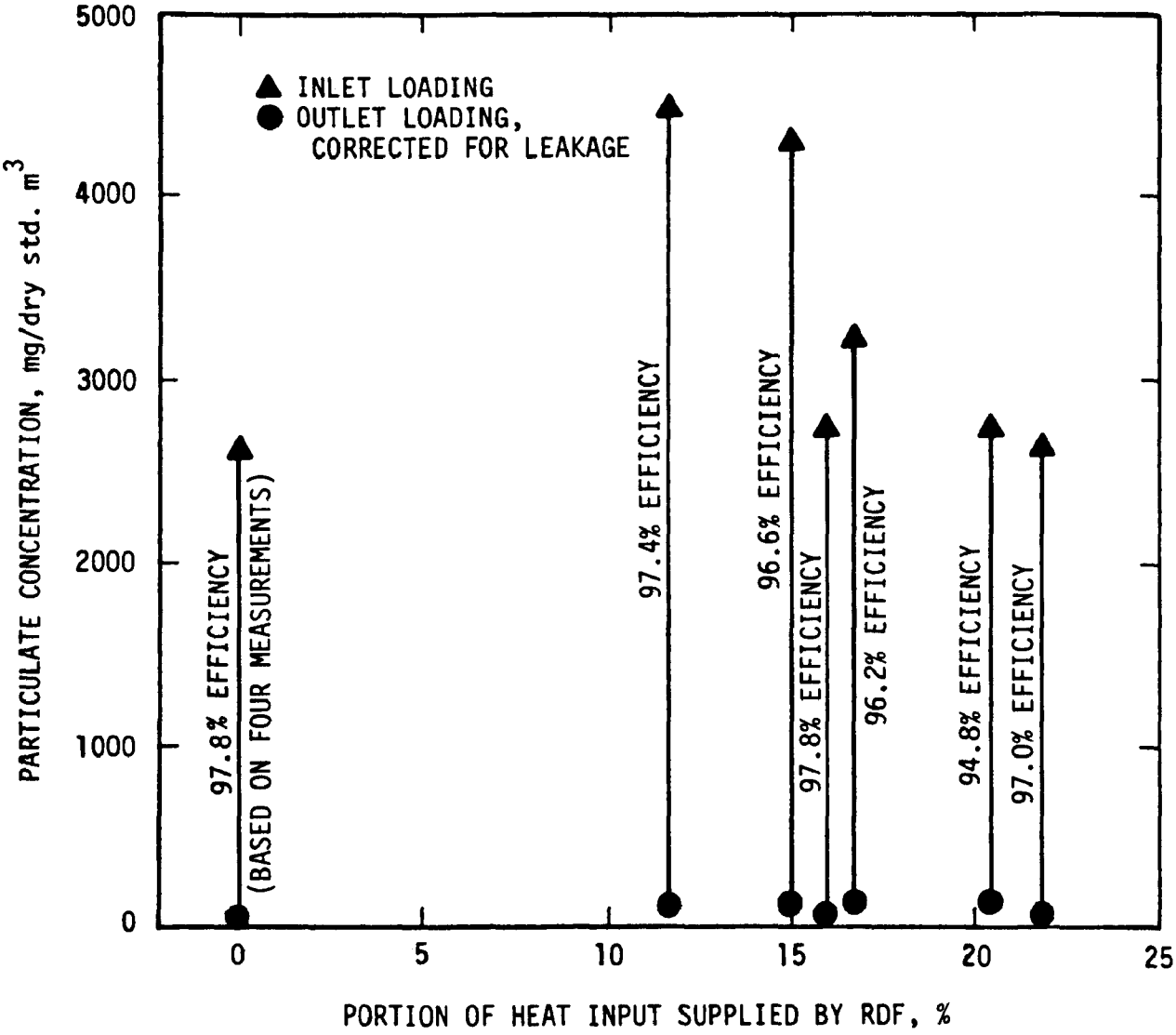

Figure 4. Efficiency of mobile ESP with SCA of 59 m^2/m^3 per second.

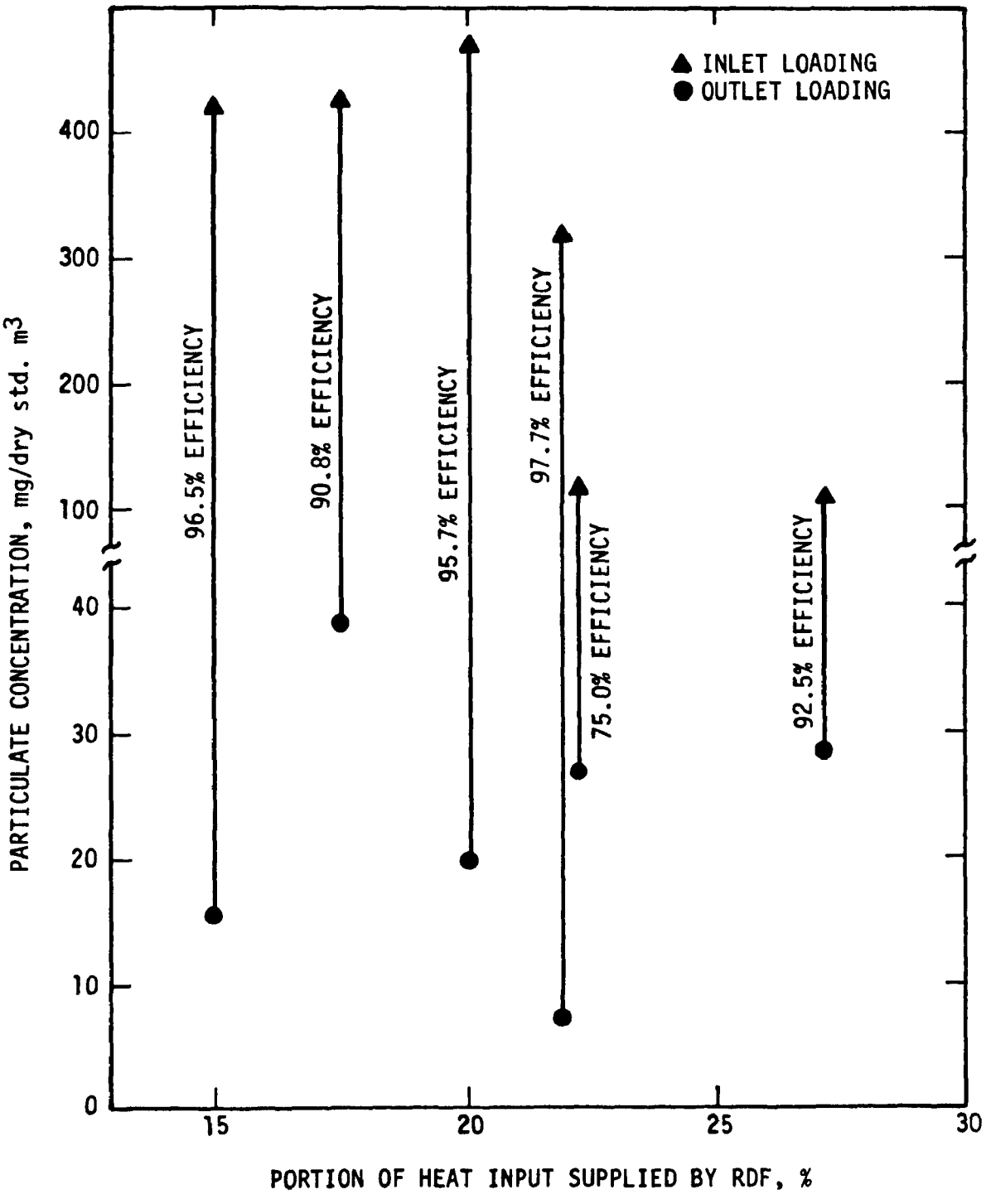

Figure 5. Efficiency of mobile scrubber as a secondary device.

Table 3. DIFFERENCES IN ELEMENTAL COMPOSITION BETWEEN COAL AND RDF FUEL SAMPLES FROM ALL TESTS[a]

	Factor by which elemental concentration in RDF differs from elemental concentration in coal
Elements more concentrated in RDF than in coal	
Copper[b]	120
Lead[b]	40
Bromine	25
Fluorine	25
Zinc	10
Manganese	10
Antimony	5
Chromium	5
Cobalt	5
Rubidium	4
Tin	3
Barium	3
Silver	3
Cadmium[b]	2
Titanium	2
Strontium	2
Phosphorus	2
Elements less concentrated in RDF than in coal	
Vanadium	50
Beryllium	25
Scandium	7
Yttrium	6
Sulfur[c]	5
Molybdenum	5
Iron[b]	4
Thallium	3
Nickel	2
Cerium	2
Lanthanum	2
Zirconium	2

[a] Based on SSMS analysis unless otherwise stated.

[b] Based on AAS.

[c] The initial determination of sulfur concentration might have been low by a factor of 3-10 because of high organic content, which necessitated low-temperature ashing of the samples.

Table 4. DIFFERENCES IN ELEMENTAL COMPOSITION BETWEEN UNCONTROLLED EMISSIONS FROM BURNING COAL PLUS RDF AND UNCONTROLLED EMISSIONS FROM BURNING ONLY COAL[a]

	Factor by which elemental concentration in emissions from burning coal plus RDF differs from elemental concentration in emissions from burning only coal[b]
Elements more concentrated in emissions from burning coal plus RDF than in emissions from burning only coal	
Gaseous chlorides	10
Lead	6
Zinc	5
Copper	3
Iron	2
Elements less concentrated in emissions from burning coal plus RDF than in emissions from burning only coal	
Zirconium	2

[a] Only elements that show definite differences are listed. Other elements, as determined by SSMS and/or AAS, show concentrations too variable to determine emission differences.

[b] Estimated from actual data and engineering judgement.

4 were too variable to determine emission differences between burning coal plus RDF and burning only coal.

Elemental concentrations in fuel do not appear directly related to elemental concentrations in uncontrolled emissions. For example, copper was measured to be 120 times more concentrated in the RDF fuel sample than in the coal fuel sample, and lead was estimated to be 40 times more concentrated. Uncontrolled emissions from burning a mixture of 75 percent coal and 25 percent RDF contain three times more copper and six times more lead than when burning only coal. The data also indicate that gaseous chloride emissions are about 10 times greater when coal and RDF are burned than when only coal is burned.

The efficiency of trace element removal was typically less with the scrubber than with the ESP. For example, lead removal efficiency was about 90 percent with the scrubber, but greater than 95 percent with the ESP.

ADDITIONAL TESTING

The use of a fabric filter as a primary control device for the removal of specific pollutants from waste-as-fuel processes is being studied. A pilot fabric filter designed and constructed for this project is currently installed at the cofiring utility in Ames. A test program of about the same scope as the program with the mobile ESP and scrubber is scheduled for completion by the end of July 1979.

Following the Ames testing program, the fabric filter is scheduled for testing at the Braintree Municipal Incinerator in Braintree, Massachusetts. The Braintree program will also involve a pilot scrubber. The scope of this test plan will be much the same as the scope of the Ames program.

REFERENCES

1. Hall, J.L. et al. Compliance Tests of Steam Generator Unit 7 for Particulate Effluent. Ames, Iowa, July 17-25, 1978.

EVALUATION OF THE CEILCOTE IONIZING WET SCRUBBER

By:

David S. Ensor
Meteorology Research, Inc.
Altadena, California 91001

and

Dale L. Harmon
U.S. Environmental Protection Agency
Office of Research and Development
Industrial Environmental Research Laboratory
Research Triangle Park, North Carolina 22711

ABSTRACT

The Ceilcote ionizing wet scrubber installed on a refractory brick kiln was evaluated with tests involving particulate mass emission, particle size distribution, and opacity. The overall efficiency was 93 percent with an average outlet opacity of 8 percent on a 1.68 m (5.5 ft) path length. The average particle cut diameter of the scrubber is 0.5 microns with a theoretical power input of 67 watts/am^3 (2.5 hp/1000 acfm). The theoretical power requirement for the ionizing wet scrubber was 41 watts/am^3 (1.54 hp/1000 acfm). A cooling tower supplying chilled water to the prescrubber required an additional 26 watts/am^2 (0.96 hp/1000 acfm) for a total system input of 67 watts/am^3 (2.5 hp/1000 acfm). It is recommended that the scrubber be considered where practical for the removal of fine particulate matter.

SECTION 1

SUMMARY AND CONCLUSIONS

The Ceilcote ionizing wet scrubber (IWS) was evaluated with field measurements of particle collection efficiency and an analysis of power consumption.

This evaluation was one of a series of such evaluations being conducted by the Industrial Environmental Research Laboratory of the U.S. Environmental Protection Agency (EPA) to identify and test novel devices which are capable of high efficiency collection of fine particles. The test methods used were not the usual compliance-type methods but were, rather, state-of-the-art techniques for measuring efficiency as a function of particle size using cascade impactors and electrical aerosol size analyzers (EASA).

The following conclusions were made from the study:

1. The emission from the refractory kiln was a submicron fume formed by condensation of volatile material baked from the raw clay. The aerosol had a mean diameter of 0.6 microns and a geometric standard deviation of 5.0 as determined with a cascade impactor assuming a particle specific gravity of 1.8 g/cm^3. The cooling of the flue gas from 150° to 50°C (300° to 120°F) doubled the concentration of particulate matter entering the ionizers.

2. The average overall mass collection efficiency was 93 percent for 3 days of testing. The average inlet concentration was 0.25 g/dsm^3 (0.0076 $gr/dsft^3$). The average outlet opacity was 8 percent over a 1.68 m (5.5 ft) path length as measured with a plant process visiometer at about 99°C (210°F).

3. The particle cut diameter (the particle diameter collected with a 50 percent efficiency) was 0.4 to 0.6 microns. The total theoretical power into the scrubber (the power required to operate the scrubber would include the efficiency of power supplies, pumps, and fans) was 67 $watts/am^3/min$ (2.5 hp/1000 acfm). The ionizers required the greatest percentage of the power input at 48.4 percent and the cooling tower required 38.4 percent. The use of energy to remove particulate matter in the scrubber is better than a theoretical high-pressure drop venturi scrubber.

It is recommended that the Ceilcote ionizing wet scrubber be considered in applications where scrubbers are practical for the removal of fine or submicron particulate matter.

SECTION 2

SITE DESCRIPTION

PROCESS

Globe Refractories, Inc., located in Newell, West Virginia, makes bloating-type refractories. These refractory products are used in the steel industry to line ladles. The term "bloating" means the refractory brick expands permanently when reheated, sealing the lining of the ladle.

The raw material is a local clay called Lower Kittanning clay composed mainly of kaolinite, quartz, illite, and pyrite. Minor constituents are organic matter, micas, and ammonium chlorides or fluorides. The clay is formed into the required shapes, including bricks, sleeves, nozzles, and pocket blocks and fired to about 1000°C (2000°F) in a tunnel kiln under a controlled temperature profile over 4 to 6 days cycle. The formed clay is loaded on tunnel kiln cars which are slowly pushed through the kiln.

The chemical reaction during firing includes oxidation of organic matter to carbon dioxide and water, oxidation of pyrite to iron oxide and sulfur oxides, decomposition of kaolinite and illite to release chemically combined water, decomposition of ammonium chloride or fluoride to form ammonia, gaseous chlorides, and fluorides. The fluxing of alkalis forms a glass bonding the brick.

The major emissions problem from the kilns is believed to be a $NH_4 HSO_4$ smoke from reaction of ammonia gas and sulfur oxides.

CONTROL DEVICE

General

The Ceilcote ionizing wet scrubber consists of five sections:

- Quench unit
- Prescrubber (with cooling tower)
- First ionizing wet scrubber
- Second ionizing wet scrubber
- Induced draft fans and stack

About 28.3 am^3/sec (60,000 acfm) of flue gas at 150°C (300°F) is piped to the scrubber through a 1.5 m (5 ft) diameter 30 m (100 ft) long duct constructed of fiberglass reinforced plastic. A diagram of the scrubber is shown in Figure 2-1.

Quench Section

In the quench section, the flue gas is reduced from 150°C (300°F) to 60°C (140°F) by evaporative cooling. The quench water is supplied at 7.6 ℓ/sec (120 gpm) at a 3.6×10^5 N/m^2 (52 psig) pressure. The unit is 2.1 m (7 ft) in diameter and 2.7 m (9 ft) long.

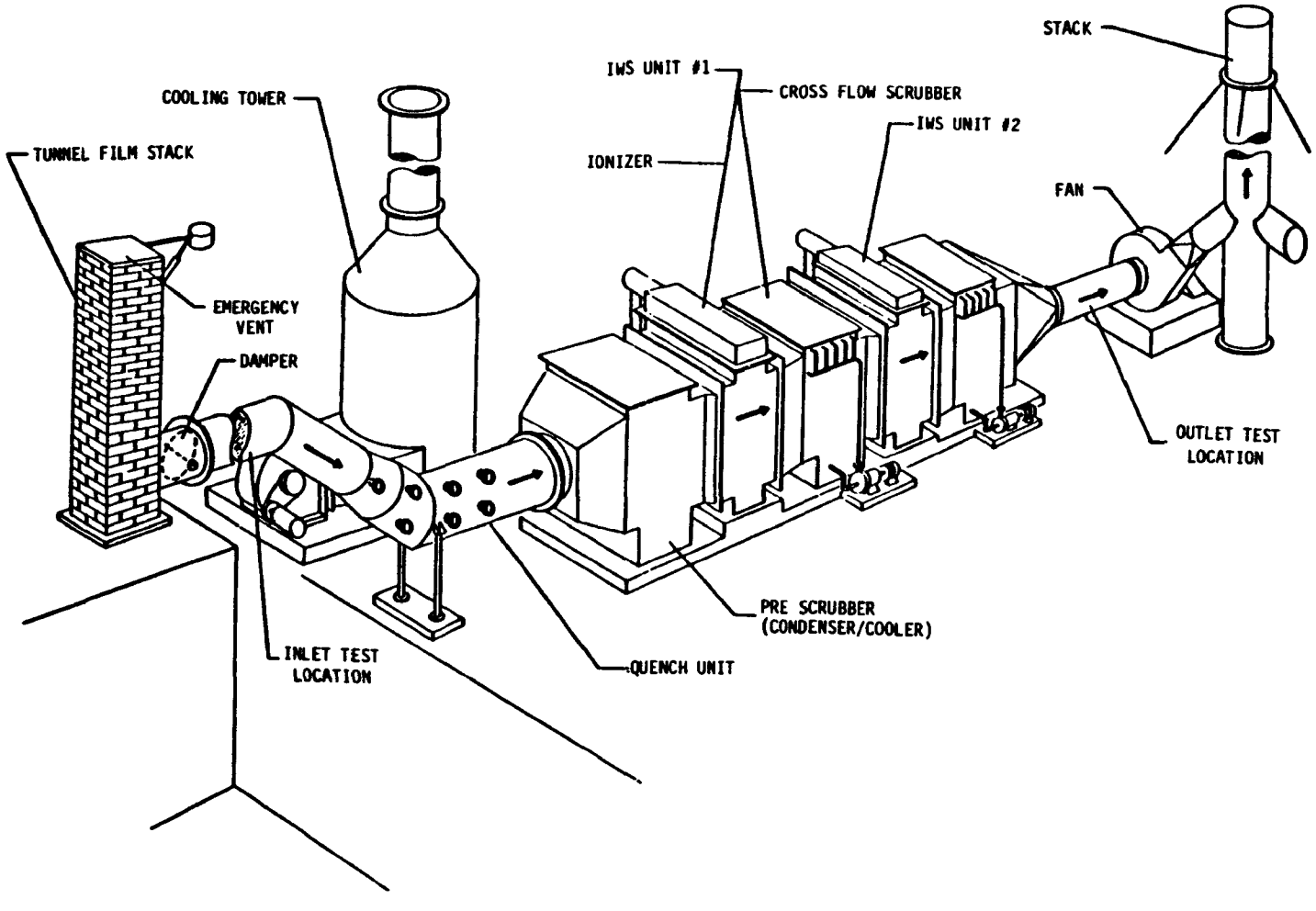

Figure 2-1. Overview of Ceilcote ionizing wet scrubber.

Prescrubber and Cooler

The gas temperature is reduced to 46°C (115°F) in the prescrubber. The prescrubber has a gas flow area 3 m x 3 m (10 ft x 10 ft) with an overall length of 5.5 m (18 ft). It is of cross-flow design with a series of inlet baffles and a 1.8 m (6 ft) deep bed of Tellerette packing. There are continuous water sprays on the inlet baffles in front of the packing and above the packed bed. Outlet baffles are sprayed on a periodic basis. Most of the water for the sprays is cooled in the cooling tower. The cooling tower reduces the temperature of the prescrubber water from 49°C (120°F) to 29°C (85°F) with a flow of 54 ℓ/sec (860 gpm) and a heat transfer rate of 3.78×10^9 cal/hr (15×10^6 Btu/hr).

The cooling tower is 3.8 m (12.5 ft) in diameter and about 6.6 m (21.5 ft) high. The tower has a stack extension for a total height of 11 m (36 ft). It has 5 cm (2 in.) Tellerette Type-R packing and the entrainment separator is 0.3 m of 5 cm (2 in.) Tellerette Type-R packing. A fan rated at 27.3 am^3/sec (58,000 acfm) at 10 cm H_2O supplies cooling air at the bottom of the tower. The cooled water is pumped to the prescrubber at 52.4 ℓ/sec (832 gpm) at a 1.8×10^5 N/m^2 (26 psig) pressure.

Ionizing Wet Scrubber (IWS)

The ionizing wet scrubber consists of two sections: an ionizer or charger and a cross-flow scrubber. The ionizer consists of charging wires suspended between irrigated grounding plates. The first ionizer operates at 30 kV with a current of 100 to 110 mA and the second operates at 31.5 kV with a current of 210 to 225 mA The scrubber contains 1.2 m (4 ft) of irrigated 5 cm (2 in.) Tellerette Type-R packing and 0.3 m (1 ft) of unirrigated packing for entrainment separation. The irrigated packing is sprayed from the front and the top. The entrainment separator is flushed periodically. The recirculation pump is rated at 36.3 ℓ/sec (575 gpm) at a pressure of 1.8×10^5 N/m^2 (26 psig).

Fan and Stack

The fiberglass reinforced polyester fan is rated at 20 am^3/sec (42,000 acfm) at 46°C (115°F) water saturated and 28 cm WC (11 in. WC) static pressure. The fiberglass reinforced plastic stack is 1.67 m (66 in.) in diameter and 46 m (150 ft) in height.

Test Locations

The test locations are indicated on Figure 2-1. Both the inlet and the outlet were located on circular ducts with sufficient length before and after the test port for smooth flow.

SECTION 3

TEST METHODS

TECHNICAL APPROACH

Measurements were conducted in three areas: aerosol characterization, gas composition, and process streams.

SIZE DISTRIBUTION MEASUREMENT

Cascade Impactor

The MRI cascade impactor is an annular jet collector type similar to that reported by Cohen and Montan. The body of the device consists of quick connect rings supporting jet plates, collection discs, and a built-in filter holder. The design permits flexibility in various sampling situations.

The tests were conducted with procedures described by Harris. The particles were collected on Apiezon grease-coated, 304 stainless steel foil collection discs. The discs were weighted to 0.01 mg on a Cahn electrobalance.

The inlet impactors were operated at duct temperature. The outlet impactors were heated to 121°C (250°F) with electrical heating jackets. The nozzles on the outlet impactors were also extended by 46 cm (18 in.) tubes which were also heated to 121°C (250°F) to dry the aerosol before entering the impactor.

The impactor data were reduced with a procedure described by Markowski and Ensor which is similar to the method described by McCain et al.

Fine Particles

The measurement of the size distribution of submicron particles was a two-stage process. First, the aerosol sample was diluted with clean, dry air; and secondly, the particulate matter in the diluted aerosol was measured with a Thermosystems Model 3030 electrical aerosol size analyzer.

Two separate dilution systems were used. The inlet dilution system consisted of a sampling probe with a cascade impactor precutter to remove particles greater than 2.5 microns followed by an out-of-stack, three-stage quantitative dilution system. The sample can be diluted with filtered dry air from 3:1 to 1000:1 by adjustment of control valves. The outlet dilution system was a single stage in-stack mixing tee. In both systems, the clean air flows are measured with orifices and the sample flows with venturis.

Thhe TSI Model 3030 electrical aerosol size analyzer (EASA) was used at both the inlet and outlet. The EASA consists of a charger, where a known charge is placed on the particles, and a mobility analyzer, where the charged particles are attached to a central collecting rod. The size of particles collected in the mobility analyzer depends on the applied voltage on the collecting rod. The aerosol passing through the mobility analyzer is detected by measuring the current transferred by the particles. The aerosol distribution in 11 logarithmic steps from 0.003 to 1 micron is measured.

OPACITY MEASUREMENT

The opacity at the inlet and outlet of the scrubber was measured with an MRI plant process visiometer (PPV). The instrument was installed on a 3-inch port and the sample was heated to reduce relative humidity. A diagram of the instrument is shown in Figure 3-1. The aerosol particles in the chamber were illuminated by a flash lamp with an opal glass filter. The scattered light was detected by a photomultiplier tube at approximately right angles to the flash lamp. The optics have been designed so that the output of the photomultiplier tube is proportional to the extinction coefficient due to scattered light. The instrument is a physical analog of the following equation:

$$b_{scat} = 2\pi \int_0^{\pi} \beta(\theta) \sin\theta \, d\theta$$

where

b_{scat} = the scattering coefficient due to scattered light

$\beta(\theta)$ = volume scattering function

θ = scattering angle

If there is no light absorption, the scattering coefficient is identical to the extinction coefficient. The extinction coefficient is related to plume opacity with the Bouger Law.

$$\text{Opacity (percent)} = \left[1 - \exp\left(-b_{ext} L\right)\right] \quad 100$$

where

b_{ext} = extinction coefficient, m^{-1}

L = stack diameter, m

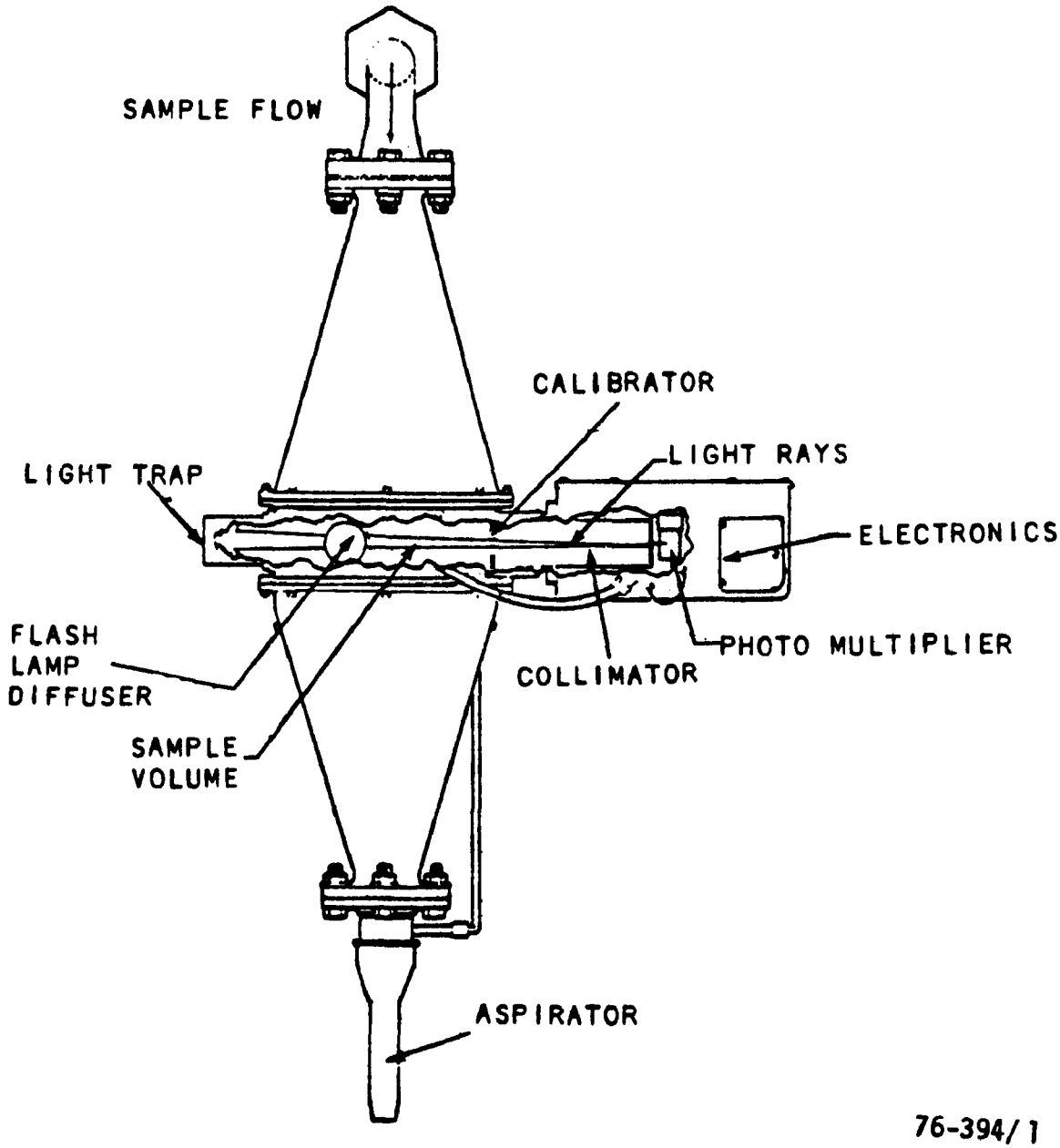

Figure 3-1. Diagram of the plant process visiometer.

The instrument is spanned with an internal calibrator consisting of an opal glass lens of known scattering coefficient. The lens was mechanically placed in the view of the detector for calibration and was retracted into a sealed chamber between calibrations. The PPV calibration opal glass is calibrated with oil smoke with reference instruments using both an integrating nephelometer and a transmissometer. The PPV is described in detail by Ensor et al.

The PPV at the inlet was mounted with the 1.9 cm (3/4 inch) probe positioned in the center of the duct. The probe was insulated and the chamber electrically heated. The PPV at the outlet was placed on the ground and a 3 m (9 ft) probe was extended into the duct from the bottom. The probe and chambers were electrically heated to about 93°C (200°F) to ensure that the gas was above the water dew point.

GAS COMPOSITION

The concentration of O_2, CO, and CO_2 was measured with an Orsat analysis following EPA Method 3. The water content of the flue gas was obtained with the impinger catch during the cascade impactor tests.

PROCESS VARIABLES

The process variables were obtained as follows:

- The velocity was determined with an S type pitot probe following EPA Methods 1 and 2.
- Pressure drop across the scrubber and pressure at the draft fan were measured using pressure transducers and recorded on a strip chart.
- Samples of water were obtained for determinations of dissolved solids.
- The water flow rates, pressure, and power required were estimated from the design specifications.

SECTION 4

FIELD TEST RESULTS

MASS COLLECTION EFFICIENCY

The overall average efficiency of the scrubber as a unit shown in Table 4-1 was 93.5 percent. The "ionizer off" test conducted on November 10, 1978, may be used as an indication of the concentration of particulate matter entering the IWS units. If it is assumed no particulate matter was removed by the IWS packing, the IWS efficiency was 98.2 percent.

TOTAL POWER INPUT

The total theoretical power input to the scrubber is summarized in Table 4-2. The electrical power to the cooling tower for air circulation and water circulation referenced to the volumetric flow of

TABLE 4-2. ESTIMATION OF THEORETICAL POWER REQUIREMENTS

Scrubber Stage	Gas watts/am^3/min (hp/1000 acfm)	Water watts/am^3/min (hp/1000 acfm)	Corona watts/am^3/min (hp/1000 acfm)	% of Total
Quench		1.97 (0.074)		3.0
Prescrubber		6.82 (0.256)		10.3
IWS 1[a]	8.47 (0.318)	4.80 (0.180)	1.82 (0.068)	22.7
IWS 2[a]	8.47 (0.318)	4.80 (0.180)	3.89 (0.146)	25.7
Cooling Tower[b]	16.7 (0.628)	8.79 (0.330)		38.4
Total	33.6 (1.264)	27.2 (1.02)	5.71 (0.214)	66.6 (2.50)[c]
Percent of Total	50.6	40.8	8.5	

(a) The gas pressure drop was divided between the two units
(b) Includes an estimate of the fan and the pump power requirements
(c) Note the total power on 11/21/78 measured with a Volt-amp meter was 149 hp or 3.02 hp/1000 acfm (80.5 watts/am^3/min)

TABLE 4-1. SUMMARY OF OVERALL MASS COLLECTION EFFICIENCY

Date (1978)	Run	Inlet Conc. mg/m^3(a) (gr/ft^3)	Run	Outlet Conc. mg/m^3(a) (gr/ft^3)(a)	Penetration (%)	Efficiency (%)	Opacity(b) (%)	Comments
11/10	25	259	16	756				
	26	256	17	471				
(c)	4a	271	46	360				IWS Power shut off
		262		529	201.9	-101.9	81	
		(0.114)		(0.231)				
11/18	27	349	18	16.9				Phase II tests after completion of repairs
	28	318	19	34.8				
		333		25.9	7.77	92.2	11	
		(0.145)		(0.0123)				
11/20	29	186	36	6.84				
	30	185	37	15.10				
(c)	5a	226	5c	7.41				
		199		9.78	4.91	95.1	3.7	
		(0.0831)		(0.00426)				
11/21	32	198	38	19.7				
	33	218	39	21.1				
(c)	66	311	6a	9.38				
		242		16.7	6.90	93.1	6.8	
		(0.106)		(0.00728)				

Note: Both impactors and in-stack filters were heated to 121° C (250° F) at the outlet.

(a) 21.1° C, 76 cm, dry
(b) 1.676 meter (5-1/2 ft) path length
(c) In-stack filter samples - the other mass concentration results were computed from the cascade impactor tests.

flue gas processed was considered as the energy input to the scrubber. Also, the gas side pressure drop of 10 cm WC was assumed to result only from the IWS units. The greatest single power input is from the gas side pressure drops (it should be noted that this input includes the cooling tower air flow). The major power input from these estimations is in the cooling tower; thus, the need to condense components of the flue gas stream in order to control the emission from the kiln results in an additional energy requirement when compared to a process which emits only solid particles. Also, the tests were conducted under atmospheric temperatures of about 4°C (40°F) which leads to efficient cooling of the water streams.

PARTICULATE MATTER FORMATION

Using the water analysis and the gas stream properties, the increase in particulate matter concentration by evaporation is shown in Table 4-3. It was assumed that the gas stream was initially cooled by evaporation under conditions of constant enthalpy to saturation, then cooled by sensible heat transfer to the observed quench temperature. It was assumed that cooling of the gas from the saturation temperature did not cause the removal of particulate matter.

The fraction of particulate matter formed by evaporation of the scrubber water is estimated from the test day of November 10 when the ionizers were shut off. Particulate matter formation from water evaporation accounts for about 30 percent, and about 70 percent results from condensation directly from gas phase for the particulate matter formed in the scrubber. The influence of the particulate matter formed by the evaporation of water is shown in Figure 4-1 with an analysis of the tests. The outlet concentration and scrubber penetration were directly related to the quantity of water evaporated in the quench section and estimated particulate matter. Thus, additional improvement in efficiency may be realized by reducing the dissolved solids in the quench water. However, the emissions were below any applicable regulation and the costs of providing fresh water for cooling the flue gas may not be warranted at the present time.

SIZE DISTRIBUTION

The impactor and EASA results were combined to obtain particle size distributions and fraction penetration curves. The last day of testing, November 21, 1978, was selected for analysis in detail. All measurements exhibited very good repeatability.

The differential size distribution is shown in Figure 4-2. The figure illustrates many of the problems experienced with obtaining fine particle data. It was noticed that the size distribution measured at the inlet was related to the life of the silica gel used to dry the dilution air. The size distribution obtained under conditions of fresh silica gel was bimodal. However, as the silica gel was depleted, the distribution grew to a single mode at 0.4 microns and appeared to match the impactor results rather than the bimodal case. It is believed that

TABLE 4-3. ESTIMATION OF AEROSOL FORMATION IN QUENCH SECTION

Date (1978)	Volumetric Gas Flow Inlet Cond. m^3/sec (acfm)	Temp. Inlet °C (°F)	Water Conc. by Volume Inlet Percent	Specific Humidity Inlet g/g (lb/lb)	Solids in Water mg/ℓ	T After Quench °C (°F)	Specific Humidity After Quench g/g (lb/lb)	Specific Humidity at Saturation g/g[a] (lb/lb)	T at Saturation °C[a] (°F)	Increase in Specific Humidity g/g (lb/lb)	Increase in Particulate Matter mg/m^3[b][c] (gr/ft^3)	Particulate Matter from Evaporation Compared to Inlet, Percent[d]	Particulate Matter from Evaporation Compared to total Generated Percent[e]
11/10	29.32 (62132)	174 (345)	7.69	0.1342 (0.1342)	2606	48 (118)	0.0755 (0.0755)	0.190 (0.190)	63 (145)	0.0558 (0.0558)	163.5 (0.0713)	63	32
11/18	22.72 (48148)	156 (313)	3.63	0.067 (0.067)	2600	43 (110)	0.06 (0.06)	0.119 (0.119)	55 (131)	0.052 (0.052)	147.0 (0.0641)	44	
11/20	25.48 (53980)	135 (275)	3.53	0.05895 (0.05895)	2830	41 (106)	0.053 (0.053)	0.095 (0.095)	52 (125)	0.0361 (0.361)	115 (0.0501)	60	
11/21	21.63 (45828)	138 (281)	5.33	0.0907 (0.0907)	2960	41 (106)	0.053 (0.053)	0.130 (0.130)	56 (132)	0.0393 (0.0393)	131 (0.0571)	54	

(a) It is assumed that the inlet gas is cooled by evaporation as a constant enthalpy process and then the gas is cooled by sensible heat transfer
(b) Obtained by the product of the water solids concentration and increase in specific humidity, it is assumed after formation, the particulate matter is not removedd by condensation in the quench section
(c) Standard conditions 21.1° C, 76 cm Hg, Dry
(d) Ratio of the increase in particulate matter formed from evaporation to that measured during the inlet tests
(e) Computed by dividing the increase in particulate matter from evaporation by the outlet of 11/10 from the average outlet concentrations from 11/18, 20, and 21. Assumes negligible removal of particulate matter in the prescrubber and deenergized IWS.

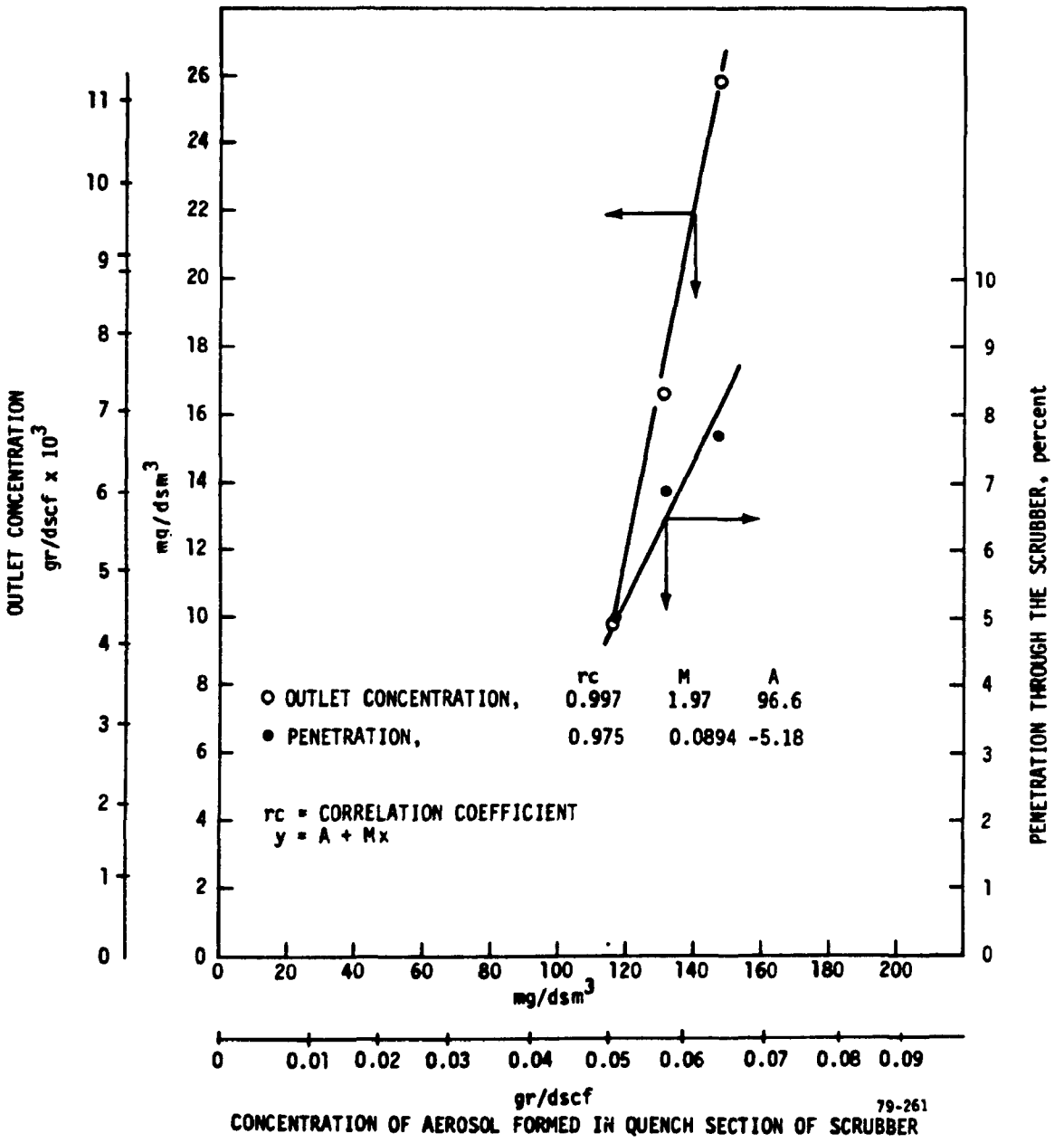

Figure 4-1. Scrubber performance as a function of scrubber-generated aerosol.

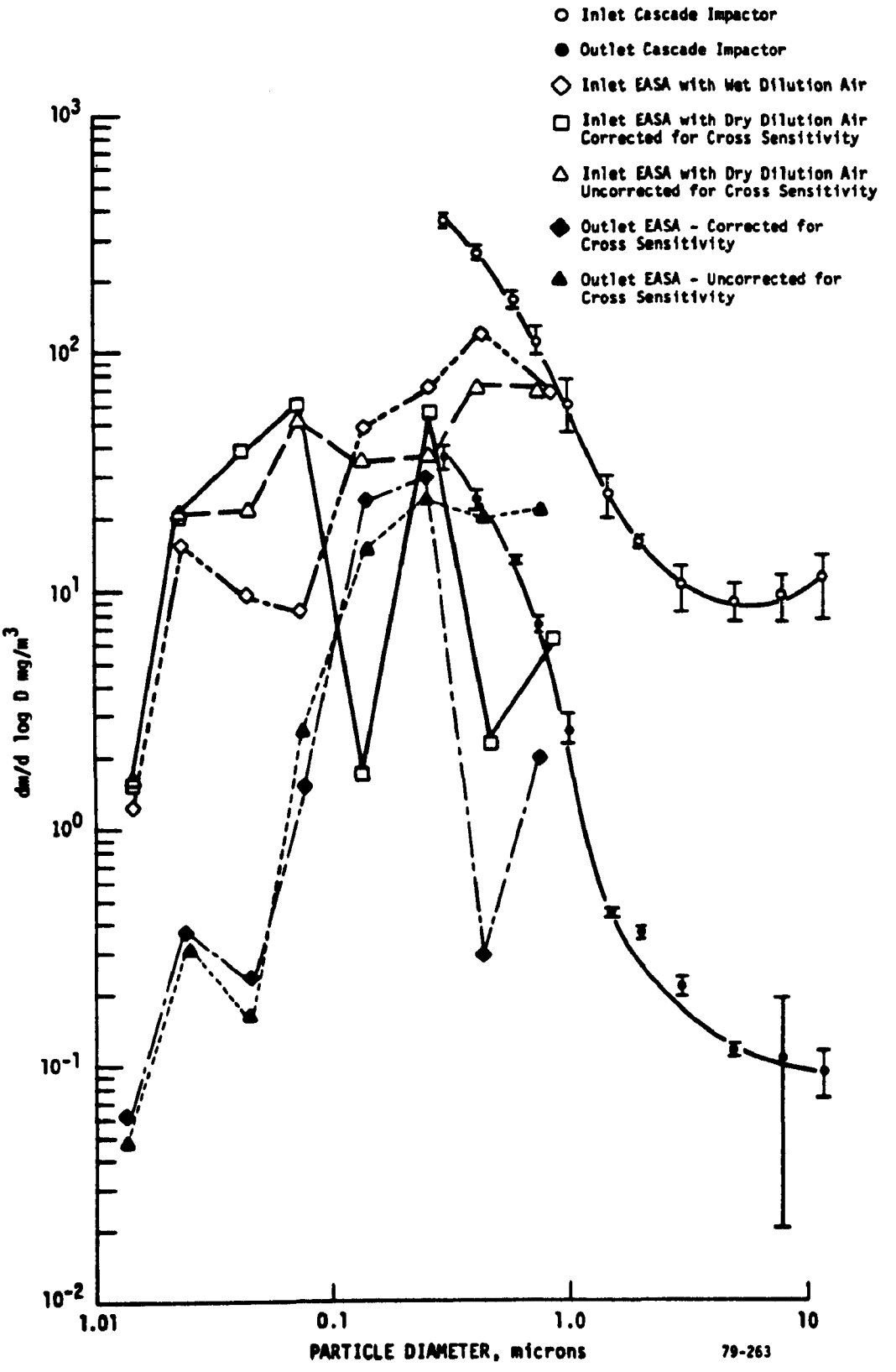

Figure 4-2. Impactor and EASA differential size distributions for 11/21/78.

the emission was very reactive with water. The dilution system was operated with dilutions of up to 1000:1; therefore, with fresh silica gel the aerosol would be measured with insignificant relative humidities (absolute humidity of 10^{-4}g H_2O/g air). The cascade impactor measured the particle size distribution under flue gas conditions of about 3 percent relative humidity. The single mode distribution is the one most likely to be present at the inlet of the scrubber. The size distributions measured by the EASA were repeatable and the humidity phenomenon was observed on other test days.

A second uncertainty is related to the data reduction procedures. The EASA has cross sensitivity errors in the last four size channels (a particle will be sensed in more than one channel). A computational procedure reported by Twomey was used to reduce the data to correct for cross sensitivity; the instruction manual method which does not correct for cross sensitivity was also used. The size distribution reported for the EASA depends on the data reduction technique.

In these tests, the instruction manual method agrees better with cascade impactor size distribution than the results corrected for cross sensitivity. However, the cascade impactors also have cross sensivity and the reduction technique used does not correct for nonideal behavior in the impactor. Therefore, agreement of EASA and impactor size distributions does not mean any particular size distribution is correct. For this reason, results from different approaches are reported. The ambiguity in reported size distribution indicates the difficulty of obtaining this information for a reactive condensible aerosol even when state-of-the-art experimental techniques are used.

PARTICLE SIZE DEPENDENT PENETRATION

In Figure 4-3, the combined impactor and EASA penetration curves are shown for November 21, 1978. The interpretation of the EASA results is an important consideration in computation of the penetration. The data obtained with partially spent silica gel at the inlet (diamond) are the most believable in the 0.1 to 0.3 micron range.

SCRUBBER PERFORMANCE

The aerodynamic diameter as defined by Calvert et al. is given by:

$$d_{aero} = d_{actual} \sqrt{C\,\rho}$$

where

C = Cunningham correction factor

ρ = Particle density, g/cm^3

d_{actual} = Actual cut diameter, microns

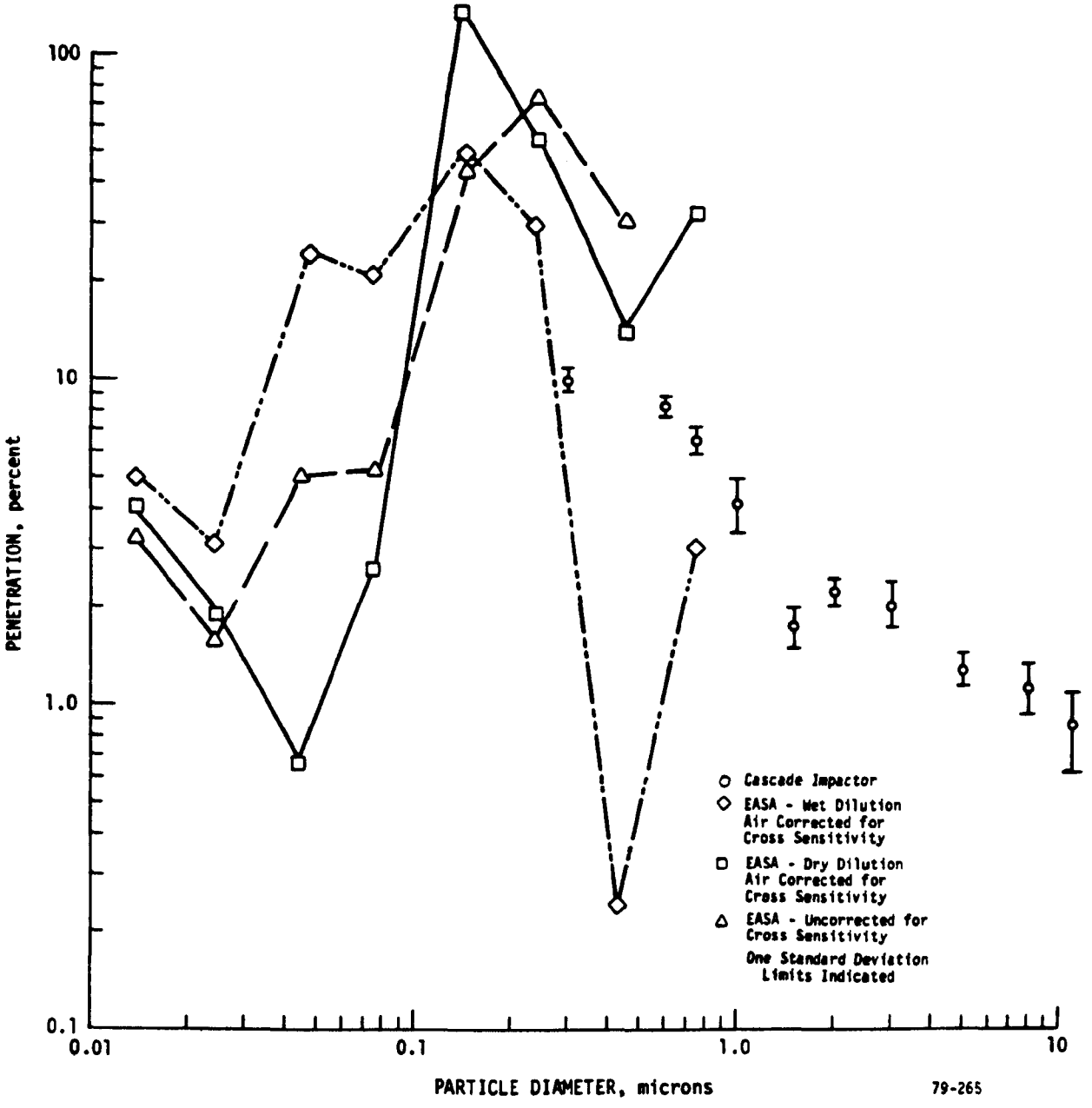

Figure 4-3. Particle size dependent penetration for cascade impactor and EASA results.

The aerodynamic cut diameters were computed from the actual diameter. The EASA size distribution was used because the cut diameter was below the resolution of the impactor.

The square root of the Cunningham correction factor and density $\sqrt{C\rho}$ was computed for the size range of interest in Figure 4-4. The actual size cut diameters were taken from Figure 4-5 and reported in Table 4-3. Depending on the measurement and data inversion technique, the aerodynamic cut diameter was from 0.4 to 0.6 microns.

TABLE 4-4. SUMMARY OF CUT DIAMETERS

Technique	Actual Diameter at 50% Penetration (micron)	$\sqrt{C\rho}$ $(g/cm^3)^{1/2}$	Aerodynamic Cut Diameter (micron)
EASA uncorrected for channel cross sensitivity	0.28	2.16	0.60
EASA inlet size distribution dry dilution air	0.24	2.28	0.55
EASA inlet size distribution water in dilution air	0.14	2.75	0.38

The aerodynamic cut diameter from Table 4-3 and theoretical power from Table 4-2 are shown in Figure 4-4. This figure has theoretical performance curves for a number of different scrubber types for comparison. These results suggest that the IWS is more efficient than a theoretical venturi scrubber.

The aerodynamic cut diameter obtained for the whole scrubber on November 21 is believed to be valid for the IWS units including the aerosol generated in the quench and prescrubber section. The generated particles are captured in the IWS in the 1 to 10 micron diameter range. The penetration in the fine particle range, less than 1 micron, appears to be unaffected by particle generation. Thus, the aerodynamic cut diameter is unaffected by this phenomenon.

OPACITY

The wide ranges of concentration and opacity between inlet and outlet conditions allowed the correlation of mass concentration and opacity as shown in Figure 4-5. The correlation coefficient of 0.96 suggests that the size distribution was fairly consistent.

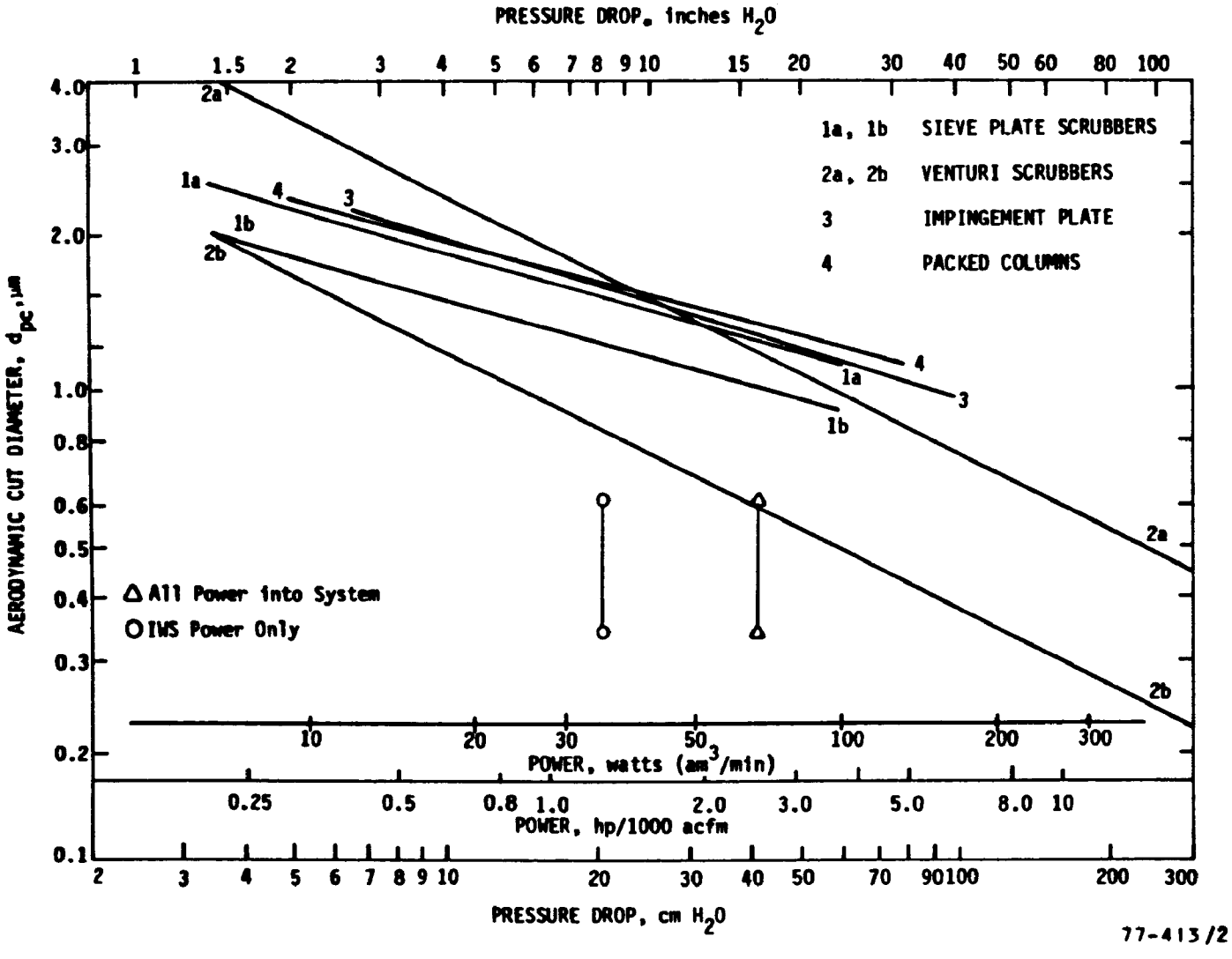

Figure 4-4. Aerodynamic cut diameters of the Ceilcote ionizing wet scrubber compared to the theoretical performance of other scrubber types (after Cooper and Anderson, adapted from Calvert).

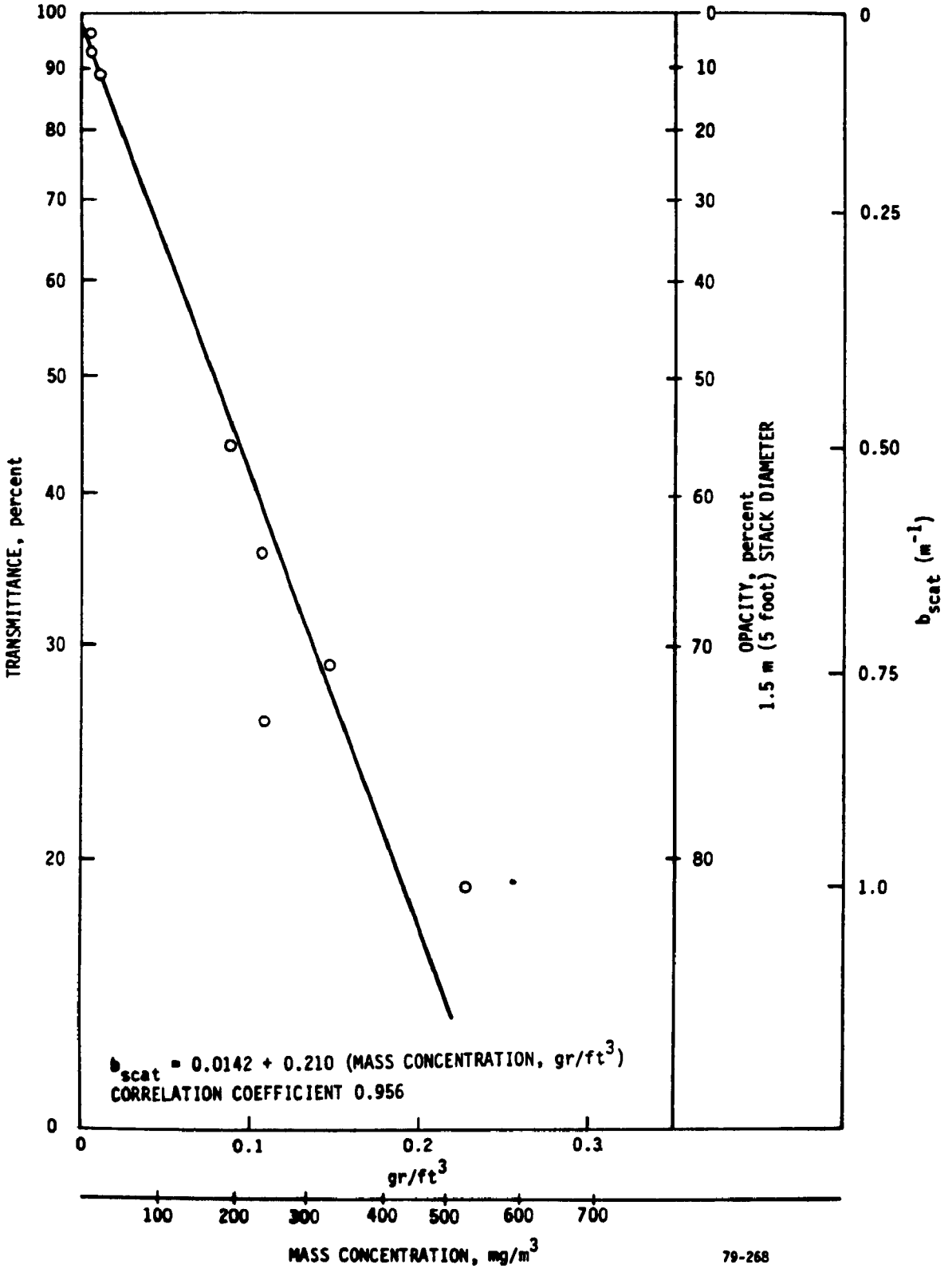

Figure 4-5. Correlation of opacity with mass concentration.

SECTION 5

REFERENCES

Calvert, S. "Engineering Design of Fine Particle Scrubbers." J. Air Poll. Cont. Assoc. 24:929-934. 1974

Calvert, S.J., J. Goldschmid, D. Leith, and D. Mehta. Scrubber Handbook. EPA-R2-72-118a, NTIS No. PB-213-016, August 1972.

Cohen, J.J., and D.M. Montan. "Theoretical Considerations, Designs, and Evaluation of a Cascade Impactor." Am. Ind. Hyg. Assn. J. 28:95-104. 1967

Cooper, D.W., and D.P. Anderson. Dynactor Scrubber Evaluation. EPA-650/2-74-083a, NTIS No. PB 243-365 U.S. Environmental Protection Agency, RTP, NC, June 1975.

Ensor, D.S., L.D. Bevan, and G. Markowski. "Application of Nephelometry to the Monitoring of Air Pollution Sources." 67th Annual Meeting of the Air Pollution Control Assoc., Denver, Colorado, Paper No. 74-110. 1974

Harris, D.B. Procedures for Cascade Impactor Calibration and Operation in Process Streams. EPA-600/2-77-004, NTIS No. PB 263-623, USEPA, RTP, NC, January 1977.

Markowski, G.R., and D.S. Ensor. "A Procedure for Computing Particle Size Dependent Efficiency for Control Devices from Cascade Impactor Data." 70th Annual Meeting of the Air Pollution Control Assoc., Toronto, Canada, June 1977.

McCain, J.D., G. Clinord, L.G. Felix, and J.Johnson. A Data Reduction System for Cascade Impactors. Proceedings: Advances in Particle Sampling and Measurement. EPA-600/7-79-065, NTIS No. PB 293-363, USEPA, RTP, NC, February 1979.

Perry, J.H. Chemical Engineer's Handbook. McGraw-Hill Book Company, Inc., New York. 1963

Strauss, W. Industrial Gas Cleaning. Pergamon Press, New York. pp. 333-334. 1974

Twomey, S. "Comparison of Constrained Linear Inversion and an Iterative Nonlinear Algorithm Applied to the Indirect Estimation of Particle Size Distributions." J. of Computational Physics. 18: 188-200. 1975

DEMONSTRATION OF A HIGH FIELD ELECTROSTATICALLY ENHANCED VENTURI SCRUBBER ON A MAGNESIUM FURNACE FUME EMISSION

by

M. T. Kearns
Air Pollution Systems, Inc.
Kent, Washington 98031

and

D. L. Harmon
Industrial Environmental Research Laboratory
U.S. Environmental Protection Agency
Research Triangle Park,
North Carolina 27711

ABSTRACT

A $566m^3/m$ (20,000 acfm) permanent installation demonstration system, consisting of the Air Pollution Systems' High Intensity Ionizer and a variable throat venturi scrubber (called the Scrub-E) has been installed on a magnesium recovery furnace. The furnace produces submicron fume particles of MgO, $MgCl_2$ and $ZrCl_4$. The system is designed to demonstrate the effectiveness of the High Intensity Ionizer versus high venturi pressure drop on the furnace emissions. The High Intensity Ionizer array operates stably at field strengths of 10-15 kV/cm and at velocities in excess of 18m/s (60 fps) while maintaining high charging efficiencies. The report covers the system design, technology, applications, and project developments. An Environmental Protection Agency proposed charged droplet Scrub-E is also discussed covering the design, technology, and proposed demonstration program.

DEMONSTRATION OF A HIGH FIELD ELECTROSTATICALLY ENHANCED VENTURI SCRUBBER ON A MAGNESIUM FURNACE FUME EMISSION

INTRODUCTION

The Particulate Technology Branch of the U.S. Environmental Protection Agency (IERL-RTP) has had for the last 5 years the responsibility to evaluate and bring to commercial feasibility, devices based on new collection principles or concepts, or new combinations of existing concepts. An emphasis has been placed on those devices that are applicable to the metallurgical industry, and that can be easily retrofitted to existing equipment. In 1977, the EPA issued a competetive procurement to "...demonstrate at pilot or small full scale the technical and economic feasibility for the most promising existing novel particulate collection system for control of fine particulate emissions from industrial sources." This competetive procurement was won by Air Pollution Systems, Inc. (APS) to demonstrate the Scrub-E which was tested in the APS laboratory under the novel device evaluation program. A contract was funded in September 1977 with APS to demonstrate the Scrub-E on a fine particulate source ($\leq$ 3μm in diameter). A magnesium recovery furnace which emits submicron particles of MgO, $MgCl_2$, and $ZrCl_4$ was selected as the demonstration site. The Scrub-E is currently erected (July 1979) with startup to occur within the next few months. (See Figure 1.)

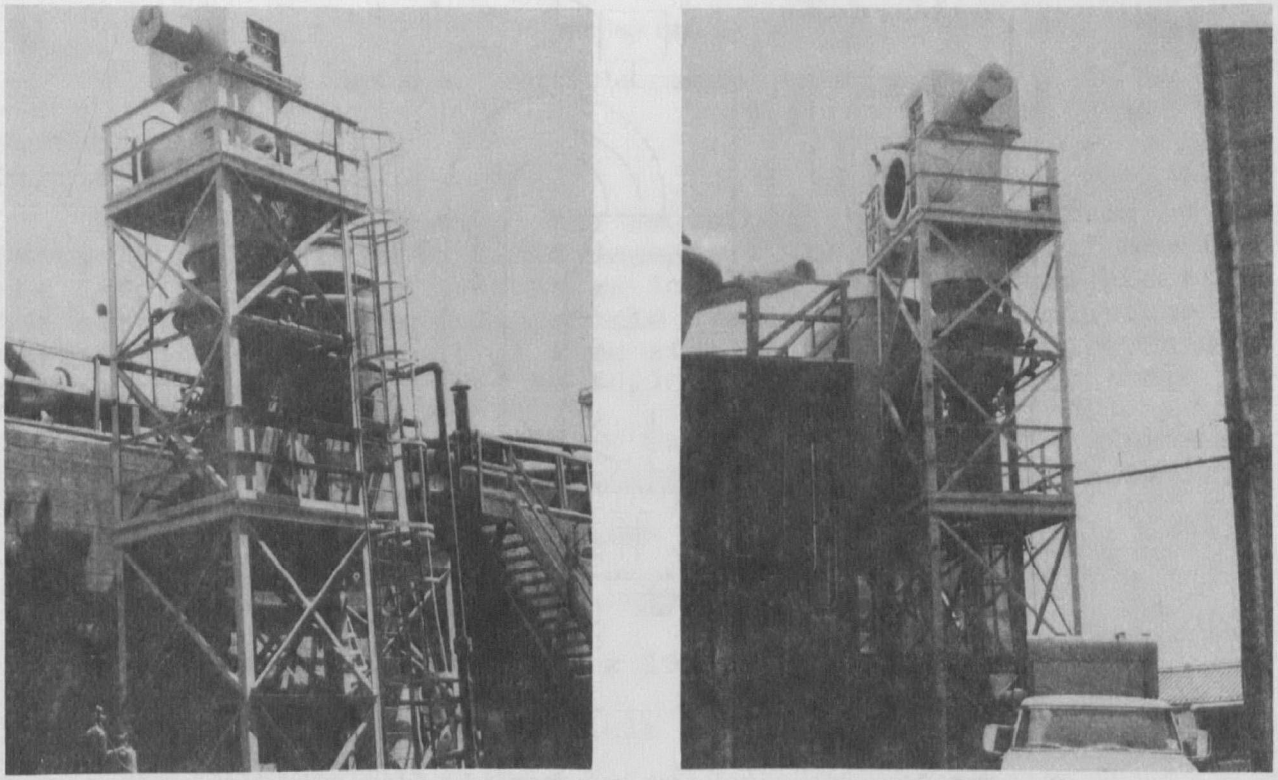

Figure 1. EPA Scrub-E demonstration system.

BACKGROUND

Substantiated research has concluded that fine particulate ($\leq$ 3μm in diameter) can result in serious environmental and health problems. The impact of fine particulates on visibility and cloud nucleation is compounded by their extremely low settling rate (mobility) and resultant persistence in the atmosphere. The above factors are compounded if the fine particulate is composed of toxic substances. This has caused increased control requirements to be set by the air pollution control agencies.

The collection of fine particulate is presently limited to equipment which is either very large and/or has high operating costs. The choices include equipment such as precipitators and baghouses which are large and have a high capital cost, or venturi scrubbers which are relatively cheap, but require very high energy consumption to collect fine particulate. The users of fine particle collection equipment are, therefore, faced with capital and/or operating costs which are becoming prohibitive, especially in the case of the venturi scrubber.

APS has taken the venturi scrubber system which represents the smallest and consequently the cheapest capital cost and attempted to reduce the operating costs to a reasonable level. The resultant system, the Scrub-E, incorporates the APS High Intensity Ionizer with the venturi scrubber system. (See Figure 2).

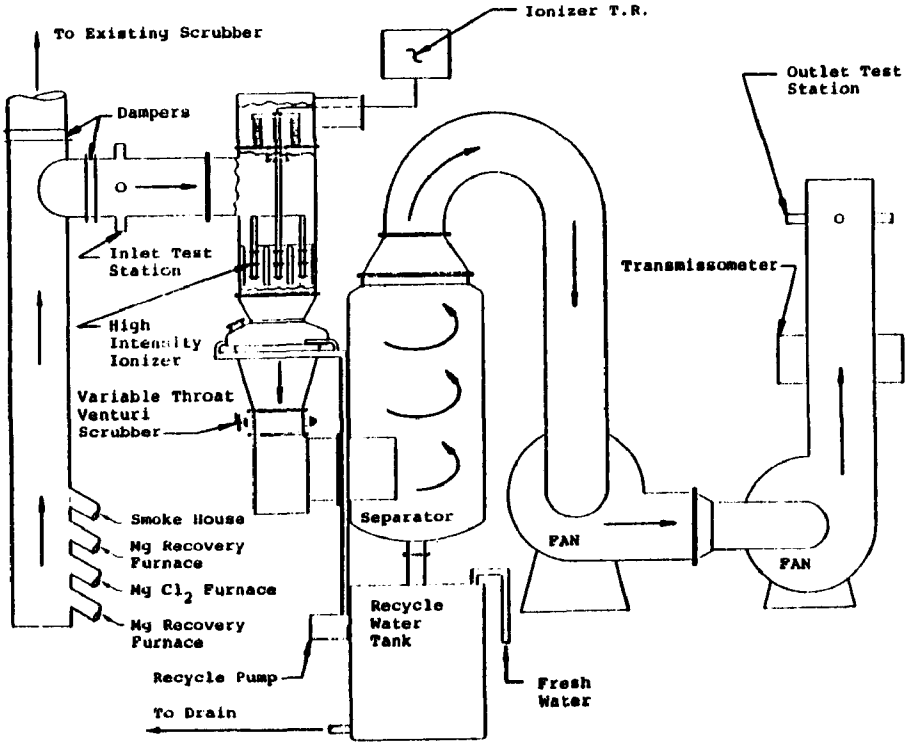

Figure 2. EPA demonstration system schematic flow diagram.

The Scrub-E utilizes the combination of electrostatic forces and inertial forces for the removal of particulate. This combination maintains an improved efficiency on fine particulate while requiring one-half to two-thirds the energy consumption of a conventional scrubber (see Figure 3). The design of the ionizing unit provides for a relatively small add-on device to precharge the particulate.

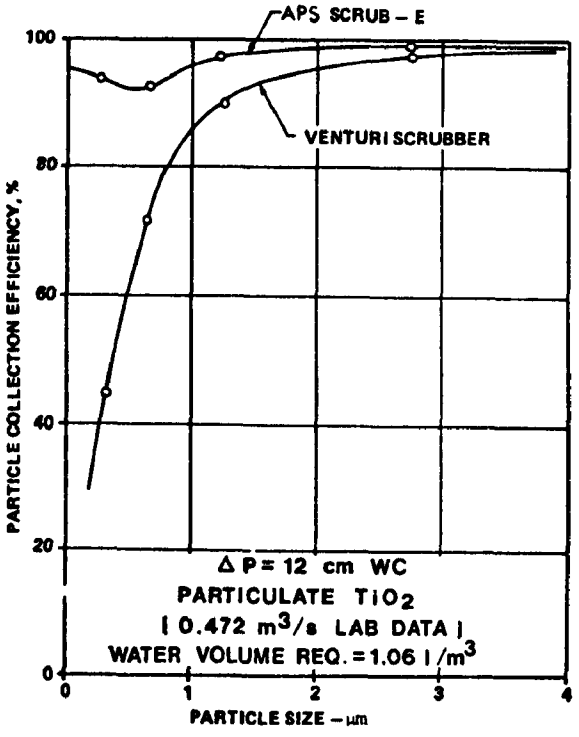

Figure 3. Particle removal efficiency.

FUNDAMENTAL THEORY

Particle Charging

From classical theory, the amount of charge collected by a particle in an electric field depends on the strength of the field, the density of charge present as ions (or in some cases electrons), the particle radius and dielectric qualities of its constituent material, and the amount of time available for charging. This is defined by Oglesby et al.[1] as follows:

the saturation charge on particles due to field charging

$$q_s = 12\,(\varepsilon/\varepsilon+2)\,\pi\varepsilon_o a^2 E_o \qquad (1)$$

where ε = relative dielectric constant

ε_o = permittivity of free space

$= 8.85 \times 10^{-12}$ farads/m

a = particle radius, meters

E_o = electric field v/m

In practice, the actual charge is time dependent. The "charging efficiency" Np can be written as:

$$Np = t/t + T \qquad (2)$$

where T is the charging time constant and depends on the ion density, N_o, and the ion mobility.

The time, t, a particle resides in the charging field depends on its velocity and the geometry of the field.

The ion density is a function of the supply current, field, and ionizer geometry so that:

$$N_o = \frac{I}{\pi\ e\ \omega\ \mu\ (R + r)\ E_o} \qquad (3)$$

where

I = supply current to ionizer - amps

ω = width of active region - meters (weighted average)

R = anode radius - meters

r = cathode radius - meters

E_o = average field V/m

μ = ion mobility m^2/V-sec.

e = electronic charge - coulombs

Further charging of a particle beyond its field saturation value can be accomplished by diffusion charging resulting from the thermal motion of ions. This process is most effective for particles in the submicron range, specifically with $r < 0.25$ µm.

Diffusion charging (White[2]) is a time function so that the charging rate is:

$$\frac{dn}{dt} = \pi\ a^2\ C\ N_o\ \exp -(ne^2/akT) \qquad (4)$$

where

n = number of ions

e = electronic charge -esu

k = Boltzmann's constant = erg/^oK

T = ^{o} Kelvin

C = rms value of ion thermal velocity

t = time-seconds

Integration yields the following formula for the diffusion component of particle charge:

$$n = \frac{akT}{e^2} \ln\left(1 + \frac{\pi a C N_o e^2 t}{kT}\right) \qquad (5)$$

The total charge on a particle is assumed to be the sum of the field charging component and the diffusion charging component. Although this is probably an over simplification, it serves as a basis for the verification of experiments.

A further component in charging should be noted if there is a free electron component in the ionizer gap. Because of the high mobility of electrons, a small percentage of free electrons can contribute measurably to particle charging with an imperceptible change in space charge. This effect was noted by Crynack and Penney[3] for fields near sparkover.

It is reasonable to assume the same effect will be found in the APS High Intensity Ionizer because of the high fields involved, but the magnitude is not known. Indications of excess current is shown in Figure 4 where excess charging of particulate was noted in charge-to-mass measurements of titanium dioxide dust.

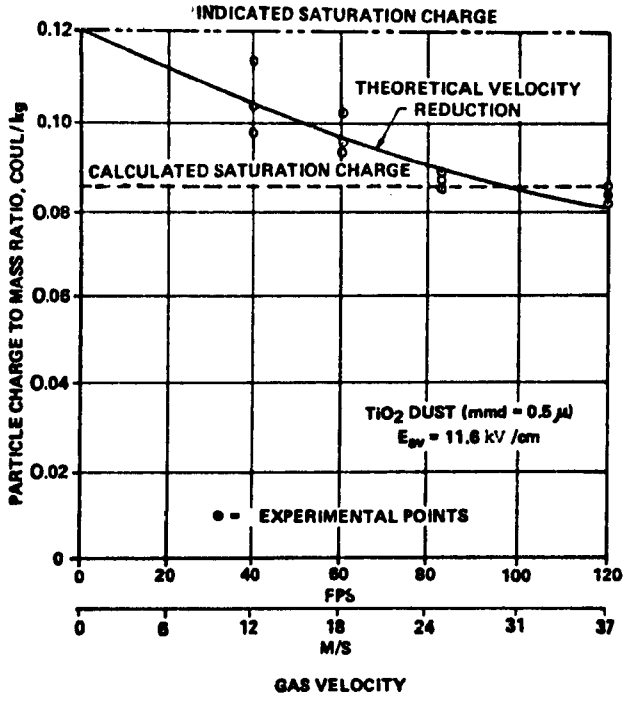

Figure 4. Effect of gas velocity on charging efficiency.

Venturi Scrubber

A venturi scrubber utilizes inertial or impaction forces to collect particulate on drops of water or scrubbing liquor. When liquor is injected into a moving air stream (as high as 122 m/sec), it is atomized or broken up into small droplets. The relative velocity between the droplets and the entrained particulates supplies the energy for collection. Aerodynamic (drag) forces act on the fine particles tending to draw them around obstructions (such as water droplets) in the air stream. Opposing the drag forces are inertial forces which resist any sudden change of direction. Since the aerodynamic drag force is proportional to the plane projected area of a particle and the inertial forces are proportional to the mass, there is a strong size dependence over which force will predominate. For a small particle the mass decreases faster than the plane area, hence for a given gas velocity there comes a natural cutoff point where impaction forces become ineffective in comparison to the drag force (see Figure 5).

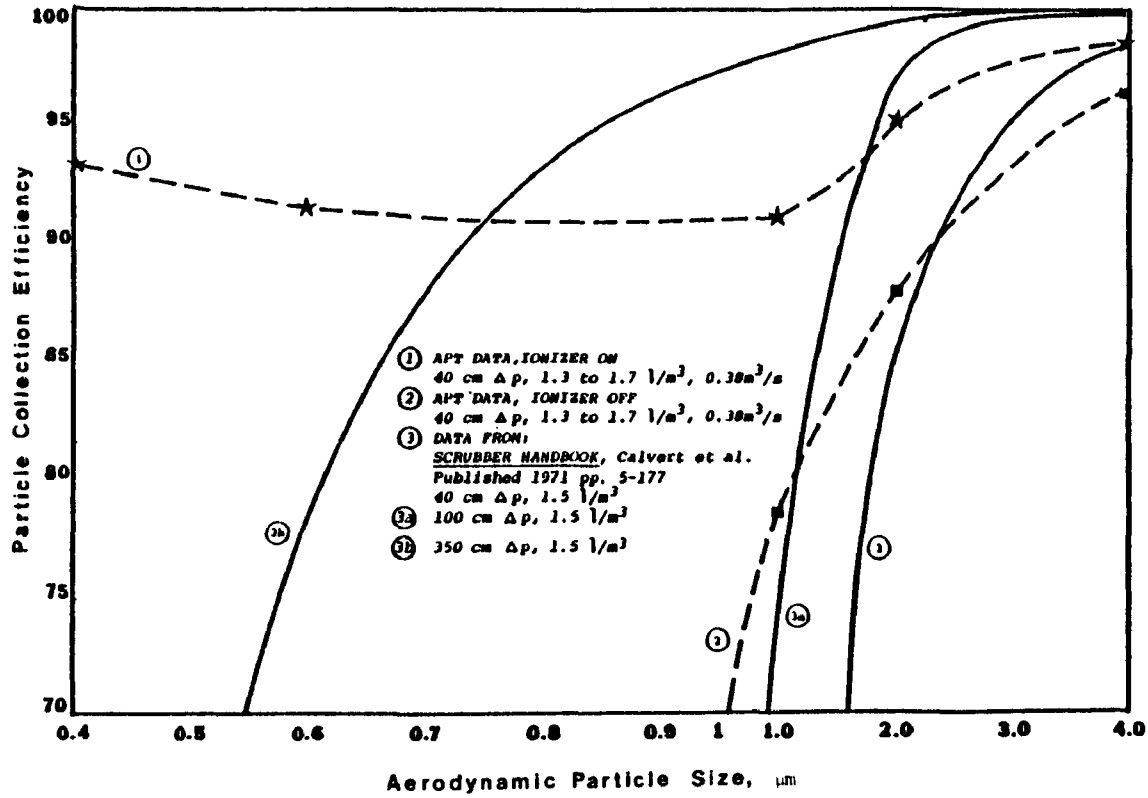

Figure 5. Particulate collection efficiency vs. size.

The above relationship can be expressed as a function of the impaction parameter $\sqrt{\psi}$ (Ranz and Wong[4]).

$$\sqrt{\psi} = \left(\frac{C\ P_p V g}{18 \eta D_c}\right)^{\frac{1}{2}} dp$$

where

V_g = gas velocity - gm/sec

P_p = particle density - gm/cm^3

C = Cunningham correction

η = air viscosity - gm/sec x cm

dp = particle diameter - cm

D_c = collector diameter - cm

Equation (6) illustrates the dependence of collection efficiency on particle size since the particle diameter dp is proportional to $\sqrt{\Psi}$. Decreasing the collector size, D_c, or increasing the gas velocity, V_g, will therefore improve collection efficiency. The collection efficiency per droplet can be considered in terms of target area or percent of the projected droplet area within which the approaching particulate will be collected by impaction or interception and not swept around the droplet. (See Figure 6.)

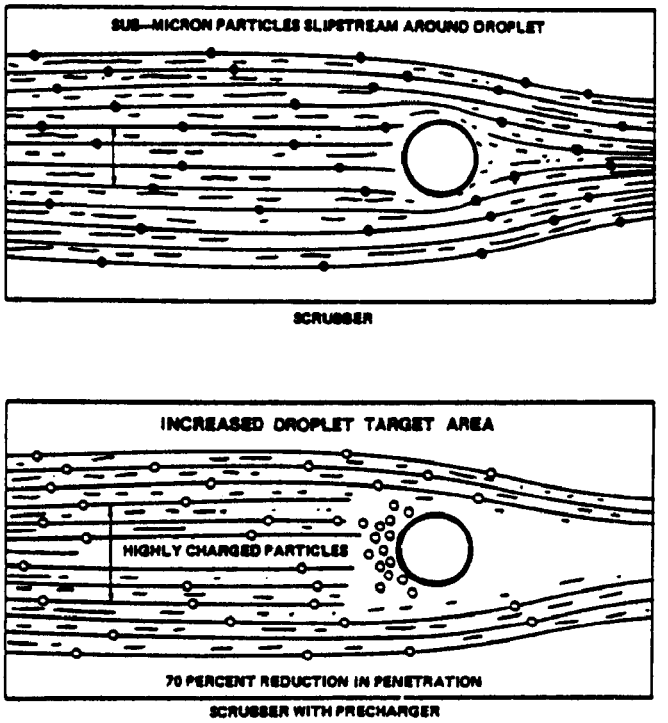

Figure 6. Mechanisms of collection in scrubbers.

The target area of a droplet is limited to the projected area of the droplet, hence the collection efficiency per droplet due to impaction alone can never be greater than 1.

Two means which can be used to achieve greater particle removal are increasing the relative velocity (resulting in greater pressure drop) or increasing the water/air ratio. Both of these means, however, have practical limitations and neither can completely overcome the reluctance of smaller particulate to be collected.

Application of Electrostatic Forces to Collection

Electrostatic forces have long been used in precipitation for dry process control and have been studied for application to scrubber collection and fiber bed collection. Of particular interest in this case is the work of Kraemer and Johnstone[5] and Zebel[6].

The total force for particle collection is the vector sum of the inertial and electrostatic forces acting on a particle. The total electrical force is the sum of all individual electrical forces acting on a particle. Strauss[7] considers the total force Fe_1 as:

Coulombic force between a charged particle and charged collector

$$F_{EC} = \frac{Qq}{4\pi\varepsilon_o r^2} \tag{7}$$

Image force of induced charge on uncharged particle by charged collector

$$F_{EI} = -\left(\frac{\varepsilon-1}{\varepsilon+2}\right)\frac{d^3Q^2}{16\pi\varepsilon_o r^5} \tag{8}$$

Image force of induced charge on uncharged collector by charged particulate.

$$F_{EM} = \frac{q^2\ D}{8\pi\varepsilon_o r^3} - \frac{2q^2\ Dr}{\pi\varepsilon_o(4r^2-D^2)^2} \tag{9}$$

Space charge force of repulsion from surrounding like charged particulate toward a relative charge void (the collector).

$$F_{ES} = -\frac{q^2D^3N}{24\varepsilon_o r^2} \tag{10}$$

where

q = charge on particle - coulombs

Q = charge on collecting body - coulombs

r = distance between particle and collector - cm

N = particle concentration per unit volume #/cm^3

ε = dielectric constant of aerosol particle

ε_o = specific inductive capacity of space

= 8.85×10^{-21} coulomb^2 dyne^{-1} cm^{-2}

Because the electrostatic forces are additive, the more positive forces that can be utilized the higher the force of collection. Furthermore, each force that can be increased in magnitude should add to the maximum. As will be explained, unusually high levels of charging are attained in the APS Ionizer by field charging (up to 15 kV/cm) with diffusion charging and electron charging components additive.

APS SCRUB-E DESIGN

Air Pollution Systems, Inc. has developed and patented a new electrode geometry (symmetry) which is successful in establishing a highly stable, intense corona discharge. The cathode is a solid metal disc supported by a structurally reliable tube section centered in a cylinderical anode arrangement. The electrode configuration produces a substantially uniform three-dimensional field which is a principal factor in the greater electrical stability. This geometry provides operating field strengths of 10-15 kV/cm compared to 3-6 kV/cm for wire electrode designs at atmospheric pressures. Figure 7 shows a typical E-I curve for the ionizer.

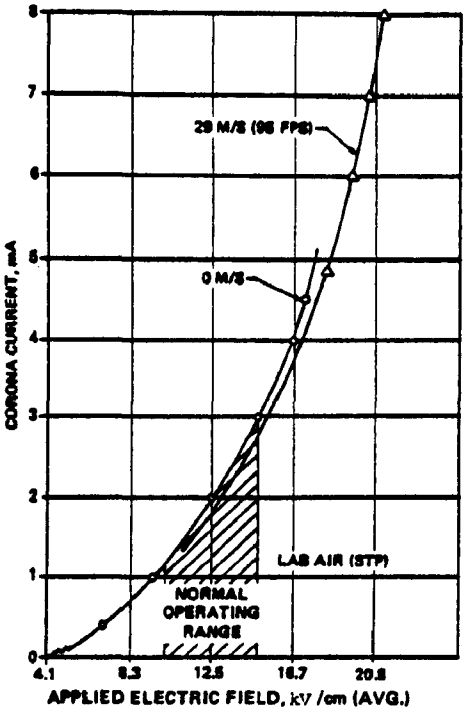

Figure 7. Typical E-I characteristics.

In addition to the very high fields, the electrode geometry produces a concentrated field with ion densities of 10^9-10^{10} ions/cc, many times that obtained conventionally. As noted above, the charge obtained on small particles is dependent on the ion density and is therefore increased with the higher ion density in the APS Ionizer. This increases the diffusional charging of the fine particulate. As a result of the higher fields and ion densities, both

the level of charge acquired by the particulate and the rate of charging are significantly higher. Particle charges approaching half an order of magnitude higher than conventional is currently being achieved. Particle charging efficiency was studied as a function of velocity (residence time). Figure 4 illustrates the effective charging of TiO2 dust (mmd = 0.5μm) in charge-to-mass measurements Q/m versus velocity for normal design ranges. The plotted theoretical and experimental data points show a good correlation in expected efficiency decrease with the increase in velocity. The saturation charge (per unit mass) was calculated to be 87μ coul/gram for an 11.6 kV/cm field. This degree of charging at higher fields was greater than predicted based on cascade impactor size distribution analysis. The charge levels above the calculated saturation charge have been theorized to be the result of direct electron charging due to the very high field strengths.

The APS High Intensity Ionizer effectively charges the particulate at velocities of 7-10 times higher than more conventional electrostatic electrode configurations. Velocities in excess of 30 m/s can be maintained past the ionizer with charging times of a few milliseconds. Figure 8 shows the velocity regime of prime concern for the ionizer versus percent saturation charge. Charging efficiency was found to be between 80% and 90% for normal operating velocities. The high current densities are also principally responsible for the capability to efficiently charge the particulate at velocities in excess of 30 m/s. This means that the particles can be charged to a higher level in a smaller volume, and as can be seen in Figure 2, the ionizer section is small compared to the overall size of the equipment.

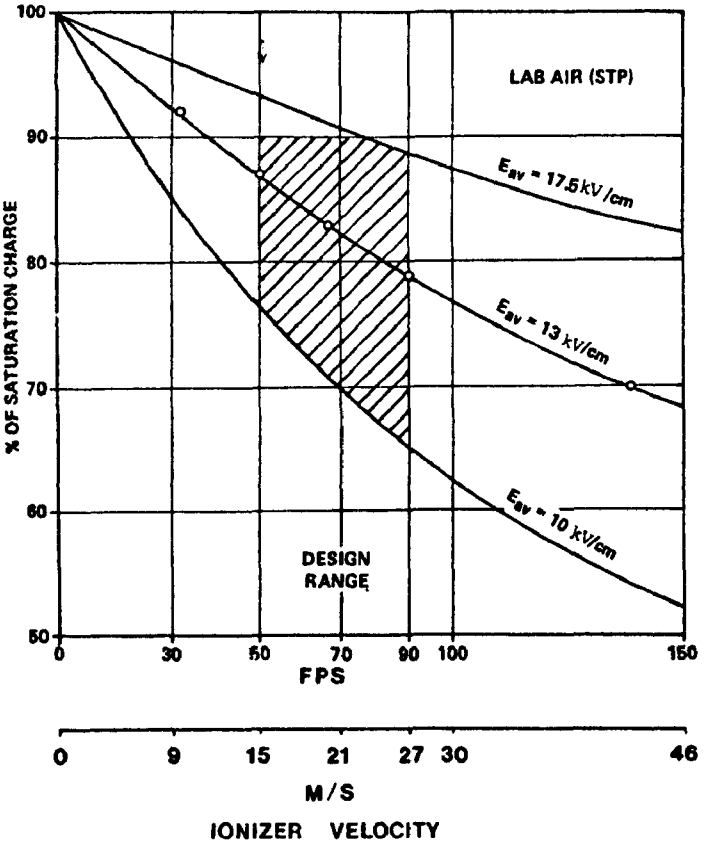

Figure 8. Calculated particulate charging efficiency.

EPA SCRUB-E DEMONSTRATION SYSTEM

Air Pollution Systems, Inc. is currently involved in the field erection phase (Task 4) on EPA Contract No. 68-02-2666. The Scrub-E is installed on a magnesium recovery furnace at Teledyne Wah Chang Albany, Albany, Oregon. (See Figure 1.) As can be seen, the venturi scrubber-separator, structural steel, and APS Ionizer module are erected. Currently (July 1979), all equipment is installed for operation with the exception of electricals, instrumentation, and ductwork. The scheduled date for startup is tentatively planned for late September or early October. (Delays have been caused at the jobsite due to the availability of materials. The ionizer emitting system, anode tubesheet, and venturi variable damper are fabricated from zirconium 702 to resist HCl acid attack. All other components are fabricated from PVC, FRP, or stainless steel.)

Figure 2 displays the demonstration system schematic flow diagram. The particulate gas stream to the Scrub-E originates at four sources. Essentially, the magnesium recovery furnaces (two each) recover nonspent magnesium metal after it has reacted to reduce $ZrCl_4$ to pure zirconium. The spent magnesium, as $MgCl_2$, is shipped to another facility for reduction to pure magnesium metal. The $MgCl_2$ furnace is a concentrator operation to recover whatever remaining magnesium that is left in pure form. The smokehouse emission is where the $MgCl_2$ crucibles are heated in a burnout operation. The magnesium furnaces produce emissions of MgO and traces of $ZrCl_4$ and $MgCl_2$ as the pure magnesium is ladled from the furnaces. All of the furnaces, although, emit primarily MgO fume. Scanning electron microscope photographs (SEM) performed on the magnesium furnace emissions have indicated the greatest proportion of particulate to be less than 1.0 μm in diameter. Cascade impactor size distribution analysis of the particulate verified the SEM data with a D_{50} by weight of 1.48 μm. This D_{50} had a standard geometric deviation of 3.0 with a linear regression correlation coefficient of 0.995.

Objectives for the demonstration program are to remove 90% of all particulate from 0.01 to 3 μm in diameter from the source gas stream. An independent testing organization will be brought on site to test the Scrub-E and to prepare a final report. Accurate particle size fractional measurements require specialty equipment. Diffusion battery techniques with condensation nuclei counters (CNC) or mobility analyzers will be used to document the concentration and size distribution of particle diameters from 0.2 to 0.01 μm. Inertial techniques (cascade impactors) will be utilized for the particle distribution measurements between 0.3 and 25 μm. The standard mass train measurement techniques (Method 5) will be used for the determination of total inlet and outlet mass loading for overall efficiencies and performance.

All of the data from the test program will be analyzed and with supportive information, a final report will be prepared documenting the system performance and economic factors pertaining to the design.

RESULTS OF PRIOR SCRUB-E TESTING

Results of APS laboratory and field testing have shown that the ionizer typically reduces the penetration through the venturi scrubber by approximately 70% or more, without changing any other parameter. These results have been verified by Air Pollution Technology (APT) of San Diego, California. They are an independent testing organization which evaluated the Scrub-E under EPA contract number 68-02-1496. These results are reported in Publication No. EPA 600/2-76-154a[8]. Typical results of the APT tests are shown in Figure 9 which compare favorably with APS lab results in Figure 3. The two curves show fractional efficiency results with and without the ionizer energized. The fractional efficiencies of particulate were determined using both cascade impactors and diffusion batteries. As can be seen in Figure 9, fractional efficiencies are very high on submicron particulate with the ionizer on. The test aerosol used was titanium dioxide with an aerodynamic mass mean diameter of 1 μm. As can be seen, the fractional efficiencies for particles < 0.8μm and > 2.0 μm were > 92% and > 99%, respectively.

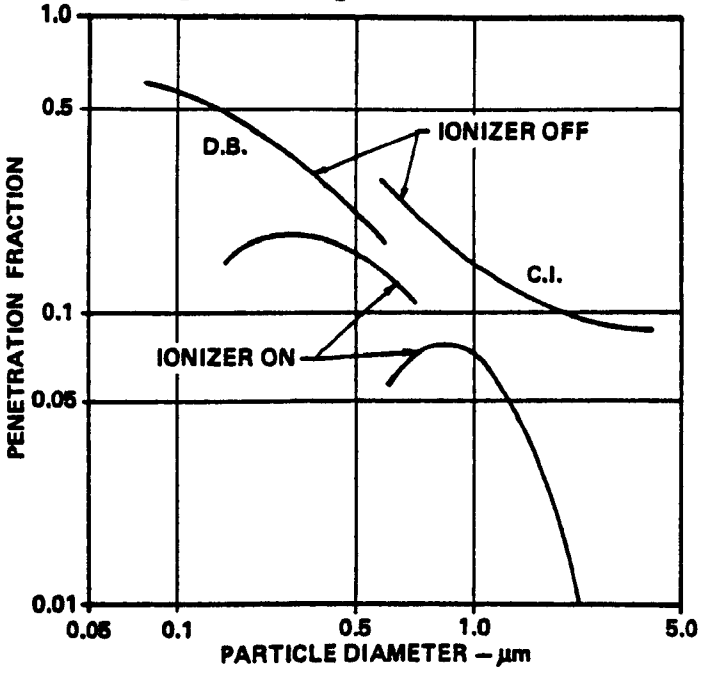

Figure 9. Penetration vs. particle diameter using both diffusion battery and cascade impactor, Run 28, A.P.T. test data.

Another significant demonstration of the Scrub-E was on a urea (carbonyl diamide) prilling tower. The particulate size distribution was 80 to 90% by weight in the 0.4 to 1.0 μm interval range with an inlet grain loading of 0.09 gm/m^3. The objective of the test program was to reduce the visible emissions to a zero level which was estimated to be about 0.0034 gm/m^3. Collection efficiencies ranged from 90.75 to 96.25% performed by the plant personnel, with a final outlet grain loading of 0.0034 gm/m^3. The pressure drop required to obtain this level was 19 cm w.g. at a flow volume of 21 m^3/min. There were no tests conducted with the ionizer off, but visual observations revealed a dense opaque plume without the electrostatics and a zero opacity or 0.0034 gm/m^3 with the ionizer on.

EPA CHARGED DROPLET SCRUB-E DEMONSTRATION PROGRAM

Initially in the performance of EPA Contract No. 68-02-2666, Air Pollution Systems, Inc. was to include in the Scrub-E demonstration system a positive polarity charged droplet vessel. However, due to the limitations of space at the job site, this was not feasible. APS proposed to the EPA to fabricate a smaller system, 85 m^3/min (3000 cfm) which would be mobile and, therefore, easily adaptable to plant space availability. The system is comprised of a single throat High Intensity Ionizer, followed by a venturi scrubber, and horizontal separator (see Figure 10). The separator vessel houses the charged droplet system which will allow liquid to gas contact residence times of 3-5 seconds, dependent on total gas flow volumes.

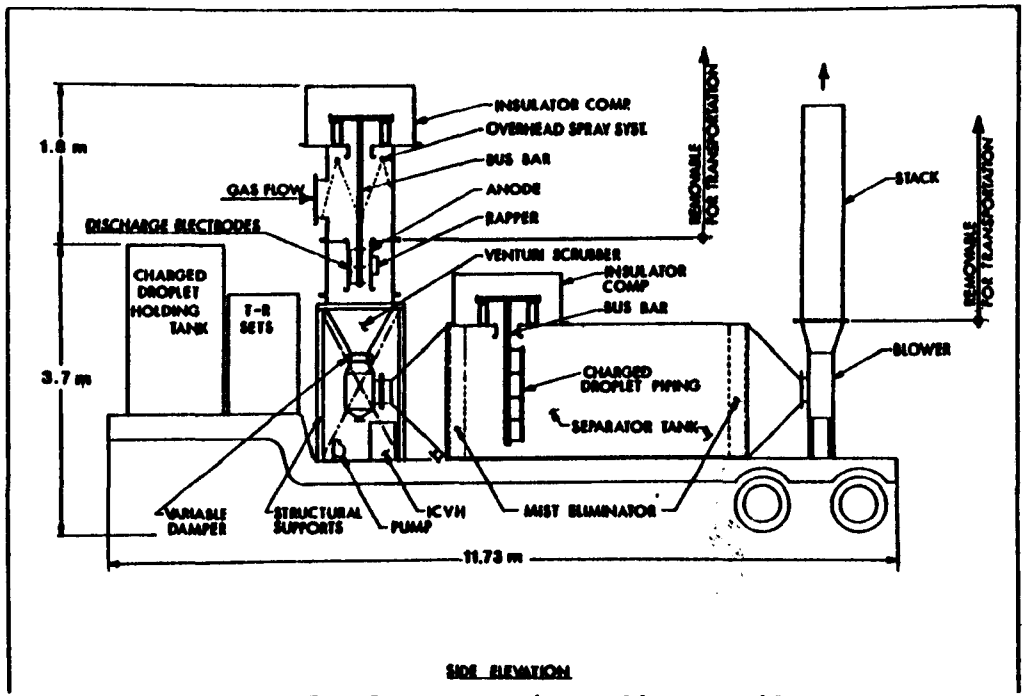

Figure 10. Charged droplet venturi scrubber trailer mounted.

The purpose of the charged droplet scrubber will be to investigate the feasibility of further reducing the pressure drop requirements of the venturi scrubber, while maintaining the high efficiency levels on submicron particulate by the introduction of charged droplets. The reduction of the liquid to gas ratio and/or the throat velocity will control the amount of charged particulate passing through the venturi into the charged droplet section for comparative efficiency measurements. Testing performed in the APS laboratory has resulted in a method of applying a substantial charging level to the water drops through the use of higher fields. The relative charge measured by APS has shown levels approximately 2-3 times higher than obtainable by methods used conventionally.

Theoretically, the objective to achieving the highest percent removal of particulate or collection efficiency with the charged droplets is to:

a) maintain the liquid-to-gas ratio most economically feasible for water consumption rate and induced pressure drop;

b) produce the smallest droplets possible that are economically feasible to provide the highest liquid surface area per quantity of liquor and per cubic meter of gas;

c) provide the most efficient charging mechanism that produces the highest charge-to-mass ratio to the droplets, and

d) provide the highest residence contact time between particles and droplets that is feasible for equipment size and, therefore, inplant space.

To achieve objective c), APS laboratory experiments have found that the use of higher fields and direct charging of the water results in a higher charge/mass ratio. It is theorized that the configuration of direct charging is more efficient since conduction of electric charges at the liquid source appears to be along the surface rather than through the bulk of liquid. This mechanism of direct charging also allows the liquid source to raise in potential until it is ejected as droplets, thereby becoming highly charged. Typical values of charging of 200 μm droplets achieved by APS are 1.43×10^{-6} coulombs/gram. This amounts to approximately one-fourth that of the Rayleigh stability limit, (see Figure 11).

Figure 11 demonstrates the Rayleigh stability curve as a function of droplet size. The field strengths were calculated knowing the charge/mass for the water droplets. The curve proves that the Rayleigh limit is equivalent to approximately 40 kV/cm, and therefore higher fields effectively produce a higher charge/mass to the water droplets.

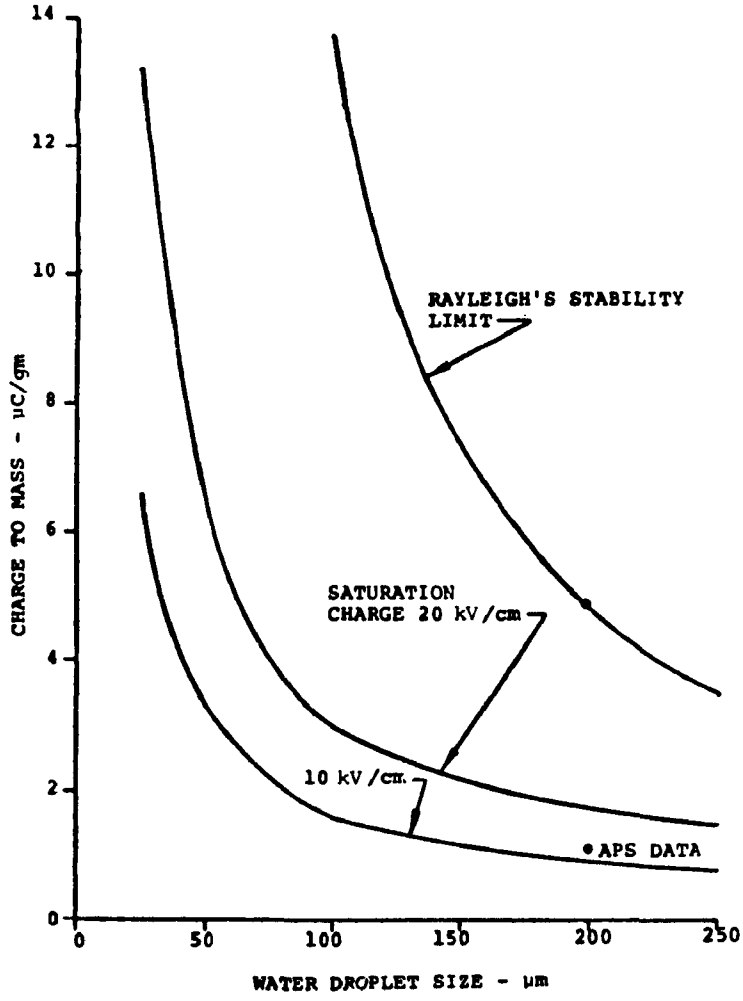

Figure 11. Water droplet charge.

Droplet surface perturbation stabilities have been predicted by Rayleigh for the maxiumum charge that a conducting water or liquid droplet with a given radius can obtain. Hendricks[9] examines Rayleigh's equation for the instability of charged liquid masses against surface displacements. Those liquid masses, in order to be stable against surface displacements, must have a charge/mass ratio of less than:

$$\underset{\text{Limit}}{(Q/m)} = \frac{10^{-6}\gamma^{\frac{1}{2}}}{p\pi^{\frac{1}{2}}r^{3/2}} \qquad (11)$$

where

Q/m = coulombs/kilogram

γ = liquid surface tension in dynes/cm

p = liquid density in kilograms/m^3

r = droplet radius in meters

This quantity is equivalent to approximately 4.83×10^{-6} coulombs/gram:

where

γ = 73.35 dynes/cm

p = 1000 kg/m^3

$r = 10^{-4}$m (100 microns)

To achieve objective d), the collection of fine particulate is usually limited by the droplet interaction lifetime unless slow velocities and hence high residence times are employed. Melcher, et al.[10] has identified the critical time constants to the collection of charged fine particles by large charged collectors (droplets).

The characteristic time required for the removal of charged particles by charged drops is given by:

$$T_C = \varepsilon_o/NQb \qquad (12)$$

The time constant given for the unipolar droplets to be electrostatically self precipitated, or the effective droplet lifetime is:

$$T_r = \varepsilon_o/NQB \qquad (13)$$

where
(MKS units)

ε_o = dielectric constant of free space

= 8.85×10^{-12} farads/m

N = drop number density

Q = drop charge coulombs

b = particle mobility which from Stokes $\simeq q/6\pi\eta_c a$

B = drop mobility which from Stokes

$$= \frac{Q}{6\pi\eta r}$$

ηc = gas viscosity (Cunningham slip by subscript)

q = particle charge - coulombs

a = particle radius - m

r = droplet radius - m

The limitations to overcome are the mobilities of the water droplets which are greater than the fine particulate (B>b). This results in a shorter characteristic time T_r than T_c. An increase in the average charge on the water droplets (Q) decreases the characteristic time T_c, which decreases the necessary residence time for higher collection efficiency. This satisfies objective d) above. An overall reduction in the liquid-to-gas ratio, or drop number density (N) by reducing the actual L/G and droplet radius will maintain T_r constant. This satisfies objectives a) and b) above.

The removal of submicron particulate has proven to be difficult due to their low mobility, diffusive nature, and unfavorable inertial properties. Because electrical forces and interactions are effective in this size range, the addition of electrical energy to charge collector sites (water droplets) is of great interest. The addition of a high positive charge to the scrubbing droplets should not only decrease the characteristic time T_c for interaction, but increase coulombic forces of attraction (equation 7) and image and space forces as well (equations 8-10). It is believed that these forces will be especially effective on the smaller particulate fraction ($\leq$1μm).

HII RETROFITTABILITY - CONCLUSION

The specialized APS electrode geometry applies an intense electrostatic field. In addition, high ion densities promote near saturation charging of particulate within a few milliseconds, thus allowing use of high gas flow rates. It is because of the short charging times that the physical size requirements of the charging system can be greatly reduced. This means that the particles can be charged to a higher level in a smaller volume and easily retrofitted to existing collection equipment.

The present uses of the Ionizer are: to precharge the particulate entering a venturi scrubber, significantly reducing the pressure drop required to obtain a specific collection efficiency (the Scrub-E); to precharge particulate entering a dry ESP, thus significantly reducing the overall size; and to be integrally incorporated into a wet ESP device called the Electro-Tube . The

Electro-Tube is a pipe type ESP (acid mist ESP) which is effective where the resistivity or stickiness of the dust prohibits the use of a conventional unit. Emissions with these characteristics are often found in the iron and steel, metallurgical, chemical, pulp and paper, and mining industries.

The utilization of electrostatics with venturi scrubbers as incorporated in the Scrub-E is expected to expand the scrubbers use into many application areas which have fine particulate emissions. As the mass mean diameter of the particulate to be controlled decreases, the Scrub-E becomes a more attractive alternative. (See Figure 9.) This is due to its small size and the high efficiencies which can be obtained on fine particulate (<3μm in diameter) at low energy levels. Traditional control equipment which can obtain high efficiencies on submicron particulate is very large and, therefore, has a high capital cost as well as utilizing a large portion of valuable plant space. The small size and relatively low capital costs, combined with the low energy requirements, favor the use of the Scrub-E for fine particle control. The EPA demonstration system will provide the necessary design criteria from data collection for an HII retrofit to any conventional venturi scrubber system.

In addition, the EPA charged droplet Scrub-E is being studied for its eventual use as an industrial air pollution control device. Such a device should have broad applicability both as a charged droplet retrofit to existing scrubbers and especially as a device where scrubbers would be suitable if the collection efficiencies were sufficiently high.

Among the manufacturers expected to be attracted to the Scrub-E are the mining, metallurgical, chemical, and paper industries, salt soaked hog fuel boilers, phosphate rock dryers, coal dryers, urea prilling towers, and electric arc furnaces.

ACKNOWLEDGEMENTS

The preparation of this paper was supported by the EPA (IERL-RTP) Contract No. 68-02-2666. Special appreciation to Gerald L. Sing and Thomas E. Nelson of Teledyne Wah Chang Albany for their support and cooperation on this project.

REFERENCES

1. Oglesby, Sabert, et al., "A Manual of Electrostatic Precipitator Technology, Part I, Fundamentals," EPA report No. APTD 0610, NTIS No. PB 196 380, August 1970.

2. White, H. J., Industrial Electrostatic Precipitation, Pergamon Press, New York, 1963.

3. Crynack, R. R. and Penney, G. W.,"Charging of Fine Particles in Negative Corona Near Sparkover", Institute of Electrical and Electronics Engineers (IEEE) Transactions on Industry Applications, Vol. 1 A-10, No. 4, July - August 1974. pp. 524-531.

4. Ranz, W. E. and Wong, J. B., "Impaction of Dust and Smoke Particles on Surface and Body Collectors," Industrial Engineering and Chemistry, Vol. 44, No. 6, pp. 1371-1381, 1952.

5. Kraemer, H. F. and Johnstone, H. F., "Collection of Aerosol Particles in Presence of Electrostatic Fields," Industrial Engineering and Chemistry, Vol. 47, p. 2426, 1955.

6. Zebel, G., "Deposition of Aerosol Flowing Past a Cylindrical Fibre in a Uniform Electric Field," Journal of Colloid Science, Vol. 20, p. 522, 1965.

7. Strauss, W., Industrial Gas Cleaning, Pergamon Press, Sydney, Australia, 1974.

8. Calvert, S., et al., "APS Electrostatic Scrubber Evaluation," EPA-600/2-76-154a, NTIS No. PB 256-335, June 1976.

9. Hendricks, Charles D., Jr., "Charged Droplet Experiments," Journal of Colloid Science, Vol. 17, pp. 249-259, 1962.

10. Melcher, J. R., et al., "Charged Droplet Scrubbing of Submicron Particulate," EPA-650/2-74-075, NTIS No. PB 241-262, August 1974.

DROPLET REMOVAL EFFICIENCY AND SPECIFIC CARRYOVER FOR LIQUID ENTRAINMENT SEPARATORS

By:

Joseph H. Gavin
Dart Environment and Services Company
Avon, Ohio 44011

and

Frank W. Hoffman
Calfran Industries, Inc.
Springfield, Massachusetts 01101

ABSTRACT

In this paper we will describe a new and highly reliable technique for determining liquid carryover in a gas stream. In addition, we are presenting a blade rating factor for ease of comparing various style liquid entrainment separator blades.

For many years various forms of blade-type liquid entrainment separators have been in use. Construction has varied from an array of simple wooden slats to complex airfoil shapes formed from plastics and metals. Blade-type separators are used in numerous applications including pollution control scrubbers and cooling towers.

Until recently, carryover of these separators was judged by visual inspection and true performance characteristics were never really obtained. As environmental considerations became more demanding, attempts have been made to monitor carryover by means of sensitized paper, materials balance and isokinetic sampling. All are prone to error and none address themselves to actual blade performance characteristics.

Prior to the discussion and data presentations, some comments are in order. Calfran Industries and Fiberglass Equipment Division of Dart Environment and Services Company have been jointly studying liquid entrainment separators for over five years. In that time both experimental and currently marketed liquid entrainment separator modules from numerous manufacturers have been studied. Also we have established a reliable technique for determining carryover and obtaining liquid entrainment separator performance characteristics.

Before proceeding, a definition of terms to be used in subsequent discussions is necessary.

SEPARATOR MODULE - A device (blades, vanes, mesh, etc.) through which the gas containing entrained liquid droplets passes and which as a device separates the liquid from the gas stream.

SEPARATOR GEOMETRY - This takes into account blade shape, size and spacing. Throughout this discussion whenever the term "separator module" is used it fixes the separator geometry. A new geometry, such as a variation in spacing or different blade, would constitute a new liquid entrainment separator module.

INPUT DROPLET DISTRIBUTION - A percentage occurrence versus droplet diameter graph giving the entrained liquid droplet size distribution contained in the gas stream prior to passing through the liquid entrainment separator.

OUTPUT DROPLET DISTRIBUTION - A percentage occurence versus droplet diameter graph giving the entrained liquid droplet size distribution contained in the gas stream after passing through the liquid entrainment separator.

REMOVAL EFFICIENCY CURVE - This is a plot of percent of droplets passed (or removed) according to micron size. The percentage is defined as the ratio of the number of droplets passing (or removed) through the separator module over the number entering the separator module for a given size class by diameter. This graph can be referred to as either the percent passage (or removed) curve. Percent removal equals 100 minus percent passage.

In order to specify the performance of any liquid entrainment separator module, the ultimate goal is to obtain a removal efficiency curve for a given set of conditions.

FACE VELOCITY - This is the average speed which the gas and entrained liquid droplets enter the separator module. Face velocity is defined as the flow of air in volume per unit time divided by the cross sectional area of the opening in which the liquid entrainment separator module is placed.

LOADING - Is the measure of the amount of liquid entrained in the gas stream before encountering the separator module.

CARRYOVER - A measure of the amount of liquid entrained in the gas stream after passing through the separator module. The unit used in this discussion is grains per cubic foot.

RE-ENTRAINMENT - This term refers to liquid removed from the gas stream, accumulated on the liquid entrainment separator surfaces, and then re-entrained in the gas stream. It is considered part of the carryover.

The objectives of this discussion are two-fold. First, a detailed description of a technique to obtain a removal efficiency curve for a liquid entrainment separator is given. This is followed by the derivation and interpretation of a liquid entrainment separator module rating factor termed "specific carryover."

It is not a goal of this paper to present all of the results. The intent here is to describe and illustrate the fundamental principles and point out the areas of concern that experience and testing has shown to be of major importance. In keeping with this line of thinking, all reference to details of a particular liquid entrainment separator module have been deliberately left out.

The method for obtaining both the input and output droplet distribution is droplet photography. Actual techniques will be discussed later. Diameters of the droplets are measured directly from the projected negatives of these photographs (Figure 1). What is produced eventually is a chart of the number of droplets into the liquid entrainment separator module and the number of droplets passing through the separator module for a given statistical size class. The ratio of droplets out to droplets in is the passage ratio or percent passage. These numbers represent the removal efficiency for that particular size class. Using information gained in a similar manner for other size classes one can generate a removal efficiency curve. This curve is a plot of removal efficiency as a function of diameter. This may be done by plotting Percent Passage versus Droplet Diameter or Percent Removal versus Droplet Diamenter. While industry classically has spoken in terms of removal percent, it will be seen later in this discussion, percent passage is mathmatically convenient and more useful in analysis and computations.

In order to generate the data we constructed a test facility. A schematic representation of the laboratory test apparatus is shown in Figure 2. Figures 3 and 4 are photographs of the horizontal and vertical test units.

Air is drawn into the intake duct by use of a variable speed centrifugal blower. Total flow of air is monitored by an annubar and inclined manometer. This system allows adjustment of the face velocity across a given liquid entrainment separator module and compensation for variation in pressure drops from module to module. Pressure drop is monitored by means of piezometric rings built into the duct.

After the blower we have a droplet source. One or more nozzles introduce a controlled water spray, co-current, counter current or both. Fine droplet nozzles are used to produce carryover and coarse droplet nozzles add sufficient spray to achieve the desired loading.

A pair of viewing ports, allowing a clear optical path across the duct, are placed before and after the separator module compartment. The camera unit and source optics may be transferred from one pair of windows to the other.

The source optics, and ultra high speed strobe unit, are located opposite the camera. An automated 35 mm camera is used and is tied into a drive unit so photographs can be taken at predetermined intervals and variable distances across the duct. All the optics are located outside the duct so nothing protrudes inside to obstruct the airflow patterns. The camera system is capable of photographing droplets of one micron diameter and larger.

For most removal efficiency testing the procedures are as follows. A liquid entrainment separator module is installed and a pressure drop versus air velocity curve is obtained. A face velocity is then selected and monitored by the inclined manometer. The desired loading is attained by adjusting the water flow rate to the nozzles and monitoring the water drain quantity from the module. Loading and face velocity can be held constant to within 5%.

Once operating conditions have been set and allowed to stabilize, photographic scans through the input and output windows are made. The set of photographs before the blades are analyzed to yield the input distribution and the set of photographs after the mist elminator module are analyzed to yield the output distribution. A computer performs the necessary calculations to generate the removal efficiency curve. Data exists on effects of loading, face velocity, spacing, spray distribution, just to name a few. Data has been taken both in the laboratory and in the field under actual operating conditions. Results have been verified and the measurement has been proven accurate and reliable.

TYPICAL DATA - For a given liquid entrainment separator module the four basic sets of data for test purposes are illustrated in Figures 5, 6, 7, and 8. Figure 5 is an input distribution curve. Not that the specific nature of the input distribution is not critical. However the droplet size and volume must allow carryover in a quantity that can be measured and provide sufficient liquid at the separator module to allow for proper loading.

The output distribution is given in Figure 6. Discrete data points from the input-output data sets are entered into a computer. This program compares the corresponding size classes and then modifies these ratios by density values. Density values are obtained from the negative drop counts. Since the same camera is used for both input and output photographs, the sampling volumes are identical. The average droplet count per frame then becomes relative density.

A plot of the ratio of percent passage versus droplet diameter appears in Figure 7. Note the excellent agreement with a semilog plot. This agreement is evident in all work done on blade type liquid entrainment separators. Deviations at the small end of the droplet spectrum can occur if sufficient "fines" are not present to insure good statistical analysis. Variations at the large diameter end may be due to re-entrainment which, when it occurs, tends to produce coarse droplets.

To obtain Figure 8, the percent removal curve, one just graphs 100 minus percent passage. Of all the data then, Figure 7, the percent passage is the most significant. The reason is two-fold. One, it contains the basic removal data while, two, being in a convenient mathmatical form, i.e. a straight line.

Accuracy and interpretation of a given removal curve are of next concern. Some basic ground rules for comparison testing are in order. The first is, the efficiency curve is very sensitive to the geometry of the liquid entrainment separator. Small variations in spacing can significantly affect the removal efficiency. Velocity will also have an effect. It will be assumed blade geometry, velocity, etc. are held constant.

What must be considered, assuming a given operating condition, are specific, statistical, and sampling accuracy for the input and output distributions. Specific accuracy is the accuracy of measuring the diameter of any droplet. With proper magnification this can be held to better than 5%. Statistical accuracy is controlled by simply measuring sufficient numbers of drops in a given sample to achieve the desired accuracy. Remember there is no magic droplet count that is sufficient but the nature of the distribution determines the statistical accuracy.

Sampling accuracy refers to sample points in the duct itself used to obtain droplet diameters. This is by far the greatest source of error. Considerable time was spent to arrive at a sampling scheme. Attempting to locate a monitor point is difficult. Unless total uniform mixing can be achieved no single monitor point is acceptable. As gas speed changes the "droplet population" moves around. The nozzle fixes the population, but the varying air speeds redistribute the droplets. On the output side different liquid entrainment separators produce different spatial variations. By experimentation, we found the most accurate sampling plan is to scan continuously across the middle of the duct in a line perpendicular to the edges of a blade system. With appropriate sampling and maintenance of operating conditions, reproducibility can be held within 10%.

Interpretation of removal efficiency curves must be done after consideration of two facts. First, the total amount of liquid removed depends on the slope of the curve as well as the y-intercept. For example, one liquid entrainment separator may have a low percentage removal with a cut-off that is sharp. Another system may have a high percentage removal, but the diameter cut-off curve is gradual. Both may remove the same amount of liquid.

Equally critical is the input distribution when trying to assess total carryover. The liquid entrainment separator is a simple filter. What actually comes out in each case is dependent on the input distribution.

SPECIFIC CARRYOVER - Specific Carryover is an attempt to compare removal efficiency curves on a common basis. This is done by using an input droplet distribution which is uniform. Simply stated, that means there is one drop of every size present from zero diameter to an infinite diameter. Using a given removal efficiency curve the normalized volume of liquid passing through is computed. This value is termed "specific carryover". Now each separator has attached to it a rating number representing its efficiency seeing this uniform input droplet loading.

Before starting the derivation it is important to point out that there are two cases. Case I represents "total cut-off" which is when the projection of the Percent Passage curve for zero micron droplet diameter falls below 100%. The "partial cut-off" or Case II is when the extension of the Percent Passage line reaches 100% at some value for droplet diameter greater than zero microns. Both situations are illustrated in Figure 9. Consider first the case of total cut-off (Figure 10).

To begin the derivation one must assume moisture removal is exponential in nature. This is certainly reasonable, based on past experience, for blade systems.

We have found that the graph of Percent Passage versus Droplet Diameter is exponentially decaying and of the form:

$$Y=Ae^{-Bx} \quad (1)$$

Where Y is the percent passage and x is the diameter in microns. A and B are shape constants and are determined by actually testing the blades under a given set of conditions.

In Figure 11, the shaded portion represents those drops which "get through". The sum of their volumes represents the amount of entrained liquid that gets through the separator. The key here is that this quantity of liquid defined as specific carryover, is fixed in amount. Two quantities determine the carryover. They are the number of drops and the volume of liquid in each drop.

SPECIFIC CARRYOVER = SUM OF (NUMBER X VOLUME)

This can be expressed as: $SC = \int_0^V f(v)dv$ (2)

where:
SC = Specific Carryover
f(v) = Droplet Passage Function
dv = Droplet Volume

In terms of the diameter "x", the differential volume is:

$$dv = \frac{\pi}{2} x^2 dx \quad (3)$$

The droplet passage function is the curve in Figure 9:

$$f(v) = Ae^{-Bx} \quad (4)$$

Thus substituting into equation (2) one obtains:

$$SC = \frac{\pi A}{2} \int_{x=o}^{x=\infty} x^2 e^{-Bx} dx \quad (5)$$

$$= \frac{\pi An!}{2B^{(n+1)}} \quad (6)$$

The integer "n" in this case is 2 so the final solution is:

$$SC = \frac{A\pi}{B^3} \quad (7)$$

Because one would like to relate absolute volume the percent must be changed to a fraction by dividing by 100.

The final answer is then: $SPECIFIC\ CARRYOVER = \frac{A\pi}{100\ B^3}$ (8)

Where A and B are the coefficients in the percent passage curve in equation (1).

The units of the constant B are in reciprocal microns thus specific carryover is a volume in cubic microns. Specific carryover is a very sensitive function and for actual cases values range from less than 100 to over 100,000.

For Case II or partial cut-off (figure 12) the integration must be done in two steps. The first terms represents total passage up to a value X_c. The second term represents the exponential decay of percent passage.

$$SC = \frac{\pi}{2} \int_0^{x_c} (1)x^2 dx + \frac{A\pi}{2} \int_{x_c}^{\infty} e^{-Bx} x^2 dx \quad (9)$$

Integrating,

$$SC = \frac{A\pi}{2} e^{-Bx_c}\left(\frac{x_c^2}{B} + \frac{2x_c}{B^2} + \frac{2}{B^3}\right) + \frac{\pi}{6}X_c^3 \quad (10)$$

Note that if x_c goes to zero this value for SC reduces to that found in Case I.

GENERAL APPLICABILITY - Removal Efficiency curves and Specific Carryover are very useful in practical evaluation of liquid entrainment separators provided they are applied properly and interpreted correctly.

The prime use of specific carryover is to compare various blade systems. The independent variable may be spacing, gas velocity, or even basic blade design. Specific carryover becomes the dependent variable. It is much easier to graph specific carryover as a function of blade spacing than it is to plot a family of curves whose y-intercept as well as slope vary greatly.

Actual carryover in grains per cubic foot can be calculated from the removal efficiency curve. What is essential is the nature and amount of the input entrainment. For the same liquid entrainment separator, the actual amount of carryover is predominately determined by the input distribution. Given this distribution and a removal efficiency curve for the operating conditions carryover in the system can easily and accurately be calculated.

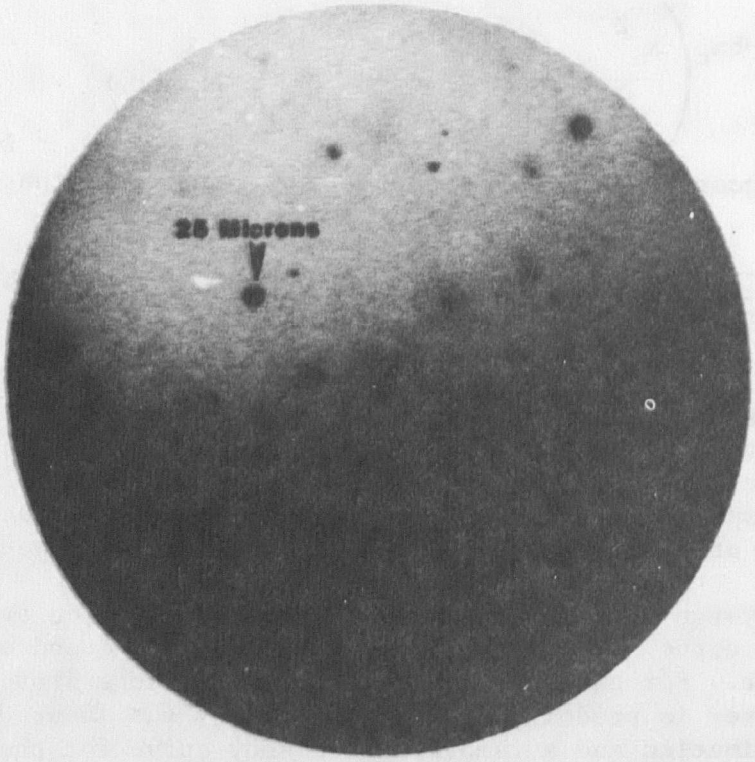

FIGURE 1

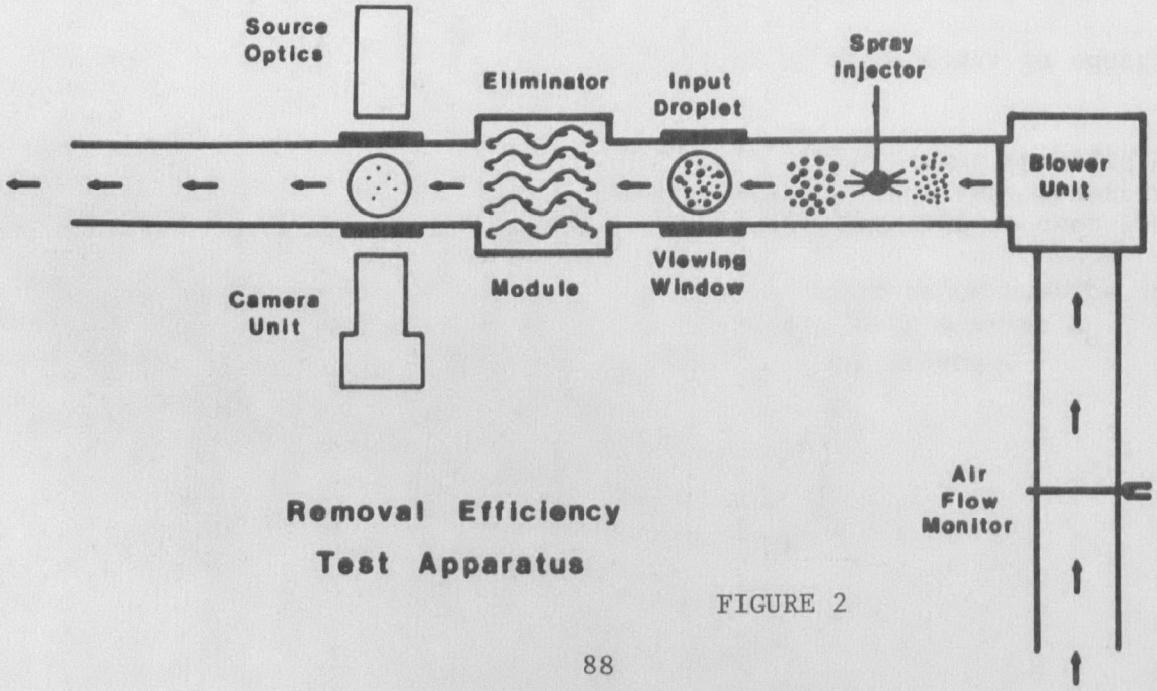

FIGURE 2

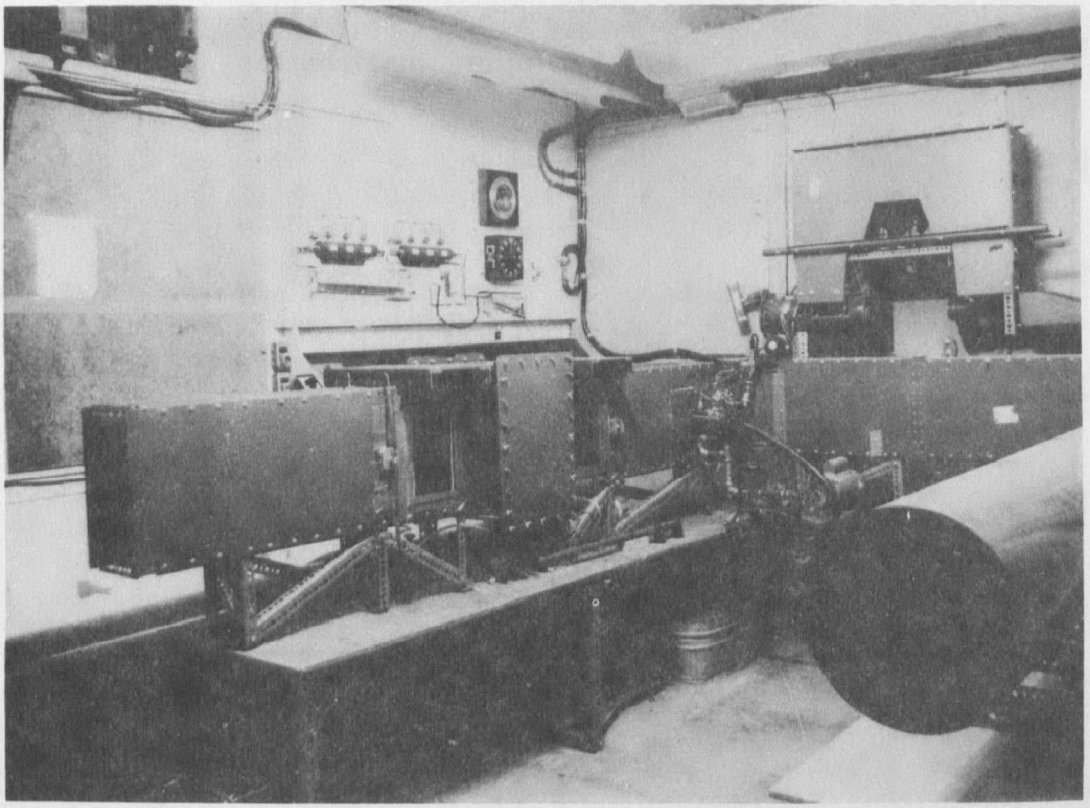

FIGURE 3

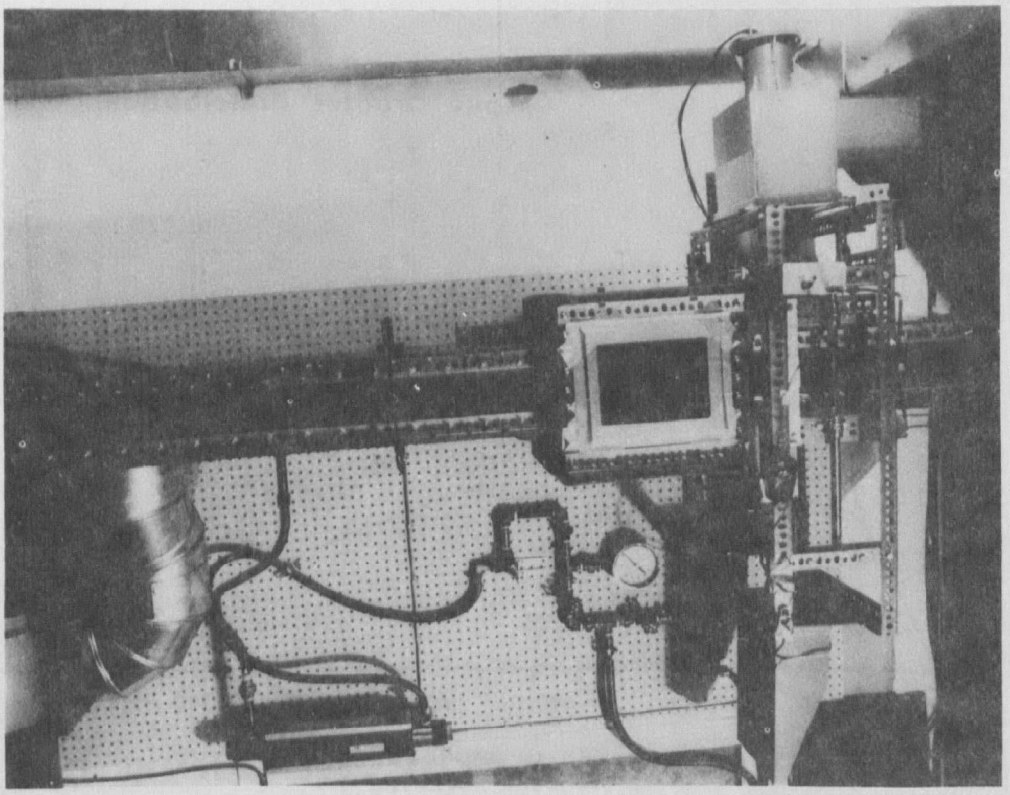

FIGURE 4

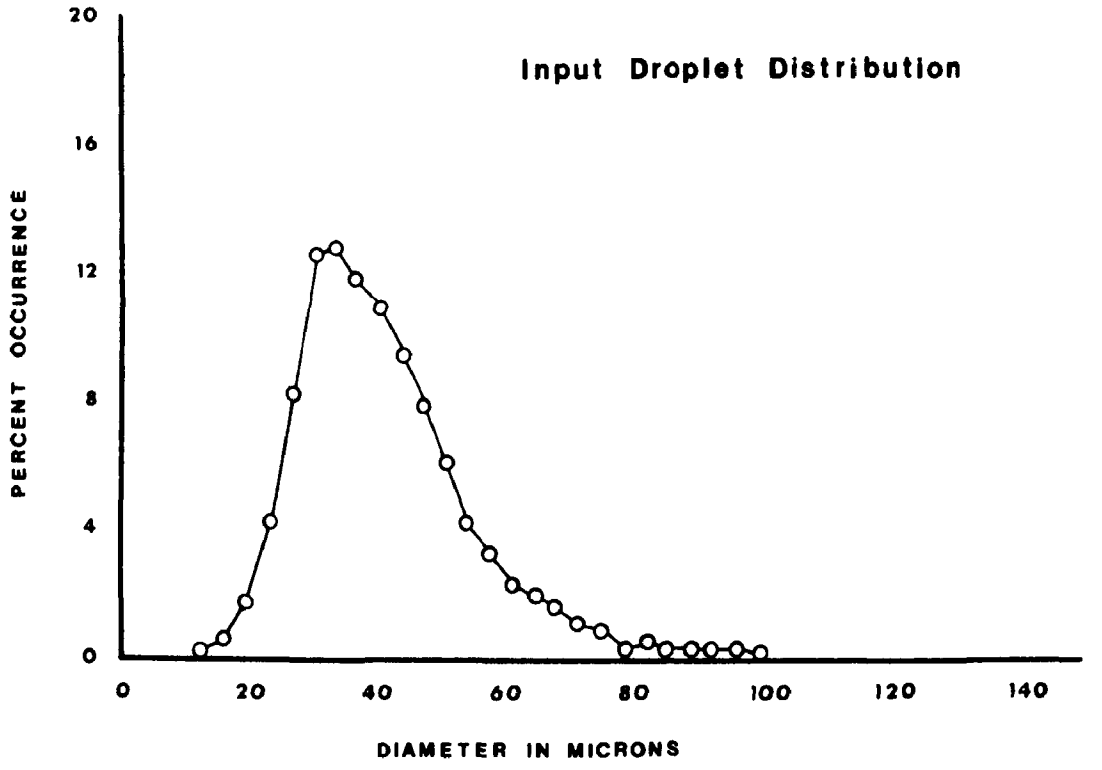

FIGURE 5

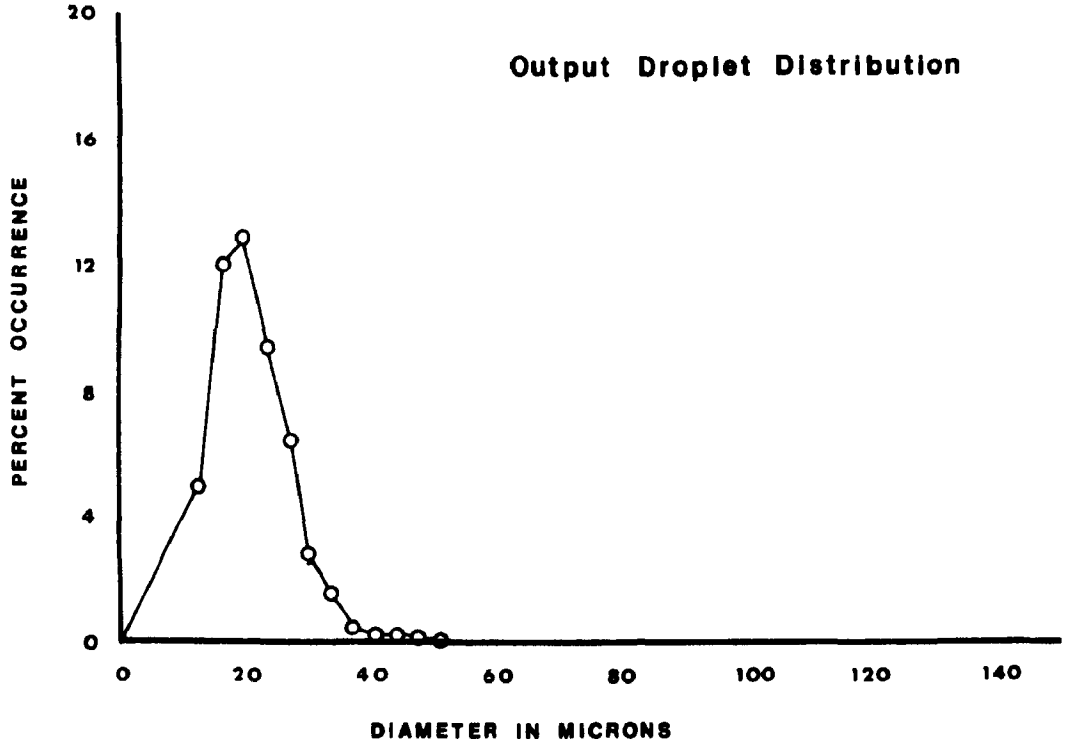

FIGURE 6

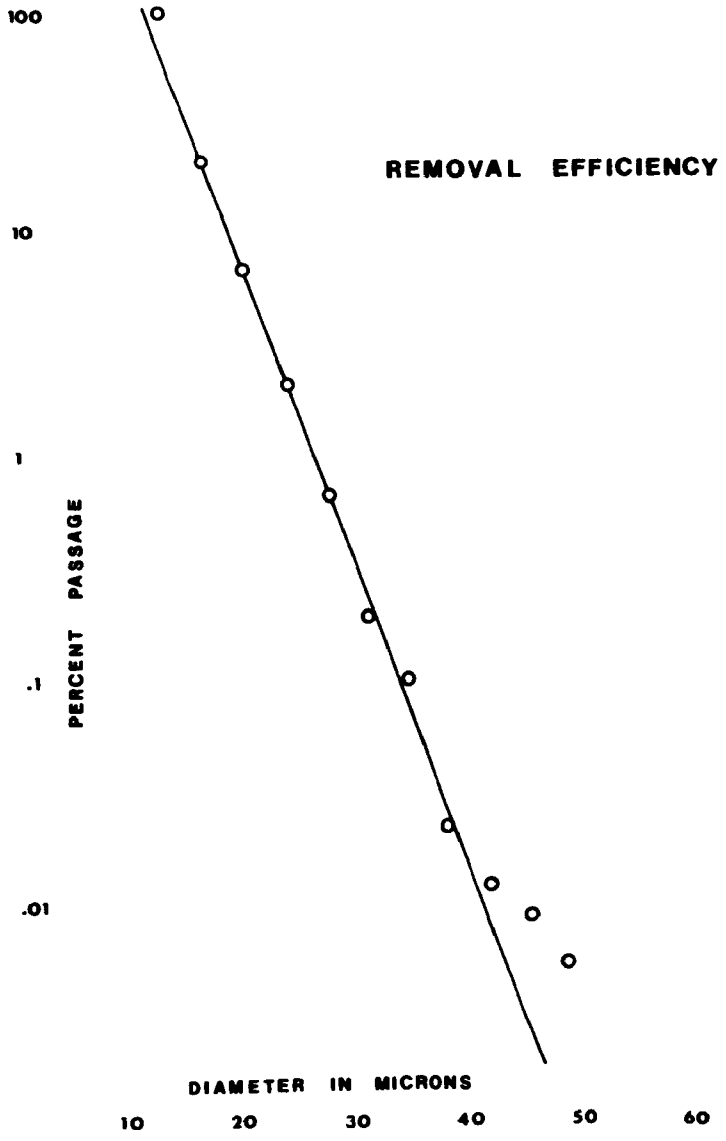

FIGURE 7

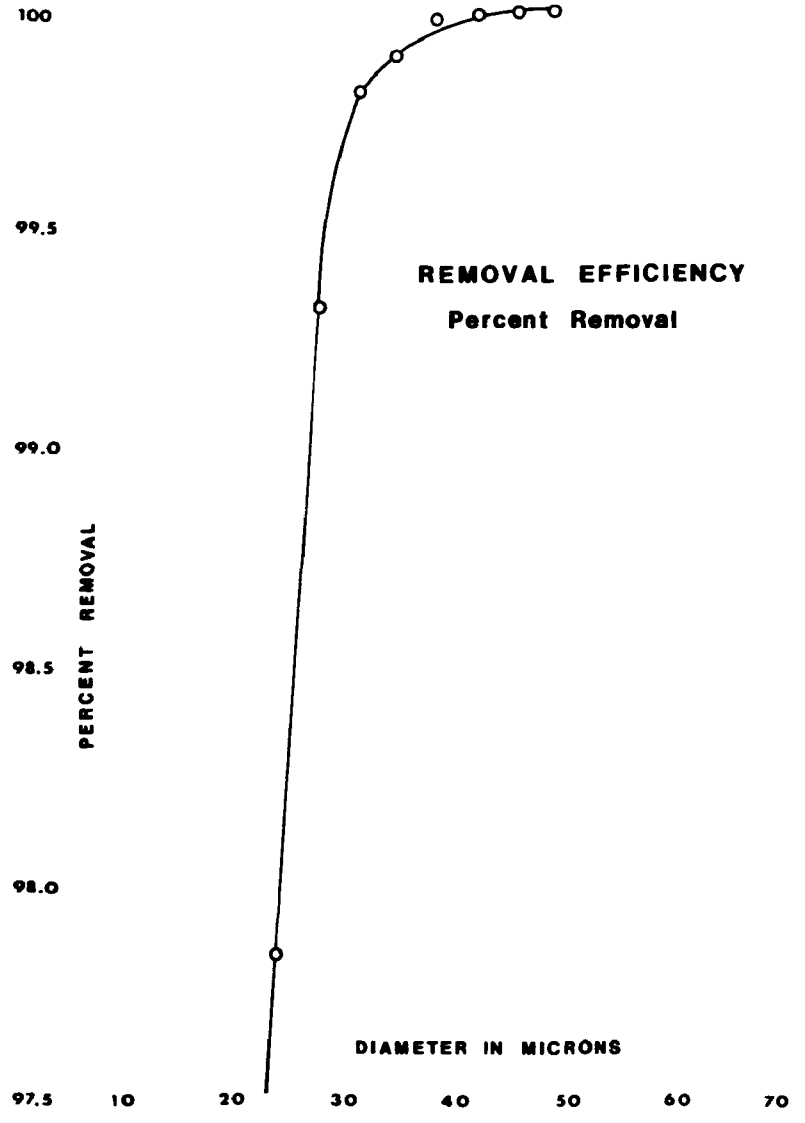

FIGURE 8

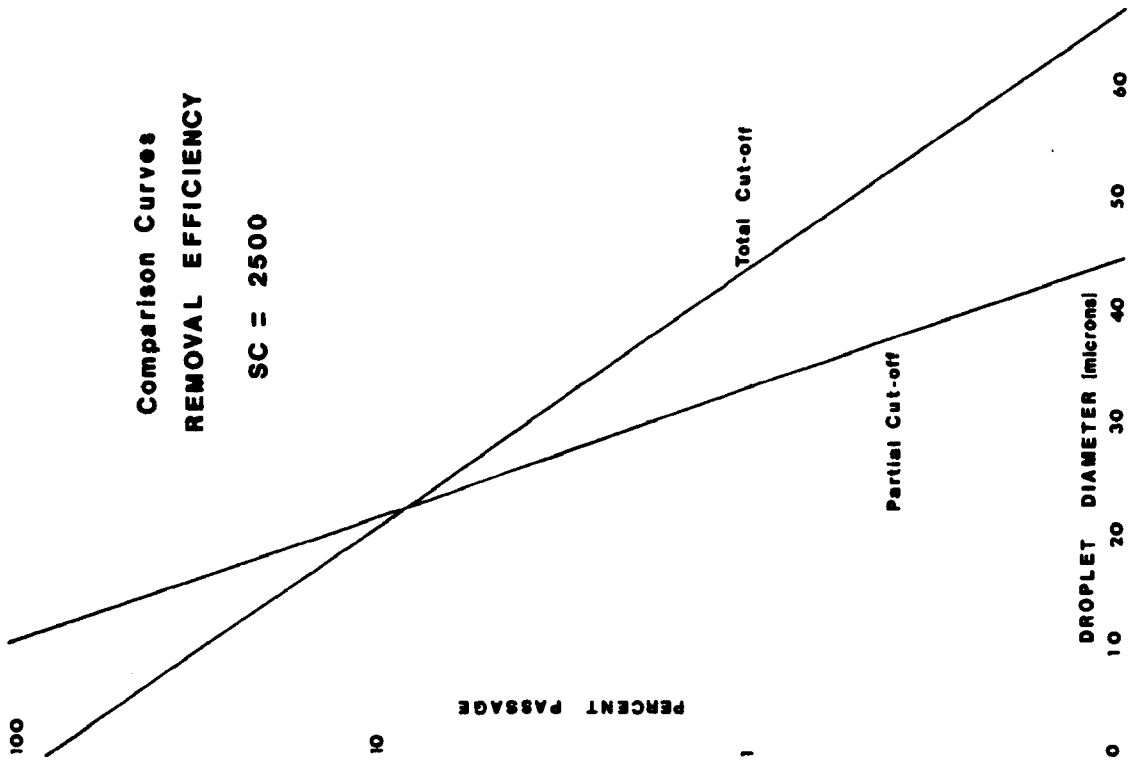

FIGURE 9

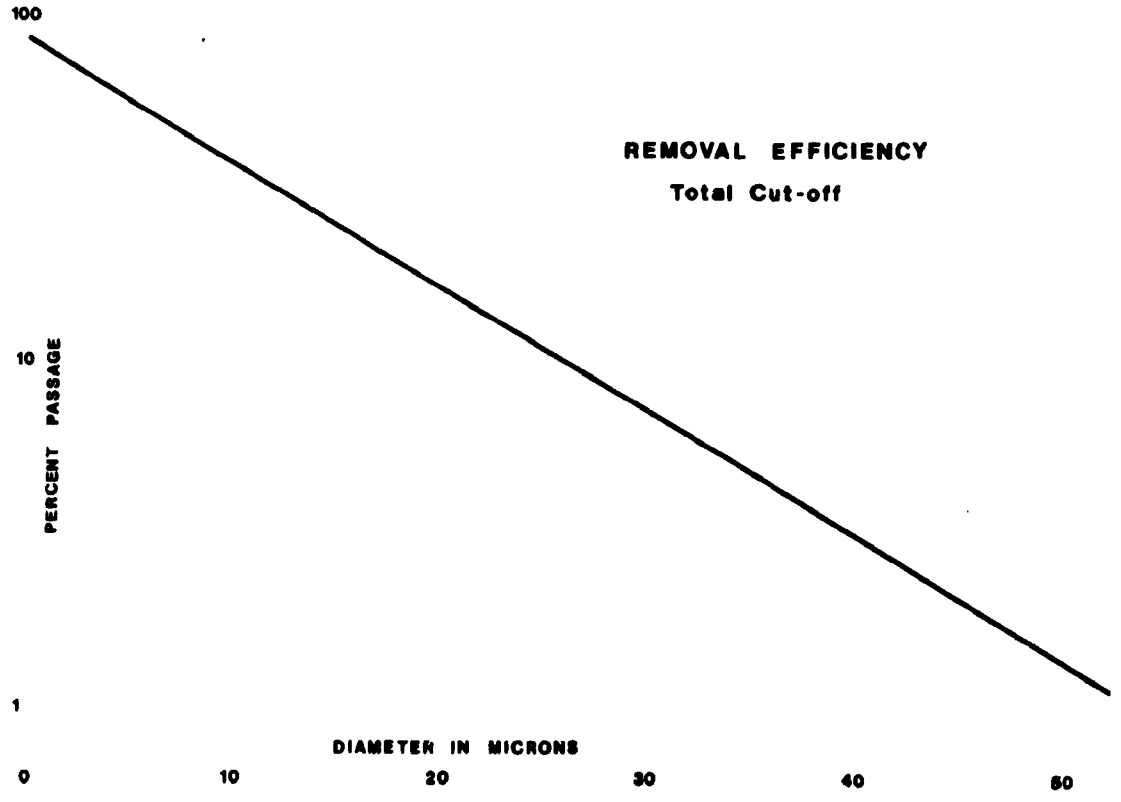

FIGURE 10

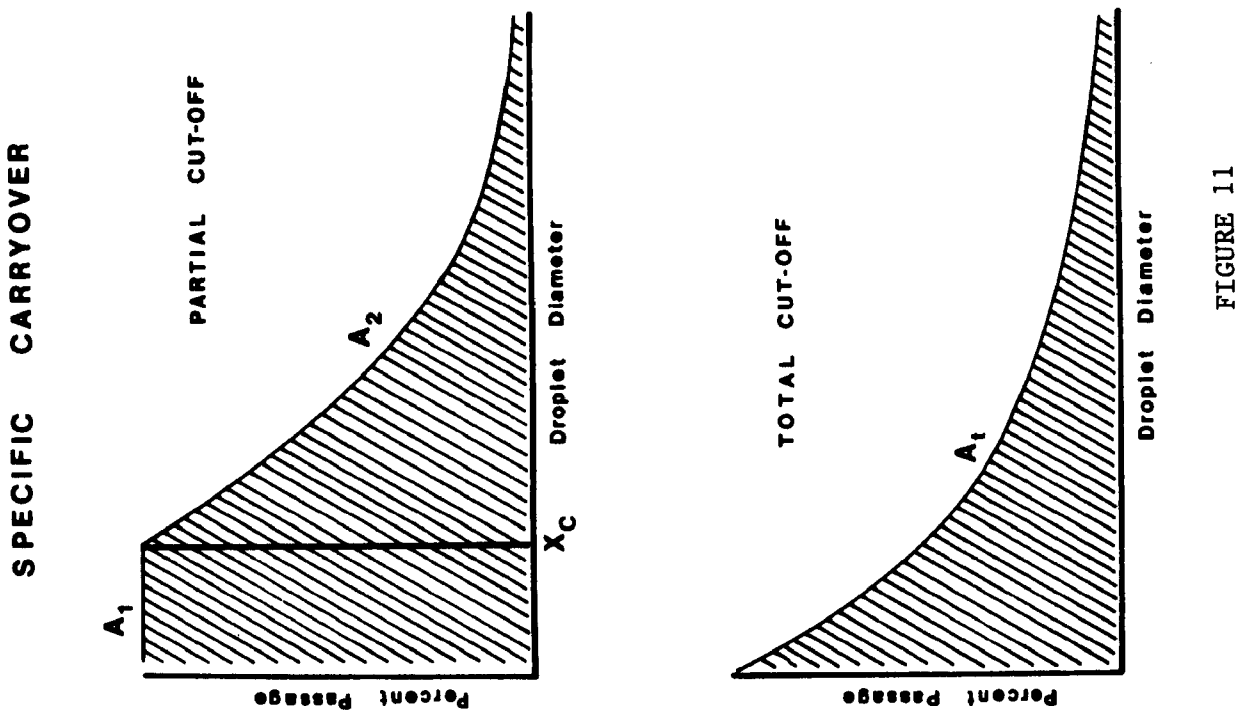

FIGURE 11

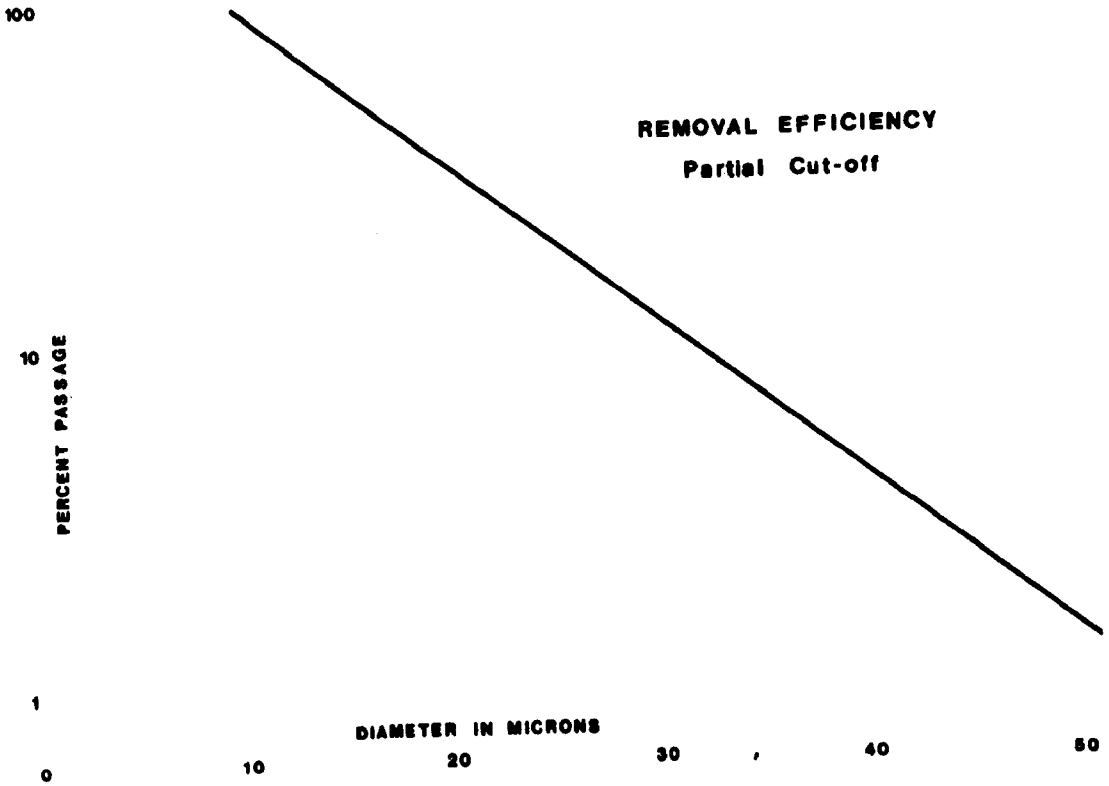

FIGURE 12

AN EVALUATION OF GRID ROD FAILURE IN A MOBILE BED SCRUBBER

By

John S. Kinsey
AeroVironment Inc.
Pasadena, California 91107

Steve Rohde
Public Service Company of Colorado
Brush, Colorado 80723

Presented at the

Second Symposium on the Transfer & Utilization of
Particulate Control Technology
July 23-27, 1979, Denver, Colorado

ABSTRACT

The body of information presented in this paper is directed to those engineers and maintenance personnel involved in the operation of mobile bed scrubbers. Materials tests were performed on three specimens of austenitic stainless steel in order to determine the possible causes of grid rod failure in a mobile bed scrubber controlling particulate emissions from a pulverized coal fired steam electric generating station. These three specimens were successively placed in an Instron universal testing machine and loaded in tension until rupture occurred. The results of these tests, in addition to other supporting data, were used in an attempt to determine the cause of the grid rod failure during actual scrubber operation. It was determined that the grade of stainless steel used, the scrubber water quality, and certain operational problems could be causes of premature failure.

AN EVALUATION OF GRID ROD FAILURE IN A MOBILE BED SCRUBBER

Standard practice for removing flyash from the fluegas of large coal-fired power plants has traditionally been by mechanical separation and/or electrostatic precipitation with fabric filtration becoming increasingly more popular. Wet scrubbers have also been used however, depending on the required application. Public Service Company of Colorado, at its Arapahoe Generating Station's Unit No. 4, has employed such a scrubber downstream of the original electrostatic precipitator for the purpose of meeting the applicable particulate emission standards promulgated by the State of Colorado. This particular scrubber, manufactured by the Universal Oil Products Company, utilizes the mobile bed concept to remove flyash from the fluegas stream prior to discharge. Figure 1 is a schematic drawing of the TCA (Turbulent Contact Absorber) scrubber installed on Unit No. 4.

Since its installation in 1973, this unit has had a history of reoccurring maintenance problems, some of which are as follows:

- Partial pluggage of presaturator sections
- Ball migration and grid failure
- Droplet carryover from the demister section
- Reheater pluggage
- Corrosion of outlet ductwork
- Inoperative guillotine isolation dampers

One of these problems, that of grid failure, will be discussed in this paper.

An experiment was conducted by the authors to compare certain physical and mechanical properties of three specimens of austenitic stainless steel rods both with each other and published values to determine possible causes of premature grid rod failure. Specimens of both exposed and unexposed stainless steel were tested, using the procedure outlined below.

DESCRIPTION OF SCRUBBER OPERATION

Fluegas from the electrostatic precipitator is pulled through the scrubber booster fan and discharged into the presaturator section. Here, moisture is introduced into the fluegas to cool the gas stream and allow for a smoother gas/liquid interface. From the presaturator, the fluegas flows into three scrubbing sections in series containing polyethylene balls. Each of these sections are separated by a grid of 3/8" diameter stainless steel rods. By the turbulent action generated by the fluegas flow, the random motion of the polyethylene balls, and a countercurrent flow of H_2O from the spray nozzles, flyash is scrubbed from the gas stream. The gas then flows to a chevron-type demister, where entrained water droplets are removed. Thereafter reheat potential is added to the fluegas by steam fed heat exchangers and directed toward the stack.

The scrubbing action described above is quite dependent on a number of factors. One of the most important of which is keeping the balls in their respective section and not "migrating" to other sections. This migration is caused by the grid rods failing and, thus,

allowing sufficient space for the balls to work through from one scrubbing section to another. If enough of this migration takes place, the following operational difficulties can occur:

- o Channeling of gas flow, hence affecting contact area versus flow.
- o Increased or decreased pressure differential across affected scrubber beds.
- o Increased ball breakage and subsequent plugging of the reheater sections or recirculation pump screens.
- o Combinations of the above.

EXPERIMENTAL

Three specimens of austenitic stainless steel were marked, using the following designation:

Specimen No. 1 - 316 stainless steel never exposed to environmental conditions inside a scrubber

Specimen No. 2 - 316 stainless steel in service inside the scrubber for approximately a six week period prior to replacement

Specimen No. 3 - 317 stainless steel never exposed to environmental conditions inside a scrubber

These three specimens were successively placed in an Instron universal mechanical testing machine, and an extensometer mounted on each specimen. The specimens were then loaded in tension until rupture occurred. A plot of load versus strain was made, using a strip chart recorder. In addition, certain other information on the chemical composition of the specimens was obtained by the authors for subsequent analysis.

The data extracted from the strip chart recordings for load versus strain for each specimen is presented in Table 1. The axial stress was calculated for each load recorded and results of these calculations are also presented in Table 1. A plot of stress versus strain, up to and including rupture, is presented in Figure 2 for Specimens 1 and 3, respectively. A similar graph for Specimen 2 was not prepared, due to the fact that rupture was premature.

The Modulus of Elasticity was determined for each specimen using a linear regression analysis of the data presented in Table 1. Results of this analysis is presented in Table 2. In addition, the tensile strength was also determined and presented in Table 2.

A chemical analysis of the 316 stainless steel used in this experiment was conducted by an independent metallurgical laboratory.[4] The results of that analysis is presented in Table 3. In addition, it was also determined that the scrubber water contains a fairly substantial concentration of chlorides and relatively low pH. Chemical analysis shows a level of 460 mg/l of chloride (as NaCl) in the water and a pH $\approx$ 2.0. The significance of this information will be discussed later.

RESULTS

The results of the calculations described above were analyzed for their significance related to the problem at hand. The published values for Modulus of Eleasticity and tensile strength for AISI (American Iron and Steel Institute) type 316 and 317 stainless steel were included in Table 2 for comparison purposes.[2] As can be seen, the Modulus of Elasticity determined from experimental data for each specimen is considerably lower than the applicable published value. In addition, it was also noted that both the tensile strength and the yield strength for all these specimens far exceeded the standard value. It should also be noted that the tensile strength of Specimen 2, which was exposed to the environment inside the scrubber, is quite a bit less than that of Specimen 1, which has never been exposed to those conditions.

The chemical analysis data obtained, along with the AISI Standard Classification Ranges, are presented in Table 3.[4] As can be seen, the chemical composition of all the specimens does conform to AISI Classification. It should be noted, however, that Specimens 1 and 2 are at the low end of the range for chromium, nickel, and molybdenum.

Upon additional research, it was discovered that cold working significantly increases both the tensile strength and yield strength of stainless steel.[2,3] Using published curves of percent cold work versus yield and tensile strength, it was determined that Specimen #1 has been cold worked approximately 15%, and Specimen #3 has been cold worked 12-18%.[2] This fact is also supported by other reference data, which gives values for certain mechanical properties of cold drawn Chromium-Nickel stainless steel wire.[2]

A careful inspection of each specimen was made prior to testing. Specimen #2 was found to have a wear pattern with alternate high and low areas. This type of wear could be caused by:

- Crevice-type pitting due to flyash buildup.[3,5]
- Simple abrasion due to friction caused by the polyethylene balls and associated flyash being forced against the bars and grinding down the metal.
- Combinations of the above.

EXPERIMENTAL ERRORS

The following experimental errors must be taken into account when evaluating the data mentioned above:

1. Only one sample of each specimen of stainless steel was tested. Duplicate samples, or even tripicate samples, are necessary to increase both accuracy and reproducibility of the data.

2. Specimen #2 ruptured prematurely at a section in the center of the specimen which appeared to have been severely affected by crevice-type corrosion. This section of rod was located at a structural member inside the scrubber. The data for this specimen is, therefore, somewhat questionable even in the elastic range.

DISCUSSION

According to one author,[1] austenitic stainless steels are not, as a general rule, highly resistant to hot sulphurous gases as would be found in a scrubber. It was also learned, however, that the addition of sufficient amounts of molybdenum gives the required

resistance to reducing environments of sulfurous acid.[3] In addition, when hot, wet SO_2 gases and quantities of H_2SO_4 are present, as found in a scrubber application, the addition of copper to the stainless steel may also be necessary.[3,6] It is also recommended that cold and hot working, including welding, should be limited to minor operations to keep the steel below a Rockwell Hardness B 96[3] in order to limit "sensitizing" the metal and causing intergranular corrosion.[6]

Also reported in the literature is that stress-corrosion cracking can occur in both 316 and 317 stainless steel when exposed to a combination of sulfurous acid and >100 ppm of metal chlorides.[3,5] As was stated above, the concentration of NaCl exceeds the 100 ppm criteria by a factor of 4.6.

CONCLUSIONS

From the information presented above, it was concluded that the following factors contribute to premature grid rod failure at Arapahoe Unit 4:

Grade of Stainless Steel. All of the specimens tested have been cold-worked or cold drawn in the range of 15%. This coupled with the low molybdenum content can significantly reduce resistance to the conditions such as found in a scrubber. The addition of a small percentage of copper to the 317 stainless steel alloy is likely to increase the service life of the rods.

Scrubber Water Quality. As the chloride (as NaCl) content of the scrubber water exceeds 100 ppm, stress-corrosion cracking of the grid rods can occur. This creates a more severe corrosion problem than would be normally present with the low pH compounding the problem.

Operational Problems. All specimens exhibit the same basic wear pattern due to a number of possible causes. If the polyethylene balls are being forced up against the grid bars on a continual basis, a problem may exist with the fluid mechanics of the fluegas flow through the scrubber.

ACKNOWLEDGEMENTS

We would like to acknowledge Mr. A.C. Bishard of the Colorado Department of Health and Dr. Robert Pearson of the Public Service Company of Colorado for their cooperation in the formulation of this paper.

REFERENCES

[1] Baumeister, Theodore, Mechanical Engineers Handbook, Sixth Edition, 1958.

[2] Mechanical and Physical Properties of Austenitic Chromium - Nickel Stainless Steel at Ambient Temperatures, International Nickle Company, 1973.

[3] Metals Handbook, American Society for Metals, Eighth Edition, Volume 1, July 1967.

[4] Test Data, Public Service Company of Colorado, December 1977.

[5] Javetski, John, "Solving Corrosion Problems in Air Pollution Control Equipment - Part I," Power, 72-77, May, 1978.

[6] Corrosion Resistance of Austenitic Chromium-Nickel Stainless Steel in Chemical Environments, International Nickel Company, 1963.

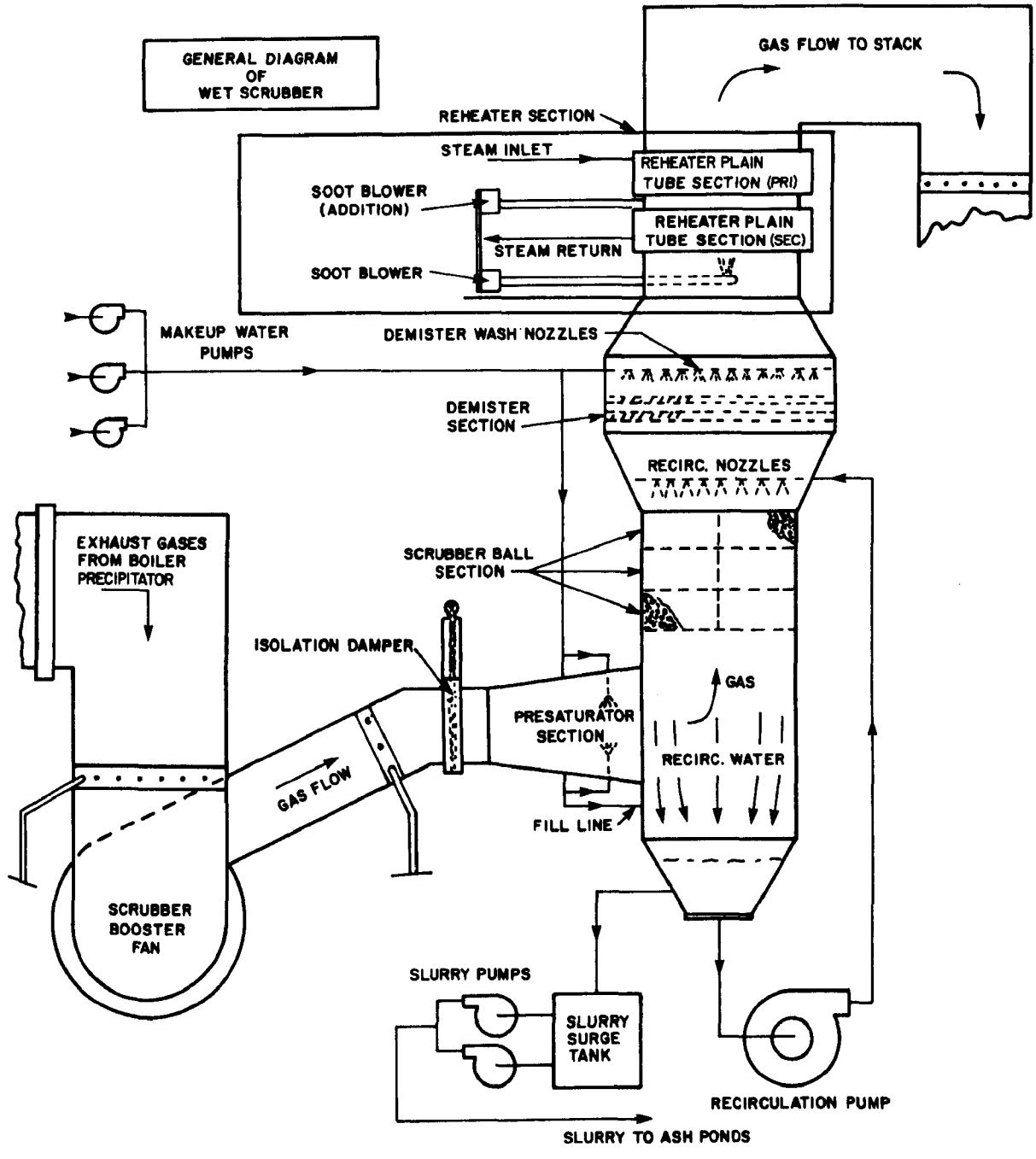

Figure 1: SCHEMATIC OF TCA SCRUBBER INSTALLED AT ARAPAHOE UNIT NO. 4.

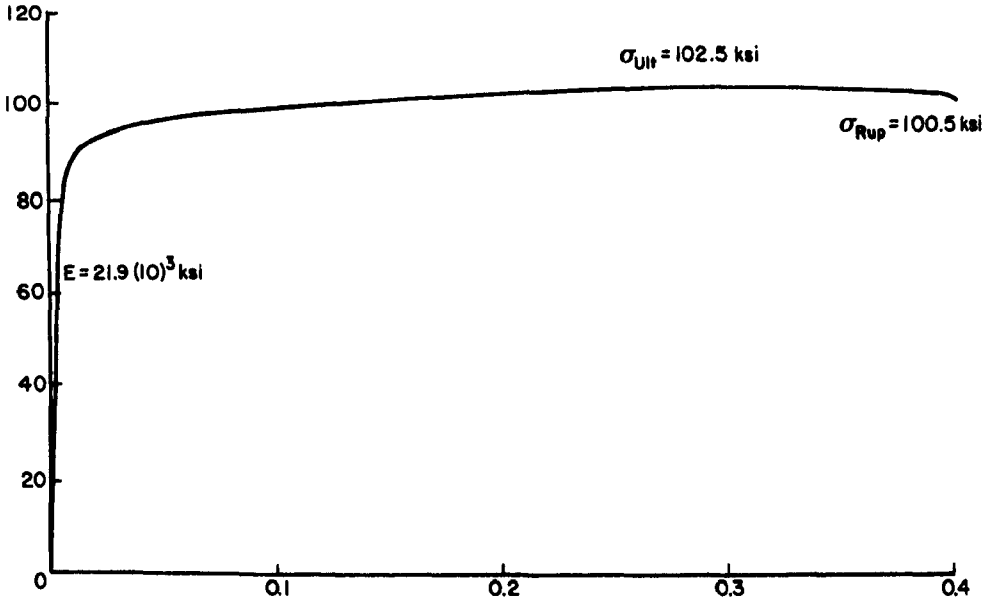

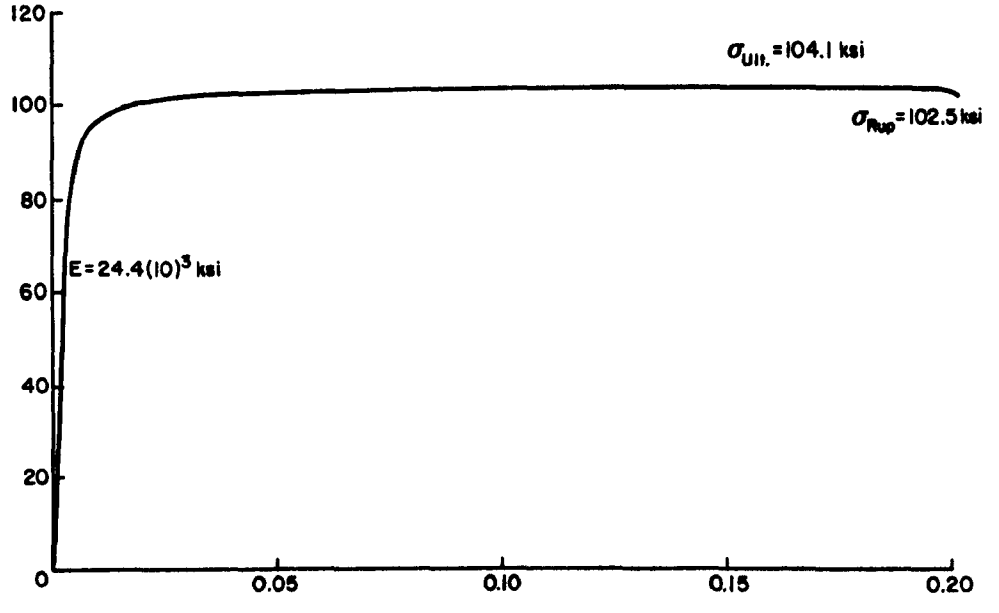

Figure 2: STRESS VS. STRAIN CURVES FOR SPECIMENS 1 AND 3.

Table No. 1: RAW DATA - SPECIMENS 1, 2, AND 3

Specimen No. 1 - 316 Stainless Steel - Low Grade - Unexposed			Specimen No. 2 - 316 Stainless Steel - Low Grade - Exposed			Specimen No. 3 - 317 Stainless Steel - 3.75% Moly-Unexposed		
Load (kips)	Stress (ksi)	Strain (inch/inch)	Load (kips)	Stress (ksi)	Strain (inch/inch)	Load (kips)	Stress (ksi)	Strain (inch/inch)
1.00	9.05	0.000165	1.00	9.05	0.000395	1.00	9.05	0.000132
2.00	18.11	0.00059	2.00	18.11	0.00079	2.00	18.11	0.00043
3.00	27.16	0.00099	3.00	27.16	0.00112	3.00	27.16	0.00086
4.00	36.22	0.00142	4.00	36.22	0.00145	4.00	36.22	0.00122
5.00	45.27	0.00182	5.00	45.27	0.00182	5.00	45.27	0.00155
6.00	54.32	0.00224	6.00	54.32	0.00224	6.00	54.32	0.00198
7.00	63.38	0.00287	7.00	63.38	0.00274	7.00	63.38	0.00251
7.58	68.63	0.00330	8.00	72.43	0.00369	8.40	76.05	0.00330
9.20	83.30	0.0066	9.00	81.49	0.00743	10.00	90.54	0.00548
10.00	90.54	0.01485	9.40	85.11	0.0132	10.36	93.80	0.00660
10.06	91.08	0.01650	9.60	86.92	0.0198	10.96	99.23	0.01320
10.22	92.53	0.0231	9.68	87.64	0.0264	11.20	101.41	0.0264
10.36	93.80	0.0297	9.70	87.83	0.0294	11.28	102.13	0.0396
10.46	94.71	0.0396				11.34	102.67	0.0528
10.60	95.97	0.0528				11.40	103.22	0.0660
10.78	97.60	0.0792				11.44	103.58	0.0792
10.80	97.78	0.0825				11.46	103.76	0.0990
10.94	99.05	0.1155				11.50	104.12	0.1650
11.08	100.32	0.1485				11.46	103.76	0.1980
11.20	101.41	0.1980				11.32	102.49	0.2086
11.32	102.49	0.2640						
11.32	102.49	0.3300						
11.22	101.59	0.396						
11.10	100.50	0.4158						

Table No. 2: COMPARISON OF EXPERIMENTAL RESULTS WITH PUBLISHED VALUES

Mechanical Property	Specimen No. 1	Specimen No. 2	Published Value for 316 Stainless Steel	Specimen No. 3	Published Value for 317 Stainless Steel
Modulus of Elasticity	$21.9(10)^3$ksi	$25.0(10^3)$ksi	$28(10)^3$ksi	$24.4(10)^3$ksi	$28(10)^3$ksi
Tensile Strength	102.5 ksi	87.8 ksi	80 ksi	104.1 ksi	85 ksi

Table No. 3: ACTUAL VS. PUBLISHED CHEMICAL COMPOSITIONS

Chemical Element	Specimen No. 1 & 2	**AISI Standard Classification Range	Specimen No. 3	**AISI Standard Classification Range
Chromium	16.18%	16-18%	*	18-20%
Nickel	10.10%	10-14%	*	11-15%
Molybdenum	2.08%	2-3%	3.75%	3-4%

*No Data Available
**Am. Iron and Steel Institute

OPERATION AND MAINTENANCE OF A PARTICULATE SCRUBBER SYSTEM'S ANCILLARY COMPONENTS

By:

P. A. Czuchra
FMC Corporation
Itasca, Illinois 60143

ABSTRACT

The proper functioning of a scrubber system is largely dependent on the operating condition of its ancillary equipment. In this paper the author discusses the common problems incurred with ancillary equipment and steps which can be taken during the design and operation of this equipment to minimize maintenance problems. The equipment discussed includes such items as fans, pumps, clarifiers, drag chain tanks, rotary vacuum filters, motors, agitators, ductwork, dampers, piping, valves, recirculation tanks, instruments and motor starters. Maintenance schedules for the various pieces of equipment are reviewed and possible solutions to such problems as corrosion, abrasion and pluggage are discussed.

OPERATION AND MAINTENANCE OF A PARTICULATE SCRUBBER SYSTEM'S ANCILLARY COMPONENTS

SECTION I. INTRODUCTION

A great deal of the operating problems associated with a particulate scrubbing system are due to the scrubber's auxiliary equipment. The auxiliary equipment includes everything it takes to make a scrubber system operate such as pumps, fans, clarifiers, vacuum filters, motors, agitators, ducts, dampers, piping, valves, recirculation tank, instruments, and motor starters. This paper will attempt to provide some basic guidelines for the maintenance of these items, and some suggestions for the correction of the more common failings of these pieces of equipment. It should be noted that this paper will serve only as a general guideline and is not intended to replace the maintenance manual of a specific vendor's piece of equipment.

As in any air pollution control system, a scrubber system is subjected to a harsh environment. The abrasiveness of some types of particulate causes equipment such as fan wheels and valves to wear away. Stack gases may also contain a variety of components that, when wetted, produce compounds which corrode equipment. This is true of any gas stream from a boiler which fires sulfur bearing fuel and of gases from many chemical processes. All scrubber components must be designed and maintained with these considerations in mind.

An important part of any maintenance program is developing a workable maintenance file. This should consist of all the individual maintenance manuals of every piece of equipment used in the system, the associated parts identification drawings, and a complete and concise maintenance schedule for all components. A record of all maintenance done on the system should also be included in the file. A common problem in setting up such a file is that most vendors supply only one type of literature with their equipment. This is a combined installation, operation and maintenance manual. The section on operation and maintenance is usually quite small in comparison to the installation section. After the installation of the system is completed this manual is often misplaced or forgotten about. If this occurs, a new manual should be ordered from the vendor as soon as possible. In order to keep the maintenance file simple and workable, it is suggested that only those pages relating to the operation and maintenance of the specific components be included in the file. All pages relating to the installation of the equipment should be kept in a separate file.

SECTION II. ROTATING MACHINERY

A. General

Rotating machinery consists of all items such as fans, pumps, clarifiers, rotary vacuum filters, motors and agitators. Because these items are in constant motion, a great deal of wear can take place. These components require some amount of regular attention to assure the proper operation of the system. Key areas of maintenance on rotating machinery are the bearings and any components rotating in the fluid stream.

There are also many other areas of maintenance unique to each type of equipment. Wherever practical, spares should be included. This is especially true for high maintenance items such as pumps. Wear resulting from any abrasive solids in the liquid stream often dictates frequent inspection and repair. When mounted before the scrubber, fan wheels may also exhibit a great deal of abrasion from the particulate in the gas stream. Unfortunately, however, it is rather impractical to utilize spare fans in a scrubber system due to the difficulties in duct arrangements and the high capital cost of fans.

A stock of the more failure-prone components should be maintained. These include such items as bearings, seals, bushings, pump housing liners (if pumps with replaceable liners are used), pump impellers, gaskets, make-up water control valves, pH control valves, pH probes, recirculation tank level control sensors, and vacuum filter cloths.

B. Fans

As in all rotating machinery, various components of the fan must be periodically lubricated. These components include all bearings on the wheel shaft, couplings and dampers. Lubrication schedules and types of lubricants should follow the equipment manufacturer's guidelines. Generally the lubrication schedule for these items ranges from quarterly to annually. The frequency of inspection of wear-prone components of the fan will vary with the severity of the application. On a fan handling relatively clean gas, the wheel and housing may go for up to one year without any need of inspection. Fans on dirty applications may require monthly or even weekly inspection. The fan wheel and housing should be inspected for signs of corrosion, abrasion and particulate buildup. If the fan is located upstream of the scrubber and the gas temperature is above 250°F, corrosion is generally not a problem. However, if the fan is downstream of the scrubber, and the gas contains any corrosive compounds, or if the fan is before the scrubber and the gas temperature is below the dew point of any corrosive components in the gas, corrosion will be a maintenance consideration. If the fan is downstream of the scrubber, moving the fan upstream of the scrubber may eliminate the problem of corrosion if the gas temperature is high enough. Should rearranging the fan not be feasible, the fan will have to incorporate more corrosion-resistant materials of construction. This requires going to a higher alloy on the fan wheel and possibly installing a corrosion-resistant liner on the housing. Attempting to reduce corrosion by collecting the corrosive gas in the scrubber system will generally not work. This is due to the fact that any condensation on the fan wheel will tend to pick up any residual corrosive gas which gets through the scrubber system. This corrosive component when collected by the condensation will eventually react with the fan materials no matter how small its concentration is.

Abrasion on the fan may be lessened by the installation of replaceable wear liners on the wheel. Replacing the existing fan with a larger fan capable of the same CFM and static pressure but at a lower RPM may help to reduce the abrasion problem. If the fan is located before the scrubber, the installation of a high-efficiency mechanical collector before the fan may help to reduce any abrasion problems. Should a mechanical collector already be installed prior to the fan, the mechanical collector's tubes should be checked for pluggage or excessive wear. Should the existing mechanical collector be found to be

working properly, consideration may be given to replacing it with a higher efficiency mechanical collector or going to a two-staye mechanical collector.

Material buildup on the fan wheel may require a spray wash system to be installed in the fan. If this fails to improve the situation enough, moving the fan upstream of the scrubber may alleviate the problem.

Fan bearings should be inspected every eight hours for oil level, oil color, oil temperature and vibration. Bearings found to be inadequately lubricated may require a greater frequency of lubrication or the installation of a forced lubrication system. The bearing housing should be inspected weekly for leaks, cracks and loose fittings. Excessive bearing wear may be caused by a higher fan operating temperature than was originally specified, or by excessive vibration due to material buildup on the fan wheel. Misalignment of the bearing mountings could also account for this problem. A major annual inspection should be made to check all bearing clearances and to detect any sign of wear, pitting or scoring on the bearings.

Dampers should be inspected semiannually for wear, corrosion, cracking or looseness. All stuffing boxes should also be inspected. Annual damper inspection should include the tightening of all fastenings. The travel of actuator and linkage versus damper leaf and linkage travel should also be checked at this time. Shaft seals on the fan should be inspected visually for wear monthly.

C. Pumps

All bearings on the pumps and pump couplings should be lubricated periodically in compliance with the manufacturer's instructions. Many pumps include oilers which should be maintained at a specified oil level. Some pumps are equipped with grease lubricated bearings. These should also be lubricated according to the manufacturer's specifications.

As with fans, the frequency of inspection will vary with the severity of the application. Normally pump bearings should be inspected at least as frequently as fan bearings with minor inspections every eight hours for bearing oil levels and for seal leaks and vibration. Semiannual inspection should be made for leaks, cracks and loose fittings. A major inspection for wear, pitting, scoring and clearance should be made at least once per year.

The pump housing and impeller along with the seals are components which are subject to abrasion and corrosion. A properly operating mechanical collector preceeding the scrubber will aid in reducing the amount of particulate to be collected by the scrubber. This in turn will reduce the amount of abrasive solids required to be pumped through the scrubber recirculation system and should reduce the abrasion on the pump.

Increasing the bleed stream from the scrubber system will also reduce the concentration of suspended solids handled by the pump. Should neither alternative be available, a pump with a replaceable rubber liner may be of benefit. This should aid in minimizing pump replacement costs. The installation of a water flush in the seals may help to reduce the wear on the seals.

Corrosion may be combatted by installing a pump constructed of a high alloy, or a rubber-lined pump, depending on the chemistry of the recirculation system. Increasing the amount of chemicals added to a scrubber system can help neutralize the recirculation stream and help preserve the equipment. However, this may require a significant expenditure for purchasing chemicals. For example, the addition of caustic will increase the scrubber's efficiency to collect a corrosive gas such as sulfur dioxide. As more sulfur dioxide is collected, the pH of the solution drops and increased amounts of caustic are needed to neutralize it until an equilibrium is reached between the scrubbing efficiency and the desired pH level. At a recirculating solution pH of about seven, the collector's efficiency of sulfur dioxide using caustic is about 90% as compared to a 60% efficiency when scrubbing with water at a pH of four. Increasing the scrubber's bleed rate may help to lessen corrosion problems by decreasing the concentration of the corrosive compounds in the recirculation system.

D. Clarifiers and Drag Chain Tanks

Clarifiers and drag chain tanks fall into a general category of gravity separation devices. A clarifier or drag chain tank may be used to remove the particulate matter from the scrubber bleed stream when the particulate is sufficiently large and has a short settling time.

Clarifiers rake the settled particulate to the center of the unit, where it is removed from the bottom in a concentrated slurry. The slurry from the clarifier is pumped to a final discharge or to an additional dewatering device if a drier final discharge is required. The pipeline from the clarifier must be periodically inspected to make sure that it is not plugged.

The rake mechanism in a drag chain tank moves the solids up an incline. As the rake breaks the surface of the liquid, water falls off the rake and a relatively dry solid is moved up the incline. The solids continue to be pushed up the incline and over the edge of the tank where they fall onto a pile along the side of the tank. The pile of solids must be regularly removed from the side of a drag chain tank at a rate dependent on the application. A front end loader may be used for this chore; however it is usually better housekeeping to have the solids discharged into a dumpster and then have the dumpster replaced and hauled away when full. The rakes of this equipment require little maintenance since the speed of rotation is very slow. However, sludge buildup may put excessive torque on the rake mechanism. If this should occur, the clarifier or drag chain tank must be shut down, drained and hosed out.

Bearings and gear reducers must be lubricated and inspected according to the vendor's schedule. This is generally done semiannually. In addition to the inspection of the bearings, the drive mechanism must be inspected for temperature rise, sprocket alignment, sprocket wear, chain tension and oil level. These inspections should generally be done after the first 100 hours of operation and every 500 hours thereafter.

E. Rotary Vacuum Filters

Rotary vacuum filters are commonly a part of concurrent sulfur dioxide and particulate control systems but may also be used on the bottom discharge

from a clarifier in a particulate control system should a more concentrated discharge be required. In a particulate control system, the fine particulate matter may pass through an ordinary rotary vacuum filter. A precoat on the rotary vacuum filter may be required for such an application. In a precoat filter a layer of filter aid is formed on the filter drum. Once the filter has been coated with the filter aid, the liquid to be clarified is fed into the unit. The knife-edge then shaves off the particulate from the filtered mass along with a small portion of the precoat. After the precoat has been removed down to a depth where it can no longer effectively filter, the filter must be shut down and recoated. Precoating of the filter may take as long as one hour and the filtering cycle may last from 16 hours to one week depending upon how fast the precoat is removed from the filter. The depth of the precoat must be visually checked periodically. A spare filter or multiple filters should be installed to insure continuous operation of the particulate removal system.

Periodic lubrication of all knife-edge bearings, filter bearings, motor bearings, gear speed reducers, and vacuum pump bearings must be done in accordance with the vendor's schedule. The filter cloth, knife-edge alignment and drive belt must be inspected occasionally and adjusted or replaced as required. The frequency of inspection will again vary with the severity of the application ranging from once per week to once per year.

F. Motors - Mechanical

Motors are basically quite simple and reliable devices from a mechanical standpoint. However, as with all rotating machinery, the bearings require some degree of care and attention. Motor bearings should be lubricated in accordance with the manufacturer's specifications. The schedule for this may vary from 750 to 8000 hours of operation depending on the motor RPM and the severity of the conditions that the motor must operate under. Extreme care must be exercised in order to avoid excessive greasing of the motor bearings. Excessive greasing can cause the bearings to overheat and can contaminate the motor's windings. When greasing motor bearings, the bearing drain or flush holes must be unplugged to help guard against over greasing. Some manufacturers supply bearings which are prelubricated and sealed for life. This is advantageous in that overlubrication is perhaps the greatest cause of motor bearing failure. Bearings should be inspected in the same manner as described for the fan and pump bearings.

G. Agitators

Agitators may be required on systems where sedimentation of the particulate in the recirculation tank is a problem, or if additional mixing is required to mix any additives into the scrubbing liquor. The bearings and gear reducers should be inspected and lubricated according to the manufacturer's specifications. The agitator's shaft and propeller should be inspected occasionally for wear and corrosion. Should the shaft or propeller exhibit excessive wear or corrosion, it should be replaced with a higher alloy. On side-entering-type agitators, the packing and seals should be inspected for signs of leakage and wear.

SECTION III. STATIC EQUIPMENT

A. Duct Work

Duct work should be visually checked occasionally for leakage and excessive flexing. The frequency of these checks will vary with the severity of the application, but should be done no less than semiannually. Holes in the duct work can be the result of a number of causes, but are most often the result of corrosion or abrasion. For duct work located after the scrubber, corrosion will be a primary cause of failure. The deterioration of the duct due to corrosion may be alleviated by lining the duct with a corrosion resistant liner. This, however, may not be possible if the duct has corroded too greatly or if the gas temperature is too high. Should this be the case, the duct will have to be replaced with an appropriate alloy or with fiber glass if the temperature is low enough. Fiber glass has proven to be an appropriate material of construction when located downstream of the scrubber. The duct can be protected from temperature excursions due to water outages in the scrubber by installing an emergency spray quench system in the scrubber and supplying it with water independent of the normal scrubbing recirculation system.

Abrasion is a problem common to duct work located upstream of the scrubber. The severity of this problem can be lessened by increasing the duct diameter, thus slowing the velocity through the duct. The addition of a mechanical collector prior to the scrubber system will lessen the particulate loading through the duct work and therefore aid in reducing duct work abrasion. Should a mechanical collector already be in the system and abrasion is a problem, the collector should be inspected to insure that it is in proper operating condition. If it is found to be working properly, consideration should be given to installing a higher efficiency mechanical collector. If excessive flexing or cracking should develop, an expansion joint should be added to the duct work at that point.

B. Dampers

Dampers, due to their infrequent operation, present special maintenance problems. Guillotine zero-leakage dampers are perhaps the most effective for air pollution control systems. Louver and butterfly dampers, however, may be appropriate for less severe or demanding service. Since the maintenance on all types of dampers is similar, concentration will be given to guillotine type dampers.

Lubrication is an important part of any damper maintenance program. The scheduling and types of lubricants should follow the manufacturer's specifications. Lubrication is normally done annually on all components of the drive mechanism and bearings. The blower motor bearings should also be lubricated at that time if one is included with the damper.

A program of regular inspection must be instituted to help insure that the damper will operate when required. The damper blades should be moved in and out of the duct six to twelve inches several times, at a frequency of no less than once per month. More severe services may require a greater frequency of this checking. Checks for leakage around the flanges should be made at least

once per month. All portions of the damper's sealing elements should be inspected for wear semiannually. Alignment and operation of the drive mechanism should also be checked semiannually. On a yearly basis, all drive components, bearings, damper blades and blowers should be inspected for wear or leakage. Please note that all these inspections should be carried out with strict adherence to the manufacturer's instructions.

Guillotine dampers should be equipped with an air purge to prevent buildup of debris in the blade seating surface trough when the blade is in an open position. It is important, to insure proper damper operation, that the manufacturer's schedule for activating these purges be followed. The frequency of these purges will depend again on the severity of the application; however, it is recommended that it be done at least daily with six air bursts of five seconds long with one to one and one half minutes between each burst.

C. Piping

Piping should be inspected at regular intervals depending on the application. Piping is prone to three common problems: abrasion, corrosion and pluggage. Abrasion is common to any scrubber system collecting a hard, insoluble particulate, such as coal-fired boiler flyash. Abrasion problems in the recirculation piping are best alleviated by reducing the concentration of the particulate that is being run through the recirculation system. This can be done by increasing the bleed rate from the system, by installing a mechanical collector ahead of the scrubber if none already exists, or by insuring the proper operation of an existing mechanical collector. Reducing the pipe velocity by installing a larger diameter pipe may also help relieve an abrasion problem. It must be noted, however, that a velocity which is too slow may promote settling and pluggage of the pipes. A pipe velocity of four to seven feet per second is a reasonable compromise between preventing abrasion and preventing pluggage.

Corrosion will be a problem in recirculation systems where the scrubber is operating on a gas stream containing corrosive gases. The methods of alleviating a corrosion problem in the recirculation system are similar to those discussed for pumps. Addition of caustic will ultimately raise the pH and neutralize the scrubber solution. Replacing the existing piping with piping constructed of a more corrosion-resistant material may be a more economical alternative in the long run. FRP pipe or plastic-lined cast iron pipe has been successfully used where corrosion is a problem and the particulate being collected is water soluble, such as sodium sulfate. Plastic-lined cast iron has an advantage over FRP in that is it is more resistant to accidents on the outside such as forklifts running into it. On a recirculation system where both corrosion and abrasion are problems, stainless steel and rubber-lined cast iron pipes have been shown to be effective.

Pluggage can be a problem on recirculation systems handling a slightly soluble particulate or if the pipe velocities are too low, thus promoting settling. On systems where the former is the problem procedures such as increasing the bleed rate or raising or lowering the pH may help to alleviate the pluggage. Should the latter be the case, an increase in the pipe velocity by decreasing the pipe diameter may help to eliminate this problem. Piping on

a system which is prone to pluggage should be flushed out with clean water on a yearly basis as a minimum. Consideration should also be given to rodding out the piping if this is possible.

D. Valves

Valves will be subject to most of the same problems which have been discussed for piping: that is, abrasion, corrosion and pluggage. The solution to these problems in valves will be similar to those solutions for the equivalent problems in piping. Installing larger diameter valves, increasing the bleed rate and installation of a mechanical collector before the scrubber will all aid in reducing abrasion. Increasing system pH and installing valves of corrosion-resistant material will help to eliminate corrosion problems. Pluggage can be alleviated by increasing the system bleed rate, adjusting pH or increasing the valve velocity in cases of settling. On a system which exhibits both corrosion and abrasion, rubber pinch valves have been found to be effective. The rubber provides resistance to corrosion, and the design of the valve provides a smooth passage for the liquid stream containing the particulate, thus minimizing abrasion.

Air-operated control valves may exhibit sticking problems. The problem may stem from one of two sources. The valve may exhibit some pluggage due to the particulate in the recirculation system, or it may have some water build up at the air connection. The latter problem may be reduced by insuring a supply of dry air to the valve or by regular inspection and drying of the air connection. The frequency of this cleaning will depend on the amount of moisture in the air supply. Since a control valve can be a rather vital component in the operation of a scrubber system, it is recommended that the piping be arranged so that any system containing a control valve can be temporarily placed on manual operation while the control valve is repaired or replaced. This is particularly important in the caustic addition system where loss of caustic may severely damage the scrubber system's components. It is also important in the scrubbing liquor make-up system where a malfunction of the control valve may cause the scrubber to run dry, thus damaging the equipment from excessive temperature. A malfunctioning control valve in the make-up line may also cause the recirculation tank to overflow. A failure of either of these control valves and the inability to resort to manual operation may require shutdown of the entire scrubbing system.

E. Recirculation Tank

The scrubbing liquor recirculation tank in most systems will require very little maintenance outside of an occasional inspection of the general condition of the tank and liquid inside. Corrosion may be exhibited on a tank handling an acidic scrubbing medium. Adding caustic, lining the tank with a corrosion-resistant liner or replacing the existing tank with one constructed of FRP or an appropriate alloy can alleviate the problem. If the scrubber is handling a large, easily settleable particulate and if the tank has a relatively long retention time, particulate may build up on the bottom of the tank. This buildup may plug the recirculation pump nozzle and foul the instrument probes. The addition of an agitator may help to solve this problem. Lowering the retention time by lowering the liquid level may also help, provided this can be done

without causing cavitation in the pump. Certain contaminants collected in the scrubber may cause a foaming problem. This problem may be reduced through lowering the scrubbing liquor pH by reducing the amount of caustic added to the system or by adding a slight amount of acid if the scrubbing solution is originally basic. Should the scrubber system not be able to tolerate a lower pH, foam-breaking sprays can be installed above the tank or anti-foaming agents may be added to the tank. Adding more freeboard to the recirculation tank may be of some benefit in relieving a foaming problem.

Pump cavitation may be a problem if the liquid level in the tank is not high enough for the pump flow rate and the diameter of the recirculation pump nozzle. A baffle or bellmouth may be used to prevent such cavitation.

SECTION IV. ELECTRICAL

A. Instruments

Instruments usually require very little maintenance. The philosophy is generally to replace them as they fail. The accuracy and calibration of analog instruments should be checked annually. All probes should be cleaned at a frequency dependent on the application. The level controller in the recirculation tank handling a highly soluble particulate may never require cleaning, whereas the pH probes on a lime slaker, should lime be used as a neutralizing agent, may require cleaning daily. It is therefore important to select types of probes which will be appropriate for the frequency of maintenance. A flange-mounted differential pressure transmitter, used for level control and located at the bottom of a recirculation tank, may be appropriate for a scrubber system operating on a highly soluble particulate. However, if the particulate tends to settle easily, this type of level controller might require that the tank be frequently drained in order to clean the probe when a sufficient amount of solids have settled around it. A top-entering float-type level controller may be more appropriate for this type of application. All pneumatic lines should be cleaned and dried of moisture regularly at intervals depending on the quality of the air supplied to them. Orifice plates should be inspected at least annually and may require more frequent inspection should the fluid contain any abrasive solids. Excessive wear on orifice plates may necessitate replacement with a harder material of construction. Ink and paper in the recorders must be checked frequently.

B. Motor Starters

Motor starter switches should be lubricated occasionally according to manufacturer's specifications. Cleaning of all electrical equipment is important to insure reliable operation. Dirt in electrical equipment may decrease heat dissipation and cause poor ventilation. Overheating and insulation breakdown may result from this. Insulation breakdown may also occur if the dust is electrically conductive. All contacts, transformer insulation and cooling fans should be inspected, cleaned and dried annually. Dirty environments may require more frequent inspection and cleaning.

C. Motors - Electrical

Motors require little attention from an electrical standpoint outside of an occasional cleaning and check of temperature rise. Dust may be removed by using dry low-pressure compressed air and a dry cloth. Grease when mixed with dirt can form a gum which is difficult to remove. Oil can cause a deterioration of the insulating varnish which in turn can lead to a burnout. Any grease or oil can be removed with a solvent such as naphtha. A fresh coat of insulating varnish should be reapplied after such a cleaning.

Measurement of the temperature rise can provide an indication of problems such as overloading, shorts or burned insulation. The three methods available to measure the temperature rise are thermometer, resistance and imbedded thermocouple. The thermometer method simply consists of placing a thermometer as close as possible to the windings and core of the motor. This may be done by removing a head bolt or eye bolt and inserting a common mercury or alcohol thermometer. The resistance method requires that a Wheatstone or Kelvin bridge be used to measure the winding resistance at room temperature and then once again after the motor has operated for four to six hours at full load. The temperature can then be calculated from the following equation:

$$T = \frac{R_H - R_C}{RC} \quad (234.5 + T_1) - (T_2 - T_1)$$

Where T = temperature rise (°C)
R_H = hot winding resistance (ohms)
R_C = cold winding resistance (ohms)
T_1 = ambient temperature, motor cold (°C)
T_2 = ambient temperature, motor hot (°C)

The embedded thermocouple method involves connecting a bridge-type instrument to a thermocouple which has been embedded in the windings. This will usually give a reading directly in degrees centigrade. The actual temperature rise should then be compared against the manufacturer's recommended temperature rise for that type of motor. A motor can be too hot to touch and still be within the proper operating temperature. Therefore it is important not to attempt to measure the motor temperature by hand. On motors 300 H.P. and above the thermocouple method should be used with the thermocouple connected to a recorder and the temperature recorded continuously.

SECTION V. SUMMARY

The ease of maintenance is often a function of proper system design. A properly designed system will often require little maintenance outside of an occasional inspection and lubrication. The effects of corrosion and abrasion must receive a great deal of consideration when designing, redesigning or maintaining the ancillary equipment of a particulate scrubber system.

An ideal scrubber system from a maintenance and operation standpoint will have a high-efficiency mechanical collector preceeding a low-RPM forced-draft fan with replaceable blade liners. Duct velocities to and from the scrubber will be between 50 and 70 feet per second. Isolation dampers are guillotine

zero leakage types. Duct work from the scrubber will be FRP or lined carbon steel with an emergency quench system incorporated into the scrubber.

The recirculation system will consist of a rubber-lined recirculation pump and an installed full spare. The lining will be of a replaceable type. The piping will be rubber lined cast iron sized for a velocity of four to seven feet per second. All valves are rubber pinch valves wherever possible. The recirculation tank will be constructed of FRP or an appropriate alloy. The bleed rate will approach that of a once-through system.

A system of this design will not be a zero maintenance system. However, proper system design and adherence to a routine maintenance program, based on the individual equipment manufacturer's specifications, will go a long way toward eliminating many of the problems which have plagued the operation of particulate scrubber systems.

SOURCES CONSULTED

Andco/Metroflex Installation, Operation and Maintenance Manual. Buffalo, 1978

Chemineer Agitators Instruction Manual. Dayton, 1978

FMC Corporation Service Manual. Itasca, Illinois 1978

Galigher Parts List and Operating Instructions. Salt Lake City, 1978

Goulds Pumps Installation, Operation and Maintenance Instructions. Lubbock, Texas 1978

Johnson, Karl E. Private Interview. Itasca, December 1978

Komline-Sanderson Installation, Operation and Maintenance Manual. Peapoc, New Jersey 1978

Leiner, Roger E. Private Interview. Itasca, December 1978

Louis Allis Instruction Manual. Milwaukee, 1971

Marinello, R. L. "The Plant Engineer's Bible: Maintenance Operating Manual." Plant Engineering, (October 26, 1978), 114-9

Moersfelder, Allan E. Private Interview, Itasca, December 1978

Susca, Vito Private Interview, Itasca, December 1978

Square D Company Instruction Manual. Middletown, Ohio, 1975

Westinghouse Corporation Installation, Operation and Maintenance Manual. Boston, September 1977

LOWERING OPERATING COSTS WHILE INCREASING THROUGHPUT AND EFFICIENCY OF REACTORS AND SCRUBBERS

By:

Richard P. Tennyson
Sheldon F. Roe, Jr., P.E.
Robert H. Lace, Sr.
The Munters Corporation
Fort Myers, Florida 33901

ABSTRACT

This paper is directed to those engineers responsible for the design, operation and/or maintenance of scrubber equipment for either quality control or chemical process improvement.

This paper reviews the unique combination of high capacity stacked wetted film contact packing with high velocity entrainment separation. The unique geometric designs of both contactor and separator permit as much as 50% or greater face velocity without the flooding, reentrainment, or excessive pressure differential to which conventional devices would be subjected.

Detailed examples of combined particulate collection and gas absorption are discussed, along with suggestions for potential applications in process and emission control - including both cross flow and counter flow systems.

Upgrading of existing systems to achieve additional capacity or improved performance efficiency are reviewed. Photos, geometric illustrations and performance characteristics are presented.

LOWERING OPERATING COSTS WHILE INCREASING THROUGHPUT AND EFFICIENCY OF REACTORS AND SCRUBBERS

1.0 INTRODUCTION

Emphasis in this paper concerns wetted film contactors, rather than auxiliary equipment such as mist eliminators and other liquid or gas handling equipment. The purpose is to provide a basic description of the wetted film contactor, and to provide some examples of its successful use.

2.0 DISCUSSION

2.1 What is a wetted film contactor?

Historically, spray towers and packed towers have been utilized for gas and particulate removal from effluent or process gas streams. It could be said, that the wetted film contactor combines the best features of spray and packed towers. It overcomes the clogging problems with packed towers, while maintaining the low pressure drop of spray towers.

However, at least two functions are added to the spray or packed towers. First, the liquid film moves sideways to the gas flow direction, as shown in Figure 1. This pays dividends in pumping head and increased residence time of the liquid. The residence time caused by this lateral movement may be twice what it is for a packing where the liquid flows straight. Second, the gas phase all must take identical flow paths in contact with the turbulent mixing action of the liquid film.

Construction is of corrugated sheets as illustrated in Figures 2 and 3. Several surface areas are available as shown in Figure 2.

2.2 How is a wetted film contactor used?

Crossflow and counterflow are the two common configurations as illustrated in Figure 4. Operating parameters must be optimized with the general selection process illustrated in Figure 5. In addition, each of the above may be used in staged separations. The Japanese have had considerable success with two stage mist elimination in crossflow. This has also proven successful in counterflow at Arizona Public Service and Texas Utilities. The first stage is coarse to prevent clogging, while the second is finer, utilizing cleaner water.[1]

Actually, some of the mist eliminators may contain approximately 25 ft^2/ft^3 of surface area in the wetted film contactor context. However, this area is arranged for higher internal gas velocities and correspondingly higher pressure drop. Some molecular transfer (SO_2, etc.) might occur, as a result of this surface area.

As applied to wetted film contactors, the staged separation technique is proposed in a similar manner to the mist elimination.

FIGURE 1

FLOW CONFIGURATION OF A WETTED FILM CONTACTOR

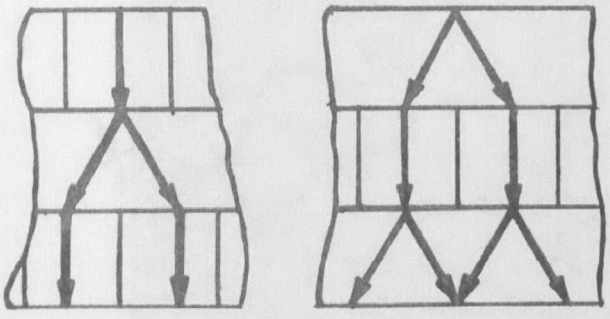

FRONT ELEVATION SIDE ELEVATION

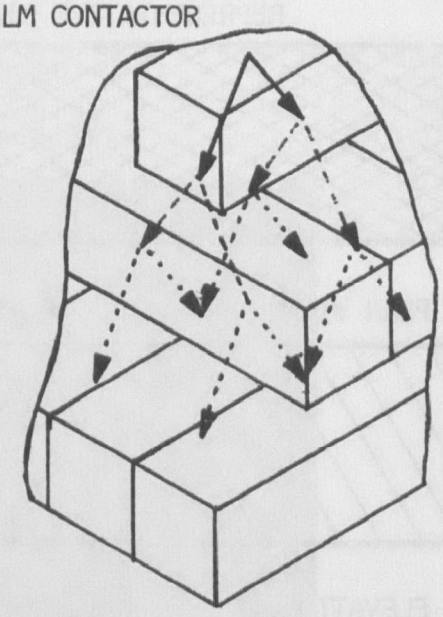

ISOMETRIC VIEW

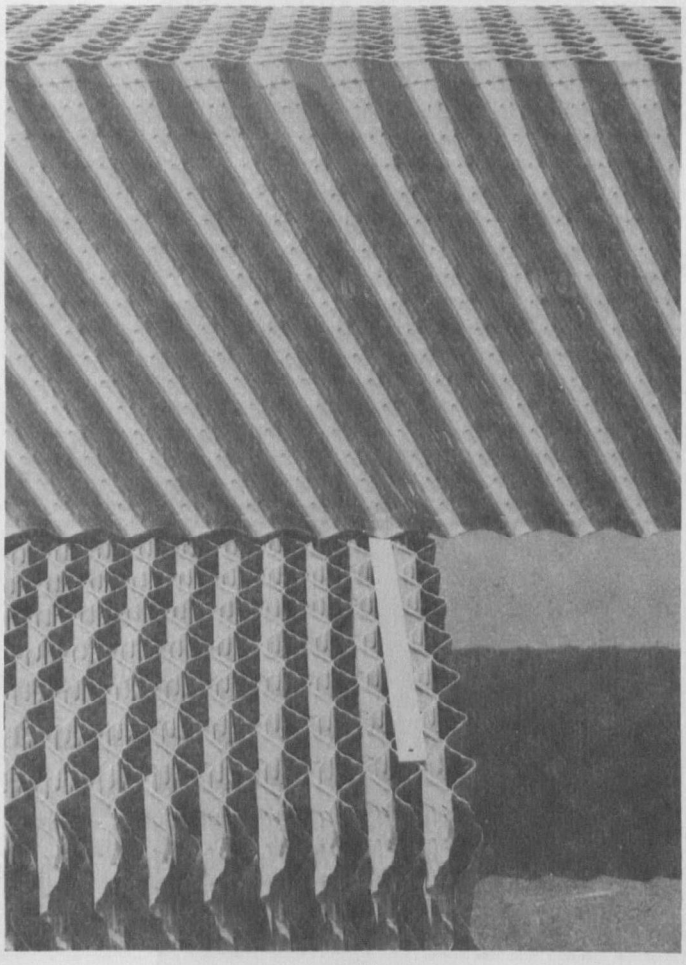

PHOTOGRAPH OF CONTACTOR MODULES ORIENTED AS IN DIAGRAM ABOVE

→ = LIQUID PATH

FIGURE 2
REPRESENTATIVE SIZES OF WETTED FILM CONTACTORS

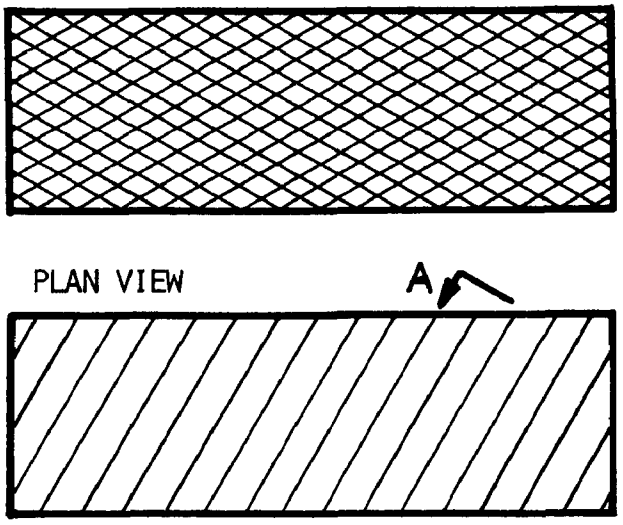

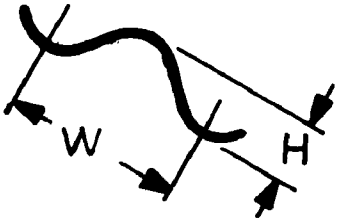

SECTION A-A

ELEVATION VIEW

DESIGNATION	12060	19060	27060
FLUTE HEIGHT			
H IN	0.46	0.75	1.07
MM	12	19	27
FLUTE WIDTH			
W IN	1.1	1.9	3.1
MM	28	48	79
SURFACE AREA			
SQ FT/CU FT	68	42	30
SQ M /CU M	223	138	98
APPROX. VOID VOLUME			
%	95.4	97.2	98.1
APPROX. MIN. FREE PASSAGE DIA.			
IN	0.4	0.7	1.1
MM	10	18	28
MAX. LATERAL LIQUID SPREAD			
IN/FT OF HEIGHT	13.9	13.9	13.9
MM/M OF HEIGHT	1158	1158	1158
PRESSURE DROP			
IN WG/FT OF HEIGHT	0.18	0.12	0.07
M BAR/M OF HEIGHT	1.5	1	0.6

AT 600 FPM VELOCITY & 8 GPM/SQ FT

FIGURE 3

COUNTERFLOW POLYPROPYLENE MEDIA
USED IN THE SO_2 SCRUBBERS AT
CHOLLA AND MARTIN LAKE POWER PLANTS

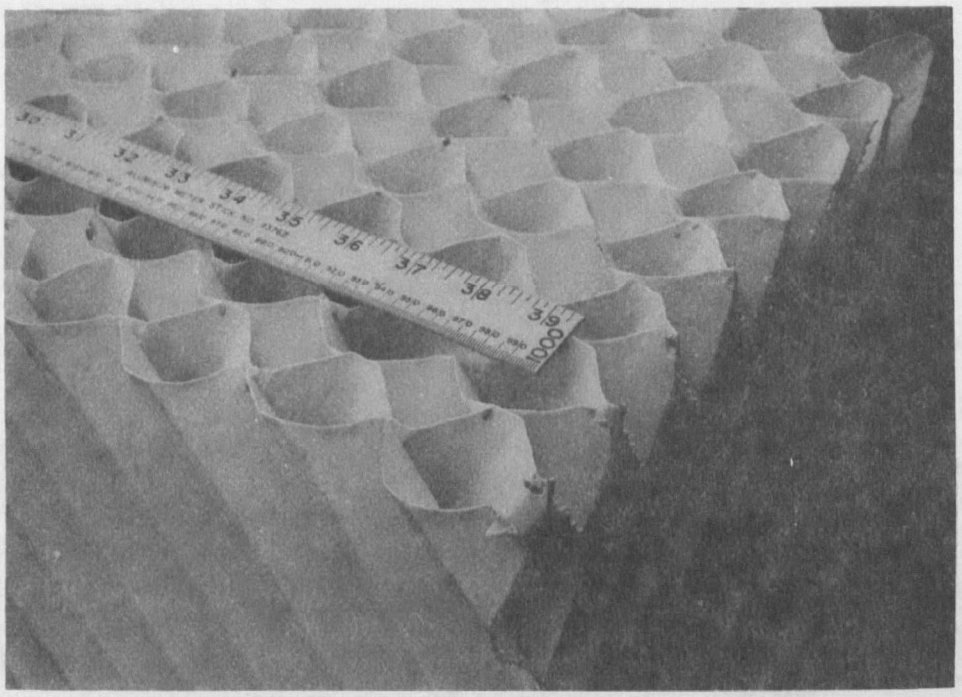

STAINLESS STEEL CONSTRUCTION

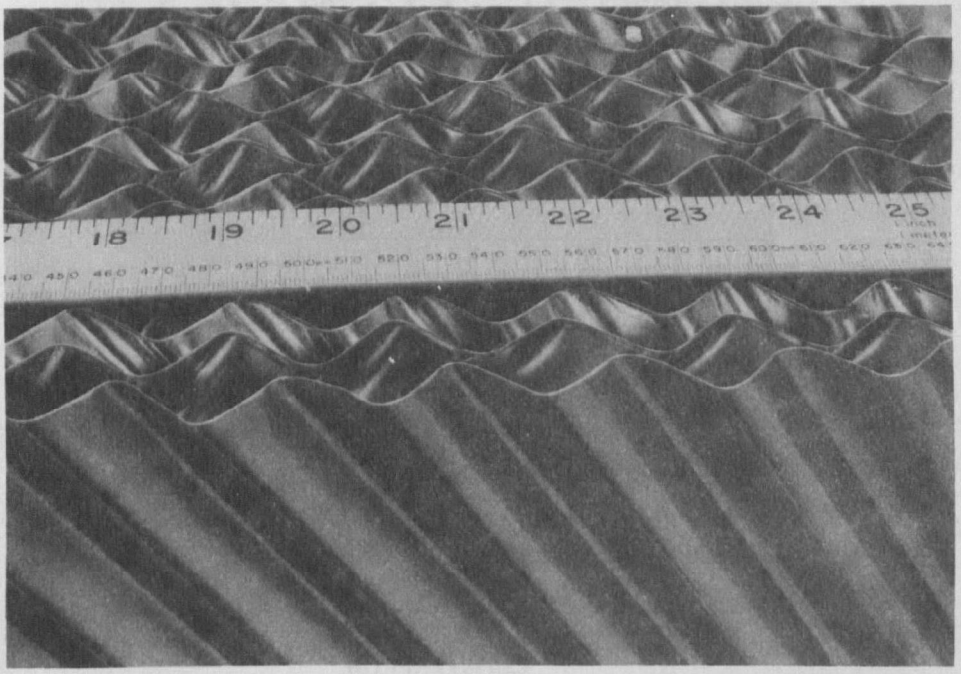

FIGURE 4
SURFACE MEDIA GENERAL
FLOW CONFIGURATION

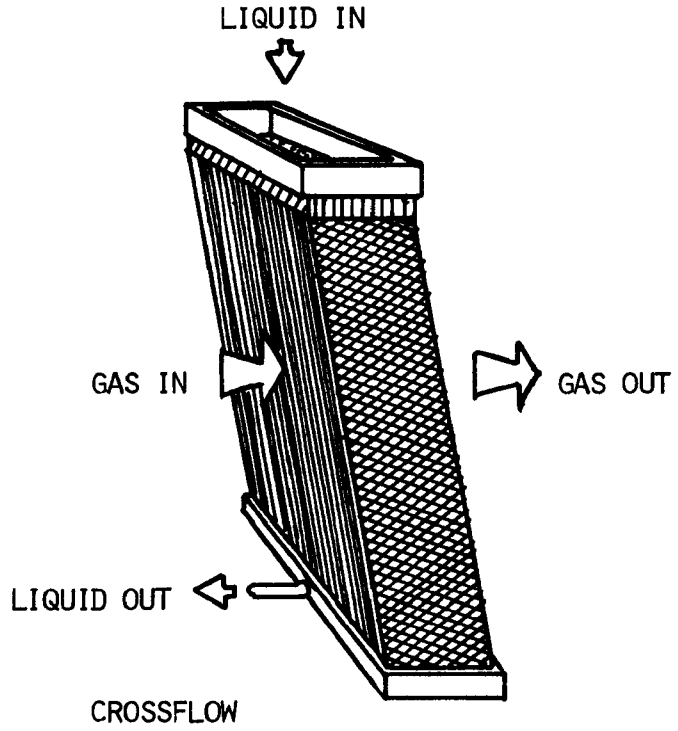

CROSSFLOW

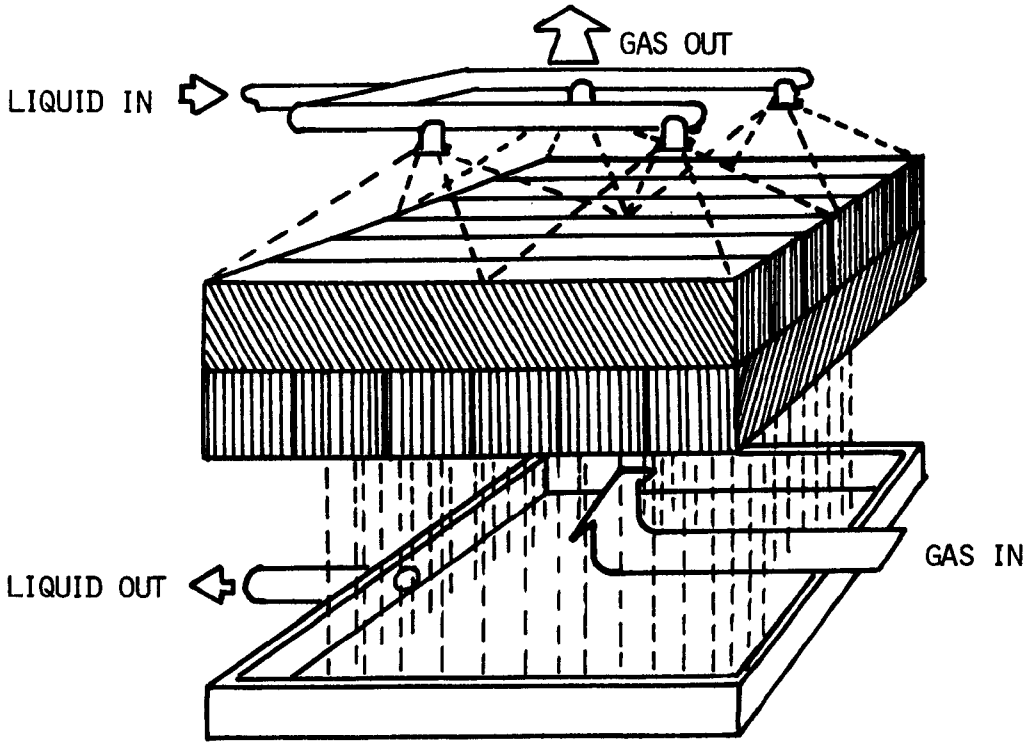

COUNTERFLOW

FIGURE 5

OPTIMIZATION OF SURFACE CONTACT MEDIA

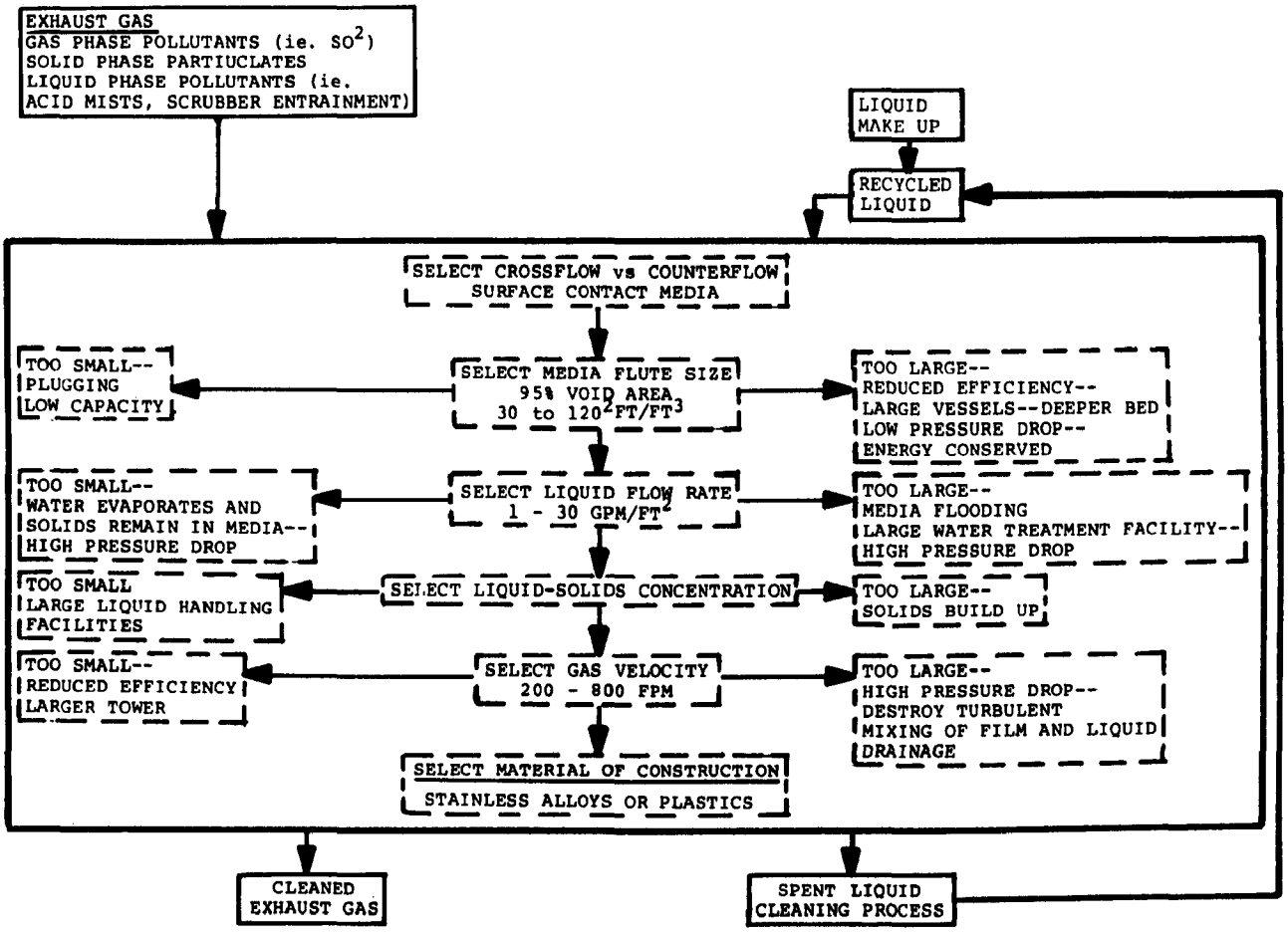

As a first stage, the media has a surface area of 30 ft^2/ft^3, and the second stage 42 ft^2/ft^3. If very clean liquid is available, the surface area could be 68 ft^2/ft^3. This fine size is utilized for acid mists as from sulfuric acid, for instance.

Since the surface contact media operates so well for gas with liquid, it is logical to expect that the surface contact media has a beneficial effect on gas flow distribution. The current practice of designing large duct diameters accentuates the problem of flow distribution.

2.3 How does a wetted film contactor affect particulate removal?

Particulate scrubbing incorporates several wellknown principles in the mechanics of particle collection, such as condensation, impaction and agglomeration. Each of these are effectively applied in the wet film contactor.

Turbulent mixing of the scrubbing liquid and the particulate laden gas will occur as frequently as every quarter inch of gas, or liquid travel through the pack. Unlike conventional packed scrubbers the gas and liquid flow through the ordered contact surfaces is uniform without localized flooded or liquid void areas, which reduce collection efficiency and increase pressure drop. In Table 1 below some published data of a prominent manufacturer of environmental control equipment using this media, as well as results of independent tests conducted on a scrubber for boiler flue gas particulate and SO_2 on oil well steam generators is presented.

Table 1

Illustration of Particulate Removal

	Gas Velocity Through Packing, fpm	Feet of Pack or Depth of Bed, ft	Pressure Drop, in w.g.	Efficiency, %
Manufacturers Data, Case 1 :	750	3	.5	99% for 6 micron particles
Manufacturers Data, Case 2 :	750	3	.5	92.5% for 4 micron particles
Flue Gas from Oil Well Steam Generator Test:	650	4	.75	83% *

*Ash content of crude oil represents 4% of total particulate collected in sampling train. Sample was subjected to combustion in which it indicated a total of 93% carbonaceous material, primarily carbon black. This would indicate that the majority of the particulate collected was in a 5 micron or less particle size range.

2.4 Field applications and operating performance.

2.4.1 Utility SO_2 application.

The basic description of surface contact media has been given before -- now some actual case histories of applications will be discussed.

One early application of wetted film contactors now has over 5 years experience, as was recently reported.[1] In this case, the polypropylene wetted film contactor pictured in Figure 3 was utilized. This system contained 4 feet height of the wetted film contactor, followed by a two stage mist eliminator. Comparisons were made with a spray tower, where the spray tower removed 14.4% SO_2, compared to 92.4% for the packed tower. Particulate removal efficiency was 99.8, and 99.7% respectively. The packed tower had an L/G ratio of 6.5 l/m^3 (48.9 gal./1000 acf) and a gas velocity of 2.1 m/s (6.9 ft/sec.).

A second example was discussed, where the towers consisted of five stages.[2] Stages 1 and 2 are sprays, while stage 3 is the wetted film contactor, pictured in Figure 3. Stages 4 and 5 are coarse and fine mist eliminators. Tower removal efficiency was 99% with 4 feet of wetted film contactor. However, throughput was increased 10% by using only 2 feet of packing with greater than 98% SO_2 removal.

It should be noted, that both of the preceding systems have been constructed of polypropylene, which has resulted in good operating records.

Part of the dependability of these units is attributed to designs allowing quick replacement from an ample supply of inexpensive spare parts. Although all plastics and stainless steels are available, polypropylene is recommended, because of its low cost and chemical resistance.

2.4.2 Pilot test.

The foregoing steam generator test also illustrates what is considered to be a major advance in the relationship of pressure drop to removal efficiency.

This example concerns a crude oil (4-5% S, 15.5° A.P.I.) fired boiler with no special modifications to the boiler and no special removal equipment, other than the scrubber.

The scrubber contained 4 feet of height of the wetted film contactor (19060 stainless steel, as described in Figures 2 and 3). Gas velocity through the wetted film contactor was 600 fpm with an inlet gas temperature of 500° F and outlet of 120° F. Liquid rates were approximately 8 gpm/ft^2 of caustic or sodium aluminate. Inlet particulate varied from 0.35 to 0.56 g/scf with analytical results indicating a fine particle size. Inlet SO_2 approximately 1500 ppm.

Results showed that, at a pressure drop of 1.25 to 1.50 in. of water, 91 to 95% removal of SO_2, and 80 to 85% removal of particulate were accomplished.

3. CONCLUSIONS

Surface contact media of the type described herein should be investigated more thoroughly with the primary goal of high mass transfer with low pressure drop.

Experience ranges from full scale utility plants with over 5 years of outstanding operating records to recent pilot tests demonstrating 80 to 85% particulate removal and 90 to 95% SO_2 removal at 1¼ to 1½ in. w.g. pressure drop.

For the future, staging, as has been demonstrated with two stage mist eliminators, is recommended. With staging it is possible to prevent clogging while providing a bed of fine structure near the final effluent point for minimum discharge. It is possible to provide large beds (1000 ft^2) of uniform "pore" size (25 $\pm$ 2 mm) where all of the gas must take identical flow paths. In this regard, surface contact media should also be of value as a flow modifier enabling economical handling of the large gas volumes being planned in today's technology.

REFERENCES

1. Heacock, F.A., R.T. Travis. Cholla Station Unit 1 FGD System 5 Years of Operating Experience. EPA Symposium on Flue Gas Desulfurization; Las Vegas, Nevada; March 1979.

2. Richman, M. Limestone FGD Operation at Martin Lake Electric Station. EPA Symposium on Flue Gas Desulfurization; Las Vegas, Nevada; March 1979.

3. Tennyson, R.P., S.F. Roe, R.H. Lace. Improved Mist Elimination Through Advanced Design Concepts. EPA Symposium on the Transfer and Utilization of Particulate Control Technology; Vol. 3, EPA-600/7-79-044c; February 1979.

OPTIMIZING VENTURI SCRUBBER PERFORMANCE THROUGH MODELING

By:

Douglas W. Cooper, Ph.D.
Department of Environmental Health Sciences
Harvard School of Public Health
Boston, Massachusetts 02115

ABSTRACT

EPA's programmable calculator version of a venturi scrubber model was used to study scrubber optimization. It showed that in the equation relating penetration (Pt) to pressure drop (Δp), $\ln Pt = -b\Delta p^a$ the exponent, a, becomes < 1 as Δp increases (at a constant liquid-to-gas ratio), which we have shown favors multiple-stage scrubbing over single-stage, for the same total Δp. An example is given for which two venturis in series would give the same collection efficiency as a single stage but require 25 percent less power. Penetration of various particle sizes for a single stage at a fairly typical liquid-to-gas ratio ($Q_L/Q_G = 1 \times 10^{-3}$) is correlated with a new dimensionless group for pressure drop, $\Delta p\tau/\mu_G$, formed from the gas viscosity (μ_G) and the particle aerodynamic relaxation time (τ). For values of Q_L/Q_G within the range of conventional practice, an example is given for which achieving the same penetration is predicted to require quite different values of Δp, in apparent contradiction of the "contacting power" hypothesis.

OPTIMIZING VENTURI SCRUBBER PERFORMANCE THROUGH MODELING

INTRODUCTION AND GOALS

Venturi scrubbers are widely used for particulate control; they are more efficient than such scrubbers as packed columns, sieve plates, and impingement plates at pressure drops greater than about 10 cm H_2O (9.8×10^3 dyn/cm^2 = 980 Pa), according to relationships given by Calvert (1977).[1] We used a programmable calculator venturi model to investigate the relationship between penetration and pressure drop, an implicit variable in the model. This penetration versus pressure drop relationship was used to study economic optimization of scrubber performance for a specific example and generalized by the introduction of a new dimensionless group for pressure drop. The relationship between penetration and pressure drop was also studied to investigate further the hypothesis (Cooper, 1976)[2] that multiple venturi stages in series would be more efficient for collecting particles than would a single stage having a pressure drop equal to the total across the multiple stages.

METHODS AND RESULTS

The Model

A programmable calculator program was prepared by Sparks (1978);[3] it uses a model for venturi scrubbers developed by Calvert et al. (1972)[9] and described by Calvert (1977).[1,4] Penetration (Pt) is predicted by

$$Pt = \exp\left[\frac{2\,Q_L u_G \rho_L d_d F(K,f)}{55 Q_G \mu_G}\right] \qquad (1)$$

where

Q_L = liquid volume flow, cm^3/s
Q_G = gas volume flow, cm^3/s
u_G = gas velocity in the throat, cm/s
ρ_L = liquid density, g/cm^3
d_d = droplet diameter, cm
μ_G = gas viscosity, poise = g/cm-s
f = empirical factor, 0.5

and

$$K = u_G C \rho_p d_p^{\,2} / 9 \mu_G d_d$$

a Stokes number, having

d_p = particle diameter, cm
C = Cunningham slip correction (approximately $1 + 0.16 \times 10^{-4}$ cm/d_p at STP)
ρ_p = particle density, g/cm^3

and

$$F(K,f) = K^{-1}\left[-(Kf + 0.7) + 1.4 \ln\left(\frac{Kf+0.7}{0.7}\right) + \frac{0.49}{Kf+0.7}\right] \quad (2)$$

Calvert (1977)[1] noted that the f factor includes the influence of other effects besides impaction, including perhaps particle growth due to water vapor condensation, presence of drop sizes different from the predicted size, maldistribution of liquid, etc.

Scrubber drop diameter is calculated from the correlation of Nukiyama and Tanasawa (Calvert, 1977):[1]

$$d_d = \frac{5.86}{u_G}\left(\frac{\sigma_L}{\rho_L}\right)^{\frac{1}{2}} + 0.0597\,\frac{\mu_L^{0.45}}{\sqrt{\rho_L \sigma_L}}\left(1000\,\frac{Q_L}{Q_G}\right)^{1.5} \quad (3a)$$

where

ρ_L = liquid density, g/cm^3
μ_L = liquid viscosity, g/cm-s
σ_L = liquid surface tension, dyn/cm.

For water this becomes (Sparks, 1978):[3]

$$d_d = \frac{50}{u_G} + 91.8\left(\frac{Q_L}{Q_G}\right)^{1.5} \quad (3b)$$

The programmable calculator uses model equations (1), (2), (3b) to predict particle penetration by integrating numerically (trapezoidal rule) over the particle size distribution, assumed to be log normal, having a mass median aerodynamic diameter of d_g and a geometric standard deviation of σ_g.

The Program

Sparks (1978)[3] implemented the venturi scrubber model above by preparing a program, designed to be written on two magnetic cards, for the Texas Instruments SR-52 programmable calculator. After the first card is read by the calculator, the user supplies all the input information (T, f, d_g, σ_g, d_i,Δd,d_f, ρ_L, Q_L/Q_G, u_G, μ_G, ρ_p) which includes specifying the temperature (T) and the integration instructions, the initial particle diameter (d_i), the final particle diameter (d_f), and the size of the steps in the integration (Δd). Sparks (1978)[3] stated that the following choices are usually adequate: Δd = 0.1 for integration from 0.1 to 1.0 μm; Δd = 0.5 for integration from 0.1 to 10 μm; Δd = 2 for integration from 10 to 20 μm. (We used integration step widths this small or smaller.) The first card gives the droplet diameter as well as the pressure drop across the scrubber due to the liquid gas interac-

tion:

$$\Delta p = 8.24 \times 10^{-4}(Q_L/Q_G)u_G^2 \quad (4)$$

where

Δp = pressure drop, cm H_2O.

After the second card is read, the user gets penetration from the integration interval initially specified; one can also get penetration for adjacent size intervals for particles which are larger than those in the initial interval without having to reprogram. (The documentation[3] should indicate the "reset" instruction must be used immediately before card 2 is read.)

The Model and Some Measurements. For the limited set of data shown in Table 1 the scrubber model and SR-52 program did very well in predicting pressure drop and penetration.

Table 1. COMPARISONS BETWEEN SCRUBBER MODEL (SR-52 PROGRAM) PREDICTION AND MEASUREMENTS (SPARKS, 1978)[3]

Plant	Pressure Drop, cm H_2O		Penetration	
	Predicted	Measured	Predicted	Measured
1	46	45.7	0.016	0.015
2	25	25	0.028	0.025
3	105	100	0.004	0.005

The model for scrubber penetration was derived from physical reasoning, measurements for single collector efficiency, and mathematical analysis. The f factor is an adjustable empirical constant, generally 0.5.[1] Thus, the model is semi-empirical. Here we compare results from the model with the experimental results reported by Semrau et al. (1977)[5,6] for their work with orifice scrubbers, which are approximately venturi scrubbers of infinitely short throat length. These results were reported in terms of the number of transfer units

$$N = -\ln Pt \quad (5)$$

versus the "effective friction loss," equivalent to the pressure drop through the scrubber due to the droplets, Δp. The experiments were run at flow rates up to 250 m^3/hr (150 ft^3/min) and at pressure drops up to 320 cm H_2O. The orifice was located in a downward flow. The test aerosol was ammonium fluorescein atomized from solution. Semrau et al. (1977) [6] stated it is nonhygroscopic, only slightly soluble in water. The two aerosols for which complete particle size data (obtained from cascade impactor measurements) were given had d_g = 1.05 μm with σ_g = 1.58 and d_g = 0.68 μm with σ_g = 1.69; these are only moderately polydisperse.

Sparks (1978)[17] compared the penetration data of Semrau et al. (1977)[6] with the predictions from this model, using the values of liquid-to-gas ratio

and gas velocity of the experiments. The predicted penetration values were within the spread of the data when plotted versus pressure drop. However, we have found that the predicted pressure drops at $Q_L/Q_G >> 1 \times 10^{-3}$ were usually about twice as high as the measured pressure drops.

It has been argued (Semaru, 1977,[7] for instance) that the penetration of a particular aerosol through a scrubber will be almost wholly a function of pressure drop alone. Calvert (1977) indicates that liquid-to-gas ratio is also quite important, with Q_L/Q_G of about 1×10^{-3} generally optimal. We used $Q_L/Q_G = 1 \times 10^{-3}$ and calculated the penetration versus pressure drop for the aerosols used by Semrau et al. (1977)[5] over the pressure drop range 10 cm H_2O to 330 cm H_2O, corresponding to gas velocities $u_G = 0.35 \times 10^4$ cm/s to 2.0×10^4 cm/s. (Other values were T = 25°C, f = 0.5, $\rho_L = 1$ g/cm^3 = ρ_p; d_i, d_f, and Δd were chosen to give three significant digits for Δp and Pt.) Figure 1 shows the two-branched lines used by Semrau et al. (1977)[5] to summarize their data and the values of penetration versus pressure drop calculated by us from the scrubber model. The excellent agreement is puzzling: The calculations were made assuming a 10^{-3} liquid-to-gas ratio. In their report, Semrau et al. (1977)[6] give Q_L/Q_G values that often were much greater than 1×10^{-3}. That the penetrations agree fairly well with the predictions at $Q_L/Q_G = 1 \times 10^{-3}$ supports the view that changing the Q_L/Q_G parameter is not very important at a given pressure drop, but that seems to contradict other results of the model which show Q_L/Q_G to be quite important.(See Appendix.)

The Two-Branched Curve

One way of correlating the data for penetration versus pressure drop is to use the transfer unit approach and the form:

$$N = -\ln Pt = b(\Delta p)^a. \qquad (6)$$

When this relationship is plotted on log-log paper, a straight line of slope a results. Cooper (1976)[2] noted that data from earlier work by Semrau and Witham (1974)[14] could be approximated not by one line but two, as in Figure 1. Further, he noted that if a relationship of the form of equation (6) held for each particle size (or for a monodisperse aerosol), it would be more efficient to use two or more scrubbers in series with total pressure drop Δp than one scrubber with the same Δp, if and only if the value of the exponent a was less than one. The extension of this principle was also presented for the two-branched curve; again, whether or not to use multiple stages depended upon whether or not the value of a was less than unity. Our calculated results for penetration versus pressure drop at $Q_L/Q_G = 1 \times 10^{-3}$ for d_g = 3.0, 1.05, 0.68 μm with $\sigma_g = 1.05$ (essentially monodisperse aerosols) are presented in Figure 2, with the lines characterizing the experimental results of Semrau et al. (1977).[5] The two-branched nature is still evident, and for the monodisperse aerosols there exists a pressure drop range for which the value of a is less than unity, the condition for which series scrubbing is attractive. The model includes only impaction as a modeled collection mechanism which changes with pressure drop, so that is is not necessary to invoke other collection mechanisms[7] to explain the existence of two branches, although the curved nature of the penetration versus pressure drop relation (approximated by the two-branched lines) may be partially due to the change in droplet diameter with

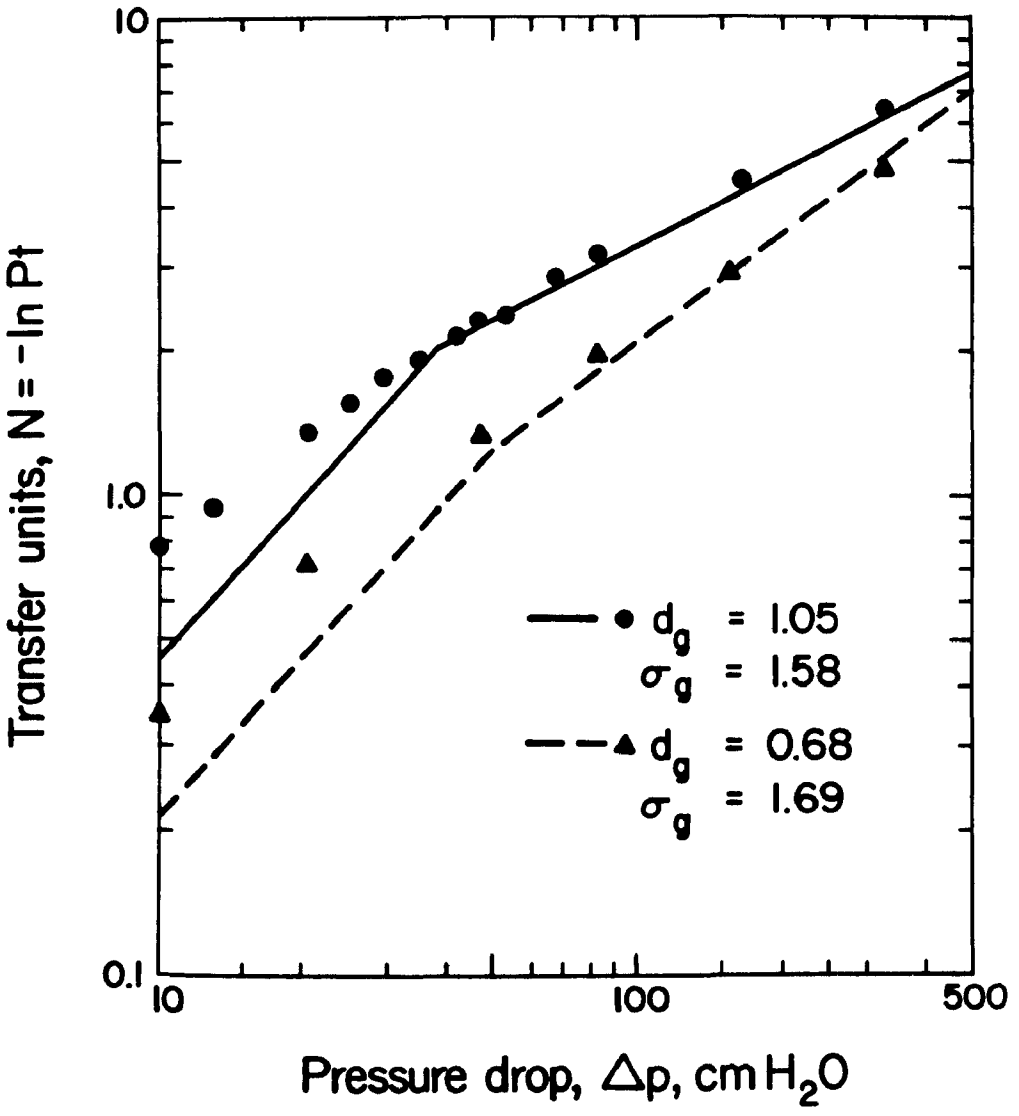

Figure 1. Penetration versus pressure drop: lines represent results of experiments with orifice scrubber by Semrau et al. (1977); circles and triangles are results of calculations with scrubber model for $Q_L/Q_G = 1 \times 10^{-3}$ and the same aerosol size distributions used in the experiments.

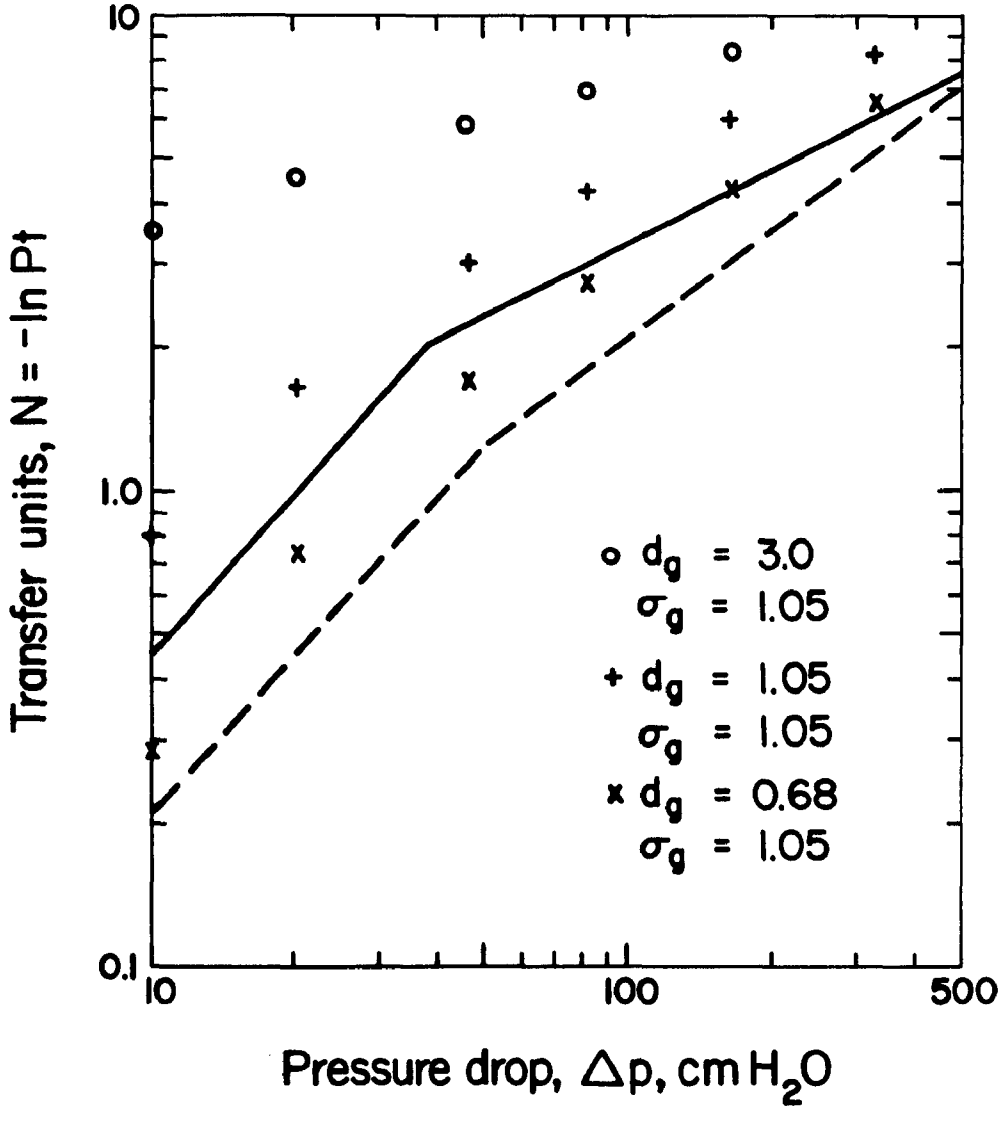

Figure 2. Penetration versus pressure drop: model calculations for monodisperse aerosol at $Q_L/Q_G = 1 \times 10^{-3}$ and the lines characterizing the experimental results of Semrau et al. (1977) for moderately polydisperse aerosols.

change in gas velocity (thus pressure drop).

Dimensional Analysis

It is generally useful to correlate data with dimensionless groups obtained from dimensional analysis. For example, pipe flow pressure drop is usually correlated with a friction factor f(Re), a function of Reynolds number. Scrubber penetration is dimensionless, so it must depend upon dimensionless groups. Using a standard method of dimensional analysis, Buckingham's Pi,[8] we found that penetration could be written as a function of some common dimensionless groups:

$$Pn = Pn(K,\ \Delta p'/\rho_G u_G^2,\ Q_L/Q_G,\ Re,\ d_p/d_d,\ d_d/D) \tag{7}$$

where

$Re = \rho_G u_G D/\mu_G$, the throat Reynolds number;
D = throat diameter (orifice diameter), cm.

(Other collection mechanisms, such as sedimentation, diffusion, electrostatic migration, would have enlarged this list of dimensionless groups.) Incorporating most of these terms make intuitive sense. The impaction parameter (K) characterizes the collection by a single droplet; the Reynolds number characterizes the flow; the ratio of the particle diameter to the droplet diameter characterizes interception; Q_L/Q_G indicates the concentration of collectors. It did not seem sensible to characterize pressure drop by $\Delta p'/\rho_G u_G^2$, however, and this led to consideration of alternate dimensionless groups.

Equation (4) indicates we could characterize pressure drop by using a combination of two dimensionless groups, $\Delta p/(\rho_G u_G^2)(Q_L/Q_G)$, which would then be constant for those conditions under which the equation (4) was applicable. Clearly, plotting Pt versus $\Delta p/(\rho_G u_G^2)(Q_L/Q_G)$ was not likely to be informative, especially where equation (4) holds and the latter group is a constant.

To obtain a more relevant dimensionless group, we turned to the equations for pressure drop and penetration in an infinitessimal collection volume of cross-section A and length dL. For N_d droplets per unit volume, the incremental pressure drop, assuming the droplets are nearly stationary,

$$d\,\Delta p' = N_d f(Re_d)\frac{\pi}{4} d_d^2 (\tfrac{1}{2}\rho_G u_G^2) dL \tag{8}$$

where

$\Delta p'$ = pressure drop, dyn/cm^2
$f(Re_d)$ = friction factor (not f)
$Re_d = \rho_G u_G d_d/\mu_G$.

The incremental change in penetration due to impaction only is:

$$d\,Pt = N_d \eta(K)\frac{\pi}{4} d_d^2\, dL \tag{9}$$

where

$\eta(K)$ = impaction collection efficiency for a droplet.

The ratio of the change in penetration to the change in pressure drop is:

$$\frac{\eta(K)}{(\frac{1}{2}\rho_G u_G^2) f(Re_d)} \tag{10}$$

which suggests that the dimensionless pressure drop should be

$$\eta(K)\Delta p'/(\tfrac{1}{2}\rho_G u_G^2) f(Re_d).$$

There are several approximate forms for f(Re) and $\eta(K)$; if one chooses Ingebo's correlation for accelerating droplets, $f(Re) = 55/Re_d$ (Calvert et al., 1972),[9] and $\eta \doteq 0.5K$ as a rough approximation for impactive efficiency, then a particularly simple form of dimensionless pressure drop results: (2/55) x $\Delta p'\tau/\mu_G$ or just $\Delta p'\tau/\mu_G$ where τ is the characteristic (or relaxation) time of the particles, the terminal settling velocity divided by the gravitational constant g. For spherical particles:

$$\tau = C\rho_p d_p^2/18\mu_G. \tag{11}$$

In Figure 3, we have re-plotted the lines characterizing the data from Semrau et al. (1977)[6] and the results of our calculations using the scrubber model. Here Pt is plotted against the dimensionless pressure drop $\Delta p'\tau/\mu_G$. Note the degree to which this helps correlate experimental results for the two aerosols, which have diameters such that the ratio of their characteristic times is $\tau(d_g = 1.05\ \mu m)/\tau(d_g = 0.68\ \mu m) = 2.2$. (Presumably, if the correlation variable for pressure drop were $\eta(K)\Delta p/f(Re_d)(\frac{1}{2}\rho_G u_G^2)$ the correlation would be even better.) The correlation shows less agreement at the higher pressure drops for both experimental and theoretical results, perhaps because the finest particles in the experiment were measured least well or diverge from the log-normal approximation, perhaps because the change in droplet diameter is not included in the correlation $\Delta p'\tau/\mu_G$ perhaps because the approximation $\eta \doteq 0.5K = \tau\mu_G/d_d$ is particularly poor here.

An alternative dimensionless group would be the ratio of the particle diameter to the scrubber cut diameter, the particle size for which the penetration is 0.50. This approach has been outlined by Calvert (1974),[10] and can sometimes be used conveniently, even though the cut diameter must be determined implicitly from equation (1). For standard conditions, graphs have been presented to simplify this (Calvert, 1974);[10] for other conditions, such techniques would have to be employed anew. It seems very convenient to know that to obtain Pt = 0.1 (at $Q_L/Q_G = 1 \times 10^{-3}$) for a given particle size requires $\Delta p'\tau/\mu_G$ of approximately 750 in any dimensionally consistent set of units and that the exponent a becomes less than 1 at $\Delta p'\tau/\mu_G \doteq 5 \times 10^2$. New values of τ and μ_G can readily be calculated for temperature and pressure conditions different from 20°C and one atmosphere pressure. (Note, for example, that $\Delta p'\tau/\mu_G$ has a μ_G^{-2} dependence.) This correlation group is not expected to work well when collection mechanisms other than impaction are important or when f(Re) is not proportional to Re^{-1}.

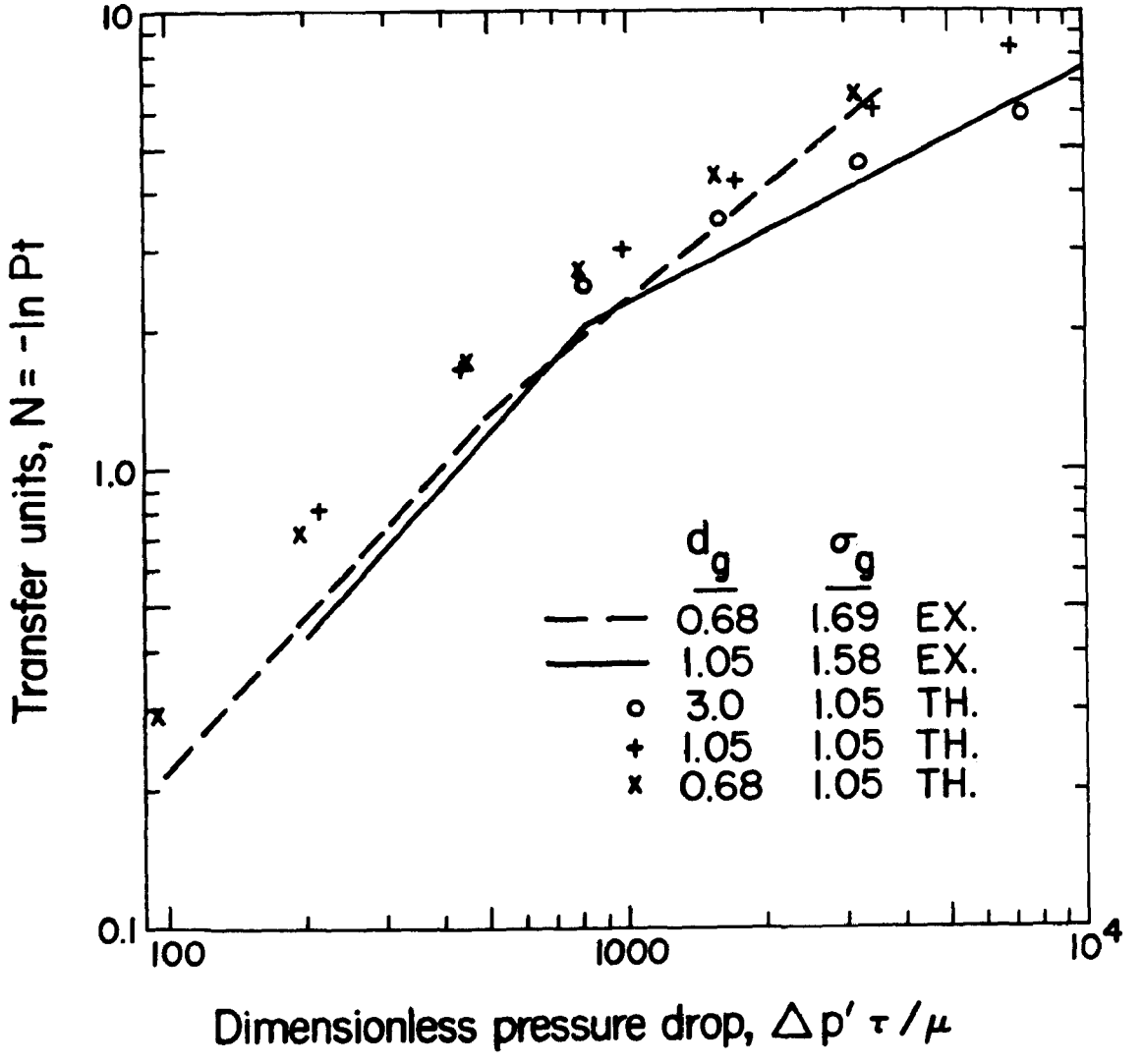

Figure 3. Penetration versus dimensionless pressure drop, $\Delta p' \tau / \mu_G$: theoretical results (TH.) for monodisperse aerosols (d_f = 0.68, 1.05, 3.0 μm) and the lines characterizing the experimental results (EX.) for polydisperse aerosols (d_g = 0.68, 1.05 μm) from Semrau et al. (1977).[5]

It has been shown by Leith (1979)[18] that at a constant pressure drop, the theoretical minimum penetration is achieved when

$$Kf = 2\tau\mu_G f/d_d = 1.10 \quad (12)$$

according to the model represented by equations (1) and (2). With equation (4), the model gives

$$Pt = \exp[-0.0155\ f^2\Delta p'\tau/\mu_G] \quad (13)$$

at the optimum combination of μ_G and Q_L/Q_G (thus optimum droplet diameter), and the number of transfer units is linearly related to the pressure drop. For f = 0.5 this equation predicts an optimal value of N = 2.9 or Pt = 0.055 in comparison with the non-optimal values shown in Figure 3 ($N \doteq 2.3$, $Pt \doteq 0.1$).

A simple example of the possible energy savings for a two-stage scrubber versus a single-stage device is found by comparing the dimensionless pressure drop needed for a single stage penetration of 0.01, $\Delta p'\tau/\mu_G \doteq 2000$, with the dimensionless pressure drop for two stages in series (each having 0.1 penetration), $\Delta p_1'\tau/\mu_G + \Delta p_2'\tau/\mu_G \doteq 750 + 750 = 1500$. Thus the two-stage device consumes 1500/2000 = 0.75 times the single-stage scrubber, a saving of about 25 percent. As is well-known, energy costs can predominate for high-energy scrubbers, so this saving could be quite significant.

Scrubber Optimization

One of the reasons for seeking penetration as a function of pressure drop is that the pressure drop times the volume flow rate divided by the fan efficiency is the power consumption of the scrubber, usually the dominant annualized cost item for high-energy ($\Delta p > 50$ cm H_2O) venturi scrubbers. Scrubbers can be designed to meet a given efficiency by specifying the throat velocity (μ_G) and the liquid-to-gas ratio (Q_L/Q_G), thus the pressure drop. These three factors, with total gas flow rate, are needed to predict capital and operating costs.

We have used the programmable calculator model to investigate the economically optimal design of a scrubber to achieve a penetration of 0.05 on the effluent from a coal-drying operation. In so doing, we have found a wide variety of pressure drops which are predicted to give the same collection efficiency, in apparent contradiction to the "contacting power theory." See, for example, Semrau (1977).[7] Table 2 from Dirgo (1979)[11] gives the result of a literature search for venturi scrubber operating conditions considered typical. The velocity range is 0.18×10^4 cm/s to 1.8×10^4 cm/s and the liquid-to-gas volume flow ratios ranged from 0.25×10^{-3} to 5.5×10^{-3}. The optimization described next was carried out within these ranges.

The conditions for the coal drying process were adapted from Calvert et al. (1972)[9] and the Particulate Pollutant System Study:[15] a gas flow of 150,000 m^3/hr at 70°C containing particles (after precleaning with a cyclone) of $\rho_p = 1.35$ g/cm^3, $d_g = 3.0$ μm and $\sigma_g = 4.4$, a very polydisperse aerosol. Table 3 shows the results of more than two score trial-and-error calculations

by Dirgo (1979)[11] seeking penetrations of 0.050 (to two significant figures). It is evident that penetration is not predicted to be a single-valued function of pressure drop within the range of throat velocities (μ_G) and liquid-to-gas ratios (Q_L/Q_G) encountered in practice. From these results, the most efficient Q_L/Q_G ratio in terms of pressure drop minimization was 1.2×10^{-3} in agreement with the recommendation of Calvert (1977).[1] The sensitivity of the penetration to changes in the pressure drop for $Q_L/Q_G = 0.9\text{-}1.25 \times 10^{-3}$ was $\Delta Pt = 0.0003$ per $\Delta(\Delta p) = 1$ cm H_2O, which indicates the predicted penetration penalty incurred by lowering the pressure drop, under these conditions.

Table 2. TYPICAL VENTURI SCRUBBER OPERATING PARAMETERS

Gas Velocity (u_G)[a]	Liquid/Gas Ratio(Q_L/Q_G)	Source
150-160 ft/s 4572-18288 cm/s	5-40 gallons/1000 ft^3 0.68-5.47 x 10^{-3} m^3/m^3	Hesketh (1974)[12]
5000-15000 cm/s	0.25-4.0 x 10^{-3} m^3/m^3	Calvert et al.(1972)[9]
3500 ft/min 1778 cm/s	3-20 gallons/1000 ft^3 0.41-2.74 x 10^{-3} m^3/m^3	(Kinley and Neveril, 1976)[13]
200-600 ft/s 6096-18288 cm/s	5-7 gallons/1000 ft^3 0.68-0.96 x 10^{-3} m^3/m^3	(NAPCA, 1969)[14]
200-400 ft/s 6096-12192 cm/s	5-20 gallons/1000 ft^3 0.68-2.74 x 10^{-3} m^3/m^3	(Calvert, 1977)[4]

[a] Parameters are reported first as they appear in the literature. They have been converted to units of cm/s for u_G and m^3/m^3 for Q_L/Q_G for purposes of comparison and because these are the units required by the SR-52 venturi scrubber model.

Rather than minimizing pressure drop at a given efficiency, one would prefer to minimize annualized costs (these include capital and operating expenses). Dirgo (1979)[11] used cost equations from Calvert et al. (1972)[9] and from Kinley and Neveril (1976),[13] with costs inflated to May 1977; he noted that his final capital cost estimates were in the high end of the range of the reported values. The annual costs were dominated by the operating costs and the operating costs were dominated by the power costs. Figure 4 has a series of budget lines for operating costs (OC) from his analysis; these show the operating costs for having the indicated Δp and Q_L/Q_G (exclusive of water pollution costs, which should depend upon liquid recycling practices). By finding the point of tangency between the budget lines and the constant penetration curve[16] one can select the operating conditions which minimize operating costs; here the predicted minimum in OC occurs for Q_L/Q_G between 1.1 and 1.2×10^{-3} and $\Delta p = 114$ cm H_2O. For high-energy venturis, the optimal conditions for minimizing operating costs will be near those for

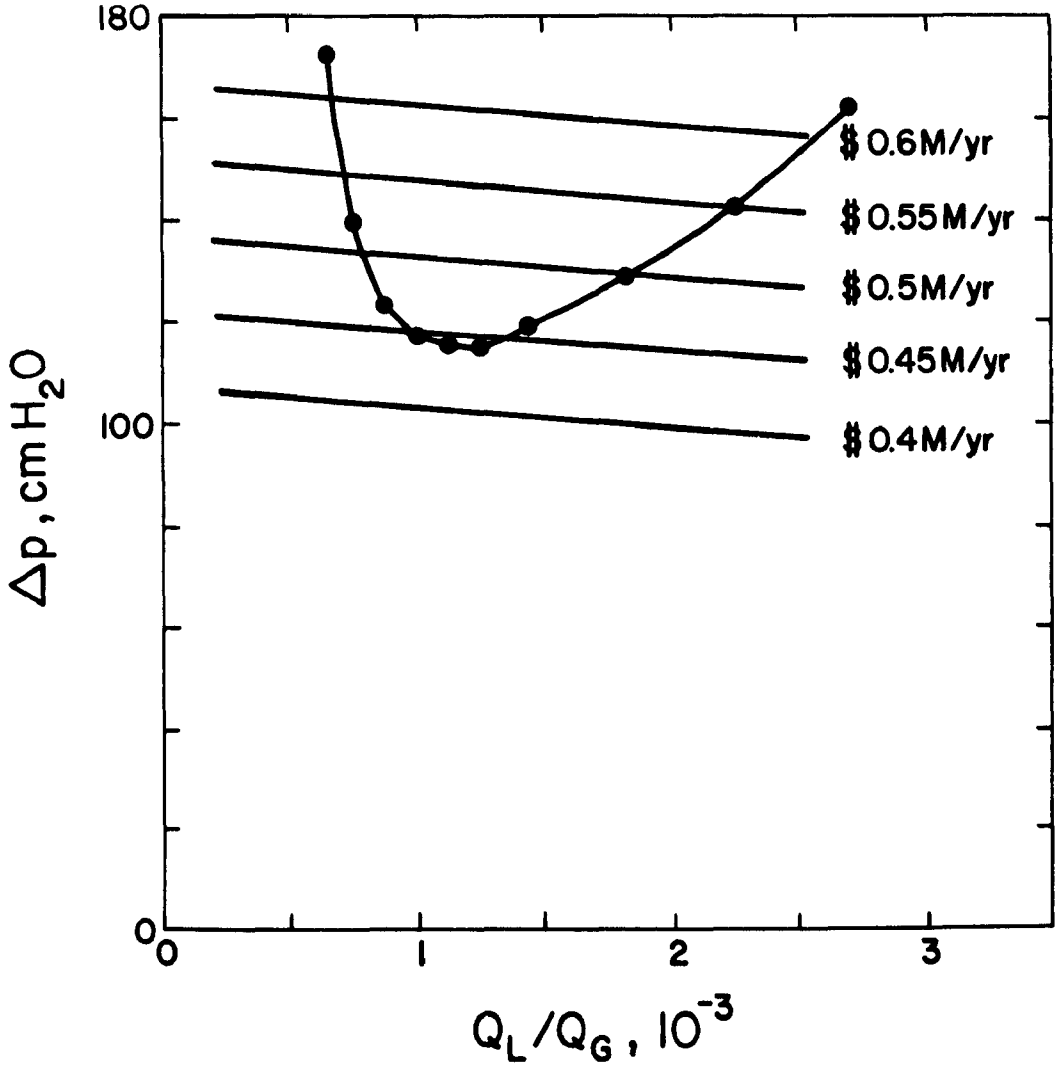

Figure 4. Locus of predicted pressure drop and liquid-to-gas ratio values giving penetration = 0.050 for coal drying process control example, along with budget lines for predicted operating costs.

minimizing pressure drop, because of the dominant cost of energy. For low-energy scrubbers other operating costs could make the budget lines less nearly horizontal in plotting Δp vs. Q_L/Q_G, and the minimum cost might be at a substantially higher pressure drop than the minimum pressure drop.

Table 3. Q_L/Q_G AND Δp FOR Pt=0.050 FOR HYPOTHETICAL COAL DRYING APPLICATION

Q_L/Q_G (10^{-3})	u_G (cm/sec)	Δp (cm H_2O)
0.645	18000	172.2
0.75	15000	139.1
0.875	13075	123.3
1.00	11900	116.7
1.125	11150	115.2
1.25	10550	114.6
1.44	10000	118.7
1.82	9250	128.3
2.25	8750	141.9
2.70	8500	160.7

For the method of steepest ascent,[19] one makes a small change from the "base" case in one variable and measures the rate of change of the penetration with respect to pressure drop, $\Delta(Pt)/\Delta(\Delta p)$. Next, the other variable is changed from the base case and the rate of change determined. A new base case is chosen, by changing either or both variables, guided by which variable gave the greatest rate of change of penetration per change in pressure drop. In Table 4, an example of a similar, simple optimization procedure is given. The first column lists the operating conditions, their changes (if any), and the results of such changes. The next columns give the values of the variables in the first column for: the first base case; the first trial; the difference between the base and trial 1; the second trial; the difference between the base and trial 2; and, finally, the new base, determined by raising the liquid-to-gas ratio by 10 percent and lowering the velocity to keep the pressure drop constant (guided by equation (4)). The example shows a decrease in penetration from 0.014 to 0.010 for this monodisperse aerosol, while the pressure drop has been returned to its original value.

DISCUSSION

This discussion will focus on the implications of these results for multi-stage versus single-stage scrubbing. As has been shown elsewhere (Cooper, 1976),[2] if the exponent in the expression $-\ln Pt = N = b\Delta p^a$ is less than one, it is optimal (for energy consumption) to use multiple venturi stages in series rather than a single stage. The same reference gives the mathematical criteria for single-stage versus multiple-stage scrubbing for a two-branched

curve; even without the criteria, it would be easy to determine through trial calculations whether or not multiple stages should be used, if Δp is high enough that the exponent a is less than one. (The penetration through the series is just the product of the penetrations through the individual stages. One can also just sum their transfer numbers.) If the change in the exponent a as pressure drop is changed were due to aerosol polydispersity, then this analysis would have been incorrect, as noted previously (Cooper, 1976),[2] but that has been shown not to be the case (see Figure 2).

Table 4. EXAMPLE OF SCRUBBER OPTIMIZATION ITERATION (d_g = 1.05 μm, σ_g = 1.05, T = 25°C, f = 0.5)

Conditions	base	trial 1	(change)	trial 2	(change)	new base[a]
u_G, 10^4 cm/s	1.0	1.05		1.0		0.953
$\Delta(u_G)$, 10^4 cm/s			0.05		0.0	
Q_L/Q_G, 10^{-3}	1.0	1.0		1.1		1.1
$\Delta(Q_L/Q_G)$, 10^{-3}			0.0		0.1	
Pt	0.0142	0.0113		0.0080		0.0104
$-\Delta$(Pt)			0.0029		0.0064	
Δp, cm H_2O	82.4	90.85		90.64		82.4
$\Delta(\Delta p)$, cm H_2O			8.45		8.24	
$-\Delta(Pt)/\Delta(\Delta p)$			0.0034[a]		0.00075[a]	

[a] $-\Delta(Pt)/\Delta(\Delta p)$ is greater for increasing Q_L/Q_G than for increasing u_G, so (Q_L/Q_G) should be increased to form new base, keeping Δp constant.

Superior collection by multiple-stage venturi scrubbers over single-stage venturis would follow from diminishing returns, in terms of collection efficiency, at high pressure drops (high throat velocities). A convenient way to picture this is to imagine that one raises the pressure drop in a test scrubber by increasing gas velocity only (constant Q_L/Q_G). If the droplets were of optimal size, then equation (13) shows that the number of transfer units will be linearly related to pressure drop. As one lowers the velocity, the number of transfer units will decrease more strongly than linearly because not only is the pressure drop decreasing, but the droplets are becoming non-optimal in size. As the velocity is increased, the number of transfer units will increase less than linearly with pressure drop because the droplets again are becoming non-optimal in size.

Calvert (1977)[1] pointed out that for large particles for which the single droplet collection efficiency is almost unity, the penetration is limited by Q_L/Q_G. A multiple-stage scrubber effectively multiplies the effectiveness of Q_L/Q_G by the number of stages employed, if all the water is added upstream of the first stage. Although a previous analysis (Cooper, 1976) showed that it was optimal in terms of pressure drop to divide the pressure drop equally

among the stages of a multiple-stage scrubber, it may not be best to have Q_L/Q_G be the same for every stage...perhaps the first stage(s) should be at low Q_L/Q_G and more water should be added immediately upstream of successive stages, to optimize the product of droplet area, collection efficiency, and path length for the particles reaching the latter stages, while keeping the same pressure drop per stage.

Another advantage of multiple-stage scrubbing not evident in this analysis is that particle growth by condensation may take place in the first stage(s), thus facilitating capture; condensation may be enhanced by expansion and cooling at the diverging portion of the first stage(s). Also, the multiple-stage device would tend to have longer contact time for gaseous and particulate diffusion.

Certainly, capital costs must be taken into account, but for submicrometer aerosols that have to be scrubbed at high energy, the power savings from multiple-stage scrubbing may outweigh increased construction costs.

CONCLUSIONS

The scrubber model developed by Calvert et al. (1972)[9] and programmed by Sparks (1978)[3] was quite useful. The two-branched nature of a log-log plot of transfer units ($N = -\ln Pt$) versus pressure drop was shown not to be an artifact due to the use of polydisperse aerosols nor to require for explanation of its shape any other collection mechanism than impaction. (Actually, the fitting of two lines to the curve of log N versus log Δp is only one of many possible approximations by any number of straight lines.) A dimensionless pressure drop, $\Delta p'\tau/\mu_G$, was found to be useful for correlating experimental data and theoretical predictions of penetration. The model predicts that penetration is sometimes not uniquely related to pressure drop, even within the ranges of gas throat velocity and liquid-to-gas ratio found in practice. It was shown that Q_L/Q_G and Δp can be adjusted to minimize operating costs with the help of the model. Results of the simulations support the hypothesis (Cooper, 1976)[2] that multiple-stage venturi scrubbers would be more efficient than single-stage venturi scrubbers for high-energy scrubbing (at the same total pressure drop).

ACKNOWLEDGMENTS

The author gratefully acknowledges the aid of Richard C. Antonelli and John A. Dirgo, both graduate students at the Harvard School of Public Health, in carrying out many of the SR-52 programmable calculator runs, and the finanical support of the U.S. Public Health Service through its program grant for environmental management,5 D04 AH 01475.

REFERENCES

1. Calvert, S. Scrubbing. In: Air Pollution. Stern, A.C.(ed.). New York, Academic Press, 1977.

2. Cooper, D.W. Theoretical Comparison of Efficiency and Power for Single-Stage and Multiple-Stage Particulate Scrubbing. Atmos Environ 10:1001-1004, 1976.

3. Sparks, L.E. SR-52 Programmable Calculator Programs for Venturi Scrubbers and Electrostatic Precipitators. EPA-600/7-78-026. U.S. Environmental Protection Agency. Office of Research and Development. Washington, D.C. 1978.

4. Calvert, S. How to Choose a Wet Scrubber. Chem Eng, August 29, 1977.

5. Semrau, K.T., C.L. Witham, and W.W. Kerlin. Relationships of Collection Efficiency and Energy Dissipation in Particulate Scrubbers. (Presented at the Second Fine Particle Scrubber Symposium, New Orleans, May, 1977. Sponsored by the U.S. Environmental Protection Agency.)

6. Semrau, K.T., C.L. Witham, and W.W. Kerlin. Energy Utilization by Wet Scrubbers. EPA-600/2-77-234. U.S. Environmental Protection Agency. Office of Research and Development. Washington, D.C. 1977.

7. Semrau, K.T. Practical Process Design of Particulate Scrubbers. Chem Eng, September 26, 1977.

8. Baumeister, T., E.A. Avallone, and T. Baumeister, III, eds. Marks' Standard Handbook for Mechanical Engineers. New York, McGraw Hill, 1978.

9. Calvert, S., J. Goldshmid, D. Leith, and D. Mehta. Scrubber Handbook. EPA-R2-72-118, NTIS No. PB-213-016, NTIS, U.S. Department of Commerce. 1972.

10. Calvert, S. Engineering Design of Wet Scrubbers. J Air Pollution Control Association. 24:929-934, 1974.

11. Dirgo, J.A. Personal communication. Harvard School of Public Health. Boston, MA. 1979.

12. Hesketh, H. Understanding and Controlling Air Pollution. Ann Arbor, Ann Arbor Science Publ., 1974.

13. Kinley, M.L. and R.B. Neveril. Capital and Operating Costs of Selected Air Pollution Control Systems. EPA-450/3-76-014. U.S. Environmental Protection Agency. Washington, D.C. 1976.

14. National Air Pollution Control Administration. Control Techniques for Particulate Air Pollutants. AP-51, United States Department of Health, Energy, and Welfare. Washington, D.C. 1969.

15. Midwest Research Institute. Particulate Pollutant Systems Study. Volume III, Handbook of Emission Properties. Contract CPA 22-69-104. U.S. Environmental Protection Agency. Washington, D.C. 1971.

16. de Neufville, R. and J.H. Stafford. Systems Analysis for Engineers and Managers. New York, McGraw-Hill, 1971.

17. Sparks, L.E. Importance of Particle Size Distribution. (Presented at the Symposium on the Transfer and Utilization of Particulate Control Technology, Denver, CO., July 1978. Sponsored by the U.S. Environmental Protection Agency.)

18. Leith, D.H. Personal communication. Harvard School of Public Health. Boston, MA. 1979.

19. Cochran, W.G. and G.M. Cox. Experimental Designs. New York, John Wiley and Sons, 1957.

APPENDIX

The similar performance of some scrubbers at a given pressure drop but different liquid-to-gas ratios (equivalently, different velocities) seemed to contradict the results in Figure 4, which showed quite different performance, for different Q_L/Q_G at the same pressure drop, on an aerosol (d_g = 3.0 μm). Using the Calvert model as given in the body of the paper, and the pressure drop group, one can write the number of transfer units as (Leith, 1979):[18]

$$N = (4/55)(\tau\Delta p'/\mu_G)K^{-1}F(K,f). \qquad (A.1)$$

Therefore, the change in the number of transfer units at constant pressure drop becomes:

$$\Delta N = (4/55)(\tau\Delta p'/\mu_G)\Delta[K^{-1}F(K,f)] \qquad (A.2)$$

The change in number of transfer units is most sensitive to changes in the bracketed group ($K^{-1}F(K,f)$) for large values of $\tau\Delta p'/\mu_G$ (large particles, high pressure drops or, simply, high collection efficiencies). For a particle of 1 μm aerodynamic diameter at $Q_L/Q_G = 1 \times 10^{-3}$ and $u_G = 0.5 \times 10^4$ cm/s, increasing the velocity by 10 percent (decreasing Q_L/Q_G by 21 percent to keep pressure drop constant)gave only a 4 percent decrease in $K^{-1}F(K,f)$, changing the number of transfer units by 0.055 and producing a penetration of 1.06 times the original, a negligible change. For the same conditions, a particle of 5 μm aerodynamic diameter would have $\tau\Delta p'/\mu_G$ be 22 times larger, $\Delta N = 1.01$, and the predicted penetration would increase three-fold, from Pt = 0.0041 to Pt = 0.011, a quite appreciable change.

THE IMPACT OF HUMIDIFICATION CHAMBER PHYSICS ON WET GAS CLEANUP SYSTEMS

By:
D. P. Bloomfield
M. L. Finson
G. A. Simons
K. L. Wray

Physical Sciences Incorporated
Woburn, Massachusetts 01810

ABSTRACT

The performance of the humidification chamber in wet gas cleanup systems is central to the effectiveness of the entire system. We have presented the theoretical analysis and the results obtained from a preliminary investigation of humidification chamber processes namely water droplet evaporation and tar condensation. The major findings of the analysis are that sharp temperature gradients and the absence of dust (seed nuclei) in the chamber lead to the formation of fine tar droplets which may be impossible to separate from the gas phase. A moderate temperature gradient will favor heterogeneous tar condensation and yields tar droplets of a more readily collectable size.

THE IMPACT OF HUMIDIFICATION CHAMBER PHYSICS ON WET GAS CLEANUP SYSTEMS

The removal of tars and particulate materials from the effluent stream of a coal gasifier is of major importance in both a power generation sense and in an environmental sense. Gas cleanup systems represent a major cost in powerplant design and their effective operation is crucial to the successful operation of coal gasifier powerplants. The wet gas cleanup system presently under study at the Morgantown Energy Technology Center is an attractive approach to tar, particulate and sulfur removal.

Figure 1 shows the relative location of components in the wet gas cleanup system. The humidification chamber in Figure 1 is a direct contact heat exchanger where the gasifier effluent is cooled by a recycle liquor spray. As the gas cools, high boiling tar condenses. Tar condensation may occur by homogeneous nucleation or heterogeneous condensation. In the former case, under conditions of intense subcooling, tar droplets form from the gas phase The nature of the process is such that a very large number of extremely fine droplets form. The formation rate can be extremely fast. Once formed, the droplets coalesce, but this process is relatively slow. As a consequence, the tar particle droplets at the exit of the humidification chamber may be too small to capture in downstream scrubbers. If the temperature profile is more gradual, and particularly if a large quantity of ash is present, heterogeneous condensation can occur. In this case, vapor phase tar condenses on dust nuclei. The resulting tar droplets can be relatively large and easier to capture in the downstream separators.

FIRST LAW ANALYSIS

Using the operating conditions specified in Ref. 1, one may determine the composition of the gas stream entering the humidification chamber. For an inlet gas flow rate of 180,000 SCFH, the total molar flow rate into the humidification chamber is about 535 lb mol/hr. In order to cool the inlet gas stream to an exit temperature of 320°F, about 167 lb mol/hr of water must be added. This effectively sets the mol fraction of water at the exit of the humidification chamber at about 38%, the total exit molar flow rate being about 702 lb mol/hr.

By setting the water vapor exit mole fraction, the heat balance also sets a limit on the system pressure. Increasing the pressure to 234 PSIA will saturate the exit stream. Above this pressure decreasing amounts of water are evaporated and exit temperature increases. In order to operate above 234 PSIA, either the gasifier steam to carbon ratio must be reduced, or the allowable exit temperature from the humidifier must be increased above 320°F.

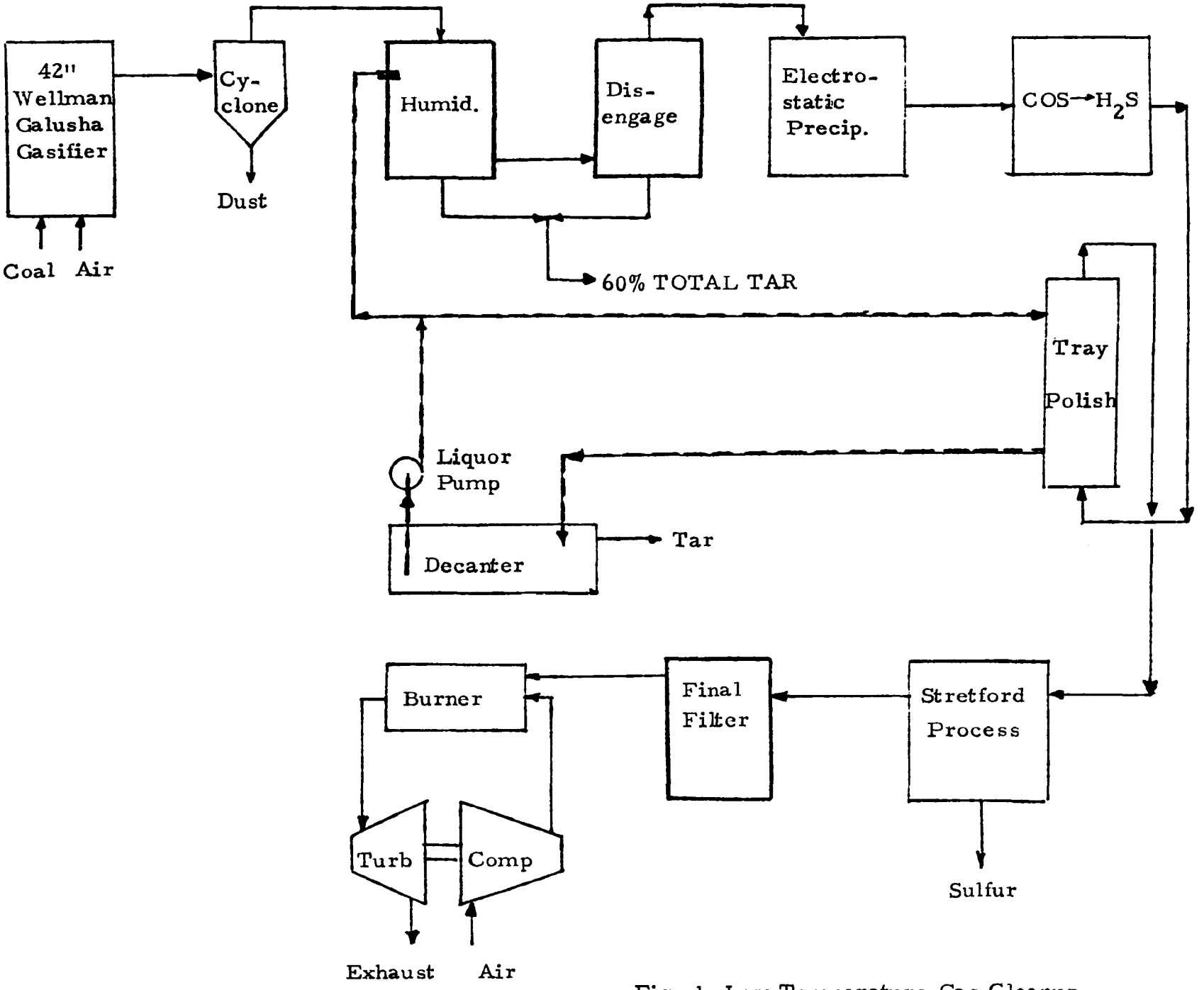

Fig. 1 Low Temperature Gas Cleanup

DROPLET EVAPORATION

A fine liquid spray is injected into the humidification chamber. The sole function of this spray is to cool the gas stream from its inlet temperature of 1100°F to a temperature of 320°F. The temperature gradient in the humidifier is created by the transfer of the gas stream's sensible heat to the water droplets of the spray.

The major difference between the humidification chamber and conventional spray towers is that the difference between the gas and droplet temperature in conventional equipment is generally small, on the order of 100°F. In the case of the humidification chamber, the difference between droplet and gas temperature is on the order of ~1000°F.

An expression for droplet evaporation at high mass flux where heat conduction to the droplet is considered rate limiting is readily derived from first law and continuity balances between the droplet phase and the gas phase. Equation (1) shows the time rate of change of droplet diameter.

$$\frac{dr}{dt} = \frac{-k}{\lambda \rho_L r} \left[T_G - T_L - \frac{\lambda}{C_p} \ln \left(1 + \frac{M_L}{M_G} \left(1 - \left(\frac{r}{r_o} \right)^3 \right) \right) \right] \quad (1)$$

where k is the gas conductivity, λ is the latent heat of vaporization, ρ_L is the liquid density, T_G is the inlet gas temperature, T_L is the inlet liquid temperature, C_p is the gas specific heat and M_L and M_G are the inlet liquid and gas mass flow rates. The results of numerically integrating the above expression are shown in Figure 2. It is apparent from Figure 2 that if the injected droplets are small.sharp temperature gradients will be formed. As we will show, this has an important bearing on tar condensation.

If we assume that the diffusion of steam away from the droplet is rate limiting, then droplet evaporation is described by Penetration Theory[3]. Using Penetration Theory, the heat and mass transfer co-efficients are calculated using the Chilton-Colburn analogy. These may be combined with a first law and continuity balance along with the properties of water in an algorithm which gives droplet radius as a function of time. The penetration theory results we show in Figures 3 and 4. Comparing the penetration theory results with the heat transfer limited case leads to the conclusion that penetration theory is applicable in the lower region of the humidification chamber and then only when saturation conditions are approached.

TAR CONDENSATION PHENOMENA

While high boiling coal tar is obviously not a pure substance, a preliminary treatment of tar droplet formation demands this type of simplification. The physical tar properties used in the analysis are shown in Table 1.

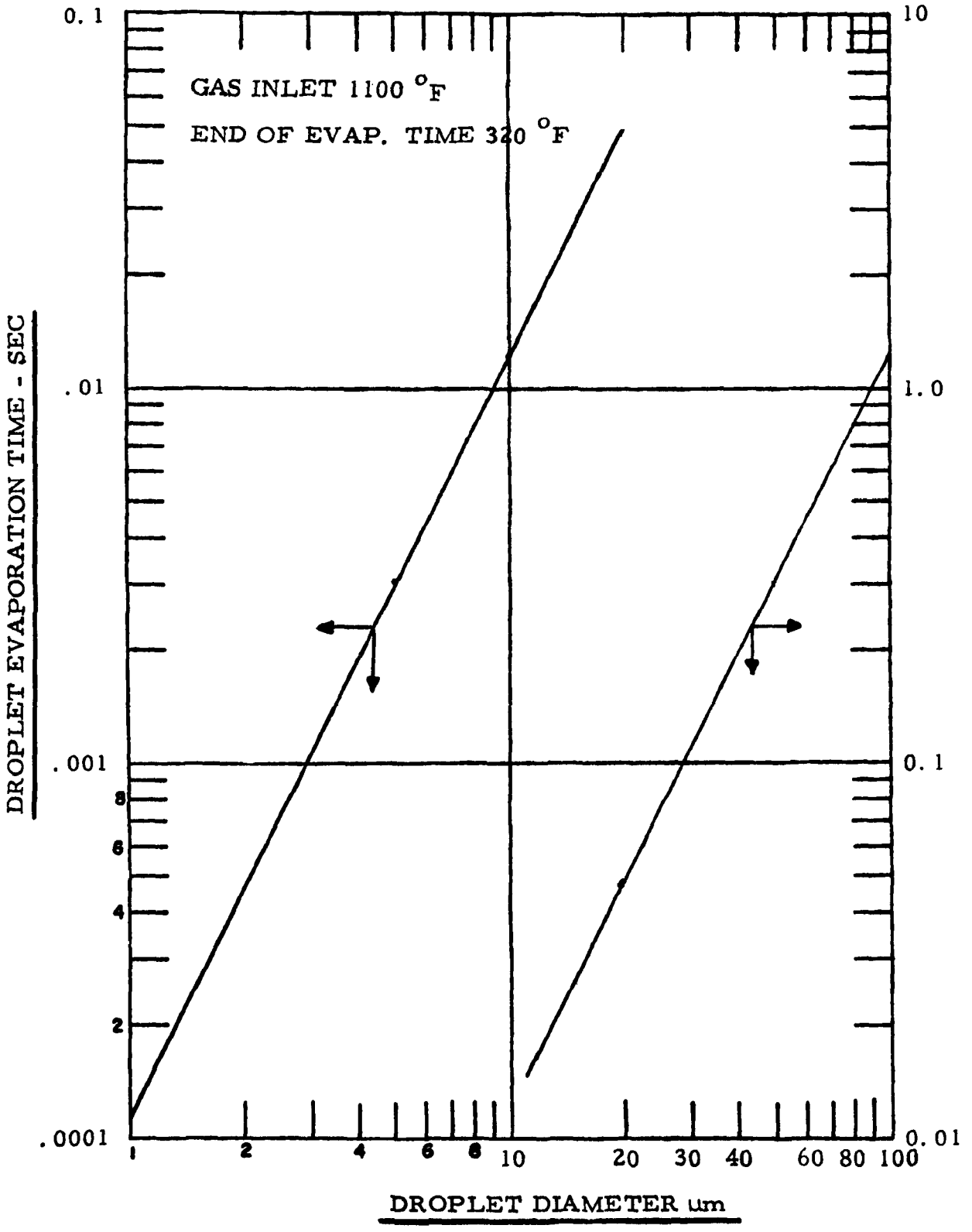

Fig. 2 Effect of Droplet Injection Diameter on Evaporation Time - Heat Conduction Limiting

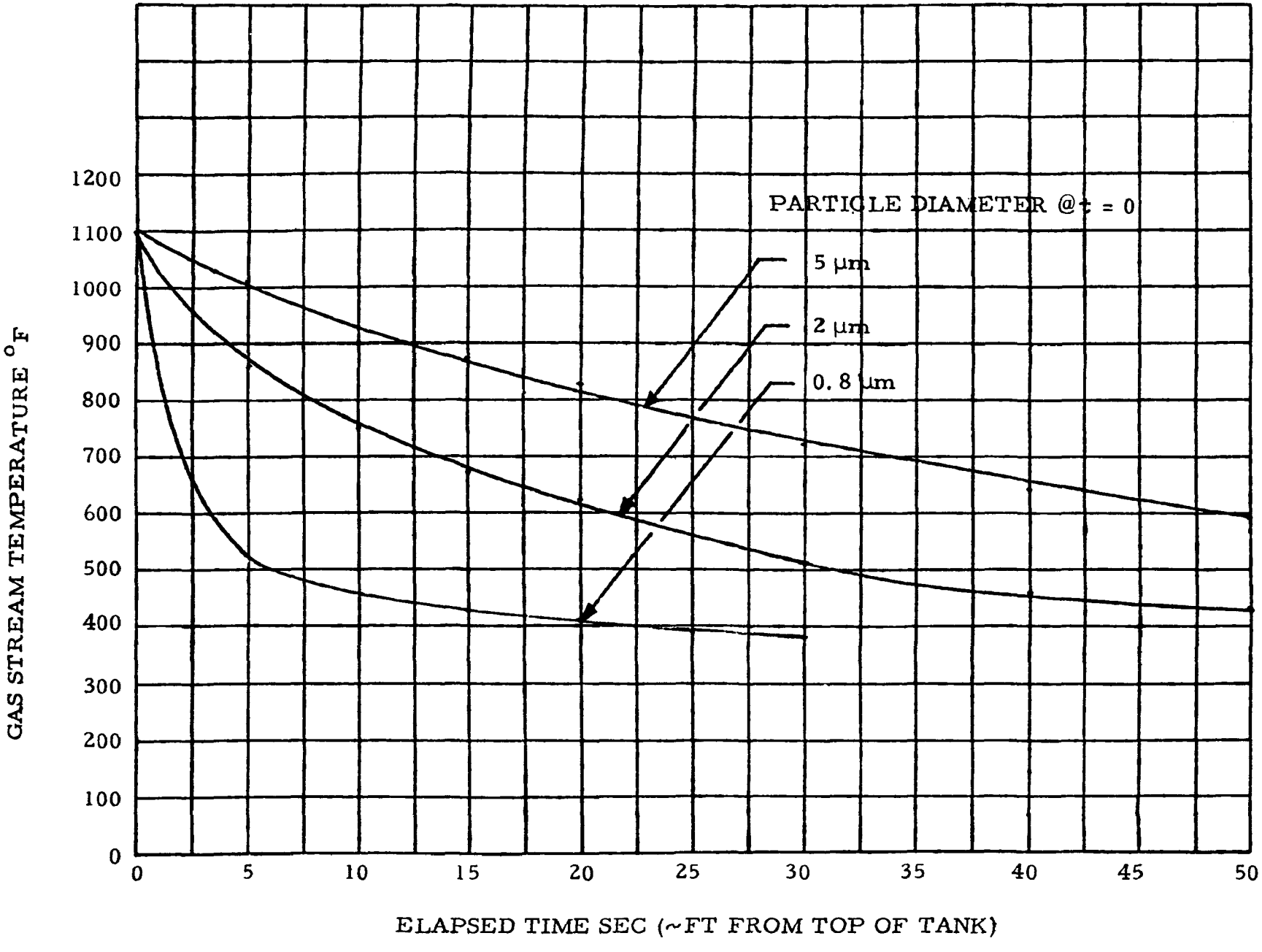

Fig. 3 Effect of Initial Particle Diameter on Temperature Profile - Penetration Theory

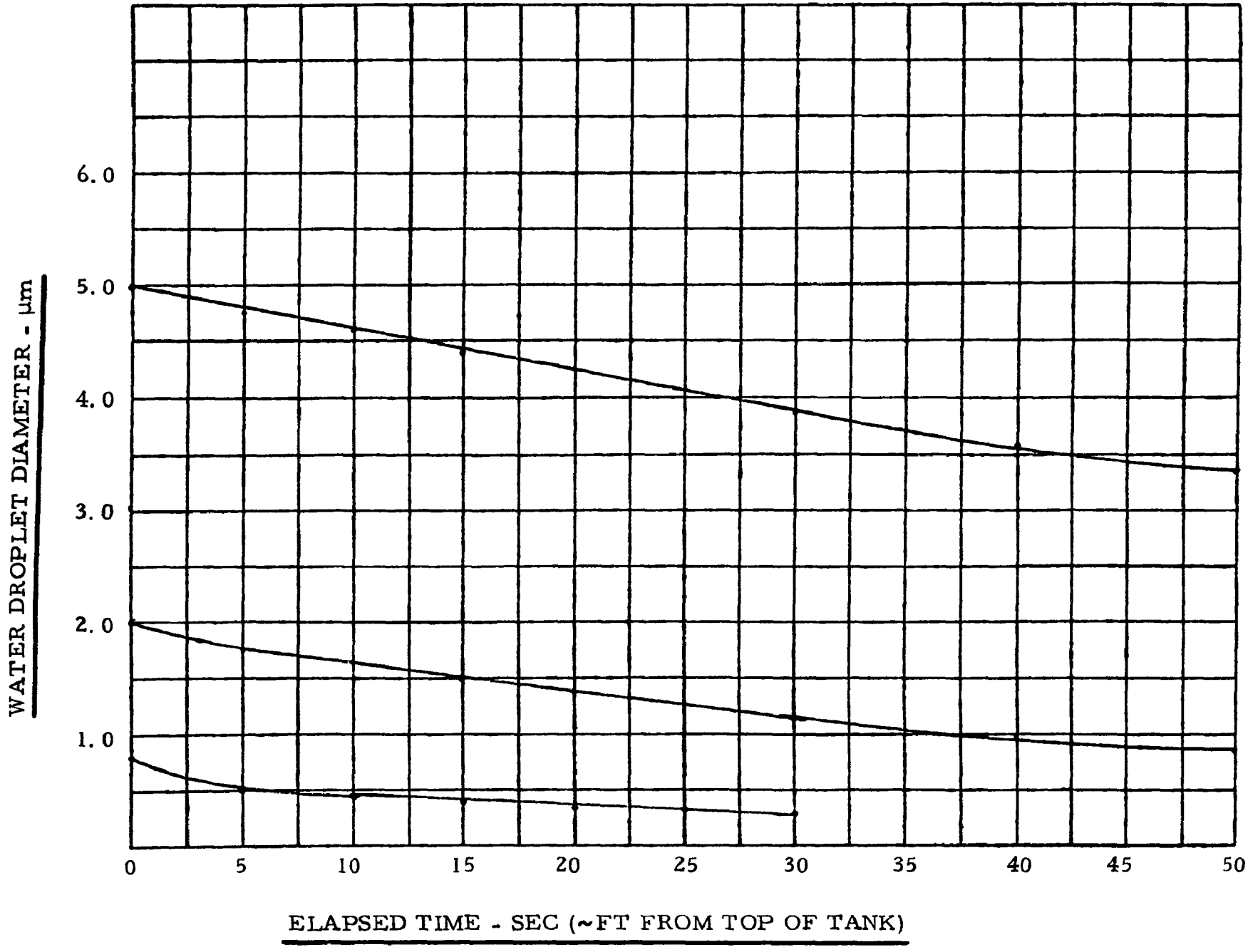

Fig. 4 Effect of Evaporation on Drop Diameter - Penetration Theory

The most significant of these properties is surface tension.

TABLE 1

PROPERTIES OF HIGH BOILING TAR [7]

Boiling Point Range

Temp °C	Tar Fraction %
250	20
250-360	15
360-450	15
450	50

Average Molecular Weight	250
Average Specific Gravity	1.1
Latent Heat of Vaporization	75 cal/gm
Surface Tension	36 dyne/cm (Temp Unknown)

In the absence of data on the surface tension at higher temperatures, this property has been treated parametrically. Tar condensation is described by two processes: nucleation and coalescence. In both of these processes, dust particles may play a significant role. It is recognized that tar emulsified in the recycle liquor may play an important role in the condensation process. In this analysis, tar injected with the recycle liquor has been ignored.

TAR NUCLEATION

While the mass of dust particles in the inlet of the humidification chamber may be significant, the number density of these particles may be quite low. When the number density of dust particles is large, heterogeneous nucleation may be dominant. If the number density of particles is small, then homogeneous nucleation is the more important phenomenon. In our preliminary treatment of homogeneous nucleation, we have examined initial rates. A more accurate analysis requires the treatment of homogeneous nucleation as a coupled phenomenon since the nucleation of liquid tar droplets will obviously influence the concentration of tar vapor. The homogeneous nucleation process requires the formation of critical radius (r*) particles. The critical radius, concentration of particles of critical radius and rate of formation of critical radius particles is determined by the gas stream temperature. In our analysis

we have used the Clausius-Clapeyron form of the Thomson equation for critical radius:

$$r^* = \frac{2\sigma v_B}{\lambda\ (1 - T/T_o)} \tag{2}$$

where σ is the surface tension, v_B is the volume per molecule of tar, λ is the latent heat of vaporization, T is the local temperature and T_o is the tar saturation temperature. The concentration of particles of critical radius (particles/cm^3) is given by:

$$Ng^* = N \exp\left(\frac{-4\pi}{3} \quad \frac{\sigma r^{*2}}{KT}\right) \tag{3}$$

where N is the total number of tar molecules per cubic centimeter in the inlet gas. The formation rate of critical radius particles (particles/sec-cm^3) is:

$$Q = Ng^* \left(\frac{v_b}{2\pi r^{*2}} \sqrt{\frac{\sigma}{KT}}\right) \frac{4\pi r^{*2} P}{\sqrt{2\pi m KT}} \tag{4}$$

where P is the partial pressure of tar and m is the mass of a tar molecule. While the errors associated with calculated homogeneous nucleation rates are sometimes large, they may be taken as the lower bound on the actual nucleation rate. Classical theory predicts onset of nucleation accurately.

An examination of Eqs (2) - (4) shows why the surface tension of the tar particle is so important. Fig. 5 shows the critical radius of tar particles as a function of gas stream temperature. It is apparent that a sharp decrease in temperature in the humidification chamber represents a high degree of subcooling of the tar vapor. Under these conditions, the critical size becomes extremely small. Further, the critical particle radius is proportional to the surface tension. Fig. 6 shows that the concentration of particles is an exponential function of the gas temperature and Fig. 7 shows the impact of gas temperature on the rate of formation of critical size tar droplets.

In the condition where the gas temperature in the humidification chamber is dropped sharply (fine water droplets), a very large number of very fine tar particles is formed very rapidly.

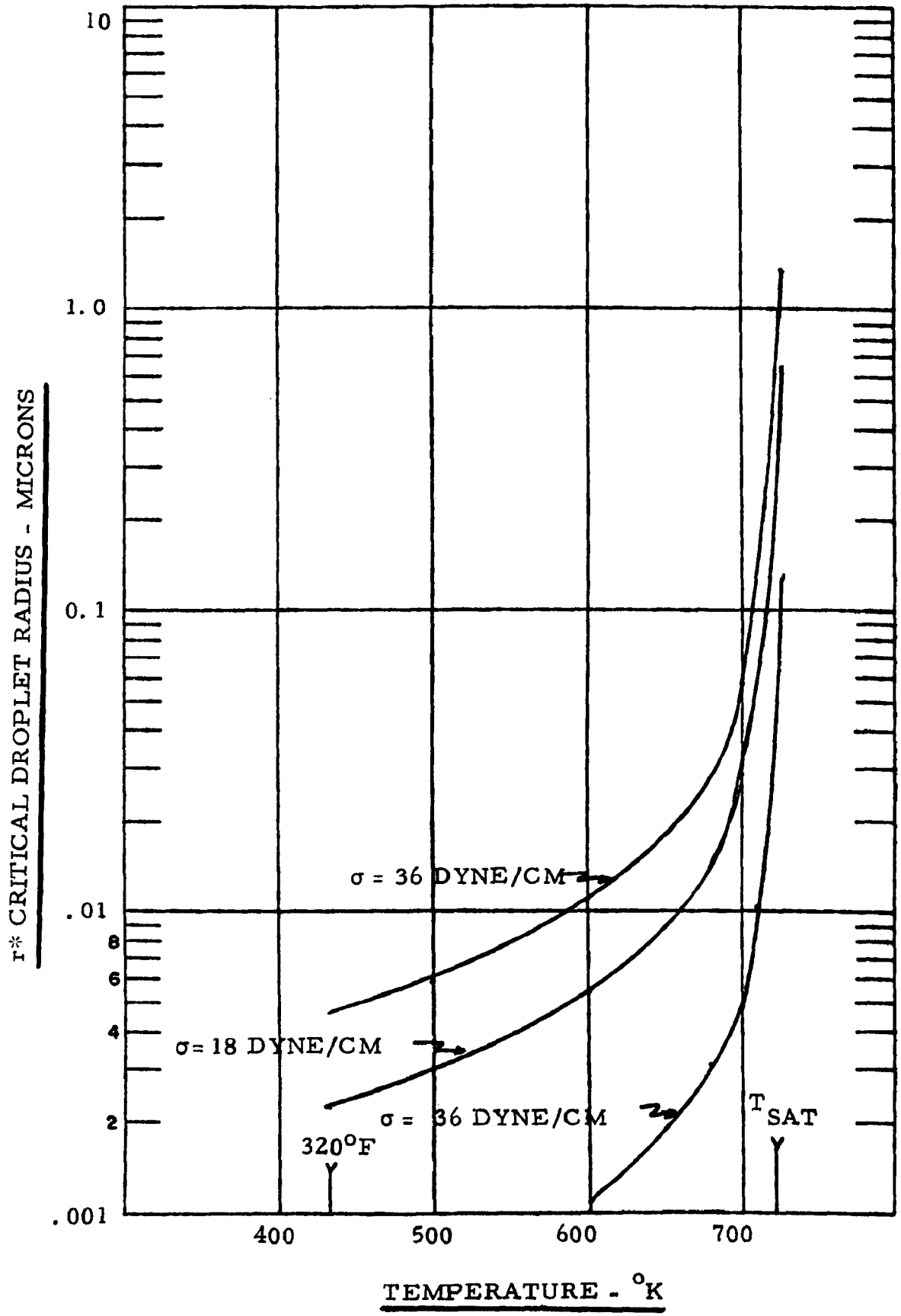

Fig. 5 Homogeneous Nucleation Effect of Temperature on Critical Drop Radius

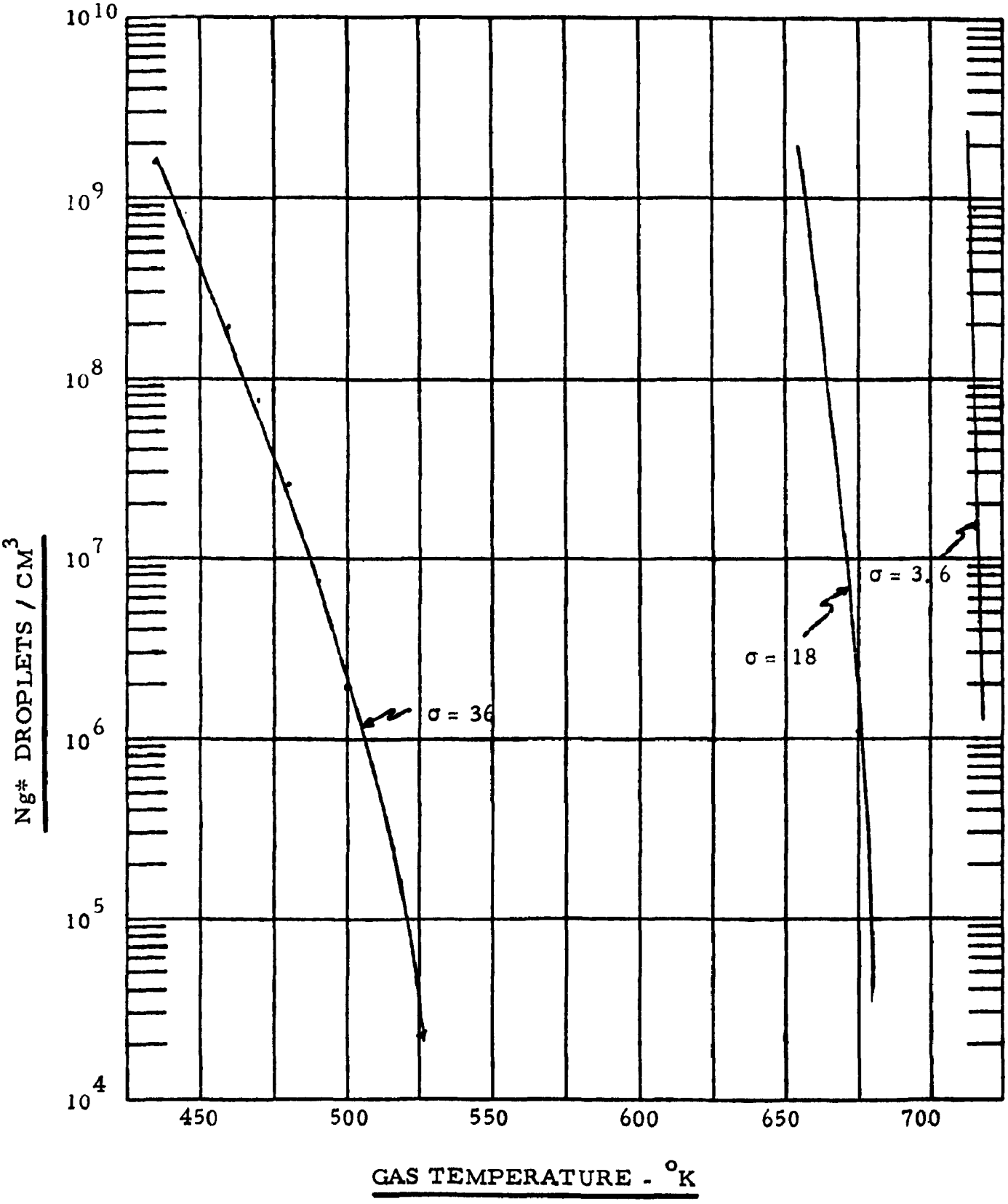

Fig. 6 Effect of Surface Tension and Temperature on Concentration of Critical Size Droplets

AGGLOMERATION

After nucleation, the tar particles grow by coalescence. This process is described in general by the theory of Smoluchowski[6]. For particle coalescence in the Knudsen regime (Knudsen No. >10) a simplified treatment has been given by Ulrich[6]. Coalescence in the Knudsen regime is somewhat faster than coalescence in the continuum regime (Knudsen No. <5). Tar particles in the humidification chamber may be in either the Knudsen or the continuum region, depending on the assumed value for surface tension. As the particles coalesce, the process of coalescence changes from Knudsen diffusion to continuum diffusion. The Knudsen number (K_N) is defined as the ratio of the mean free path (L) in the gas phase to the diameter of the particle.

$$K_N = L/2r \tag{5}$$

$$L = (KT/\sqrt{2}\pi d^2) \tag{6}$$

where K is the Boltzmann constant, d is the diameter of gas molecules, the gas P is the total pressure in atm and T is the absolute gas temperature. For a total pressure of 100 PSIA (6.9 atm), a temperature of 320°F (433°K) and assuming the diameter of gas molecules is 4×10^{-8} cm^3, the mean free path is 0.05 μ. In this case, the particle radius can grow to .014μ. Further growth is via continuum diffusion. The coalescence of tar particles in the region of Knudsen numbers greater than 10 takes the form:

$$N = N_o(1 + 3.4 \times 10^{-12} T^{1/2} C_o N_o^{5/6} t)^{-6/5} \tag{7}$$

where N is the number of tar droplets per cm^3 at time t, N_o is the initial droplet concentration, T is temperature, and C_o is the initial tar molecule concentration in the gas phase. The coefficient 3.4×10^{-12} is obtained from substituting tar properties into the coalescence equations. Note that at longer times the number density of tar droplets is independent of the initial droplet density.

With an expression for the number of tar particles, a simple mass balance shows that the radius of the exit tar particles is a function of the -2/5 power of the coalescence time.

In the continuum diffusion regime, the expression for the rate of particle coalescence is derived from Smoluchowski theory using the Stokes-Einstein form of the diffusivity[5]. In this case, the number of particles is related to the coalescence time by the equation.

$$N = \frac{N_o}{1 + N_o \left(\frac{2}{3} \frac{KT}{\mu} t\right)^{-1}} \tag{8}$$

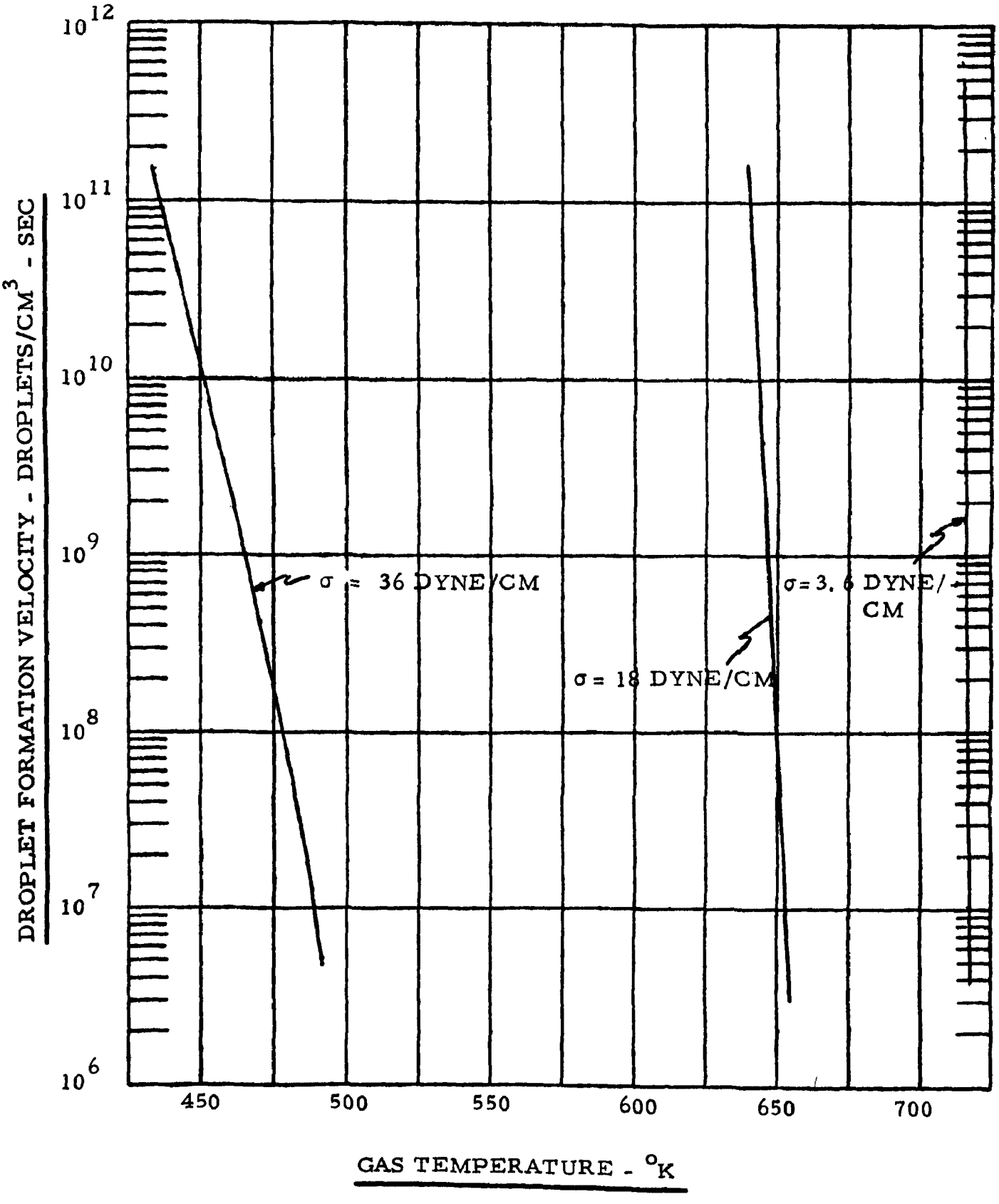

Fig. 7 Effect of Surface Tension and Temperature on Formation Rate of Critical Size Droplets

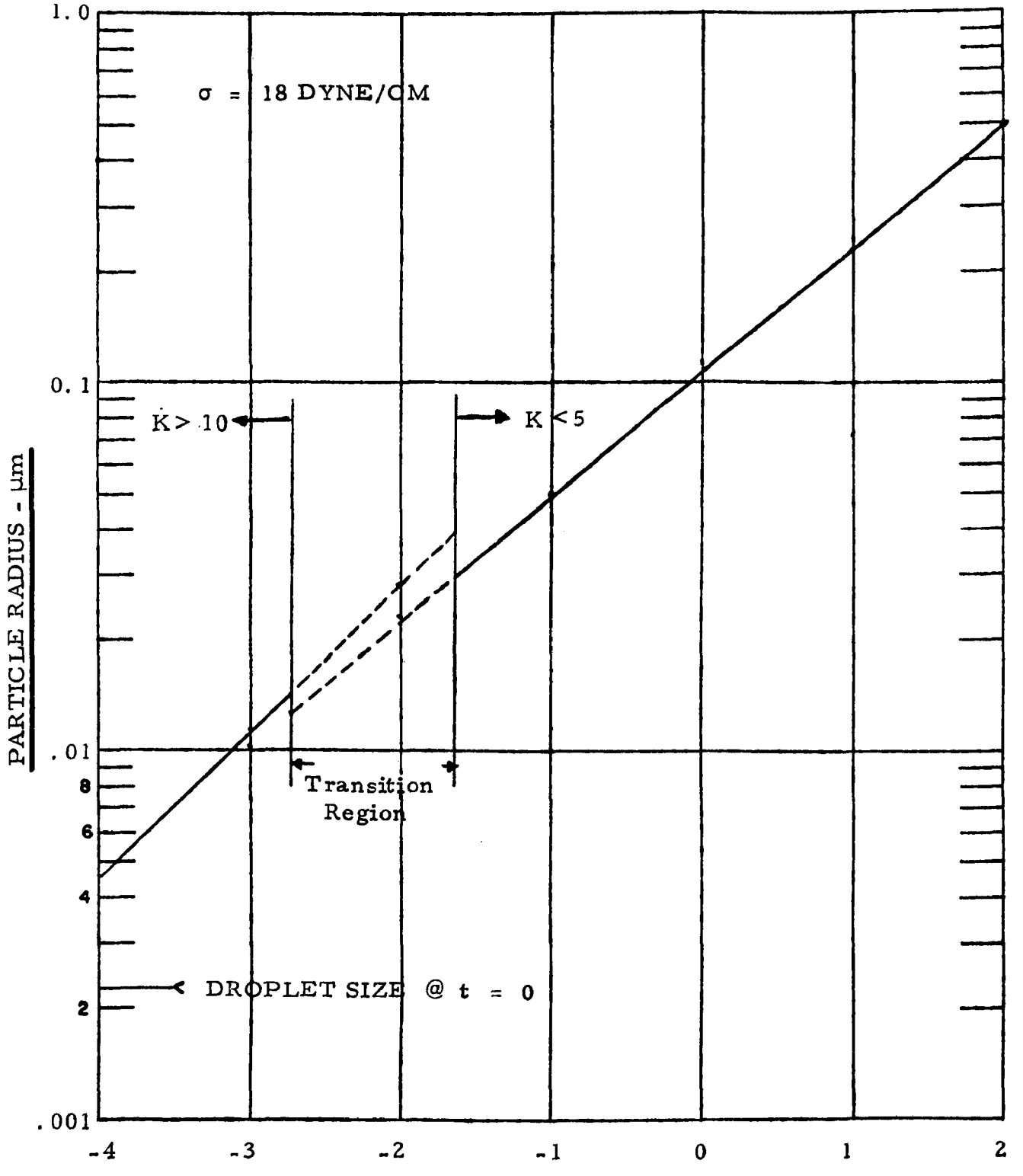

Fig. 8 Tar Droplet Growth Rate

where μ is the viscosity of the gas.

The particle radius (r_t) at some time after the onset of coalescence is determined by the number density (N) at that time, and the particle radius and number density at the initiation of coalescence by a simple mass balance.

$$r_t = r_o \, (N/N_o)^{1/3} \quad . \tag{9}$$

Fig. 8 shows the rate of particle growth assuming the nucleation of tar droplets for a surface tension of ~18 dyne/cm. The tar droplet grows from an initial radius of .0023μ to a radius of .0143μ in about 2 msec. At this point, the transition from the Knudsen diffusion to continuum diffusion occurs. At about .02 sec., the particle has grown to a radius of .023μ. Growth in the continuum diffusion region progresses slowly. At 100 sec., the particle diameter has only grown to ~1μ.

HETEROGENEOUS CONDENSATION

Because of tar/dust interactions, heterogeneous condensation is a somewhat more complex phenomenon than homogeneous nucleation. We have made a preliminary estimate of the condensation rate to form tar particles of a readily collectable size (~10μ). To do this, we assume the dust loading in the gas is $\sim 10^{-3}$ gm dust/gm air. We further assume that the dust has the composition of coal ash (~3gm/cm^3). For dust particles much larger than the mean free path, the rate controlling process is the diffusion of tar molecules to the surface of the dust particles. An estimate of the tar diffusion coefficient was made using the Chapman-Enskog equation ($D = 2.7 \times 10^{-2}$ cm^2/sec). Finally, the process was analyzed at the tar saturation temperature (~450°C). The concentration of tar particles in the gas stream is then:

$$C_{TAR} = C_{TAR,\,O} \exp(-2\pi D \, d_{DUST} \, C_{DUST} \, t) \quad . \tag{10}$$

where $C_{TAR,O}$ is ~3.6 x 10^{15} molecules/cm^3, D is the diffusion coefficient, d_{DUST} is the dust particle diameter, and t is in sec. Substituting coefficient values into the above expression we obtain (setting $d_{DUST} = 10\mu$):

$$C_{TAR} = 3.6 \times 10^{15} \exp(-.32t). \tag{11}$$

The results of this equation are shown in Fig. 9. To reduce the tar vapor concentration to 4% of the inlet value, a condensation time of ~10 sec is required. Note that increasing the dust loading will reduce the time scale exponentially. While 10 sec is not an especially long time, the gas must not be appreciably subcooled during this period. If the gas is subcooled during the process, then

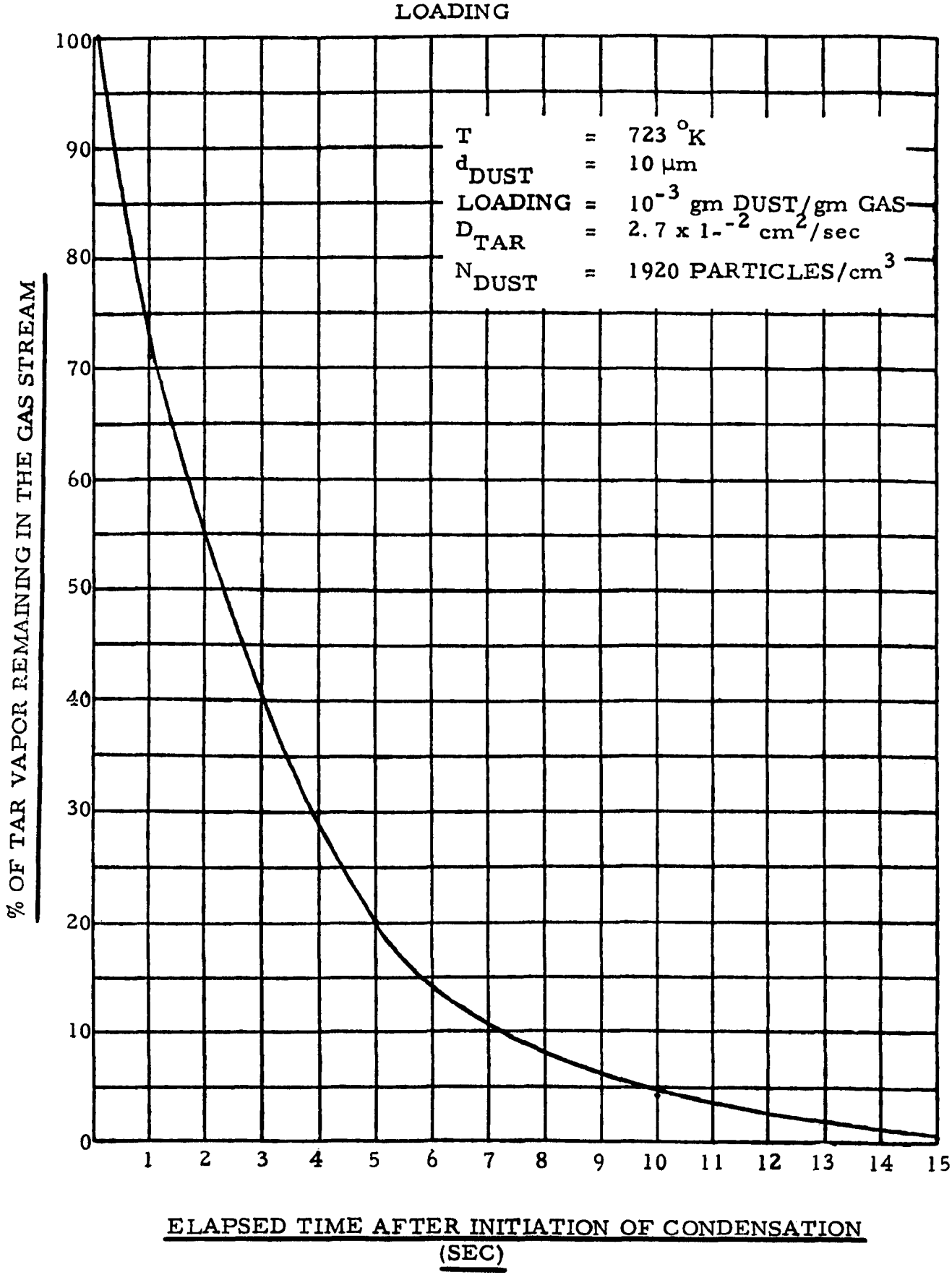

Fig. 9 Heterogeneous Condensation

homogeneous nucleation will proceed concurrently with heterogeneous condensation. This will, in turn, reduce the amount of tar collected on the dust particles.

ACKNOWLEDGEMENT

We are grateful to the U.S. Department of Energy, Morgantown Energy Technology Center, for their support of this work. Funding was through DOE Contract No. DE-AT21-78MCO8450.

REFERENCES

1. Cleaning Producer Gas from MERC Gasifier, A. Moore, IR No. 96 May, 1977.

2. Wet Scrubber System Study, Volume 1, ATP Inc. to Environmental Protection Agency, July 1972, NTIS PB-213 016.

3. Transport Phenomena, R. Bird, W. Steward, E. Lightfoot, John Wiley & Sons, 1960.

4. Kinetic Theory of Liquids, J. Frankel, Doren Publications Inc. 1974.

5. Stochastic Problems in Physics and Astronomy, S. Chandrasekhar, Reviews of Modern Physics, Vol. 15, No. 1, Jan 1943.

6. Particle Formation in High Temperature Systems, G. Ulrich, WSCI 71-37.

7. High Temperature Tar, J. Weiler, Chemistry of Coal Utilization Supplementary Volume, H. H. Lowry Ed., John Wiley & Sons, 1963.

IMPROVING THE EFFICIENCY OF FREE-JET SCRUBBERS

By:
Donald A. Mitchell
Hydro-Sonic Systems
P.O. Box 4138, Lone Star, Texas 75668

ABSTRACT

A free-jet scrubber is an innovative gas cleaner in which the primary liquid/gas contacting takes place in the turbulent mixing zone emanating from a jet nozzle. The first such devices, powered by supersonic steam or air ejectors, were exceptionally effective cleaners but were criticized as being high-energy users. A great reduction in the energy consumption of free-jet scrubbers has been accomplished in the last four years, a feat which may seem in contradiction to the "contacting power rule". An explanation of what is happening in these devices must take into account the effectiveness with which energy and water are utilized, thereby leading one to a somewhat circular definition of "effective contacting power". The theoretical implication of this analysis is primarily to remind us that there are many paths between two states and some are more energy efficient than others. The practical value is that such analysis generates information which aids in choosing between several design options, a direct benefit of the various free-jet configurations.

IMPROVING THE EFFICIENCY OF FREE-JET SCRUBBERS

Several recognized methods for capturing particulate and noxious vapors involve the generation of fine water droplets and frictional forces which aid in vigorous liquid/gas contacting. One class of cleaners utilizing this concept, the gas-atomized systems, provide the means for this "scrubbing" action by pumping the polluted gases through a restriction where the increased flow velocity atomizes water as it is sprayed across the path of the high-velocity gas. The relative energy of motion between the water spray and the polluted gas is responsible for the frictional forces which atomize the water drops and induce pollutant capture. This energy is dissipated as heat due to the irreversibility of frictional processes. The presently accepted theory of particulate capture says that the performance of all such cleaners is basically a function of energy dissipated by turbulence during liquid/gas contacting, a relationship called the "contacting power rule", and which may be written as follows:

$$N_t = f(P_t) \sim \alpha P_t^{\gamma} \quad (1)$$

or

$$\eta = 1 - \exp[-f(P_t)] \quad (2)$$

Where N_t = Number of transfer units = $-\ln(1-\eta)$
η = Fractional efficiency
P_t = Total contacting power
α, γ = Constants peculiar to an aerosol

The implication of this theory, which is strongly supported by experiment, is that an equal energy input to two differently configured scrubbers should give equal cleaning performance. Of course some devices may fall below optimum performance due to irreversible energy losses whenever water atomization and droplet distribution are less than ideal or when the relative momentum is partially reduced due to a poor flow pattern. This paper describes an innovative class of gas-atomized scrubbers in which the basic operating principle permits one to choose between designs in which there is a wide range in energy and water options, the best choice depending on the particulars of a given application.

The essential distinguishing feature of free-jet scrubbers is that liquid/gas contacting takes place in the turbulent mixing zone created by compressible fluid flow through a jet nozzle. There are several ways in which this may be accomplished. Several arrangements will be described, followed by a comparison of their performance characteristics.

The first free-jet cleaner (Figure 1) was called the "Steam-Hydro". In this device, a steam ejector pulls the process gas around the nozzle where water is sprayed around the steam jet, resulting in violent shattering of the water and ejection of high-velocity droplets through the polluted gas. Exceptionally effective capture is achieved with a minimum of water usage (about 0.35 kg/kg of gas). Additionally, the system can be operated with a compressed air ejector with no loss in performance, a fact which demonstrates that steam condensation is not the primary cleaning mechanism as has been suggested by some. However, it can be seen that only a portion of the kinetic energy of the steam or air can be effectively utilized in the contacting process. This is because the water does not penetrate into the supersonic jet core, but remains in the mixing zone where the flow is subsonic and thus of lesser kinetic energy. The result of this energy loss is apparent from the performance data to be described later.

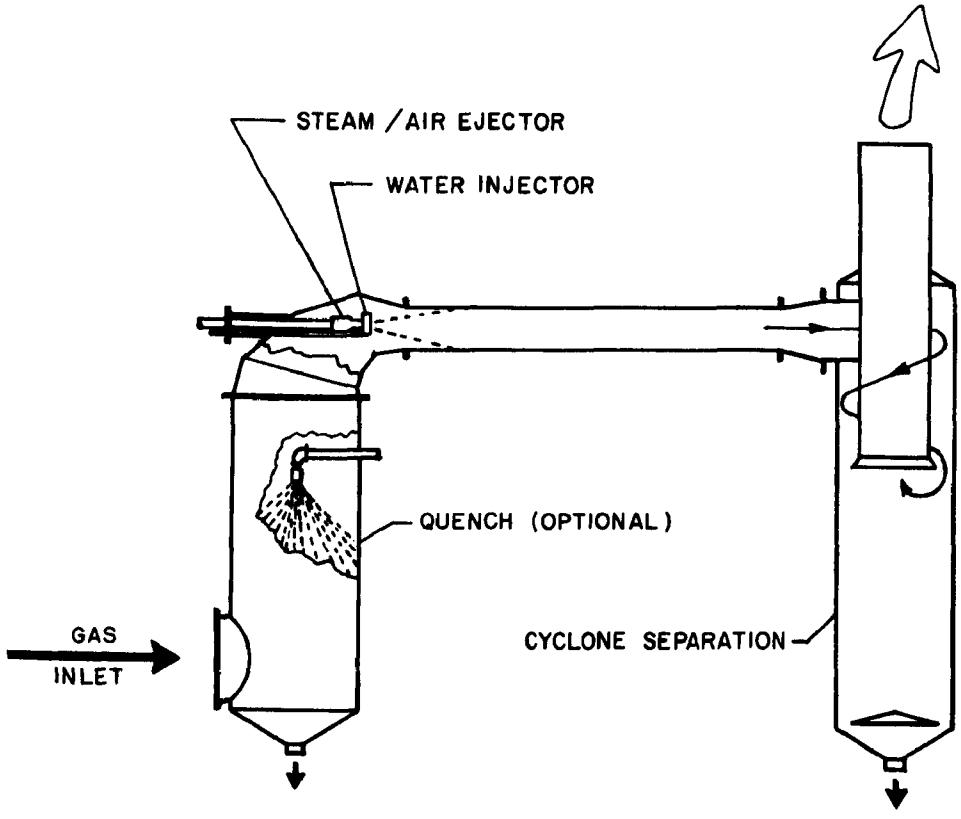

Figure 1 Free-jet scrubber with ejector drive.

The "Fan Coalescer" (Figure 2) is an entirely subsonic free-jet design in which maximum benefit can be made of kinetic energy. In this arrangement, a fan is used to pump the gas through a nozzle where it flows out in a diverging cone as shown. The inner cone retains its velocity and serves as the energy source for atomization and pollutant capture. As with all free-jet configurations, however, the contacting takes place in the turbulent mixing zone, although some water may penetrate into the core. However, our experience has been that any attempt to inject water into the core or into the nozzle throat will result in somewhat poorer performance.

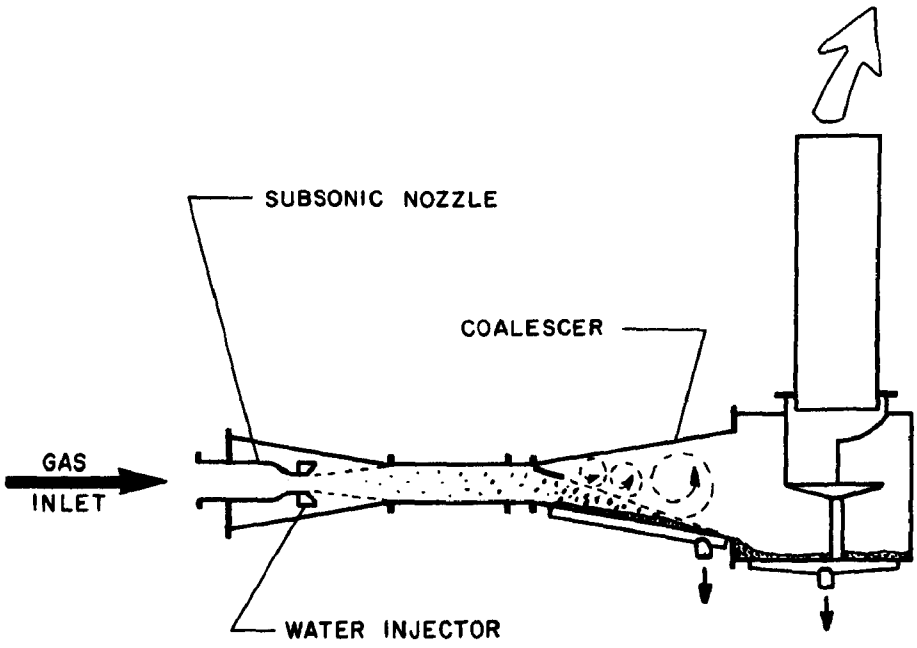

Figure 2 Single stage fan-driven "Coalescer" cleaner.

For control of fine particulate and noxious vapors, the "Tandem Nozzle" arrangement (Figure 3) is normally significantly better than the single nozzle design. Dividing the contacting process into two parts allows better utilization of energy and water, primarily due to enhanced saturation, adiabatic expansion, condensation, and droplet growth. The two-stage free-jet shows its greatest advantage for processes in which emissions consist of very fine, low density particles, especially where oily hydrocarbons are known to be present.

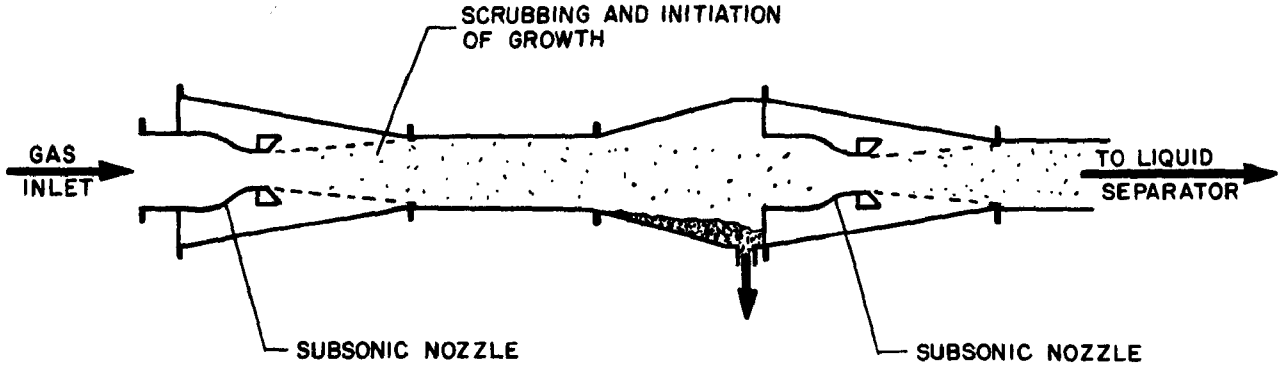

Figure 3 Two stage subsonic free-jet arrangement.

The "SuperSub" (Figure 4) is a hybrid which incorporates a single subsonic nozzle and a small steam or air ejector. A combination of energy sources allows one to achieve efficient performance under normal conditions and to enhance fine particulate capture during upset conditions simply by activating the small ejector. It requires only a 10% increase in water flow beyond that required by a single subsonic nozzle design.

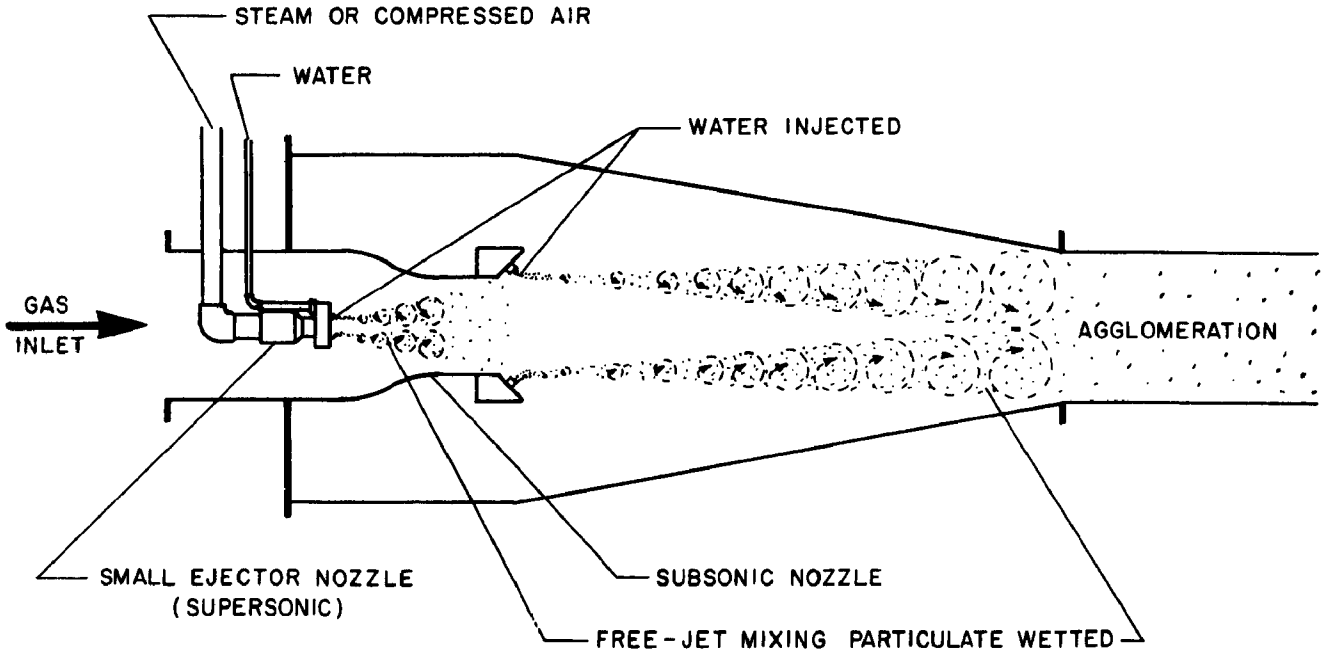

Figure 4 Hybrid supersonic/subsonic free-jet arrangement.

In comparing the performance of free-jet scrubbers, it is convenient to plot efficiency or emissions versus equivalent pressure loss. The pressure drop therefore indicates the power input per unit volumetric flow rate. The problem arises as to how to compute an equivalent pressure loss for the ejector drive. Actually it is a simple procedure, although the values assigned to gas densities and efficiencies are somewhat arbitrary. However, the general features are not very sensitive to these estimates. The equivalent pressure loss for an ejector unit is obtained by finding the available energy loss for the ejector flow and computing the pressure drop across a fan system necessary to drive the same process gas while expending the same total available energy. Therefore, for the steam or air ejector cleaners, the performance curve is not really a plot of performance as a function of effective contacting power since one can only accurately compute the kinetic energy of the ejector media, not the energy effectively utilized in scrubbing. This is because of the unknown amount of energy lost due to irreversibilities in the transition from supersonic to subsonic flow. However, if one simply estimates the effective energy at sonic conditions, a value comparable to that for the fan-driven cleaners will be obtained.

The open hearth steel refining process is one in which emissions are fairly repeatable (Figure 5). While the absolute value of controlled emissions is noteworthy, the more instructive feature is the great difference in cleaning between the units at typical energy levels. As expected, the Steam-Hydro consumes much more energy than the fan-driven units. However, it uses the least quantity of water (about 3 gal/1000 SCF). The other cleaners also achieve high cleaning, but do so with considerably less available energy expenditure, although they do require three or more times the water rate. Note that the stack sample measurement for the single nozzle system suggests that its performance is the same as that for the SuperSub, a somewhat misleading result. Although no stack samples were obtained for the single stage system at higher pressure losses, it was obvious from the stack opacity that the higher performance could not be achieved even at much greater energy levels and water rates. This is partly due to the fact that the tandem unit induces condensation growth of submicronic fumes and partly due to the fact that a single stage cannot effectively utilize an unlimited quantity of water—that is, excessive water will tend to destroy the free-jet action.

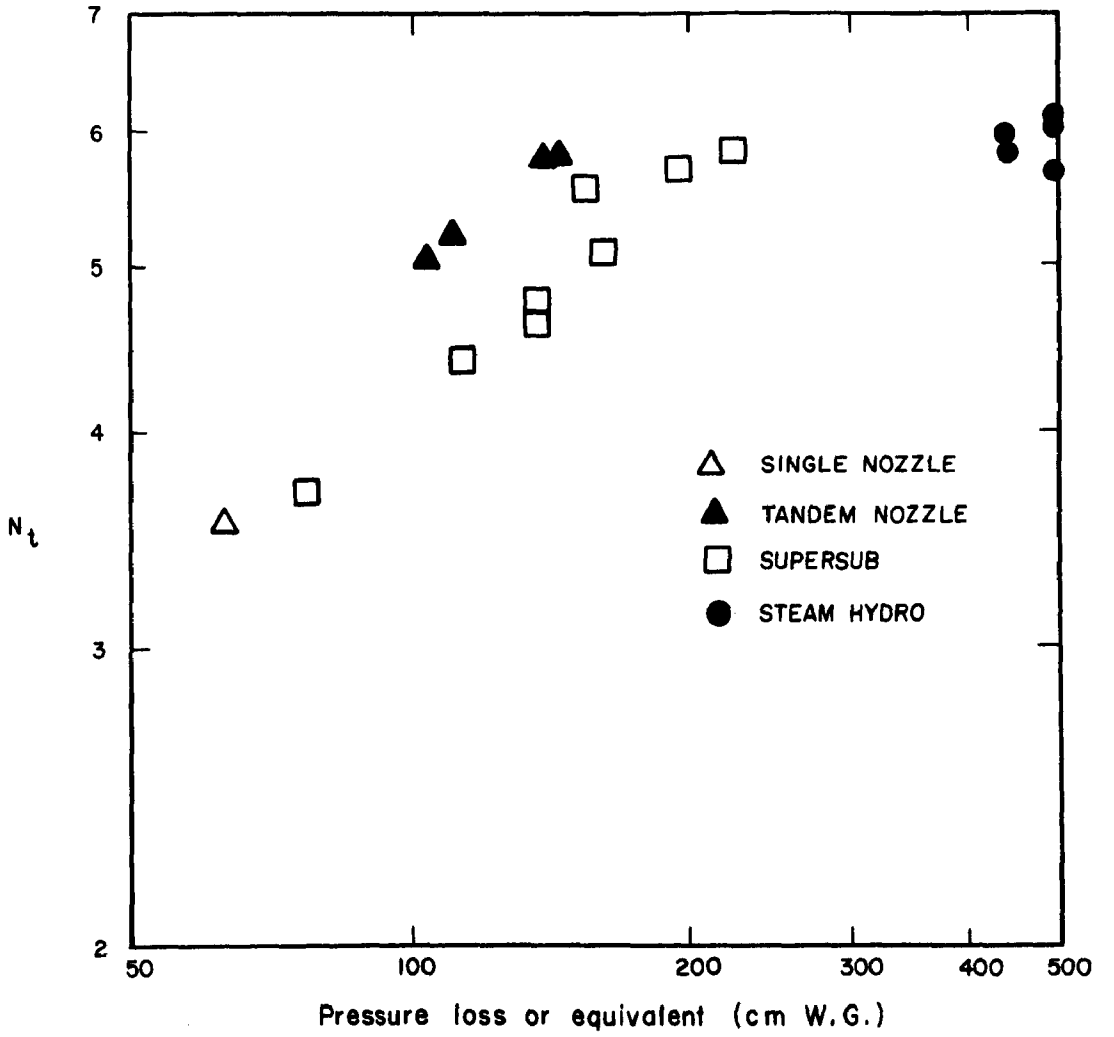

Figure 5 Performance of free-jet scrubbers on an open hearth furnace.

A second series of curves (Figure 6) illustrates the dramatic difference between performance on a process with more limited particle emission types and sizes, such as steel refining, and a process with a wide range of emissions, such as for a gray iron cupola. The most obvious feature for this process is that the devices requiring less energy can give remarkably better performance than the devices needing higher energy, with the exception of the single nozzle scrubber. (Data for the single stage unit appear as discrete points to illustrate an apparent non-conformity with simple theory.) What this data set suggests is that water utilization and condensation growth are dominating factors when one is scrubbing an off-gas with a large fraction of submicronic, low density emissions, especially where condensible hydrocarbons are present.

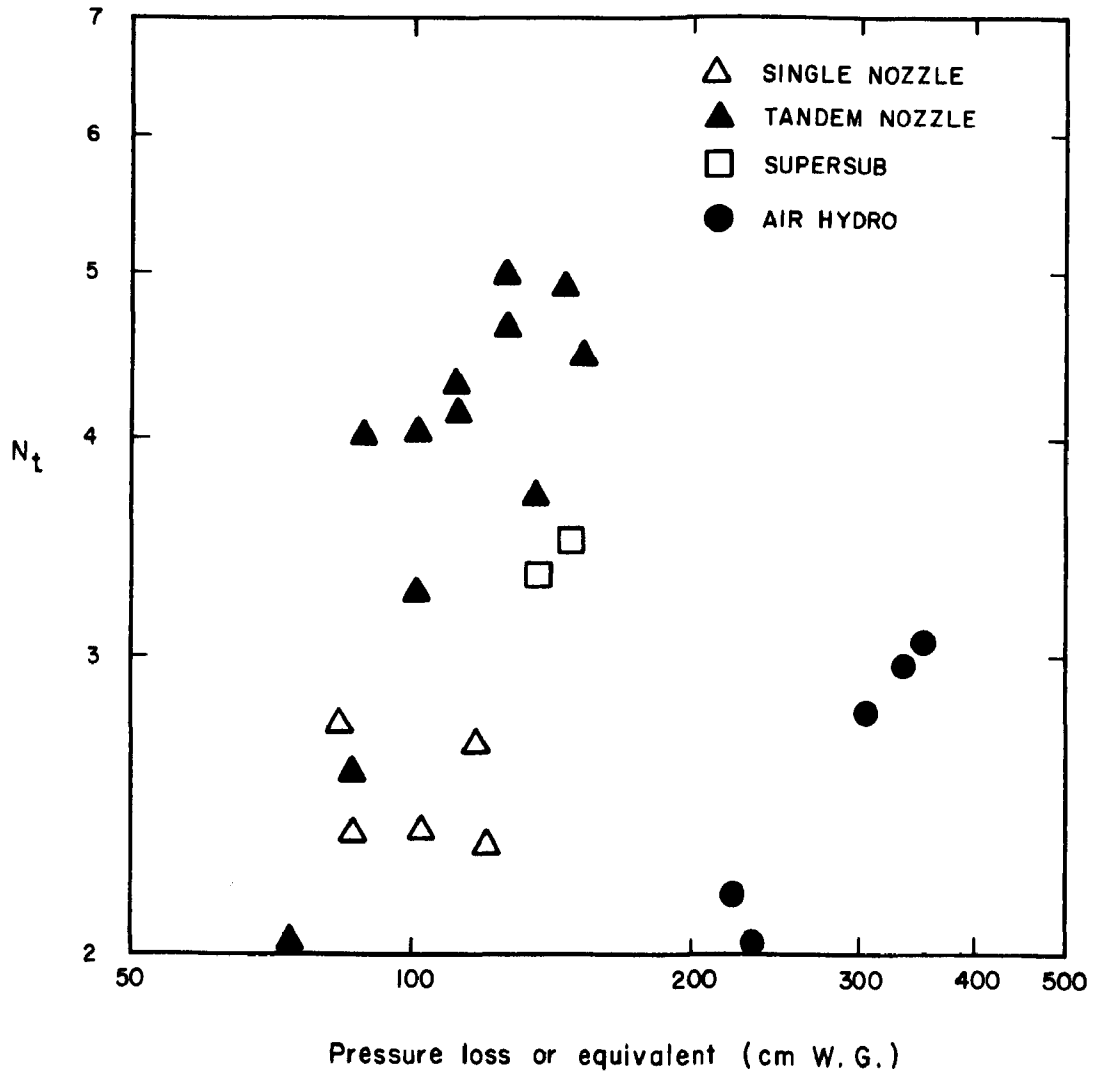

Figure 6 Performance of free-jet scrubbers on a gray iron cupola.

The selection of a particular free-jet configuration is greatly aided by utilization of performance data as given in Figure 7. These curves indicate something about the nature of the particulate as well as the relative advantage of one particular type cleaner over another. However, such curves do not indicate the influence of certain process variables and do not alleviate the need to predict absolute emission levels. Furthermore, it is quite hazardous to extrapolate efficiency from very low to high energy levels necessary for opacity control unless a given device has been shown to have the capability to achieve high performance. It is the ability of a cleaner to get the last bit of fine particulate which really counts in opacity-limited processes, and this is where the free-jet gas cleaners are unsurpassed.

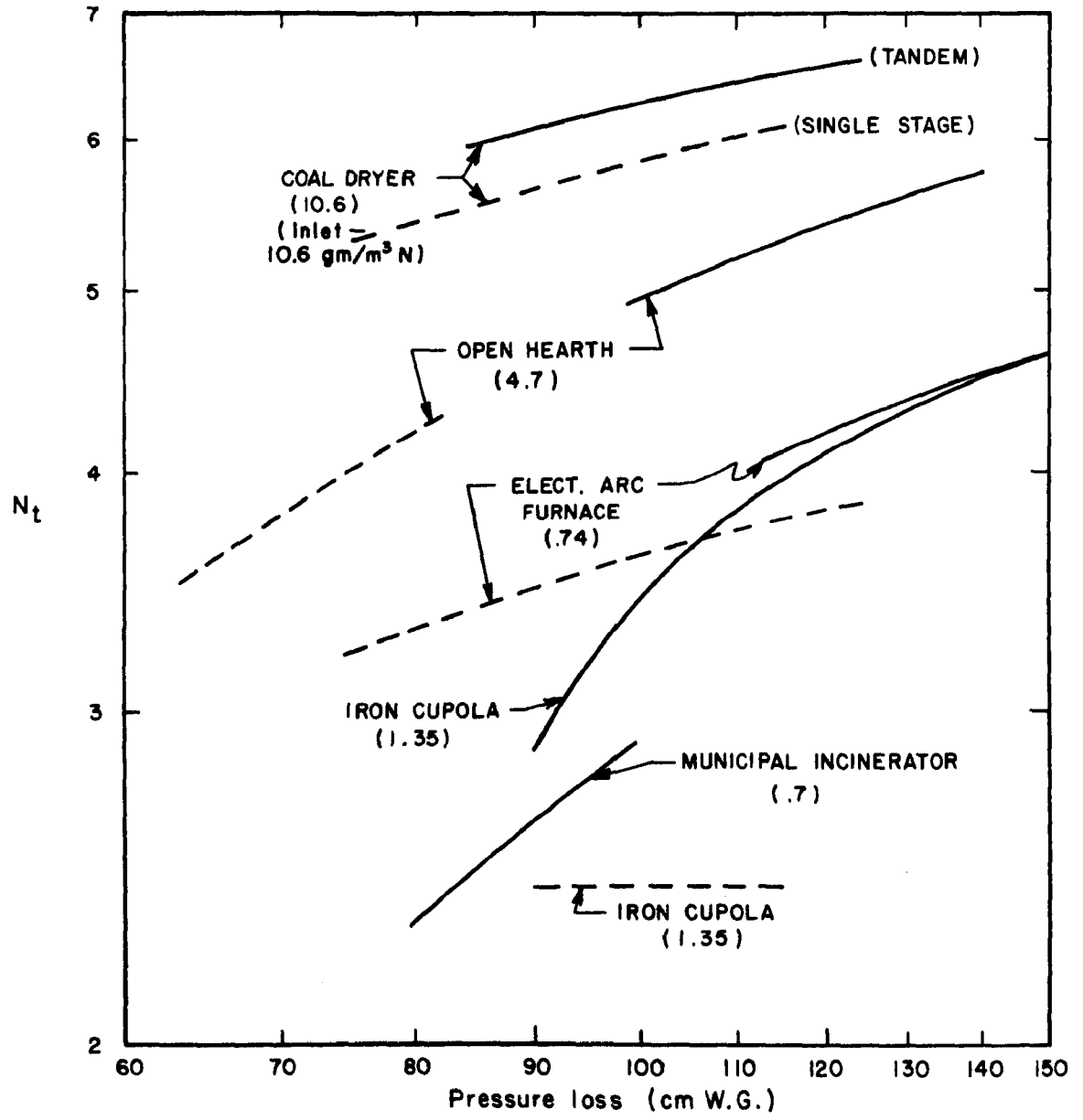

Figure 7 Performance curves for selected processes.

To summarize the characteristics of free-jet scrubbers which account for their operation at sustained optimum performance, the following features are fundamental:

1. The nozzles are designed to achieve maximum benefit of relative momentum.

2. The free-jet produces a turbulent mixing cone which extends the length of the liquid/gas contacting region and increases the time of interaction.

3. The water is sprayed into the turbulent mixing region where pressure gradients enable it to be used to maximum benefit, this effect being most pronounced for the ejector-driven units.

4. Beyond the high-velocity core, water droplets are agglomerated, thus aiding in liquid separation and minimizing mist carry-over.

In conclusion, the application of accepted theory to free-jet scrubbers gives some insight into the performance characteristics of the free-jet scrubbing process. However, it adds little to the theory itself, except to remind us that there are many energy paths and physical mechanisms possible between the inlet and outlet of a gas cleaner. Also, it is humbling to remind ourselves of how little available energy could be used to do the same job by the most efficient process, a value which can be easily calculated using the methods of statistical mechanics. In principle, on the order of about 10^{-7} joule could "clean" a cubic meter of typical off-gas. While such a low value may never be approached in practice, it should serve to point out the biting truth of just how far we all have to go to achieve the ideal.

HIGH VELOCITY FIBROUS FILTRATION

By:

Michael J. Ellenbecker, John M. Price, David Leith, and Melvin W. First
Harvard School of Public Health
Department of Environmental Health Sciences
665 Huntington Avenue
Boston, Massachusetts 02115

ABSTRACT

The particle collection characteristics of fibrous beds at low filtration velocities are well understood; many experiments have confirmed the collection efficiencies predicted by theory. In this study, the particle collection characteristics of a stainless steel fibrous material collecting resuspended fly ash were investigated at very high superficial filtration velocities (i.e., 1-10 m/s). Under these conditions the theoretical collection efficiency due to impaction should have approached 100% for all but the smallest particles present. Previous investigators have found, however, that penetration in this velocity range can be higher than predicted by theory, presumably due to particle bounce and/or resuspension.

Collection efficiency was measured against particle size and filtration velocity. Test results indicate that, under certain conditions, penetration can increase both with velocity and with particle size. The possible use of these anomalous collection characteristics in a unique fly ash collection device is discussed.

HIGH VELOCITY FIBROUS FILTRATION

INTRODUCTION

Mats of fibrous materials have been used for many years to collect particles from gas streams.[1] Several different collection mechanisms, including diffusion, impaction, and interception, can contribute to the overall collection efficiency of fibrous mats. These collection mechanisms are well understood, and the theories describing them can be used to accurately predict collection efficiency over a wide range of filter and operating characteristics.

The theory and experiments described here are concerned with a set of filtration conditions which are outside the range of "normal" filtration. The predominant characteristic of this filtration regime is the very high filtration velocities used - in the range of 1-10 m/s (200-2,000 fpm). These filtration velocities, when combined with the tested filter materials (randomly oriented 8 um stainless steel fibers) and dust (resuspended fly ash), result in particle collection characteristics which cannot be described satisfactorily by classical filtration theory.

This combination of particle sizes, fiber diameter, and filtration velocities results in particle collection predominantly by impaction, even for very small particles. Just as importantly, the kinetic energy of large particles and the drag forces on collected agglomerates are sufficiently large so that particle bounce and reentrainment can be expected.

This research was undertaken to investigate fly ash collection characteristics in the high inertia regime. In particular, the research is aimed at determining combinations of fiber beds and filtration conditions where small particles are effectively collected by impaction while large particles bounce through or are reentrained. Since the large particles which would penetrate such a filter can be collected by other simple devices (e.g., cyclones), this penetration characteristic could possibly form the basis for a two-stage, high efficiency collection device.

THEORY

Particle Collection Mechanisms

Introduction. Filtration theory attempts to predict overall particle removal in a filter based on an understanding of the interaction of particles with a single filter element. This element can be an isolated fiber or previously collected dust particles.

The single element efficiency, η_s, is defined as the number of particles collected by a filter element divided by the number of particles whose centers

pass through the element's projected area as the particles approach it.[2] The major mechanisms by which particles collect in a filter element are inertial impaction, diffusion, interception, gravity settling, and electrostatic deposition.[2]

A single element collection efficiency due to any one mechanism, η_i, can be estimated for each of the fundamental collection mechanisms; however, this paper is concerned with sets of operating conditions where the impaction mechanism dominates all the others. Under such conditions, the contribution of all other collection mechanisms is insignificant and can be disregarded.

Inertial Impaction. As the gas flows past a collector element, the streamlines curve around the collector. Near the collector surface, inertia will cause particles to deviate from the streamlines. Particles with sufficient inertia can cross streamlines and hit the collector. Inertial impaction has been found to be proportional to the dimensionless impaction parameter,[2] ψ:

$$\psi = \frac{\rho_p d_p^2 v C_c}{18 \mu d_f} \tag{1}$$

where: ρ_p = particle denisty (kg/m^3)
d_p = particle diameter (m)
v = superficial filtration velocity (m/s)
C_c = Cunningham slip correction factor
μ = gas viscosity (Pa·s)
d_f = fiber diameter (m)

Much experimental and theoretical work has been devoted to determining the relationship between the impaction parameter, ψ, and the single fiber collection efficiency from impaction, η_I. One widely accepted empirical formula was derived from experiment and theory by Landhal and Herrman.[3] It was developed for a fiber Reynold's Number of 10 and can be expressed as:[2]

$$\eta_I = \frac{\psi^3}{\psi^3 + 0.774^2 + 0.22} \tag{2}$$

Typical Calculations. Theoretical impaction collection efficiencies can be calculated for values of the variables used in this study, which are summarized in Table 1. All experiments were conducted using 8 μm diameter fibers. Figure 1 plots single fiber collection efficiency η_I as a function of particle size for the lowest velocity (1 m/s) and the highest velocity (10 m/s) used here. Note that a significant fraction of even very small particles will impact a fiber at these velocities.

Other Collection Mechanisms. Since the fibers used in this study were very small (8 μm diameter), interception might be thought to be important. However, velocities were sufficiently high so that impaction always completely overshadowed interception. The theoretical single fiber collection efficiency from impaction and interception combined was calculated assuming that the mechanisms are independent but that a particle caught by one mechanism cannot

be caught by the other;[4] the combined collection efficiency never exceeded the single fiber collection efficiency from impaction alone by more than 1%. Likewise, particle collection from diffusion was negligible under the conditions considered.

Overall Collection Efficiency

Dorman[5] gives the overall collection efficiency for a filter of thickness L and solidity α as:

$$\eta = 1 - \mathrm{Exp}\left[\frac{-4L\alpha\eta_s}{\pi d_f(1-\alpha)}\right] \tag{3}$$

where η_s is the combined single fiber collection efficiency from all effects. In this study, impaction dominates all other collection mechanisms so that

$$\eta_s \simeq \eta_I \tag{4}$$

Equation 3 is difficult to apply in this case, because at the high velocities used here the filter mats compress and L changes in a manner which is difficult to measure and/or predict. However, Equation 3 can be modified by making use of the definition of solidity, α, defined as the ratio of fiber volume to total filter volume:

$$\alpha = \frac{V_f}{V_T} = \frac{m_f/\rho_f}{LA} \tag{5}$$

$$\alpha = \frac{m_f}{\rho_f LA} \tag{6}$$

where ρ_f is the filter density and m_f and A are the filter mass and cross-sectional area, respectively. Solving Equation 6 for filter thickness L and substituting into Equation 3:

$$\eta = 1 - \mathrm{Exp}\left[\frac{-4m_f\eta_I}{\pi\rho_f d_f A(1-\alpha)}\right] \tag{7}$$

The overall theoretical filter collection efficiency can thus be calculated from easily measured filter bed parameters (m_f, ρ_f, d_f, A), the theoretical single fiber collection efficiency from impaction (η_I), and filter porosity ($1-\alpha$). Porosity changes with filtration velocity; however, the porosity of a filter with no airflow can be measured using pycnometry, and changes in porosity with filtration velocity can be estimated from the slope of the measured pressure drop versus velocity curve.

EXPERIMENTAL APPARATUS

Apparatus

Figure 2 is a diagram of the experimental high velocity filtration system. It contains a 30 cm square filter holder by which fibrous materials can be packed to depths of up to 15 cm. A movable 4 mesh screen upstream and a stationary 4 mesh screen downstream provide rigid support at high filtration velocities. A downstream centrifugal blower draws the test aerosol through the 20 cm round entry duct, the filter holder, and the Venturi meter which measures the airflow rate. A Dwyer photohelic gauge is used with a motor driven blastgate to maintain a constant airflow rate.

A National Bureau of Standards (NBS) dust feeder[6] generates the fly ash aerosol at mass rates from 3 to 125 g/min. The test dust is an electrostatically precipitated fly ash with a count median diameter (CMD) of 0.14 μm and a geometric standard deviation (GSD) of 1.9. A polydisperse (CMD = 0.7 μm, GSD = 2.05) dioctyl phthalate (DOP) aerosol can also be generated using a DeVilbiss nebulizer (The DeVilbiss Co., Somerset, PA). The test aerosol and inlet air are thoroughly mixed before entering the filled section by a Stairmand disk[7] located at the inlet duct.

Simultaneous up and downstream isokinetic samples are taken to determine aerosol penetration of the filter medium. Microscopic and gravimetric analyses of the sample filters determine particle size distribution of the fly ash and downstream of the filtering section as well as overall collection efficiency. Eight stage Anderson impactors (Anderson-2000 Inc., Atlanta, Georgia) are also used up and downstream for particle sizing. DOP penetration is measured using a Particle Measuring Systems, Inc., laser scattering aerosol spectrometer (PMS Model CSASP-100).

Procedures

Upon packing a filter material into the filter housing and setting the airflow rate, test aerosol is generated and directed to the filter. Inlet dust concentration is held constant and after the filter reaches maximum pressure drop (about 7.5 kPa) the filter is removed for inspection and cleaning. During the dust loading, pressure drop across the filter is recorded and aerosol samples are taken at regular intervals. Cleaning of the filter material can be done by blowing compressed air through the upstream side of the filter, striking the filter and filter frame against a rigid surface, or shaking the filter manually. After cleaning, the filter is placed in the filter housing and retested at original flow rate and dust loading.

EXPERIMENTS

The fractional penetration of fly ash through filter mats of 8 μm stainless steel fibers was measured at five filtration velocities: 1.5, 2.9, 3.2, 6.9 and 8.0 m/s. The characteristics of the fly ash and filter material are given in Table 1. At the lower velocities the filtration time between cleanings was long enough so that adequate Anderson impactor samples could be collected in one cleaning cycle, while at the higher velocities multiple cycles

were needed to obtain sufficient impactor deposits.

The fractional penetration of the polydisperse DOP aerosol was also measured over the same velocity range. The DOP concentration was extremely low, so that the filter exhibited no loading effects during the DOP tests.

RESULTS

Fractional penetration curves for fly ash collected at five different filtration velocities are presented in Figure 3. Increased penetration with both velocity and particle size is evident.

Similar measurements were made with the liquid DOP aerosol at six velocities; the fractional penetration curves for these experiments are shown in Figure 4. Shown also for comparison in Figure 4 are the 1.5 and 8.0 m/s fly ash penetration curves from Figure 3. In contrast to the fly ash, the DOP aerosol penetration follows the trends predicted by classical impaction theory, decreasing with both velocity and particle size.

Dust concentration downstream of filters loaded with fly ash using clean inlet air were also measured and found to be insignificant at these velocities.

DISCUSSION

Particle Bounce

Equation 7 is a theoretical formula which predicts overall filter collection efficiency (η) from the single fiber collection efficiency (η_I) and gross filter parameters (m_f, ρ_f, d_f, A, $1-\alpha$). However, Equation 7 can also be used to calculate experimental single fiber collection efficiencies (η'_I) from experimental filter collection efficiency data (η'). Such numbers are more useful than overall collection efficiencies in comparing results to theory because they are independent of the particular filter configuration tested and should only be a function of the particle-fiber impaction parameter (Equation 2).

Solving Equation 7 for η'_I,

$$\eta'_I = -\frac{\pi \rho_f d_f A(1-\alpha)\ln(1-\eta')}{4m_f} \tag{8}$$

and substituting the filter parameters from Table 1 gives:

$$\eta'_I = -0.145(1-\alpha)\ln(1-\eta') \tag{9}$$

where the solidity, α, is a function of filtration velocity. As discussed earlier, changes in α with velocity can be estimated from the clean filter pressure drop curve; in any case, the quantity $1-\alpha$ is always close to unity in these tests so that changes in α have little effect on the calculation of η'_I.

The empirical formula of Landall and Herrmann relating impaction parameter (4) and η_I (Equation 2) is plotted in Figure 5. Also plotted are the experimentally determined single fiber collection efficiencies for the lower test velocity (1.5 m/s, α = 0.0085) and the highest test velocity (8.0 m/s, α = 0.0285). The values for intermediate velocities are similar and have been omitted for simplicity. As shown in Figure 5, the experimental and theoretical single fiber collection efficiencies are in agreement only for the smallest Anderson impactor fly ash size category, when the fiber impaction parameter is approximately equal to 1. As impaction parameter increases the experimental η'_I decreases; when η_I equals 0.99 ($\psi \simeq 100$), η'_I equals only 0.2 for the lowest velocity and 0.05 for the highest velocity.

Experimental single fiber collection efficiency data for the liquid DOP aerosol are also shown in Figure 5. In contrast to the fly ash data, the DOP η'_I values closely fit the Landell and Herrmann curve. These data strongly suggest that fly ash particles do impact the fibers but bounce through the filter at high velocities. Indeed, for particles larger than 4 μm the data indicate that approximately 80% of the particle-fiber collisions result in particle bounce at 1.5 m/s and that 95% result in particle bounce at 8 m/s.

Adhesion Probability

The amount of particle bounce for different velocities and particle sizes is indicated by the particle adhesion parameter, h, which is defined as the probability of a particle adhering to a fiber after colliding with it.[8] Theoretically, the probability of particle adhesion can be calculated from a consideration of the energies involved. A particle will not adhere to a fiber upon collision if the kinetic energy of the particle on rebound is greater than the energy of attraction (primarily due to London van der Waals forces).[9] Loffler[8] and and Dahneke[9] present the energy balance equation and the procedures for calculating critical conditions necessary for bounce to begin. As pointed out by Dahneke[9] and Esmen, et al.,[10] the equations are difficult to solve for a polydisperse, irregular dust such as fly ash and a multilayer fiber filter, so that adhesion probability cannot be predicted as a function of particle size and velocity. However, experimentally measured adhesion probability should show a correlation with particle kinetic energy.

The adhesion probability can be obtained from experimental data by taking the ratio of the experimentally measured single fiber collection efficiency to the theoretical single fiber collection efficiency. Since impaction predominates in this study,

$$\eta = \frac{\eta'_I}{\eta_I} \tag{10}$$

The adhesion probabilities calculated for all of the data points in Figure 3 are plotted against particle kinetic energy in Figure 6. The expected decrease in adhesion probability with increasing kinetic energy is evident. The data fall on a straight line (log-log plot) at low energies (high adhesion probability) but exhibit increasing scatter at higher energies (low adhesion probability).

The spread in data at high energies may be caused by the complex particle impaction and rebound pattern which would exist in this regime. High energy particles, after bouncing, will accelerate until reaching gas velocity; during acceleration they may impact another fiber and rebound again or they may adhere, depending on the velocity at impact. A very complex collection pattern can thus be expected for a polydisperse dust in a multilayer filter for particles with large kinetic energy. However, this mechanism cannot account for the very low adhesion probabilities measured on two experiments ($v = 5.2$ m/s and 8.0 m/s) when the particle kinetic energy exceeded 10^{-13} J. Additional data will be collected in an attempt to clarify these results.

Relative humidity can have a great effect on particle adhesion,[11] and thus could have contributed to the differences in adhesion probabilities measured in different experiments. Relative humidity ranged from 20-50% during the experiments, but the adhesion data could not be correlated with the relative humidity data.

A regression line was fit to the data of Figure 6 and is plotted in Figure 7. Also plotted are data of Loffler[8] and Esmen, et al.[10] Loffler's data were collected for 1.8-10.0 μm diameter NaCl particles collected on 20 μm diameter polyamide fiber filters while Esmen, et al., impacted 4.4 and 8.8 μm diameter uranine spheres on a flat brass substrate. Considering the different particles and substrates used, the agreement among the various experiments is good. Figure 7 indicates a region of particle inertial energy where particle adhesion can be expected to be very good ($E_K < 10^{-15}$J) and a region where particle adhesion can be expected to predominate ($E_K > 10^{-13}$J). In the intermediate energy regime, (10^{-15}J $< E_K < 10^{-13}$J), particle adhesion probability will be a strong function of the particular particle and filter used.

Practical Design Implications

The penetration characteristics reported here suggest that a novel, compact, high efficiency particle collector may be feasible. The device would operate at high gas velocities, and would collect particles over a wide size range by impaction. It would consist of two stages: 1) a fibrous media filter, which would efficiently collect small particles but allow some large particles to bounce through or reentrain; and 2) a cyclone, which can efficiently collect large particles. When operated in series, the two devices should collect all particle sizes with high efficiency.

Such a device would have many desirable properties. Our experiments indicate that the pressure drop across a clean fibrous bed, when operated at high velocities, (e.g., 1.5 m/s), is about the same as across a cyclone: 0.5-1 kPa. The total pressure drop across the device would thus be fairly low - on the order of 2 kPa. The device would be extremely simple in design and easy to operate; the only area where moving parts may be needed is in the filter cleaning system, and that would depend on the cleaning method chosen. The device, by operating at high gas velocities, would be very compact. It would collect all types of aerosols (solid and liquid) and would use relatively small amounts of energy.

The design and testing of such a two-stage device is now in the planning stage. An important design consideration now being addressed is the selection of an optimum fibrous material. The ideal material would have a fractional penetration similar to the stainless steel fiber beds but would be cheaper and easier to clean in situ. Materials such as felts and sintered fiber mats are being tested in preparation for the construction of a pilot two-stage device.

SUMMARY AND CONCLUSIONS

Particle bounce has been shown to play an important role in the collection of fly ash by mats of stainless steel fibers. The penetration of fly ash particles through 8 μm fiber filters in the 1-10 m/s velocity range increased with both particle size and velocity; since impaction was the controlling collection mechanism, these results run contrary to classical filtration theory.

Particle adhesion probability was found to be inversely proportional to particle kinetic energy. This result is in general agreement with previous adhesion studies, which were performed with monodisperse aerosols under controlled laboratory conditions. This study demonstrates that the particle adhesion properties of a polydisperse dust (fly ash), under conditions similar to those encountered by practical filters, can also be related to the particle kinetic energy.

These results have important implications for the operation of fibrous filters at high velocity, and may help explain cases where penetration is higher than anticipated. These experiments also suggest the possible use of a novel two-stage inertial collection device to take advantage of the high velocity particle penetration characteristics noted here.

ACKNOWLEDGEMENT

This work was funded by the Environmental Protection Agency under grant 804-700, James H. Turner, project officer.

NOMENCLATURE

A	filter cross-sectional area, m^2
C_c	Cunningham slip correction factor
d_f	fiber diameter, m
d_p	particle diameter, m
h	adhesion probability
L	filter thickness, m
m_f	filter mass, kg
v	superficial filtration velocity, m/s
V_f	total fiber volume, m^3
V_T	filter volume, m^3
α	filter solidity
η	theoretical filter collection efficiency
η'	experimental filter collection efficiency
η_I	theoretical single fiber impaction efficiency
η'_I	experimental single fiber impaction efficiency
η_S	combined single fiber collection efficiency
μ	gas viscosity, Pa·s
ρ_f	fiber density (kg/m^3)
ρ_p	particle density (kg/m^3)
ψ	inertial impaction parameter

REFERENCES

1. Davies, C.N. Air Filtration. New York, Academic Press, Inc., 1973.

2. Pich, J. Theory of Aerosol Filtration by Fibrous and Membrane Filters. In: Aerosol Science, Davies, C.N. (ed.). New York, Academic Press, Inc., 1966.

3. Landahl, H.D., and R.G. Herrman. Sampling of Liquid Aerosols by Wires, Cylinders, and Slides, and the Efficiency of Impaction of the Droplets. J. Colloid Sci. 4(2):103-136, 1949.

4. Strauss, W. Industrial Gas Cleaning. 2nd ed. Oxford, Pergamon Press, 1975. p. 287.

5. Dorman, R.G. Filtration. In: Aerosol Science, Davies, C.N. (ed.). New York, Academic Press, Inc., 1966.

6. Dill, R.S. A Test Method for Air Filters. Trans. Amer. Society of Heating and Ventilating Engin. 44:379-386, 1938.

7. Stairmand, C.J. Sampling Gas-Borne Particles. Engineering. 41:141-143, 181-183, 1941.

8. Loffler, F. Adhesion Probability in Fibre Filters. Clean Air. 8(4), 1949.

9. Dahneke, B. The Capture of Aerosol Particles by Surfaces. J. Colloid Interface Sci. 37(2):342-352, 1971.

10. Esmen, N.A., P. Ziegler, and R. Whitfield. The Adhesion of Particles Upon Impaction. J. Aerosol Sci. 9:547-556, 1978.

11. Corn, M. The Adhesion of Solid Particles to Solid Surfaces, I. A Review. J. Air Poll. Control Assoc. 11(11):523-528, 1961.

Table 1. VALUES OF TEST VARIABLES USED IN THIS STUDY.

Dust	
Type	resuspended fly ash
Count median diameter	0.14 μm
Geometric standard deviation	1.9
Particle density (ρ_p)	2.2×10^3 kg/m^3
Filter	
Fiber type	310 stainless steel
Fiber diameter (d_f)	8 μm
Fiber density (ρ_f)	7.92×10^3 kg/m^3
Filter cross-sectional area(A)	0.093 m^2
Filter mass, m_f	0.032 kg
Filtration velocity (V)	1 - 10 m/s

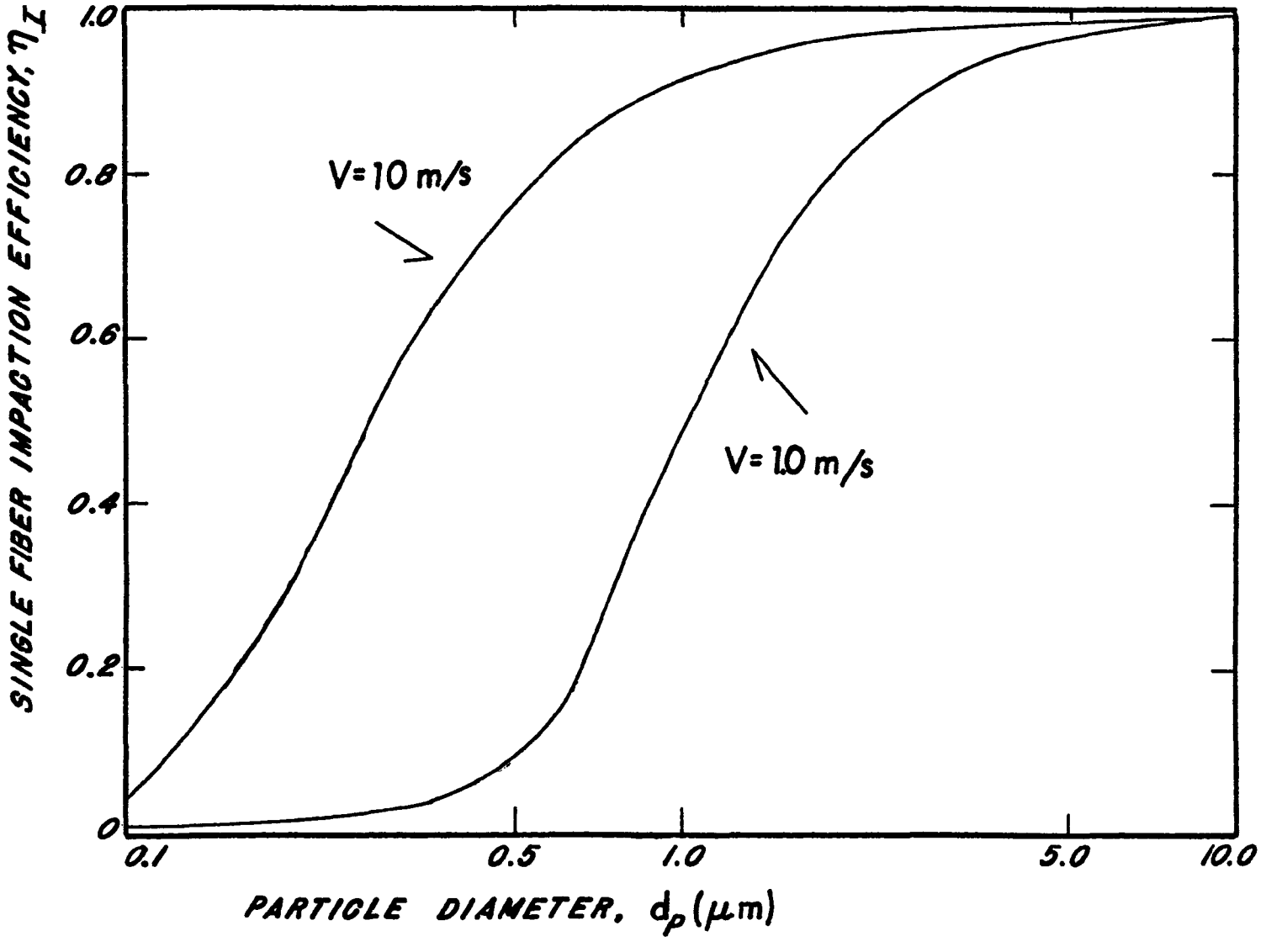

Figure 1. Theoretical single fiber impaction efficiency vs. particle diameter at 1 and 10 m/s filtration velocities.

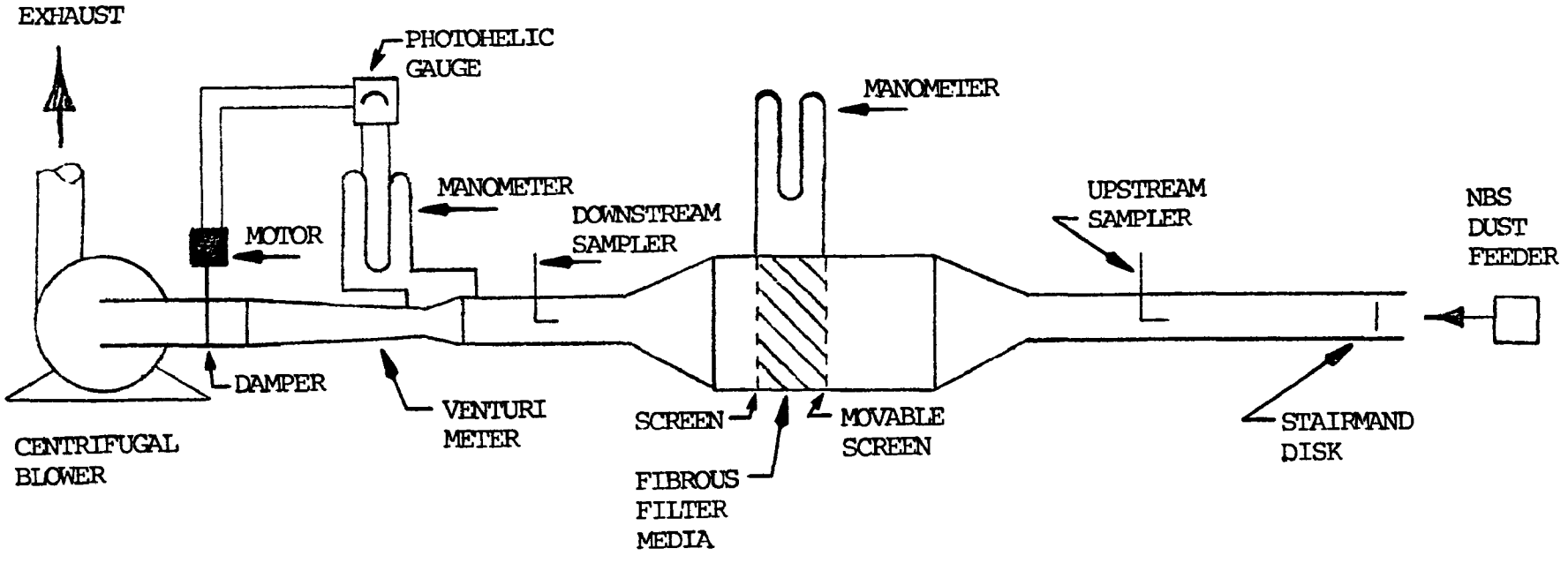

Figure 2. High velocity filtration apparatus.

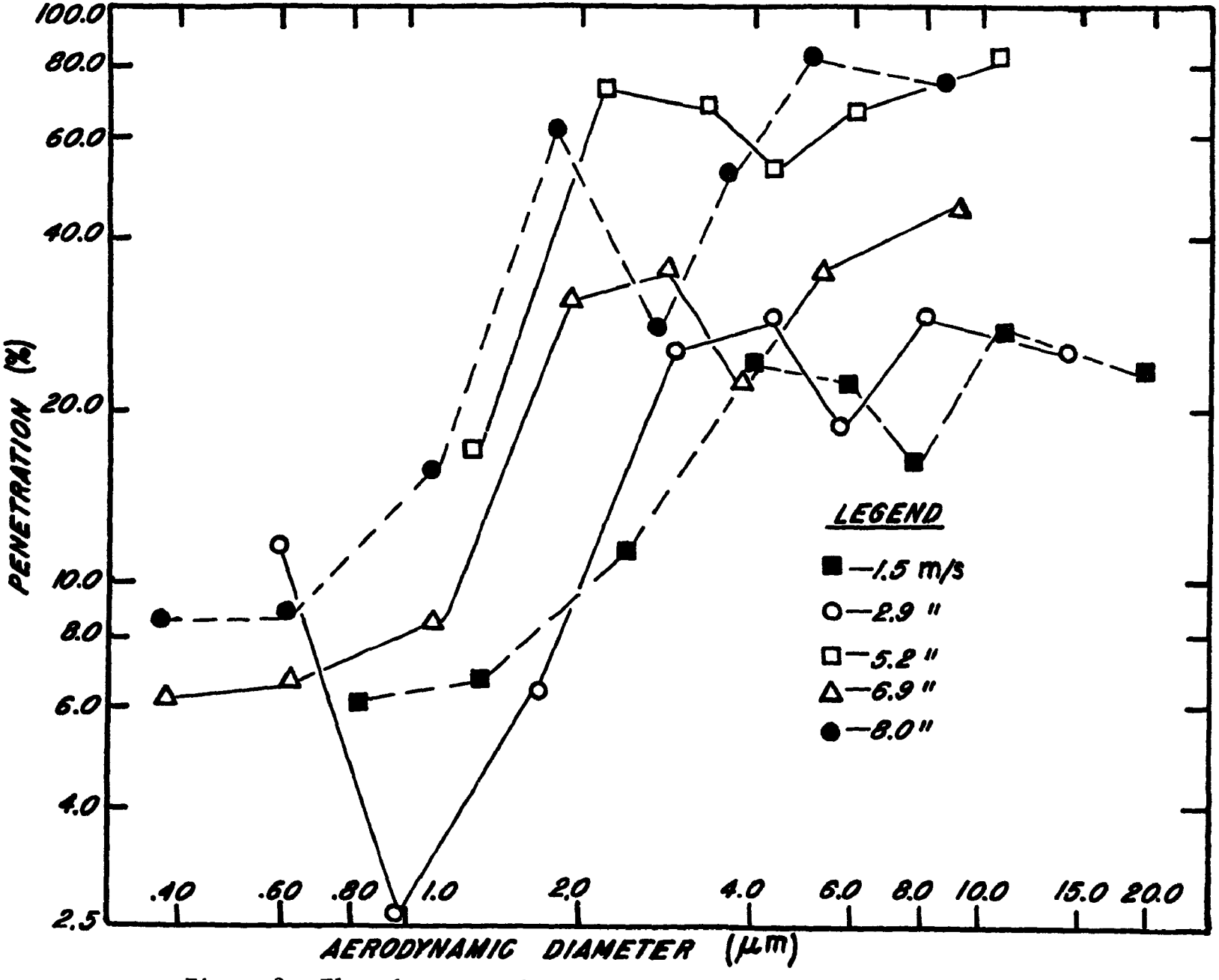

Figure 3. Fly ash penetration vs. particle size at five filtration velocities.

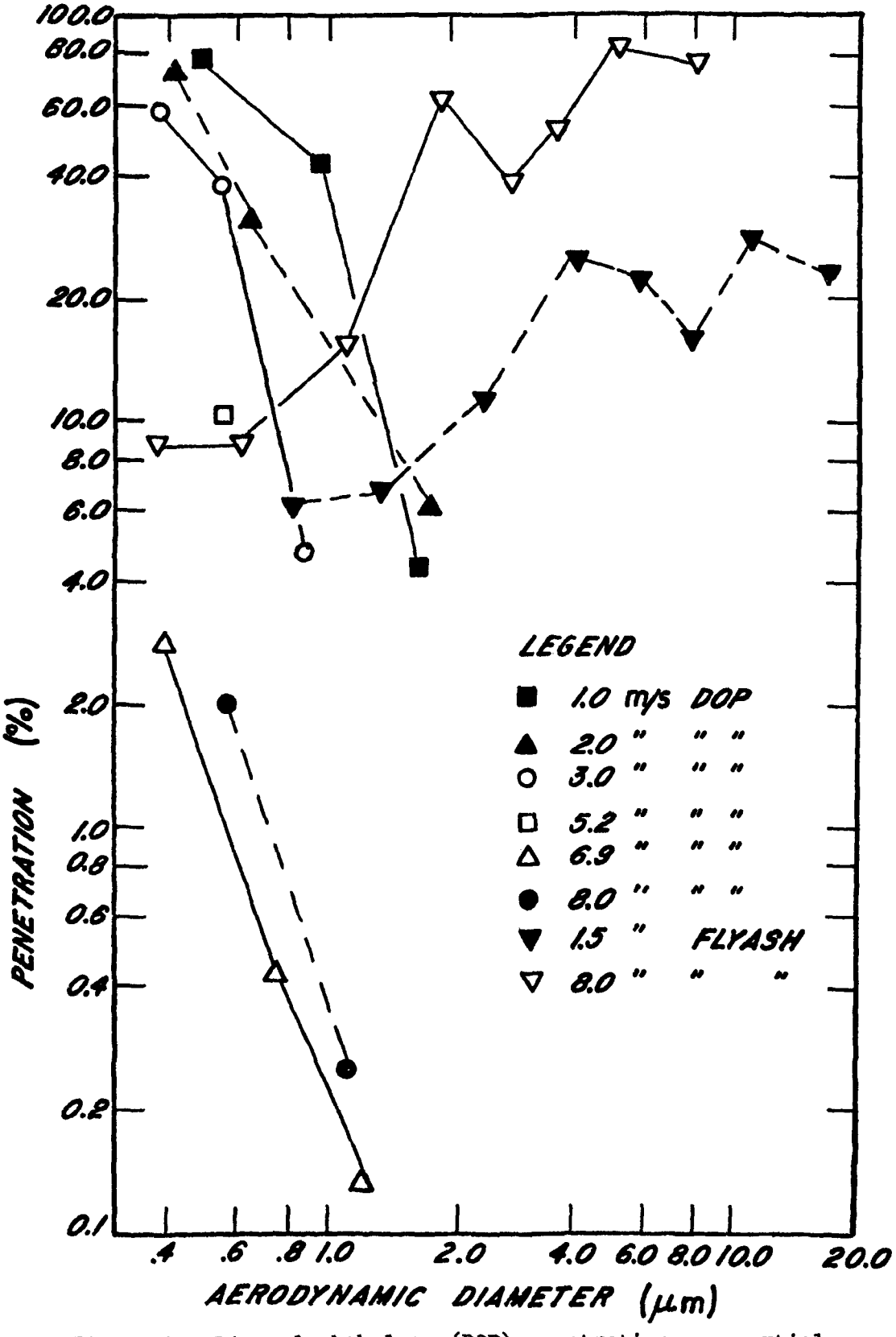

Figure 4. Dioctyl phthalate (DOP) penetration vs. particle size at six filtration velocities.

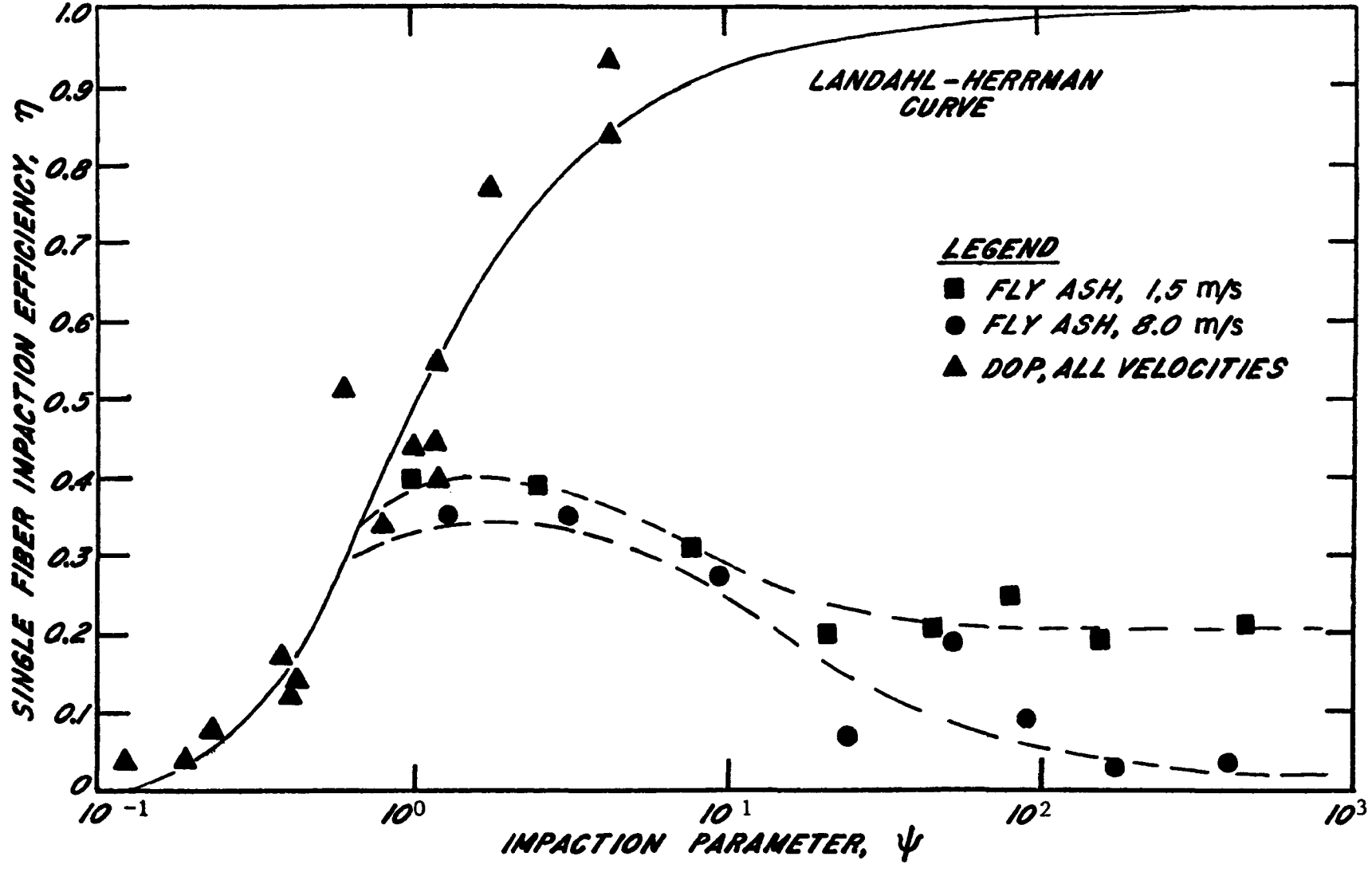

Figure 5. Theoretical and experimental single fiber impaction efficiencies vs. impaction parameter for DOP and fly ash.

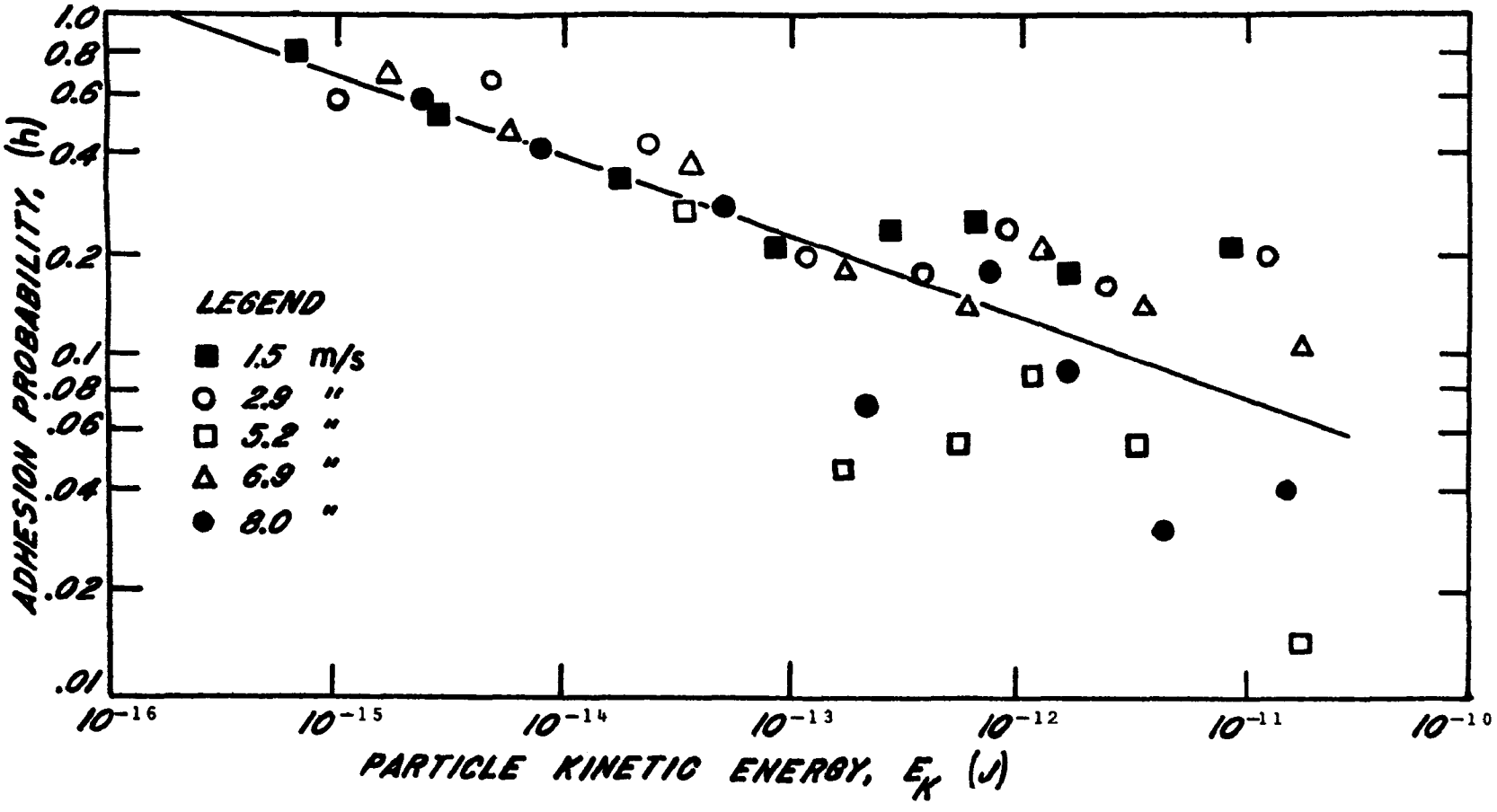

Figure 6. Fly ash adhesion probability vs. particle kinetic energy.

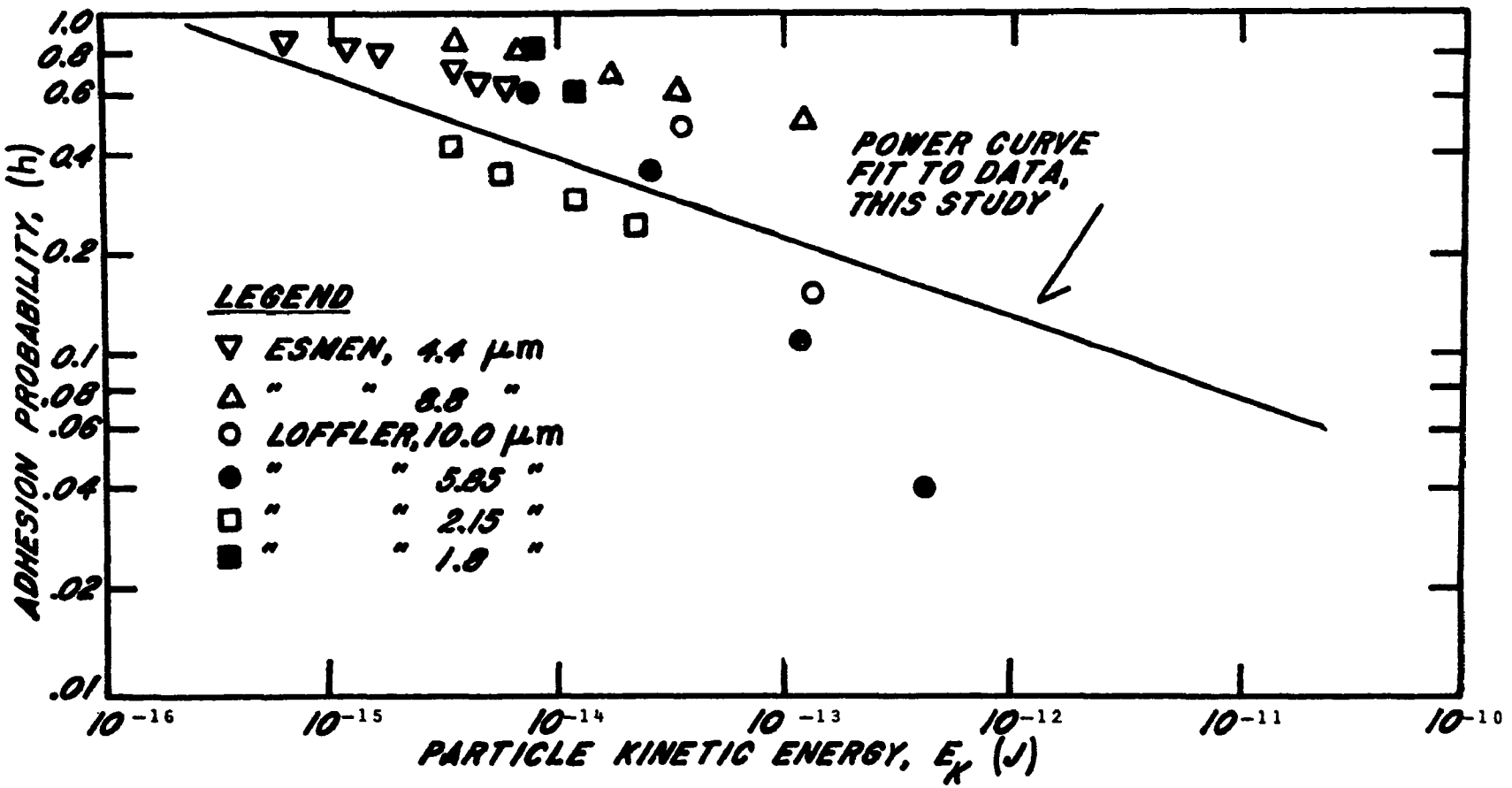

Figure 7. Comparison of adhesion probability data from this study with those of other investigators.

THE EFFECT OF DUST RETENTION ON PRESSURE DROP IN A HIGH VELOCITY PULSE-JET FABRIC FILTER

By:

Michael J. Ellenbecker and David Leith
Harvard School of Public Health
Department of Environmental Health Sciences
665 Huntington Avenue
Boston, Massachusetts 02115

ABSTRACT

Pulse-jet fabric filters exhibit abnormally high pressure drops when operated at higher than normal superficial filtration velocities. The causes of high pressure drop are investigated for a pilot-scale pulse-jet filter collecting fly ash at 50, 75, 100, 125, and 150 mm/s filtration velocities.

The measured equilibrium pressure drops ranged from 0.35 kPa (1.4 in H_2O) at low velocity to 10.2 kPa (40.8 in H_2O) at high velocity. Retention of a large mass of dust on the fabric was found to have a significant effect on equilibrium pressure drop at all of the tested filtration velocities.

The dust deposit's distribution, total mass, and specific resistance (K_2) all remained essentially constant at lower filtration velocities, but changed dramatically at the highest test velocity. At the 150 mm/s velocity the total dust mass doubled, the dust distribution equalized over the surface of each bag, and K_2 increased by a factor of 4.7.

THE EFFECT OF DUST RETENTION ON PRESSURE DROP IN A HIGH VELOCITY PULSE-JET FABRIC FILTER

INTRODUCTION

Fabric filters have been widely used for particle collection because they operate with high efficiency, and will find increased future use as particle emission regulations become more stringent. Pulse-jet filters may be well suited for both new and retrofit applications because they operate at higher superficial filtration velocities (air-to-cloth ratios) than do reverse-air or shaker-cleaned systems, and are correspondingly smaller. It is tempting to increase filtration velocity through a pulse-jet system still further, since the decreased installation cost may more than compensate for the increased cost associated with operating at a higher pressure drop. Occasionally, space limitations may make a high velocity pulse-jet system the only option which will both fit and provide the necessary collection efficiency.

However, increases in filtration velocity above the values commonly used are associated with large increases in system pressure drop,[1,2] which tend to make high velocity operation both uneconomical and impractical. Fabric filtration theories do not relate this increased pressure drop to system operating variables.

Redeposition of the dust deposit following a cleaning pulse has been identified[2] as one cause of increased pressure drop at high velocity. Redeposition occurs when dust agglomerates removed from a fabric surface by a cleaning pulse are recaptured on the same bag or a neighboring bag before they can fall into the hopper. Another cause of increased pressure drop is the failure to remove part of the dust deposit from the fabric during cleaning.[3] Unremoved and redeposited dust have the same effect on the system--excessive dust on the fabric. In this paper they will not be distinguished, and their total effect will be termed "mass retention." The mass retained on a fabric after cleaning will be called "residual" mass.

Mass retention causes the dust deposit to build up from cleaning cycle to cleaning cycle until the system reaches an equilibrium condition in which the total mass of dust on the bag is much greater than the mass of dust collected during one cleaning cycle. The pressure drop across this large dust deposit is much greater than the pressure drop across a deposit which consists solely of the dust collected during one cleaning cycle. Mass retention becomes very significant at high filtration velocities, presumably because of the increased tendency to drag dust agglomerates back to the bag surface as filtration resumes after cleaning.[2] Therefore, it appears that redeposition-caused dust deposit retention may be a key factor in preventing the economical use of high velocity pulse-jet filter systems.

The research described here was undertaken to quantify the factors which contribute to increased pressure drop when a pulse-jet fabric filter is operated at high superficial filtration velocities. The relative contributions of changes in filtration velocity, magnitude and distribution of the dust mass, and dust deposit specific resistance were determined.

THEORY

Pressure Drop

Darcy's law, which is often applied to fabric filter systems, states that the rate of flow through a porous medium is directly proportional to the pressure gradient causing flow.[4] In fabric filtration, the total pressure drop Δp can be divided into the pressure drop across the clean fabric Δp_f and that across the dust deposit Δp_d:

$$\Delta p = \Delta p_f + \Delta p_d \tag{1}$$

Darcy's Law then takes the following form:[5-8]

$$\Delta p = K_1 v + K_2 v w \tag{2}$$

in which K_1 is the clean fabric resistance, K_2 is the dust deposit specific resistance, v is superficial filtration velocity, and w is the areal density of the dust deposit.

Most filtration models define K_1 for a "conditioned" fabric rather than a clean or unused fabric. K_1 is then the resistance of a fabric which has been conditioned by dust which lodges <u>within</u> the fabric itself and is not removed by cleaning, while K_2 characterizes the resistance of the actual dust cake which forms <u>on</u> the fabric. In high velocity pulse-jet systems, however, large amounts of dust are always present within the structure of the felted material, and a true dust cake is not always formed on the surface.[7,9,10] It is thus not possible to distinguish the dust which is conditioning the fabric and the dust which is forming the cake; under these circumstances, it seems more appropriate to consider the clean fabric separately and account for all of the dust in the dust deposit specific resistance, K_2.

Theoretical calculations of pressure drop in a fabric filter system are usually based on the assumption that the cleaning mechanism employed is 100% effective in removing the dust deposit added since the last cleaning cycle.[8,11-13] Under this assumption, the pressure drop immediately <u>after</u> cleaning is the pressure drop across the (conditioned) fabric only, Δp_f:

$$\Delta p_a = K_1 v \tag{3}$$

In this case the pressure drop just <u>before</u> a cleaning pulse is equal to Δp_f plus the pressure drop across the dust deposit added since last cleaning:

$$\Delta p_b = K_1 v + K_2 v w_0 \tag{4}$$

where w_0 is the incremental dust deposit added during one cleaning cycle.

If dust mass is retained on the fabric, however, the model must be modified to include the pressure drop across this deposit. The residual dust mass in a fabric filter can be characterized by the mass retention coefficient, γ, defined as the fraction of the dust mass which remains on the bag after pulse cleaning.[3] If a fabric filter system is operated to equilibrium with a dust deposit retention of γ, the pressure drop before a cleaning pulse is:[3]

$$\Delta p_b = K_1 v + K_2 v w_0 \left(\frac{1}{1-\gamma}\right) \tag{5}$$

The pressure drop after a cleaning pulse is:[3]

$$\Delta p_a = K_1 v + K_2 v w_0 \left(\frac{\gamma}{1-\gamma}\right) \tag{6}$$

Dust Deposit Profiles

Mass retention phenomena can lead to an uneven distribution of the residual dust mass along and among the bags in a fabric filter system,[3,14] which will lead to a corresponding uneven velocity profile along each bag (assuming a constant specific resistance). Since the pressure drop is the same at all points on each bag, a bag area with a small dust deposit will have a higher local filtration velocity than an area with a large dust deposit.

The effect of dust deposit profiles can be investigated by dividing the bag into n segments, each with a constant dust deposit areal density. Assume that K_1 and K_2 are constant from segment to segment, and that the segments are numbered consecutively from one end of the bag.

The total pressure drop across all segments is equal:

$$\Delta p = v_i (K_1 + K_2 w_i) \tag{7}$$

The total airflow through the bag must equal the sum of the flows through the individual segments:

$$Q = vA = \sum_{i=1}^{n} v_i A_i \tag{8}$$

Substituting Equation 7 into Equation 8 and rearranging,

$$\Delta p = vA \left[\sum_{i=1}^{n} \frac{A_i}{K_1 + K_2 w_i} \right]^{-1} \tag{9}$$

Equation 9 states that pressure drop can be calculated from the harmonic average of the local dust deposit areal densities.[15]

Factors Affecting Pressure Drop

Equation 9 gives the pressure drop across the dust and fabric for an unevenly distributed dust deposit; an examination of this equation reveals the factors which can cause a change in the pressure drop. These factors include:

1) changes in v;
2) changes in the magnitude of the w_i values (i.e., changes in the average dust deposit areal density, $\overline{w}$);
3) changes in the distribution of the w_i values;
4) changes in the fabric resistance, K_1; and
5) changes in the dust deposit specific resistance, K_2.

The possible contributions of changes in each factor listed above to changes in pressure drop will be discussed.

Changes in Velocity. Equation 2 predicts a direct proportionality between pressure drop and superficial filtration velocity. If K_1 and K_2 are not functions of velocity and the dust deposit is constant, a doubling of the filtration velocity will cause a doubling in the pressure drop. Conversely, any change in Δp other than a doubling when v is doubled will reflect a change in the magnitude of the dust deposit, the distribution of the dust deposit, K_1, and/or K_2.

Changes with Dust Deposit Profile. Changes in the profile of the dust deposit can influence pressure drop. Solutions in Equation 9 reveal that, for a given mass of dust, the highest pressure drop occurs when the dust is evenly distributed over the fabric surface.[16] The wider the variation in w_i, the lower the pressure drop.

Changes with Dust Deposit Magnitude. Changes in the magnitude of the average dust deposit have a direct effect on pressure drop. Equation 2 states that a doubling of the average dust deposit areal density will cause a doubling of Δp, assuming constant v, K_1, and K_2.

Changes with K_1 and K_2. K_1 may also vary with filtration velocity, perhaps due to a compression of the fibers comprising the felt. In many cases, however, the pressure drop across the fabric is much smaller than the pressure drop across the dust deposit; when this is so, changes in K_1 will have little effect on the total pressure drop.

Previous work has shown the dust deposit specific resistance, K_2, to be a function of the superficial filtration velocity. Billings[7] summarizes data which seem to indicate a linear relationship between filtration velocity and specific resistance; i.e., "increases of velocity by factors of 2 or 3 tend to produce similar increases in K_2." Dennis[17] found K_2 to be proportional to $v^{0.5}$ for fly ash collected on woven fabrics. Rudnick[18] found K_2 to vary with $v^{0.2}$ in his laboratory-scale tests of woven fabrics, while Borgwardt[15] measured values of K_2 in laboratory and field tests of fly ash on woven fiber glass which varied with $v^{1.5}$.

K_2 is usually determined by solving Equation 2, using a calculated or

measured average value for the dust deposit areal density. If the dust deposit is not evenly distributed, however, this procedure will give an apparent value for K_2, K_{2a}, which is the value K_2 would take if the dust deposit were evenly distributed and the pressure drop were the same as the value measured. The actual value of K_2 can only be determined if the dust deposit profile on each bag is known. K_2 can then be calculated by solving Equation 9 for K_2.

EXPERIMENTS

Pressure drop and dust deposit profiles were measured on a pilot-scale pulse-jet fabric filter.[19] The fabric filter contained three commercial-scale bags manufactured from polyester needled felt. The test dust was resuspended fly ash, fed at a constant mass rate to the filter inlet. Three experiments were performed at each of five superficial filtration velocities: 50, 75, 100, 125, and 150 mm/s.

After each experiment, the dust deposit profiles along each bag were measured using a beta gauge areal density measurement system.[19] The bags were 2.4 m long, and areal density measurements were taken every 0.1 m. The pressure drops were measured with time, and each experiment was run until equilibrium was reached.

Manometer fluid was accidentally deposited on one bag during the third experiment, making it necessary to wash the bags. The dust deposit profiles and equilibrium pressure drops were found to be significantly different before and after washing.[19] Since this difference confounds the data, the results of the first three experiments are not included in the following discussion.

RESULTS

Dust Deposit Profiles

The dust deposit profiles from the fifteen experiments were described and analyzed previously,[19] and are summarized here. Figure 1 shows the dust deposit areal density profiles for each superficial filtration velocity, averaged over the last twelve experiments. The average dust deposit areal density is plotted against filtration velocity in Figure 2.

Pressure Drop

The equilibrium total pressure drop was measured at the conclusion of each experiment. The total pressure drop (Δp_t) includes the pressure drop across the dust deposit (Δp_d), the pressure drop across the clean fabric (Δp_f), and the pressure drop across the venturi nozzle (Δp_n). The pressure drop appearing in the theoretical relationship of Equation 9 is the pressure drop across the fabric and dust deposit (Δp_{f+d}), and can be determined by subtracting Δp_n from Δp_t.

Δp_n was measured at each filtration velocity by operating the baghouse

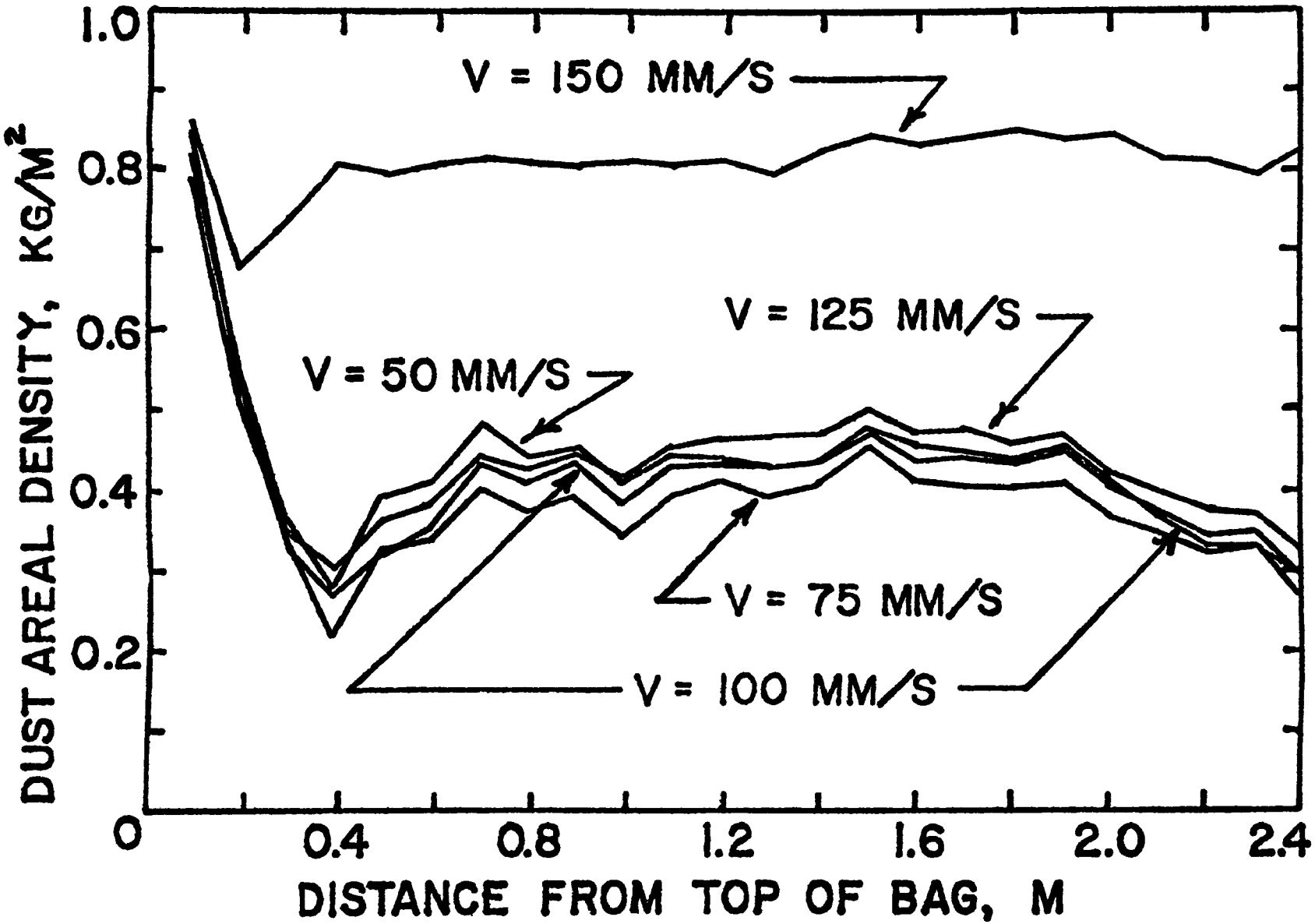

Figure 1. Average dust deposit areal density profile at each filtration velocity.

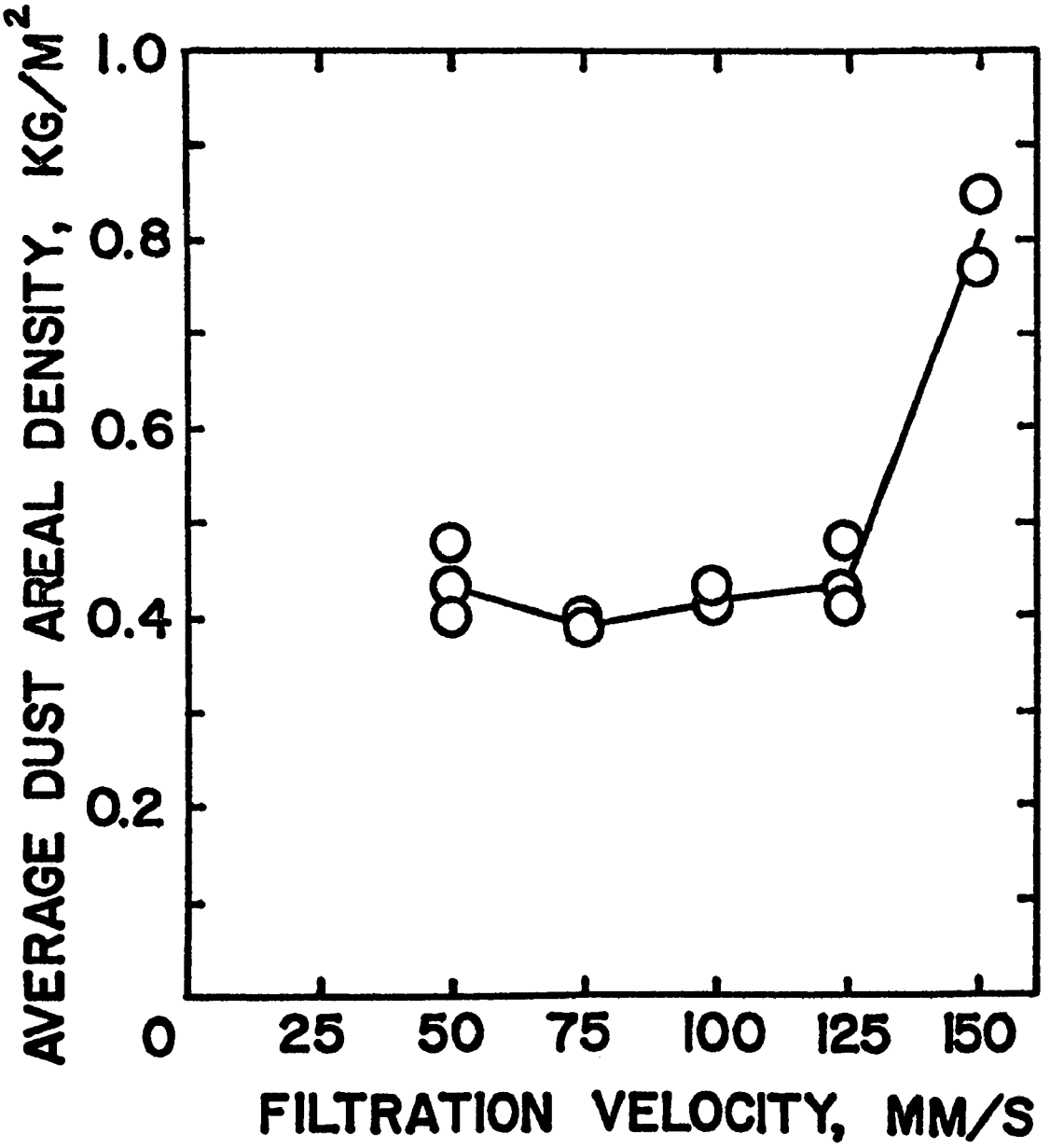

Figure 2. Average dust deposit areal density for each of the last twelve experiments.

without bags installed. The pressure drop across the fabric and dust deposit, obtained by subtracting Δp_n from Δp_t at each filtration velocity, is plotted against superficial filtration velocity in Figure 3.

According to Darcy's law, the pressure drop across the clean fabric is a linear function of velocity (Equation 2). The fabric resistance (K_1) of the test fabric was 850 Pa-s/m (0.02 in H_2O/fpm), giving values of Δp_f which range from 40 Pa (0.2 in H_2O) for the lowest test velocity to 130 Pa (0.5 in H_2O) for the highest velocity. These values are small compared to the pressure drops across the fabric and dust combined, as shown in Figure 3.

DISCUSSION

Summary of Factors Affecting Pressure Drop

The equilibrium system pressure drops, Δp_t, measured in these experiments ranged from 350 Pa (1.4 in H_2O) for one experiment at a filtration velocity of 50 mm/s to 10.2 kPa (40.8 in H_2)) for one experiment at a filtration velocity of 150 mm/s. The first number represents an acceptable pressure drop at a fairly high air-to-cloth ratio (10 cfm/ft^2), while the second number represents a very high pressure drop at a very high air-to-cloth ratio (30 cfm/ft^2). The dust deposit measurements taken during this series of tests make it possible to determine the relative contributions of changes in filtration velocity, dust deposit magnitude and distribution, and specific resistance to this increase in pressure drop at higher velocities.

The factors contributing to a change in Δp when the superficial filtration velocity is changed are summarized in Tables 1 and 2. Table 1 quantifies those factors contributing to a change in Δp_d when the filtration velocity is increased from one lower velocity (75 mm/s) to another lower velocity (100 mm/s). Table 2 quantifies the factors contributing to the dramatic change in Δp_d when going from the 125 mm/s filtration velocity to 150 mm/s The specific resistances listed in these tables are the actual K_2 values calculated from Equation 9, not K_{2a} values from Equation 2.

When going from the 175 mm/s filtration velocity to 100 mm/s, the pressure drop across the dust deposit increases by a factor of 1.64. Most of this increase is accounted for by the increase in velocity itself, since Δp_d should increase by a factor of 1.33 according to Darcy's law. Changes in the dust deposit distribution, dust deposit magnitude, and K_2 all account for a small fraction of the increase.

The causes of the nearly elevenfold increase in Δp_d when going from the 125 mm/s velocity to 150 mm/s are given in Table 2. The increase in filtration velocity and the change to a flatter dust distribution cause relatively small increases in Δp_d. The average areal density of the dust deposit nearly doubles, accounting for almost a factor of two increase. The most important cause of the increase, however, is the factor of 4.69 increase in the dust deposit specific resistance.

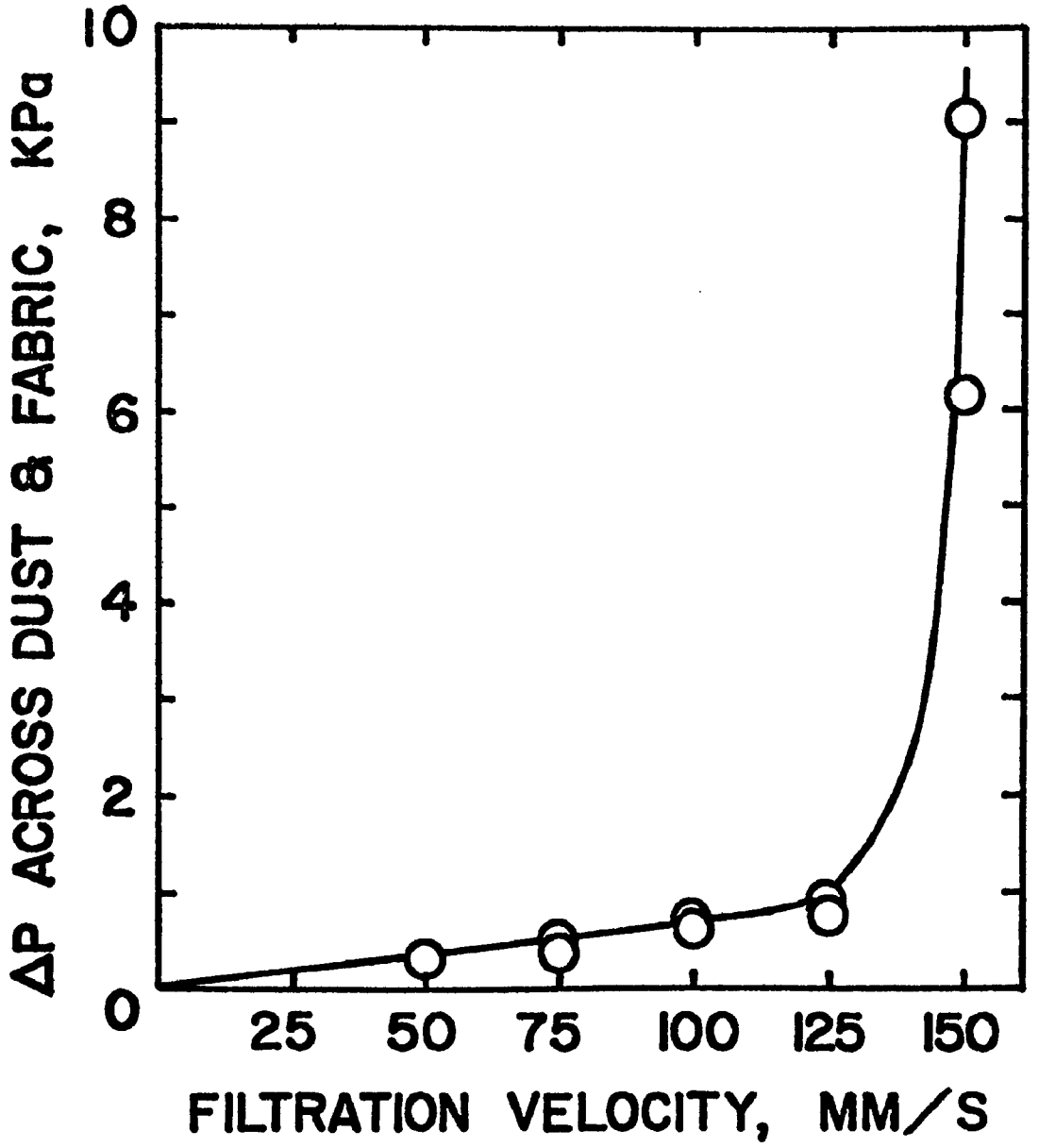

Figure 3. Measured pressure drop across the dust and fabric vs. filtration velocity.

Table 1. FACTORS CONTRIBUTING TO THE CHANGE IN Δp_d AT LOWER FACILITIES

Factor Contributing To The Change In Δp_d	Superficial Filtration Velocity (mm/s)		Ratio Of Values At The Two Velocities
	75	100	
Δp_d(Pa)	330	540	1.64
v(mm/s)	75	100	1.33
Distribution Of w_i values*	0.951	0.969	1.02
Magnitude Of $\bar{w}(g/m^2)$	394	420	1.07
K_2 (s^{-1})	11,740	12,460	1.06

*Ratio of the measured Δp_d to the value Δp_d would take if the dust deposit was evenly distributed.

Table 2. FACTORS CONTRIBUTING TO THE CHANGE IN Δp_d AT THE HIGHEST VELOCITIES

Factor Contributing To The Change In Δp_d	Superficial Filtration Velocity (mm/s)		Ratio Of Values At The Two Velocities
	125	150	
Δp_d(Pa)	680	7,455	10.96
v(mm/s)	125	150	1.20
Distribution Of w_i Values*	0.946	0.998	1.06
Magnitude Of $\bar{w}(g/m^2)$	439	807	1.84
K_2 (s^{-1})	13,100	61,440	4.69

*Ratio of the measured Δp_d to the value Δp_d would take if the dust deposit was evenly distributed.

Total Dust Mass

The previous discussion centered on the change in pressure drop at different superficial filtration velocities. It should be noted, however, that a very large mass of dust remained on the bags after cleaning for all filtration velocities. This large dust mass contributed a great deal to the high pressure drops measured in some of these experiments. As shown in Figure 2, the average dust deposit areal density ranged from 0.39-0.44 kg/m^2 at the lower filtration velocities, and doubled to an average value of 0.81 kg/m^2 at the highest velocities. These values, when combined with the incremental dust deposit used in these tests (w_o=3.1 g/m^2), resulted in mass retention coefficients (γ) of 0.993 at lower velocities and 0.996 at the highest velocity.

The increase in pressure drop due to mass retention can be determined by solving Equation 4 to give Δp with no mass retention and comparing the values obtained with the pressure drops measured with retention. The results of such calculations at each filtration velocity are presented in Figure 4. The curve labelled "no mass retention" represents the lowest possible pressure drop at each velocity which could be obtained on the pilot system with the experimental conditions used. The "measured mass retention" curve represents the pressure drops measured during the experiments; the difference between the two curves represents the increased pressure drop caused by retention of the dust deposit.

The curves show that mass retention at velocities through 125 mm/s, while significant, did not cause the system pressure drop to rise to levels higher than 2,000 Pa, or 8 in H_2O . Mass retention would have to be reduced significantly at 150 mm/s, however, to give a pressure drop in this range.

Dust Deposit Specific Resistance

Magnitude. At velocities below 150 mm/s, pressure drops measured in these experiments were relatively low, even though a large mass of dust was deposited on the fabric. This reflects the relatively low specific resistance (K_2) values measured here, compared to those measured on woven fabrics.[7,10,17,18] The K_2 values measured at 150 mm/s, while much higher than the others measured here, are still lower than typical values for woven fabrics. Lower specific resistance is due to the nature of the dust deposit on non-woven materials, where some particles are deposited within the material on more-or-less isolated fibers.[20] The porosity of this type of deposit is much greater than when the same particles form a particle-to-particle dust layer on the surface of a woven fabric.

Dust Profile Effects. The actual and apparent dust specific resistance values, K_2 and K_{2a}, are compared at each filtration velocity in Table 3. The values listed are the averages from the experiments at each velocity. The actual values were calculated by substituting the 72 areal densities measured on the three bags during each experiment into Equation 9 and solving for K_2 using Newton's method.

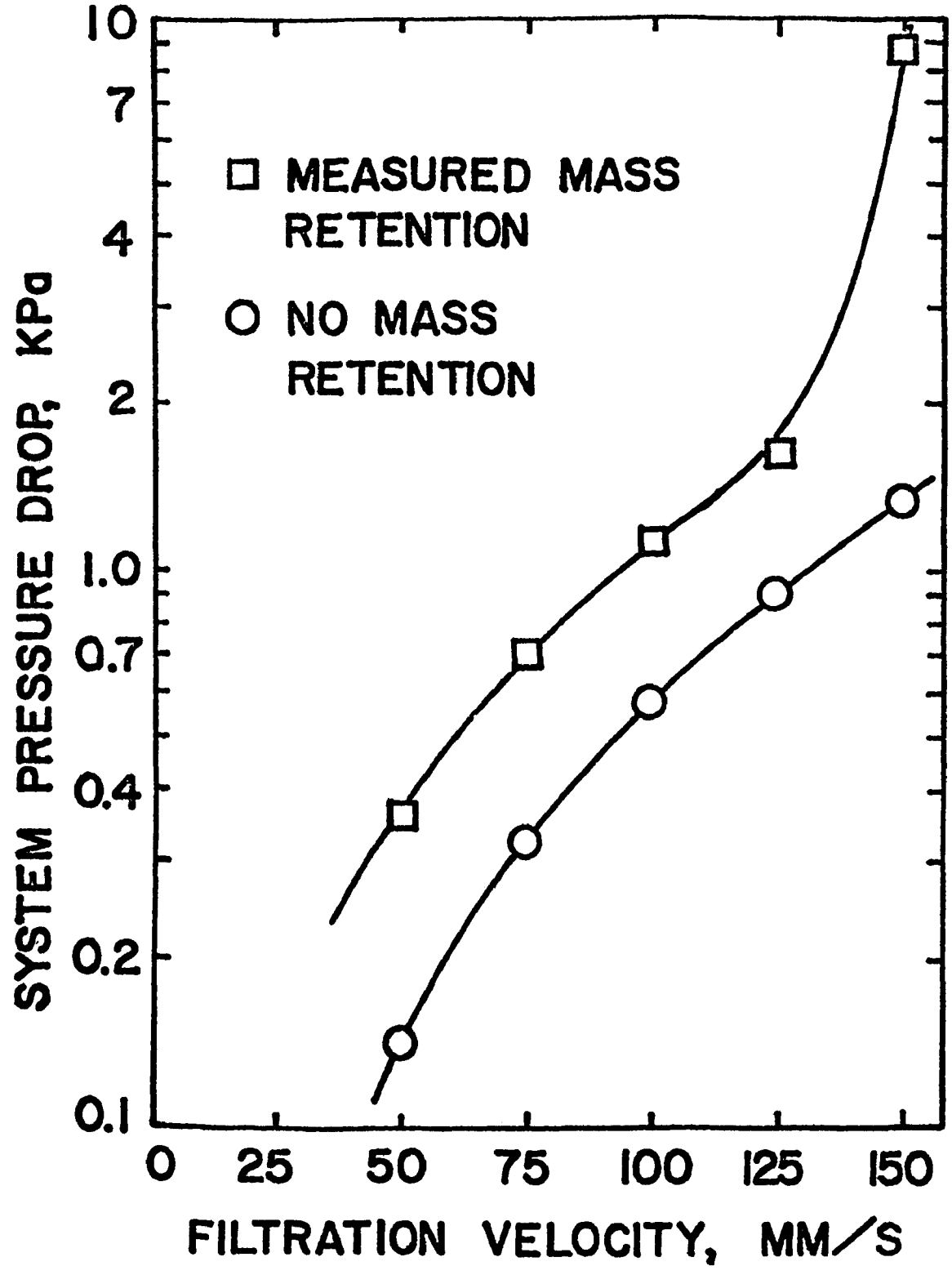

Figure 4. Pressure drop with measured mass retention and pressure drop with no mass retention vs. filtration velocity.

Tables III. COMPARISON OF APPARENT AND ACTUAL VALUES OF DUST DEPOSIT SPECIFIC RESISTANCE.

Superficial Filtration Velocity (mm/s)	Dust Deposit Specific Resistance, s^{-1}		% Error
	Apparent	Actual	
50	10,400	10,800	4.1
75	11,200	11,700	4.6
100	12,800	13,400	4.9
125	12,500	13,100	4.9
150	61,200	61,400	0.5

The errors in the apparent values of K_2 at lower velocities ranged from 4 to 5%, while the error at 150 mm/s was only 0.5%. The low error at the highest velocity reflects the essentially flat profiles measured at that velocity, while the higher errors reflect the characteristic profiles measured at lower velocities. Greater variations in dust deposit along the bags would cause greater errors in K_{2a}.

Changes in Filtration Velocity. The changes in K_2 with filtration velocity do not follow the pattern noted by others,[7,15,17,18] who found K_2 to be proportional to v^a, where $0.2 \leq a \leq 1.5$. Here, K_2 increased only slightly at the lower test velocities, showing a 20% increase when the filtration velocity was raised from 50 to 125 mm/s. The nature of the dust deposit was evidently only slightly affected by the deposition velocity over this range.

The dust-fabric structure changed dramatically at the highest test velocity, however, as indicated by the nearly five-fold increase in K_2 accompanied by an almost doubling of $\overline{w}$. The sudden change in the dust deposit and specific resistance seem to indicate that a fundamental change in the dust deposit occurs when the filtration velocity is raised above some critical value. It seems probable that the same factor which was responsible for the doubling of the amount of dust retained on the fabric was also responsible for the increased flow resistance of the deposited dust. The amount of dust deposited at the 150 mm/s velocity may have been sufficient to form a true dust cake on the surface of the felt; such a cake could account for the higher K_2 values measured at that velocity. Alternatively, some "collapse" mechanism may have occurred, causing the dust-fabric structure to become more firmly packed, making the dust more difficult to remove, and increasing K_2.

SUMMARY AND CONCLUSIONS

Dust deposit retention had a significant effect on equilibrium pressure drop at all of the tested filtration velocities. The measured values of the mass retention coefficient (γ) ranged from 0.993 to 0.996, indicating that over 99% of the dust deposit was not removed by each cleaning pulse. It would be desirable to identify basic changes in the cleaning process which will increase the cleaning efficiency.

The dust deposit's distribution, total mass, and specific resistance all followed the same pattern with changes in superficial filtration velocity. They remained essentially constant at all lower velocities, but changed dramatically at the highest test velocity. At the 150 mm/s velocity the total mass doubled, the distribution equalized over the surface of each bag, and the specific resistance increased by a factor of 4.7. A fundamental difference in the dust deposit formation and removal process must exist at the highest velocity to account for these changes.

The measured equilibrium pressure drops ranged from very low (0.4 kPa, 1.4 in H_2O) to very high (10.2 kPa, 40.8 in H_2O). All of these values could have been reduced if mass retention would have been reduced; the highest pressure drops were due more to the increase in specific resistance, however.

A test program is planned to measure pressure drop and areal densitites at many velocities between 125 and 150 mm/s, in an attempt to determine the precise manner in which the dust profile and K_2 change over this range. Tests are also planned to determine the relative contribution of cleaning efficiency and redeposition to mass retention, and to measure local variations in K_2.

ACKNOWLEDGMENTS

This work was supported in part by the Bird Companies Charitable Foundation, Inc., and in part by EPA grant 804-700.

NOMENCLATURE

Symbols

A	area of filter bag
K_1	clean fabric resistance
K_2	dust deposit specific resistance
K_{2a}	apparent dust deposit specific resistance
Δp	pressure drop
n	number of bag segments
Q	air flow rate
v	superficial filtration velocity
w	dust deposit areal density
γ	mass retention coefficient

Subscripts

a	after cleaning pulse
b	before cleaning pulse
f	fabric
n	venturi nozzle
t	total
0	incremental quantity (one cleaning cycle)
1,2,...,n	bag segments

REFERENCES

1. Leith, D., S. N. Rudnick, and M. W. First. High Velocity, High Efficiency Aerosol Filtration. EPA Report EPA 600/2-76-020. National Technical Information Service, Springfield, Va., 1976.

2. Leith, D., M. W. First, and H. Feldman. Performance of a Pulse-Jet Filter at High Filtration Velocity - II. Filter Cake Redeposition. J. Air Poll. Control Assoc. 27(7):636, 1977.

3. Ellenbecker, M. J. and D. Leith. Effect of Dust Cake Redeposition on Pressure Drop in Pulse-Jet Fabric Filters. Proceedings of 3rd International Powder & Bulk Solids Handling & Processing Conference. Rosemont, Ill., May 1978.

4. Carman, P. C. Flow of Gases Through Porous Media. New York, Academic Press, 1956.

5. Williams, C. E., T. Hatch and L. Greenburg. Determination of Cloth Area for Industrial Air Filters. Heat. Piping Air Cond. 12(4):259, 1940.

6. Silverman, L. Filtration Through Porous Materials. Heat. Vent. 47(7): 67, 1950.

7. Billings, C. E. and J. Wilder. Handbook of Fabric Filter Technology. National Technical Information Service Publication No. PB-200 648. Springfield, Va., 1970.

8. Davis, W. T., P. J. LaRosa and K. E. Noll. The Generation and Evaluation of Fabric Filter Performance Curves From Pilot Plant Data. Filtr. Sep. 13(6):555, 1976.

9. Davies, C. N. The Separation of Airborne Dust and Particles. Proc. Inst. Mech. Eng. London. 1B(1):185, 1952.

10. Holland, C. R. and E. Rothwell. Model Studies of Fabric Dust Filtration: 1. Flow Characteristics of Dust Cakes Uniformly Distributed on Filter Fabrics. Filtr. Sep. 14(1):30, 1977.

11. Walsh, G. W. and P. W. Spaite. An Analysis of Mechanical Shaking in Air Filtration. J. Air Poll. Control Assoc. 12(2):57, 1962.

12. Robinson, J. W., R. E. Harrington, and P. W. Spaite. A New Method for Analysis of Multicompartmented Fabric Filtration. Atmos. Environ. 1(4): 499, 1967.

13. Theodore, L., J. Reynolds, A. Corvini and A. Buonicore. Particulate Control by Pulsed-Air Baghouse Filtration: Describing Equations and Solution. Proceedings of 2nd Specialty Conf. on: The User and Fabric Filtration Equipment. Buffalo, N.Y.,1975. p. 90-103.

14. Stephan, D. J. and G. W. Walsh. Residual Dust Profiles in Air Filtration. Ind. Eng. Chem. 52(12):999, 1960.

15. Borgwardt, R. H., R. E. Harrington, and P. W. Spaite. Filtration Characteristics of Fly Ash from a Pulverized Coal-Fired Power Plant. J. Air Poll. Control Assoc. 18(6):387, 1968.

16. Ellenbecker, M. J. Pressure Drop in a Pulse-Jet Fabric Filter. Sc.D. Thesis. Harvard School of Public Health, 1979, Appendix C.

17. Dennis, R., R. W. Cass and R. R. Hall. Dust Dislodgement from Woven Fabrics Versus Filter Performance. J. Air Poll. Control Assoc. 28(1): 47, 1978.

18. Rudnick, S. N. and M. W. First. Dust Cake Compaction in Fabric Filtration. Paper 78-62.7 presented at the 71st Annual Meeting of the Air Pollution Control Association. Houston, Texas, June 1978.

19. Ellenbecker, M. J. op. cit., Manuscript II.

20. Rothwell, E. Fabric Filter Failures--Relating Laboratory Observations to Practice. Paper presented at the Filtration Society's Conference on Filtration, Productivity and Profits at the Dust Control, Air Filtration & Gas Cleaning Exhibition. London, England, Sept. 1977.

ROLE OF FILTER STRUCTURE AND ELECTROSTATICS IN DUST CAKE FORMATION

By

George E. R. Lamb and Peter A. Costanza
Textile Research Institute
Princeton, New Jersey 08540

ABSTRACT

This study has examined the relationship between filter performance and dust cake formation. The latter is found to be dependent on filter structure and on electrostatic effects. An important feature of the dust cake is the distribution of mass with distance from the fabric surface. When the cake forms close to the upstream surface, lower dust retention and lower pressure drop result, as well as better capture efficiency. This upstream concentration of the dust cake can be achieved by proper choice of the fibers of which the filter is made, by certain layered constructions of the filter, and by application of an electric field at the filter surface.

ROLE OF FILTER STRUCTURE AND ELECTROSTATICS IN DUST CAKE FORMATION

INTRODUCTION

At TRI a program of research aimed at studying basic mechanisms of gas-particulate filtration has been active for several years. Various approaches to the optimization of filter performance have been taken. These have included modification of the component fibers and of the fabric structure, as well as the application of D.C. electric fields between suitably located electrodes. The changes in performance due to these modifications are assumed to be accompanied by changes in the structure of the dust cake. This structure, however, is difficult to observe and quantify. Microphotographic analysis has, in general, not yielded useful data [Miller et al. (1978)[1]; Leith et al. (1976)[2]]. The approach taken in the present studies has been to use filters formed of a number of thin layers. By weighing these before and after filtration, the distribution of dust mass with depth into the filter can be characterized. This macroscopic technique has given useful indications of the changes in cake structure accompanying filter modification, which are invisible to an observer looking at the filter surface. Such information should aid the design of better filter fabrics.

EXPERIMENTAL METHODS

All measurements were made with "patch" filters 12.5 cm x 12.5 cm. These were clamped in holders that exposed a 10-cm diameter circle to the aerosol stream. The aerosol was generated by feeding pulverized coal flyash into the path of a compressed air jet. The aerosol stream moved upwards in a 10-cm duct towards the filter at the top, so that larger particles and agglomerates with a settling velocity greater than the upward flow fell to the bottom and were not part of the measured dust cake. Dust penetrating the test filter was collected on a full-flow membrane filter. Efficiencies were determined from the mass of dust collected on both filters. Pressure drop across the test filter was measured using a pressure transducer and recorder, as well as a liquid manometer.

FIBER GEOMETRY

The effects of the geometry of the component fibers on the performance of a filter fabric has been studied extensively [Miller et al. (1977)[3]]. It has been shown that variations in the diameter of the fiber (at constant filter weight and density) bring about

considerable response in both capture efficiency and pressure drop. However, these variations offer only a trade-off, since a gain in one response is accompanied by a loss in the other. Changes in fiber cross-sectional shape, however, have been shown to result in both increased efficiency and lower pressure drop. This is illustrated in the "performance curves" in Figure 1, which compare filters made of fibers having different lobed cross sections. A performance curve is obtained by plotting pressure drop (ΔP) vs. penetration (mass fraction of dust coming through the filter) for filters operating under a standard set of conditions. Each curve contains points for filters made of fibers with equivalent cross-sectional shapes but different linear densities; that is, the curve is characteristic of the fiber shape. Ideal performance is represented by a point at the origin, and the closer a curve is to the origin, the better its relative performance. Figure 1 compares filters made of fibers with round and trilobal cross sections. The variations in lobe depth are characterized by the "aspect ratio" (AR), which is the ratio of the diameters of the circumscribed to the inscribed circles (Figure 2). It can be seen that as the aspect ratio increases, the performance improves. The greater efficiency would be expected because the projected area of a lobed fiber increases (at constant linear density) with increasing aspect ratio. Electrostatic effects, however, also appear to play a significant part. It has been shown theoretically [Miller et al. (1978)[1]] that in an electric field, lobed fibers have greater capture efficiency than round ones, and that the efficiency increases with the number and depth of the lobes. In any filter, local electric fields must be created by charges on fibers and captured particles. It is possible, therefore, that differences in efficiency caused by changes in fiber shape are due to the different responses of the fibers to these local fields.

The following experiments in which local differences in electric potential were eliminated by coating the fibers with metal appear to support the above hypothesis. Felts were made with nylon fibers of round and of shallow (AR = 1.4) and deep (AR = 2) trilobal cross sections. The surface conductivity of one set was increased by vacuum deposition of gold. In Figure 3 penetration is plotted as a function of number of conditioning cycles. Without a gold coating, as expected, penetration is lower through the deep-lobed samples. With the gold coating, this improvement disappears, and in addition, the penetration for all three samples increases sharply at about the 20th cycle. It appears, therefore, that electrical effects play a part both in capture and in the stability of the dust cake.

It might not be apparent why fiber cross-sectional shape should influence pressure drop. If anything, increased lobe depth should, by offering greater resistance to air flow, bring about pressure drop increases. However, the observed lower pressure drops associated with lobed fibers are attributable to differences

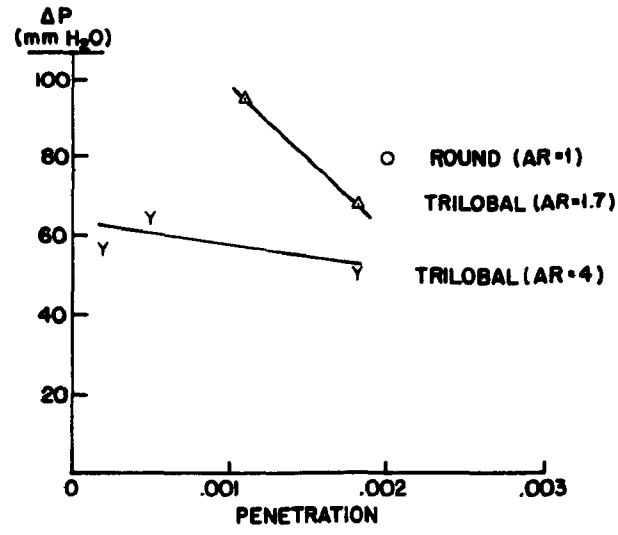

Figure 1. "Performance curves" comparing filters made of fibers with different aspect ratios (AR).

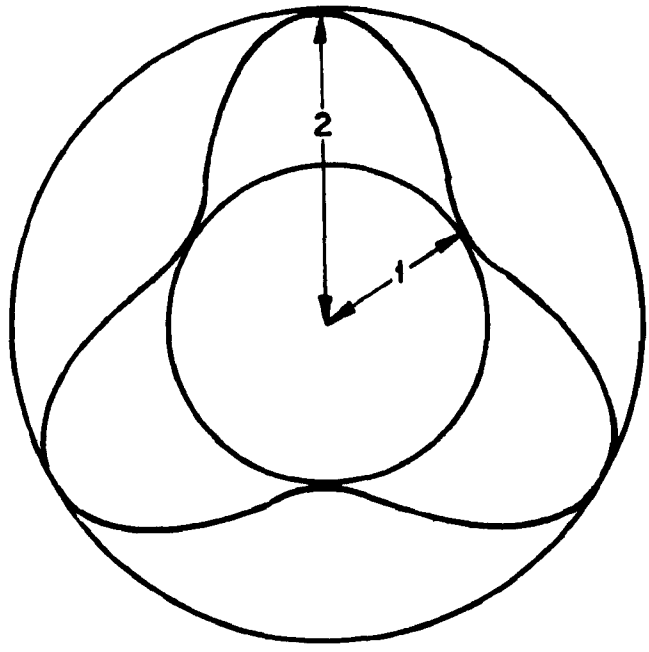

Figure 2. Cross section of fiber with aspect ratio 2.

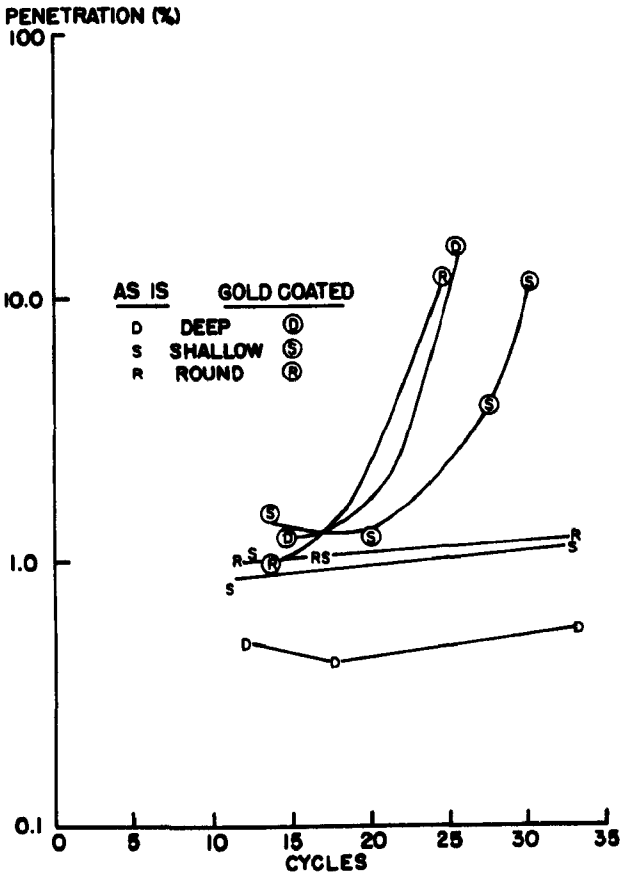

Figure 3. Penetration through fabrics made of fibers with different aspect ratios, with and without gold coating.

in the way dust distributes with respect to depth into the filter. Table 1 shows amounts of dust captured in various layers of clean 4-layer filters. It is seen that the trilobal filter collects a greater fraction in the upstream layers. This results in more thorough cleaning, as indicated in Figure 4 which shows the amounts left in the various layers as the layered filters are progressively conditioned. It is seen that the residual cake mass is lower in the trilobal filters.

The improved cleanability of trilobal filters also appears to be partly electrostatic in origin. Table 2 shows the effect of gold coating on the pressure drop after conditioning obtained with round fiber and trilobal fiber filters. Whereas with the control filter the trilobal one gave a lower pressure drop, gold coating makes the difference vanish. The difference in the mass of residual cake likewise disappears.

Table 1. DISTRIBUTION (%) OF DUST CAKE MASS IN VARIOUS LAYERS OF FOUR-LAYER FILTERS MADE OF TRILOBAL AND OF ROUND FIBERS.

Layer number	Trilobal	Round
1	93.0	88.3
2	3.4	6.3
3	1.5	3.0
4	0.8	1.0
Penetration	1.2	1.5

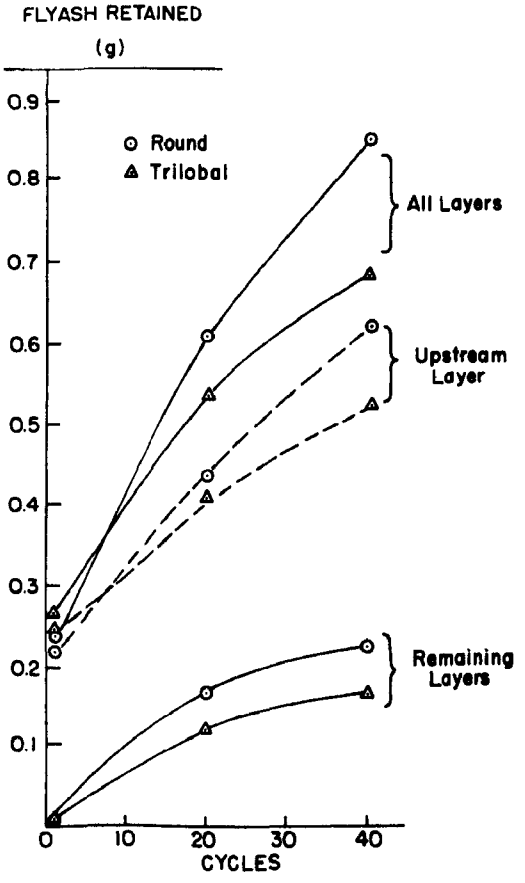

Figure 4. Retention of dust cake in layers of multilayer filters made of trilobal and round fibers in first forty cycles of conditioning.

Table 2. FILTRATION PERFORMANCE OF GOLD-COATED POLYESTER FILTER FABRICS AFTER 50 CYCLES OF CONDITIONING.

	Pressure drop (mm H_2O)	Residual cake after cleaning (% of filter mass)
Round (control)	145	122
Round (gold-coated)	145	102
Trilobal (control)	115	75
Trilobal (gold-coated)	142	104

COMPOSITE FILTERS

The above findings, namely that collection in the upstream regions of a filter promotes improved performance, suggested that other means (besides use of lobed fibers) of causing a similar collection pattern might result in similarly enhanced performance. A simple modification of fabric structure which would be expected to achieve this end consists of forming the fabric in layers, and arranging that the upstream layers are made of finer fibers.

Card webs containing minor proportions of fibers having low softening points were prepared. Composite felts were then made by combining layers of fine and thicker fibers and compacting them by pressing at 120°C. The effects on filtration performance of varying the thickness of the upstream layer, and also of reversing the order of the layers, were examined using the eight samples described in Table 3.

Table 3. COMPOSITION OF TWO-LAYER FILTERS MADE FROM 3 AND 6-DENIER FIBERS.

Upstream	/ Downstream
100% 6d	0% 3d
83% 6d	17% 3d
50% 6d	50% 3d
17% 6d	83% 3d
100% 3d	0% 6d
83% 3d	17% 6d
50% 3d	50% 6d
17% 3d	83% 6d

Experimental conditions were as follows:

Fabric weight	:	0.25 kg/m^2 (7.3 oz/yd^2)
Fabric density	:	0.130 g/cm^3
Fiber type	:	Polyester
Face Velocity	:	60 mm/s (12 ft/min)
Inlet concentration	:	3.5 g/m^3
Cycle time	:	5 min

Measurements were made not only of the penetration and the pressure drop of these filters, but also of the residual dust after cleaning (expressed as percentage of the base filter mass).

Figures 5,6, and 7, respectively, show these measurements as a function of %6d/%3d in the two-layer composite filters; that is, percentage of 6-denier fibers upstream increases to the right, whereas percentage of 3-denier fibers upstream increases to the left. It can be seen now that the composites with 3-denier fibers upstream allow less penetration and also exhibit a lower pressure drop than those with 6-denier fibers upstream or with 100% 3-denier fibers. The 17% 3d upstream/83% 6d downstream composite appears to be the best combination. These effects may be explainable by the correlation between the curves of Figures 5 and 6 with those of Figure 7. It appears generally that penetration and pressure drop are directly related to the amount of dust retained after cleaning. Finer 3d fibers upstream prevent dust from lodging deeper into the filter whence it cannot be blown back. This in turn keeps the penetration lower and, since unremovable dust increases resistance to air flow,also keeps the pressure drop lower.

ELECTRIC STIMULATION

The mechanisms whereby a fiber collects particles from an aerosol stream more efficiently when an electric field is present are well known [Zebel (1965)[5]]. Less clear are the reasons why in some circumstances the presence of an electric field also causes a reduction in pressure drop. It appears that, as in the cases examined above, the pressure drop response is associated with changes in the cake structure.

Figure 8 shows the distribution of cake mass in the different layers of a filter made up of thin separable nonwoven fabric. These were weighed after five minutes of filtering a 3-g/m^3 flyash aerosol. One set of results was obtained with no applied field. The second (marked 4 kV/cm) was obtained with 6 kV applied to alternate parallel wire electrodes resting on the upstream surface of the upstream layer (no. 1). With the applied field, there is a measurable shift in the distribution in an upstream direction. At the same time, there is a large reduction in the penetration (from

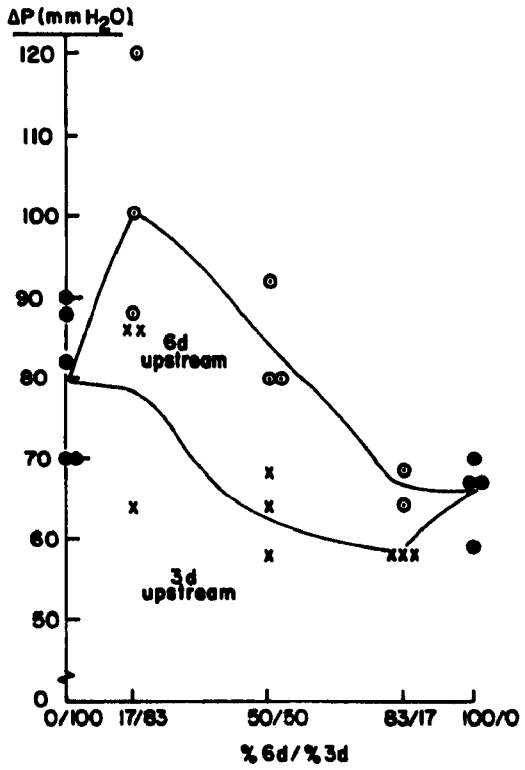

Figure 5. Pressure drop across composite polyester filters having different proportions of 3 and 6-denier fibers in two layers.

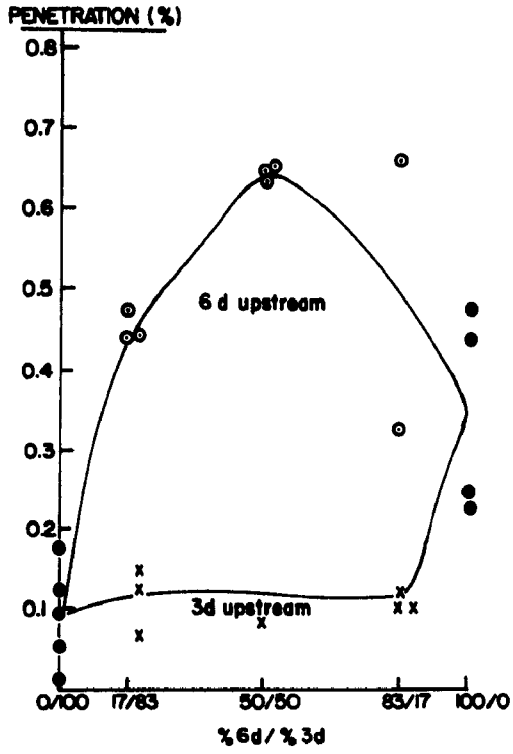

Figure 6. Penetration for the composite filters of Figure 5.

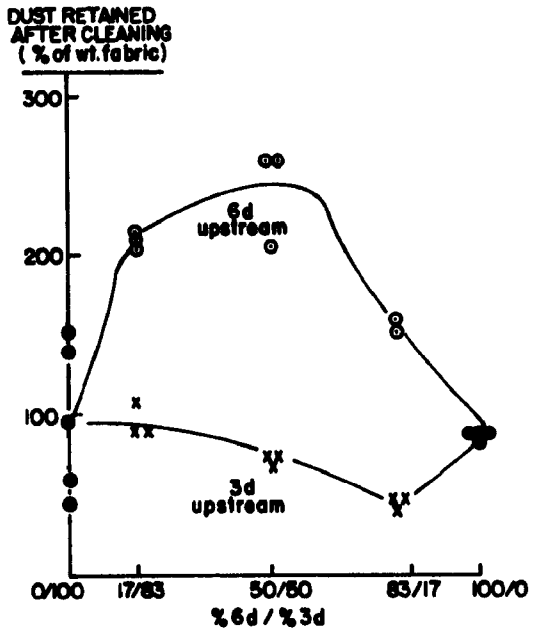

Figure 7. Residual dust after cleaning the filters in Figure 5.

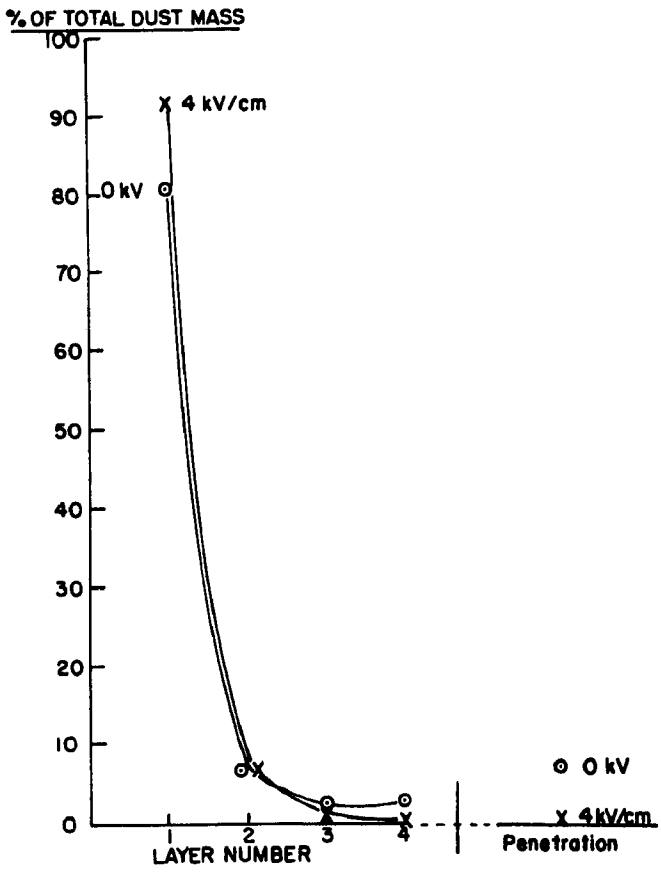

Figure 8. Distribution of dust cake mass and overall penetration for four-layer filter with and without applied electric field.

7% to 0.2%) and also a decrease in pressure drop. The above result appears paradoxical, since if in the presence of an electric field the dust accumulation in a fabric is shifted in an upstream direction, the greater mass concentrated in the first layer would be expected to lead to greater pressure drop. In fact the opposite occurs, and we must conclude that cake formation in the uppermost layer is modified by the presence of the field.

Figure 9 shows photographs of the upstream surface of a needled polyester commercial filter fabric after 6 minutes of filtering a 5-g/m^3 flyash aerosol without an applied field (Figure 9a) and with a 6-kV/cm field (Figure 9b). In contrast with the compact cake seen in Figure 9a where surface fibers are free of dust, in Figure 9b there is heavy deposition on these surface fibers. Final pressure drop measured with the cake in Figure 9a was 18 mm of water; with the cake in Figure 9b it was 3 mm of water. The explanation of the paradox is thus that the dust cake, on being

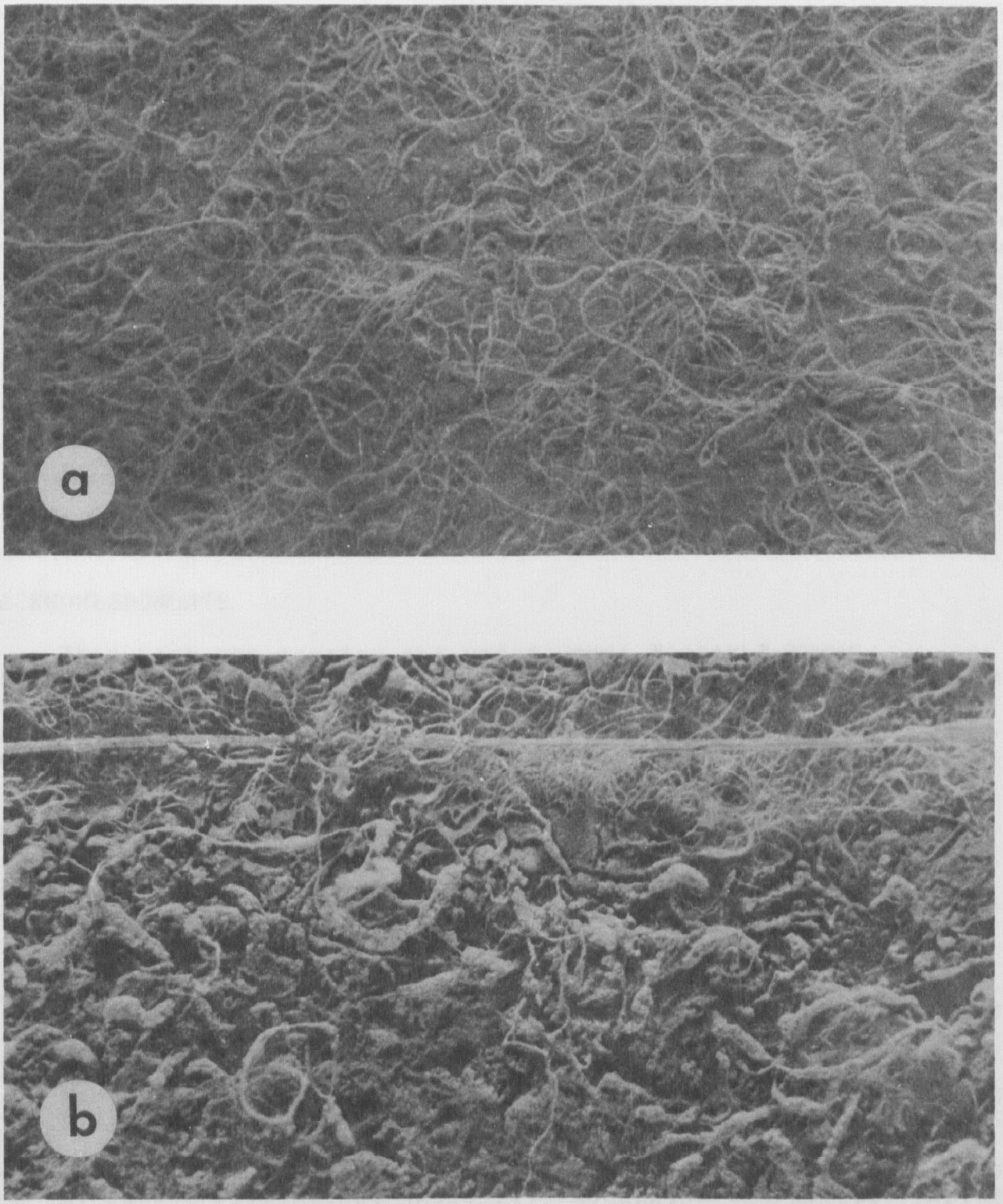

Figure 9. Photographs of dust on the surface of a nonwoven fabric.

a) Dust collected with no field.
b) Dust collected with 6-kV/cm field.

shifted upstream by the field, is also made to form in a region of the fabric where the packing density (or volume fraction of fibers) is lower. It follows that pressure drop reduction by an applied field depends on the presence on the upstream surface of the filter of a region of low packing density.

Accordingly, the dependence of pressure drop reduction on the packing density α of the surface layer was studied using a series of two-layer composite fabrics in which the upstream layers (bonded by a thermoplastic binder) were made with different packing densities by being formed at different pressures. Figure 10 shows plots of pressure drop ratios (PDR) versus applied voltage for the different composites. PDR is the ratio of the pressure drop obtained with the applied field to that without a field. It can be seen that the response is indeed strongly dependent on the packing density of the upstream layer. These results have a significant influence on the power consumption accompanying a certain level of pressure drop reduction, as seen in Figure 11 for two of the composites in Figure 10. The lower surface density is seen to be associated with much lower power levels.

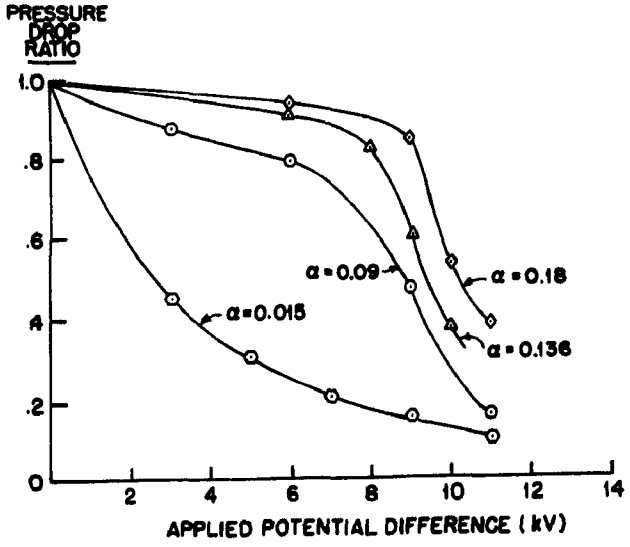

Figure 10. Dependence of PDR on applied voltage for filters with surface layers of indicated packing density α. Face velocity 6 cm/s.

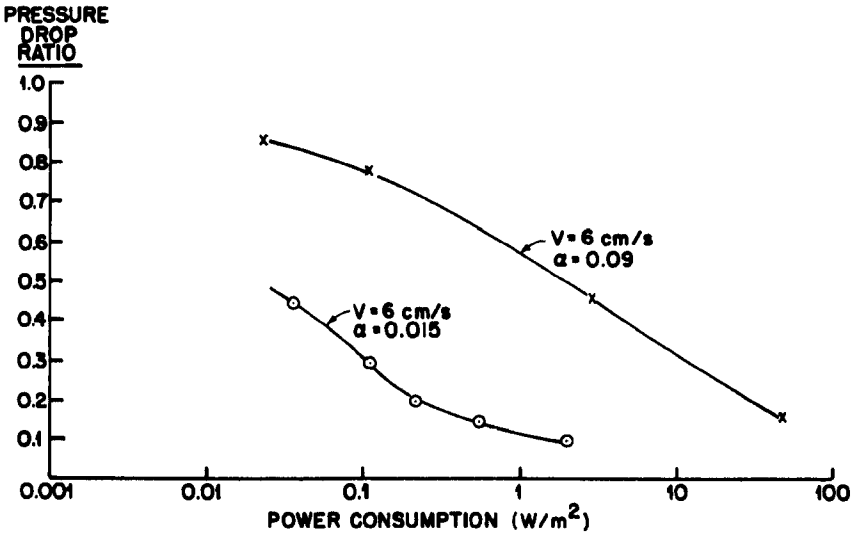

Figure 11. Pressure drop ratio vs. power needed to obtain it for two surface layer packing densities.

ACKNOWLEDGMENTS

This work was carried out under Grant Number R-804926 from the Environmental Protection Agency (Project Officer: James H. Turner), and the TRI research project "New Technology for Filtration of Gases by Fibrous Media," supported by a group of Corporate TRI Participants.

REFERENCES

1. Miller, B., G. Lamb, P. Costanza, D. O'Meara, and J. Dunbar. Studies of Dust Cake Formation and Structure in Fabric Filtration. EPA-600/7-78-095, June 1978.

2. Leith, D., S. Rudnick, and M. First. High Velocity, High-Efficiency Aerosol Filtration. EPA-600/2-76-020, January 1976.

3. Miller, B., G. Lamb, P. Costanza, and J. Craig. Nonwoven Fabric Filters for Particulate Removal in the Respirable Dust Range. EPA-600/7-77-115, October 1977.

4. Lamb, G., P. Costanza, and D. O'Meara. Electrical Stimulation of Fabric Filtration. Part II: Mechanism of Particle Capture and Trials with a Laboratory Baghouse. Textile Res. J. 48: 566-573, October 1978.

5. Zebel, G. Deposition of Aerosol Flowing Past a Cylindrical Fiber in a Uniform Electric Field. J. Colloid. Sci. 20: 522-543, 1965.

PRESSURE DROP IN ELECTROSTATIC FABRIC FILTRATION

By:

Teoman Ariman
Department of Aerospace and Mechanical Engineering
University of Notre Dame
Notre Dame, Indiana 46556

and

Dennis J. Helfritch
APITRON Division
American Precision Industries
Charlotte, North Carolina

ABSTRACT

Fabric filtration systems have been employed in industry for over a century with relatively few technological modifications. However, with the recent substantial increase in energy costs, conservation in energy consumption has become vitally important. As a result, the filtration systems of yesteryear may not be the best approach for future applications. Recently, an external electrical field was considered in fabric filtration of industrial dust with very promising initial results. An increase in the collection efficiency, particularly for fine particulates, and a decrease in the pressure drop was observed. In this paper the further results of an experimental program in the investigation of pressure drop in the electrostatic fabric filtration in industrial dust control are presented. The basic apparatus, a bench-side electrostatic fabric filtration system, creates a representative dust cake under specific conditions of operating parameters and charge levels. The results clearly indicate that filter and dust cake resistance, or pressure drop, decreases substantially with the increased electrostatic field strength for all industrial dust samples tested, regardless of fabric type and other relevant parameters.

1. INTRODUCTION

The energy consumption of a fabric filter air pollution control system is a function of the pressure drop across the fabric-dust cake combination and of the work required to remove collected dust from the fabric. Billings and Wilder (1970)[1] in a survey of operational systems in the field noted that the average pressure drop across a fabric filter is approximately 6 inches of water, a value which creates an electrical cost of 35¢ cfm-year (assuming a charge rate of 3.5¢/kw-hr). The cost of energy for bag cleaning varies greatly depending upon the cleaning technique and other variables; however, for pulse jet systems the electrical energy consumed in compressing the cleaning air is at least 25% of that spent in overcoming the pressure drop. It has been estimated that in 1969 an average of 75 x 10^6 cfm of air was passed through fabric systems. Assuming that the quantity of air processed has doubled since that time, approximately 788 million dollars per year is being spent nationally to cover energy costs for fabric filtration.

Buttersworth (1964)[2] presented data which showed that an electrical charge on the fabric can greatly reduce the pressure drop associated with a given dust load on the fabric. For example at a fixed velocity an uncharged fabric with a dust load of 2 oz/ft^2 exhibited a pressure drop of 13 inches of water where - as a charged fabric with the same dust load required only 3 inches of water pressure differential to produce the same flow (see Figure 1). In addition, it may be noted from Figure 1 that not only is the pressure loss less for charged fabric systems, but also the rate of change of pressure drop with dust load is reduced. Thus, it would appear that considerably less frequent fabric cleaning could be employed in charged fabric systems with a resulting energy savings and also an extension of bag life. This latter factor is an important consideration since a typical expenditure of 30¢/cfm-year is required for labor and materials to replace fabrics (which typically last for a year),(Billings and Wilder (1970)[1]).

In this paper an experimental program to investigate pressure drop in electrostatic fabric filtration of industrial dust is discussed. The results clearly indicate that pressure drop decreases substantially with the increased electrostatic field strength for all industrial dust samples tested regardless of fabric type and other relevant parameters.

2. STATE OF THE ART

Fabric filtration systems have been employed in industry for over a century with relatively few technological modifications (Strauss (1966)[3]). Indeed, there have been in recent years only a few advances of note: introduction of fabrics capable of withstanding higher temperatures and development of pneumatic cleaning techniques. For the most part, there was in the past little incentive for improvement—the collection of the systems was satisfactory and the units were inexpensive to purchase. However, with the recent substantial increase in energy costs attention should now be given to operating expenses (e.g.,energy consumption). As a result, the filtration systems of yesteryear may not be the best approach for future applications.

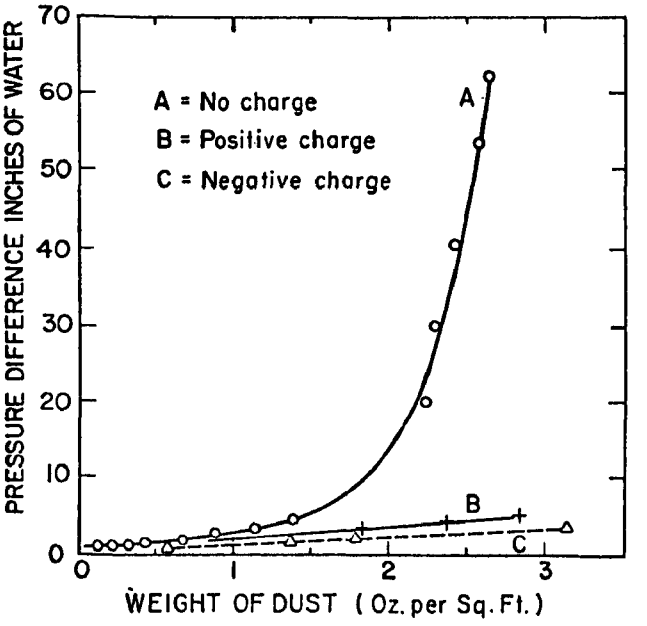

Figure 1

From both the theoretical and experimental standpoints, the application of electrostatics to fabric filtration systems tends to augment the already comparatively high value of collection efficiency (with the obvious exception of a case in which particles and fabric-dust cake are unipolarly charged). However, work is needed to advance the state-of-the-art in formulating and predicting pressure losses across the fabric-dust cake system. In particular, as indicated in the work of Buttersworth (1964)[2], Ariman and Lane (1972)[4], Ariman and Helfritch (1977)[5] and Ariman (1978)[6], (1979)[7] there have been few if any initial attempts to show the energy savings associated with the application of electrostatics. It appears that there is tremendous potential for significant advances in both modelling and in experimental work in this area.

When dealing analytically with the collection of dust from an air stream past a cylindrical fiber, inertia, interception, sedimentation and diffusion of particles are generally taken into consideration. Electrostatic effects are mostly neglected although they often occur and may play an important role as indicated by Ariman et al (1973)[8], Fuchs (1966)[9], Davies (1973)[10] and Frederick (1961)[11]. The difficulty of including electrostatic considerations in modelling of ordinary fibrous filters is that it is usually impossible to make any statements about the electrical charge on fibers. Theoretically, this difficulty is eliminated by placing a filter in an electrical field. In this spirit, Kraemer and Johnstone (1955)[12] made a comprehensive analytical and experimental study of aerosol collection on a spherical collector. They obtained computer solutions assuming potential flow around the collector and they also derived several approximate equations for the collection efficiency of isolated cylindrical fibers. Dawkins (1958)[13] extended Kraemer's computer solutions to cylinders in potential flow, but was unable to solve the viscous

flow case. Natanson (1957)[14] dealt with the deposition of charged and uncharged aerosol particles on a single uncharged fiber; coulombic and polarization forces, as well as image forces, were taken into account. For essentially isolated spheres and cylinders comparisons of the collection efficiency for electrical forces with that due to other mechanism shows that for low velocities, the electrical collection may be clearly dominant. An experimental confirmation of this prediction was given by Lundgren and Whitby (1965)[15]. Natanson's problem has also been dealt with by Yoshioka et al (1968)[16] who computed numerical solutions. They carried out experiments on the filtration efficiency of homogeneous aerosols with particle radius of 0.5 μm charges from 0 to 70 electrons per particle.

Rossano and Silverman (1954)[17] and Goyer et al (1954)[18] experimentally measured the effect of fiber charge and particle charge on filtration. Their results show an increase in efficiency due to particle charge, fiber charge, and filter packing density. Silverman et al (1956)[19] investigated the effect of electrostatic charge on the filtration of atmospheric dust. The continual motion of a fabric over a fibrous filter was used to produce a continually charged filter. Their results show filter efficiency increases inversely with velocity and directly with fiber charge. Rivers (1962)[20] compared some experimental data with theoretical calculations on a commercial electrified filter. His results show an increase in filter efficiency can be obtained by placing a strong electrical field across the filter. An extensive review of the subject of the electrical behavior of aerosols is given by Whitby and Liu (1966)[21]. Gillespie (1955)[22] obtained rough estimates of deposition on a cylinder in potential flow under the action of electrostatic forces. Neglecting inertia and making assumptions for the net effective charge on fibers, he was able to obtain a reasonably good agreement between theory and experiment. For different degrees of electrification of filter and particles, he presented penetration versus particle size curves. The collection on a single fiber model by electrostatic mechanisms was also investigated by Thomas and Woodfin (1959)[23], Sweitzer (1961)[24], Dennis et al (1958)[25], Anderson and Silverman (1958)[26], and Lapple (1970)[27].

Havlicek (1961)[28] and Silverman et al (1952)[29] have markedly improved the efficiency of conventional fiber filters through application of an external electrical field. Walkenhorst and Zebel (1964)[30] and Zebel (1966)[31] adopted a different course. They did not place the conventional fiber filter between sievelike electrodes but employed an open arrangement of some 30 to 100 layers of regularly arrayed fibers. The strong electrical field was thus homogeneous compared with other experiments, so that all fibers and aerosol particles were uniformly polarized. The experimental results showed that a satisfactory deposition was obtained. Because of the large distance between fibers it was not necessary to have recourse to terms such as porosity, packing and density. Zebel (1968)[32] theoretically investigated the deposition of uncharged and charged aerosol particles from an air stream upon an isolated circular cylindrical fiber perpendicular to the stream in a homogeneous electrical field. The particle trajectories were calculated for both potential and viscous flows by Lamb's formulation. It should be noted that if higher collection efficiencies are present, the single fiber model generally overestimates deposition as indicated by Ariman et al (1978)[3] and Ariman (1979)[33].

Recently Ariman and his co-workers have (1973)[8] developed an improved model for fabric filters. This model assumes several layers of evenly arranged fibers of cylindrical cross section of radius b. The axes of the electrical field E_o is assumed. All cylindrical fibers and spherical dust particles are assumed to be uniformly polarized by the electrical field. The flow and electrical fields in the vicinity of an individual fiber influence the motion of a particle. These fields are in turn subject to the interference of the two immediately neighboring fibers. Here two cases were considered, the first for $Fu << 1$, where $Fu = 2b/d (0 < Fu < 1)$, and the second for $Fu<1$; and in each case the interference effects were taken into account by the method of images (Scheidegger (1960)[34]) for velocity and electrical fields.

In a following investigation Ariman and Tang (1976)[35] have studied the similar problem for charged fibers but non-charged dust particles. In both papers the critical trajectories of the particles are calculated by numerically solving the governing equation for the particle trajectories. The effect of various parameters on collection efficiency is presented. Numerical results confirm that when higher collection efficiencies are present, the commonly used single-cylinder model significantly overestimates the collection efficiency.

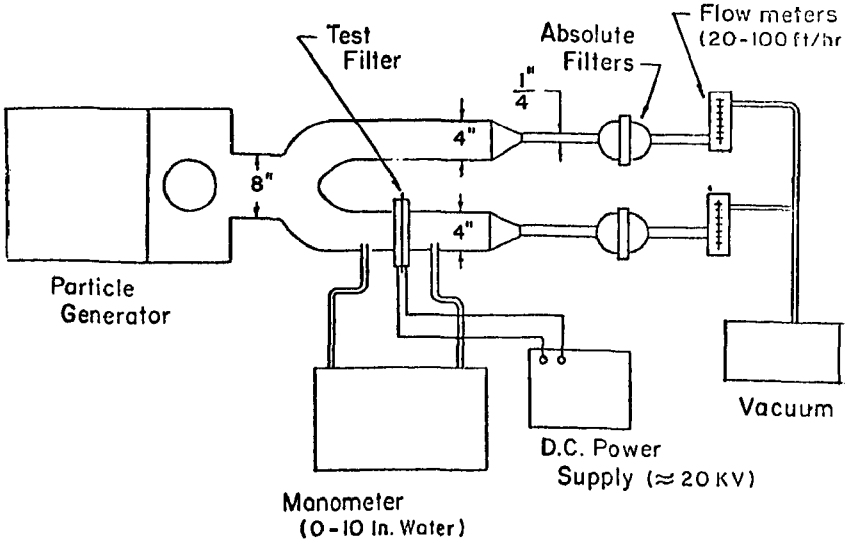

Figure 2.

Ariman and Lane (1972)[4] set up an experimental system, Figure 2, and conducted filtration tests both with and without a superimposed electric field. The fabric filter was charged by placing aluminum screens on both sides of the fabric sample and applying a DC voltage. A wide variety of different fabric materials were employed to determine the effect of fabric upon collection efficiency and pressure drop for a particular test dust. It was observed that the application of an external electric field considerably improved the efficiency of fine particle collection. In addition, the pressure drop across the filter was reduced substantially when an electric field was applied. These interesting initial observations suggested that substantial savings in energy costs could result from incorporation of electrostatics into fabric filtration systems and they provided the basis for the reported investigation.

3. EXPERIMENTAL PROGRAM

The basic apparatus which was employed in the experimental program is shown schematically in Figure 3. Primarily, it consists of a means for creating a representative dust cake on a fabric sample under varying conditions of relative humidity and charge levels. At constant face velocity, suspended dust particles were filtered by an initially clean fabric filter. The particles were charged prior to deposition by means of passage through a corona discharge (Figure 4). Degree of charge was controlled by the magnitude of the field strength, and pressure drop was recorded after a specified weight of dust had been deposited. Then the similar testing is performed for different dust/fabric type combinations.

Air flow rate through the system is measured with the aid of a laminar flow element and a pressure gage. Relative humidity is sensed with an electric hygrometer and the temperature in the sample holder is monitored with the aid of a thermocouple system. Pressure drop across the filter is measured by an inclined manometer. The system permits a variation in the flow rate over a range such that a filtering velocity range of 0-15 ft/min can be obtained and that relative humidity can be controlled over the range of 15-80 percent. The electric field strength is varied between 0-12 kv/in.

Nine dust samples provided by Apitron division of the API were utilized in the bench-scale tests. The resulting extensive data were used in the formulation of the effects of electric field strength, flow rate, dust type, fabric type, etc. or pressure drop. The dust samples were:

a. Electric Furnace Fume
b. Limestone
c. Asphalt Plant Rock Dust
d. Phosphate
e. Gypsum
f. Calcium Carbide
g. Asbestos
h. Wedron Silica
i. Fly Ash

Some selected results are presented in the following section.

3. BENCH SCALE TEST RESULTS

In Figure 5, pressure drop values in inches of water are presented as a function of the filtering velocity (ft/min) for charged and non-charged gypsum. Fabric type was wool felt with a weight of 16 ounce per square yard and relative humidity and temperature were kept at 36% and 81°F respectively during the test runs. Three tests were performed at 5, 10 and 15 ft/min filtering velocity with approximately the same amount of gypsum. Thus in the graph CW represents the cake weight and is determined by weighing the initially clean flat fabric filter sample (9" x 11.5") before and after the test. The fabric filter sample was cleaned for each test by a brush. It is seen that in all tests electric charge on particles causes particularly for U = 15 ft/min a

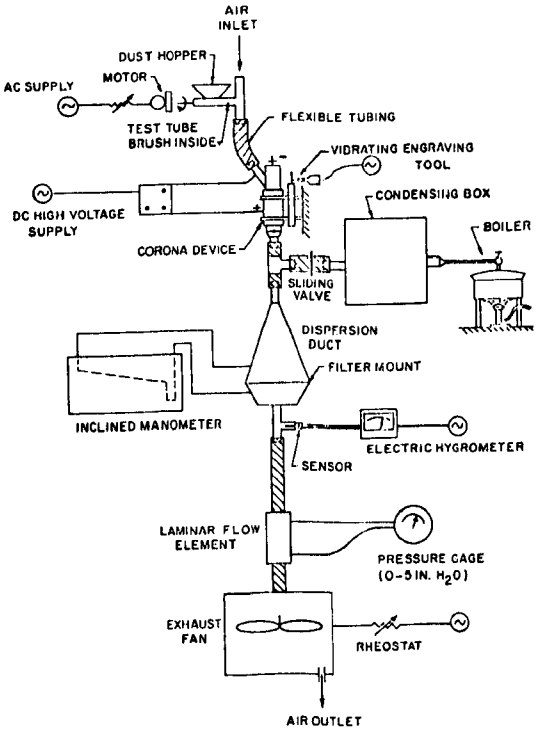

Figure 3

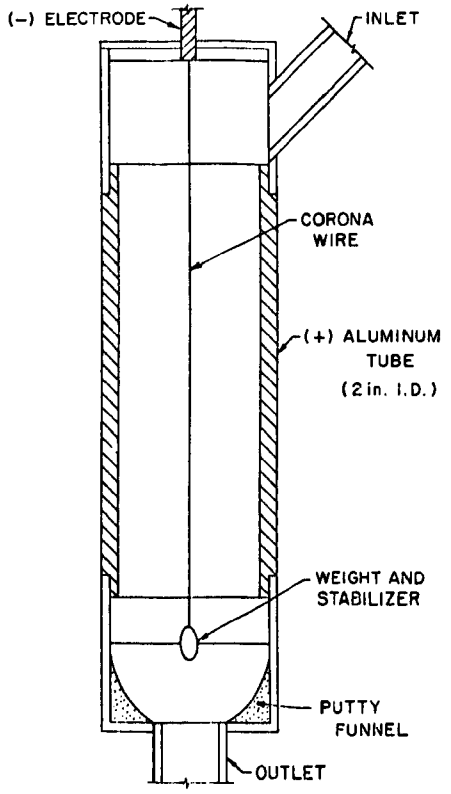

Figure 4

considerable decrease in pressure drop or filter resistance. It appears that the majority of the decrease takes place for V = 7 kv/in with little additional decrease with V = 10 kv/in. This situation more or less was valid for all dust samples tested.

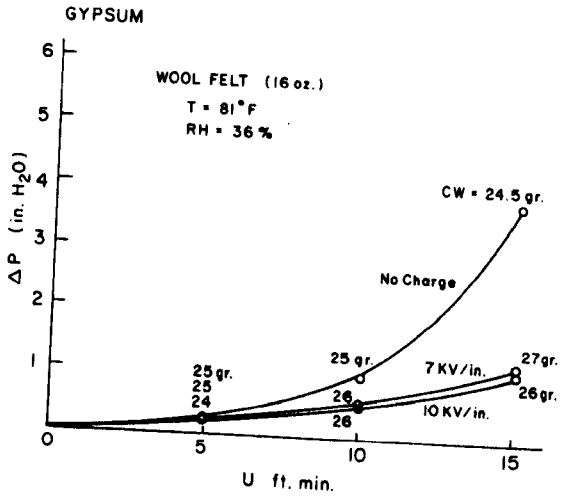

Figure 5

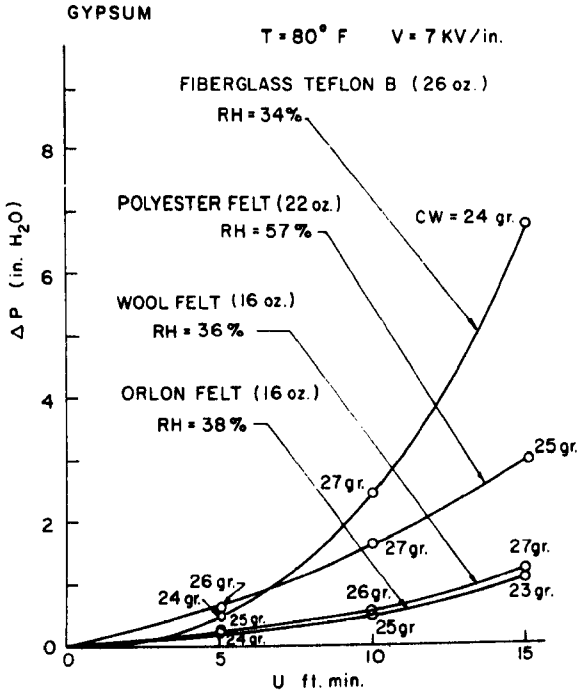

Figure 6

The effect of fabric type on pressure drop for the charged case of V = 7 kv/in is demonstrated in Figure 6. Orlon felt, wool felt, fiberglass teflon B and polyester felt fabric samples were utilized in the tests. It appears that under the similar operating conditions orlon felt (16 oz) and wool felt (16 oz) were the best performers and fiberglass teflon (26 oz) was the worst one from the pressure drop point of view.

Figure 7 represents the pressure drop variations for limestone and for non charged and charged cases with Polypropylene (15 oz) and Orlon (16 oz) at the filtering velocities of 5, 10 and 15 ft/min. For all tests it is observed that electric charge on limestone particles causes a substantial decrease in pressure drop particularly for higher filtering velocity values of 10 and 15 ft/min.

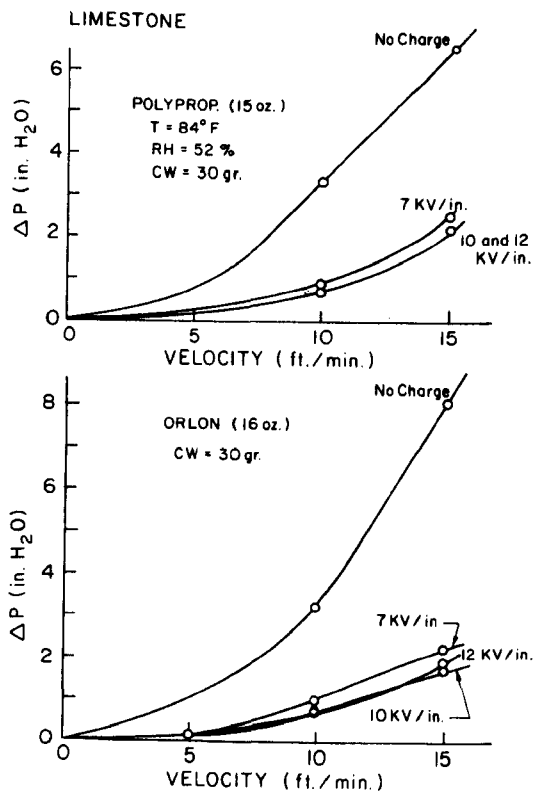

Figure 7

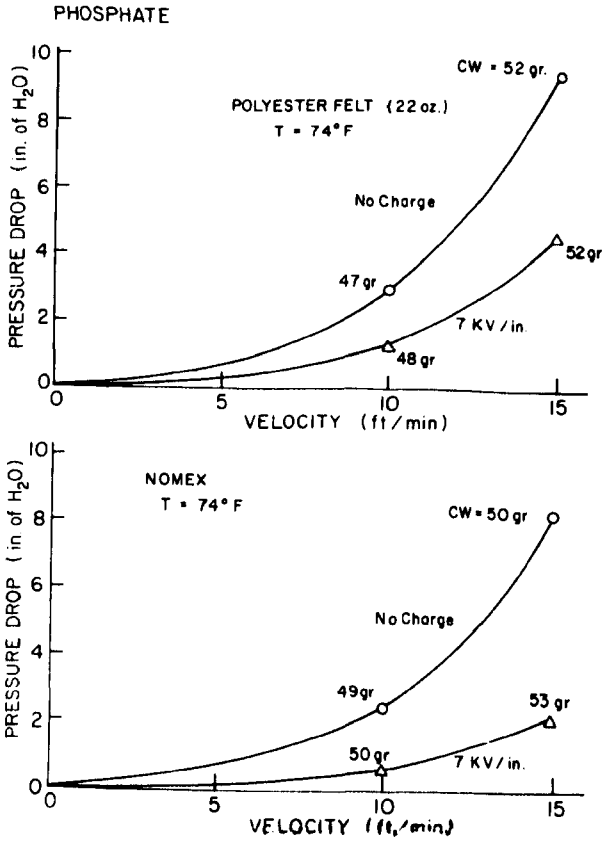

Figure 8

As stated earlier the degree of charge was controlled by the magnitude of the field strength, namely through the voltage values of V = 7, 10 and 12 kv/in cases the tests were performed for a dust cake weight of 30 grams. It is remarkable to notice that for the Orlon 16 oz filter sample and noncharged case pressure drop is 8.2 inches of water while for the charged case of 7 kv/in the corresponding pressure drop value is substantially lower, namely 2.1 inches of water. It is therefore estimated that by charging limestone particles, the filtration rate per unit fabric area of a given fabric can be increased by a factor of up to four. This implies that with the aid of electrostatics it might reasonably be expected fabric filters can be reduced in size by a factor of four, while achieving better collection efficiency. It is further seen from the figure that there was no noticeable difference for the cases of 10 kv/in and 12 kn/in. Again the majority of the decrease in the pressure drop takes place for v = 7 kv/in case.

Figure 8 presents pressure drop results for phosphate and for Nomex (9 oz) and Spun Nomex (9 oz) fabrics again for two difference face velocities of 10 and 15 ft/min for charged (7 kv/in) and non-charged cases. In accordance with the test results of the previously stated dust samples, a considerable decrease in pressure drop is again observed due to the effect of electric charge on particles.

Pressure drop - face velocity relation is presented in Figure 9 for electric

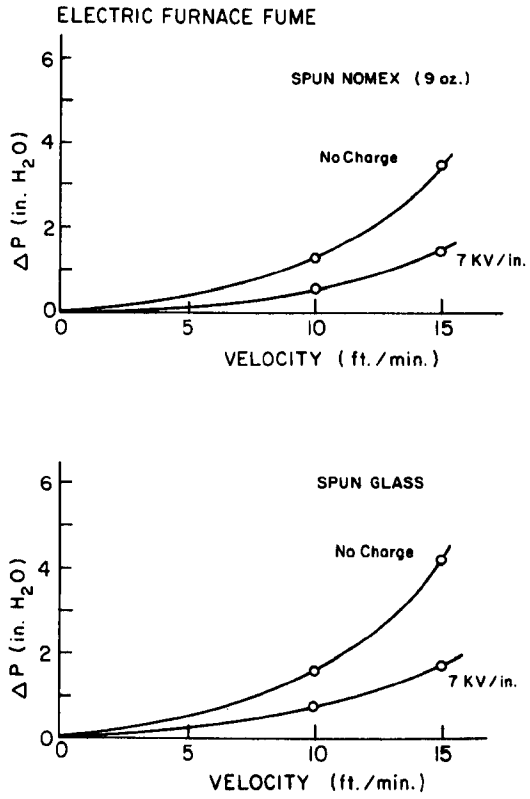

Figure 9

furnace fume. In accordance with the procedure of the previous tests no charge and charged (7 kv/in) cases were investigated. Nomex (14 oz) and Spun Nomex (10 oz) were utilized for the tests of Figure 9. As expected a considerable decrease took place in pressure drop for the charged case. It is further noted that for the similar operating conditions Spun Nomex fabric filter causes somewhat higher pressure drop as compared to that for Nomex fabric filter. Namely 3.6 inches of water for Spun Nomex versus 3.2 inches for non charged limestone particles and 1.6 inches versus 1.3 inches for the charged case. Note that this interesting observation was made despite the fact that Nomex (14 oz) filter is heavier than the Spun Nomex (10 oz) one. Therefore it appears that in addition to the fabric weight, fabric characteristics need also to be considered in the pressure drop investigations.

In order to investigate the effect of the increase in the charge on particles in a continuous form, a series of tests were performed with Wedron Silica by using Orlon (16 oz) fabric filter sample at the face velocities of 10 and 15 ft/min and with no charge and V = 5, 6 and 7 kv/in cases (Figure 10). For the higher face velocity between V=0 and V=5 kv/in no noticeable change took place in the pressure drop. However, following the formation of the corona discharge around 5.3 kv/in, a sudden decrease in the pressure drop was observed. Namely from 3.8 to 2.1 inches of water for V=6 kv/in. A further decrease with less magnitude also took place when V was increased to 7 kv/in. A continuous decrease in pressure drop with an increased rate was observed wity higher V values for the face velocity of U=10 ft/min.

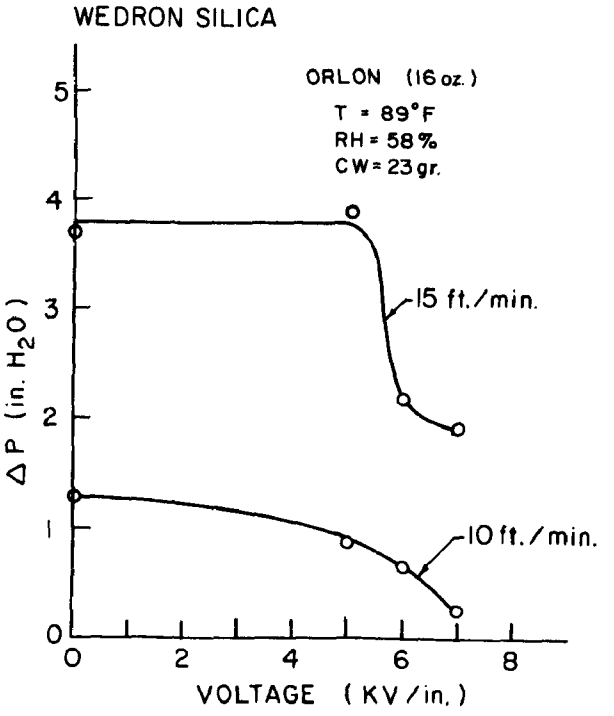

Figure 10

ASPHALT PLANT ROCK DUST

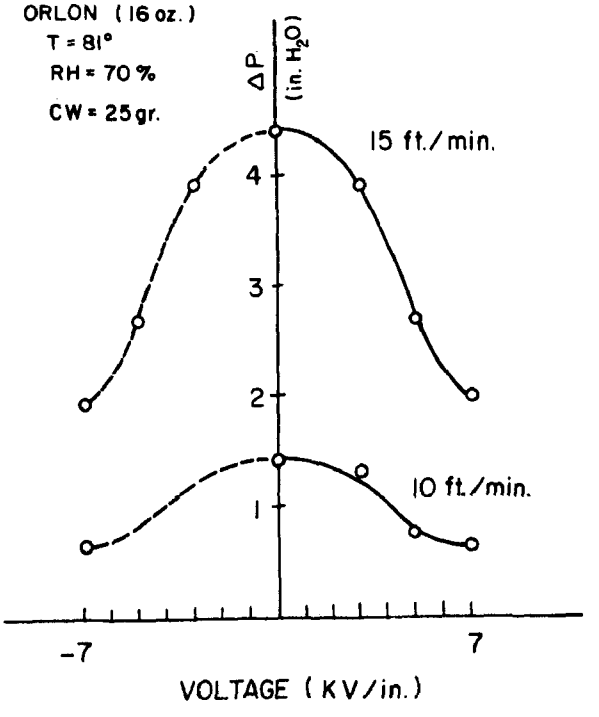

Figure 11

Finally the effect ot the change of sign of corona discharge field was also investigated for an Asphalt Plant Rock Dust and Orlon (16 oz) filter. It is quite interesting to note that for both filtration velocities of 10 and 15 ft/min there is no noticeable difference on pressure drop with the change of the sign of the electric field (Figure 11).

5. CONCLUDING REMARKS

An experimental program was carried out for the investigation of pressure drop of electrostatic fabric filtration in industrial dust control. The results of the experimental program clearly indicate that filter and dust cake resistance or pressure drop decreases substantially with the electrostatic charge on particles. Although there are quantitative differences in the magnitude of the effect of charge on dust particles prior to filtration, the effect is qualitatively identical for all industrial dust samples tested.

For a possible explanation of the substantial reduction in the pressure drop, the microstructure of each dust cake sample was studied under a microscope. As a characteristic example two pictures of an asbestos cement dust cake for the uncharged (Figure 12) and charged (Figure 13) are presented here. It appears from the comparison of these pictures that the microstructure of the dust cake of the charged asbestos cement dust differs a great deal from the noncharged cake. The dust cake formed on an industrial fabric sample with the deposition of charged asbestos cement particles looks much more porous and fluffy than the one formed with the deposition of uncharged particles on the same type of fabric sample. In turn it is quite clear that more porous dust cake would give rise to a small resistance against the dust laden gas flow. Note that a substantial increase in the porosity of the charged dust cake was observed for all the dust and fabric samples used in the test programs.

Furthermore it also appears that again due to the quite loose and fluffy microstructure of the charged dust, it would be easier to clean an industrial bag when an external electric field is present. Thus, it would appear that considerably less frequent fabric cleaning could be employed in electrostatic fabric filter systems with an additional energy savings and also an extension of bag life which typically lasts for a year. This latter factor is an important consideration since a typical expenditure of 20¢/cfm - year is required for labor and materials to replace fabrics.

It is shown in this research program that the electrostatics appears to have a profound effect on the flow resistance of fabric filters. It is seen that by charging industrial dust a decrease in the pressure drop up to 80% is obtained. Thus, it appears that substantial savings could be achieved in the energy costs from incorporation of electrostatics into bag house filtration in industrial dust control. Furthermore a considerable increase in the collection efficiency especially for fine particulates, mass mean diamter less than 3 micron, is another important outcome of the electrostatic fabric filtration.

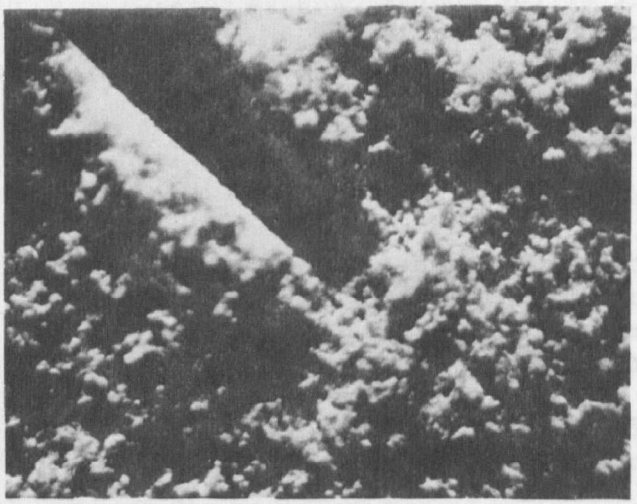

UNCHARGED ASBESTOS CEMENT DUST
DEPOSITED ON FABRIC - 5X MAGNIFICATION

Figure 12

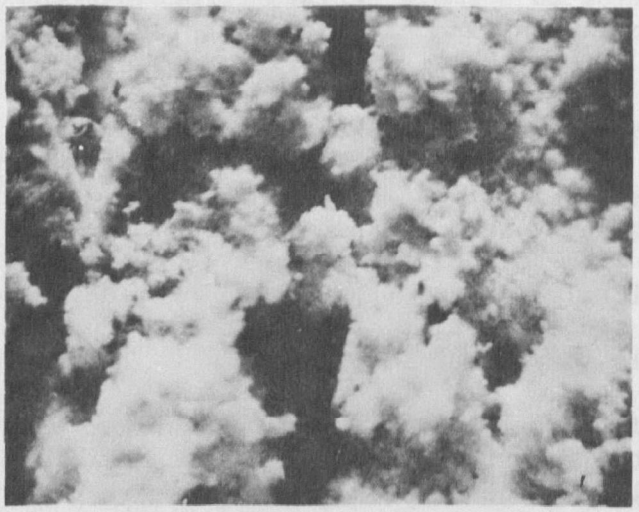

CHARGED ASBESTOS CEMENT DUST
DEPOSITED ON FABRIC - 5X MAGNIFICATION

Figure 13

REFERENCES

1. Billings, C.E. and Wilder, J. Handbook of Fabric Filter Technology, Volumes I-IV, GCA-TR-70-17-G, prepared for NAPCA (EPA)(1970).

2. Butterworth, E., Manufacturing Chemist, 65, Feb. (1964).

3. Air Polution Control, Part 1, Edited by W. Strauss, 337, Pergamon Press, New York (1966).

4. Ariman, T. and Lane, M.J., "On Experimental Determination of Collection Efficiency and Pressure Drop in Fabric Filters in an Electrostatic Field," unpublished report, (1972).

5. Helfritch, D.J. and Ariman, T., "Electrostatic Filtration and the Apitron Design and Field Performance," Novel Concepts, Methods and Advanced Technology in Particulate/Gas Separation, Teoman Ariman, Editor, University of Notre Dame.

6. Ariman, T., "Pressure Drop in Electrostatic Fabric Filtration," UND, Final Report, December (1978).

7. Ariman, T., "Electrostatic Fabric Filtration in Industrial Dust Control - A Review," UND-DOW-EFF TR. No. 1, April (1979).

8. Ariman, T., Rao, K.S., Yang, K.T. and Hosbein, R.L., "Collection of Dust by Fabric Filtration in an Electrostatic Field," Proceedings of the Second Annual Environmental Engineering and Science Conference, p. 555 (1973).

9. Fuchs, N.A., The Mechanics of Aerosols, Pergamon Press, Oxford (1966).

10. Davies, C.N., Air Filtration, Academic Press, New York (1973).

11. Frederick, E.R., Chem. Eng., 68, 107 (1961).

12. Kraemer, H.F., and Johnstone, H.F., Ind. Engng Chem., 47, 2426, (1955).

13. Dawkins, G.S., Technical Report No. 15, Engineering Experiment Station, University of Illinois (1958).

14. Natanson, G.L., Proc. of the Academy of Science, U.S.S.R., Physical Chemistry Section, 112, 95 (1957).

15. Lundgren, D.A.. and K.T. Whitby, I and E.C. Fund (1965).

16. Yoshioka, N., Emi, H., Hattori, M., and Tamori, I., Kagaka Kugaku, Chem. Eng. Japan, 32, 815 (1968).

17. Rossano, A.J., Jr., and Silverman, L., AEC NYO-1594. Air Cleaning Laboratory, Harvard School of Public Health (1954).

18. Goyer, G.G., Gruen, R., and LaMer, V.K., J. Phys, Chem., 58, 137 (1954).

19. Silverman, L., Conners, E.W., Jr., and D.M. Anderson, AEC NYO-4610, Air Cleaning Laboratory, Harvard School of Public Health (1956).

20. Rivers, R.D., ASHRAEJI, 4, 37 (1962).

21. Whitby, K.T. and B.Y.H. Liu, Aerosol Science, Academic Press (1966).

22. Gillespie, T., J. Colloid, Sci., 10, 299 (1955).

23. Thomas, J.W. and Woodfin, E.J., Applic. and Industry, (AIEE)(1959).

24. Sweitzer, D., "Electrets, Literature Search" No. 308, Jet Propulsion Laboratory, Cal. Inst. of Tech., (1961).

25. Dennis, R., Kristal, E., and Silverman, L., AEC NYO-4614, Air Cleaning Laboratory, Harvard School of Public Health (1958).

26. Anderson, D.M., and Silverman, L., AEC NYO-4615, Air Cleaning Laboratory, Harvard School of Public Health (1958).

27. Lapple, C.E., Advances in Chemical Engineering, 8, Academic Press, New York (1970).

28. Havlicek, V., Int. J. Air Water Pollution, 4, 225 (1961).

29. Silverman, L., Billings, C.E., and Bennis, R., AEC NYO-1592, Air Cleaning Laboratory, Harvard School of Public Health.

30. Walkenhorst, W., and Zebel, G., Staub, 24, 444 (1964).

31. Zebel, G., J. of Colloid Sci., 20, 522 (1965).

32. Zebel, G., Staub, (English Translation) 26, 18 (1966).

33. Ariman, T., "Collection of Dust by Fiber Filters in an Electrostatic Field," Survey Article, to be published.

34. Scheidegger, A.E., The Physics of Flow Through Porous Media, The Macmillan Company, New York (1960).

ACKNOWLEDGEMENT

This investigation has been supported by the APITRON division of American Precision Industries and also by the Department of Energy, Industrial Energy Conservation under the contract EC-77-S-2-4428 to the University of Notre Dame. The senior author acknowledges the encouragement and interest of Mr. John R. Rosmeissl, the project monitor during the course of this research program.

EXPERIMENTAL ADVANCES IN FABRIC FILTRATION TECHNOLOGY IN JAPAN

- Effects of a Corona Precharger and Relative Humidity on Filter Performance -

By:

Koichi Iinoya and Yasushige Mori
Department of Chemical Engineering
Kyoto University
Kyoto, Japan 606

ABSTRACT

1. The effects of a corona precharger on the performance of a fabric filter have been studied experimentally in air with controlled humidity. Test dust, fine calcium carbonate powder, is precharged and then ducted to a filter fabric. The charged dust for the most part reduces both the pressure loss and the particle penetration through the filter, on which the same amount of dust is collected as in the experiments without the precharger.

2. Fundamental experiments have been conducted to clarify the effects of air humidity on the performance of a fabric filter. Three kinds of test dust (calcium carbonate, Kanto-loam and flyash) are used. In general, the humidity of air does not have much of an effect on the pressure loss and the particle penetration, when the agglomerated particles size distributions of the airborne dusts are controlled so as to be almost constant in spite of the different humidity of air.

1. EFFECT OF CORONA PRECHARGER ON FILTER PERFORMANCE

There are several experimental reports on the performance of a combination dust collector of an electrostatic precharger and a fabric filter, which reduces the pressure loss.[1)-5)] However, they are mostly concerned with the qualitative results of fundamental experiments or the overall performance of a pilot scale filter. A preliminary but quantitative experiment on the hybrid filter is conducted herein by use of a bench scale test facility.

1.1 Experimental Apparatus and Procedure

Figure 1 shows a flow diagram of the experimental apparatus. Fine calcium carbonate is uniformly fed to a mixer type disperser as a test dust by a Micro Feeder (Sankyo Dengyo Co.), and is ducted to the test filter through both a corona precharger and a settling (or mixing) chamber. The test section is a series combination of a test fabric filter and a back-up high performance Millipore filter, and is followed by an orifice flow meter and a suction pump. The air flow rate is controlled so as to be constant during a test period by use of an automatic regulator, and is recorded on a chart with the pressure loss of the loaded test filter.

The corona precharger is a kind of a short electrostatic precipitator, which is constructed with 8 discharge electrodes of tungsten wire (0.2 mm x 100 mm) and 10 plate electrodes (11 mm x 100 mm). The distance between the above two electrodes is 12 mm. The applied voltage is about 7 kV D.C., and the electric current is kept constant between 3 and 4.5 mA. during a test period.

The dust collection area of a test fabric is about 50 cm^2, and the fabric is a polyester (Tetron) felt, of which the weight is 640 g/m^2 and the air permeability is 15 cm/sec for the pressure loss of a half inch of water column. Electrostatic charge of dispersed test dust is measured just before the test filter by use of a Faraday cage with a glass fiber filter.

Penetration of test dust is calculated from the ratio of dust weight collected by the test filter and the weight by the back-up filter. Figure 2 shows particle size distributions of dispersed test dust sampled just before the test filter by use of a slit type cascade impactor (Shimadzu CI50). The size distributions of charged dust are almost the same as those of uncharged dust, because a part of electrostatically agglomerated particles may settle down in the settling chamber. The filtration velocity is 3.1 m/min for all of the test runs.

1.2 Experimental Results[6)]

Figure 3 shows a picture of the ragged surface of the charged dust bed collected on a test fabric. Figure 4 is also a picture of a rather smooth surface of the charged dust bed on the same fabric. Figure 5 is another picture of the smooth surface of the uncharged dust bed on the same fabric. In the case of Figure 3, pressure loss of the loaded test filter is much lower than that of the case of Figure 5. However, the pressure loss of Figure 4 is nearly the same as that of the uncharged dust bed shown in Figure 5.

Figure 6 shows a relation between drags (pressure loss divided by filtration velocity) and dust loads deposited on a test filter for various relative humidity of filtered air. The ragged (nodular deposit) surface often takes place at a relative humidity of 50 to 75%. The reduced pressure loss is apparently due to the uneven nodular deposits of test dust collected on the fabric by the electrostatic charge effect.

Figure 7 shows the cumulative collection efficiencies by weight for the same experimental conditions as those in the pressure loss. The efficiencies of charged dust are usually higher than those of uncharged dust and have no correlation with the air humidity nor the shape of the powder bed surface.

Figure 8 shows the measured electrostatic charges of test dust just before a test filter at various air humidities. The lower points mostly represent the charges just before the test period, and accordingly the upper points correspond to those just after the test period. The charges at an air humidity of 60 to 70% are somewhat higher than those at lower or higher humidities.

1.3 Conclusion

Pressure loss of a fabric filter may be reduced by use of electrostatic corona precharger in front of the fabric filter at an appropriate condition. The reduced amount is less than half of the original pressure loss for the equal dust load deposited on a filter.

On the other hand, collection efficiency of a fabric filter is usually improved with a corona precharger. Penetration of dust is reduced up to 10 to 50% of the original values. Therefore, the precharger seems to be a promising device for improving the performance of a fabric filter, if the economic cost is allowable.

References

1) Helfritch, D.J. Performance of an Electrostatically Aided Fabric Filter. Chem Eng Prog. 73:54 - 57, August 1977.

2) Lamb, G. E. R., and P. A. Costanza. Improving Performance of Fabric Filters. Chem Eng Prog. 73:51 - 53, January 1977.

3) Lamb, G. E. R., and P. A. Costanza. Electrical Stimulation of Fabric Filtration. Textile Res J. 47:372 - 380, May 1977.

4) Penney, G. W. Using Electrostatic Forces to Reduce Pressure Drop in Fabric Filters. Powder Tech (Netherlands). 18:111 -116, 1977.

5) Penney, G. W. Electrostatic Effects in Fabric Filtration: I. Fields, Fabrics, and Particles. EPA - 600/7 - 78 - 142a., September 1978.

6) Costanza P.A., G.E.R. Lamb, and J.B.Dunbar. Electrical Stimulation of Fabric Filtration (ESFF) for Cotton Dust Control. J Eng for Ind, Trans ASME. 101: 65 - 68, February 1979.

II EFFECT OF HUMIDITY ON FILTER PERFORMANCE

There are few experimental reports about the effect of relative humidity on the pressure loss of a fabric filter. Higher relative humidity seems to reduce the pressure loss because of particle agglomeration[1)-3)]. However, two previous papers present different experimental results[4)5)], in one of which humidity does not have much of an effect on both the pressure loss and dust dislodgement of a filter when calcium carbonate is used as a test dust. Therefore, we have tried again to confirm the effect by use of our experimental facility and three kinds of test dust.

2.1 Experimental Apparatus and Procedure

Figure 9 shows a flow diagram of the experimental apparatus. A test dust is uniformly fed into a mixer type disperser by a Micro-Feeder (Sankyo Dengyo Co.) and is ducted to a test filter section through a settling or mixing chamber with a bipolar ion generator as an electrostatic charge neutralizer. The test filter is followed by two back-up Millipore filters in series, of which the latter serves to calibrate the humidity effect on the blank weight. The air flow rate is measured by an orifice meter and controlled so as to be constant during a test period by an automatic regulator. Finally, a suction pump induces air flow with suspended dust through the whole system.

The collection surface of the test filter is round and has an area of about 32 cm^2, and the fabric is a polyester (Tetron) felt, of which the weight is 640 g/m^2 and the permeability is about 15 cm/sec at the pressure loss of 12.7 mmH_2O.

Dust penetration is calculated from both the dust weight collected on a test filter and that on a back-up filter. Local penetrations of oversized particle fractions are measured by use of a light scattering particle counter (Bausch-Lomb) and a flow sampling line. Local penetrations of the whole size range of test dusts are also measured by use of a piezo-electric mass balance (Thermo System Inc.). Electrostatic charges of test dusts are also measured by use of a Faraday cage with a filter just after the settling chamber. Three kinds of test dust are fine calcium carbonate, Kanto loam (JIS No.8) and fly ash (JIS No.5). The filtration velocity is constant at 2.7 m/min for all test runs.

2.2 Experimental Results and Discussions

2.2.1 Pressure Loss. Figures 10, 11 and 12 show the drags of a filter against dust loads deposited on a test fabric for three kinds of test dust respectively. Relative humidity of filtered air does not have much of an effect on the pressure loss of a filter and these tendencies are different from the results obtained by others.[1)-3)] This experimental discrepancy may be due to the difference of the agglomerated size distributions of test dust just before the test filter, as given in the next section.

2.2.2 Particle Size Distributions of Test Dusts. Particle size distributions of three kinds of test dust, measured by a cascade impactor just before the settling chamber, depend on the relative humidity of air as shown in Figures 13, 14 and 15. The higher the relative humidity, the coarser the

particle size. Higher humidity seems to promote particle agglomeration.

However, particle size distributions of the same test dusts, measured by an impactor just after the settling chamber, do not show much of a change for a wide variation in air humidity, as shown in Figures 16, 17 and 18. This seems to be due to the sedimentation of agglomerated coarse particles in the settling chamber.

2.2.3 Collection Efficiency or Particle Penetration. Figures 19, 20 and 21 show particle penetrations against dust loads on a fabric for three kinds of test dust respectively. Relative humidity of filtered air does not have much of an effect on the collection performance of the filter. The reason seems to be the unchanged size distributions for a wide range of humidity just after the settling chamber, as mentioned in the previous section.

Figures 22, 23 and 24 show local number penetrations of particles above one micrometer against dust loads on the filter for three kinds of test dust respectively. The effect of relative humidity on the number penetration has no definite tendency, and it depends on the kind of test dusts.

2.2.4 Electrostatic Charge of Test Dust. Electric charges of dispersed test dusts sampled just before the test fabric are measured by use of a Faraday cage with a glass fiber filter and a high sensitivity electrometer. Figure 25 shows that these electrostatic charges of three kinds of test dust depend on humidity in the air. However, these data show no definite tendency.

2.2.5 Moisture Content of Test Dust. Moisture contents of three test dusts change with air humidity, as shown in Figure 26. The moisture content is nearly proportional to relative humidity.

2.3 Conclusion

Both pressure loss and collection efficiency of a fabric filter are not affected by the relative humidity of filtered air, when particle size distributions of any test dust in the air do not change with humidity just before the test filter. However, the moisture contents of test dusts are nearly proportional to humidity, and electrostatic charges of the test dust are in the order of 10^{-6} to 10^{-7} coulomb/g.

References

1) Ariman, T., and D.J. Helfritch. How Relative Humidity Cuts Pressure Drop in Fabric Filters. Filtration & Separation (London). 14:127-130, March / April 1977.

2) Ariman, T., and D.J. Helfritch. Effect of Humidity on Pressure Drop in a Baghouse Simulator. A I Ch E, Symp Series. 74: No.175 10-15, 1978.

3) Durham, J.F., and R.E. Harrington. Influence of Relative Humidity on Filtration Resistance and Efficiency of Fabric Dust Filters. Filtration & Separation (London).8:389-398, July / August 1971.

4) Donovan, R.P., B.E. Daniel, and J.H. Turner. EPA Fabric Filtration Studies: 3. Performance of Filter Bags Made from Expanded PTFE Laminate. EPA-600/2-76-168c., December 1976.

5) Iinoya, K., and Y. Mori. Fundamental Experiments of Fabric Filters. EPA-600/7-79-044b. Symposium on the Transfer and Utilization of Particulate Control Technology: Vol.2, Fabric Filters and Current Trends in Control Equipment.

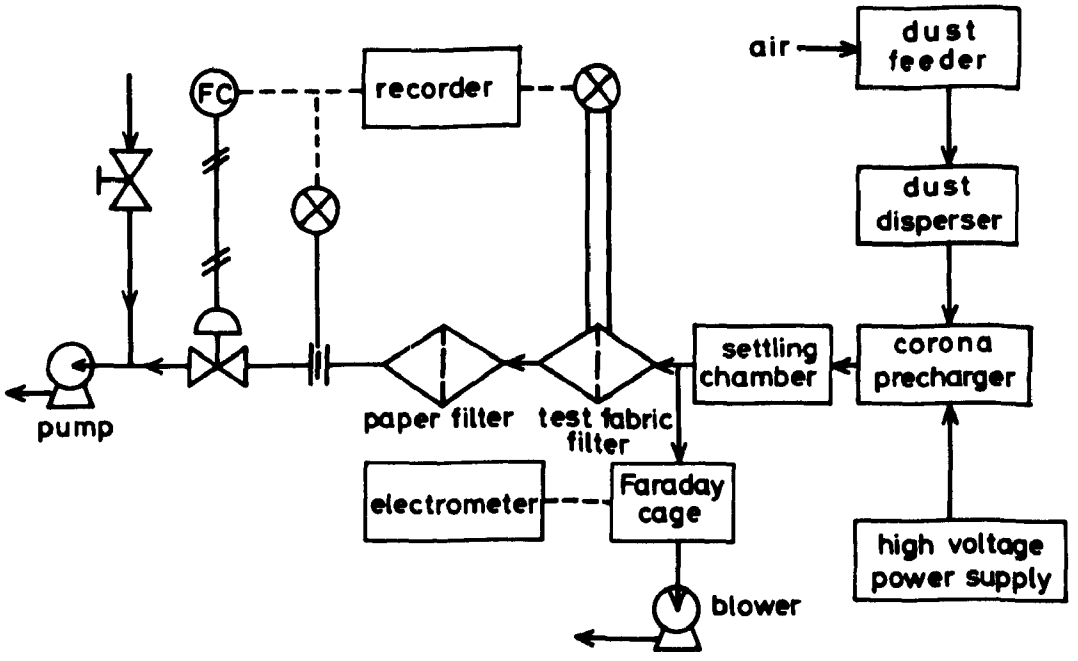

Figure 1 Experimental apparatus for electrostatic effects in fabric filtration

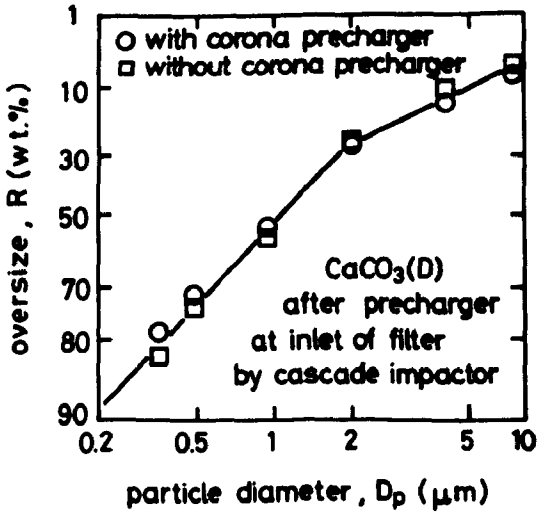

Figure 2 Particle size distributions of test dust

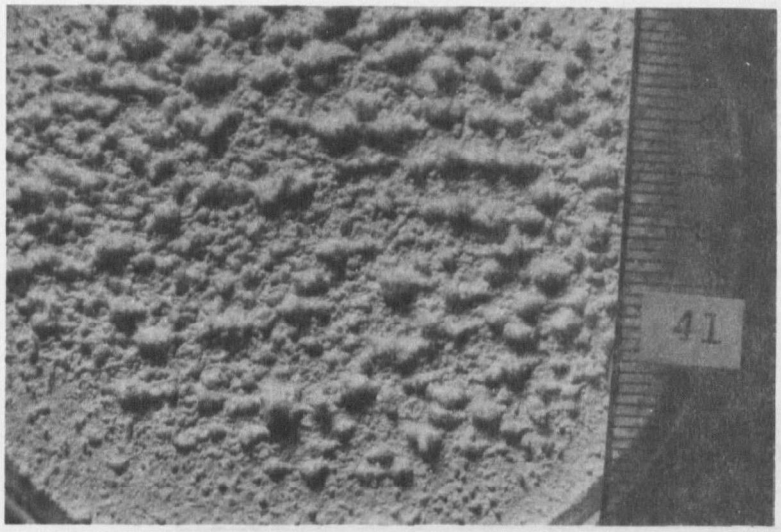

Figure 3 Photograph of ragged surface of deposited dust with corona precharger, $m = 83,5\ g/m^2$, R.H. = 73 %

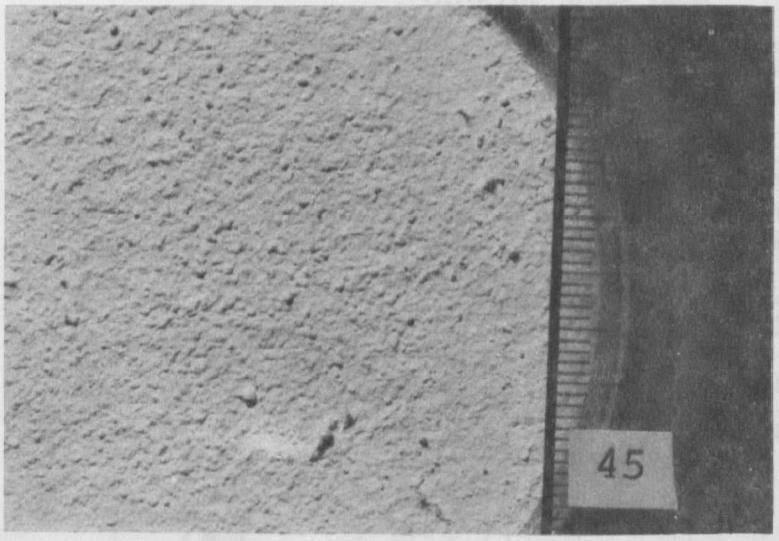

Figure 4 Photograph of smooth surface of deposited dust with corona precharger, $m = 86.7\ g/m^2$, R.H. =83 %

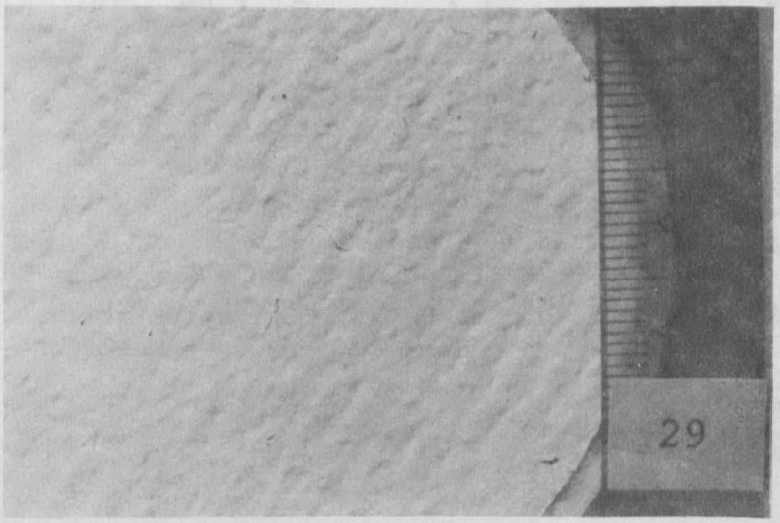

Figure 5 Photograph of smooth surface of deposited dust without corona precharger, $m = 138\ g/m^2$, R.H. = 55 %

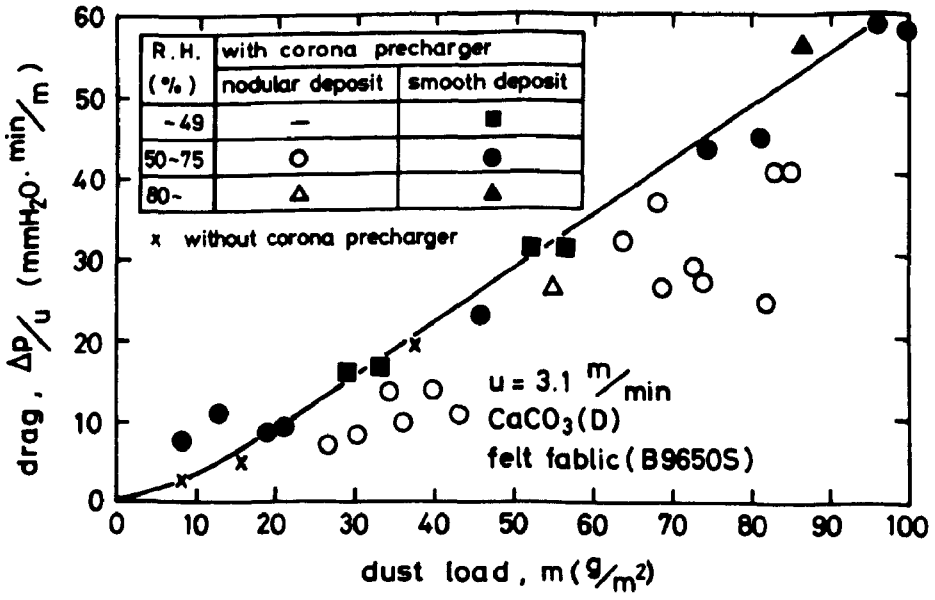

Figure 6 Relation between drags and dust loads on a filter

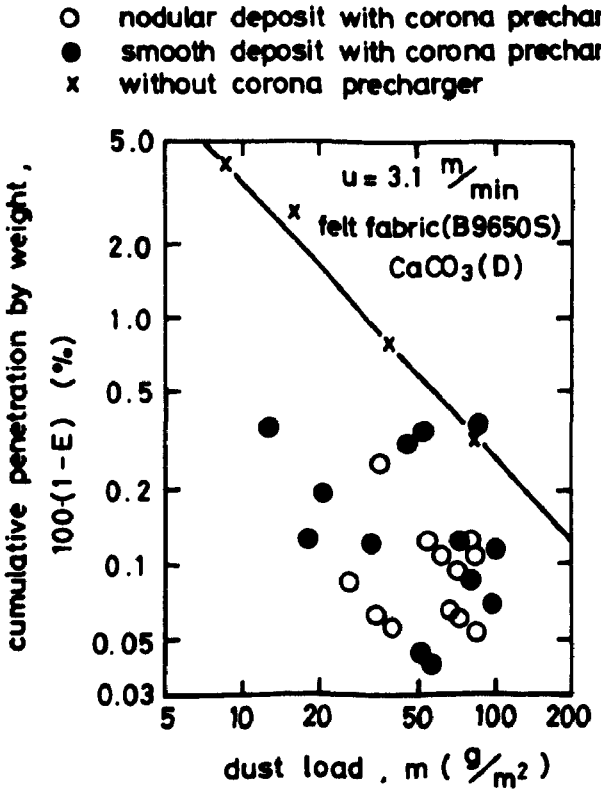

Figure 7 Relation between cumulative penetrations and dust loads on a filter

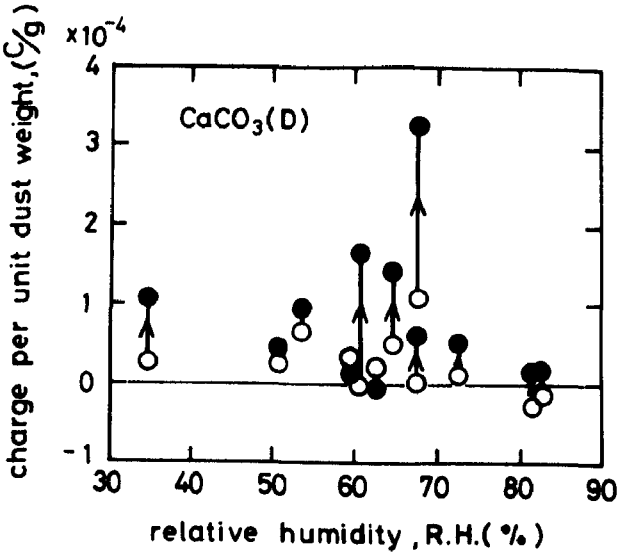

Figure 8 Effect of relative humidity on electrostatic charge by corona precharger

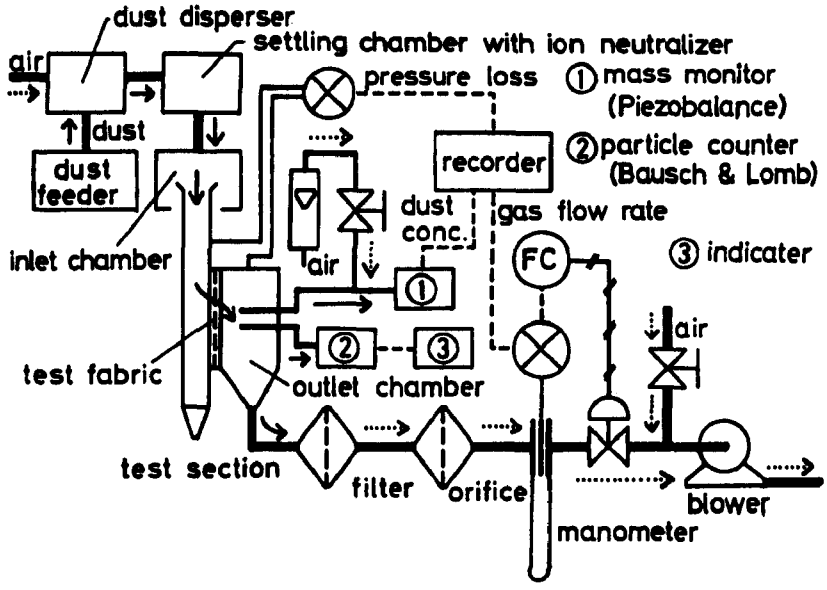

Figure 9 Experimental apparatus for effect of humidity on filter performance

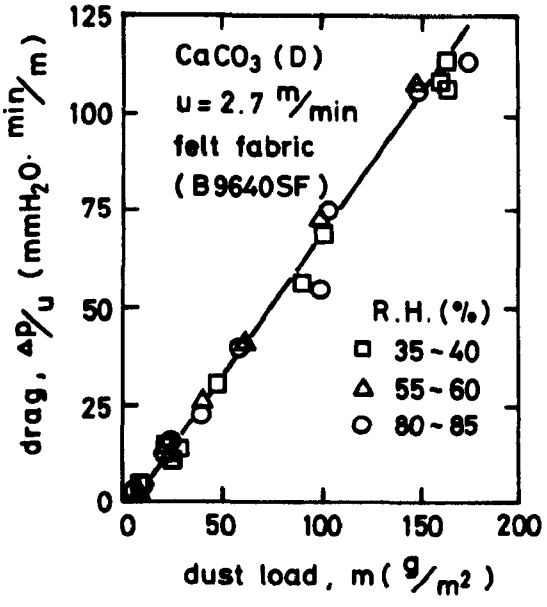

Figure 10 Relation between drags and dust loads for fine calcium carbonate at various relative humidity levels

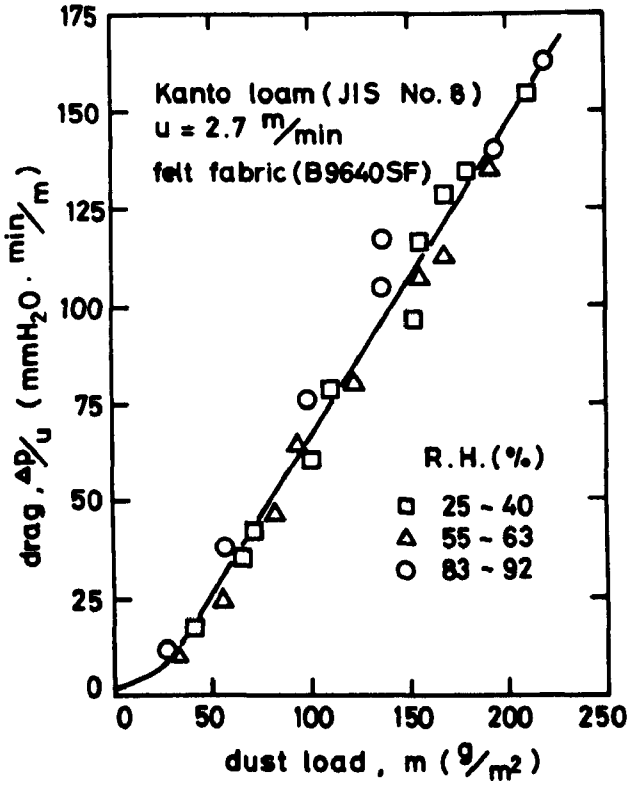

Figure 11 Relation between drags and dust loads for Kanto loam (JIS No.8) at various relative humidity levels

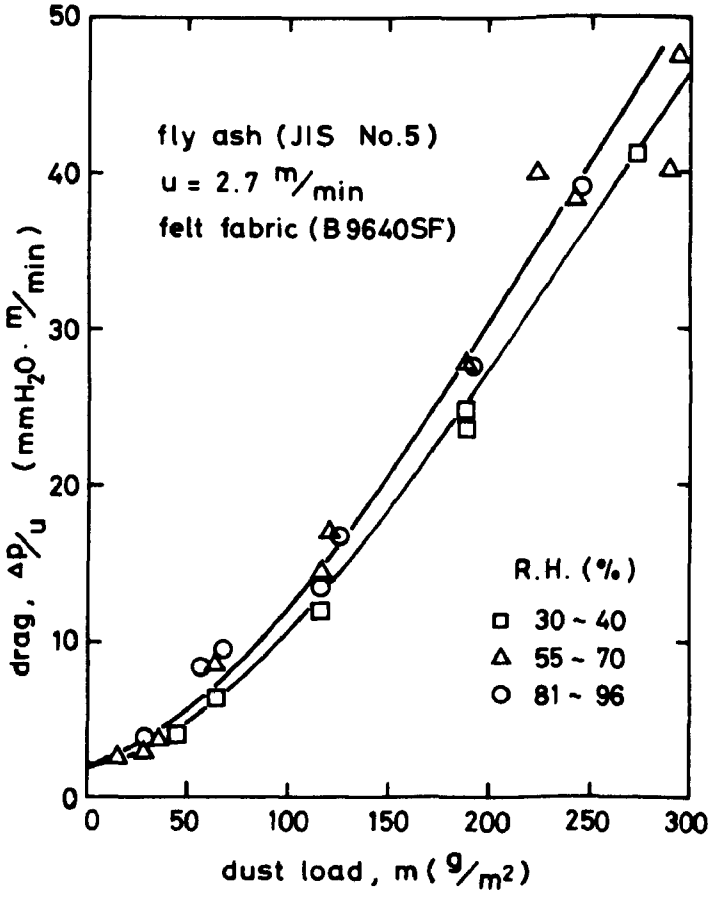

Figure 12 Relation between drags and dust loads for fly ash (JIS No.5) at various relative humidity levels

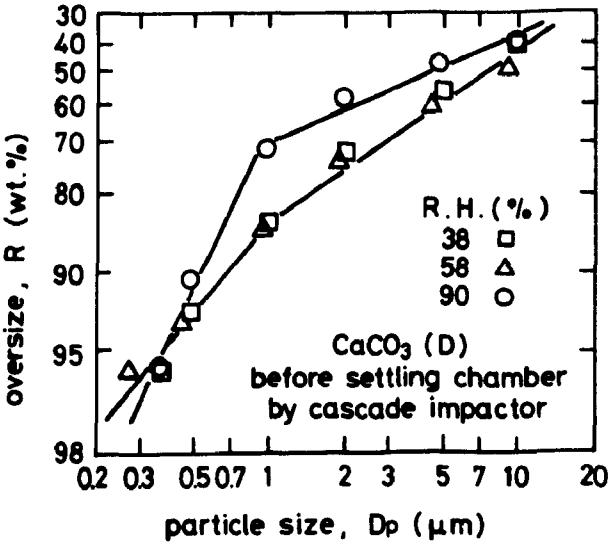

Figure 13 Particle size distributions of fine calcium carbonate before settling chamber at various relative humidity levels

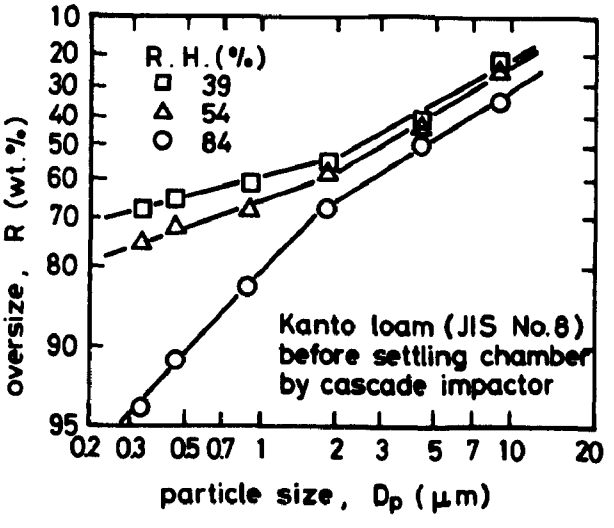

Figure 14 Particle size distributions of Kanto loam (JIS No.8) before settling chamber at various relative humidity levels

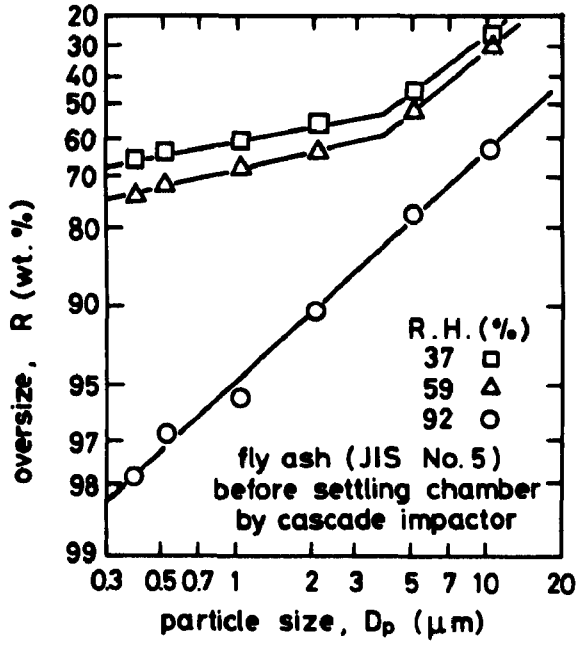

Figure 15 Particle size distributions of fly ash (JIS No.5) before settling chamber at various relative humidity levels

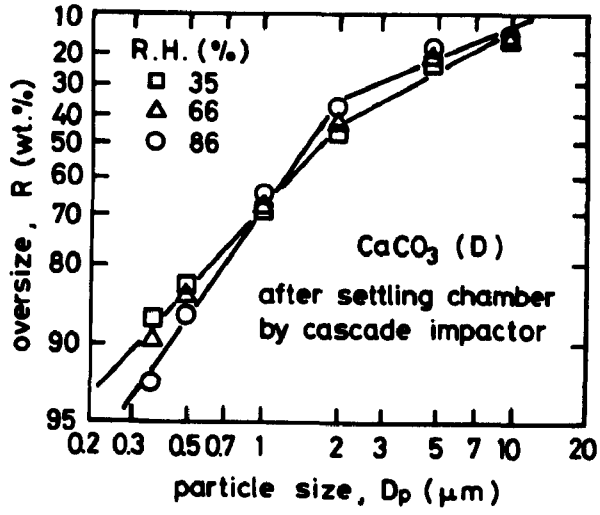

Figure 16 Particle size distributions of fine calcium carbonate after settling chamber at various relative humidity levels

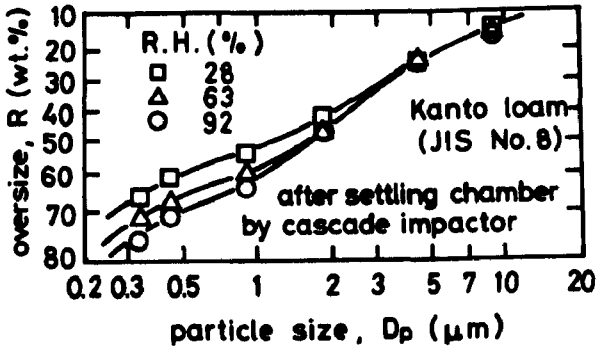

Figure 17 Particle size distributions of Kanto loam (JIS No.8) after settling chamber at various relative humidity levels

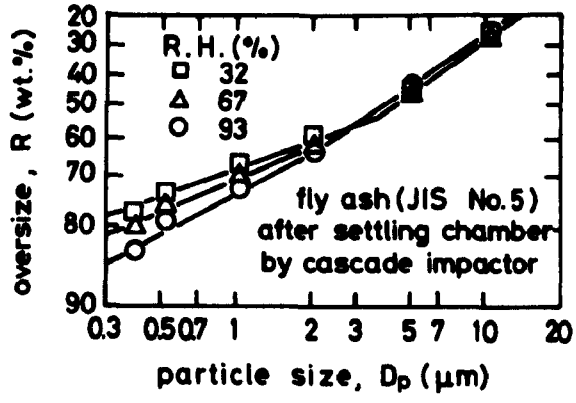

Figure 18 Particle size distributions of fly ash (JIS No.5) after settling chamber at various relative humidity levels

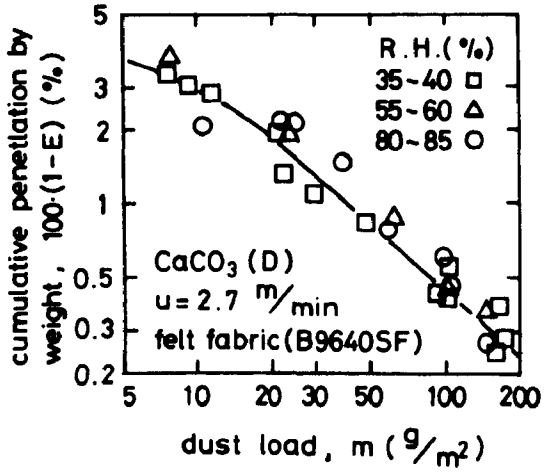

Figure 19 Relation between cumulative penetrations and dust loads for fine calcium carbonate at various relative humidity levels

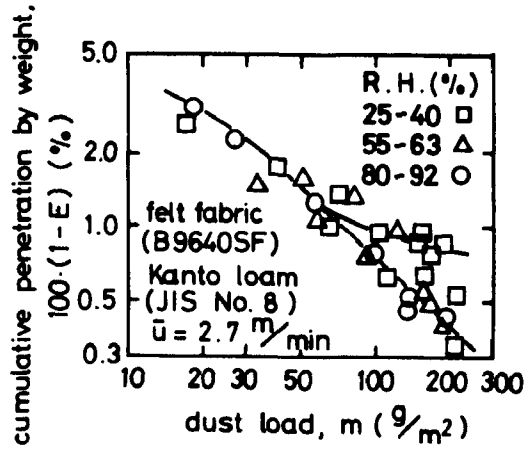

Figure 20 Relation between cumulative penetrations and dust loads for Kanto loam (JIS No.8) at various relative humidity levels

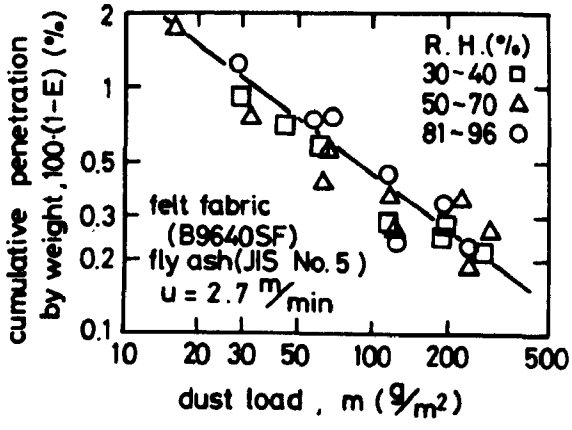

Figure 21 Relation between cumulative penetrations and dust loads for fly ash (JIS No.5) at various relative humidity levels

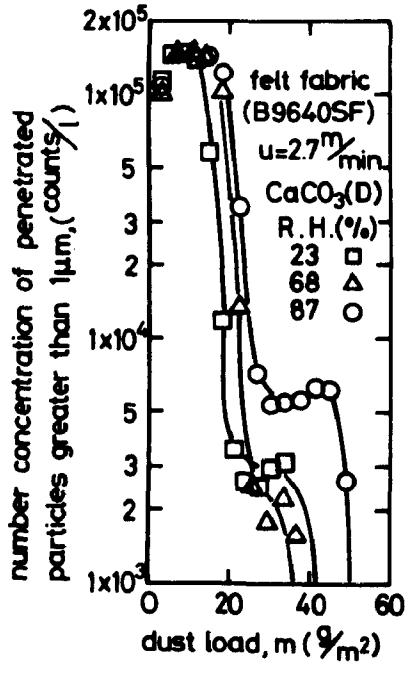

Figure 22 Relation between local penetrations and dust loads for fine calcium carbonate at various relative humidity levels

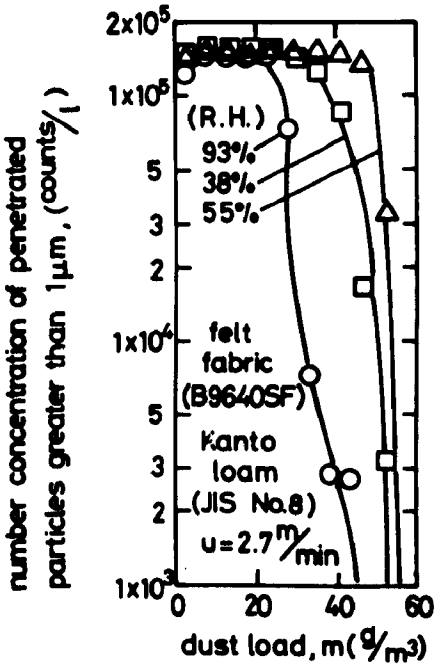

Figure 23 Relation between local penetrations and dust loads for Kanto loam (JIS No.8) at various relative humidity levels

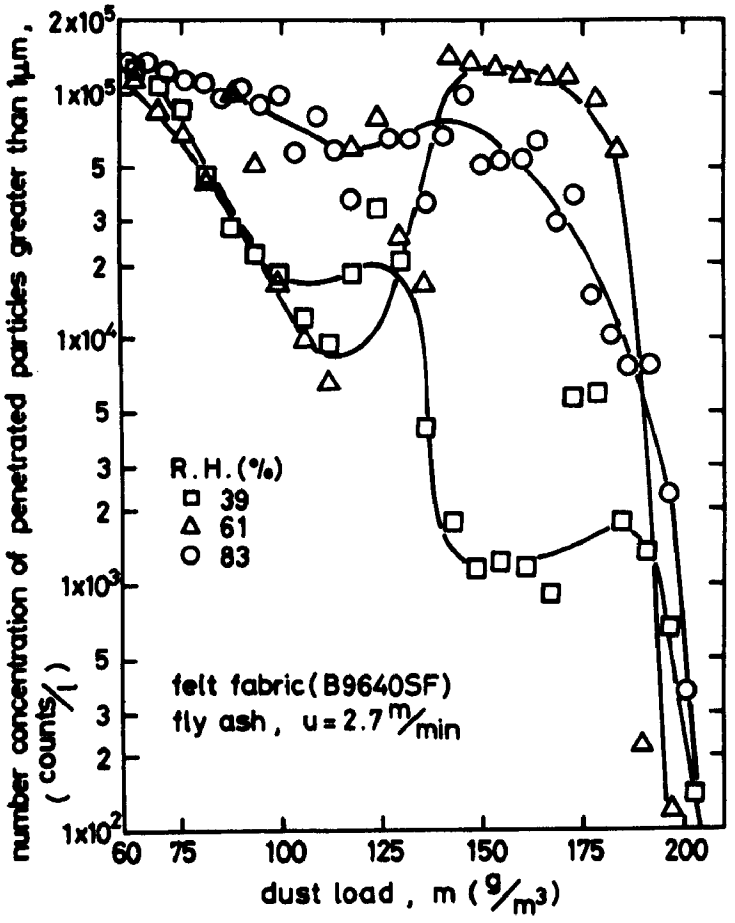

Figure 24 Relation between local penetrations and dust loads for fly ash (JIS No.5) at various relative humidity levels

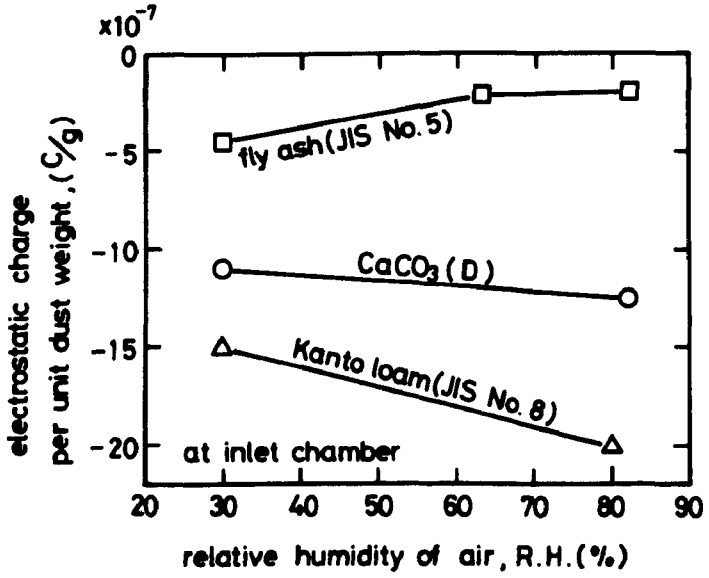

Figure 25 Relation between electrostatic charge and relative humidity

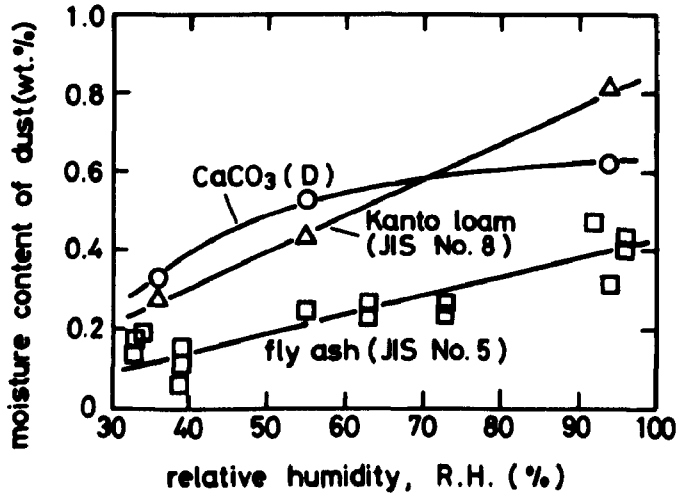

Figure 26 Relation between moisture contents of test dusts and relative humidity

BAGHOUSE OPERATING EXPERIENCE ON

A NO. 6 OIL-FIRED BOILER.

BY:

David W. Rolschau, President
DaVair, Inc.
Minneapolis, Minn. 55405

ABSTRACT

In June 1977, the University of Illinois, Chicago, Illinois, went operational on the nation's first high ratio, reverse gas, glass bag baghouse operating on a No. 6 oil-fired HTHW boiler. This paper discusses factors influencing baghouse design and selection, capacity control, furnace pressure stability, decision to eliminate pre-coating, cold start procedures, operating experience, and maintenance costs.

BAGHOUSE OPERATING EXPERIENCE ON A NO. 6 OIL-FIRED BOILER.

PROBLEM.

The University of Illinois, Circle Campus, downtown Chicago, Illinois, operates four 75 MBTU/hr, HTHW gas-oil fired boilers. In 1975, when gas was in short supply, the decision was made to install a stack baghouse system so as to make possible the burning of low sulphur No. 6 oil in a residential setting. The boilers were currently operating within code limits except during soot blowing, which occurred once every fourth hour at full load.

SOLUTION.

The decision was made to manifold a single baghouse system, sized for 75 MBTU/hr gas capacity (35,000 ACFM @ 450° F), to all four stacks and to valve the system as shown in Figure 1, such that the baghouse system would operate continuously on one of the four stacks and would be manually alternated between stacks in order to clean full stack capacity during soot blowing. The baghouse, therefore, was to handle approximately four times normal particulate loading.

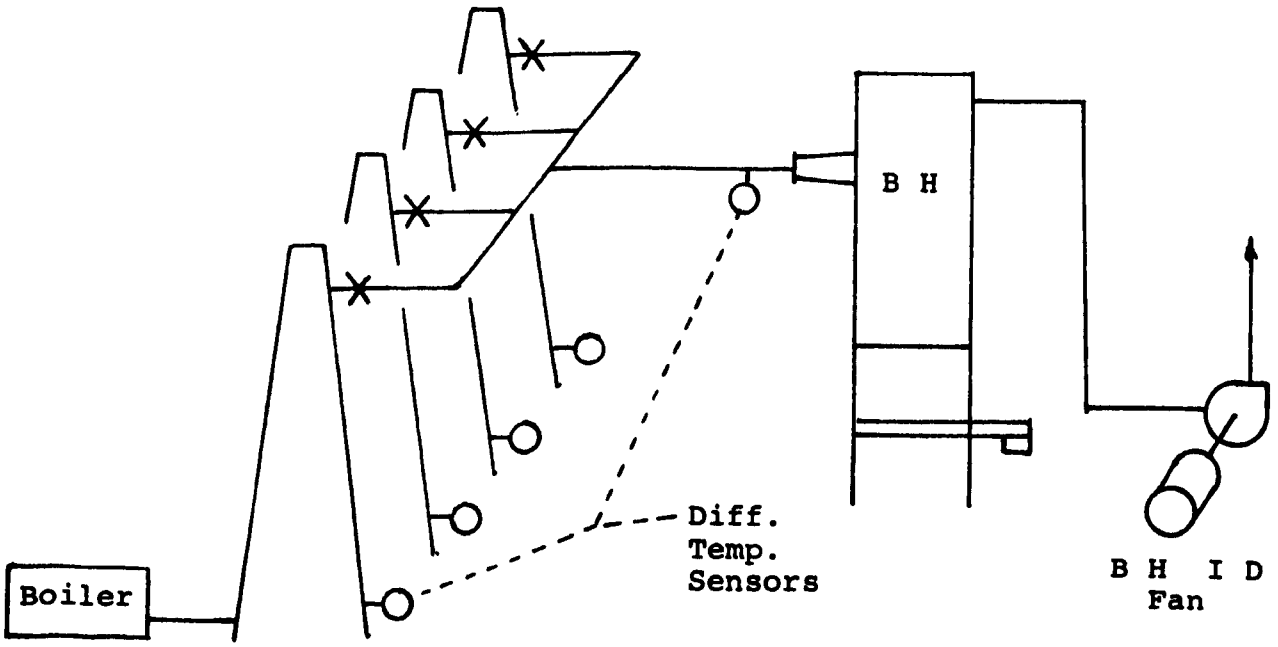

Figure 1.

BOILER - BAGHOUSE SCHEMATIC

No other baghouse system had ever been put in operation in the country on No. 6 oil-fired boiler service.

A baghouse capacity control system was needed to match the baghouse to the stack being cleaned. A baghouse gas dilution capacity control system was designed to couple the baghouse to any one of four different capacity stacks. The system matched boiler and baghouse gas capacity by mixing stack gas with 5 per cent atmospheric stack downflow air for dilution cooling, and sensed the resulting difference between stack and mixed gas temperature. The baghouse inlet temperature sensor was interlocked with one of the four stack temperature sensors and with one of the four inlet manifold valves to provide automatic baghouse volume control by regulating the I D fan to maintain stack temperature 25° F higher than mixed gas temperature.

Since each HTHW boiler had an operating turn-down ratio of 10:1, a DC motor driver was specified for the baghouse I D fan.

The system specification, prepared by Murphy Engineering of Chicago, Illinois, addressed the unknowns of oil-fired operation by requiring performance guarantees with substantial penalties in the following areas:

1. Gas effluent quality better than 0.015 Gr/ACF.

2. Noise level 65 dbA or less at customer's property line.

3. Abrasive wear for one year.

4. Labor and material cost for bag failure and/or excessive pressure loss at rated capacity, for one year.

5. Assigned responsibility for selection and sizing of the baghouse I D fan and D C motor driver to the baghouse manufacturer.

The bid by Independent Mechanical Industries, Chicago, Ill., using a DaVair DCR 200-15 baghouse at 4.5:1 cloth ratio was accepted based on lowest first cost, compliance with all performance guarantees, and technical confidence in the unique bag cleaning features of the patented reverse gas design. A diagram of a DaVair DC Series baghouse is shown in Figure 2.

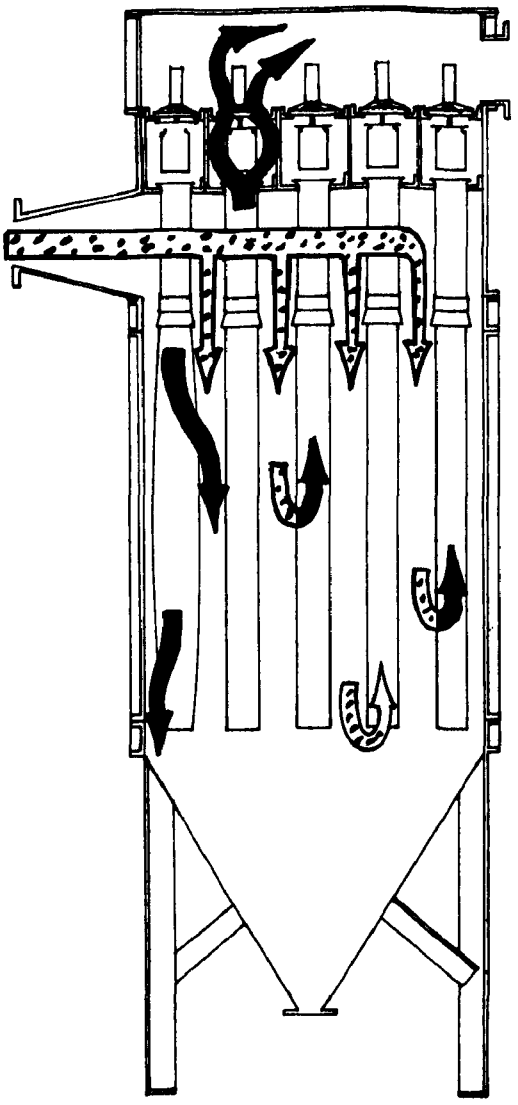

Figure 2.

DAVAIR DC BAGHOUSE.

Each DaVair DC Series baghouse compartment is a totally self contained unit, complete with its own head mounted reverse gas fan and automatic bag cleaning system. The highly sectorized design is particulary well suited for small boiler service because the pressure drag variations, which occur as all baghouses cycle into and out of cleaning mode, are so small that furnace pressure normally varies less than 0.1 in. W C from set point.

The DC Series design creates downflow of the dirty gas stream. Particulate removed from the bag during cleaning cycle is transported to the hopper by this downflow. Baghouse performance is not dependent upon the ability of the particle to agglomerate to a larger size, nor is performance adversely affected by the increased gas viscosity of high temperature operation. Refer to Figure 3, Stokes Law, terminal velocity of ash particles in flue gas.

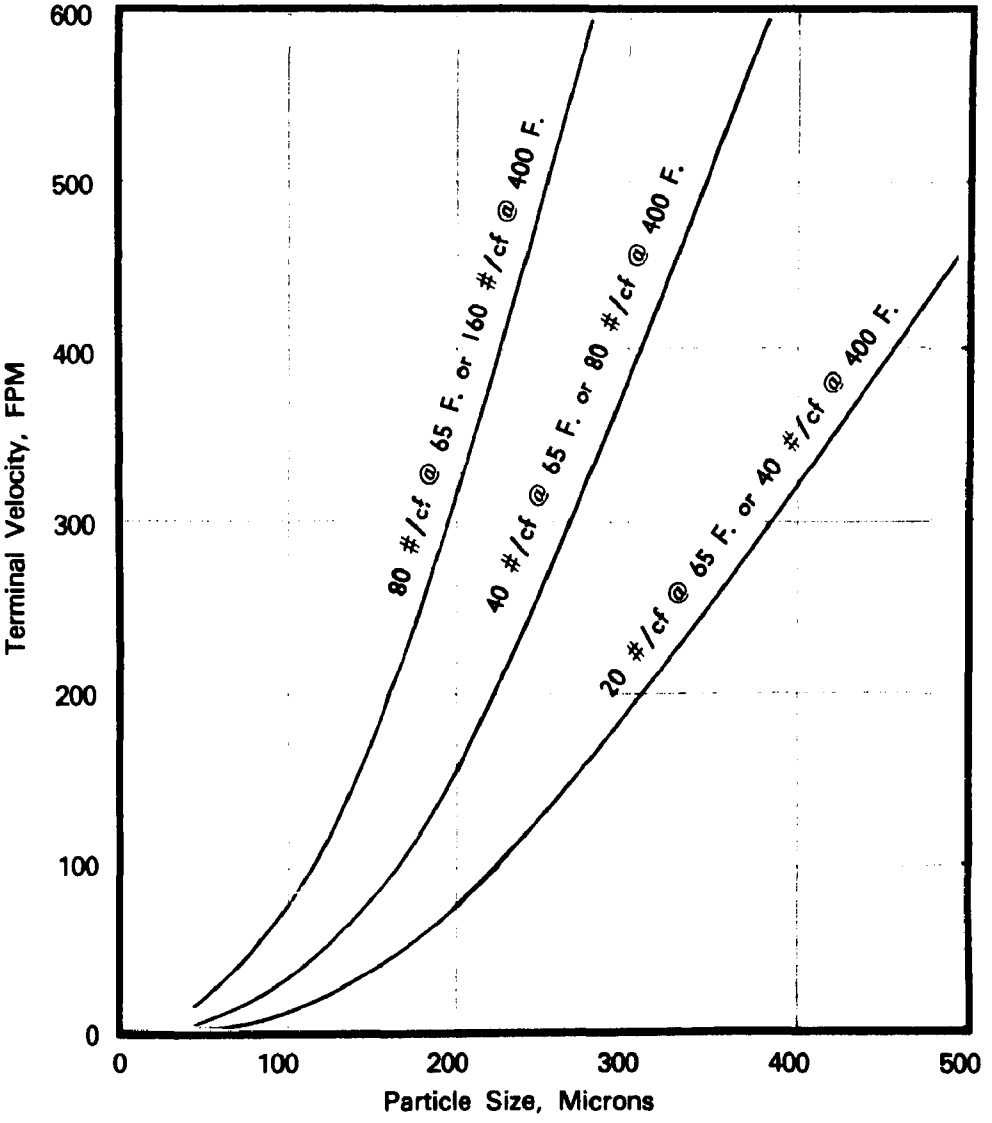

Figure 3.

TERMINAL VELOCITY OF PARTICLES IN FLUE GAS.

The DC Series baghouse operates with a design bag cleaning velocity of 8 FPM. This velocity, which is approximately four times higher than found in conventional reverse gas designs, allows operation with heavier weight fiberglass bags to improve bag life, and assures adequate cleaning energy availability for maintaining cake porosity with sticky particulate, such as is typically found in oil-fired service.

OPERATING EXPERIENCE.

Pre-Coating.

Based on our experience with the DC Series high energy cleaning system, we recommended that no bag pre-coating system be installed or used. (A pre-coat is normally recommended if the baghouse manufacturer anticipates that particulate stickyness will exceed the capability of the bag cleaning system). That decision proved to be correct. All four boilers have been routinely brought on line from cold start-up many times since the system went into operation in June 1977. No bag blinding has occurred.

Operation Below Dew Point.

During the first five months of operation, the baghouse ran continuously on one boiler, firing at ten per cent load. Baghouse outlet temperature never exceeded 240° F, which is substantially below acid dew point on 0.9 per cent sulphur oil. No adverse bag effects were detectable, although considerable amounts of sulphur salts condensed on the metal surfaces of the baghouse clean gas plenum.

Bag Life.

The first set of 200 fiberglass bags was destroyed by fire after nine months of continuous operation. No bag failures had occurred within that time; in fact the bag section had not been opened for any reason at any time prior to the fire.

The baghouse was not used during the 1978-79 season. No additional data on bag life is available from this installation.

The bags have performed as guaranteed in the specification.

Pressure Drag.

During initial operation, a partial failure occurred in the DaVair designed air cylinders which operate the cleaning system. Sufficient reserve energy existed in the cleaning system, such that the boiler-baghouse system operated at full load for three winter months within the capability of the I D fan.

Normal pressure drag is 4 in. W C, flange to flange, during cleaning cycle, at 4.5:1 cloth ratio (35,000 ACFM). Drag stability is 0.4 in W C.

Baghouse Capacity Control.

Heat radiation losses from the insulated baghouse and breeching system prevent the automatic baghouse capacity control system from functioning at boiler capacities below 40 per cent load. Manual speed control of the baghouse I D fan is necessary at the lower load conditions. An explanation of the situation is shown graphically in Figure 4.

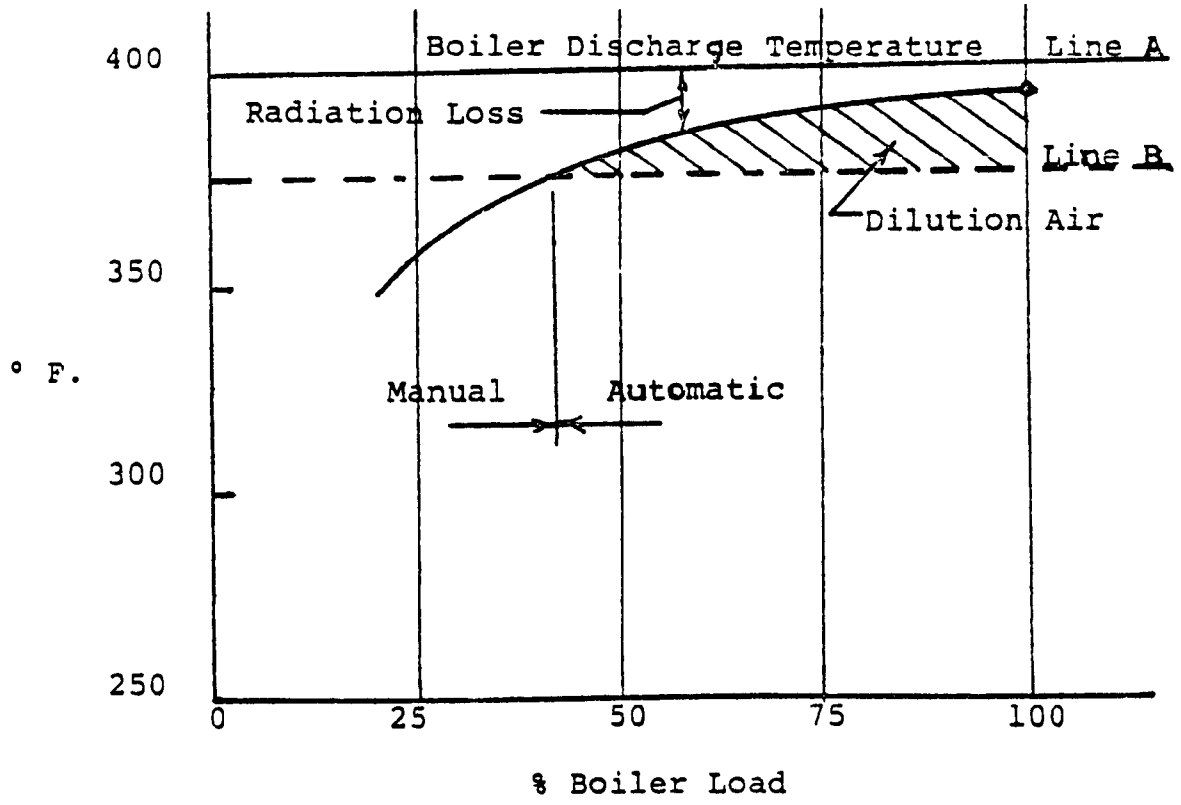

Figure 4.

BAGHOUSE CAPACITY CONTROL.

The differential temperature between boiler and baghouse depends upon both heat radiation losses from the ductwork and dilution mixing of the stack gas with atmospheric air. If the stack gas is cooled 10° F by radiation loss at full load, that cooling will be 20° F at half load, 40° F at one quarter load, and 80° F at one eighth load. When the radiation loss curve crosses line B, the differential temperature sensor, sensing cold baghouse inlet, shuts down the I D fan. Switching the I D fan control to manual mode at low load allows continued operation of the baghouse, but increases the possibility of high oxygen content in the stack gas and the risk of a baghouse fire.

Part Load Radiation Losses.

The specific value of the radiation loss curve in Figure 4 is that it graphically depicts the problem of maintaining baghouse temperatures above acid dew point on installations where the baghouse is subject to high turn down ratios, such as occurs when more than one boiler is breeched into a single baghouse system.

Baghouse Fire.

On March 31, 1978, a baghouse fire occurred which consumed the bags only. The baghouse structure survived, intact, without deformation of the tube sheet. The baghouse can be put into operation at any time, and is budgeted to go into service this year, but increased availability of natural gas in the Chicago area may cause postponement of that decision.

The fire occurred during an aborted cold start on a boiler that was being brought on line after extended maintenance. The baghouse was hot at the time, and had a larger than normal quantity of high carbon ash stored in its hopper. A higher than normal oxygen content exists in the gas stream during start-up, and this also increased the risk of fire.

Costs.

The 1976 installed cost of the particulate control system described was approximately $12. per ACFM.

Operating costs during the first nine months of operation consisted of power costs for operating the I D and reverse gas fans, plus ash disposal costs. Bag and equipment maintenance costs were zero.

Probable bag life, based on experience, should exceed two years.

Conclusion.

The DaVair DC Series baghouse has demonstrated the ability to provide compliance effluent quality at 4.5:1 cloth ratio, without pre-coating, withlow pressure drag, good drag stability, and good bag life, on No. 6 oil-fired boiler service.

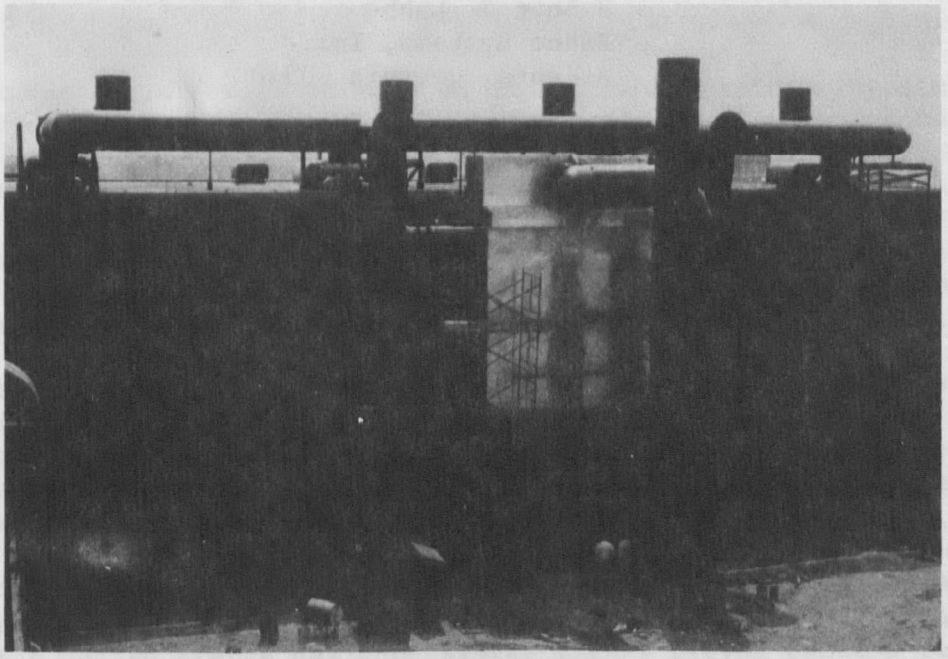

Figure 5.

OIL-FIRED BAGHOUSE.

NEW FABRIC FILTER CONCEPT PROVEN MORE FLEXIBLE IN DESIGN, EASIER TO MAINTAIN AND UNSURPASSED FILTRATION

BY:

Bengt Carlsson
Bahco Systems, Inc.
Atlanta, Georgia 30340

Robert J. Labbe
Bahco Systems, Inc.
Atlanta, Georgia 30340

NEW FABRIC FILTER CONCEPT PROVEN MORE FLEXIBLE IN DESIGN, EASIER TO MAINTAIN, AND UNSURPASSED FILTRATION

The United States is well recognized for its advanced technology in many fields. There is an old American saying, "necessity is the mother of invention". Both the United States and Europe share the necessity of meeting government regulations in air pollution. However, European governments' regulations seem to be more rigid. I think this is largely due to the rigorous enforcement imposed by the pollution control agencies.

When industry is forced to make an unprofitable capital investment like a dust collector, (I base this statement on general calculations for return on investments), the total investment, i.e. capital investment plus maintenance expense must be compared for the available alternatives.

If, in addition to the economical consideration, we evaluate the difficulty and willingness of the worker to maintain a baghouse from the inside, features of any alternative system become highly significant.

I want to quote something that I read in the Fabric Filter Newsletter - "If the dilute emission of flyash (which has been identified as a suspected carcinogen) to the atmosphere is considered harmful to the general public, then why would a corporation allow their men inside a confined space in a concentrated atmosphere to change out bags?"

Outside maintenance and compactness have been achieved by almost all manufacturers through the use of compressed air cleaning. This method of cleaning is a United States designed system with a proven success record established in the last several years. What is Europe able to contribute to fabric filter technology? Is it possible to achieve or even increase capacity of a fabric filter utilizing the compact design with outside maintenance? Questions arise as to: the life of the fabric with high air to cloth ratios? Bag blinding as a problem? The following should give some answers to these problems:

A very important consideration in the design of the fabric filter is the gas inlet. (Figure 1). A well designed gas inlet will prevent abrasion caused by coarse dust impinging on the fabric media. It is established and proven that using "off line" cleaning allows us to use higher air to cloth ratios with a minimum of risk of blinding, and improved fabric life expectancy. For several reasons, European manufacturers of fabric filters have tried several configurations other than the conventional bag. For example, the envelope, pocket and cassette. A description of the conventionally used bag filter cleaning technique is required to demonstrate the reason for the above referenced different configurations.

Clean, dry and oil free compressed air is introduced through a header located in the clean air plenum of the baghouse. (Figure 2). Because this header is located in the clean gas plenum, secondary air is induced into the venturi by the high pressure compressed air jet. This high velocity air moves down the bag in a wave fashion causing the fabric to expand extremely rapidly. (Figure 3). This very rapid expansion of the fabric will cause the dust cake to penetrate into the fabric. The major portion of the dust cake is shocked loose. (Figure 4).

When the fabric has reached the most expansive point, it then returns striking against the cage like a "whip lash". The dust penetrating the fabric is discharged into the clean air side of the bag during this "whip lash" phenomenon. The fact that the fabric is flexing from a maximum to a minimum with dust penetrating into the fibers means that the fibers are mechanically abraded by this penetrated dust. We are all aware that a dirty suit will not last as long as a clean suit.

This fabric dust penetration phenomenon was discovered after several laboratory tests while flexing a conventional bag. The same tests were performed on the rigidly designed cassette where minimum flexing was experienced and dust penetration was substantially reduced. (Figure 5). The emission after the bag was ten times greater than the emission measured after the cassette.

Employing the fabric filter as the dust collector on a coal fired boiler has become more and more common today, due to the fact that a very high efficiency is required and capable of being achieved - 99.9 plus per cent. This alternative, when considering efficiency performances on western low sulphur coal, is usually more desirable than the electrostatic precipitator option.

Recognizing that high efficiency and continual cleaning performance is achievable on the fabric filter, the key question left to be answered is: what type of fabric has to be used? Several test programs have been performed with all kinds of experts involved. An annotated summary of the state of the art findings might look something like this ...

WOVEN GLASS, WITH DIFFERENT COATINGS:

Plus	Minus
High temperature resistance	The fabric is rather fragile and has low mechanical abrasion resistance
Good acid resistance	
Long time experience from different installations available	Limited capacity per square foot which makes it difficult to be used in higher air to cloth ratio units.

FELTED GLASS:

Plus	Minus
High temperature resistance	Fragile material with low mechanical abrasion resistance
Good acid resistance	Limited experience from installations available
Good capacity and able to be used on rather high air to cloth ratio units	

TEFLON FELTED:

Plus	Minus
High capacity	High initial cost
High temperature resistance	Limited mechanical abrasion resistance
High acid resistance	
Experience data available to some extent	

CHEMICALLY TREATED NOMEX:

Plus	Minus
High capacity	Limited experience data available
Good mechanical abrasion resistance	
Acid resistance	Temperature limitation to 400 degrees Fahrenheit

With the continued rapid development of fabrics suitable for filtering fly ash generated by coal fired boilers, the resultant increased number of fabric filter installations shall create a focal point on maintenance and operation. The older technology low ratio shaker and reverse air fabric collectors, which have been recently, and are presently being installed on coal fired boilers, are very expensive to operate and maintain. Even though these low ratio collectors have a high capital cost and operating cost, the reliability and long term experience is the basis of their present usage.

The high ratio compact cell filter design, allowing for complete external maintenance, will definitely have an impact on fabric filter systems for coal fired boilers.

Because of the more stringent pollution control regulations, the low maintenance mechanical dust collectors no longer suffice as a viable control alternative. Also, electrostatic precipitators that must operate on low sulphur coals at very high efficiencies become economically not feasible in many cases. The fabric filter alternative becomes virtually the only viable solution. With this thought in mind, it becomes an essential mission of both the consulting engineer and the manufacturer to inform the user of the importance and cost of maintenance and operating procedures for the various fabric filter alternatives.

Figure 1

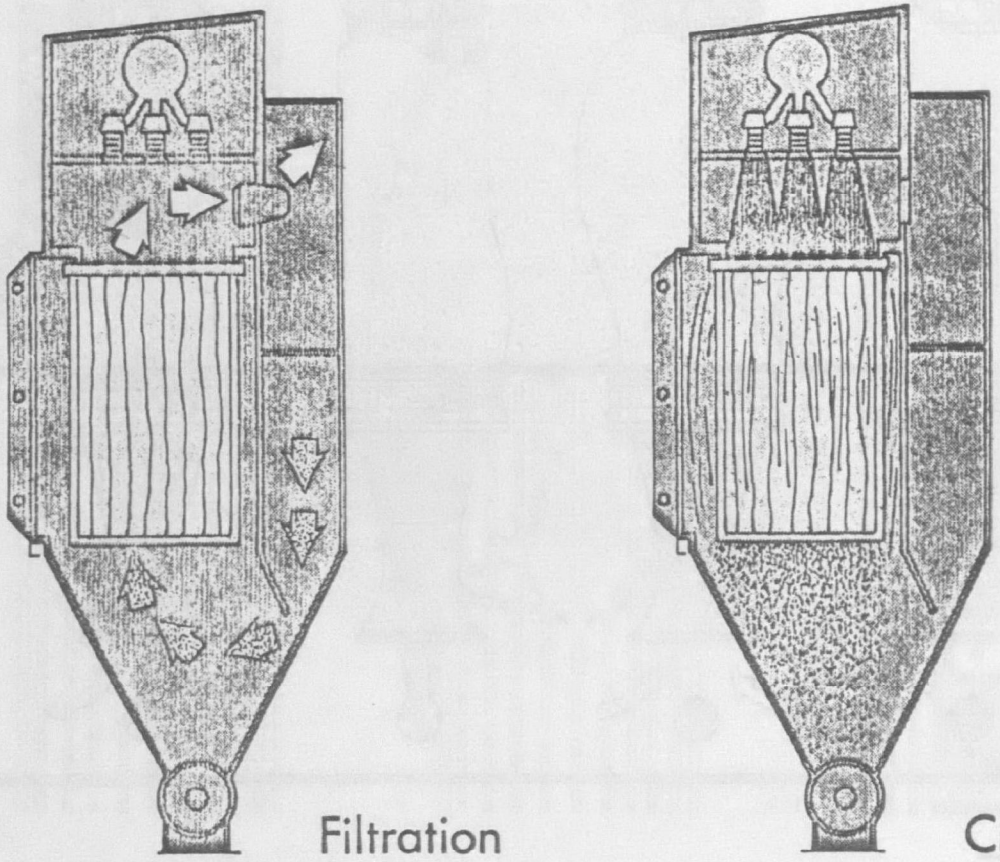

Filtration

Cleaning

Figure 2

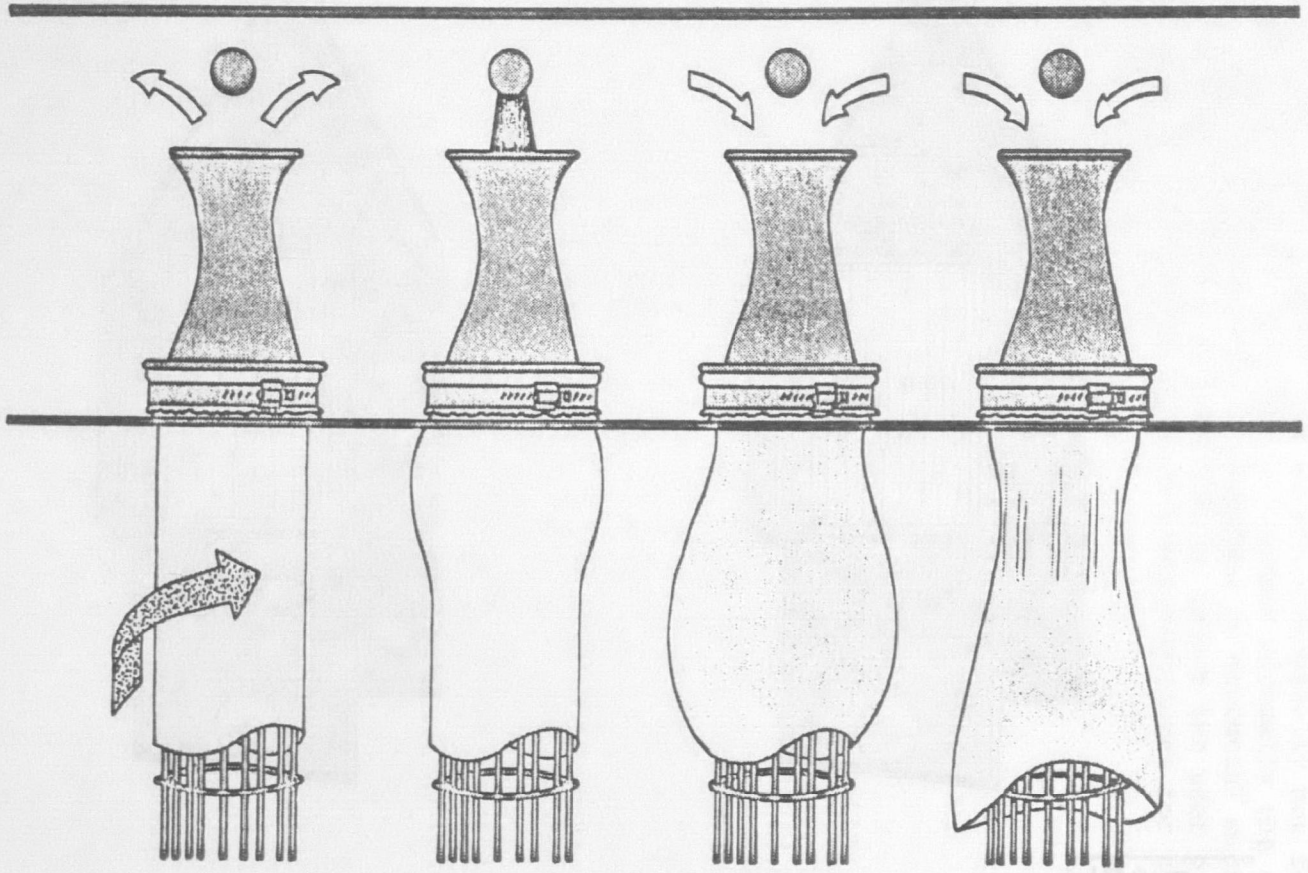

Figure 3

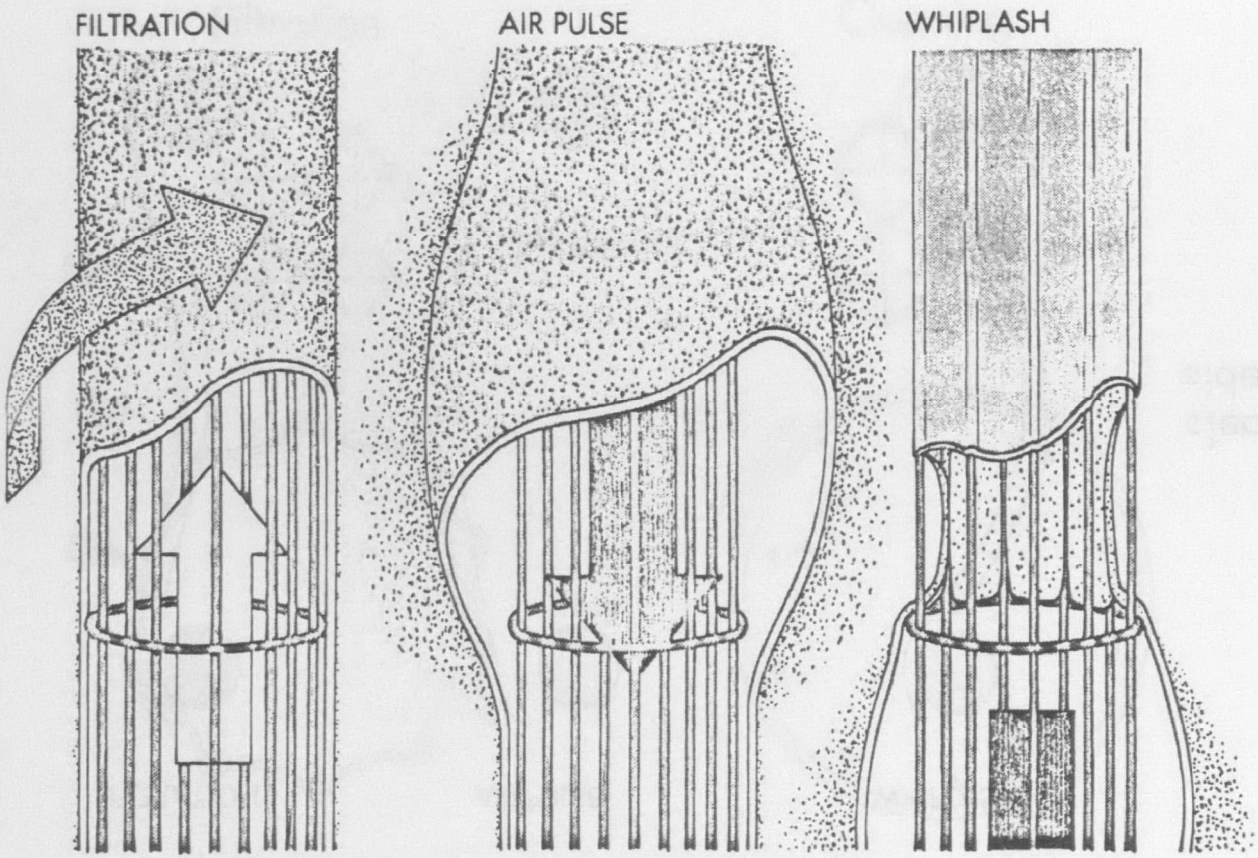

Figure 4

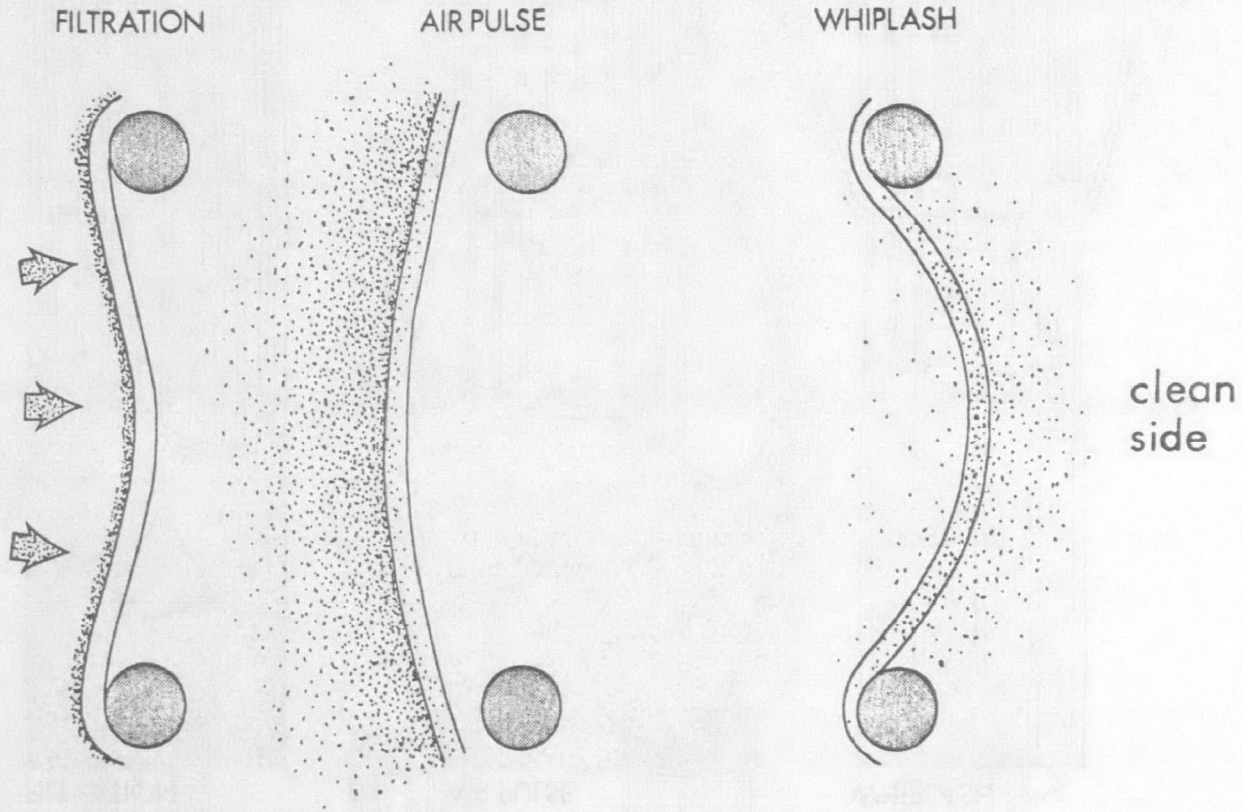

Figure 5

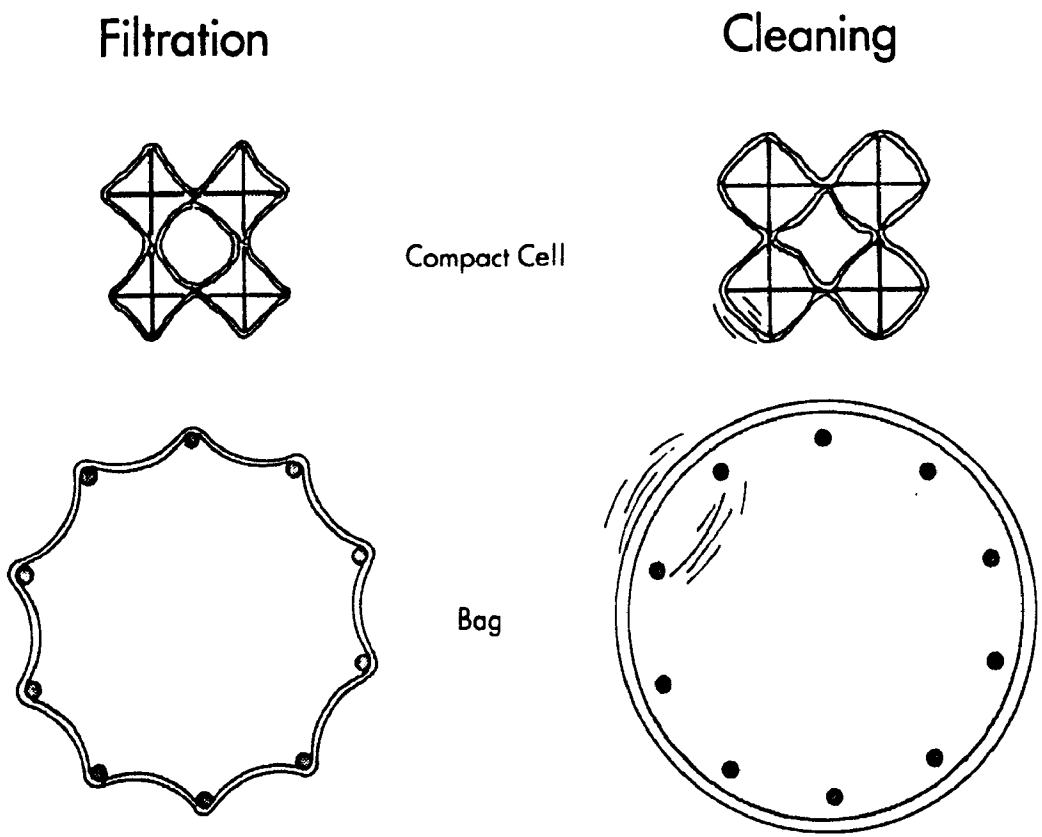

EPRI's FABRIC FILTER TEST MODULE PROGRAM:

A REVIEW AND PROGRESS REPORT

R.C. Carr
Electric Power Research Institute
Palo Alto, California 94301

John Ebrey
Lodge-Cottrell Operations/Dresser Industries, Inc.
Houston, Texas 77005

ABSTRACT

The use of fabric filters (baghouses) for control of particulate emissions from pulverized-coal fired utility boilers is a young but rapidly evolving technology. To insure that the electric utility industry has accurate design and operational information available, the Electric Power Research Institute (EPRI) has initiated a major fabric filter pilot plant research program. The program consists of the design, fabrication, installation and testing of a 850 m3/min four compartment fabric filter pilot plant at the EPRI Advanced Particulate Control Test Facility in Denver, Colorado. The pilot plant design reflects the range of commercially available technology offered by the major equipment vendors. An extensive series of tests will be performed to quantify and optimize the effects of air-to-cloth ratio, cleaning techniques, fabric type, bag geometry and gas flow distribution on operating pressure drop, reliability, stack opacity and total/fine particulate control. This paper provides a progress report on the project including objectives, schedule, fabric filter hardware specifics and proposed test plan.

INTRODUCTION

A key environmental problem facing the electric utility industry is the increased emphasis by regulatory agencies on application of high efficiency particulate control devices to pulverized-coal fired boilers. This increased emphasis is manifested by the revised New Source Performance Standard of 12.89 grams/10^9 Joules (0.03 lb./10^6 BTU) recently promulgated by EPA. In addition, considerable attention is being focused on control of fine particulates (less than 2 micron diameter), trace element emissions and plume opacity.

In response to these constraints the utility industry, through the Electric Power Research Institute (EPRI), is conducting a major research program to improve existing technologies and develop cost effective alternatives which promise high efficiency particulate control. One such research effort defining the optimum design and operating parameters of fabric filters (baghouses) is described in this paper.

Although baghouses have been in commercial use for many years, their application to the electric utility industry is a relatively new technology. For example, the first units to come on line were the Sunbury and Nucla station baghouses in 1973 and 1974, respectively. The Sunbury station, owned and operated by Pennsylvania Power and Light Company, consists of four baghouses installed on four nominally 44 Mw p-c boilers firing an anthracite/petroleum coke/bituminous coal mix. The Nucla station, owned and operated by Colorado - Ute Electrical Association, consists of three baghouses installed on three 13 Mw spreader-stoker boilers firing a submituminous coal. Although both installations have reported very successful baghouse operation, [Ensor Et. Al. (1976)[1] Wagner, (1978)[2]] they are not considered typical of utility boilers due to their small size, firing method and/or type of coal fired. More recently, baghouses have been applied to larger more typical pulverized - coal fired utility boilers ranging in size from 25-550 Mw. Preliminary results reported [Beaton (1978)[3], Faulkner, Ladd (1978)[4]] for many of these installations have been mixed, i.e. some units are experiencing excessively high pressure drops (up to 250 mm) whereas other exhibit more acceptable pressure drop characteristics (50 - 100 mm).

The specific reasons behind the anomalous baghouse performance observed to date are unclear, although there are several possible explanations which immediately come to mind: much of the initial experience was gained on atypical units which may not be applicable to more conventional utility boilers; several vendors have entered the market offering baghouses with wide ranges in hardware design and recommended operating philosophies; an inability to measure or control critical parameters; underestimation of the importance of gas flow distribution; laboratory performance data obtained with resuspended flyash which may have led to erroneous scale-up conclusions due to subtle changes in particle size distribution and subsequent filter cake dynamics; and a lack of comprehensive pilot scale research on utility boiler flue gas streams.

Consideration of the current situation leads to the conclusion that there is an urgent need to provide the electric utility industry reliable design and operating baghouse specifications. Accordingly, EPRI has initiated a baghouse

pilot plant program which is governed by the following constraints: pilot plant of sufficient scale to properly simulate a full scale baghouse; the use of fly ash and flue gas from a pulverized-coal fired utility boiler; hardware which permits a complete and systematic evaluation of all the major design and operating parameters without restriction to a particular manufacturer's design; and well controlled and characterized operating conditions. Following this line of reasoning, EPRI has contracted with Lodge-Cottrell/Dresser Industries, Inc. to design fabricate and assist in testing a 850 m^3/min., four compartment baghouse pilot plant which is currently being installed at the EPRI Advanced Emissions Control Test Facility. The pilot plant will form the basis for an extensive series of tests with the ultimate objective to define the optimum design and operating criteria as well as identify cost effective improvements for fabric filters applied to pulverized - coal fired utility boilers.

SPECIFIC OBJECTIVES

The electric utility industry have currently installed or committed to over 5000 Mw of baghouses on pulverized - coal fired utility boilers. Based upon the range of design and operating criteria evident in the baghouses purchased to date (e.g. air-to-cloth ratios from 0.5 - 1.0 m/min), it appears that choices are being made by utilities with less than complete information at their disposal. This situation is likely in many cases to lead to higher capital and operating costs than necessary without any assurance of satisfying regulatory constraints. Accordingly, it is the intent of this project to produce results which will remove the intuitive aspects from baghouse design and quantify the design and operational factors necessary for optimum performance. It is expected that this characterization program will enable the utility industry to prepare optimized baghouse specifications for both retrofit and new coal-fired boilers. Specific areas of interest are:

- Establish criteria for proper gas flow distribution in inlet/outlet manifolds, hoppers and cell plates.
- Define the most effective method of fabric cleaning.
- Establish the dependence of pressure drop and particulate penetration on air-to-cloth ratio, time between cleaning and inlet concentration.
- Determine the importance of bag aspect ratio ($^{L}/D$)
- Evaluate different levels of compartmentalization
- Examine the effect of filter cake particle size distribution on pressure drop and particulate penetration.
- Determine optimum start-up and shut down techniques.
- Identify improved fabrics or methods of cleaning which require less off-line cleaning time.

TEST FACILITY DESCRIPTION

The EPRI Advanced Emissions Control facility is a pilot plant test facility designed to evaluate advanced concepts in both particulate and gaseous emission control for pulverized-coal fired utility boilers. The facility is located on the 110MW unit 4 at the Arapahoe Station of Public Service Company of Colorado and consists of five flue gas slip streams ranging in size from 142-991 m^3/min. (1-10 MW) as shown in figure 1. The slip streams are directed to five pilot plants which are involved in a wide variety of testing. Unit 1 is a nominal 142 m^3/min. pilot plant electrostatic precipitator used primarily as a technology screening tool. Unit 2 is a nominal 991 m^3/min. precipitator which is used for prototype evaluation of promising design and operating improvements. Unit 3 is a nominal 283 m^3/min. pilot plant which is used to evaluate more novel concepts such as granular bed filtration and electrically augmented fabric filters. Unit 5, the unit of interest here, is a nominal 850 m^3/min. fabric filter pilot plant described in more detail below. Unit 6 is a 283 m^3/min. pilot plant designed to assess the impact of integrating the various emission control technologies currently available into a reliable, cost effective system.

UNIT 5 FABRIC FILTER PILOT PLANT

The design of the fabric filter pilot plant (FFPP) presented some interesting and formidable problems since it was decided at the outset that the most meaningful results would be obtained from a flexible research facility which also retained the representative character of current commercial utility baghouses. After evaluating several configurations, the general arrangement shown in figures 2, 3 and 4 was selected. This particular design consists of a four compartment, hopper inlet, inside bag collector similar to existing utility baghouses. However, there the similarity ends as described below:

General Specifications

To maximize the flexibility of the FFPP, each of the four compartments is capable of independent operation and control, which explains the intricate system of ducts shown in figures 2, 3 and 4. The ducting arrangement shown for each compartment includes a dirty gas inlet, compartment bypass, reverse gas cleaning, clean air preheat and clean outlet gas ducts, respectively. Refer to figure 2 showing the process flow control diagram.

An important feature of this arrangement is the bypass duct, which maintains constant volume flow conditions through the on line compartments when a fourth compartment is removed from service. Accordingly, the FFPP can be operated as one four compartment baghouses or four-one compartment baghouses depending upon the particular situation. Note that flow control and measurement of the inlet (dirty) gas is accomplished by calibrated venturi flow meters rather than orifice plates to minimize the potential for dust fouling and flow disturbances. Although requiring a more elaborate duct arrangement, the venturis were placed on the inlet rather than the outlet to permit flow control during compartment bypass situations, which by definition eliminates flow in the outlet duct. All flow control dampers depicted in figures 2, 3 and 4 are cast iron wafer type round dampers designed for a maximum leakage rate of below 1%.

Table 1 summarizes the major design specifications for FFPP. Note that sufficient lattitude is provided to evaluate the wide range in hardware design and operating philosophy currently available in commercial baghouses. Before proceeding further, a comment on the range in air-to-cloth ratio ($^{A}/_{C}$) reported in Table 1 is appropriate. With all full size bags (304 mm diameter x 10.4 m long) and compartments in service the maximum A/C ratio possible is 0.6 m/min with the existing booster fan. However, higher A/C ratios will be achieved by capping an appropriate number of bag thimbles in each compartment, thus driving the gas through the remaining elements at A/C ratios as high as 1.2 m/min. Similar levels of A/C ratio can also be achieved by operating with one or two compartments out of service. A combination of techniques will permit testing at even higher A/C ratios, if desired. In any event, the fan and cleaning system are sized to adequately handle operational excursions of this nature.

It should also be noted in table 1 that inlet particulate concentrations ranging from 0.5 - 16 grams/m^3 are possible. The wide range in inlet concentration is accomplished by use of either a multiclone or flyash re-injection system incorporated into the FFPP. (The particulate concentration for the Arapahoe Boiler averages roughly 2.3 - 4.6 gram/m^3). In addition, provisions have been made for the injection of water, SO_x compounds, and dry alkali reagents for possible future evaluation of dry SO_2 removal technology, operation of baghouses downstream of wet SO_2 scrubbers and/or high-sulfur coal baghouse applications.

TABLE 1

	Minimum	Maximum
Flow, m3/min	425	850
Temperature, °C	93	177
Dust Loading gram/m^3	0.5	16
Flue gas moisture, % vol.	7.6	15
Static Pressure at inlet, mm H_2O	-380	Ambient
Air-To-Cloth Ratio, m3/m2/min.	.3	1.2
No. compartments	-	4
Bags compartment	-	36
Bag Length, m.	6.7	10.4
Bag Diameter, mm.	150	304
Cleaning	Shaker, reverse air, or shaker/reverse air	

Filter Bag Types And Dimensions

Each module of the FFPP is approximately 3 meters square by 13.7 meters high and will contain 36 bags in a 6x6 array, each on square 355 mm centers for testing nominal 304 mm diameter bags. The entire bag support assembly is adjustable, thus permitting evaluation of 6.7, 7.9, 9.1 and 10.4 meter long bags. In addition, extra cell plates are available having appropriately sized thimbles to permit evaluation of 150 and 203 mm diameter bags. These additional cell plates retain the 355 mm center spacing. It is believed this combination of bag lengths and diameters will allow a quantitative determination of the effect of bag aspect ($^{L}/_{D}$) ratio on particulate penetration and pressure drop.

For ease of substitution, the dust hopper under each module is supported independent of the housing and fitted with an 0.5 meter high spool piece to the underside of the cell plate. To test different diameter bags, the spool piece will be unbolted, top and bottom, and slid out to one side. The existing cell plate may then be lowered, thus providing clearance above the thimble tops, and exchanged for a cell plate serving bags of the desired diameter.

The initial bags to be installed in the FFPP will be 10.4 meter long, 3x1 twill, silicone-graphite - teflon (Tri Coat) coated fiberglass bags manufactured by Globe Albany, Inc. Follow-on testing will include other combinations of bag size, coating and weights.

Bag Cleaning

Since effective bag cleaning is an essential ingredient to efficient baghouse operation, unusual flexibility has been incorporated into the FFPP to permit complete characterization of this important aspect of the technology. A variable reverse flow system is provided at rates ranging from 0.18 to 1.8 m/min. using filtered flue gas. Shut-off, modulating and by-pass dampers along with the associated ductwork are included to insure that the operating conditions in the three on-line compartments are not affected during cleaning (see figures 2, 3 and 4).

In addition, a novel shaking mechanism will be installed. This mechanism can be adjusted in finite increments to provide predominantly vertical or horizontal movements, the maximum for either movement being 476 mm with numerous intermediate combinations. As delivered, this mechanism will be adjusted to provide natural spring-loaded, dampened frequency oscillation of the bags after snap release. The frequency of activation can be varied from 2 to 40 cycles per minute during this mode of shaker cleaning, as required. To evaluate the more conventional method of shaking used in several of the currently operating utility baghouses, the shaker can be easily modified to reinforced oscillation with a frequency range of 10-200 cycles per minute.

Finally, combinations of reverse-air and shaker are possible, since the systems are fully independent.

Instrumentation And Controls

The prerequisite of operating four independent baghouse compartments has dictated the use of monitoring, control logic and supervisory equipment far exceeding ordinary commercial requirements, Combined with the necessity of obtaining data on numerous operating variables from multiple stations simultaneously, these aspects of the program were seen as a limiting constraint on both the accuracy and time required to collect data if the FFPP were operated and tested in a conventional manner. Fortunately, reliable micro-processor hardware and technology is now available which makes management of such complex situations both cost effective and efficient.

The micro-processor utilized has the capability of performing ladder logic, mathematical functions and proportional-integral-differential loop control. This system provides for 224 discrete inputs/outputs, 12 analog inputs and 16 analog outputs. If desired, this system may be expanded at the job site.

To examine, control and record the baghouse operating variables the following major instrumentation and control systems are provided:

Qty. (5) - Flow control systems consisting of

- Venturi metering tube
- Differential pressure transducers for input into micro-processor
- Thermocouple input into micro-processor

Qty. (4) - Cell Plate - differential pressure display

Qty. (1) - System differential pressure display

Qty. (6) - Temperature displays

Qty. (1) - Reverse air control system

Qty. (4) - Recorder channels for compartment gas volume

Qty. (1) - Recorder channels for reverse air gas flow

Qty. (50)- Mode selection switches for shake and reverse air cycles

Qty. (8) - Event recorder channels for shake and reverse air system in each compartment.

Qty. (4) - Manometers

Qty. (1) - Air pre-heater system

Qty. (1) - Graphics display panel

Qty. (4) - Variable speed shaker motor systems

TEST PROGRAM

The FFPP will be operated and characterization tests performed during an initial fifteen month test period. The major test variables include types of bags and fabrics, cleaning mechanism and duty cycle, gas volumetric flow rate (A/C ratio), inlet/outlet concentration and pressure drop as summarized in table 2. The test program will be working under the hypothesis that for a given fabric cleaning technique, an optimum combination of A/C ratio and cleaning cycle exists which yields a minimum pressure drop for the required level of outlet concentration. In addition, a second premise is that with proper characterization of the FFPP the results will be of direct application to full scale utility units constructed by different manufacturers and handling various types of flyash.

Although not yet finalized the FFPP test plan is currently divided into four basic sequences: 1) Air-Load testing; 2) Start-up and conditioning tests; 3) First year characterization tests; and 4) Long term testing of more advanced concepts.

This comprehensive test effort will remain flexible to respond to results as they become available.

1. Air Load Testing

Prior to start-up of the FFPP with flue gas, an air-load will be performed to insure that all systems are functional. This will include a verification that all fans, dampers, motors and controls operate properly; leak testing of each module; calibration of all transducers and instrumentation; and determination of clean bag weights. In addition, the pressure drop across each cell plate and the entire FFPP will be measured as a function of volumetric flow both with and without bags. And finally, the velocity profile across the bottom of the cell plate (bag inlets) and in the inlet duct work will be measured as a function of volumetric flow rate to verify proper flow distribution. It is appropriate to mention here that 1/4 scale laboratory gas flow distribution tests are being conducted at the Lodge-Cottrell Model Test Facility, to ensure that the capability is available to assess the impact of gas flow mal-distribution on baghouse performance.

2. Start Up And Conditioning Tests

One aspect of utility baghouse operation which is currently in a state of uncertainty is the optimum method of start-up, particularly with respect to the need and appropriate procedures for pre-coating of the bags. To address this issue, the FFPP start-up testing will include a bag pre-coat with resuspended flyash on at least two of the four compartments. The FFPP will then be operated with flue gas on a continuous basis to condition the bags. The inlet and outlet streams will be monitored continuously during this period for pressure drop, volumetric flow, and opacity. The cleaning technique to be used during start-up has yet to be selected, although a reasonable approach may be to use shaker/reverse air assist on two compartments and reverse air only on the remaining compartments. A major objective of this phase of the test is to determine the long range effects of the

start up procedure, i.e. will the differences in method of start-up be detectable when all compartments eventually stabilize, or will the effect of a lack of pre-coat at the outset persist in the form of high pressure drop well after start-up.

3. First Year Characterization Test

This series of tests will be directed toward quantifying the effects of cleaning cycle parameters, bag conditioning, bag aspect ratio ($^{L}/_{D}$), A/C ratio and inlet particulate concentration and size distribution on operating pressure drop and outlet concentration. As outlined earlier the primary objectives are to establish the following:

- The effectiveness of shaker, reverse air or shaker/reverse air combination cleaning.
- The optimum cleaning cycle for each method of cleaning (i.e. shaker frequency, shaker direction of motion, reverse air gas volume, times for dwell, null, overlap, rate of compartment re-pressurization, etc).
- Relationship between particulate penetration and the fundamental controlling parameter of bag ash loading (product of inlet concentration, face velocity (A/C) and time between cleaning).
- Relationship between pressure drop across the bags and bag ash loading.
- Significance of bag aspect ratio ($^{L}/_{D}$).
- Importance of inlet velocity distribution on pressure drop, particulate penetration, and cleaning effectiveness.
- Identify the most successful fabrics from the standpoint of minimum pressure drop and filter cake release.
- Effect of inlet concentration on pressure drop, bag cleaning and particulate penetration.

The importance of items 3 and 4 (above) cannot be over-emphasized. Although the relationship of particulate penetration and pressure drop has in the past been correlated with A/C ratio, recent work by [Drehsen and Ensor (1979)[6], Dennis and Surprenant (1978)[7]] has shown that the fundamental controlling parameter is bag ash loading. This parameter includes the effects of cleaning cycle time, inlet concentration and A/C ratio and more properly characterizes baghouse operation. Accordingly, it is believed that establishment of quantitative pressure drop and particulate penetration versus bag ash loading performance curves will provide the necessary information for utilities and manufacturers alike to utilize in specifications of baghouse design for optimum performance.

Long Term Testing

The specific nature of these tests will be dependent upon the results of previous testing of the FFPP as well as new developments in baghouse technology. However, some general items of interest include evaluation of new types of fabrics, dry SO_2 removal technology, evaluation of the role of electrostatics, and advanced bag cleaning concepts which require less off-line cleaning time.

Test Schedule

Air load testing is due to start in November 1979, with start-up and conditioning tests commencing during late 1979 early 1980. It is anticipated that characterization tests will be conducted in 1980. However the ultimate test time will be highly dependent upon results obtained. Schedules for the long term testing program will be developed at a later date. In order to expedite the transfer of information to the electric utilities intermediate reports will be issued as meaningful information becomes available.

MEASUREMENT METHODS AND PHILOSOPHY

Fabric filters have several unique operational characteristics which require special consideration when conducting emission testing. First, the very efficient collection capability places a heavy demand on the ability to measure gas streams with a 10,000 fold difference in particulate concentration. Outlet concentrations as low as 0.23 milligrams/cubic meter have been measured in the field, thus requiring long sampling times with high flow rate test equipment and very sensitive instrumentation. Also, complex data reduction schemes are required to compute particle size dependent penetration under these conditions.

A second unique aspect of fabric filtration is that the behavior is similar to a "batch process" because of the need to periodically remove compartments from service and clean the collected particulate matter from the fabric. Accordingly, the outlet emissions will vary significantly as compartments are removed from service and cleaned, which dictates the need for careful testing and characterization of the cleaning cycle.

A final important factor which must be considered is the long time constants associated with baghouse operation. The response of a baghouse to operational changes is not instantaneous and in some cases several days may be required to attain steady state. The parameters requiring the longest time to achieve steady state are those dependent upon the ash layer on the bags. For example, it is not uncommon for new bags to require several weeks of conditioning to reach a stabilized level of pressure drop and collection efficiency. Other process changes such as variable volumetric flow or cleaning cycles can also introduce significant time lags prior to achieving equilibrium.

The consequences of these generic characteristics of fabric filtration are that the FFPP operating conditions must be carefully controlled, monitored and characterized on a continuous basis. This will be accomplished by equipping the FFPP with real time continuous aerosol instrumentation, gaseous species monitors and pressure transducers to track the dynamic behavior of the FFPP. The specific instrumentation and methodology used will be similar to that reported for previous particulate control device testing supported by EPRI [Ensor et. al. (1976)[1], Drehsen and Ensor (1976)[6], Ensor, et. al. (1979)[8]].

The testing of the FFPP will include both routine day-to-day monitoring and intensive test periods to examine in detail specific operating conditions which require more extensive resources and concentrated effort. The routine monitoring will be performed between the intensive test periods to screen various operating conditions, determine when steady state conditions are achieved and evaluate the operating trends of the FFPP over long time periods. Measurements will include continuous recording of gaseous species and the important baghouse parameters of cell plate and flange-to-flange pressure drop, flue gas and reverse air volumetric flows, temperature, static pressure, fan motor currents, damper settings, and cleaning cycle sequences. In addition continuous inlet and outlet opacity instrumentation will be used to detect operating problems and provide a qualitative indication of aerosol penetration.

The intensive tests will focus primarily on the characterization test sequence described above. The measurements conducted will include inlet velocity distributions, particulate mass penetration, size dependent penetration from 0.01-20 micron particle diameter, SO_3, and size dependent trace element analysis. Where possible information will be data logged to provide a common time base which is useful in correlating parameters and detecting subleties in the data.

A summary of measurement techniques is provided in table 3.

SUMMARY

A 850 m^3/min four compartment fabric filter pilot plant (FFPP) is currently being installed at the EPRI Advanced Particulate Control Test Facility in Denver, Colorado. The FFPP will be the subject of an extensive test series with objectives to quantify the design and operational factors necessary for reliable and cost effective performance. Specific areas of interest include determination of gas flow distribution effects; most effective fabric cleaning techniques and cycle; relationship of pressure drop and particulate penetration on air-to-cloth ratio, time between cleaning and inlet concentration; appropriate start-up and shut-down techniques; effects of bag aspect ratio and fabric characteristics. It is expected that the program will produce results to enable the utility industry to prepare optimized baghouse specifications for both retrofit and new coal-fired boilers.

REFERENCES

1. Ensor, D.S., R.G. Hooper, and R.W. Scheck. Determination of the Fractional Efficiency, Opacity Characteristics, Engineering and Economic Aspects of a Fabric Filter Operating on a Utility Boiler. EPRI Report FP-297. November, 1976.

2. Wagner, N.H. Current Status of Bag Filters at Pennsylvania Power and Light Company. Third International Fabric Alternatives Forum Proceedings. September, 1978. pp. 3-1 to 3-32.

3. Beaton, R.J. Continuing Operation and Maintenance Experience of the Four Reverse Air Fabric Filters at the Kramer Station. Third International Fabric Alternatives Forum Proceedings. September, 1978. pp. 1-1 to 1-20.

4. Faulkner, G.R. and K.L. Ladd, Jr. Start-up, Operation and Performance Testing of Fabric Filter System at Harrington Station Unit Number 2. Septemper, 1978. pp. 2-1 to 2-15.

5. Green, G. Personnel Communications. Public Service Company of Colorado. Cameo Baghouse Start-up Performance. June, 1979.

6. Drehsen, M.E. and D.S. Ensor, Evaluation of the Kramer Baghouse - Phase II B. MRI Report to EPRI. February, 1979.

7. Dennis, R., and N.F. Surprenant. Particulate Control Highlights. Research on Fabric Filtration Technology. U.S. Environmental Protection Agency Report No. EPA - 600/8-78-005d. June, 1978.

8. Ensor, D.S., et al. Evaluation of the George Neal Electrostatic Precipitator. EPRI Project RP 780-1, Final Report. Publication date July, 1979.

Table 2

FFPP MAJOR TEST VARIABLES

Variable	Independent Controllable	Uncontrolled	Fixed by Design	Dependent
Type of baghouse			X	
Bags			X	
Area of bags	X			
Cleaning equipment			X	
Cleaning cycles	X			
Fabric			X	
Gas Volumetric flow rate	X			
Gas composition	X			
Gas temperature	X			
Concentration In	X			
Size distribution In		X		
Particle composition		X		
Opacity In	X			
Concentration Out				X
Size distribution out				X
Ash loading on bags				X
Pressure drop				X
Opacity Out				X
Collected Ash				X

Table 3
MEASUREMENT SUMMARY

PARAMETER		TECHNIQUE	COMMENTS
1. O_2	C	Electrochemical	Important to monitor boiler operation and dilution in duct
2. NO_x	C	Electrochemical	Important to monitor boiler operation and dilution in duct
3. SO_2	C	Electrochemical	Important to interpret resistivity measurements
4. CO. CO_2	C	Nondispersive infrared detector	Monitor boiler operation and dilution in duct
5. NO/NO_2	C	Chemiluminescence	
6. CO_2. O_2. CO	C	Orsat	Obtain average molecular weight of stack gas
7. H_2O		Impinger catch during Impactor Test	
8. Opacity	C	Plant Process Visiometer Light Scattering	Inlet of baghouse to monitor boiler operation
			Outlet of baghouse to monitor real-time variations in baghouse performance, i.e., cleaning cycles, approach to equilibrium, leaks, etc.
9. Total Particulate Mass and Trace Elements		Method 5 Train with volatile trace element absorbing solutions	
10. Velocity		S-Type Pitot Probe	Gas volumetric flow rate, flow distribution

Table 3 (Cont'd)

PARAMETER		TECHNIQUE	COMMENTS
11. Total Particulate Mass		Thimble	Resistivity Measurements in laboratory
12. In situ Resistivity		Point to plane probe	
13. SO_3		Goksoyr/Ross controlled condensation	Inlet, Outlet
14. Particle Size Distribution 0.5 to 20 um		Cascade impactor	In situ - Inlet-Outlet
15. Trace Element 0.5 to 20 um		Cascade Impactor with Kapton Substrates, Ion-Induced X-Ray Analysis, Neutron Activation Analysis	In situ - Inlet-Outlet
16. Particle Size Distribution 0.05 to 0.5 um	C	Electrical Aerosol Size Analyzer	Aerosol removed from duct and diluted in-stack (inlet) and out-of-stack at outlet
17. Particle Size Distribution and Trace Elements 0.05 to 20 um		Low Pressure Cascade Impactor Kapton Substrates, Ion-Induced X-Ray and Neutron Activation Analysis	Alternative size distribution and trace element technique. Inlet and outlet.
18. Compartment ΔP	C	Pressure Transducer	Real-Time continuous pressure drop monitoring

NOTES: C - Continuous analyzer recorded on strip charts and a magnetic tape logger.
Inlet/Outlet impactor measurements simultaneous

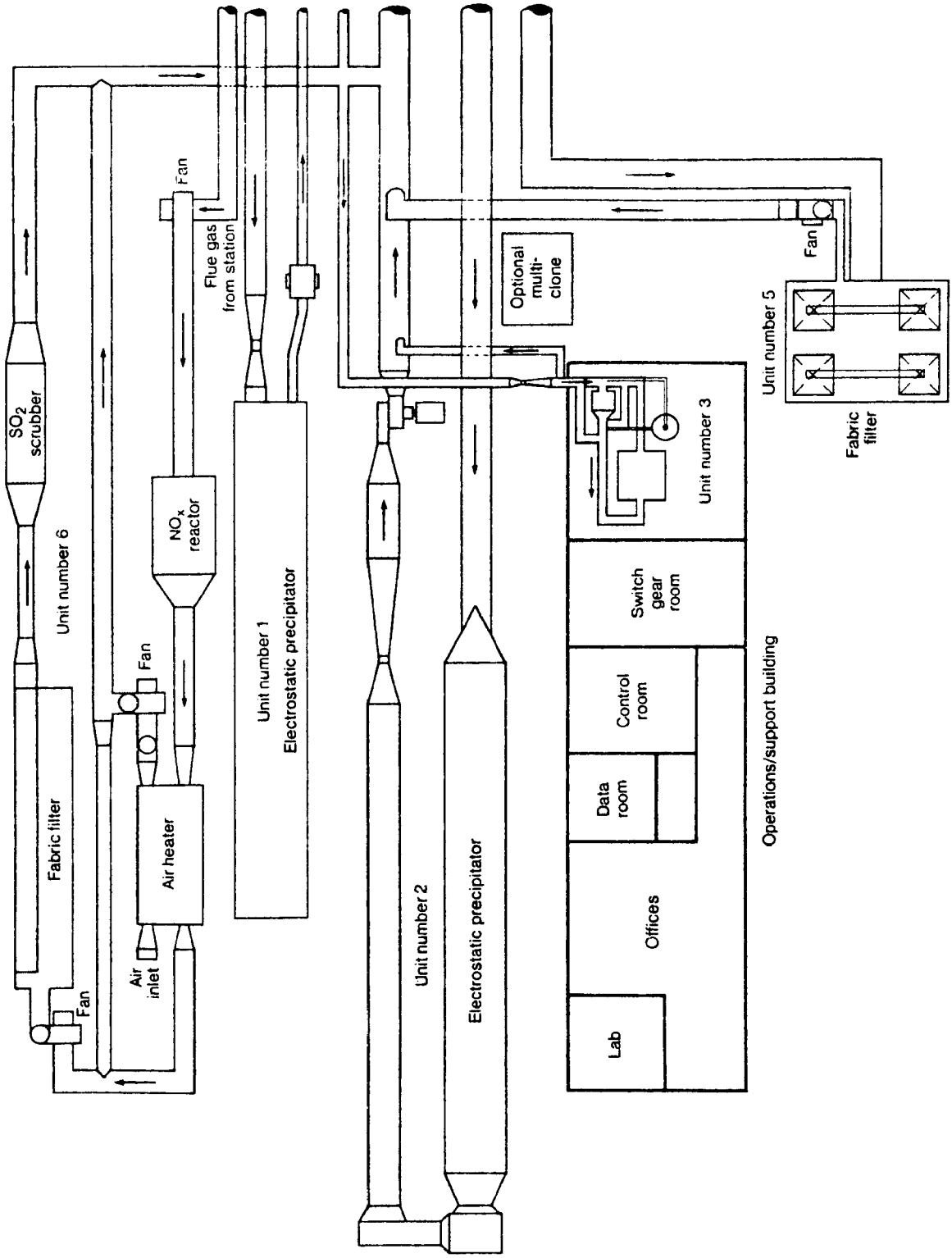

Figure 1

Plant layout - Arapahoe Unit 4.

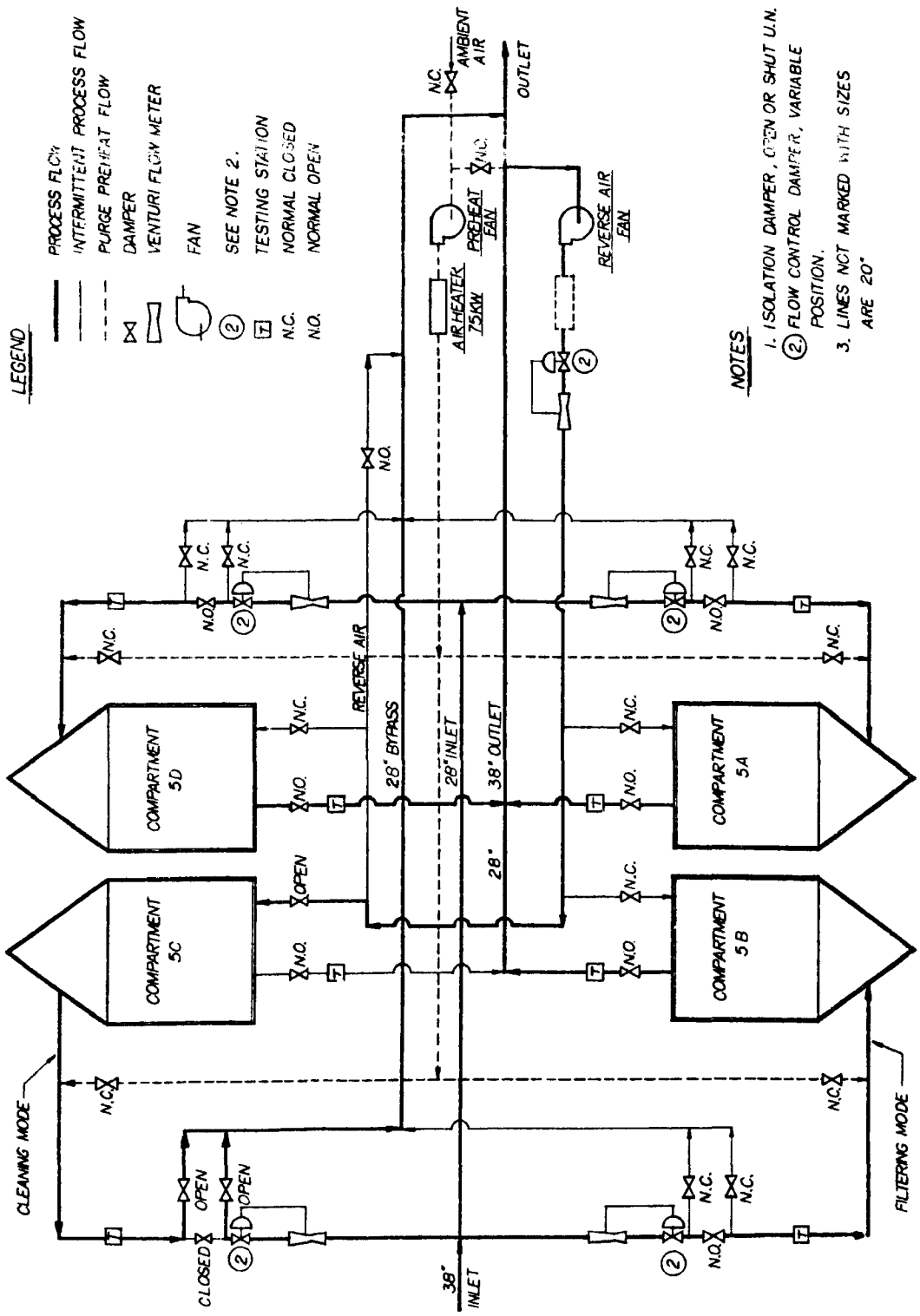

Figure 2

Flow diagram.

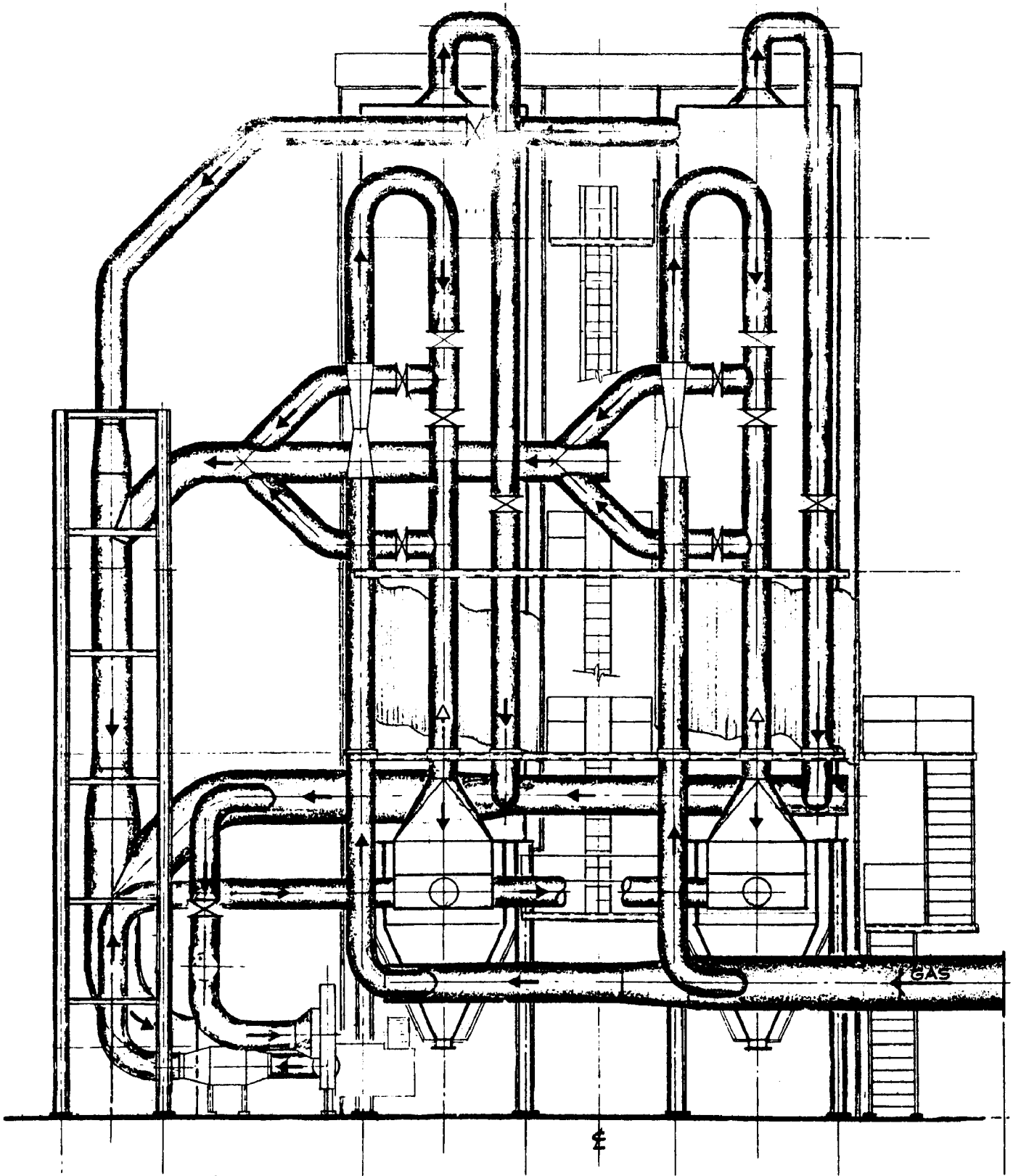

Figure 3

Elevation.

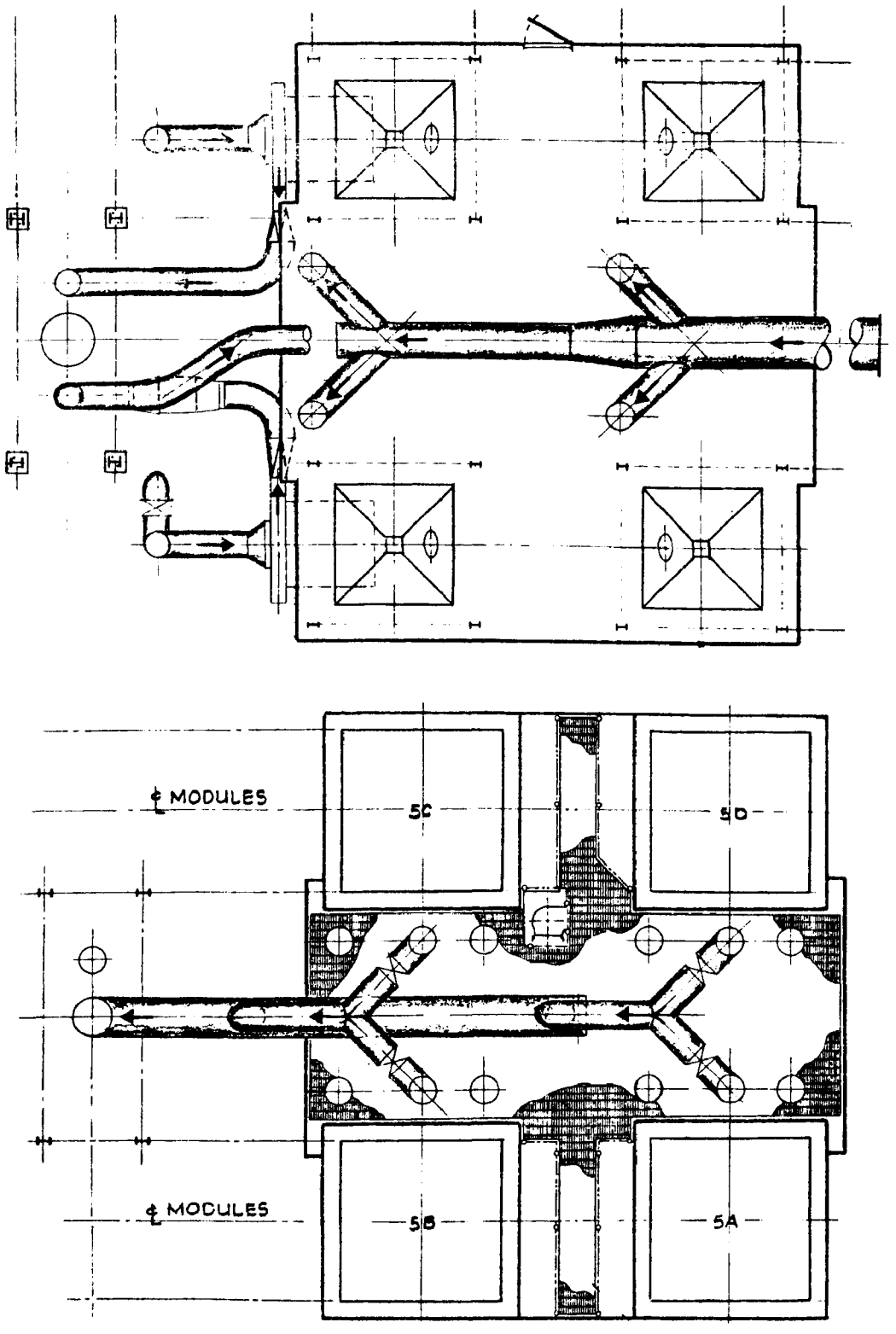

Figure 4

Plan view inlet and outlet.

ELECTROSTATIC ENHANCEMENT OF MOVING-BED GRANULAR FILTRATION

Dale S. Grace
John L. Guillory
Fernando M. Placer

Combustion Power Company, Inc.
Menlo Park, California

ABSTRACT

The electrostatic granular filter developed by Combustion Power Company combines a moving-bed filter with an electrostatic grid for high-efficiency collection of particulate. The coulomb charge occurring naturally on particulate from combustion or other processes in which tribocharging occurs is sufficient such that imposition of an electric field substantially enhances mechanical collection in the packed filter. A mathematical model is presented which accounts for the major parameters affecting electrostatic performance. Experimental data developed in an industrial unit retrofitted with electrostatic equipment and a pilot-scale filter demonstrates dramatic improvement in opacity and outlet loading; the industrial unit achieved 99% collection efficiency with less that 4 Iwd pressure drop. Data from the pilot-scale filter has shown that collection of micron-size particulate is especially enhanced with the electric field and has confirmed the 99%+ overall collection capability demonstrated in the industrial unit. The design of a 420,000 acfm system being installed at Weyerhaeuser Company's Longview, Washington plant is also discussed.

INTRODUCTION

Combustion Power Company's first commerical moving-bed granular filter, the Dry Scrubber™, was installed in 1974. Although granular filters have been used for industrial processes since the early 1900's, they were usually of the fixed bed type, requiring intermittent cleaning of the filter media and often disrupting the process. The Dry Scrubber was first conceived for use with CPC's process research on fluid bed combustors and later developed for industrial applications, in part as a response to new and more stringent regulations on particulate emissions. Indeed, interest in the

environment has become more intense in recent years, and the public has come to realize that further degradation in air quality is unacceptable. Industrial capacity continues to grow, albeit at a slower rate than the first half of the decade, and more efficient control of pollution is necessary. Since society bears the cost of pollution in any case—whether damage to public health in the community, workers' health in the plant, or damage to property and aesthetic values—a high degree of control is mandated. It is in this context that the moving-bed granular filter is used and finding many applications. The granular filter concept was designed with these objectives in mind: to meet specific particulate control performance while minimizing total annual cost. Design objectives include: moderately low pressure drop, high volume flow, low operating and maintenance costs, and dry operation. A filter utilizing both mechanical and electrostatic mechanisms, the Electroscrubber™, was developed as an extension of this concept.

DESCRIPTION

Figure 1 shows the general schematic of the Electroscrubber granular filter. The system consists of a cylindrical vessel containing two concentric, cylindrical louvered screens. The annulus between the screens is filled with 1/8 x 1/4 (pea sized) gravel media. Particulate-laden gas enters the filter and travels through the inner screen into the media at velocities ranging from 100-150 feet per minute. The particulate is removed from the gas stream by contact with the media. Clean gas exits through the outer screen and through the appropriate breeching to an exhaust stack. Note that the gas flow may be reversed for some applications.

The filter media moves continuously downward by gravity to prevent a filter cake from forming on the face of the filter and to prevent a high pressure drop. To provide complete cleaning of the louver face, the louvers are designed so that some of the media falls through each louver opening, thus preventing any bridging or buildup of particulate material. The particulate-laden media is continuously removed at the bottom of the granular filter where it is transported by a pneumatic conveying system to the air/particulate de-entrainment section of the system. Media recirculation rate is controlled through the use of an L-valve, shown in Figure 2. The injector air forces the media into the main lift air flow, transporting the media up the lift pipe. The lift air velocity is approximately 80 feet per second and the media velocity is less than 15 feet per second. The media and air then enter the de-entrainment vessel, shown in Figure 3. The ash or dust is removed from the media by the mechanical interaction of the media as it is being conveyed up the lift pipe and by the scrubbing action of the air as it lifts the media. The clean media then drains by gravity to the top of the filter unit for another cycle. The particulate is pneumatically conveyed to a particulate separator and storage silo.

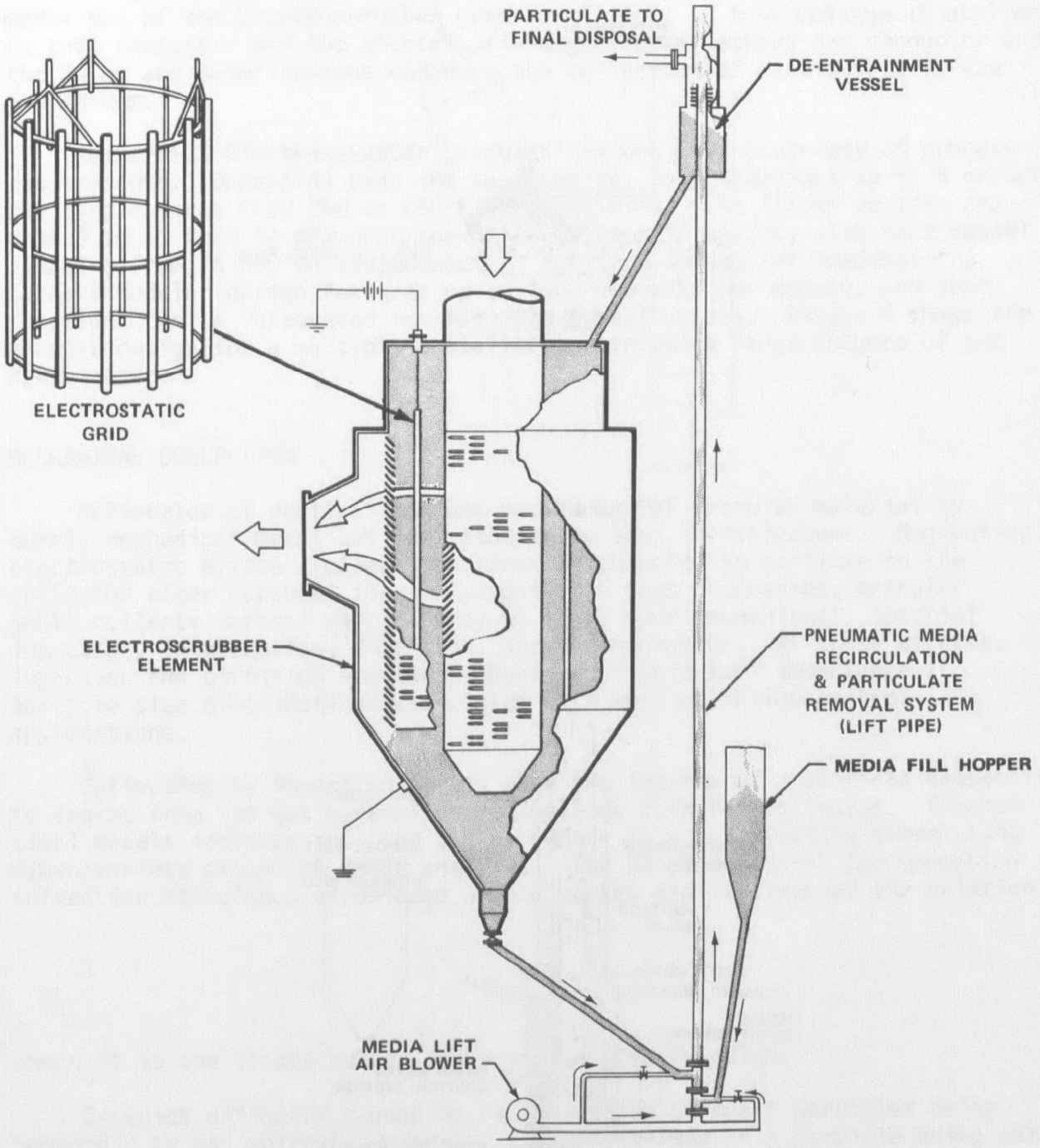

Figure 1 Electroscrubber Granular Filter Schematic

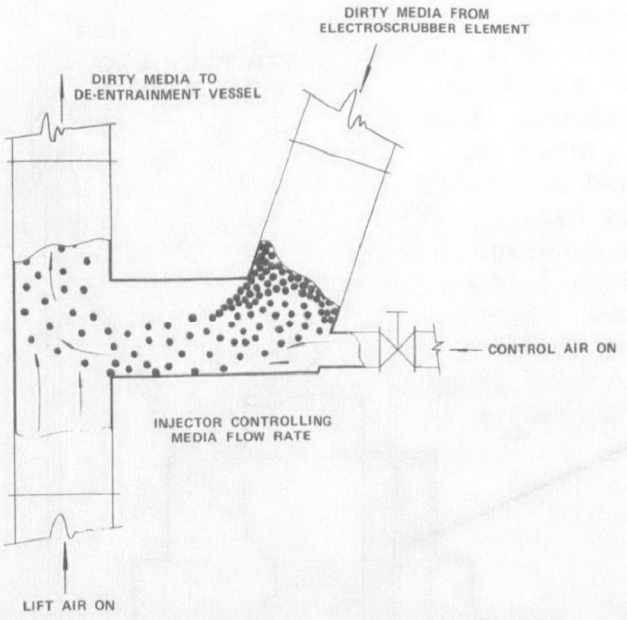

Figure 2 L-valve.

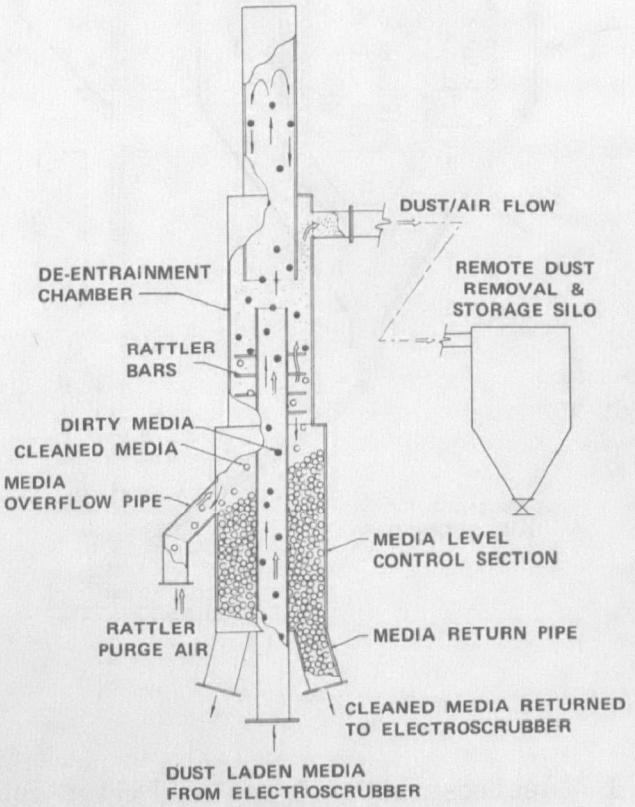

Figure 3 De-entrainment vessel.

The electrostatic grid, in the form of a cage, is positioned within the media bed of the Electroscrubber granular filter. A high voltage is applied to this conductor and the electric field generated between the conductor and the inner and outer screens enhances the collection of particulate in the gas stream.

Commercial Electroscrubber granular filters meet a variety of process requirements. Depending upon the application, inlet loadings up to 5 gr/acf and temperatures from 250 to 850 F are specified. The filter vessels are from 9 to 13 feet in diameter and 35 to 60 feet in height, with each vessel cleaning from 25,000 to 125,000 acfm. For very low outlet loadings the current modular design features up to four elements per module, and some functions can be integrated for multiple installations. Figure 4 shows the modular design for a multiple installation, in which large volumes of gas are cleaned.

MECHANICAL COLLECTION

Collection of particulate in a packed bed of granular material by purely mechanical means has been studied by many investigators. Neglecting electrostatic effects (other than those which hold the particle to the collector after capture) for the purposes of this discussion, granular media collects aerosol particles by at least four mechanisms: inertial impaction, interception, diffusion, and sedimentation. Of these effects, impaction and diffusion are the mechanisms of principal importance in particle size distributions associated with most pollution control applications.

Collection by impaction occurs when the inertia of a particle causes it to depart from the gas streamline and collide with the collector. Theoretical models indicate that the Stokes number is a satisfactory correlating dimensionless group for these analyses. The Paretsky model[1] for impaction collection efficiency associated with a packed bed is given by the relation:

$$\eta_{imp} = \frac{St}{\epsilon}$$

where St is the Stokes number and ϵ is the void fraction.

Brownian diffusion caused by random motion of small particles being bombarded by gas molecules enhances the possibility of a particle being collected. Even though the particle may be generally following a gas streamline, random motion occasionally allows the particle to approach a collector surface and causes it to contact that surface and be captured. Friedlander[2] recommends that collection efficiency for a single isolated collector by diffusion can be expressed as:

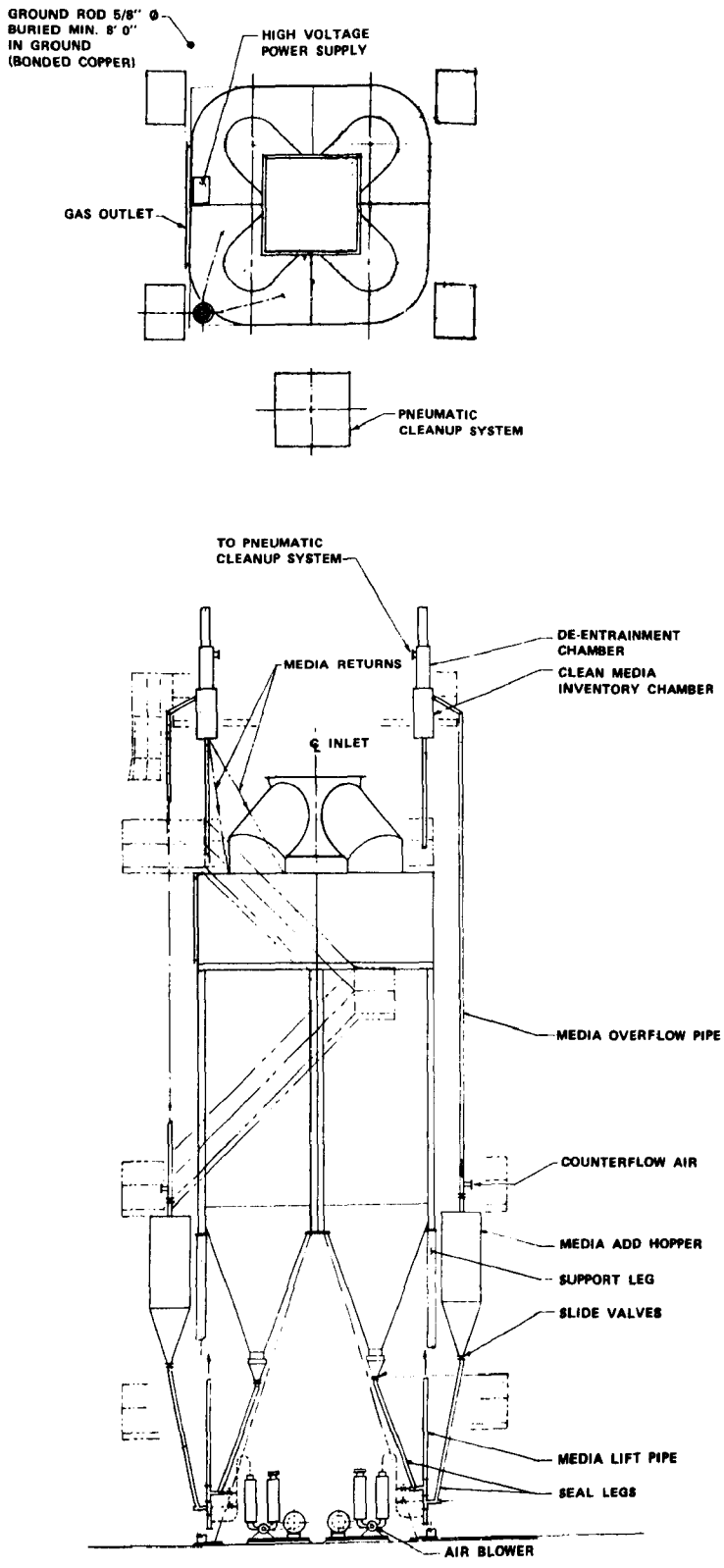

Figure 4 Electroscrubber Granular Filter Modular Design

$$\eta_{diff} = \frac{4.36 Pe^{-2/3}}{\epsilon}$$

where Pe, the Peclet number, is related to the ratio of bulk to diffusive mass transport and , like the Stokes number, is a simple function to dimensions and properties.

From the physical description of these phenomena, it can be seen that inertial impaction most effectively operates on larger particles (with a significant mass/area ratio) whereas diffusion is more effective on small particles whose trajectory can be influenced by molecular motion. The other effects, interception (a limiting case of impaction wherein a particle grazes the collector surface) and sedimentation (which describes the effect on gravitation on particle trajectory) are small and will not be discussed here. Reference 3 treats these phenomena more thoroughly.

Considering the various collection mechanisms to represent n "stages" (each of efficiency η_i) which operate successively on the original dust load, the overall collection efficiency $\bar{\eta}$ can be written as:

$$(1-\bar{\eta}) = \prod_{i=1}^{n} (1-\eta_i)$$

or, considering the two mechanisms discussed above,

$$(1-\bar{\eta}) = \left[1 - \left(\frac{St}{\epsilon}\right)^m\right]\left[1 - \frac{4.36}{\epsilon} Pe^{-2/3}\right]$$

where m is an empirically determined exponent which depends upon the Stokes number range.

ELECTROSTATIC COLLECTION

In addition to the mechanical collection mechanisms, the electrostatically enhanced granular filter utilizes an electric field in the media for particulate collection. In an electrostatic precipitator (ESP) a corona discharge is created between a high voltage wire and a ground electrode. The field used to generate the corona collects particulate which has been charged by the same corona. The Electroscrubber granular filter differs from the ESP in that there is no corona. Collection due to

electrostatic forces relies on the particulate charge which occurs naturally from upstream processes. Frictional charging (or tribocharging) will occur in flow through pipes and cyclones and in high mixing environments. Collection occurs when the direction of travel of charged particulate is charged by virtue of the electrostatic force, in opposition to the fluid flow field and viscous forces, and moves through the fluid toward a collection surface. Although the force is directed perpendicular to equipotential surfaces, the particulate undergoes many changes in direction through a packed media bed, and has many opportunities to come in contact with the media. The electrostatic collection in the granular filter is similar to an electrostatic precipitator with very narrow and winding walls and therefore increased effective surface area. Of course, the mechanical collection mechanisms of impaction and diffusion contribute significantly to the overall collection.

The electric field strength in the filter is a function primarily of applied voltage and geometry of the electrodes. Secondary effects include presence of the media and the gas as highly resistive dielectrics. Thus, within the well-defined overall field there are local changes in field strength and direction due to the media and, on a smaller scale, the particulate. Local gradients in field strength provide another small force on the particulate resulting in dielectrophoresis. The collection of particulate is therefore related to a number of factors. The actual collection is affected by one or more of the collection mechanisms: impaction, interception, diffusion, and electrostatic forces. The one or two mechanisms that dominate in an electrostatically enhanced granular filter will depend on the following physical parameters: particulate size, density, charge, collector size, and fluid velocity. In addition, re-entrainment, the rubbing off and recapture of particulate from the media, affects the net collection efficiency.

MATHEMATICAL MODEL

Some investigators have attempted to model the electrostatic effects on particulate[4,5]; however, there are few theoretical models describing the behavior of charged particles in a complex flow field. Besides solving for the fluid flow field, a detailed model must account for inertial effects and small variations in the electric field within the granular filter. The following simple model includes the major parameters affecting particulate collection, while assumptions are made regarding geometry and particulate loading.

It was shown previously that the total penetration is equal to the product of the penetrations due individual mechanisms. For a system in which both mechanical and electrical effects are important,

$$(1-\bar{\eta})_{tot} = (1-\eta)_{elec}\,(1-\eta)_{mech}$$

In order to include the electrostatic effect within the system of equations, an expression is needed for the collection efficiency as a function of particle charge, average electric field, etc. An approach similar to the Deutsch equation[6] first developed for standard ESP's is used: the force on a charged particle due to an electric field is equated with the viscous force when it reaches terminal velocity. Relating this migration velocity to the geometry of the collecting surface and flow field yields:

$$\eta_{elec} = 1 - \exp\left[\frac{\frac{-1}{3\pi\mu}\, q_p\, C\, A_c E}{Q_f\, d_p}\right]$$

E = Average Electric Field Strength

A_c = Collection Area

Q_f = Volumetric Gas Flow Rate

C = Cunningham Correction Factor

q_p = Particle Charge

d_p = Particle Diameter

μ = Gas Viscosity

Considering the geometry of a granular bed, A_c/Q_f is approximated as:

$$A_c/Q_f = \frac{6(1-\varepsilon)t}{d_g\, U}$$

U = Gas Superficial Velocity

ε = Void Fraction

t = Bed Thickness

d_g = Media Granule Diameter

Substituting,

$$\eta_{elec} = 1 - \exp\left[\frac{\frac{-2}{\pi\mu}(1-\varepsilon)t\, E\, q_p\, C}{U\, d_g\, d_p}\right]$$

From the above it is noted that increased efficiency can be obatined by increasing: electric field strength, particulate charge and filter thickness, or by decreasing: flow velocity and media granule diameter. An increase in temperature is seen to reduce efficiency through the increase in gas viscosity. According to the model, larger particles actually have increased efficiencies, as the particle charge is assumed proportional to the square of the diameter (surface area).[7]

Two factors of importance in utilizing the electrostatic concept are the particulate charge and the media resistivity. Tribocharging of the particulate to nominally 10% of saturation is more than sufficient to provide the desired electrostatic performance. Media resistivity is important because it affects the power required by the grid.

EXPERIMENTAL DATA

Substantial testing has been performed on full-size and pilot-scale moving-bed granular filters. Both gravimetric and impaction classifier data have been obtained for a veriety of operating conditions. The Snoqualmie Falls Electroscrubber, located at a Weyerhaeuser mill in Washington, is a Dry Scrubber retrofitted with an electrostatic grid. The Low-Outlet-Loading Electroscrubber is a pilot unit located at Combustion Power Company's Menlo Park facilities.

Snoqualmie Falls Installation

The Snoqualmie Falls installation brought on line in 1974 consists of a Dry Scrubber designed to handle 45,000 ACFM of gas flow from a hog-fuel fired boiler. This unit has an 18-in thick media bed and the cleaning/transport system consists of a feeder-screener and bucket elevator rather than a pneumatic lift system.

CPC undertook a development program with a full-scale installation that would demonstrate the dramatic increase on filtration performance due to electrostatic effects within the filter bed of a moving-bed granular filter. For this purpose the Dry Scrubber was upgraded and retrofitted with an electrostatic grid placed in the filter media. The electrostatic grid is energized by a high voltage power supply capable of delivering 60 ma at 25 KV DC. Figure 5 is a schematic of the installation after it was retrofitted.

After completion of the high voltage system installation, a test program was initiated with the objective of evaluating the concept of electrostatic cleanup on an operating industrial system, determining any functional problems and collecting data on the enhancement of the filter collection efficiency as a function of grid voltage.

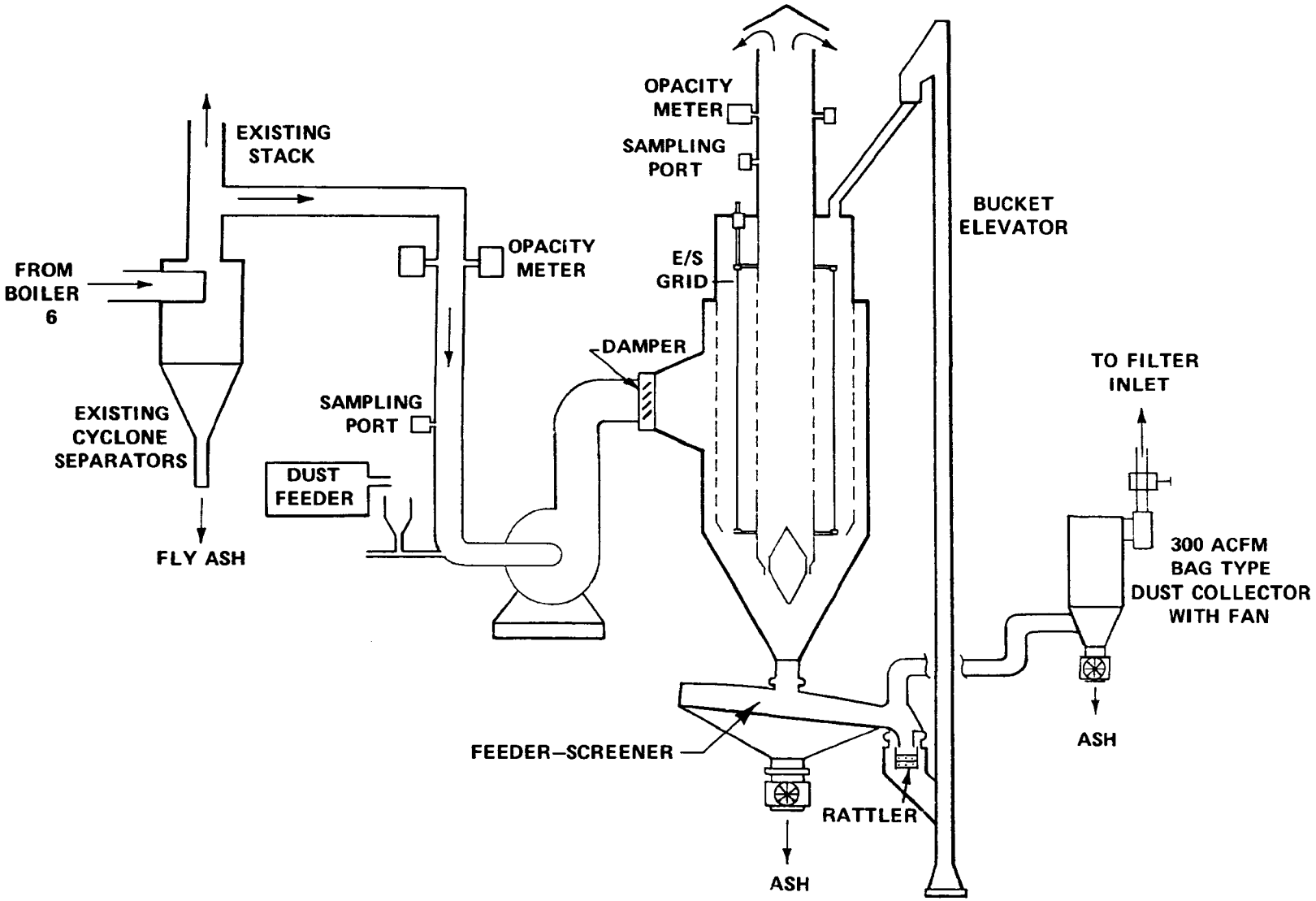

Figure 5 Snoqualmie Falls Electroscrubber Granular Filter

Table 1 is a summary of the test results. Inlet loadings range from .138 gr/sdcf to 1.128 gr/sdcf (12% CO_2). The high inlet loadings were obtained by dust injection to supplement the loading generated by the boiler. The outlet loadings ranged from .006 gr/sdcf with the electrostatic grid energized (20 KV) to .050 gr/sdcf with the electrostatic grid completely de-energized. Efficiencies of 99% are achievable.

Figures 6 and 7 show the effect of grid voltage on outlet loading and opacity. It is shown that mass outlet loading and outlet opacity can be reduced by a factor of 5 or more from baseline values by energizing the grid to 20 KV DC.

From the particle size distribution samples the fractional efficiencies were calculated. Figure 8 shows the fractional efficiency for the Snoqualmie Falls unit for different grid voltages. From these curves two basic conclusions can be drawn: electro-enhancement increases (65% to 95%) the collection efficiency for submicron particles, and electrostatics tends to flatten the fractional efficiency curve, i.e., makes particle collection efficiency less dependent on particle size.

Another way of representing the data that has been found useful is the plot of particulate penetration through the filter as a function of a dimensional grouping that characterizes the filter performance. Figure 9 is a plot of penetration versus $\Delta PL_i/M$, where ΔP is the pressure drop (Iwd), L_i is the particulate inlet loading (gr/acf) and M is the media circulation rate (lb/min). The best straight line curve fit was obtained from a least-squares analysis of the points. The substantial decrease in penetration is most apparent from this figure.

Low-Outlet-Loading Electroscrubber

Experimental data was also obtained from a pilot-scale unit, the Low-Outlet-Loading Electroscrubber granular filter (LOL), shown in Figure 10. This unit was designed with a media circulation system similar to the system on the elements being installed on Weyerhaeuser Company's boiler unit at Longview, Washington. The inner screen has an inside diameter of 17-1/2" and an active screen height of 10 feet thereby providing a flow area of 45.8 ft^2. The media bed thickness is 24 inches.

The media circulation and cleaning system is pneumatic and has a capability of lifting 300 lb/min of 1/4 x 1/8 filter media to 60 feet and returning the cleaned media to the test unit through two return pipes. The particle-laden air is separated from the media and passed through a small baghouse and exhausted to atmosphere. The principal air supply is a 50 Hp induced draft blower with manual inlet vanes control. Air flow capability is 7000 acfm @ 14 Iwd and 200 F. The air is heated before passing through the media bed by a packaged natural gas burner capable of increasing the inlet air temperature to approximately 300 F.

Table 1 SNOQUALMIE FALLS DATA

TEST NUMBER	GRID VOLTAGE (K Volts)	GRID CURRENT (ma)	FILTER D/S ΔP (IWd)	OUTLET GAS FLOW (acfm)	SINGLE PASS OPACITY (%)	COLLECTION EFFICIENCY (%)
1	0	0	2.8	24889	5-6	83.3
2	10	3	2.8	28890	2	89.6
3	10	13	3.0	26971	4	94.1
4	10	4	2.7	26467	2	89.1
5	15	9	3.0	25945	1	94.2
6	15	14	3.2	25009	1.2	94.2
7	15	6.5	3.3	26887	1	93.5
8	20	16-30	3.2	25910	1-5	95.2
9	20	14	3.0	24762	1-3	97.1
10	0	0	2.7	25105	12	80.8
11	10	6-9	2.8	25144	2.5	94.3
12	0	0	2.4	25685	5	73.6
13	20	(3-2)	5.4	37073	1-1.5	95.8
14	20	16-24	2.7	24156	1-1.5	95.8
15	20	7.5-13.5	2.3	25729	.5-1	95.8
16	20	14-16	2.8	23376	.5-1	96.8
17	20	20-29.5	2.5	24303	--	97.4
18	20	19-39	4.9	36736	1.5	93.5
19	20	36-53	3.3	26851	1.5	99.0
20	20	20-56	3.5	28439	1.7	98.6
21	10	14-16	6.4	47740	5-6	88.6
22	20	14-28	4.6	38552	1.5	96.1
23	0	0	2.1	23872	7	79.3
24	10	11.5-13.5	4.0	27656	8	98.0

Note: Efficiency calculated using front half loadings by EPA Method 5 at inlet and outlet of filter.

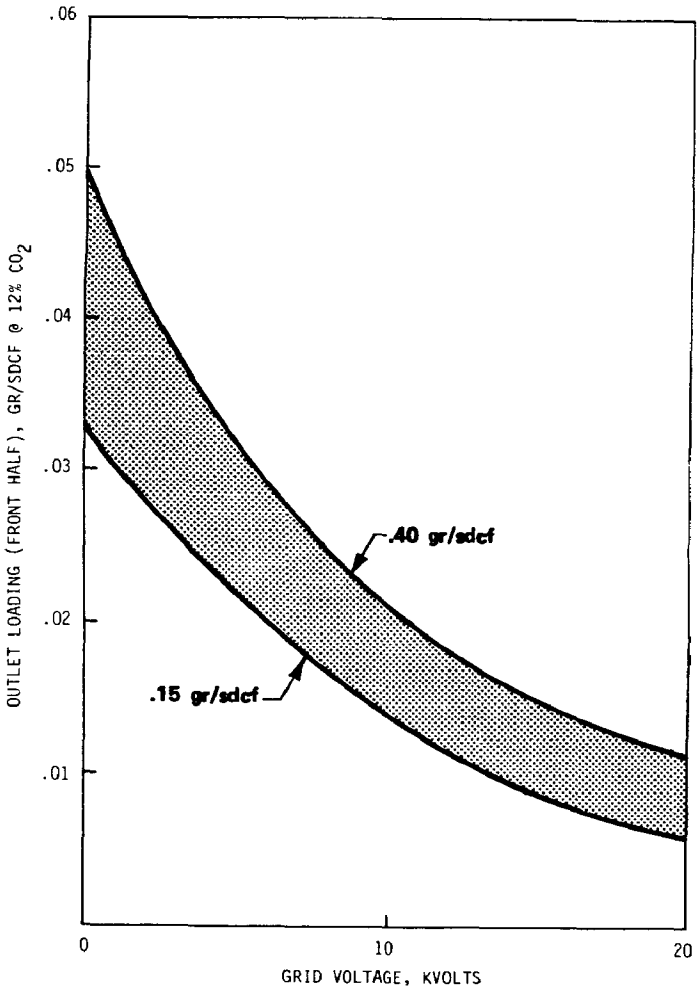

Figure 6 Snoqualmie Falls test results - outlet loading vs. grid voltage and inlet loading.

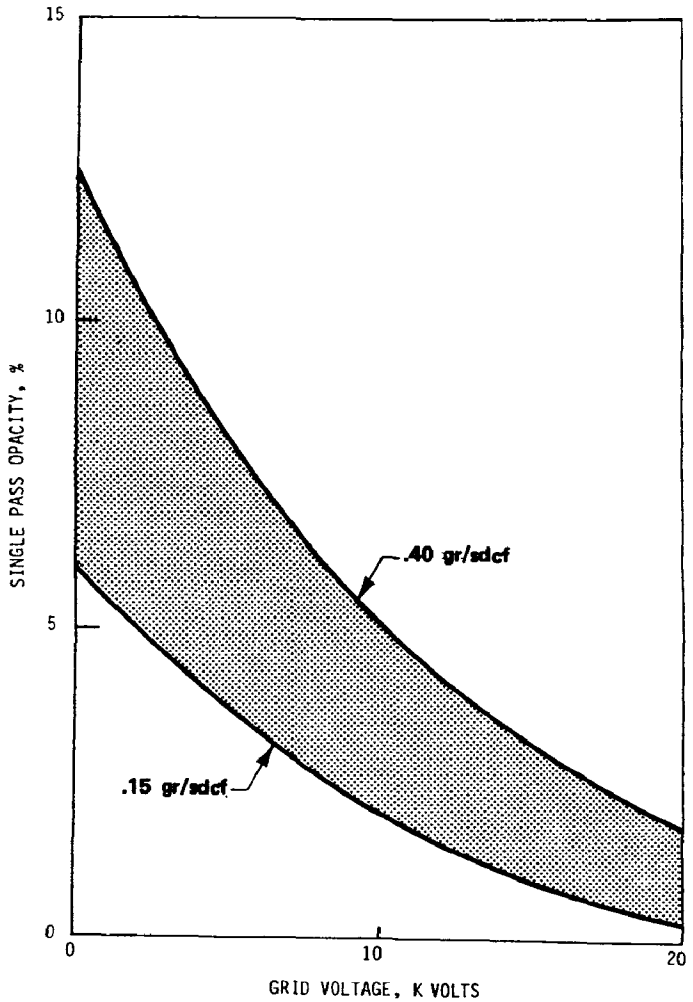

Figure 7 Snoqualmie Falls test results - single pass opacity vs. grid voltage and inlet loading.

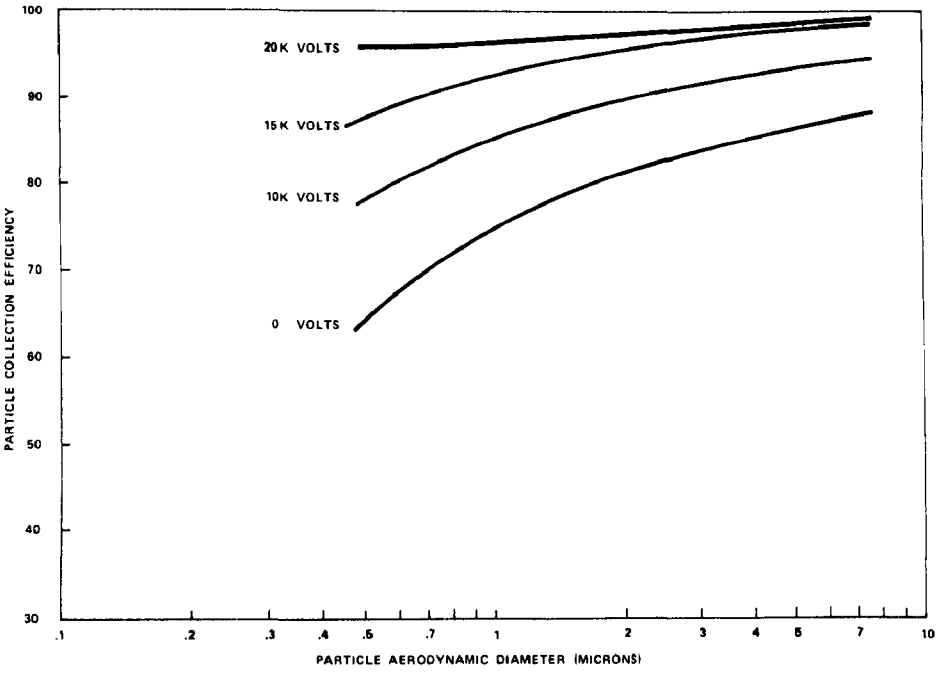

Figure 8 Fractional Efficiency, Snoqualmie Falls Electroscrubber Granular Filter

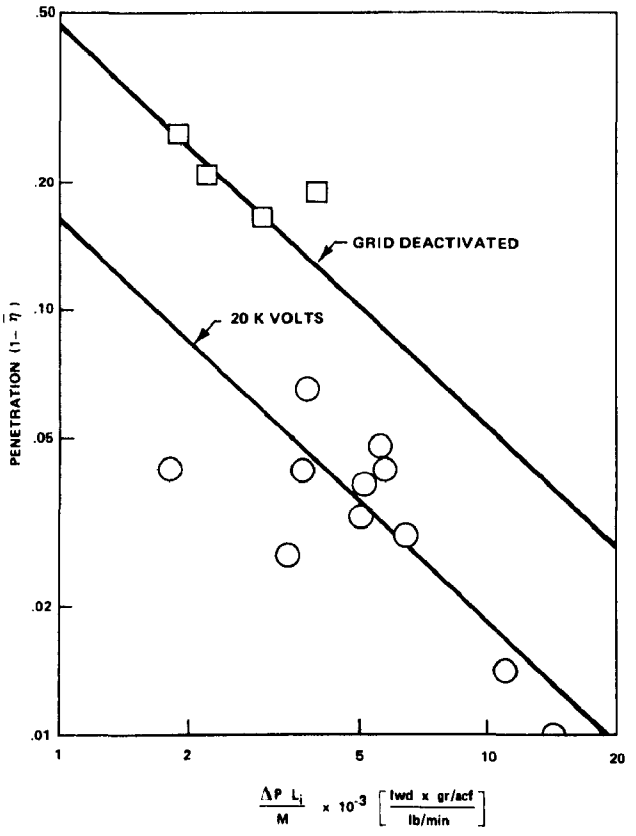

Figure 9 Penetration vs. Filter Parameter, Snoqualmie Falls Electroscrubber Granular Filter

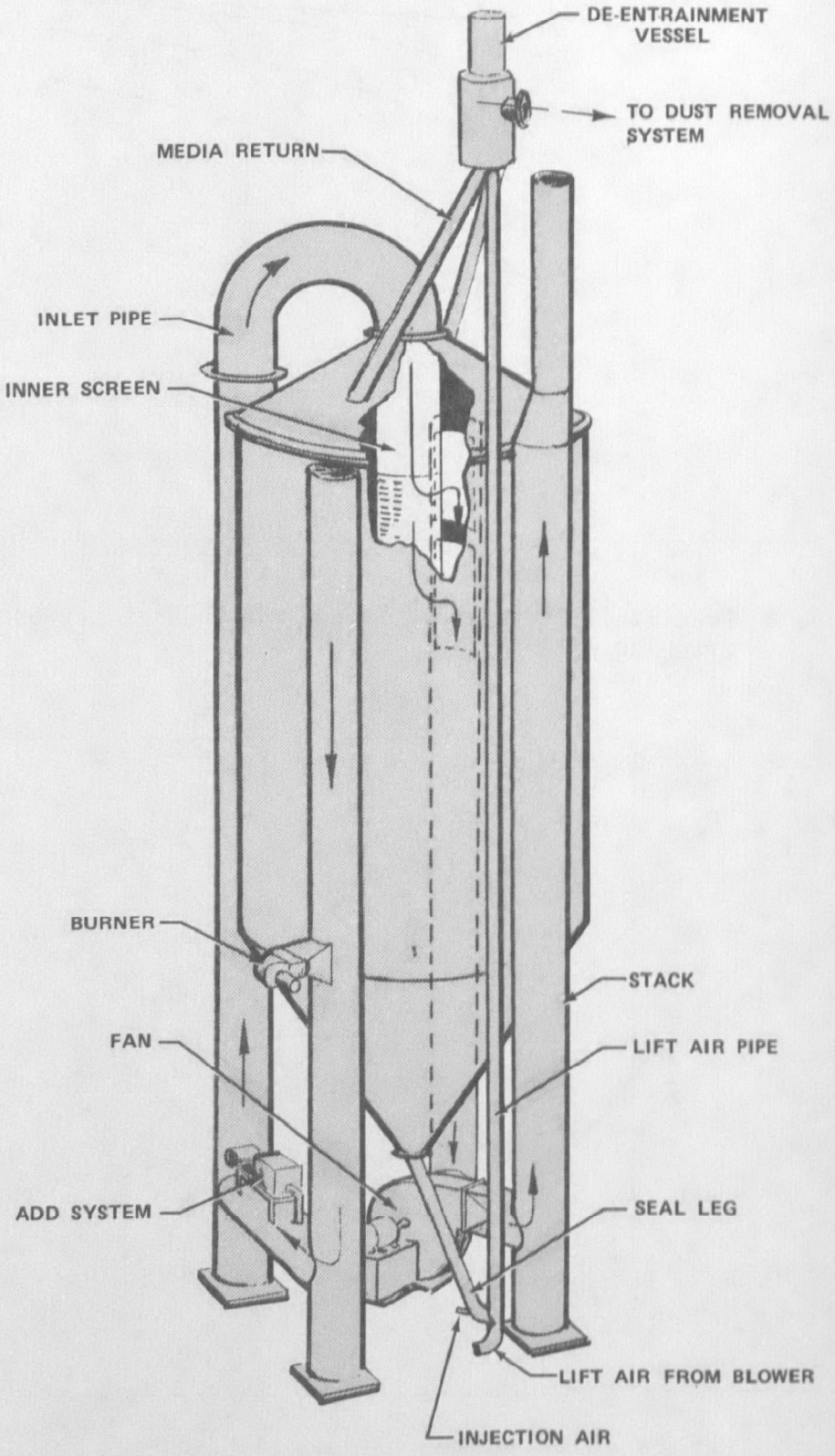

Figure 10 Low-outlet-loading Electroscrubber Granular Filter Test Facility

The dust injection system uses the vacuum generated by the induced draft blower to inject any type of dust into the system inlet. Dust is introduced by a screw feeder at a mass rate dependent on the physical properties of the dust being injected and the feed speed. An electrostatic grid consisting of a series of vertical pipes is installed in the media cavity. A 75 kilovolt high voltage power supply (15 ma max) supplies the potential for the gird. The system has been operated a total of over 800 hours in a series of functional and performance tests. Particular attention was given to tests of the pneumatic system to explore actual capabilities of the system for media lifting and cleaning.

Filtration performance of the system was evaluated by collecting simultaneous inlet and outlet total loading samples using standard EPA Method 5 procedures. The inlet and outlet particle size distributions were obtained by sampling with an Andersen 2000 Mark III impaction classifier. The baseline conditions with the grid voltage at 0 kv were obtained first, sampling simultaneously at the inlet and the outlet. The grid was then energized to 20 kv and an outlet sample taken without changing upstream conditions. This data indicates that, for those operating conditions, the outlet loading can be reduced over 90% by applying a voltage of 20 kv to the grid. Dramatic increase of collection efficiencies for particles smaller than 1 micron was noted. Increasing the voltage beyond 20 kv does not provide significant increase in efficiencies. The particulate used in these tests was collected by an existing Dry Scrubber installed on a hogged-fuel fired boiler. Further tests are planned using lime-kiln dust and coal-fired boiler ash. Also, further tests are planned for a thinner (12") media bed.

Figure 11 is a plot of penetration versus the dimensional parameter $\Delta PL_i/M$. The straight line is from a least-squares analysis. As found previously with the Snoqualmie Falls data, this grouping satisfactorily characterizes the filter operation performance. These curves again demonstrate the substantial decrease in penetration when using electrostatic enhancement.

LONGVIEW ELECTROSCRUBBER

Figure 12 is a photograph of the new Electroscrubber installation at Weyerhaeuser Company's Longview, Washington plant. Figure 13 is an isometric drawing showing some of the details of the installation. The electrostatically-enhanced granular filer system is configured as described earlier in Figures 1, 2, and 3. The unit is designed to handle up to 420,000 acfm of gas from a hog-fuel fired boiler at temperatures of 350 F and inlet particulate loadings up to .4 gr/sdcf corrected to 12% CO_2. The installation consists of 12 elements, each capable of handling 35,000 acfm arranged in 3 modules with each module having an exhaust stack. Each element has a separate media pneumatic lifting/cleaning system. Each module has a separate baghouse to which the particulate-laden air is pneumatically

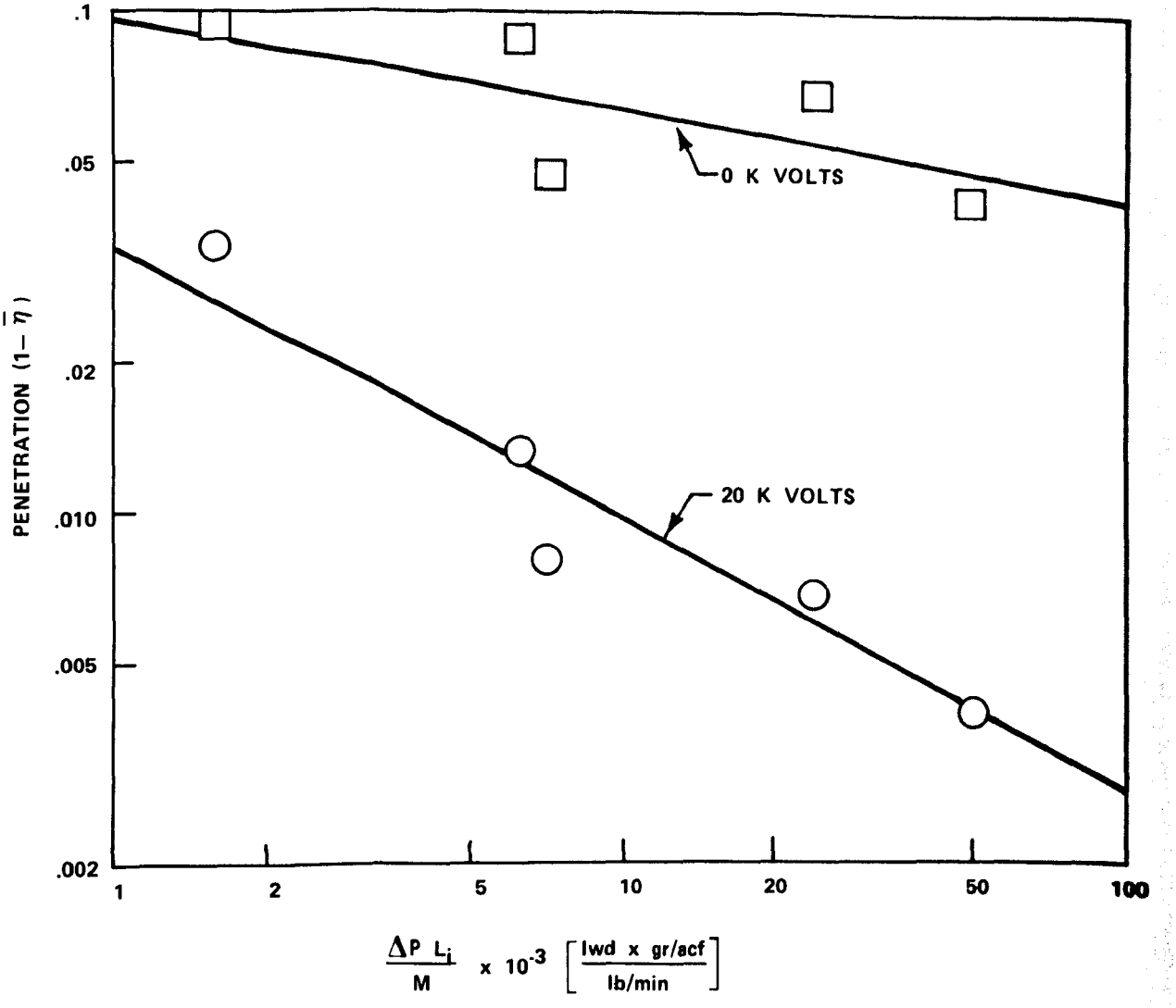

Figure 11 Penetration vs. Filter Parameter, Electroscrubber Granular Filter Test Facility

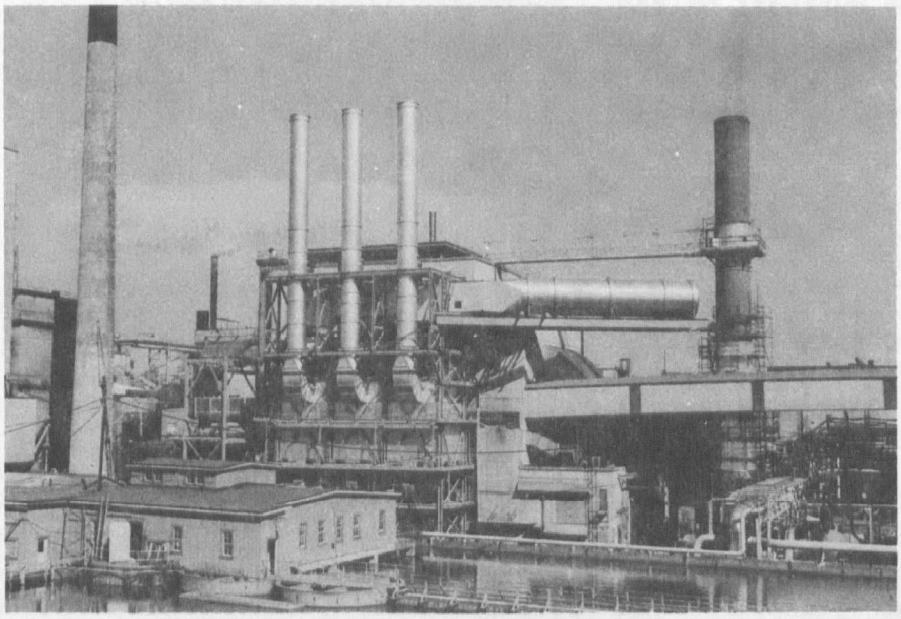

Figure 12 Longview Electroscrubber.

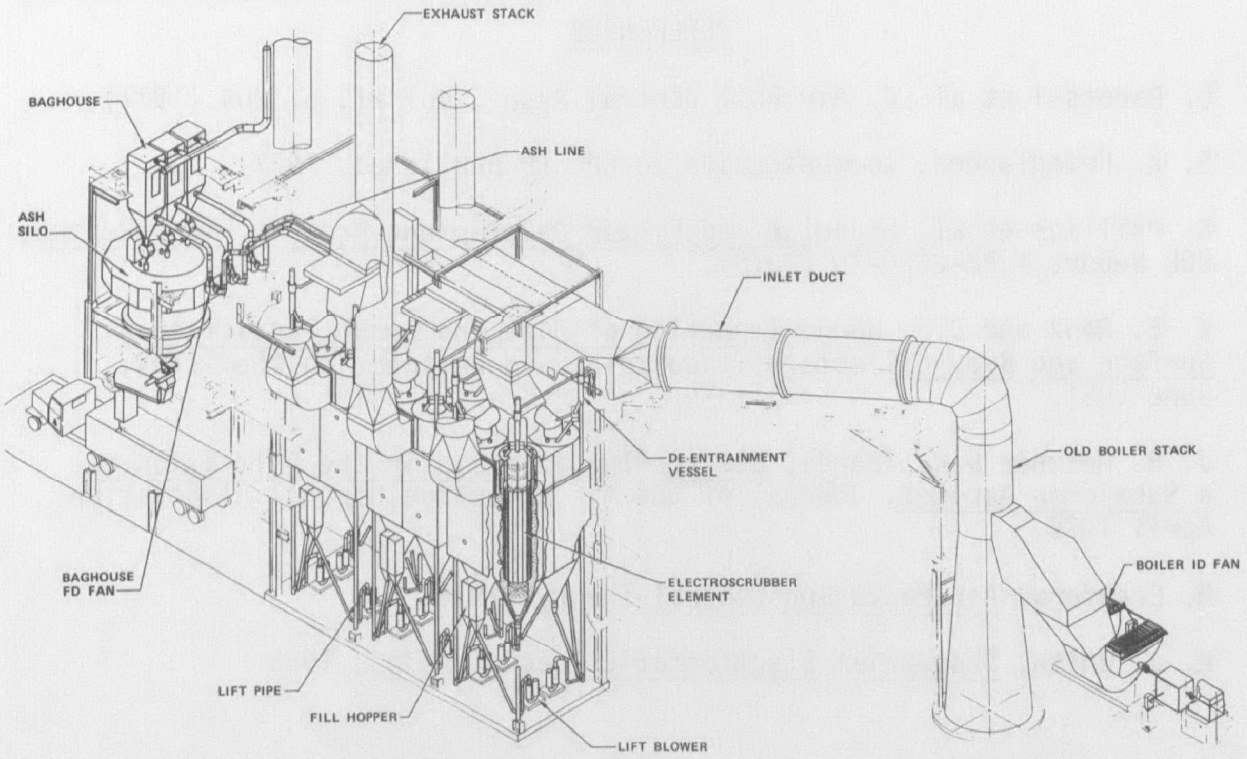

Figure 13 Longview Electroscrubber schematic.

conveyed. The exhausts of the 3 baghouses are manifolded to a single exhaust stack. Each element has its own electrostatic grid powered by a power supply capable of delivering 120 ma at 30 kv dc. The elements are filled with 1/4 x 1/8 gravel and the pneumatic circulation systems will circulate the filter media.

SUMMARY

The utilization of electrostatic forces in granular filters provide an additional mechanism for collection of particulate and is especially effective on micron-size particles. Data obtained from an industrial unit retrofitted with electrostatic equipment and a pilot-scale filter has demonstrated a considerable increase in collection efficiency using electrostatic enhancement. Besides the mechanisms of impaction and diffusion, the electrostatic mechanism provides an important means for improving filter performance at minimal additional capital and operating expense. Unlike electrostatic precipitators which depend on corona-charging of the particulate, the Electroscrubber granular filter uses the interaction of the tribocharged particles with the electric field and small-scale electric field effects to enhance contact of the particulate with the media. The use of electrostatically enhanced moving-bed granular filters offers a relatively new and effective means of meeting the particulate control objectives of the next decade.

REFERENCES

1. L. Paretski et al, J. Air Poll Control Assn., Vol 21, p. 204 (1971).

2. S. K. Friedlander, Communication to CPC (Unpublished, 1977).

3. K. Phillips et al, Granular Bed Filter Development Program Final Report, DOE Report # FE-2579-19 (1978).

4. W. E. Ranz and J.B. Wong, Impaction of Dust and Smoke Particles on Surface and Body Collectors, Industrial and Engineering Chemistry, June 1951.

5. J. R. Melcher & K. Zahedi, Electrofluidized Bed in the Filtration of a Submicron Aerosol, Journal of the Air Pollution Control Association, April 1976.

6. M. Crawford, Air Pollution Control Theory, 1976.

7. H. J. White, Industrial Electrostatic Precipitation, 1963.

ELECTRICAL AUGMENTATION OF GRANULAR BED FILTERS

S. A. Self, R. H. Cross and R. H. Eustis
High Temperature Gasdynamics Laboratory
Stanford University
Stanford, California 94305

A study of the enhancement of the collection efficiency of granular bed filters by electrical means is reported. By applying electric fields of a few kV/cm (dc or ac) across a bed of insulating granules, the efficiency for submicron charged aerosol is greatly increased, to the point where the efficiency minimum normally observed with such filters in the size range 0.1-1 μm is removed. The performance of such filters is explored as a function of granule size, applied field, face velocity and charge state of the entering aerosol with both a bench-scale flow system (to 40 ft^3/min) and a wind tunnel (to 600 ft^3/min). Some theoretical estimates are made to identify the most likely physical mechanism of electrical enhancement, and a number of potential application possibilities are discussed.

INTRODUCTION

A great variety of air filtration devices for particulate emission control have been explored and developed over the years, varying from purely mechanical devices such as cyclones, scrubbers and fabric, fiber and granular bed filters, to purely electrical ones exemplified by electrostatic precipitators. Because electrical forces can be so much stronger than mechanical ones, it appears that incidental electrical effects often play an unrecognized role in nominally mechanical devices. In recent years, various attempts have been made to capitalize on this fact, and enhance the collection efficiency of basic mechanical devices by deliberately incorporating electrical features. Examples include electrified scrubbers[1,2], electrified fiber[3] and fabric[4] filters, and electrified granular beds, both packed and fluidized[5-7]. An overview of electrostatic devices for control of submicron particles has been made by Melcher et al.[8].

In the present work, the enhancement of the collection efficiency of a packed granular bed filter by electrical means has been explored. The work has been primarily experimental, utilizing a bench scale flow apparatus operating at throughputs of up to 40 ft^3/min; some additional experiments were made in a tunnel facility at throughputs up to 600 ft^3/min. In addition some preliminary theoretical work has been undertaken concerning the nature of the electrical interaction.

To provide a background framework for interpreting this work, a summary is given in the next section of the present state of understanding of filtration by granular beds in the absence of electrical effects. More extensive reviews of this topic have been given by Spielman[9], by Tardos et al.[10] and by Schmidt et al.[11].

FILTRATION BY GRANULAR BEDS

Filtration is characterized by the simultaneous action of forces of fluid mechanical, inertial and gravitational origin, together with electrical forces acting between the particles and the collectors. These combined forces govern the particle trajectories, which determine whether particles intercept the collectors and are retained. A rational approach to understanding filtration in an electrified bed is to first consider the mechanisms operative in the absence of electrical effects, and then consider the modifications due to their inclusion.

The theory of filtration neglecting electrical effects is usually discussed in two steps. First, collection by an isolated filter element (sphere or cylinder) is considered. This subject is well established and is summarized below. Second, collection by fibrous or granular bed filters is developed from the theory for isolated collectors, but modified to give the efficiency per representative element taking account of the flow modifications produced by the surrounding elements. This approach, outlined below, is less firmly established, and is better justified for tenuous media (fibrous or fluidized bed filters) than for dense media such as fabric filters or packed granular beds.

Aerodynamic Capture by an Isolated Sphere

This is based on the solution for flow past a sphere, which is well documented for the cases of viscous creeping (Stokes) flow (Re << 1) and potential flow (Re >> 1). Solutions for intermediate values of Reynolds numbers are listed by Tardos et al.[10].

As discussed in the classic text by Fuchs[12] and the more recent one by Friedlander[13], the collection efficiency is then calculated as the sum of four physical processes, namely, interception, impaction, diffusion and gravitational settling, though the latter is often neglected. These processes determine whether a particle reaches the collector surface; however, whether it is permanently captured depends on the balance of attaching forces (van der Waals, capillary, electrical, etc.) against the fluid mechanical forces tending to re-entrain it. The overall collection efficiency then depends on the net effects of collection and re-entrainment.

The cross section for <u>interception</u> is taken as the area normal to the incoming flow, extending from the axial streamline out to the radius of the limiting streamline which passes within one particle radius of the collecting sphere's surface. The collection efficiency is then taken as this area divided by the projected area of the sphere. For potential flow, Fuchs[12] and Ranz and Wong[14] suggest the following efficiency formula, with coefficients β of 2 and 3/2, respectively:

$$\eta_{int}(p) = \beta (a_p/a_c) \tag{1}$$

where a_p and a_c are the particle and collector radii, respectively. For viscous flow, Fuchs[12] amd Paretsky[15] suggest the formula

$$\eta_{int}(v) = \frac{3}{2} (a_p/a_c)^2 \ . \tag{2}$$

Since (a_p/a_c) is << 1, eq. (2) yields very much lower efficiencies than eq. (1). In either case η_{int} is independent of velocity, viscosity and particle density.

<u>Impaction</u> relates to the departure of the particle trajectories from the fluid streamlines due to inertia. For a given flow field the trajectories can be computed and the cross-section for impaction is then the area normal to the upstream flow extending from the axis out to the limiting trajectory which just intercepts the sphere surface. As for interception, the efficiency is then the ratio of this area to the sphere's projected area. According to theory, for a given Reynolds number, the efficiency should be a function only of the Stokes parameter

$$Stk = \frac{2\rho_p a_p^2 u}{9\mu a_c} \tag{3}$$

where ρ_p is the particle density, u is the free stream velocity and μ is the gas viscosity. For example, for air at STP, $\mu \sim 1.8 \times 10^{-5}$ Kg/m·s, and for the typical value $\rho_p = 2 \times 10^3$ Kg/m^3, $a_p = 10$ μm, $a_c = 1$ mm and $u = 1$ m/s, $Stk \approx 2.5$.

For both potential flow and viscous flow, calculations show that the efficiency for impaction η_{imp} is zero below some critical Stokes parameter Stk_{cr}, increases rapidly through values of Stk of order unity, and asymptotes to unity (100%) for $Stk \gtrsim 10$. For potential flow, Langmuir[16] gives $Stk_{cr} = 0.083$ and the approximate formula for $Stk \geq 0.2$

$$\eta_{imp}(p) = \left(\frac{Stk}{Stk + 0.5} \right)^2 . \tag{4}$$

For viscous flow, he found $Stk_{cr} = 1.214$ and the approximate formula

$$\eta_{imp}(v) = \left[1 + \frac{0.75 \ \ell n \ (2Stk)}{Stk - 1.214} \right]^{-2} . \tag{5}$$

Later workers have obtained similar results which indicate that impaction is very efficient for large particles but is insignificant for small particles, with a rapid dependence on particle size. The collection site for impaction is concentrated around the upstream facing surface of the collector.

Diffusion due to Brownian motion of submicron particles promotes their deposition during flow past a collector. The diffusion coefficient for Brownian motion is given by the Stokes-Einstein formula

$$D = \kappa TC/6 \pi \mu a_p \tag{6}$$

where κ is the Boltzmann's constant, 1.38×10^{-23} J/K, T is the absolute temperature, and C is the Cunningham correction factor to Stokes' law when a_p is comparable to or less than the mean free path λ:

$$C = 1 + \frac{\lambda}{a_p} \left[1.26 + 0.40 \ \exp(-1.10 \ a_p/\lambda) \right] . \tag{7}$$

The steady state convective diffusion equation

$$\vec{u} \cdot \nabla n = D \ \nabla^2 \ n \tag{8}$$

where n is the concentration of particles in a given narrow size range, has been solved by several workers[17-19] with very similar results for the efficiency for diffusive collection by an isolated sphere:

$$\eta_{diff} \approx 4.0 \left(\frac{D}{2a_c u}\right)^{2/3} \approx 4.0\ (Pe)^{-2/3} \approx 4.0 \left[\frac{\kappa TC}{12\pi\mu a_p a_c u}\right]^{2/3} \qquad (9)$$

where Pe is the Peclet number. For instance, for air at STP, a_c = 1 mm, a_p = 0.1 μm and u = 1 m/s, we have C = 1.87, D = 1.22 x 10^{-10} m^2/s, Pe = 1.64 x 10^7 and η_{diff} = 6.8 x 10^{-5}. It may be noted that the Brownian diffusion coefficient is typically very small, and that eddy diffusion due to weak turbulence in flows of low Reynolds number may in practice be comparable to or larger than that due to Brownian motion.

The calculated fractional efficiencies versus particle size for an isolated sphere by interception, impaction and Brownian diffusion for typical conditions of interest are shown in Figure 1. Also shown are the total fractional efficiencies for the cases of potential flow and viscous flow. Both show a minimum efficiency due to the fact that, with increasing size, diffusive capture decreases while capture due to interception and impaction increases. Such a minimum, usually falling in the size range 0.1-1.0 μm is characteristic of packed bed and other filters. For potential flow, the minimum is at ~0.08 μm, while for viscous flow the minimum is at ~2.0 μm and about an order of magnitude smaller in value. The case illustrated has a Reynolds number of ~70 so that one would expect a rigorous treatment to yield a solution falling between these limiting cases of viscous and potential flow. Langmuir suggested the interplation formula for impaction

$$\eta_{imp} = \frac{[\eta(v) + \eta(p)(Re/60)]}{[1 + (Re/60)]} . \qquad (10)$$

Aerodynamic Filtration by a Packed Bed

Model computations of the collection efficiency of fibrous and packed bed filters are based on the theory for collection by isolated cylinders and spheres, respectively, but modified to give an average efficiency per representative element (cylinder or sphere) which takes account of the modification of the flow by the surrounding elements. Such models are called cell models, and are inevitably of dubious validity because they endeavor to account for the interference effect of the neighboring collectors in only a very approximate way. In the case of typical fibrous filters, where the packing fraction is very low (0.01-0.1), this approach has greater validity than for a close packed array of spherical collectors with a typical packing fraction of 60-70%.

The overall fractional efficiency of the bed as a function of particle size is then obtained by integrating the following differential relation for the decrease in particle concentration

$$\frac{dn}{dx} = -\frac{3\alpha\eta\, n}{4a_c} \qquad (11)$$

where η is the total fractional efficiency per cell, α is the packing fraction, and x is the flow direction. The fractional penetration P for a bed of thickness L is then given as a function of particle size by

$$P = \frac{n(L)}{n(0)} = \exp - \frac{3\alpha\eta\, L}{4a_c} \tag{12}$$

and the fractional efficiency of the bed is then

$$\eta_B = 1 - P. \tag{13}$$

Equation (12) allows effective fractional efficiencies per cell, or sphere, to be calculated from measured values of the penetration.

The total mass collection efficiency for a given input aerosol size distribution is given by integrating the mass-weighted fractional efficiency over the size distribution.

The most widely used cell model is that of Happel and Brenner[20], which treats a representative sphere occupying the center of an idealized cell. The cell consists of two concentric spheres, an inner one representing the collector, and an outer sphere representing a fluid envelope having a free surface, i.e., having no tangential stress. The ratio of the volumes of the inner and outer spheres is taken equal to the packing fraction of the real bed. The viscous flow equations are solved for the cell, which allows the pressure drop or specific flow resistance to be evaluated. The flow field also serves as the basis for calculating particle capture.

Numerical solutions for the efficiency of impaction per sphere using Happel's cell model with viscous flow were obtained by Paretsky et al.[15]. In the limit $\alpha \to 0$, for an isolated sphere, they reproduce the result of Langmuir for viscous flow with $Stk_{cr} = 1.214$. With increasing packing fraction, the efficiency curve (see Figure 1) is translated to lower Stokes numbers; for instance for $\alpha \sim 60\%$, Stk_{cr} is reduced by about an order of magnitude to ~0.1. This is probably attributable to the effect of fluid jets in the flow passages increasing the effective Stokes parameter above that calculated on the basis of the superficial velocity.

The collection efficiency per sphere by diffusion was evaluated by Pfeffer[21] for viscous flow as

$$\eta_{diff} = \frac{5.0(Pe)^{-2/3}}{[\rho(\alpha)]^{1/3}} \tag{14}$$

where

$$\rho(\alpha) = [2 - 3\alpha^{1/3} + 3\alpha^{5/3} - 2\alpha^2]/(1 - \alpha^{5/3}). \tag{15}$$

In the limit of an isolated sphere, $\alpha \to 0$, $\rho \to 2$, and eq. (14) reduces to eq. (9). For a close packed bed with $\alpha = 0.6$, $\rho(\alpha) \sim 1.15$, so that the Pfeffer model gives a very modest increase in efficiency per sphere over that for an isolated sphere.

As Spielman[9] comments, "there is considerable disagreement among workers as to which, if any, of the different models is best suited to predict particle capture by fibrous and granular filters." Cell models completely ignore the tortous flow passages associated with the topology of a real packed bed. Payatakes et al.[22] disapprove of representative sphere models for densely packed beds. As an alternative they discuss a constricted tube model which requires numerical solution to predict particle capture. It would appear that some such model, which takes a more realistic view of the actual geometry of a packed bed will be necessary to obtain more useful formulae for the capture efficiency in close-packed beds. Such a model would also appear to be necessary to deal realistically with electrified beds where, as discussed below, the electric field is very inhomogenous.

Experimental

A number of experiments on filtration by packed beds have been reported, as reviewed by Tardos et al.[10]. However, the data often covers only limited parameter ranges and is not particularly well correlated with theory. Measurements of penetration are commonly made as a function of superficial velocity for a fixed monodisperse aerosol. When plotted as fractional efficiency versus aerosol diameter, the data typically shows a minimum in the size range 0.1-1 μm. Recent work by Goren[23] extends over a wider range and is empirically correlated in dimensionless plots of single grain efficiency against Stokes number, Peclet number and also a gravity number $Grv \equiv 2 \rho_p a_p^2 Cg/9\mu u$, where g is the gravitational acceleration. Nevertheless, the correlation of theory and experiment leaves much to be desired. To quote Tardos et al., "There is still considerable work to be done in order to explain the operation of granular filters. This includes theoretical models that will take account of electrical forces, the entrainment of dust from the collection surface, unsteady characteristics of the filter, and lastly comparison of these theoretical results with well-designed experiments."

Despite being imperfectly understood, granular bed filters are, in practice, effective filters for particulate emission control, and are being investigated[24], along with other devices, for high temperature applications.

For conventional stack gas temperatures, commercial-sized units (to 200,000 acfm or more), known as dry scrubbers, are manufactured by Combustion Power Company, and have been installed on a number of hog fuel boilers and other systems where they are competitive with alternative devices such as electrostatic precipitators.

In this form the bed of gravel granules (1/8" - 1/4") occupies the annulus between two concentric vertical louvered steel cylinders. The dusty gas flows radially through the bed from an input plenum, and the cleaned gas exhausts upwards through the outlet duct. The gravel medium moves slowly downwards in

approximate plug flow and exits at the bottom, where it is cleaned of dust and recycled to the top of the bed. Such filters are sometimes used with a pre-cyclone inertial separator to remove the bulk of the large size fraction to avoid loading the bed unduly. The optimum design of the cyclone-filter combination depends on the particle size distribution and involves trade-offs between the pressure drops and collection efficiencies of the two components.

Recent reports[25] of field tests of such a granular bed filter, fitted with high voltage electrodes in the bed, indicate a dramatic decrease in plume opacity on a hog fuel boiler, and are attributed to a significant electrical enhancement of the efficiency for submicron particles.

ELECTRIFIED BEDS - THEORETICAL CONSIDERATIONS

A considerable variety of distinguishable electrical effects are possible, depending on the charge state of the entering aerosol and the configuration of the bed with regard to the electrical properties of the granules, the electrode configuration, the magnitude and character (dc or ac) of the applied voltage, etc. Furthermore, the electrical states of both the particles and the bed can change as a result of their mutual interaction.

Here we consider first the field (and charge) distribution in the bed alone, and then the interaction of particles with the bed in terms of several distinct electrical mechanisms.

Field Distribution in an Electrified Packed Bed

We consider a packed bed of semi-insulating granules immersed between electrodes between which an external voltage is applied. The electrodes are assumed to have large radii of curvature relative to the granule size, so that they do not support corona discharges, and the scale of the field variation is determined primarily by that of the granules and not of the electrodes. Because, even for a perfectly close-packed bed of uniform spheres, the geometry is quite complex, the analysis is restricted to the simple case of a regular cubic array of contacting spheres between external electrodes located along principal lattice planes (Figure 2(a)). This model has been discussed by McLean[26] in connection with the resistance of precipitated ash layers in electrostatic precipitators. Though idealized, it apperas that the model describes the essential features of the field distribution in practical beds.

Several points should be made at the outset. First, it is important to recognize that no insulator is perfect, so that in a steady state there will be a (small) current flow, and the distribution of potential and electric field is determined by the bed's resistive properties, i.e., it is a problem in resistive current flow rather than one of electrostatics for perfect dielectrics. Furthermore, if the bed is used to filter an aerosol carrying a net charge, the bed resistance must be low enough to leak off the current due to the collected particles without producing fields comparable to those applied. Otherwise the bed will charge up, bias off the applied field, and be self-limiting. Even for an aerosol which is grossly neutral, but is bipolarly charged, the resistance must be low enough to allow current flow between the collection sites of the oppositely charged particles without inducing fields

comparable to those externally applied. Fortunately, it appears that these conditions will be met unless highly insulating granules are used under very dry conditions, so that in practice any modification of the bed field due to the aerosol is negligible.

Second, there are two modes of current conduction through the bed: (i) through the volume of the media and (ii) on the surface of the media. In general both contribute to determining the potential distribution, but it seems likely, especially in moist combustion gases, that surface conduction predominates.

Third, as discussed below, the contacts between the individual bed elements are critical, because the resistance is primarily determined by the contact area, and the electric fields are concentrated around the regions of contact. There is evidence that localized intermittent discharges occur in the narrow gaps around the contact points. It also seems probable that these regions of strong field play an important role in the filter action.

The basic element of the array of spehres shown in Figure 2(a) is a single sphere with current entering at one pole, $\theta = 0$, and leaving at the opposite one, $\theta = \pi$, as shown in Figure 2(b). An analysis of the potential distribution for the cases of volume conduction and surface conduction can be then given as follows:

Volume Conduction. For a sphere of radius a, volume resistivivity ρ and for a total current, I, the potential at any interior point is given[27] by

$$V = \frac{\rho I}{2\pi}\left\{\frac{1}{R_o} - \frac{1}{R_\pi} - \frac{1}{2a}\,\ell n\left[\frac{R_o\,(1+\cos\alpha_o)}{R_\pi\,(1+\cos\alpha_\pi)}\right]\right\} \tag{16}$$

where R_o and R_π are the distances from the poles, and α_o and α_π are the angles to the polar axis (Figure 3(a)).

For a point on the surface, $r = a$, we have (Figure 3(b)) $R_o = 2a\sin(\theta/2)$, $R_\pi = 2a\cos(\theta/2)$, $\alpha_o = (\pi/2)-(\theta/2)$, $\alpha_\pi = (\theta/2)$. Then

$$V(a,\theta) = \frac{\rho I}{4\pi a}\left\{\frac{1}{\sin(\theta/2)} - \frac{1}{\cos(\theta/2)} - \ell n\left[\frac{\sin(\theta/2)(1+\sin(\theta/2))}{\cos(\theta/2)(1+\cos(\theta/2))}\right]\right\} \tag{17}$$

$$\equiv \frac{\rho I}{4\pi a} F(\theta) \quad \text{(say)}. \tag{18}$$

Thus the diametral plane $\theta = \pi/2$ is the equipotential $V = 0$, and the potential has a simple pole at each contact point.

$$V \xrightarrow[R_o \to 0]{} \frac{\rho I}{2\pi R_o} = \frac{\rho I}{2\pi a\theta}\,. \tag{19}$$

Around the contact points the equipotentials are approximately spherical centered on the contact point, and of value inversely proportional to their radius. The function $F(\theta)$ is graphed in Figure 4.

The case of a finite contact area between the two spheres can be modelled by assuming a perfectly conducting sphere of radius $R_o = \delta << a$ surrounds the contact point. The potential across the half-sphere is then

$$V_o = \frac{\rho}{2\pi\delta} \approx \frac{\rho I}{2\pi a\theta_o} \tag{20}$$

where θ_o is the polar angle of the contact circle.

The equipotentials and field lines appear approximately as shown in Figure 3(c).

To calculate the field surrounding a cubical lattice of spheres, assuming zero conduction in the surrounding space, we should solve Laplace's equation $\nabla^2 V = 0$, subject to the boundary conditions that V is given by eq. (17) on the surface of the sphere and that the diametral planes are equipotentials. However, this is rather complex. For our purposes, a satisfactory solution is obtained by assuming that the field is given approximately by the potential difference divided by the gap height.

Now the gap half-height (Figure 3(d)) is

$$h = a(1 - \cos\theta) \approx a(\theta^2/2), \tag{21}$$

and the field in the gap at polar angle θ is

$$E(\theta,\theta_o) = \frac{V(\theta) - V(\theta_o)}{h} . \tag{22}$$

For small angles this can be written

$$E(\theta,\theta_o) \approx \frac{E_{av}\theta_o}{\theta^2}\left[\frac{2}{\theta_o} - \frac{2}{\theta}\right] \approx 2E_{av}\frac{(\theta - \theta_o)}{\theta^3} . \tag{23}$$

This has a maximum when $\theta = 3\theta_o/2$ of value

$$E_{max} = \frac{8}{27}\frac{E_{av}}{\theta_o^2} . \tag{24}$$

Here E_{av} is the potential drop across the sphere divided by its diameter.

Thus the field enhancement around the contact region can be very large and scales inversely as the square of the diameter of the contact region.

For instance, for $a = 3$ mm (~1/4" diameter balls) and a contact radius of $\delta = 0.05$ mm (~0.002"), $\theta_o \sim 1°$, so that $(E_{max}/E_{av}) \sim 1000$. For an average applied field of 3 kV/cm, the maximum field would be 3 MV/cm.

Clearly, with such large fields, there would be a partial (intermittent) breakdown of the gap, which would effectively increase the contact area and lower the maximum field. For instance, if we assume the gap breaks down for $E > 30$ kV/cm, then with $E_{av} = 3$ kV/cm, we should have an enhancement of 10 and $\theta_o \sim 10°$, $\delta \sim 0.5$ mm (~0.020").

Surface Conduction. Consider now a sphere, radius a, with surface resistivity s (ohms/square) with current entering and leaving at the poles $\theta = 0, \pi$ as before. The volume resistivity is assumed to be infinite.

The potential on the surface can be shown to be[28]

$$V = \frac{sI}{2\pi} \tanh^{-1}(\cos\theta) \equiv \frac{sI}{2\pi} G(\theta) \quad \text{(say)}. \tag{25}$$

For $\theta = \pi/2$, $V = 0$, on the diametral plane. For small θ

$$V \to \frac{-sI}{2\pi} \ell n(\theta/2). \tag{26}$$

Thus unlike the case of volume conduction, where V has a simple pole at $\theta = 0$, the case of surface conduction gives a logarithmic pole at $\theta = 0$. The function $G(\theta)$ is plotted for comparison with $F(\theta)$ in Figure 4.

If the contact is a circular area subtending a half-angle θ_o at the center of the sphere, then the potential drop across the half-sphere is

$$V_o = \frac{sI}{2\pi} \tanh^{-1}\left(\cos\theta_o\right) \sim - \frac{sI}{2\pi} \ell n\left(\frac{\theta_o}{2}\right). \tag{27}$$

For two spheres in contact over the angle out to $\theta = \theta_o$, the electric field in the gap is given approximately by

$$E(\theta,\theta_o) = \frac{sI}{2\pi} \frac{[\tanh^{-1}(\sec\theta_o) - \tanh^{-1}(\sec\theta)]}{a(1 - \cos\theta)}. \tag{28}$$

For small angles this may be written

$$E(\theta,\theta_o) \approx - \frac{2E_{av}}{\theta^2} \frac{\ell n(\theta/\theta_o)}{\ell n(\theta_o/2)}. \tag{29}$$

This has a maximum when $\ell n(\theta/\theta_o) = 1/2$, i.e., when $\theta = \theta_o e^{1/2} \approx 1.65\,\theta_o$. The maximum value is

$$E_{max} = \frac{E_{av}}{e\theta_o^2 \, \ell n(2/\theta_o)} \quad . \tag{30}$$

Comparing this with the case of volume resistance, it is seen that the numerical factors are similar (1/e compared with 8/27), but in the surface conduction case the fields are smaller by the factor $\ell n(2/\theta_o)$ in the denominator.

For instance, for $\theta_o = 1°$, this factor is 4.7, so that $E_{max}/E_{av} \sim 200$ instead of 1000 in the volume conduction case. To make the comparison another way, if we require $E_{max}/E_{av} = 10$, set by the incidence of discharge, then for the volume conduction case $\theta_o \sim 9.9°$ whereas for the surface conduction case $\theta_o = 6.5°$.

Thus if the conduction mode is via the surface, the field enhancement is somewhat less, and the breakdown strength of the gap will be exceeded out to a rather smaller radius from the contact point than for volume conduction.

The foregoing analysis reveals that in an electrified packed bed, the field is highly inhomogeneous and is locally enhanced around the contact points by a large factor. In practice the enhancement is probably limited by the occurrence of intermittent microdischarges which effectively increase the contact area out to where the field is no greater than a factor ~10 over the average field values (~3 kV/cm) typically applied to the bed experimentally. Near the sphere's surface, away from the contact points, the field is reduced somewhat below the average value.

In the region of contact, the fields are directed to the surfaces, across the gaps, whereas away from the contact points the fields are more generally parallel to the surfaces. These facts suggest that the regions around the contacts between the granules probably play a dominant role in the collection of fine particles in an electrified packed bed.

The presence of intermittent localized discharges around the granule contact points, which will give rise to a degree of gaseous ionization, might play some role in particle collection, for instance by discharging particles. However, at the small currents likely to be met in practice, such effects are probably negligible.

Interaction of Particles with an Electrified Bed

The state of charge of the entering aerosol is clearly important in determining the interaction of particles with the granular bed. This applies not only when the bed is externally electrified, but even when it is uncharged (grounded), because of the existence of image forces.

In general an aerosol consists of particles having a distribution of charge magnitudes extending over both polarities, which depends on how it was formed and its subsequent history, and is in general correlated with its size distribution. The net aerosol charge may be characterized by the net charge/mass ratio as determined by a sampling Faraday cage filter. However, it is important to recognize that aerosols having little or no net charge may often have significant levels of bipolar charge.

To establish a rough quantitative scale for the charge magnitudes likely to be encountered, we may use the fact that there is a limit to the charge that a particle can carry, set by the condition that the electric field E_s at its surface becomes large enough to cause breakdown of the carrier gas. For a spherical particle of radius a and density ρ, the limiting charge is given by

$$q_\ell = 4\pi a^2 \varepsilon_o E_s, \tag{31}$$

while the charge/mass ratio is

$$\frac{q_\ell}{m} = \frac{3\varepsilon_o E_s}{\rho a} . \tag{32}$$

For instance, taking $E_s = 3 \times 10^6$ V/m, $2a = 1$ μm and $\rho = 2$ kg/m^3, we find $q_\ell \sim 8 \times 10^{-17}$ C, or $\sim$500 electron charges, while $(q_\ell/m) \sim 8 \times 10^{-2}$ C/kg, or $\sim$ 80 μC/g. The limiting value of $q \propto a^2$, while the limiting value of $(q/m) \propto (1/a)$.

This limiting charge, set by breakdown, can be compared with the saturation charge due to field (bombardment) charging in a monopolar corona discharge.

$$q_b = 12\pi a^2 \varepsilon_o \left(\frac{\varepsilon}{\varepsilon+2}\right) E_c a^2 . \tag{33}$$

Here E_c is the charging field and ε is the relative permittivity of the particle. It is clear that for $E_c \sim 5 \times 10^5$ V/m, typical of single stage precipitators $q_b \lesssim q_\ell$.

There is relatively little documentation of the state of charge of aerosols produced by various processes, but it is probably true to say that, more often than not, they are significantly charged relative to the limiting value, unless special measures are taken to neutralize them.

For instance, when powders are dispersed in air by various means to form an aerosol, it appears that the resulting aerosol commonly has a significant level of bipolar charge due to deagglomeration of the powder. In addition, a net aerosol charge may be induced by tribocharing if the particles make contact with surfaces in the dispersal process[29,30].

Further, measurements by White[31] using a charge analyzing probe on the fine particle effluent from electrostatic precipitators fitted to coal-fired power plants show monopolar charge/mass ratios ranging up to 100 μC/g. More importantly, measurements of the input aerosol, i.e., the exhaust from the combustor, showed that while it was approximately grossly neutral, bipolar charge/mass ratios of the order $\pm$ 10-20 μC/g existed. The origin of this bipolar charge condition, and whether it is a typical or universal condition for fly ash emissions from coal combustors, is unknown, but it is clearly an important factor to be reckoned with in designing particulate control devices.

Turning now to the question of the electrical interaction of aerosol particles with a granular bed, it is clear that we should consider the possibilities of the particles being uncharged or charged to either sign, and also the possibilities of the aerosol being grossly neutral or having a net charge.

Thus there are several distince physical situations and corresponding mechanisms that can play a role in producing electrical forces on the particles. We discuss these in turn and then compare their relative magnitudes.

(i) Uncharged particles situated in an electric field E_o have an induced dipole moment

$$M = 4\pi\varepsilon_o \frac{(\varepsilon-1)}{(\varepsilon+2)} E_o a_p^3 \tag{34}$$

where ε_o is the vacuum permittivity and ε is the relative permittivity of the particle (~2 for fly ash). In a uniform field there is no net force on the particle, but in a nonuniform field there is a force $M\nabla_{||}E_o$ where $\nabla_{||}E_o$ is the field gradient along the field direction. For the purposes of estimation, the value of $\nabla_{||}E_o$ due to the inhomogeneous field in an electrified bed may be taken as $\sim(E_o/a_c)$ where E_o is the average field and a_c is the collector radius. Then the force is of order

$$F_1 \approx 4\pi\varepsilon_o \frac{(\varepsilon-1)}{(\varepsilon+2)} E_o^2 \frac{a_p^3}{a_c} \quad . \tag{35}$$

(ii) In the case of an aerosol having a net charge, there is a self field E_s, due to the space-charge of the particle cloud with which each particle interacts causing the cloud to disperse towards the surrounding collector surfaces. Poisson's equation gives

$$\nabla \cdot \vec{E}_s = \frac{nq}{\varepsilon_o} \tag{36}$$

where q is the average charge on the particles. Taking the characteristic dimension of the interstices of the bed as of order a_c we have for the self force qE_s on the particles near the collector surfaces

$$F_2 \approx \frac{n\,q^2}{\varepsilon_o} a_c \quad . \tag{37}$$

(iii) Charged particles also experience an image force when close to the collector. If the bed is conducting, the image force is

$$F_3 = \frac{1}{4\pi\varepsilon_o} \frac{q^2}{(2d)^2} \tag{38}$$

where d is its distance from the conductor. In the case of an uncharged dielectric collector of relative permittivity ε_c, this force is modified by the factor $(\varepsilon_c-1)(\varepsilon_c+1)$.

(iv) Finally, in an external field a charged particle experiences a force

$$F_4 = q\, E_o. \tag{39}$$

To compare the relative magnitudes of these four forces, we must estimate some typical magnitudes for the quantities involved. For the particle charge, we assume it is given by eq. (33) for bombardment charging which is valid for particles down to at least ~ 1μm diameter. Also, the particle concentration can be expressed as

$$n = \frac{3L}{4\pi\rho_p a_p^3} \tag{40}$$

where L is the mass loading.

Using eqs. (33) and (40) in eqs. (35), (37), (38) and (39) neglecting factors involving ε which are of order unity, and putting $E_c \approx E_o$, we have for the four forces

$$F_1 \sim \varepsilon_o E_o^2 a_p^2 \left(\frac{a_p}{a_c}\right) \tag{41}$$

$$F_2 \sim \varepsilon_o E_o^2 a_p^2 \left(\frac{a_c}{a_p}\right)\left(\frac{L}{\rho_p}\right) \tag{42}$$

$$F_3 \sim \varepsilon_o E_o^2 a_p^2 \left(\frac{a_p}{d}\right)^2 \tag{43}$$

$$F_4 \sim \varepsilon_o E_o^2 a_p^2 \tag{44}$$

It is clear that F_1, the force on an uncharged particle in a nonuniform field is smaller than F_4, the force on a charged particle in an applied field by the ratio $(a_p/a_c) \sim 10^{-3}$. Also, F_3, the image force on a charged particle only becomes comparable with F_4 when $d \sim a_p$, i.e. when the particle is within distance of the order of the particle radius of the collector. Relative to F_4, the self force F_2 has a factor $(a_c/a_p) \sim 10^3$ and a factor $(L/\rho_p) \ll 1$ which is proportional to the aerosol mass loading. For a typical value $L \sim 2$ gram/m^3 (~ 1 grain/ft^3) and $\rho_p \sim 2$ kg/m^3, the factor $(L/\rho_p) \sim 10^{-3}$ and we find F_2 comparable to F_4.

Thus we should expect F_1 and F_3 to be negligible compared with F_4, while F_2 becomes comparable with F_4 at high loadings for monopolarly charged aerosols.

There are three practical situations of interest where these estimates of electrical forces can be applied, as follows. For an electrified bed and uncharged particles, the only force is F_1; for an unelectrified bed with charged particles, the relevant forces are F_3 and also F_2 if the aerosol is monopolarly charged; for an electrified bed and charged particles the relevant forces are F_4 and also F_2 if the aerosol is monopolarly charged.

From the foregoing estimates one concludes that the strongest electrical augmentation should be observed with charged particles and an electrified bed, and the effect should be maintained at vanishingly small dust loadings (due to F_4). Significant augmentation should be observed for monopoalrly charged particles and an unelectrified bed, but the effect should fall off with dust loading, i.e., the later layers of the filter become progressively less effective. With uncharged particles and an electrified bed one should expect, in comparison, negligible augmentation.

These general predictions are borne out by experimental comparisons of the enhancement of collection efficiency with and without pre-charging and with and without voltage applied to the bed, described in the next section.

ELECTRIFIED BED - EXPERIMENTAL WORK

Most of the experimental work was performed in a bench scale flow system at throughputs of up to 40 ft^3/min as described below. Some exploratory work was also done in a test tunnel facility at throughputs up to 600 ft^3/min, and is described below.

Bench Scale Apparatus

The bench scale test rig employed for most of this work is shown in Figure 5, and consisted of a vertical, square section (4" x 4") duct of plexiglass containing a fixed bed 8" high of alumina balls 1/4" in diameter. The bed was contained between grounded metal screens at the top and bottom and had a similar grid at the central section which served as a high voltage electrode.

Ambient air entered via a diffuser section and was exhausted at the top via a fan. The flow velocity was in the range 1-6 ft/sec corresponding to pressure drops between 0.4" and 4" water across the bed. Fly ash was fed from a screw feeder via an "Air-Vac" aspirator to disperse the ash, at grain loadings in the range 1-20 gr/ft^3.

The aspirator incorporates a coaxial sonic nozzle, fed by compressed air at 60-80 psi, and very effectively deagglomerates the ash due to the rapid acceleration of the ash-laden aspirated air and the presence of shocks and a high level of small scale turbulence. In the process, it produces a significant level of bipolar charge in the aerosol which is approximately grossly neutral.

No quantitative study was made of the charge state of the aerosol, but measurements with a charge analyzing probe[32] developed subsequently, have indicated bipolar charge levels in the range 10-20 μC/g with this type of dispersal system used with fly ash.

Ahead of the bed was fitted a corona discharge particle-charging device, consisting of two fine wires situated between three ground planes. By selecting the polarity of the high voltages applied to the wires, the charger could be operated to give positively or negatively charged particles. Also, by applying alternating voltages, it could be used to neutralize the tribo-charged dust delivered by the dust dispersal system.

Sampling probe stations were located immediately upstream and down of the bed. Since the principal interest in this study concerned the collection of submicron particles, extensive use was made of an electrical aerosol analyzer (EAA) (TSI model 3054) to measure grain loading and efficiency. This was supplemented by measurements with a cascade impactor for the size range 0.36-4.4 μm and also a Coulter counter for the range 1-30 μm.

The ash used in these studies was fly ash from the Black Dog power plant. This was relatively coarse, having a mass mean diameter of ~ 15 μm and only ~2% by mass below 1 μm. Consequently the EAA was used with a pre-cyclone having a D_{50} cut point at 2 μm, and a dilution system to prevent overloading the instrument. The EAA indicated that there was a negligible component of ash below ~0.06 μm after it was dispersed in the test rig. It is not known whether the ash as delivered was deficient in such particles or whether deagglomeration was ineffective for very fine particles. In any event, this set a lower limit to efficiency measurements of ~0.1 μm.

Experiments with Tribo-charged Ash

In an initial series of experiments, the particle charger was not used, and measurements were made of the filter's total mass efficiency and fractional efficiency as a function of particle size, as other parameters were varied, notably the voltage applied to the bed, the flow velocity, and the dust loading.

Figure 6 compares the efficiency η as a function of particle size of the electrified bed (E = 4 kV/cm) with that of the unelectrified bed, at a superficial velocity of 2 ft/sec and an input grain loading of ~4 gr/ft^3. The overall mass efficiency was 79% for the unelectrified bed, increasing to 85% for a field of 4 kV/cm, produced by applying 40 kV dc to the central grid. It will be noted that the unelectrified bed has an efficiency of $\eta \sim 80\%$ for particle diameters $D \gtrsim 3$ μm, but it falls rapidly to $\eta \sim 20\%$ for $D \lesssim 1$ μm. This is characteristic of most filters and is due to the rapid onset of collection by impaction for Stokes parameters increasing through a value of order unity. The expected increase in efficiency due to diffusive collection for small particles is not seen here, but can be expected to occur for $D < 0.1$ μm.

The most significant feature displayed by the data of Figure 6 is the dramatic enhancement of efficiency in the submicron range brought about by application of the field. The large drop in efficiency for submicron particles exhibited by the unelectrified bed is completely removed, and the efficiency remains high (~80%) down to $D \sim 0.1$ μm.

The foregoing filter efficiency measurements were made by measuring sequentially with the sampling probe stationed first before the bed and then after the bed. This procedure poses some uncertainties related to ensuring that the flow and sampling conditions are constant and identical for the two measurements. A simpler procedure, which avoids some of these uncertainties and isolates the effect of electrifying the bed, is to sample sequentially with the probe downstream of the bed, first with no field and then with the field applied. This simpler, quicker procedure was adopted for the measurements described below, where various parameters were varied.

Two related measures of the enhancement of filter efficiency due to application of the field can be defined in terms of the flux P of particles penetrating the filter, as follows:

Electrical Effectiveness
$$\varepsilon = \frac{P(E=0) - P(E)}{P(E=0)} \tag{45}$$

Electrical Factor of Improvement
$$F = \frac{P(E=0)}{P(E)} \, . \tag{46}$$

In either case the penetrating flux P can be a number flux or a mass flux, and can be for a specified size range or integrated over the prevailing distribution. Clearly, the two measures are related by

$$\varepsilon = 1 - (1/F) \tag{47}$$

or

$$F = 1/(1 - \varepsilon) \, . \tag{48}$$

Thus, as the electrical enhancement increases from zero to the maximum possible, ε runs from zero to unity while F runs unity to infinity.

Figure 7 shows the effectiveness ε (based on the number flux of particles < 1 μm) as a function of applied field E (positive polarity of applied voltage) for conditions otherwise the same as in Figure 6. It is seen that ε increases with E and asymptotes to a saturation value of $\varepsilon \sim 75\%$ for $E \sim 5$ kV/cm.

Figure 8 shows the factor of improvement as a function of particle diameter from measurements with the mobility analyzer, cascade impactor and Coulter counter. There is some lack of numerical agreement among the three techniques, which is hardly surprising in view of their widely differing principles of operation, but the trends are in consonance. A factor of improvement in the range 3-5 is indicated for submicron particles, whereas a value $F \sim 1$ (no significant electrical enhancement) is indicated for particles above $D \sim 3$ μm, where the efficiency of the unelectrified filter is already high (~80%).

Figures 9 and 10 show the effectiveness ε, (based on the number flux of particles < 1 μm) as a function of grain loading and superficial velocity, respectively. It is seen that ε is a weakly increasing function of grain loading, while it decreases with velocity from $\varepsilon \sim 80\%$ at $u \sim 1$ ft/sec to $\varepsilon \sim 55\%$ at $u \sim 6$ ft/sec.

Figure 11 compares the effectiveness (based on submicron particle number flux) as a function of field strength for steady applied voltages (of either polarity) and a 60 Hz alternating voltage. It is clear that for the same rms field, ac is as effective as dc, which has obvious practical consequences of economy in large scale application.

Figure 12 compares the effectiveness, based on submicron particle number flux, for fine TiO_2 powder (0.2 μm mass mean diameter), with that for the Black Dog fly ash, and shows that there is no significant dependence on the presence of large particles.

Figure 13 compares the effectiveness, based on submicron particles, for two different sizes of alumina spheres used for the bed.

Finally, in Figure 14, a comparison is made of the collection efficiency with and without applied voltage for two different electrode geometries, namely the original screen geometry and one in which the screens were replaced by rows of rods (~0.1" dia). The latter configuration (with vertical rods) was expected to be more suitable for use in a bed moving slowly down in plug flow. As expected, for the same applied voltage, the rods yield an enhancement only slightly less than the screens.

It should be emphasized that in all the aforementioned experiments, the precharging corona discharge was not energized, though it was known that the particles were significantly tribo-charged in the ash dispersal system, and that this was likely to be important to the observed electrical enhancement effect.

Experiments with Pre-charged and Neutralized Ash

To investigate the effect of the state of charge of the ash entering the filter, a series of experiments were made utilizing the two-wire, three-plate, corona pre-charger shown in Figure 5. Such a charger also acts as a single-stage precipitator. Figure 15 shows its efficiency for submicron particles as a function of negative corona current, measured with the EAA at the lower sampling station by switching the current on and off. No problem was experienced with back corona, even with the highest current densities, because the Black Dog ash is of low resistivity and the relative humidity was high (~60%).

In Figures 16-19 the filter efficiency in terms of the number flux of particles in the size range 0.24-1.0 μm is plotted as a function of electrical conditions. Figure 16 shows the efficiency as a function of the current to the pre-charger for an unelectrified bed (the electrodes grounded). It indicates that although the efficiency increases with particle charge, it does not attain the high values observed with tribo-charged particles and an electrified bed.

Figure 17 shows the efficiency for submicron particles with both the precharger energized (to 50 μA) and the bed electrified, as a function of field applied to the bed. The four combinations of the precharger and bed polarities show essentially identical results and indicate efficiencies in excess of 95% for submicron particles at $E \sim 4$ kV/cm. This is higher than that observed for the tribo-charged ash (~85%) and is also higher than the overall mass efficiency (i.e., including the bulk of the ash above 1 μm) for these conditions.

These results suggested that the nominally uncharged ash used in the earlier experiments was, in fact, quite strongly tribo-charged bipolarly, although it was grossly neutral, as indicated by measurements with a Faraday cage total filter. To elucidate this matter, measurements were made with 60 Hz high voltage applied to the corona charging wires. It is well known that such an ac corona discharge contains roughly equal concentrations of positive and negative ions, and is effective in neutralizing aerosol charges.

Figure 18 compares the efficiency for submicron particles as a function of field applied to the bed, with the charger off and with it energized with ac. It clearly demonstrates that the high efficiencies (~80% at E ~ 4 kV/cm) observed with nominally uncharged particles is due to their actually being bipolarly tribo-charged, since when the ash is charge-neutralized the efficiency is much lower.

Finally, a comparison was made of the collection efficiencies, with pre-charged ash, of an unelectrified insulating bed and a grounded bed of conducting steel balls of the same size. Figure 19 shows that while the conducting bed is somewhat better than the insulating bed, it falls far short of the electrified insulating bed.

In summary, the foregoing results show conclusively that to obtain the large enhancement of collection efficiency in the submicron range requires a strong field applied across an insulating bed combined with a significant charge on the incoming aerosol. This is in agreement with the theoretical considerations discussed in the previous section.

Experiments in a Test Tunnel

To explore the concept of the electrified granular bed filter at a larger scale, and under more realistic conditions, that might be extrapolated to a pilot scale, a filter was constructed to fit into a wind tunnel facility built for studies of electrostatic precipitation. This facility consists basically of a tunnel of rectangular cross section 10" wide by 30" high, with a flow capability of up to 2000 ft^3/min, and has provisions for heating and humidifying the air flow to simulate conditions of a power plant exhaust stack. Fly ash can be injected and dispersed using a screw feeder and aspirator arrangement, similar to that employed for the bench scale rig but of larger scale, at ash loadings of up to ~10 gr/ft^3.

A plan view of the filter is shown in Figure 20. The shell is constructed of particle board and the filter media is contained between grounded wire mesh screens having a separation of 18" in the flow direction.

In a practical granular bed filter it is necessary to arrange for the granules to move slowly under gravity in plug flow, to allow their extraction for cleaning and re-use. Accordingly, the electrode system was chosen in the form of vertical rods to be compatible with bed motion. As shown, three rows of 1/4" diameter rods were used, with the center row grounded and the other two rows connected to a bus-bar for electrical energization.

Because it was judged that the high quality alumina spheres employed in the bench-scale rig might be too costly for large-scale application, the use

of a lower grade bed material was investigated. Alumina granules or nuggets of a grade commonly used for grinding were employed. These were irregularly shaped, of approximately 1/4" mean size, and of a dark grey color, in contrast to the white alumina spheres. The color is attributed to impurities. Their suitability as an insulating bed material was first tested in the bench-scale rig. It was found that they were limited to lower average electric fields than the pure alumina spheres by the onset of electrical breakdown. The maximum field was found to be ~2.1 kV/cm, compared with ~5 kV/cm with the pure alumina spheres. By chemical cleaning the nuggets the maximum field could be increased to ~3 kV/cm.

Figure 21 compares the efficiency based on the number flux of sub-micron particles, as a function of average applied field, for the nuggets and the spheres, measured in the bench-scale rig using tribo-charged fly ash. It is seen that the efficiencies tend to the same asymptote (~85%), but that the efficiency for the nuggets approaches saturation more rapidly with increasing field. Thus the lower maximum field for the nuggets may not be a disadvantage in practice.

A series of experiments were then made with the filter, filled with alumina nuggets, in the test tunnel. A single wire-plate corona charging unit was fitted upstream of the filter, and sampling ports were provided at stations immediately upstream and downstream of the filter.

Figure 22 shows, as a function of face velocity, the pressure drop and also the total mass efficiency for tribo-charged Black Dog fly ash, as measured with a total filter sampling probe. No significant difference in total mass efficiency was detectable whether the bed was electrified or not. However this is to be expected, because the enhancement with an electrified bed occurs for the submicron fraction which comprises only 1-2% by mass of the fly ash. The rather rapid decrease in total mass collection efficiency for face velocities greater than 1-2 ft/sec must be attributable to re-entrainnment of impacted ash from the granules.

The electrical enhancement effects observed for submicron particles are shown in Figure 23, where the efficiency for submicron particles is plotted against face velocity for three cases; tribo-charged ash with and without the bed electrified, and with corona-charged ash with the bed electrified at 1.2 kV/cm, dc. In the latter case, the submicron efficiency was 90-95% for face velocities of 1-2 ft/sec.

During these experiments the ambient relative humidity varied by about 10 percentage points and it was observed that the bed current was a sensitive function of humidity. At 60% relative humidity the filter drew 4 mA at 15 kV (1.2 kV/cm), falling to 1.2 mA at RH ~ 55%. This supports the view that the bed resistance is controlled by the surface resistivity rather than the bulk resistivity of the granules.

To investigate this effect, the gas temperature was varied up to 150°F by operating the natural gas burner in the tunnel test facility, which reduced the relative humidity considerably. At this temperature the bed current was reduced to the very low value of ~10 μA at 1.2 kV/cm field. The current tended to be unstable under these conditions, and it appeared as though the filter were charging up and then breaking down to leak off the accumulated charge.

The electrical effectiveness for submicron particles is compared in Figure 24 for ambient and hot-flow conditions. Tribo-charged dust was used with a filter field of 1.2 kV/cm in both cases. It is seen that under hot conditions, the effectiveness is reduced by a factor ~2. It is not clear whether this is due entirely to the change in bed resistance, or whether it involves also the ash resistivity which is also a strong function of temperature and humidity. From resistivity cell measurements it is estimated that the Black Dog ash resistivity increases from ~10^9 ohm-cm at room temperature to ~10^{11} ohm-cm at 105°F. The hopper of the screw-feeder was heated in all the experiments reported, so that the state of charge of the dispersed ash should be independent of the main tunnel gas temperature, although its resistivity can be expected to rapidly assume that corresponding to the tunnel gas temperature and humidity. Thus the principal effect of ash resistivity can be expected to be on the bed resistance, as the bed accumulated dust, especially around the contacts between granules.

For a face velocity of ~2 ft/sec, a grain loading of ~5 gr/ft^3 and a bipolar charge/mass ratio of $\pm$ 20 μC/g, the bipolar current intercepted by the bed is ~$\pm$20 μA. This is comparable with the external current through the bed, and it seems probable that the reduced effectiveness at the elevated temperature is due to the high bed resistance. Under these conditions, the bed fields due to the applied voltage are reduced or biased off due to charge deposited by the captured ash, which cannot leak off fast enough.

This is a critical point for operation of a granular bed in stack gases and needs further investigation.

DISCUSSION

The principal result of this work is that the collection efficiency of a granular bed filter for submicron particles can be dramatically enhanced by electrical augmentation. The bench-scale experiments and theoretical considerations indicate that electrification of an insulating bed to average fields of a few kV/cm, together with significant levels of particle charge are necessary to achieve the maximum effect, where the usual rapid fall off in efficiency of granular beds for submicron particles is completely removed.

The potential of electrified granular bed filters for large-scale application to particulate control will depend on an engineering evaluation of a number of factors not fully addressed in this preliminary study. These include the trade-offs between the face velocity, pressure drop and efficiency loss due to re-entrainment, the problems and cost of auxiliary equipment for recycling the bed material, efficiency loss associated with relative motion of the granules in a moving bed, and optimization of the bed resistance to avoid, on the one hand, unnecessarily large power consumption, and on the other, electrical biasing of the applied field with too high a bed resistance.

Its potential will also clearly depend on the particular application and how it is integrated with other equipment. For conventional coal-fired power plant applications, it might be used with an inertial pre-separator or electrostatic precipitator to remove the bulk of the coarse fly ash fraction, which

would greatly simplify the bed cleaning problem. In this sense it might be attractive as retrofit equipment to control submicron emissions on existing devices which do not meet the impending stricter requirements for such emissions. It may also have potential for hot gas clean up for coal-fired gas turbines, if suitable bed materials are available with low enough resistivities at high temperatures.

The electrified bed filter has a number of inherent advantages over various competing devices. It is rugged and fireproof so that, compared with bag filters, it is immune to boiler upset. Moreover, it works equally well with ac and dc voltages, which implies a considerable saving in power supply costs relative to precipitators.

An intriguing and potentially important possibility, is that the ash emitted by combustion systems may be sufficiently highly bipolarly charged that one might eliminate the need of a pre-charging stage, with a consequent saving in complexity and cost. The evidence on this point[31] is inadequate, and further work is necessary to characterize the charge state of the particulate emissions from common combustion systems and other industrial processes. However, the fact that dramatic reductions in plume opacity have been reported[25] on hog-fuel boilers with electrification of the granular bed indicates that the emissions were most likely significantly charged in that case.

ACKNOWLEDGEMENT

It is a pleasure to record the useful advice and contributions of Prof. M. Mitchner, Dr. L. Collins and Mr. E. Kushner to this work. This work was supported by the Electric Power Research Institute.

REFERENCES

1. Pilat, M. J., "Collection of Aerosol Particles by Electrostatic Droplet Spray Scrubbers," J. APCA, 25, 176-178 (1975).

2. Nielson, K. A. and Hill, J. C., "Capture of Particles on Spheres by Inertial and Electrical Forces," I&EC Fund., 15, 149-157, (1976).

3. Bergman, W., Taylor, R. D., Miller, H. H., Bierman, A. H., Hebard, H. D., daRosa, R. A., and Lum, B. Y., "Enhanced Filtration Program at Lawrence Livermore Laboratory--A Progress Report," 15th DOE Air Cleaning Conference, Harvard, August 1978 (Preprint UCRL-81512).

4. Lamb, G.E. and Custanza, P.A., "Electrical Stimulation of Fabric Filtration," Textile Research J., 47, 372-380 (1977).

5. Zahedi, K. and Melcher, J. R., "Electrofluidized Beds in the Filtration of a Submicron Aerosol," J. APCA, 26, 345-352 (1976).

6. Zahedi, K. and Melcher, J. R., "Collection of Submicron Particulate in Bubbling Electrofluidized Beds," I&EC Fund., 16, 248-254 (1977).

7. Alexander J. C. and Melcher, J. R., "Alternating Field Electrofluidized Beds in the Collection of Submicron Aerosols," I&EC Func., 16, 311-317 (1977).

8. Melcher, J. R., Sachar, K. S. and Warren, E. P., "Overview of Electrostatic Devices for Control of Submicrometer Particles," Proc. IEEE, 65, 1659-1669 (1977).

9. Spielman, L. A., "Particle Capture from Low-Speed Laminar Flows," Ann. Rev. Fluid Mech., 9, 297-319 (1977).

10. Tardos, G. I., Abuaf, N. and Gutfinger, C., "Dust Deposition in Granular Bed Filters: Theories and Experiments," J. APCA, 28, 354-363 (1978).

11. Schmidt, E. W., Gieseke, J. A., Gelfand, P., Lugar T. W., and Furlong, D. A., "Filtration Theory for Granular Beds," J. APCA, 28, 143-146 (1978).

12. Fuchs, N. A., The Mechanics of Aerosols, Pergamon Press, New York, 1964.

13. Friedlander, S. K., Smoke, Dust and Haze, Wiley-Interscience, New York, 1977.

14. Ranz, W. E. and Wong, J. B., I&EC, 44, 1371 (1952).

15. Paretsky, L., Theodore, L., Pfeffer, R., and Squires, A. M., "Panel Beds for Simultaneous Removal of Fly Ash and Sulphur Dioxide: II Filtration of Dilute Aerosols by Sand Beds," J. APCA, 21, 204-209 (1971).

16. Langmuir, I., J. Meteor., 5, 175 (1948).

17. Levich, V., Physico-Chemical Hydrodynamics, Acad. Sci., USSR, Moscow, 1952, English Translation, Prentice-Hall (1962).

18. Friedlander, S. K., "Mass and Heat Transfer to Single Spheres and Cylinders at Low Reynolds Numbers," J. AICHE, 3, 11 (1957).

19. Aksel'rud, G., Zh. Fiz. Khim., 27, 1445 (1953).

20. Happel, J. and Brenner, H., Low Reynolds Number Hydrodynamics, Prentice Hall (1962).

21. Pfeffer, R., "Heat and Mass Transfer in Multiparticle Systems," I&EC Fund., 3, 380 (1964).

22. Payatakes, A. C., Tien, C., and Turian, R. M., J.AICHE, 19, 58, 67, 1036, (1972).

23. Goren, S. L., "Aerosol Filtration by Granular Beds," Symposium on Transfer and Utilization of Particulate Control Technology, Denver, Colorado, 24-28 July, 1978, Session C3.

24. Geffken, J., Guillory, J. L. and Phillips, K. F., "Performance Characteristics of Moving-Bed Granular Filters," Ibid., Session C3.

25. Reese, R. G., "The Electroscrubber, An Electrostatic Granular Bed Filter," Combustion Power Company, Menlo Park, Calfiornia.

26. McLean, K. J., "Cohesion of Precipitated Dust Layer in Electrostatic Precipitators," J. APCA, 27, 1100-1103 (1977).

27. Smythe, W. R., Static and Dynamic Electricity, 2nd ed., McGraw-Hill (1950), ch. 6, p. 239.

28. Ibid., p. 243.

29. Smy, P. R., "Role of Gas Breakdown in the Charging and Discharging of Macron Clouds," Proc. IEE, 120, 523-526 (1973).

30. Cheng, L. and Soo, S. L., "Charging of Dust Particles by Impact," J. Appl. Phys., 41, 585-591 (1970).

31. White, H. J., Industrial Electrostatic Precipitation, Addison-Wesley, (1963) p. 152, also private communication 1979.

32. Self, S. A., Paul, P. and Kushner, E., "A Charge Analyzing Probe for Aerosol Flows," IEE-IAS Conference, Cleveland, October 1979 (to be presented).

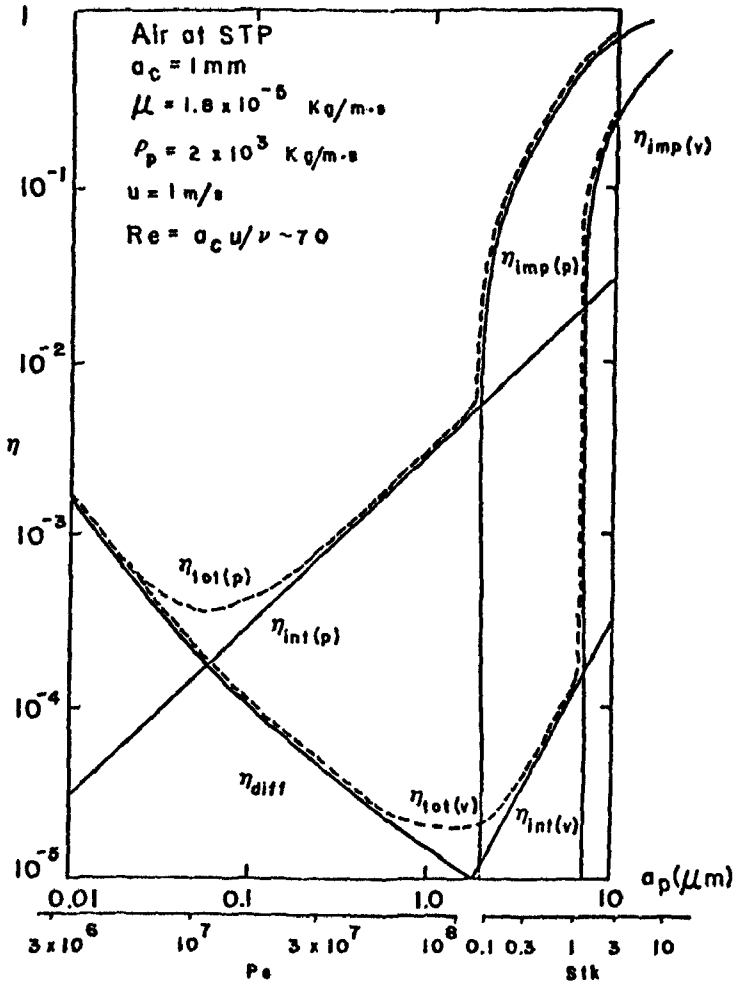

Figure 1. Theoretical collection efficiency by isolated sphere for potential(p) and viscous(v) flow.

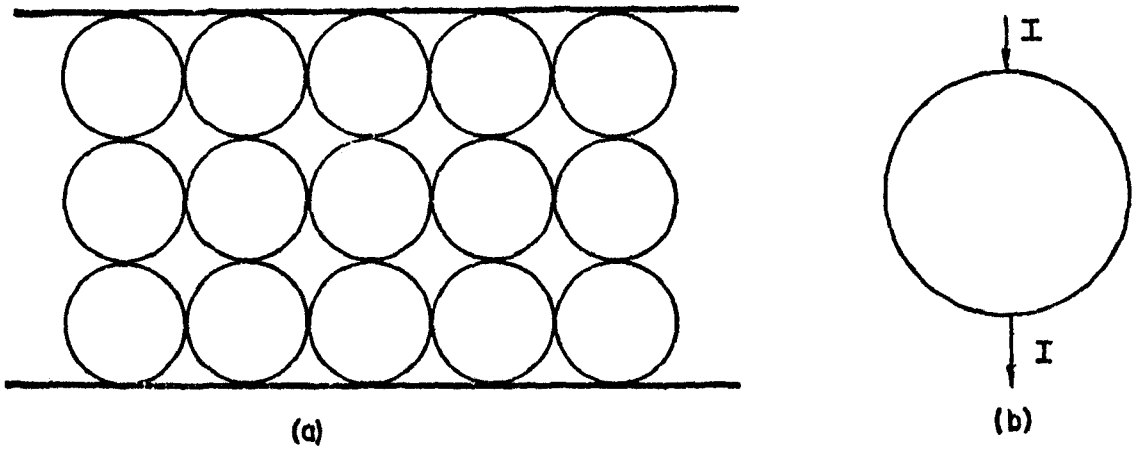

Figure 2. (a) Cubic array of spheres between plane electrodes
(b) Sphere with current entering and leaving at opposite poles.

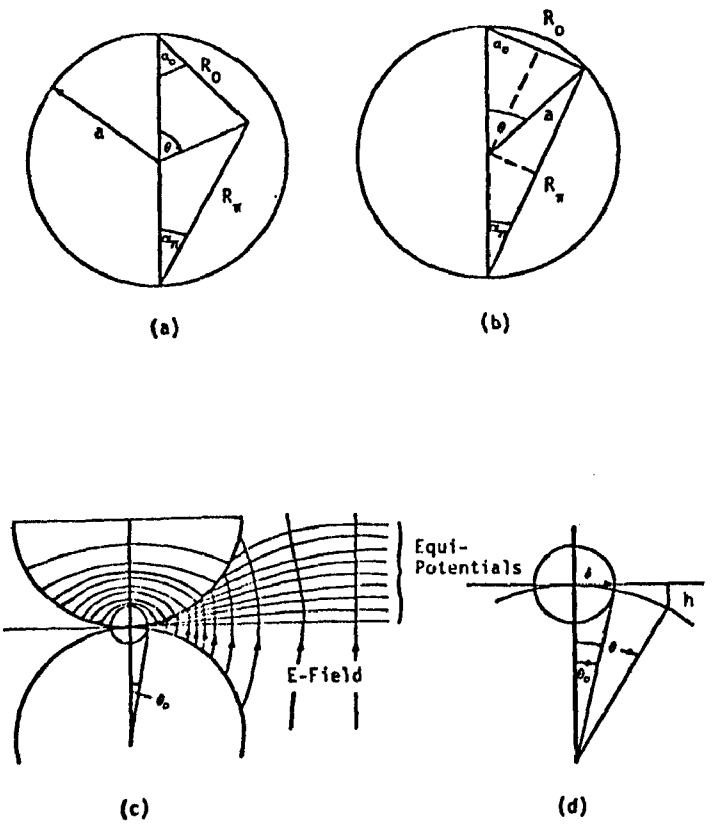

Figure 3. Geometry for current flow through resistive spheres.
(a) volume conduction, (b) surface conduction,
(c) potential and field distribution, and
(d) geometry in contact region.

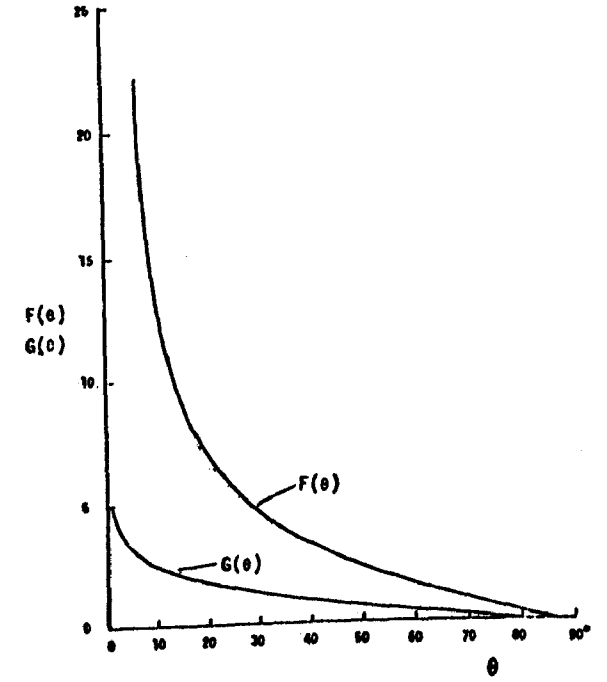

Figure 4. Functions F(θ) and G(θ) for potential distributions for current flow across a sphere.

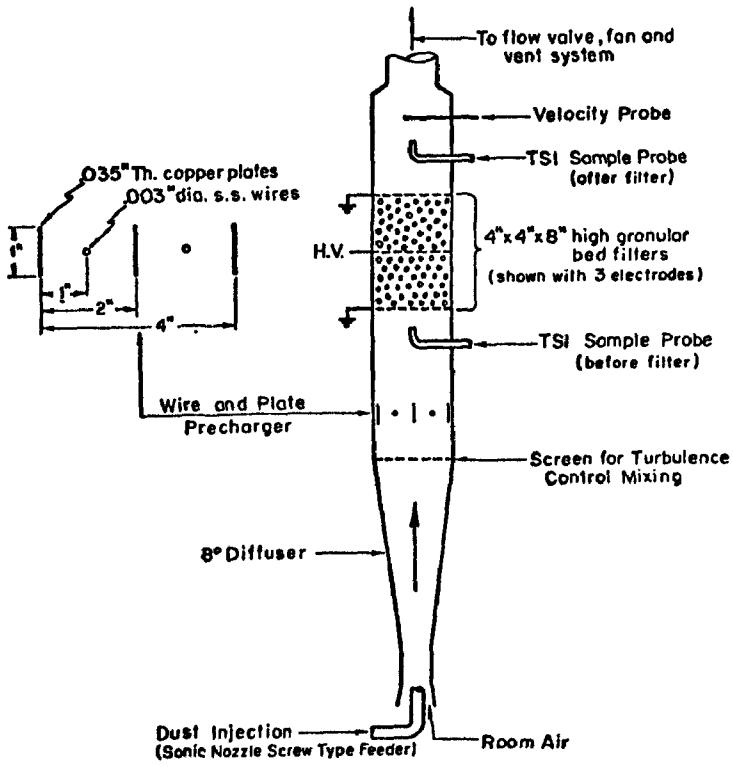

Figure 5. Bench scale test apparatus.

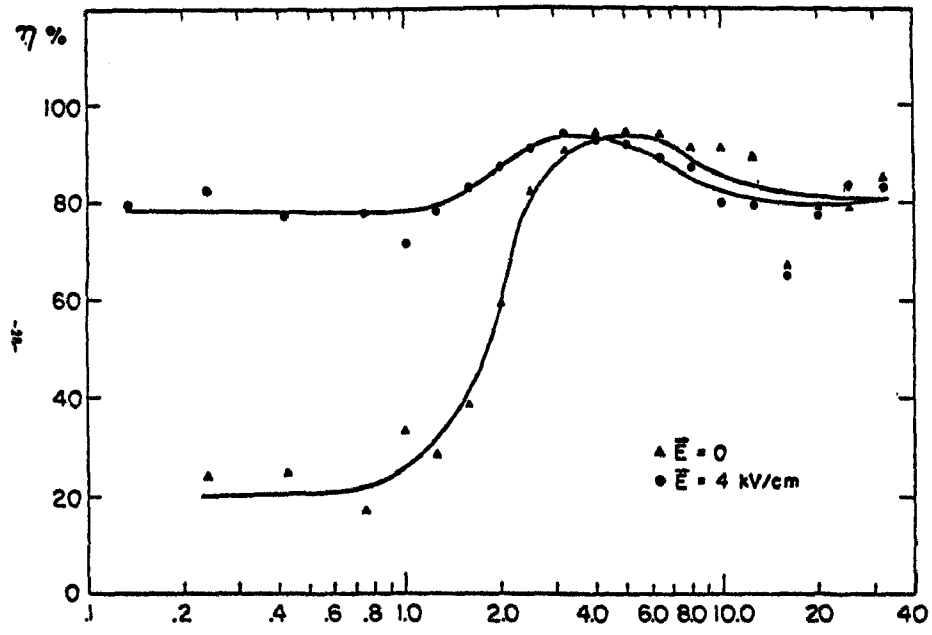

Figure 6. Filter efficiency as a function of particle size, combined results Coulter Counter (> 1 μm) and Electrical Aerosol Analyzer (< 1 μm).

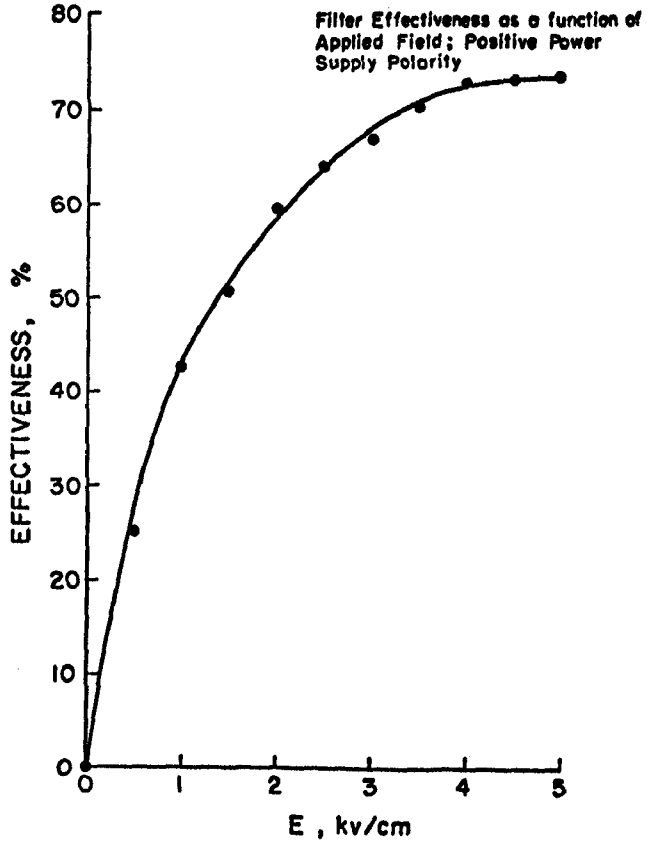

Figure 7. Filter effectivenss, ε, as a function of applied field strength.

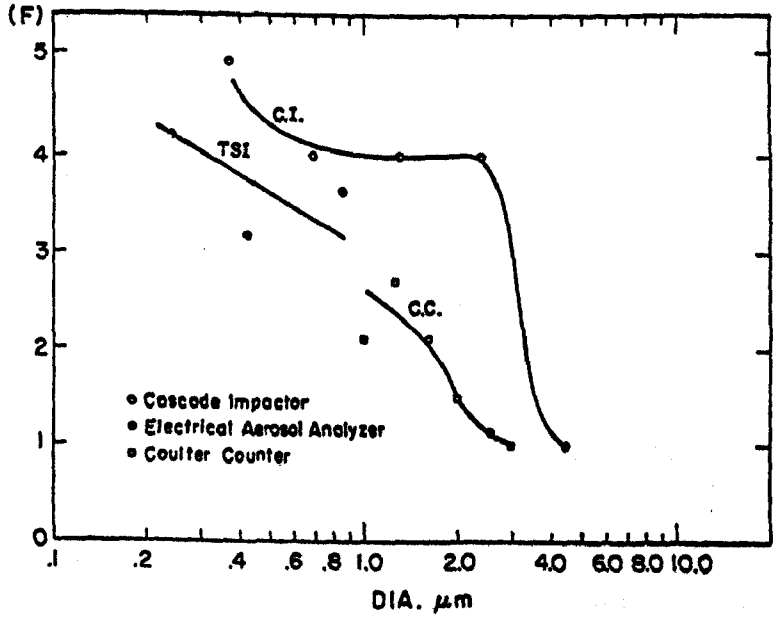

Figure 8. Factor of improvement (F) in collection of fine particles with applied field of 4 kV/cm as a function of particle size as measured with the TSI Electrical Aerosol Analyzer, the Cascade Impactor and the Coulter Counter.

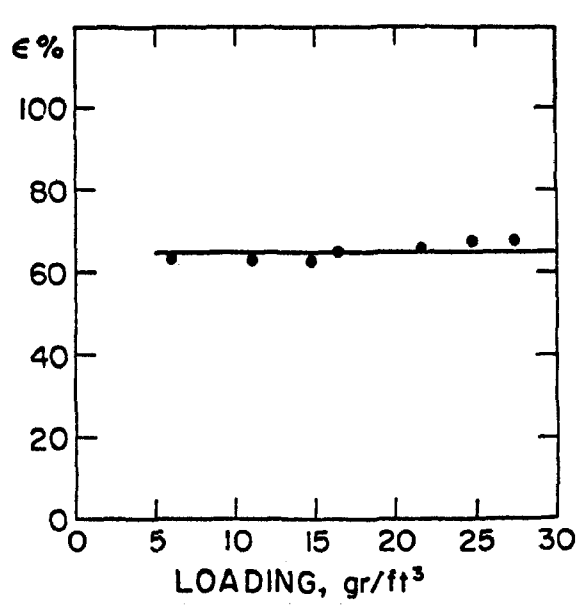

Figure 9. Filter effectiveness (ε) as a function of dust loading using an applied field of 4 kV/cm with a free stream velocity of 2 ft/sec.

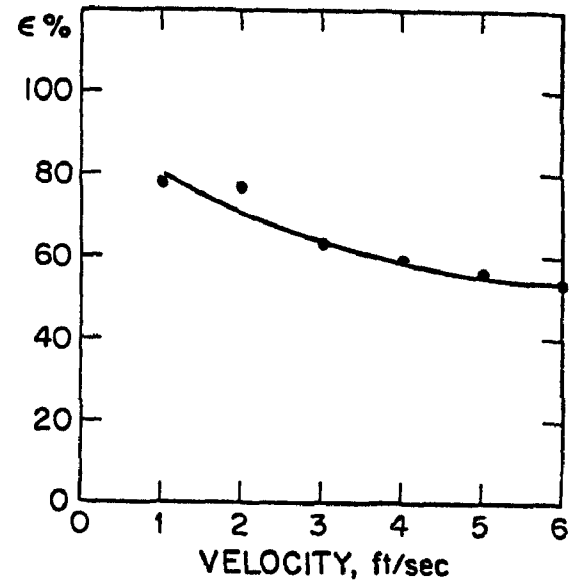

Figure 10. Filter effectiveness (ε) as a function of superficial velocity.

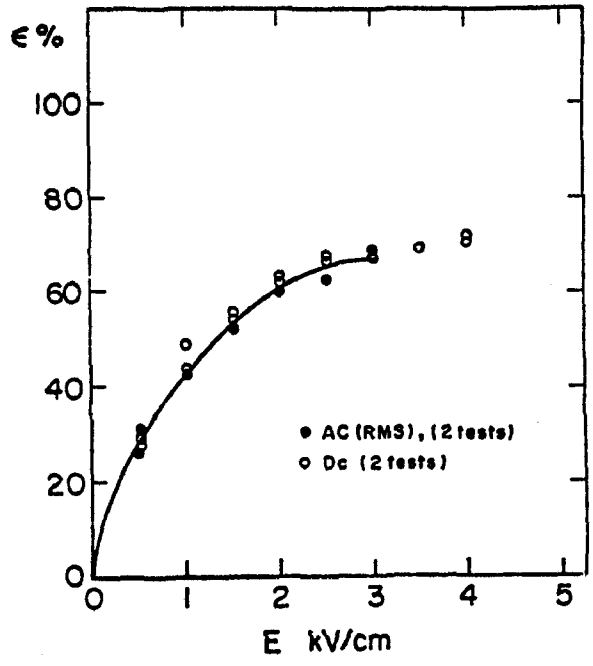

Figure 11. Comparison between AC (RMS) and DC operation of similar filters under similar conditions. Effectiveness (ε) vs. applied field.

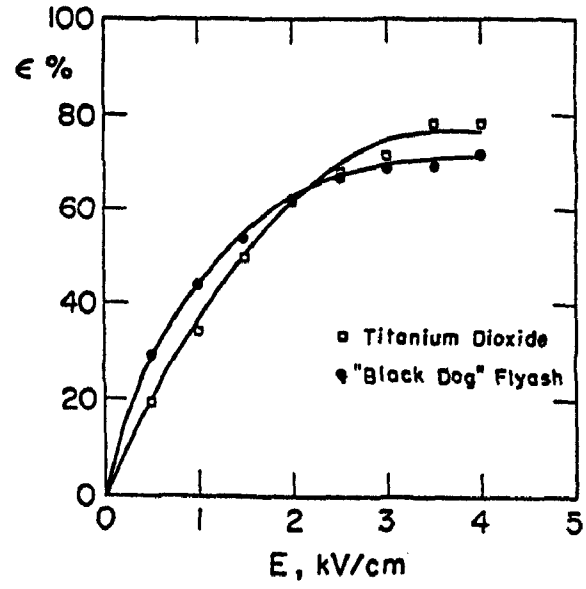

Figure 12. Comparison between filter effectiveness (ε) as a function of field strength observed with submicron titanium dioxide and Black Dog Power Station fly ash.

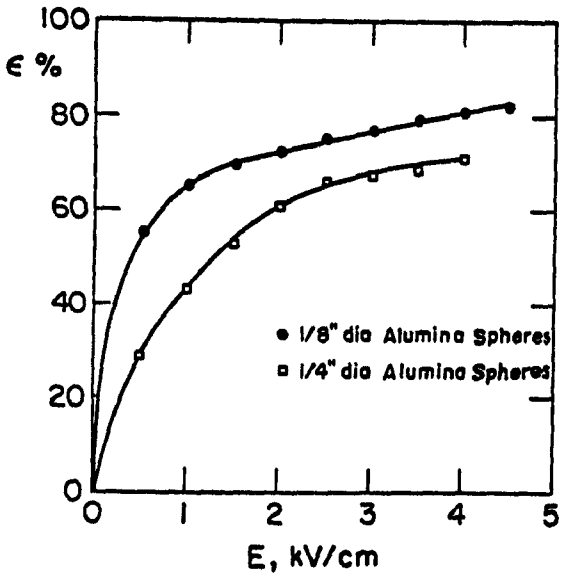

Figure 13. Effectiveness (ε) as a function of applied field with two different filter media sizes.

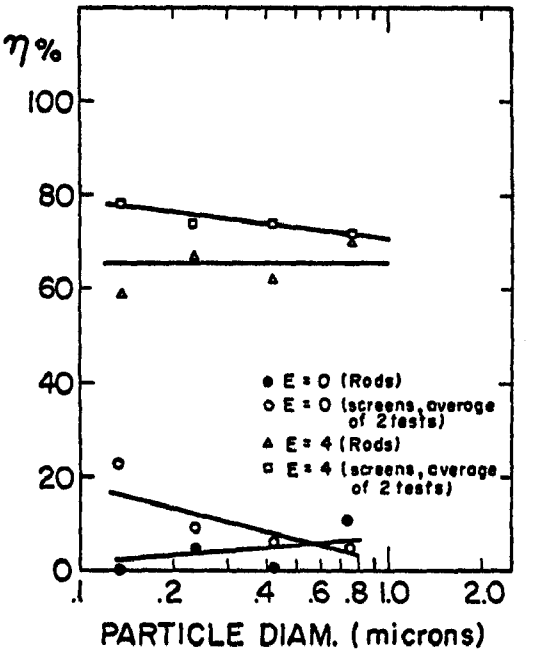

Figure 14. Filter efficiency, a comparison between rod and screen electrodes as a function of particle size.

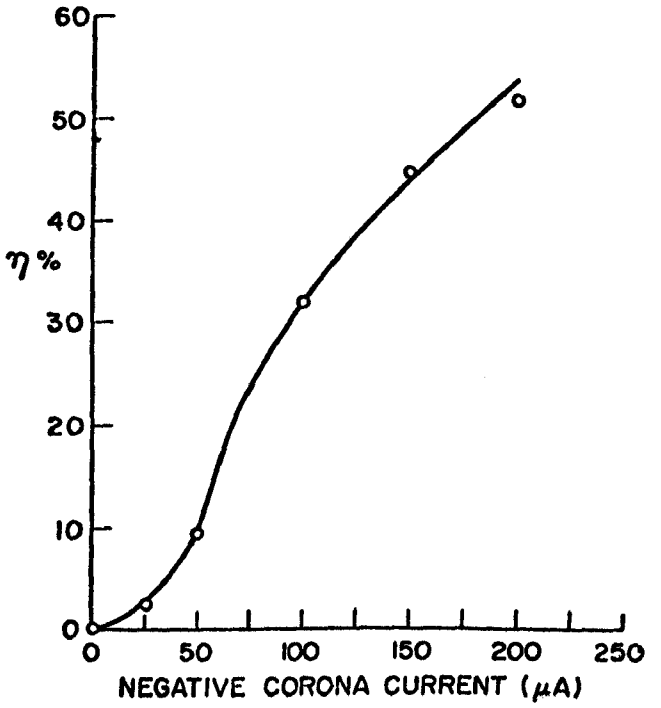

Figure 15. Charger's collection efficiency for particles between 0.24 and 1.0 μm diameter.

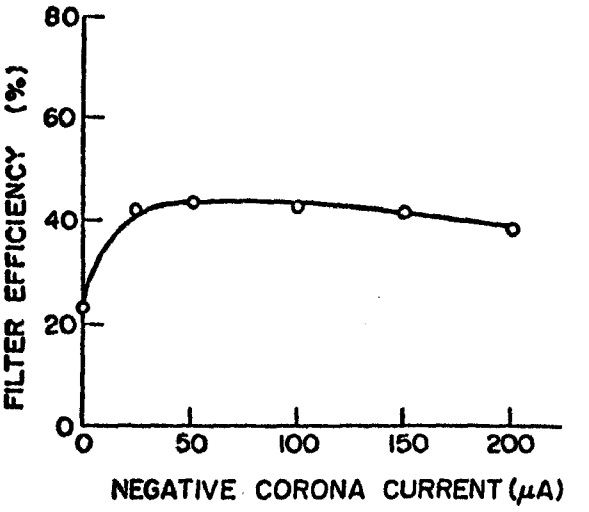

Figure 16. Filter collection efficiency as a function of precharger current. Electrodes in filter grounded. Size range of measurement = 0.25 → 1.0 μm.

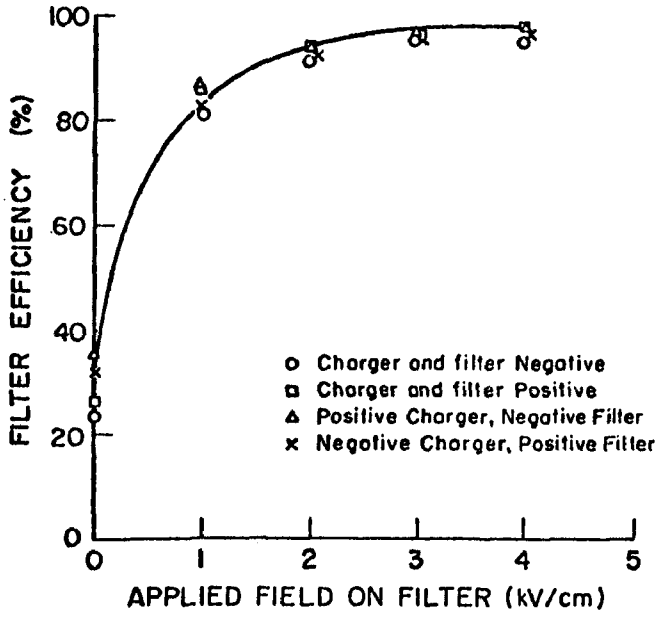

Figure 17. Filter efficiency as a function of applied field with precharged fly ash. Corona current = 50 μA. Size range of measurement = 0.24 → 1.0 μm.

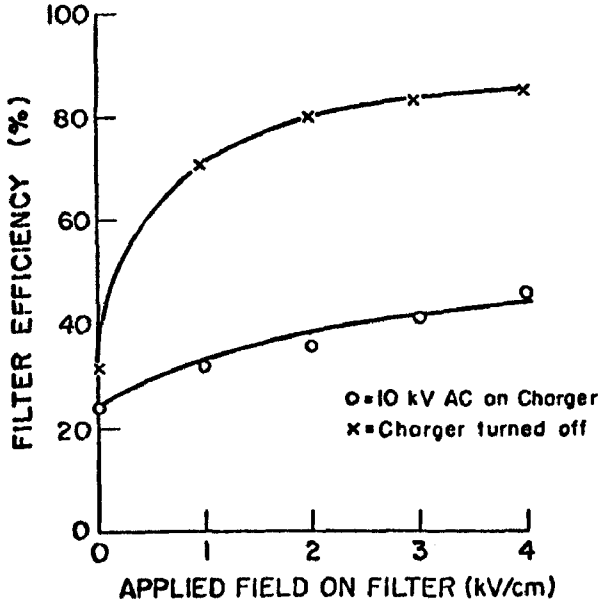

Figure 18. Efficiency as a function of applied field—comparison between neutralized and tribo-charged fly ash. Size range of measurement = 0.24 → 1.0 microns.

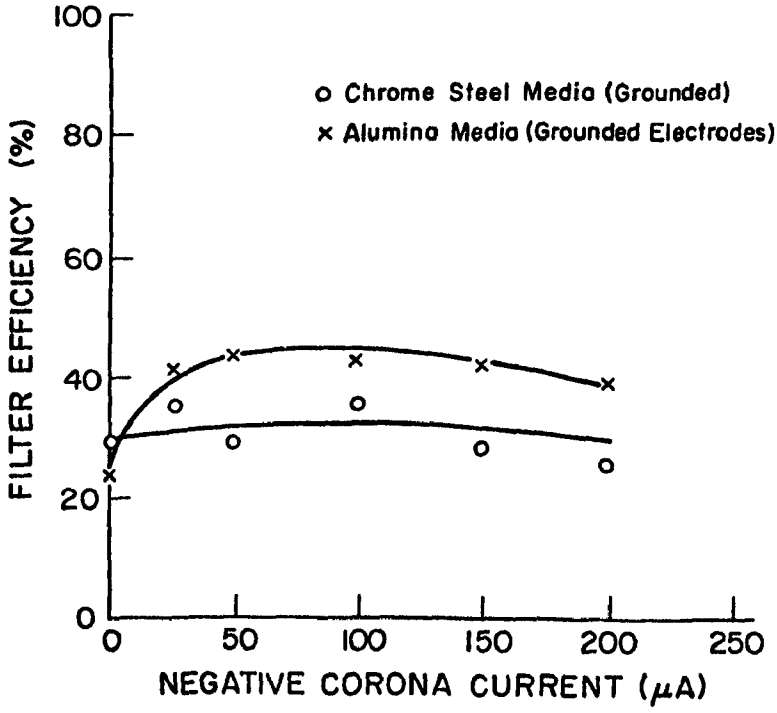

Figure 19. Filter collection efficiency as a function of charger current. Comparison between steel and alumina media (0.25"). Size range of measurement, 0.24 → 1.0 μm.

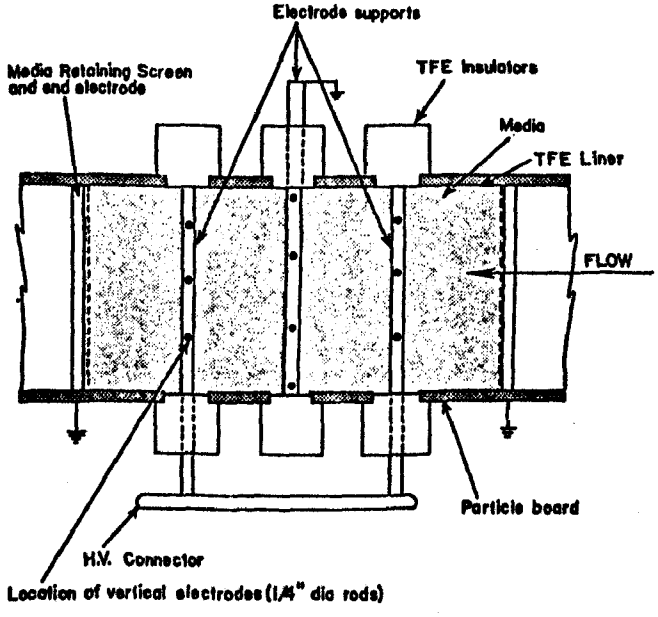

Figure 20. Top view of granular bed filter portion of test section for ESP test facility (18" long in flow direction, 29.5" high, 9.84" wide) shows location of vertical electrodes used to provide electric field.

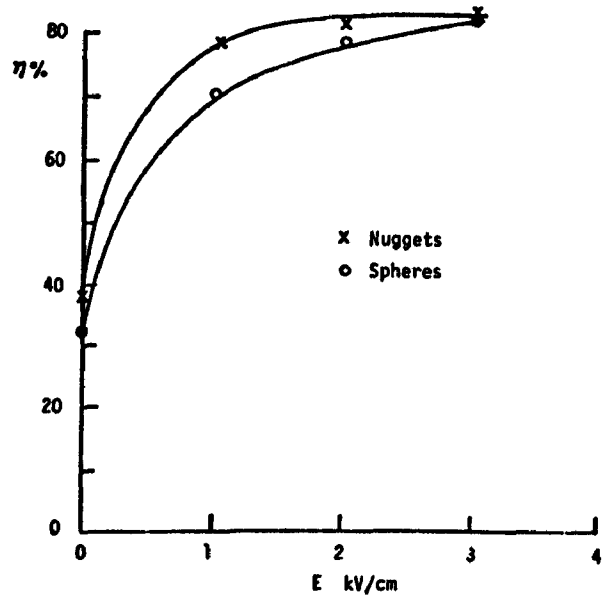

Figure 21. Comparison between alumina spheres and Aluminum Oxide Nuggets in bench scale test apparatus--submicron efficiency vs. applied electric field.

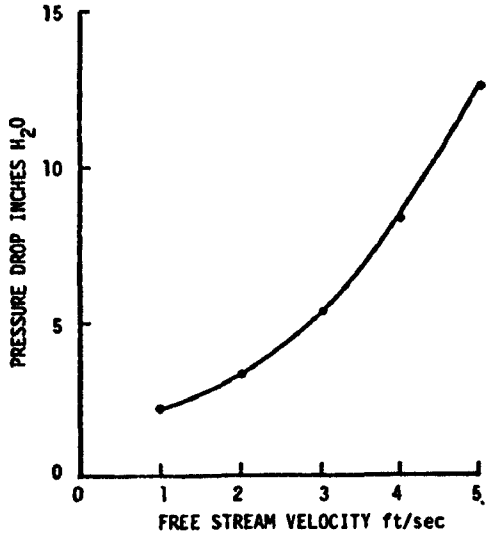

Figure 22a. Pressure drop as a function of free stream velocity in the granular bed filter in the ESP test facility.

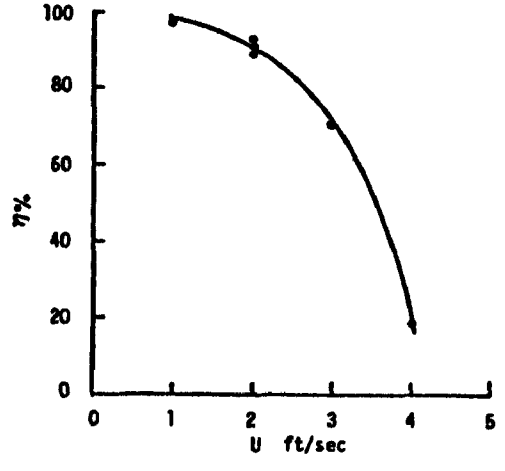

Figure 22b. Mass efficiency of granular bed filter in ESP test facility as a function of velocity.

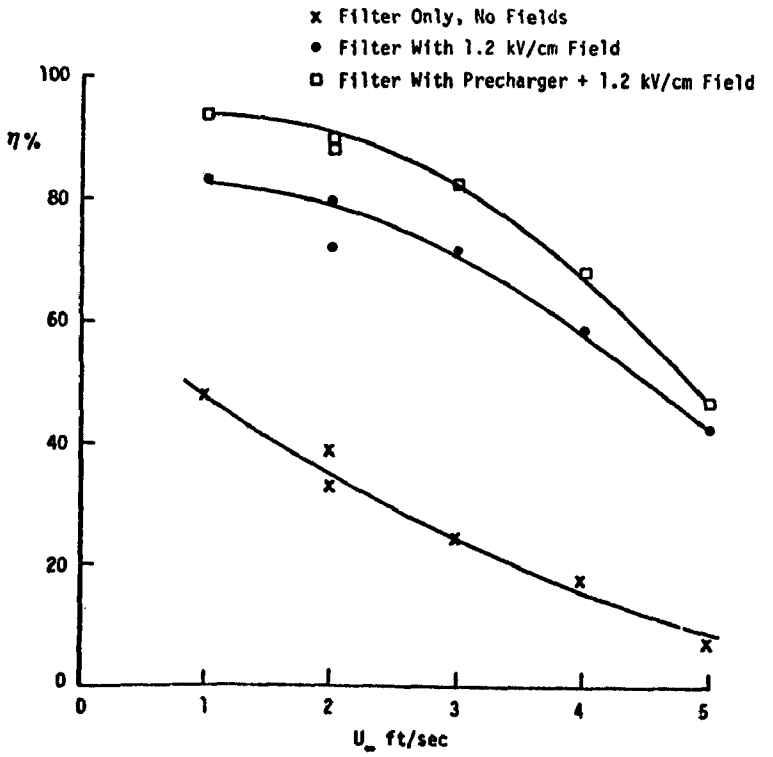

Figure 23. Comparison between baseline filter performance and electrified performance in ESP test facility for submicron particles. Efficiency vs. velocity.

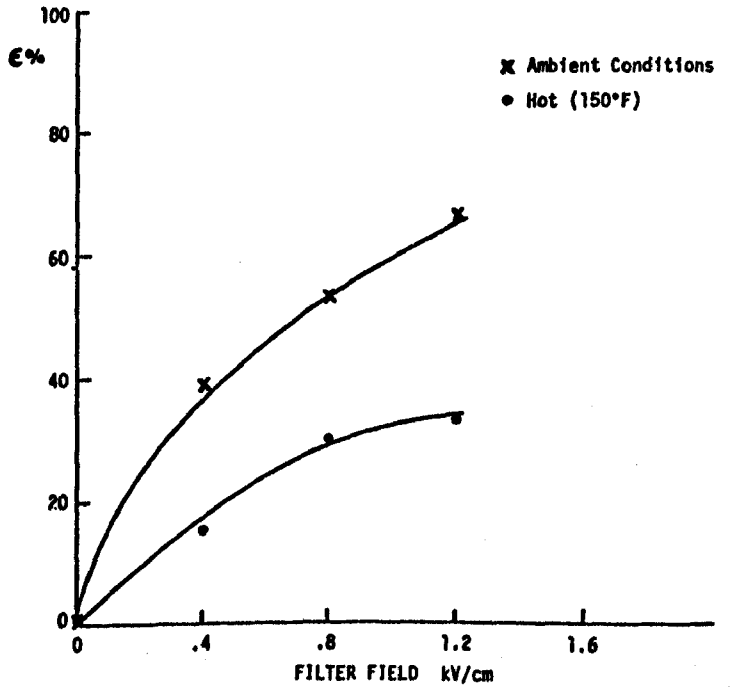

Figure 24. Filter performance in test facility with heated airstream. Shows effect of dust resistivity, hence bed current upon electrical enhancement effect. No precharger.

THEORETICAL AND EXPERIMENTAL FILTRATION EFFICIENCIES IN ELECTROSTATICALLY AUGMENTED GRANULAR BEDS

G.A. Kallio, P.W. Dietz, and C. Gutfinger*
General Electric Company
Corporate Research & Development
Schenectady, New York 12301

ABSTRACT

Filtration efficiencies for fine particles by electrically-enhanced granular beds are computed and compared with available experimental data. Collection efficiencies of a single bed sphere in a "unit cell" are calculated by numerically solving the equations of particle motion which incorporate the effects of inertial impaction, interception, and charged particulate-imposed electric field interaction in both Stokes and potential flows. The "unit cell" model enables one to include the effects of surrounding bed particles on the collection process. Total efficiency is computed by integrating the single-sphere collection efficiency over the bed volume. These calculated total bed efficiencies compare satisfactorily with data obtained from an existing granular bed facility. Both theory and experimental data show that the electrical force significantly enhances particulate collection in granular beds.

*Faculty of Mechanical Engineering, Technion - Israel Institute of Technology, Haifa, Israel

THEORETICAL AND EXPERIMENTAL FILTRATION EFFICIENCIES IN ELECTROSTATICALLY AUGMENTED GRANULAR BEDS

I. INTRODUCTION

Increasing attention is being directed toward the emission of fine particles because of their potential responsibility for adverse health effects. Since fine particles (below 5 - 10 μm in diameter) are predominantly formed by condensation, their chemical composition is often distinctly different than that of coarse particles which are usually formed by mechanical processes. For example, studies have shown that certain heavy metals are more concentrated in fine particles (Natusch and Wallace (1974)[1]). Because these fine particles pass through conventional pollution control devices uncollected and are also the most likely to be deposited in the respiratory tract, the potential for serious health problems is clearly established and air quality standards may soon be promulgated which require removal of these particles.

One device which has the demonstrated ability to remove particles as small as 0.2 μm in diameter is the electrostatically-enhanced granular bed filter or electrofluidized bed (EFB) (Zahedi and Melcher (1976, 1977)[2,3]; Zahedi (1976)[4]). The fundamental mechanism responsible for this high collection efficiency can be easily understood. Before entering the EFB, the fine particles are electrically charged. Upon entering the bed, the particles experience an electrical force due to the electric field between the particles. Essentially, the bed particles act like the plates of miniature electrostatic precipitators (ESPs). As can easily be seen from the classic Deutsch equation for ESP performance, the consequence of many small ESPs is high efficiency.

Numerous authors (Whipple and Chalmers (1944)[5]; Kraemer and Johnstone (1955)[6]; George and Poehlein (1974)[7]; Nielsen and Hill (1976)[8]) have studied the electrostatically-enhanced collection of fine particles on isolated spherical collectors. In 1976, Zahedi proposed a model for the collection of charged fine particles in a granular bed with an imposed electric field. This model assumed that each particle in the granular bed acted like an isolated sphere and, thus, its collection could be modeled by the Whipple and Chalmers result. Recently, Dietz (1979)[9] developed an analytic model for the collection of fine (inertialess) particles in a granular bed with an imposed electric field. This model is based on the identification of a "single filter element" or "unit cell" which consists of a single bed particle and the adjacent gas. The flow in the vicinity of this element is then calculated and single element efficiencies are computed. The overall efficiency of the granular bed can thus be obtained by integrating over all of the collecting bed particles.

This general approach to modeling the flow through granular beds has been employed by Happel (1958)[10] and Kuwabara (1959)[11] to predict the pressure

drop through granular beds, and by Gutfinger, Tardos, and Abuaf (1974, 1978, 1979)[12,13,14] to predict the mechanical collection of fine particles by granular beds.

In the present paper, the concept of a unit-cell is employed to predict the collection of inertial particles in an electrified granular bed. The differential equation describing the motion of fine particles is numerically integrated based on assumed fluid flow models. The resultant particle trajectories are used to compute single element efficiencies and, subsequently, overall bed efficiencies.

The results of these calculations are compared with data obtained by Alexander (1978)[15]. In conclusion, model extentions are suggested future work.

II. THEORY

A. Equation of Motion

The equation of motion for a solid, spherical, fine particle of radius r_p and mass density ρ_p in a gas flow can be approximated as

$$\frac{4}{3}\pi r_p^3 \rho_p \frac{d\bar{V}}{dt} = 6\pi\mu r_p (\bar{U} - \bar{V}) + \bar{F}^e \qquad (1)$$

where $\bar{U}$ = local gas velocity
$\bar{V}$ = fine particle velocity
μ = gas viscosity
$\bar{F}^e$ = arbitrary electrical force

The assumptions and considerations incorporated into Eq. (1) are:

1) The mass of the displaced gas is negligible;

2) Stokes drag law is valid ($Re_p < 1$);

3) The fine particles do not perturb the gas streamlines;

4) The fine particles are large enough that mass diffusion, or Brownian movement, can be neglected;

5) Gravity is neglected.

B. Bed Model

The granular bed is modeled as a homogeneous assemblage of equal "cells"; each cell consisting of a bed particle of radius a_2 surrounded by a concentric shell of gas with radius ℓ (Tardos, et al, (1974)[12]). See Figure 1. The effect of void fraction upon filtration is incorporated into the model by prescribing the shell radius ℓ to be such that the void fraction within the

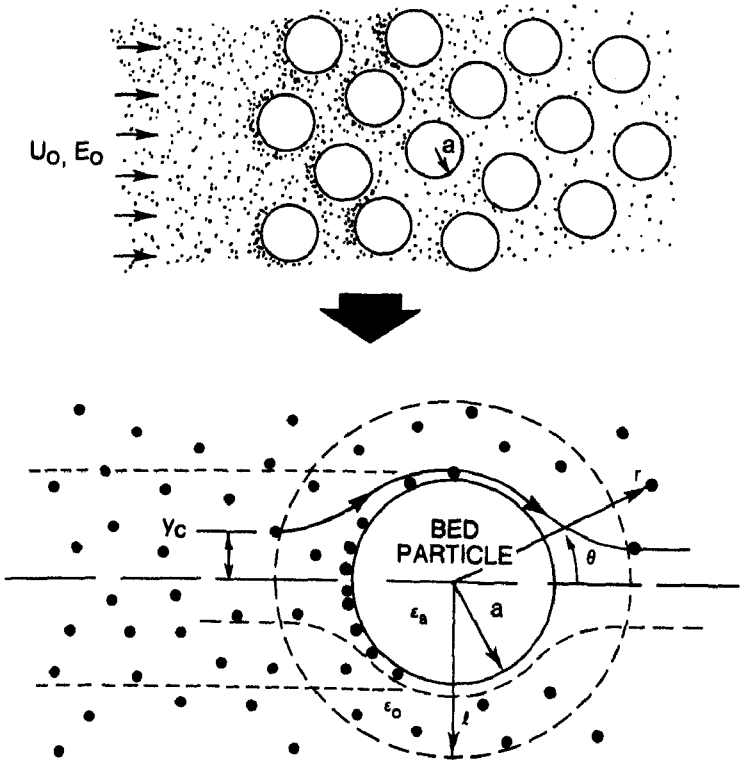

Figure 1. Unit cell model for granular bed.

cell equals the average void fraction α of the bed:

$$\ell = a(1-\alpha)^{-1/3} \tag{2}$$

In this way, the effect of neighboring bed particles upon the collection rate can be modeled. Also, this approach establishes a boundary at which initial conditions can be set without having to specify the location of all the bed particles.

C. Gas Flow Models

The gas flow throughout the bed is assumed laminar. Two velocity fields ($\bar{U}$) are used in Eq. (1): Stokes flow ($Re_a << 1$) and potential flow (zero vorticity, $Re_a >> 1$) for which the corresponding axisymmetric stream functions have been derived by Kuwabara (1959)[11] and Lamb (1945)[16]:

Stokes flow

$$\psi = (A/r + Br + Cr^2 + Dr^4) \sin^2\theta \tag{3}$$

where $A = \frac{-U_o a^3}{4k}\left(1 - \frac{2a^3}{5\ell^3}\right)$ (4a)

$B = \frac{3U_o a}{4k}$ (4b)

$C = \frac{-U_o}{2k}\left(1 + \frac{a^3}{2\ell^3}\right)$ (4c)

$D = \frac{3U_o a}{20\ k\ell^3}$ (4d)

and $k = \frac{1}{5}\left(\frac{a}{\ell}\right)^6\left[5\left(\frac{\ell}{a}\right)^6 - 9\left(\frac{\ell}{a}\right)^5 + 5\left(\frac{\ell}{a}\right)^3 - 1\right]$ (4e)

Potential flow

$$\psi = \frac{-U_o}{2}\left(\frac{\ell^3}{\ell^3 - a^3}\right)\left(r^2 - \frac{a^3}{r}\right)\sin^2\theta \quad (5)$$

Figure 1 displays the coordinate system employed in the analyses. The components of the gas velocity are given by

$$u_r = -\frac{1}{r^2 \sin\theta}\frac{\partial \psi}{\partial \theta} \quad (6a)$$

$$u_\theta = \frac{1}{r \sin\theta}\frac{\partial \psi}{\partial r} \quad (6b)$$

D. Electrical Force Model

The electrical force ($\overline{F}^e$) is due to a uniform external electric field of strength E_o interacting with electrically charged fine particles and neutral bed particles. A voltage is applied across the granular bed between two parallel grids to create the field which is defined to be collinear with the superficial gas flow. The imposed field polarizes the bed particles (i.e., induces a charge separation) to produce an attractive force between the charged fine particles and the leading hemispheres of the bed particles. The following assumptions apply:

1) The bed particles are semi-insulating, and retain a zero net charge;

2) Space charge effects due to the charged fine particles are negligible;

3) The image force between charged particles and neutral collectors is neglected;

4) Dipole interactions are neglected.

The particulate efflux is charged by a high voltage corona source prior to entering the bed. For this analysis, the fine particles are assumed to

be conducting and charged to saturation (Melcher and Sachar (1974)[17]), thus:

$$q_p = 12\pi\epsilon_o r_p^2 E_c \tag{7}$$

where q_p is the charge acquired by one particle and E_c is the corona charging electric field strength. Therefore, the total electrical force experienced by a fine particle is

$$\overline{F}^e = q_p \overline{E}(r,\theta) \tag{8}$$

where $\overline{E}(r,\theta)$ is the local (intensified) electric field within the bed.

The derivation of $\overline{E}(r,\theta)$ for the cell model is analagous to that of the gas flow field. Specifying the potential, Φ, on the surface of the unit cell to be the average potential at that position, the potential within the cell can be computed:

$$\Phi = \frac{E_o}{3+\alpha(K-1)} \left[(K+2)r - (K-1)r^{-2}\right]\cos\theta \tag{9}$$

where $K = \epsilon_a/\epsilon_o$. The corresponding electric field components are given by:

$$E_r = -\frac{\partial \Phi}{\partial r} \tag{10a}$$

$$E_\theta = -\frac{1}{r}\frac{\partial \Phi}{\partial \theta} \tag{10b}$$

E. Normalization

The mathematics can be more easily managed by normalizing all distances with respect to a, all velocities with respect to U_o, and the electric field with respect to E_o, for example

$$\overline{V} = U_o \overline{V}^* \tag{11a}$$

$$\overline{U} = U_o \overline{U}^* \tag{11b}$$

$$\overline{E} = E_o \overline{E}^* \tag{11c}$$

$$r = ar^* \tag{11d}$$

therefore

$$t = at^*/U_o \tag{11e}$$

Eq. (1) can now be written concisely as two coupled second-order differential equations to describe the trajectory of a fine particle:.

Radial

$$\frac{dv_r^*}{dt^*} = (u_r^* - v_r^*)/St + GE_r^* \tag{12a}$$

Tangential

$$\frac{dv_\theta^*}{dt^*} = (u_\theta^* - v_\theta^*)/St + GE_\theta^* \qquad (12b)$$

where

$$St = \frac{2}{9}\,\frac{\rho_p r_p^2 U_o}{\mu a} \qquad (13)$$

$$G = 9\,\frac{\varepsilon_o a E_c E_o}{\rho_p r_p U_o^2} \qquad (14)$$

The Stokes number, St, is a dimensionless quantity which relates the ratio of the fine particle's inertia to the viscous drag it experiences. Therefore, a large, dense particle would correspond to a high Stokes number. The dimensionless electrical parameter, G, relates the ratio between the electrical force and inertial force on the fine particle. These two parameters play an important role in describing the particles' trajectory.

III METHOD OF SOLUTION

A. Initial Conditions

In order to compute the trajectory of a given fine particle approaching a bed particle, initial velocity conditions must be imposed at the cell boundary $r = \ell$. Here the velocity of a fine particle is assumed to be equal to the sum of the local gas velocity and the velocity due to electrical attraction:

$$\overline{V} = \overline{U} + b\overline{E} \quad \text{at } r = \ell \qquad (15)$$

where b is the fine particle's electrical mobility, defined as

$$b = \frac{q_p}{6\pi\mu r_p} \qquad (16)$$

This statement is equivalent to neglecting acceleration in Eq. (1). Incorporating normalized quantities, Eq. (15) becomes:

$$\overline{V}^* = \overline{U}^* + (St)(G)\overline{E}^* \quad \text{at } r = \ell \qquad (17)$$

B. Collection Efficiency

Collection, or capture, of a fine particle is assumed to occur when it contacts the surface of a bed particle. Thus, since the fine particles are of a finite size, any particle whose trajectory passes within one radius (r_p) of the surface of the bed particle is collected. The "critical trajectory"

is defined to be that trajectory which just grazes the bed particle. This trajectory is characterized by the initial height, y_c, at which it enters the cell (see Figure 1). All fine particles entering the cell within y_c are collected (a "capture window"), while those entering beyond y_c are swept around the bed particle. Since the particulate flux is assumed to be uniform upon entering the unit cell, the single-sphere collection rate, Γ, can be computed by

$$\Gamma = n_o U_o \pi y_c^2 \tag{18}$$

where n_o is the inlet concentration density of the fine particles. A single-sphere collection efficiency, η', can be defined as the ratio of this collection rate to the total rate at which particles would pass through the area occupied by the bed particle in its absence. Thus

$$\eta' = \Gamma / n_o U_o \pi a^2 = y_c^2 / a^2 \tag{19}$$

Then, the single-sphere efficiency can be directly computed once the critical trajectory height, y_c, has been found from the governing differential equations (Eqs. (12a) and (12b)). Since these equations are highly non-linear, they have been numerically integrated on the computer using a Kutta-Merson predictor-corrector routine.

Figures 2, 3 and 4 show computer-drawn trajectories (pathlines) of fine particles approaching the leading hemisphere of the bed particle. Each figure demonstrates a particular collection mechanism that has been accounted for in the efficiency calculations. In Figure 2, no electrostatics are applied and the fine particles are assumed inertialess, so their trajectories identically follow the gas flow streamlines. Collection can only occur in such a case when the fine particles follow streamlines which pass within one radius (r_p) of the surface of the bed particle. This mode of collection is termed "interception" and dominates at low Stokes numbers. Note that the subsequent capture window is quite small. Figure 3 shows how the trajectories of fine particles with finite inertia deviate from the gas flow. Such collection is called inertial impaction, which generally leads to greater efficiencies than interception. In Figure 4, an external electric field is applied. Charged particles will follow these attractive trajectories in the absence of gas flow. Note that the capture window is large, resulting in single-sphere collection efficiencies that may exceed 1.0.

Once the single-sphere efficiency has been determined for a particular situation, the collection efficiency of the entire bed, η, can be computed. An expression for η is derived by equating the change in particulate flux across a thin bed layer to the collection rate of the enclosed bed particles as determined by η' (Dietz, (1979)[9]). Integration of the resulting differential equation over the bed length L yields

$$\eta = 1 - \exp\left[-\frac{3(1-\alpha)}{4a} \eta' L \right] \tag{20}$$

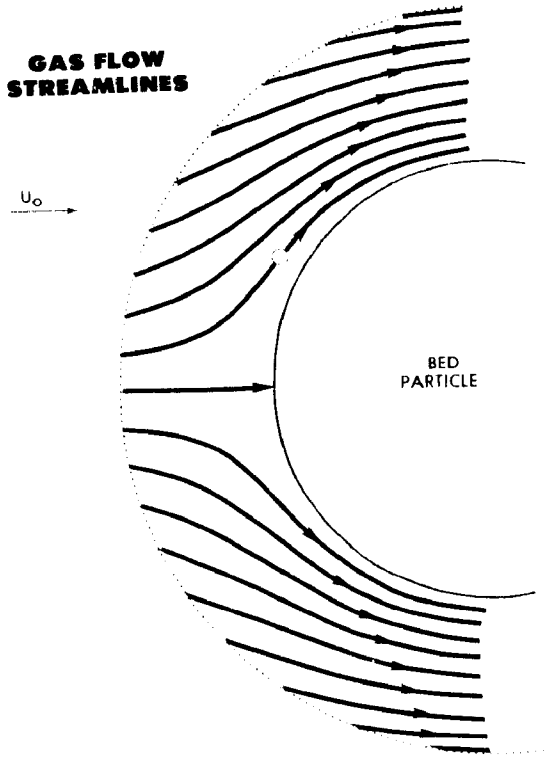

Figure 2. Trajectories of inertialess fine particles for Stokes flow.

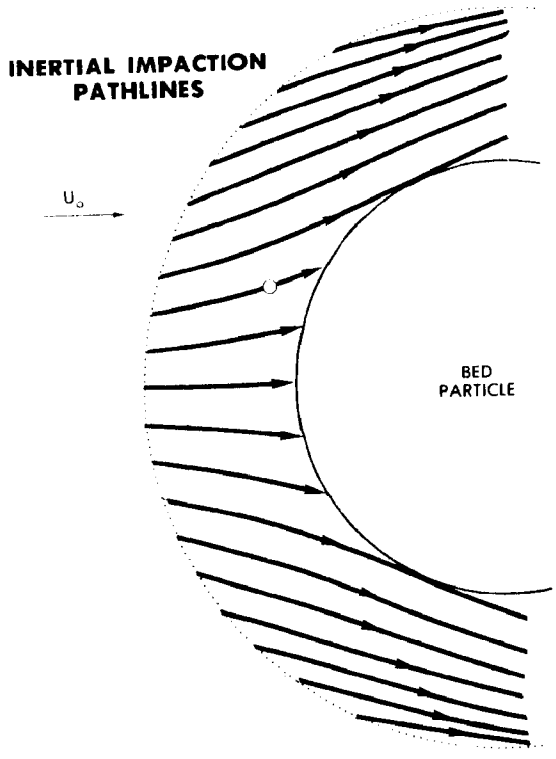

Figure 3. Trajectories of inertial fine particles for Stokes flow.

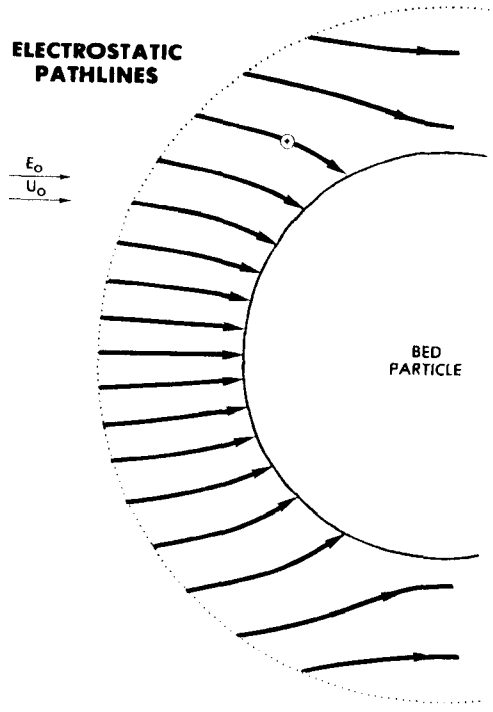

Figure 4. Trajectories of charged fine particles with an applied electric field.

IV. RESULTS AND DISCUSSION

A. Theory

Figures 5 and 6 display single-sphere collection efficiencies as a function of Stokes number for both Stokes and potential flow models. The effectiveness of the various collection mechanisms — interception, inertial impaction, and electrostatic attraction — can be seen. The ratio r_p/a indicates the extent to which interception plays a role. For $r_p/a = 0.001$, corresponding to the lower curve in both figures, interception is essentially nonexistent and thus inertial impaction is the only collection mode. When $r_p/a = 0.05$, interception does indeed become significant — being dominant at low St as shown by the middle curves. One might expect lowest efficiency when $St \to 0$, however, a minimum is observed between St = 0.01 and 0.1. For these Stokes numbers, computer results show that a fine particle traveling along the critical trajectory closely follows the gas streamlines as it starts to accelerate around the bed particle. However, at some point beyond the inflection of the trajectory, the fine particle's inertia becomes great enough in the accelerating gas flow that it deviates from the gas flow and moves away from the bed particle. Consequently, lower collection efficiencies are predicted.

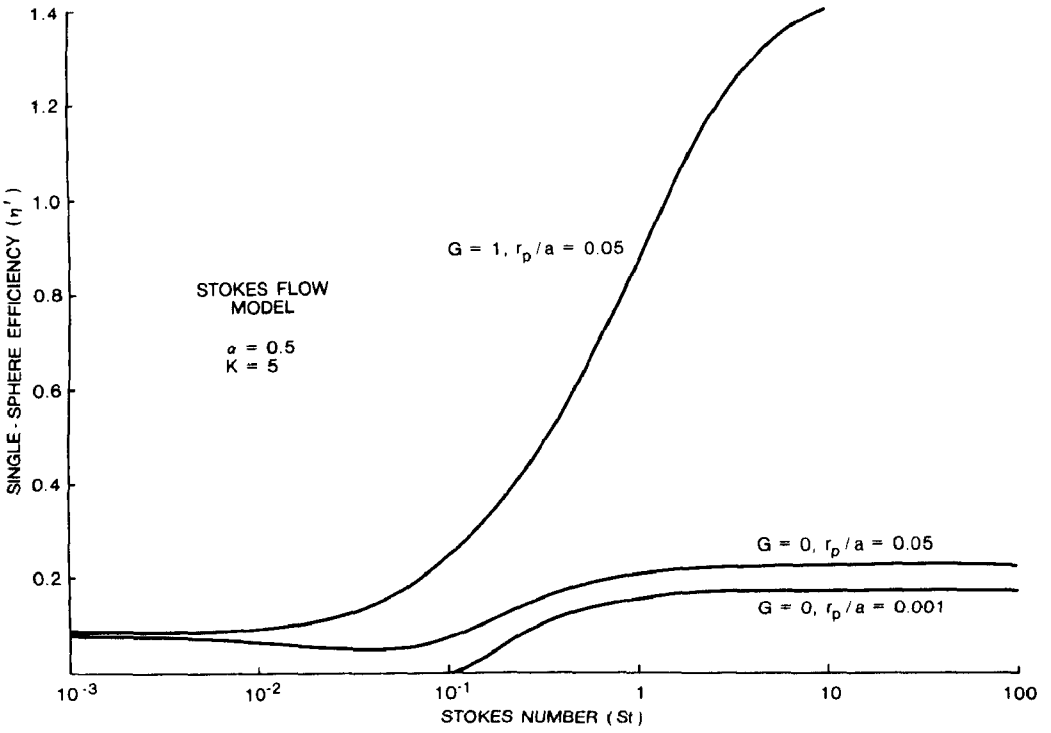

Figure 5. Single-sphere efficiency vs. Stokes number for Stokes flow.

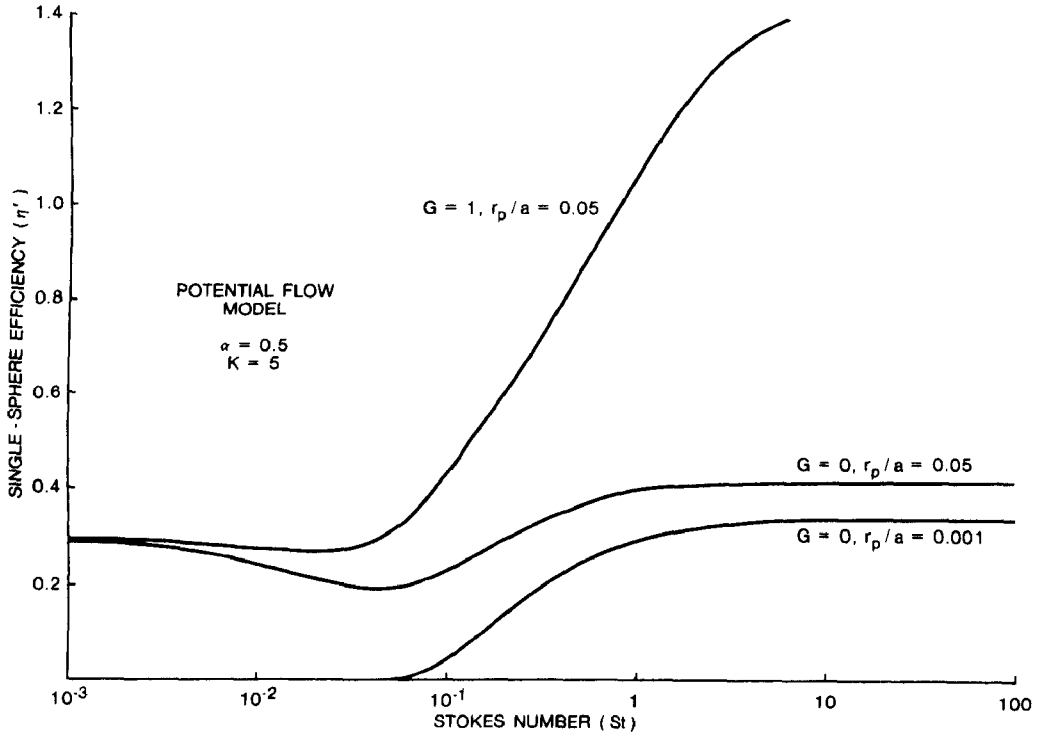

Figure 6. Single-sphere efficiency vs. Stokes number for potential flow.

The upper curves of Figures 5 and 6 show the significant enhancement that an external electric field can incur upon the collection of charged particles. The degree of electrical attraction is quantified by G, where G = 1 represents a typical situation. Note that η' exceeds 1.0 for large values of the Stokes number. Also note that the minimum discussed previously is essentially masked out by the electrostatic effects.

The single-sphere efficiencies obtained for potential flow are consistently higher than those using Stokes flow. This is due to the fact that potential flow predicts higher local gas velocities in the vicinity of the bed particle. Consequently, both inertial impaction and interception are increased. Therefore, collection efficiencies are sensitive to the choice of flow solution, with Stokes flow and potential flow setting the lower and upper limits, respectively, to efficiency. Stokes flow should be applied where $Re_a < 1$ and potential flow applied where $Re_a \gtrsim 50$. Intermediate Reynolds numbers are better approximated by Oseen flow and other solutions (Gutfinger, et al (1979)[14]).

Since St, G, and r_p/a contain common terms, Figures 5 and 6 are difficult to use to predict the sensitivity of collection efficiency to certain parameters. Figures 7 and 8 show <u>total</u> bed efficiency (Eq. (20)) plotted versus fine particle radius with and without an applied electric field. Here, bed parameters have been specified and trends can be better observed. Besides fine particle radius and electric field strength, the dependence of collection efficiency upon bed particle radius and superficial gas velocity has been shown also. In both figures, the potential flow solution has been used to model the local gas velocity. Reynolds number (Re_a) ranges from 1 to 50 for the bed values specified. Therefore, the efficiencies presented in Figures 7 and 8 can be considered "best-case" predictions based upon the flow model.

There are several important trends that these plots reveal:

1) Predicted efficiencies are 0.99+ for fine particles with radii greater than 2 μm.

2) Below 2 μm, the unelectrified bed shows drastically reduced efficiencies. This drop is characteristic of such beds due to the rapid onset of collection by inertial impaction for St > 0.1.

3) Collection efficiency is dramatically enhanced in the submicron range by the application of an electric field and the charging of fine particles. In fact, 0.99+ efficiency is predicted throughout the 0.1 μm to 10 μm size range for moderate-to-high field strengths.

4) A bed consisting of smaller particles is more efficient.

5) A <u>lower</u> superficial gas velocity enhances collection in an electrostatically-dominated bed due to an increased residence time of the charged fine particles (note that G is proportional to U_o^{-2}).

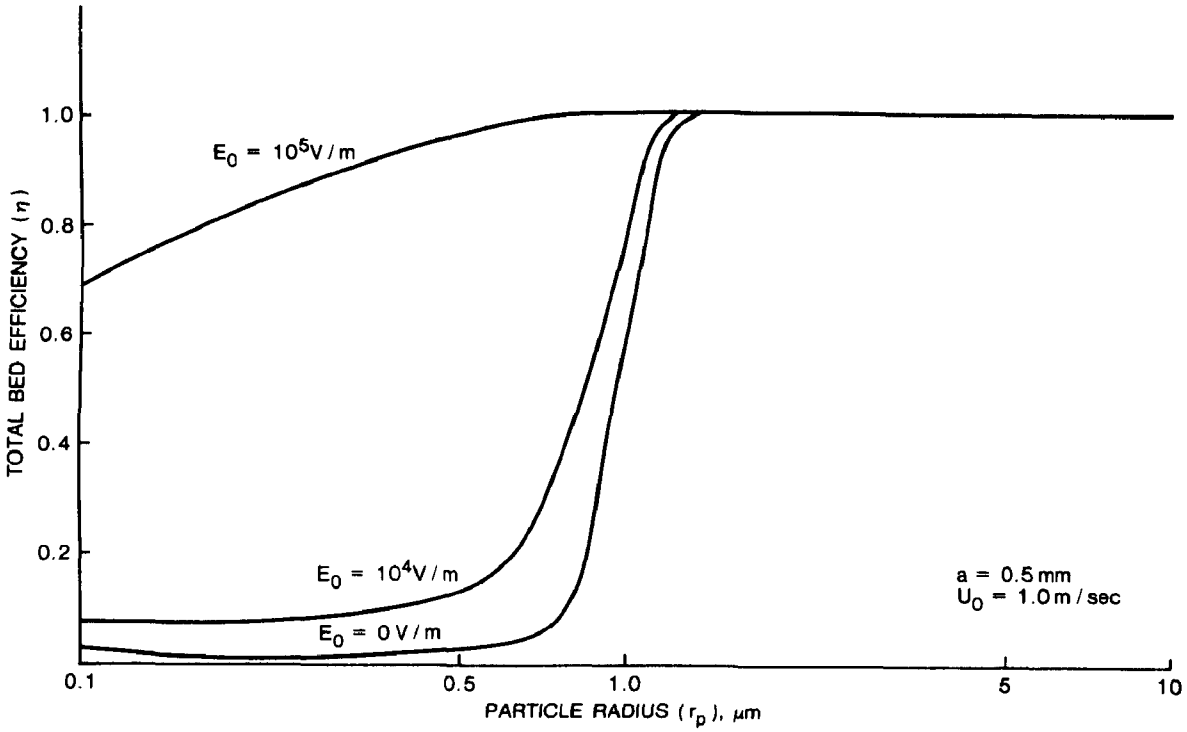

Figure 7a. Overall bed efficiency vs. fine particle radius.

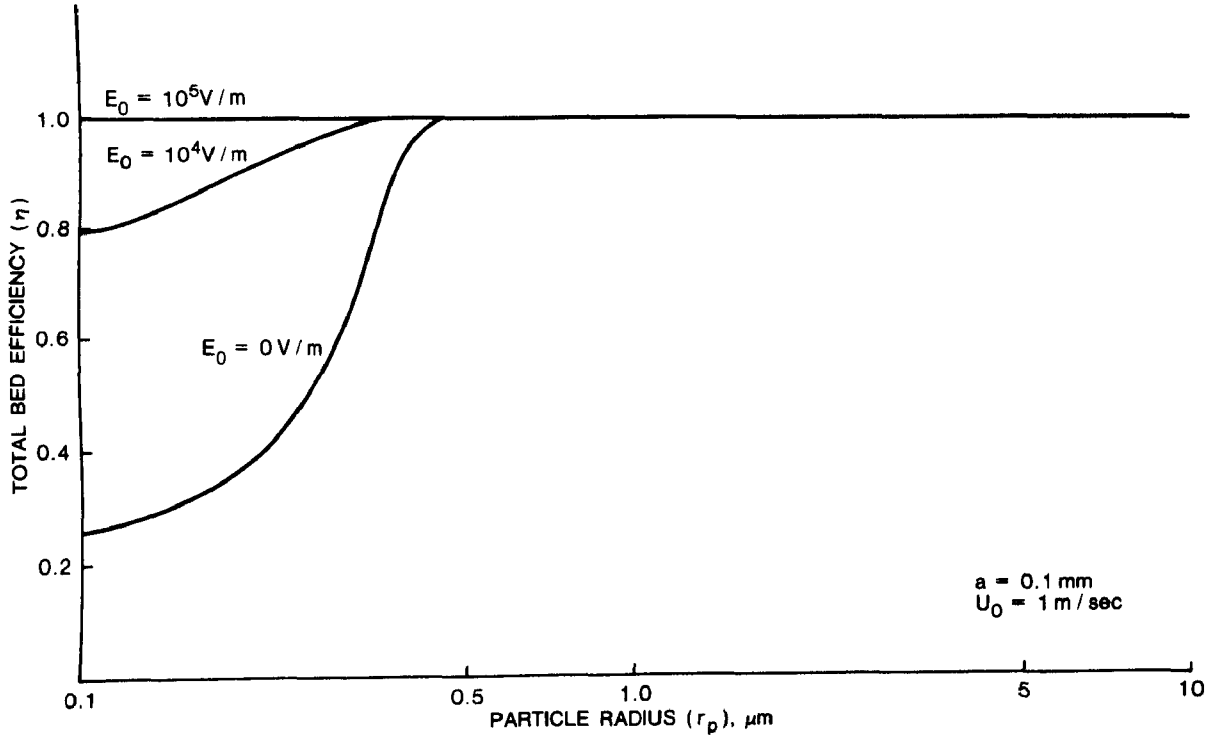

Figure 7b. Overall bed efficiency vs. fine particle radius.

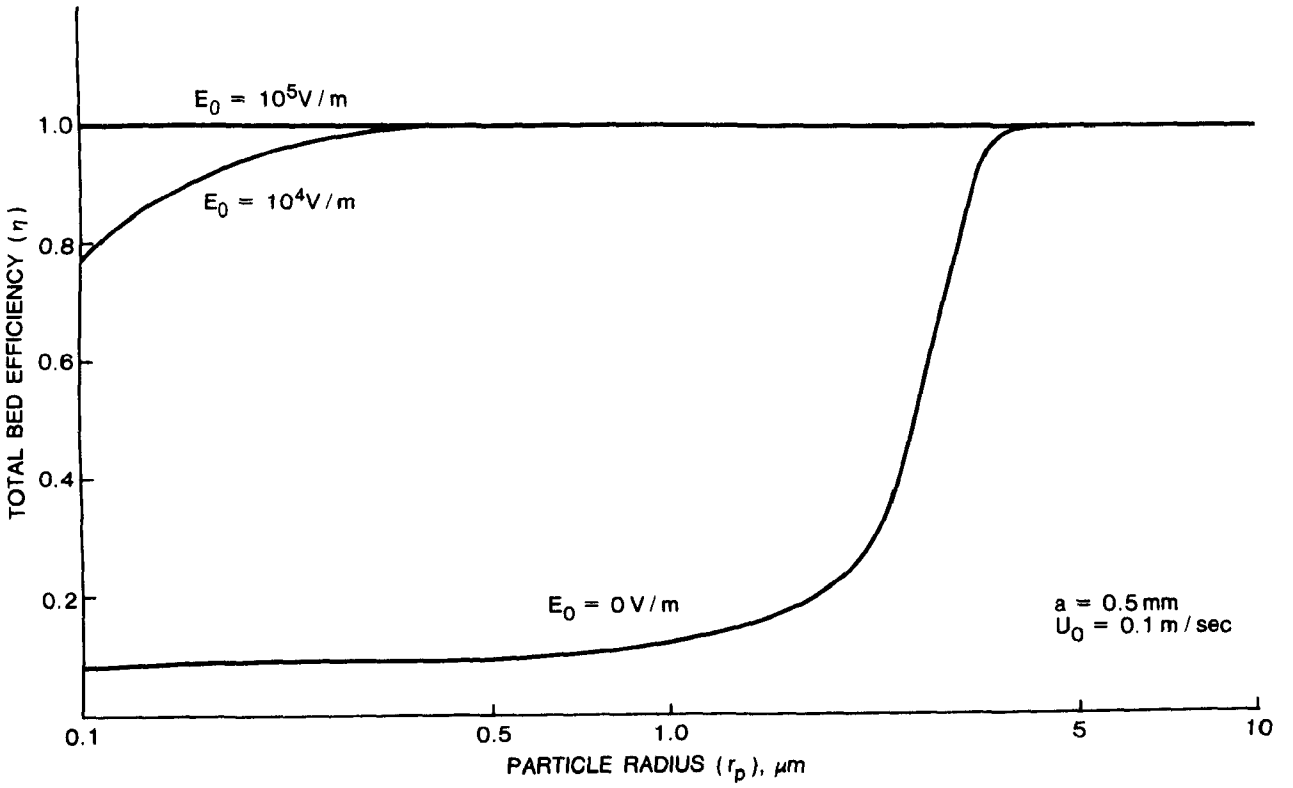

Figure 8a. Overall bed efficiency vs. fine particle radius.

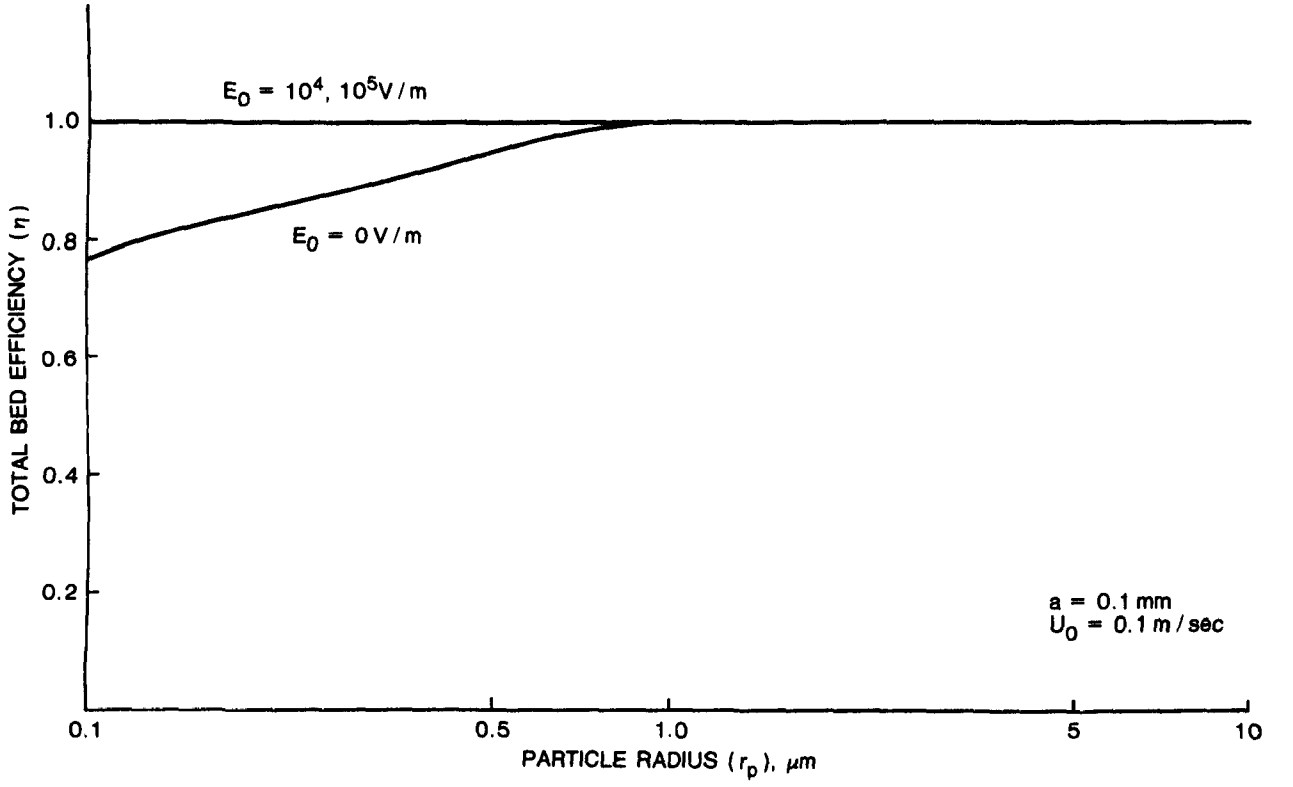

Figure 8b. Overall bed efficiency vs. fine particle radius.

6) A lower gas velocity in a mechanically-dominated bed (inertia and interception) usually decreases collection efficiency; however, if the bed is operating near the minimum in Figure 6, an increase in efficiency may be obtained.

Parameter values used in Figures 7 and 8 are:

$$L = 10 \text{ cm}$$
$$\alpha = 0.5$$
$$E_c = 5 \cdot 10^5 \text{ V/m}$$
$$K = 5$$
$$\rho_p = 2 \cdot 10^3 \text{ kg/m}^3$$
$$\mu = 2 \cdot 10^{-5} \text{ kg/m} \cdot \text{sec}$$

B. Data Correlation

Figure 9 displays electrofluidized bed data taken independently at MIT by Alexander (1978)[15]. In these experiments, monodisperse aerosols of liquid dioctylphthalate (DOP) were collected in granular beds of New Jersey sand and efficiencies were measured with a TSI mass monitor. The use of a liquid aerosol insured adhesion to the bed particles, thus, no reentrainment could occur. Uniform DOP droplets were generated by nebulization and optically sized. The droplets were charged by ion impact and electrical mobilities measured by a small, laminar-flow ESP. An electric field was applied collinear to the fluid flow with a series of screen electrodes placed across the bed.

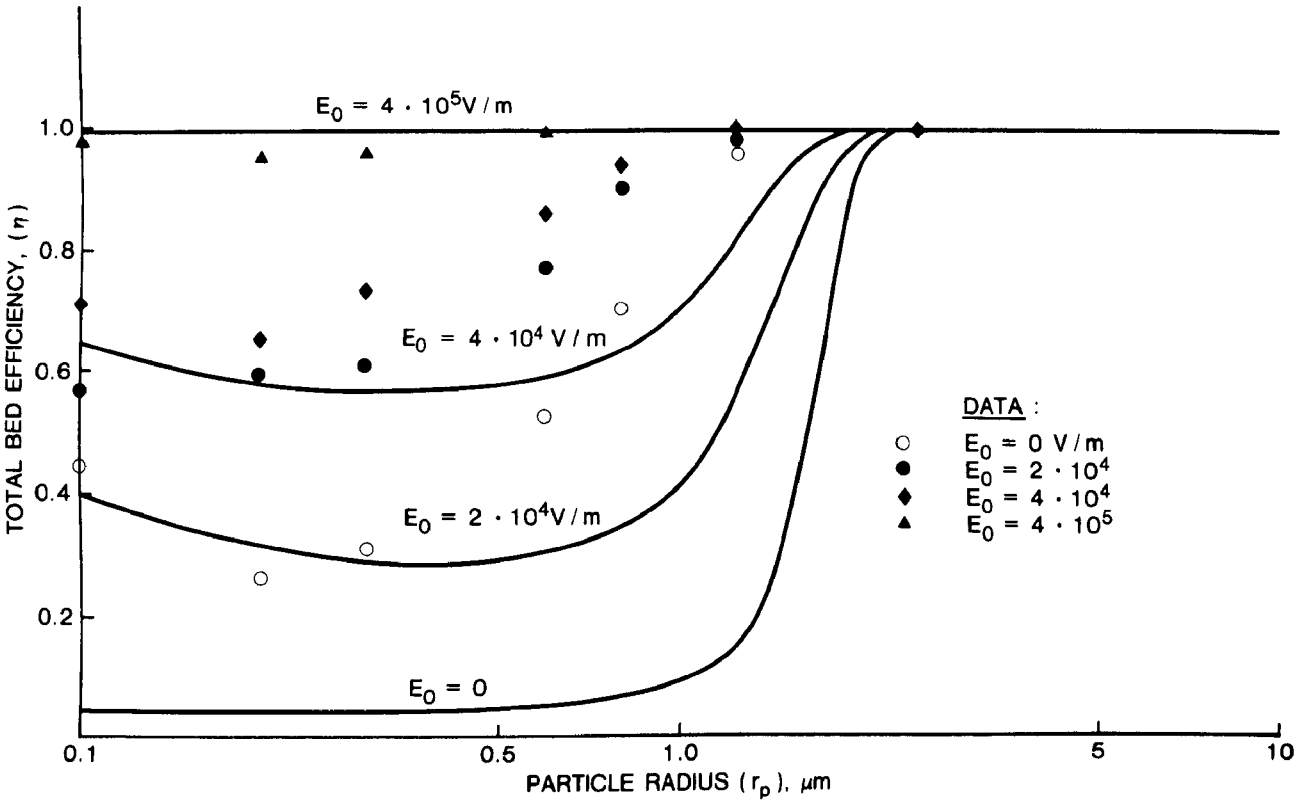

Figure 9. Alexander's EFB data correlation.

The efficiency data shown in Figure 9 is plotted versus fine particle (aerosol) radius as in Figures 7 and 8 with applied electric field as a parameter. The experimental EFB was typical of the parameters expected in practical systems:

$a = 0.5$ mm
$U_o = 1$ m/sec
$L = 10$ cm
$\alpha = 0.5$

also
$K = 5$
$\rho_p = 10^3$ kg/m^3
$\mu_p = 2 \cdot 10^{-5}$ kg/m·sec

The curves in Figure 9 represent the corresponding theory as predicted by Eq. (20) and computer results. Note that both theory and data predict 0.99+ collection efficiency regardless of electrostatics for particle radii greater than approximately 2 μm. Below this value, however, there exists significant variability between different field values. This size range corresponds to those particles which tend to lodge in the lower respiratory tract so their collection is of greater importance (Miller, et al (1979)[18]). Data and theory show that modest electric field strengths can greatly improve bed efficiency in this region.

The theory presented here generally under-predicts the data gathered at MIT for fine particles less than 2 μm. However, the curve shapes and relative magnitudes compare favorably. The discrepancy is attributed to two causes:

1) The model does not include collection due to the image force between a charged fine particle and neutral bed particle. This separate electrostatic effect would increase predicted efficiencies.

2) Collection due to diffusion, or Brownian motion, is not included in the model. This mechanism generally becomes significant below particle radii of about 0.2 μm.

It is believed that the incorporation of the above mechanisms into the model will better predict EFB performance.

REFERENCES

1. D.F.S. Natusch and J.R. Wallace, "Urban Aerosol Toxicity: The Influence of Particle Size," Science, 186, 695 (1974).

2. K. Zahedi and J.R. Melcher, "Electrofluidized Beds in the Filtration of a Submicron Aerosol," JAPCA, 26, 345 (1976).

3. K. Zahedi and J.R. Melcher, "Collection of Submicron Particles in Bubbling Electrofluidized Beds," I&EC Fund., 16, 248 (1977).

4. K. Zahedi, PhD Thesis, Massachusetts Institute of Technology, Cambridge, MA (1976).

5. F.J.W. Whipple and J.A. Chalmers, "On Wilson's Theory of the Collection of Charge by Falling Raindrops," Quart. J. Roy. Met. Soc., 70, 103 (1974).

6. H.F. Kraemer and H.F. Johnstone, "Collection of Aerosol Particles in Presence of Electrostatic Fields," I&EC EDE, 47, 2426 (1955).

7. H.F. George and G.W. Poehlein, "Capture of Aerosol Particles by Spherical Collectors: Electrostatic, Inertial, Interception and Viscous Effects," Environ. Sci. and Tech., 8, 49 (1974).

8. K.A. Nielsen and J.C. Hill, "Capture of Particles on Spheres by Inertial and Electrical Forces," I&EC Fund., 15, 157 (1976).

9. P.W. Dietz, "Electrostatic Filtration of Inertialess Particles by Granular Beds," in preparation, 1979.

10. J. Happel, "Viscous Flow in Multiparticle Systems: Slow Motion of Fluids Relative to Beds of Spherical Particles," Am. Inst. Chem. Eng. J., 4,197 (1958).

11. S. Kuwabara, "The Forces Experienced by Randomly Distributed Parallel Circular Cylinders or Spheres in a Viscous Flow at Small Reynolds Numbers," J. Phys. Soc. Japan, 14, 527 (1959).

12. G. Tardos, C. Gutfinger and N. Abuaf, "Deposition of Dust Particles in a Fluidized Bed Filter," Israel J. Tech., 12, 184 (1974).

13. G. Tardos, N. Abuaf and C. Gutfinger, "Dust Deposition in Granular Bed Filters: Theories and Experiments," JAPCA, 28, 355 (1978).

14. C. Gutfinger, G. Tardos, and N. Abuaf, "Analytical and Experimental Studies on Granular Bed Filtrations," Proceedings of the Symposium on the Transfer and Utilization of Particulate Control Technology, 3, 243 (1979).

15. J.C. Alexander, PhD Thesis, Massachusetts Institute of Technology, Cambridge, MA (1978).

16. H. Lamb, Hydrodynamics, Articles 93-95, 6th Edition, Dover Publications, New York (1945).

17. J.R. Melcher and K.S. Sachar, "Charged Droplet Scrubbing of Submicron Particulate," Environmental Protection Technology Series EPA-650/2-74-075 (1974).

18. F.J. Miller, et al, "Size Considerations for Establishing a Standard for Inhalable Particles," JAPCA, 29, 610 (1979).

NOMENCLATURE

A,B,C,D,k	-	constants used in Eqs. (3) and (4)
E_o	-	external electric field
E	-	local electric field
E_r, E_θ	-	radial and tangential components of local electric field
E_c	-	charging electric field
F^e	-	arbitrary electrical force
G	-	dimensionless electrical parameter
K	-	bed particle dielectric constant
L	-	granular bed length
Re_a	-	bed particle Reynolds number
Re_p	-	fine particle Reynolds number
St	-	Stokes number
U_o	-	superficial gas velocity
U	-	local gas velocity
u_r, u_θ	-	radial and tangential components of local gas velocity
V	-	fine particle velocity
v_r, v_θ	-	radial and tangential components of fine particle velocity
a	-	bed particle radius
b	-	electrical mobility
ℓ	-	unit cell radius
n_o	-	inlet fine particle concentration
q_p	-	fine particle charge
r,θ	-	polar coordinates
r_p	-	fine particle radius
t	-	time
y_c	-	critical trajectory height
U^*, V^*, r^*, etc.	-	normalized parameters
α	-	bed void fraction
Γ	-	fine particle collection rate
ε_a	-	bed particle permittivity
η'	-	single-sphere collection efficiency
η	-	total bed collection efficiency
μ	-	gas viscosity

ρ_p - fine particle mass density

Φ - electric potential function

ψ - gas stream function

AEROSOL FILTRATION BY A CONCURRENT MOVING GRANULAR BED: DESIGN AND PERFORMANCE

By:

Thomas W. Kalinowski and David Leith
Department of Environmental Health Sciences
Harvard School of Public Health
Boston, Massachusetts 02115

ABSTRACT

Aerosol filtration by a concurrent moving granular bed filter has been investigated. The effect of an intergranular dust deposit on mass penetration and pressure drop is described. A 2^4 factorial experiment was conducted to identify significant control variables, including: superficial velocity (100 and 250 m/s), bed depth (130 and 230 mm), granule size (2.1 and 2.7 mm), and the intergranular dust deposit expressed as percent by weight of collected dust in the bed (1% and 5%). The test aerosol was resuspended utility boiler fly ash. All tests were conducted at ambient temperatures and pressure. A static, intergranular dust deposit produced high filtration efficiency (>99%) at the low superficial velocity; granular motion produced reentrainment.

AEROSOL FILTRATION BY A CONCURRENT MOVING GRANULAR BED: DESIGN AND PERFORMANCE

INTRODUCTION

In a concurrent moving granular bed filter (CMGBF), aerosol passes downward through a descending bed of granules while clean granules are added continuously at the bed top. To the aerosol, the slowly moving bed functions as a graded media filter with coarse collectors (clean granules) encountered first followed by an increasingly dense deposit of fine collectors (previously captured dust). By adjusting the granule flow rate and the superficial gas velocity, the intergranular dust accumulation can be controlled. A unique feature of the CMGBF is the controlled formation of an intergranular dust deposit to enhance filtration. Particle collection in the CMGBF more closely resembles cake filtration than filtration by a bed of clean granules, in that particle collection depends more upon the nature of the intergranular deposit than on the clean granules.

The CMGBF offers advantages over alternative granular bed configurations. In continuously moving cross-flow filters, formation of a uniform dust deposit is not possible so that efficiencies greater than 98% are found only with thick beds (390 mm) or small granules (0.8 mm); this leads to pressure drops in excess of 2.5 kPa (10" H_2O) according to Wade *et al*. (1978).[1] In intermittently moving beds, cake formation at the bed surface provides high efficiency (> 99%) but periodic cleaning by reverse air or high pressure pulsed air is required. McCain (1978)[2] found increases in outlet concentration associated with periodic backflushing in an intermittently cleaned granular bed filter. Even if such periodic peaks in outlet concentration do not degrade average performance, they may be unacceptable for applications involving downstream gas turbines. The CMGBF offers the advantages of high efficiency provided by the intergranular particle deposit and continuous operation without bypassing for cleaning.

This study was undertaken to determine the fundamental mechanisms by which an intergranular dust deposit forms in a CMGBF and the manner in which this deposit influences bed efficiency and pressure drop. This paper describes the CMGBF experimental apparatus and reports the results of a screening experiment to investigate the effects of superficial velocity, (V), bed depth, (B), granule diameter, (D), and the amount of intergranular dust deposit (K) expressed as percent by weight of collected dust in the bed. The first three factors are important in clean-bed filtration theory; the last reflects the condition of the dust-laden bed.

EXPERIMENTAL APPARATUS

A schematic diagram of the CMGBF experimental apparatus is shown in Figure 1. The test aerosol is electrostatically precipitated coal fly ash

from a utility boiler. The ash was sieved through a screen with 348 μm openings to remove large particles, then stored at 150°C. The fly ash had a mass median aerodynamic diameter of 6.2 μm and geometric standard deviation of 2.4. The fly ash was resuspended by a National Bureau of Standards dust feeder (Dill 1938).[3] The aerosol passed through a charge neutralizer using a 50 mCi ^{90}Sr source designed according to the criteria of Cooper and Reist (1973).[4]

The air flow rate through the CMGBF was always greater than that coming from the aerosol generator, with the difference provided by room air. Flow was measured by a calibrated Stairmand disk at the inlet, which also mixed the aerosol to provide a uniform inlet concentration (Stairmand 1941).[5]

Air flow was controlled by a globe valve in the outlet pipe and a bypass valve as shown on Figure 1. Downstream were a surge tank and type AF24 Roots blower. Relative humidity was determined by dry bulb and wet bulb temperatures downstream of the bed.

Upstream and downstream isokinetic sampling were identical and consisted of fixed 4.7 mm diameter probes center-line mounted in the inlet and outlet pipes. Each probe was connected to a pair of 47-mm filter holders. One filter was used at the start of sampling for purging the probe and setting flow. As shown in Figure 1, a solenoid valve diverted flow from the purge filter to the sample filter during sampling. Mass samples were collected on MSA 1106 BH glass filters.

The CMGBF consisted of three gas-tight sections: a granule storage bin, the bed column, and a granule control mechanism. Granules flowed by gravity from a 39 L storage bin mounted on top of the column. The bin was flanged to an aluminum distribution plate from which four funnel spouts, each 19 mm in diameter and 460 mm long, extend downward into the column. The storage bin-funnel assembly could move up or down on external support rods.

The moving bed was retained in a 203 mm diameter column made from acrylic plastic. The inlet pipe entered the column wall above the bed surface. Inlet screen plugging has been reported for other granular filter designs (Wade et al. (1978)[1] and Hoke and Gregory (1977)[6]), but was not found in the CMGBF which had no inlet screens as aerosol passed directly into the top of the bed.

The bed outlet consisted of a nearly continuous circumferential port located 200 mm from the bottom of the column. This port was sufficient to provide an average exit velocity equal to the superficial gas velocity through the bed, thereby preventing gas acceleration at the exits which could contribute to reentrainment of collected dust. The granules were retained by a stainless steel screen with 0.3 mm openings. The exit port area was contained within an enclosed annulus from which the outlet pipe exited.

Two rows of pressure taps were located 90° from each other along the column wall at 20 mm intervals; three more taps were located in the outer ring of the exit annulus. Using these taps, total pressure drop across the bed and pressure drop at intermediate bed depths could be obtained.

The bed depth, B, was defined as the distance between the end of the funnel outlets and the center line of the gas exit ports. Bed height was varied by adjusting the elevation of the storage bin-funnel assembly. Mounding of granules at the funnel outlets caused the top of the bed to be uneven; this led to slightly lower pressure drops than would have been obtained had the bed surface been flat. Based on pressure drop, bed depth as defined above was found equivalent to that of a full right cylindrical bed approximately 30 mm shorter than the depth defined by the funnel outlets. Pressure drop data are reported as pressure drop per unit bed depth ($\Delta P/B$) based on averages of intermediate pressure drop measurements to remove end effects of the uneven bed surface and the outlet screen.

Takahashi and Yanai (1973)[7] found that a turntable located at the column bottom provided plug flow in granular beds. Plug flow was highly desirable, to minimize granule-to-granule motion. As shown in Figure 1, a 298 mm diameter turntable was centered directly below the column and enclosed in a hopper with acrylic front and back plates. The 200 mm bed height below the gas outlet screen was provided to ensure a depth to diameter ratio greater than one for all bed depths, to enhance plug flow and to prevent the bed from rotating as a solid body on the turntable. The turntable was calibrated for mass flow rates between 60 and 1000 grams per minute against motor RPM. These calibrations were used as guides, and actual granule flowrates were obtained for each run by weighing collected granules. The dirty granules were collected in collection bottles below the hopper.

Two sizes of high density (ρ_g = 3.25 g/cc) alumina granules were obtained from Electrorefractories and Abrasives Division of Ferro Corporation in East Liverpool, Ohio. Ferro Corporation currently markets these granules as "Arlcite" in 8-12 mesh and 6-8 mesh sizes which were found to correspond to a mean diameter of 2.1 mm for the 8-12 mesh size and 2.7 mm for the 6-8 mesh size.

To simulate the loose packing porosity in a moving granular bed, the Happel(1949)[8] slow re-inversion method was used. The porosity calculated using this procedure was found to be 0.41 for both granule sizes. Happel (1949)[8] found this method to be within one percent of the flowing bulk density of moving catalyst beds. For uniform, smooth spheres in the absence of wall effects, Eastwood *et al.* (1969)[9] found the random loose porosity to be 0.43 $\pm$ 0.02. Generally, porosity was found to be less for non-uniform granules, as was found for the Arlcite granules in these tests.

The pressure drop characteristics of the unused alumina granules are shown in Figure 2, a plot of $\Delta P/B$ against superficial velocity, V. Pressure drop was linear with bed depth, and each experimental data point in Figure 2 is the slope of the least squares linear regression of the ΔP versus B data over a range of 50 to 300 mm depth. The Ergun (1949)[10] pressure drop equation fitted these data well if bed porosities of 39% and 38% were used for the 2.1 mm and 2.7 mm granules, respectively. These porosities may be within the range of experimental error for the 41% porosity measurements made using the Happel slow inversion technique.

After use, the collected dirty granules were screened and reused. The cleaned granules were not entirely free of fly ash as indicated by an observed average increase of 0.2 Pa/mm in the pressure drop per unit depth over that for new granules; however, complete separation of collected dust from the granules may not be necessary or even important for effective operation of the CMGBF. Lee (1975)[11] found higher collection efficiency for cleaned sand compared to new sand in a panel bed filter where cake formation was also desired. Recycle of dusty granules may allow the intergranular deposit to form faster than would occur with completely clean granules.

INITIAL PERFORMANCE TESTS

A screening experiment identified significant control variables which affect particulate mass removal efficiency and pressure drop in the CMGBF. A randomized 2^4 factorial experiment was performed with the variables listed in Table 1. The experiment consisted of a total of 16 runs conducted at room temperature and atmospheric pressure.

The low superficial velocity of 100 m/s was limited by the NBS dust feeder air flowrate. The high velocity of 250 mm/s was selected to be sufficiently below the 350 mm/s velocity reported by Goren (1978)[12] to cause bounce and/or reentrainment of 3.91 μm potassium bipthalate particles in a static bed of 2 mm alumina granules. Granule size was limited by the two available sizes of Arlcite granules. The bed depths were selected to be in a range that would produce moderate efficiency (< 97%) according to clean-bed theory for these test conditions. Furthermore, the time to reach steady state as measured by bed volume replacement became excessive for depths greater than about 230 mm.

The fourth factor, K, was selected as a measure of the intergranular dust deposit and defined as:

$$K\% = \frac{W_d}{W_g} (100) \qquad (1)$$

where W_d = dust mass feed rate, g/min
W_g = granular mass flow rate, g/min.

This assumes complete retention of inlet dust within the filter. Dust mass feed rate was calculated from repeated inlet concentration measurements made during each run and volumetric air flowrate. Inlet dust concentrations ranged from 1.8 to 23 g/m^3 to provide the required K values.

For these experiments, granular mass flowrate, W_g, was held constant at 88 grams per minute. At a bulk density of 1.93 g/cc, the mean granular velocity was 0.023 mm/s, three to four orders of magnitude less than the superficial gas velocity. Wade et al. (1978)[1] report granular velocity to be a significant factor in cross-flow granular bed filters, and subsequent experiments will investigate the effect of granular velocity in the CMGBF.

The outcome variables in the 2^4 factorial experiment were mass penetration and pressure drop per unit bed depth at the time of two bed volume replacements. The number of bed volumes refers to the number of times that

portion of the bed between the bed surface and bottom of the gas exit ports was replaced. The time for bed volume replacement was calculated from the dimensions of the column, the bed depth, and granular mass flowrate. At the end of two bed replacements, steady state operation was expected and was found in some runs as indicated by leveling off of penetration and pressure drop. Although it is not certain that a true steady state was achieved in all cases, two bed replacements appeared adequate for the purposes of these screening experiments.

Mass penetration and pressure drop measurements were made throughout each run, at quarter bed volume increments. Granular mass flowrate, W_g, was determined three times per run by weighing collected granules. Relative humidity was determined from dry bulb and wet bulb temperatures early in each run before the wet bulb wick became dirty. At the end of each run special penetration measurements were made as described later. Upstream and downstream samples were also taken at two bed volumes for particle size analysis by scanning electron microscopy (SEM). Isokinetic samples were collected on 0.2 μm pore diameter Nuclepore filters. Particle size analyses will be reported in a subsequent paper.

RESULTS

The experimental conditions and outcome variables for each of the 16 runs are listed in Table 2. Analysis of variance was used to identify significant control variables and their interactions. The sums of squares for 3-way and 4-way interactions were pooled to estimate the error mean square, or error variance. Where appropriate, significant control variables were used in multiple regression equations to summarize results.

Overall mass penetration ranged from 2.6% to 24%. Analysis of variance identified the intergranular dust deposit, K, superficial velocity, V, and bed depth, B, to be significant ($p < 0.001$, 0.001, and 0.01, respectively). The first order interactions KV and VB were highly significant ($P < 0.001$). The KB and KVB interactions were also significant ($P < 0.05$). The effects on penetration of K, V and B and their interactions were positive, i.e., penetration increased as each of these factors increased. The effect of granule diameter, D, was also positive, i.e., penetration increased as D increased, but was not significant at the 5 percent level. The presence of the interactions, particularly KVB, indicate a multiplicative, rather than a simple additive effect.

Figure 3 shows the least squares regression fit ($r^2 = 81\%$) of the mass penetration data at two bed volumes to the interaction term KVB:

$$Pt(\%) = 2.42 + 0.69 \times 10^{-4} \text{ KVB } (\% - mm^2/s). \qquad (2)$$

Slight improvement in the correlation coefficient is possible by adding the separate significant terms in a multiple regression equation; however, considering the size of the experiment and the large r^2 provided by the single interaction term, the simplicity of equation 2 appears appropriate. It should be noted that the powers of K, V, and B in equation 2 may be other than one, but

a two level factorial experiment cannot reveal them. Relative humidity ranged from 25 to 48 percent and was not statistically significant.

The pressure drop per unit bed depth ($\Delta P/B$) ranged from 1.7 to 18.7 Pa/mm. For $\Delta P/B$ at two bed volumes, the analysis of variance revealed K, V and D to be highly significant ($P < 0.001$). Only the KV and KD interaction terms were significant at $P < 0.05$. The K, V, and KV terms had positive effects, increasing pressure drop. The effect of D was negative, as was the KD effect. Bed height, B, and its interactions showed no significant effect, as would be expected for the normalized $\Delta P/B$ variable.

Figure 4 shows the correlation ($R^2 = 96\%$) between observed pressure drop data and values predicted by the simple additive model for the effects of K, V, and D for the dust laden CMGBF:

$$\Delta P/B(\text{Pa/mm}) = 8.44 + 3.05(K\%) + 0.0099(V \text{ mm/s}) - 4.39(D \text{ mm}). \quad (3)$$

Only a slight improvement in the multiple correlation coefficient is possible by inclusion of the two significant interaction terms.

The outlet screen, which was designed to retain granules much finer than those used in this experiment, was subject to plugging in some runs as indicated by pressure drop rise across the outlet screen. Equation 3, however, is based on intermediate bed depths and as such does not include pressure drop across the outlet screen.

DISCUSSION

The numerical value of the coefficients in regression equations 2 and 3 are of less importance than the trends indicated by signs on the coefficients and by the terms found to be significant. This section compares these results with conventional static, clean granular bed theory and identifies some of the unique aspects of the CMGBF.

The penetration relationship, equation 2, is surprising because it opposes what would be predicted by clean-bed theory and because it is opposite what was expected from knowledge of cake filtration. Conventional clean-bed theory predicts decreasing penetration with increasing bed depth, B, and with decreasing granule diameter, D. Present data show an opposite effect for bed depth and no significant effect of granule diameter. Although the difference between the two granule sizes used was not great, it appears that granule size is of less importance in the CMGBF than might be predicted by conventional theory.

For the granule sizes the fly ash used in these experiments, inertial impaction should be the dominant collection mechanism (in the absence of substantial electrostatic effects). Thus, penetration should decrease as gas velocity increases. It was expected that particle removal would be greatly enhanced beyond that expected from impaction on the granules alone, due to presence of the intergranular dust deposit. Using a 50 mm diameter bed of Na_2CO_3 pellets at a superficial velocity of 100 mm/s, Rudnick *et al.* (1976)[13] observed fly ash penetrations less than 0.02 weight percent in a CMGBF of

somewhat different design.

The time trend of outlet concentration, shown in Figure 5 for a typical run, is useful in understanding the apparently anomalous penetration data. Figure 5 shows outlet concentration as a function of the number of bed volume replacements. Outlet concentration decreased at first, as expected due to intergranular deposit formation. However, at approximately three-quarters bed volume, outlet concentration rapidly increased and then leveled off for the remainder of the run. Three-quarters bed volume corresponded to the point at which the loaded bed reached the upper edge of the outlet screen. This breakthrough suggests reentrainment of previously collected dust at the outlet screens. Wade et al. (1978)[1] found reentrainment to occur in a continuously moving cross-flow granular bed filter. Accordingly a series of end-of-run penetration measurements were conducted to identify the significance of possible penetration processes including:

(1) straight through
(2) air scouring
(3) scouring by granular motion.

After the normal penetration measurements were completed, bed motion was stopped and penetration was immediately measured again. This dust-on/bed-stopped situation measured the penetration straight through the loaded, static bed. Next the dust feeder was stopped and the downstream concentration was determined with the bed still stopped, to measure the effect of air scouring at the superficial velocity of the run. Finally, the bed motion was restarted but with no dust fed. This dust-off/bed-moving situation allowed sampling of the collected dust reentrained from the loaded bed as the result of granular motion.

The results of these experiments are presented in Table 3. Expressed as a percentage of the outlet mass concentration, the straight through case (1) for the static, loaded bed averaged 17%. Air scouring, case (2), at the superficial velocity averaged 2.7% but was essentially zero for the low velocity runs. Case (3), reentrainment due to granular motion, was found to represent an average of 72% of the outlet concentration. Recognizing that air scouring case (2) is probably a component of both case (1) and case (3), these averages sum to roughly 90%, representing a closure error of 10 percent. Because of the disruptive effect of stopping and restarting the bed to make the case (3) measurement, errors in the summation are understandable. The significant conclusion here is that the fraction of outlet concentration attributable to granular motion was always greater than that due to straight through penetration and generally was about four times greater.

Visually, the downstream samples for case (1) and case (3) were quite different. Penetration of the static, loaded bed generally produced a uniform discoloration of the downstream sample filter. However, the downstream samples from case (3) situations often showed distinct, large particles or agglomerates scattered across the filter surface. These observations will be verified by analysis of SEM samples which were also taken for each run; these analyses are currently underway and results will be reported later.

Based on the data in Table 3, penetration through the static, loaded bed averaged less than 0.5% by weight at 100 mm/s and 3.0% at 250 mm/s, ignoring the levels of the other factors. Increased penetration at the higher velocity may be largely due to air scouring. Efficiencies in excess of 99.5% at the lower velocity for the relatively fine test aerosol indicate the potential for high efficiency if reentrainment due to granular motion is reduced or eliminated.

Reentrainment may be reduced by lowering the granular velocity. If granular motion at the gas outlet screens is the major cause of reentrainment in the present design, an alternative outlet configuration in which the gas exits through a layer of stationary or more slowly moving granules may improve performance. However, the increased penetration with increased bed depth indicates that reentrainment at the outlet screens is not the only adverse effect of granular motion. The presence of the bed depth, B, in equation 2 suggests that reentrainment increases even within the bed as the amount of dust available (KB interaction) for reentrainment increases. A cascading effect can be envisioned by which collected dust agglomerates break off and are redeposited or are reentrained throughout the bed.

Even without major modification, it may be possible to operate the CMGBF as an agglomerating filter which can capture greater than 95 percent of the entering fly ash mass. In addition, a significant portion of the reentrained agglomerates might be collected in a cyclone downstream.

Finally, it is recognized that the alumina granules used in this experiment offer advantages with regard to mechanical and thermal properties but that their relatively large size and smooth surface may preclude adequate adhesion by the fly ash particles and agglomerates. Na_2CO_3 pellets used by Rudnick et al. (1976)[13] were softer and subject to humidity problems but may have superior fly ash adhesion properties so that reentrainment was reduced.

Equation 3 for pressure drop indicates expected trends. Pressure drop across a granular bed is known to increase as superficial velocity increases and as granule diameter decreases, as predicted by the Ergun equation for clean beds. Similar trends are confirmed in this experiment for loaded granular beds. In addition, equation 3 shows that the amount of intergranular dust deposit, K% by weight, has a significant positive effect on pressure drop.

In this experiment for a given combination of superficial velocity and granule size, increasing K from 1% to 5% generally produced five-fold increase in $\Delta P/B$. However, based on experiments at two levels of K, it cannot be concluded that the effect of K is linear. Additional experiments over a range of values for the intergranular dust deposit will be required to determine this relationship. Because pressure drop is very sensitive to bed porosity, pressure drop should rise as increases in the intergranular dust deposit reduce bed porosity.

Based on the pressure drop measurements made at intermediate bed depths, a uniform intergranular dust deposit is established within a few centimeters of the bed surface. It appears advantageous to operate the CMGBF with a shallow bed to reduce overall pressure drop without significantly affecting efficiency.

SUMMARY

An experimental apparatus has been constructed to investigate aerosol filtration by a concurrent moving granular bed. Screening experiments have been performed to identify significant control variables. Initial results show that conventional collection theory for static, clean granular beds is inadequate to describe the performance of loaded, concurrently moving beds. This is indicated by trends of increasing mass penetration with increases in superficial velocity and bed depth, opposite to what is predicted by clean-bed theory. Granule diameter was found to have little effect on penetration in a bed with an established intergranular dust deposit.

Formation of an intergranular dust deposit results in performance characteristics that are significantly different from those of comparable clean beds. It appears that the intergranular dust deposit functions as a highly efficient filter for collection of dust in the inlet stream. The collection efficiency of the static, loaded bed averaged 99.5% by weight at 100 mm/s superficial velocity and 97% by weight at 250 mm/s superficial velocity. However, agglomeration and reentrainment of collected dust were significant when the bed was moving. Over the range of conditions in this experiment, about three quarters of the penetrating dust resulted from reentrainment of collected dust caused by granular motion.

Experiments are under way to investigate these and other effects further. Fractional efficiency data will also be analyzed to determine fine particle collection efficiency, extent of particle agglomeration within the CMGBF, and nature of reentrained dust.

ACKNOWLEDGEMENT

This work was supported by the National Science Foundation, grant number ENG 77-26975.

REFERENCES

1. Wade, G.L., et al. Granular Bed Filter Development Program: Final Report. Department of Energy Report FE-2579-29, April 1978.

2. McCain, J.D. Evaluations of Novel Particulate Control Devices. Environmental Protection Agency Report EPA-600/7-78-093, June 1978. p. 33-62.

3. Dill, R.S. A Test Method for Air Filters. Trans. Amer. Society of Heating and Ventilating Engin. 44:379-386, 1938.

4. Cooper, D.W. and P.C. Reist. Neutralizing Charged Aerosols with Radioactive Sources. J. Colloid and Interface Science. 45:18-26, October 1973.

5. Stairmand, C.J. Sampling Gas-Borne Particles. Engineering. 41:141-143, 181-183, August 22, 1941.

6. Hoke, R.C. and M.W. Gregory. Evaluation of a Granular Bed Filter for Particulate Control in Fluidized Bed Combustion. In: Proceedings of the EPA/DOE Symposium on High Temperature High Pressure Particulate Control, Washington, D.C., September 1977. Environmental Protection Agency Report EPA-600/9-78-004. p. 112-131.

7. Takahashi, H. and H. Yanai. Flow Profile and Void Fraction of Granular Solids in a Moving Bed. Powder Technology. 7:205-214, 1973.

8. Happel, J. Pressure Drop Due to Vapor Flow Through Moving Beds. Industrial and Engineering Chemistry. 41:1161-1174, June 1949.

9. Eastwood, J., et al. Random Loose Porosity of Packed Beds. British Chemical Engineering. 14:1542-1545, November 1969.

10. Ergun, S. Fluid Flow Through Packed Columns. Chemical Engineering Progress. 48:89-94, February 1952.

11. Lee, K. Filtration of Redispersed Power-Station Fly Ash by a Panel Bed Filter with Puffback. Ph.D. Thesis. The City University of New York, April 1975.

12. Goren, S.L. Aerosol Filtration by Granular Beds. In: Proceedings of the First EPA Symposium on the Transfer and Utilization of Particulate Control Technology, Denver, May 1978. Environmental Protection Agency Report EPA-600/7-79-044c. p. 459-469.

13. Rudnick, S.N. Particulate Collection in a Low Level Radioactive Waste Incinerator. In: Proceedings of the 14th ERDA Air Cleaning Conference, Sun Valley, Idaho, August 1976. ERDA Report CONF-760822. p. 80-101.

Table 1 FACTORS IN 2^4 FACTORIAL EXPERIMENT

Control Variables	Level	
	Low	High
K - Intergranular dust deposit	1	5% by wt.
V - Superficial velocity	100	250 mm/s
B - Bed depth	130	230 mm
D - Mean granule diameter	2.1	2.7 mm

Table 2 RESULTS OF 2^4 FACTORIAL EXPERIMENT

Run No.	Conditions* K	V	B	D	Penetration @ 2 Bed Volumes (% by weight)	ΔP/B @ 2 Bed Volumes (Pa/mm)
1	-	-	-	-	4.63	2.5
2	+	+	+	+	24.0	13.3
3	-	-	-	+	4.67	2.2
4	-	+	+	-	7.28	3.6
5	+	-	+	+	4.00	10.0
6	+	+	+	-	22.0	18.7
7	+	+	-	-	12.3	17.4
8	-	+	-	+	6.94	2.8
9	-	-	+	-	2.60	1.8
10	-	-	+	+	3.06	1.7
11	+	-	-	+	5.03	11.2
12	-	+	-	-	5.50	3.7
13	+	-	+	-	4.73	15.4
14	-	+	+	+	12.1	2.7
15	+	+	-	+	15.4	13.7
16	+	-	-	-	6.79	16.2

* Levels shown in Table 1; high level as + and low level as -.

Table 3 END-OF-RUN PENETRATION TESTS

Run No.	Outlet Concentration (g/m^3)				% of C_{2BV}*			Penetration Case (1)
	C_{2BV}*	$C_{(1)}$	$C_{(2)}$	$C_{(3)}$	(1)	(2)	(3)	(% by weight)
1	0.204	0.027	0.000	0.072	13.2	0.0	35.3	0.51
2	1.31	0.600	0.072	1.64	45.8	5.5	125.	7.66
3	0.166	0.030	0.004	0.121	18.1	2.4	72.9	0.86
4	0.133	0.002	0.000	0.153	1.5	0.0	115.	0.12
5	1.02	0.053	0.026	0.735	5.2	2.5	72.1	0.20
6	1.87	0.292	0.034	1.10	15.6	1.8	58.8	3.20
7	1.05	0.170	0.049	0.646	16.2	4.7	61.5	2.65
8	0.150	0.040	0.012	0.107	26.7	8.0	71.3	1.59
9	0.085	0.015	0.000	0.072	17.6	0.0	84.7	0.41
10	0.134	0.008	0.000	0.115	6.0	0.0	85.8	0.17
11	1.24	0.072	0.004	0.738	5.8	0.3	59.5	0.41
12	0.101	0.030	0.002	0.082	29.7	2.0	81.2	1.66
13	1.27	0.080	0.004	0.250	6.3	0.3	19.7	0.27
14	0.268	0.030	0.008	0.167	11.2	3.0	62.3	1.76
15	1.38	0.451	0.153	1.63	32.7	11.1	118.	5.29
16	1.43	0.251	0.015	0.481	17.6	1.0	33.6	0.69
				Average	16.8%	2.7%	72.3%	
				SD	11.9	3.2	29.8	

*Outlet concentration under normal operating conditions at the end of two bed volume replacements.

(1) Straight through -- dust-on/bed-stopped
(2) Air scouring -- dust-off/bed-stopped
(3) Scouring by granular motion -- dust-off/bed-moving

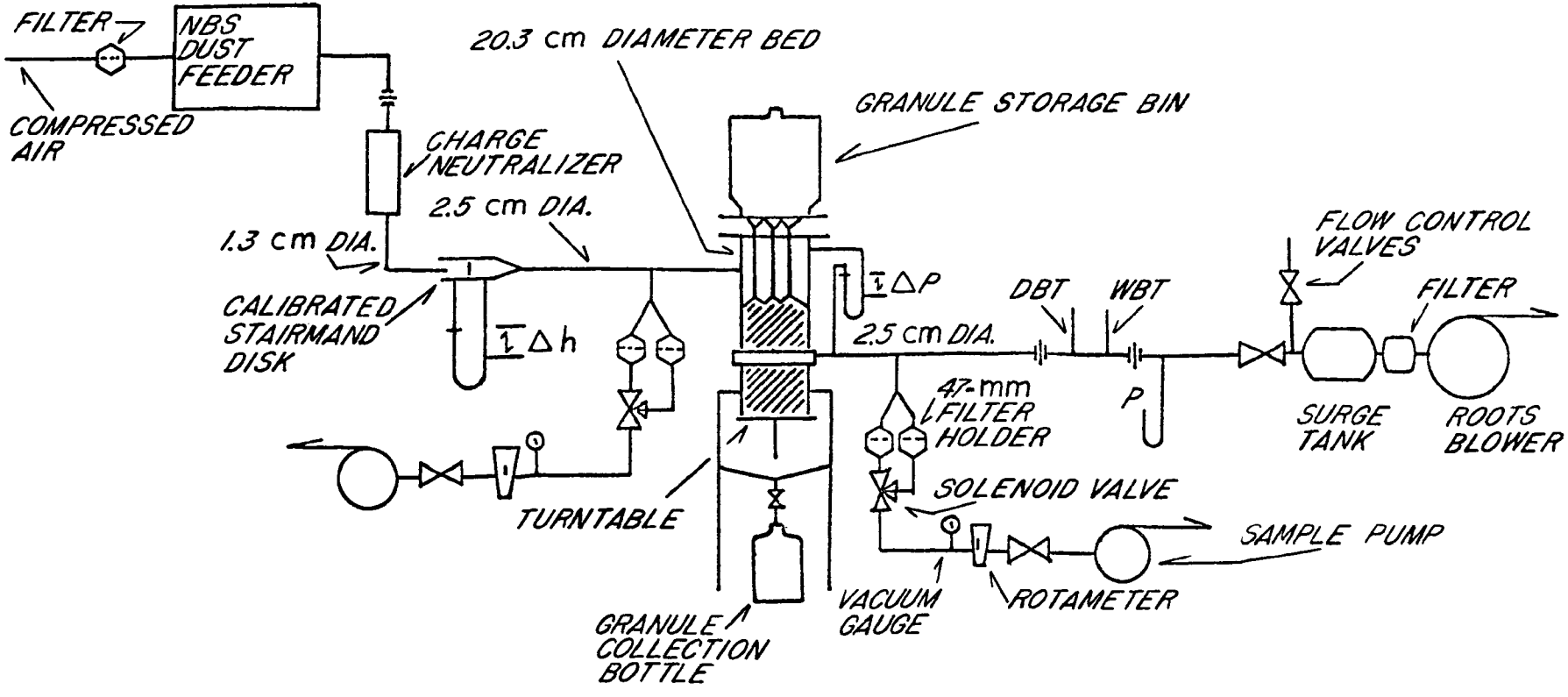

Figure 1 Concurrent moving granular bed filter experimental apparatus .

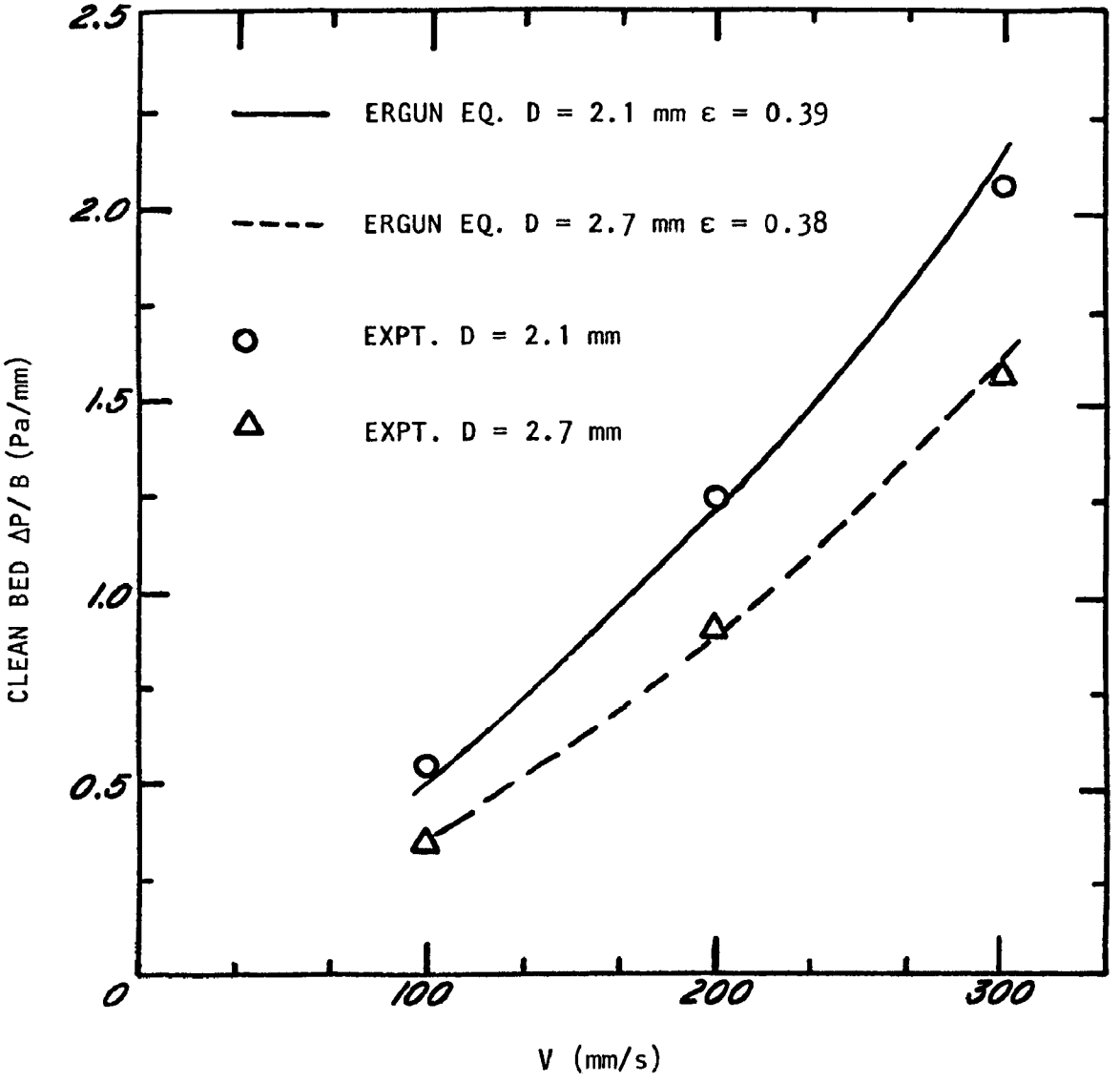

Figure 2 Clean bed pressure drop versus superficial velocity.

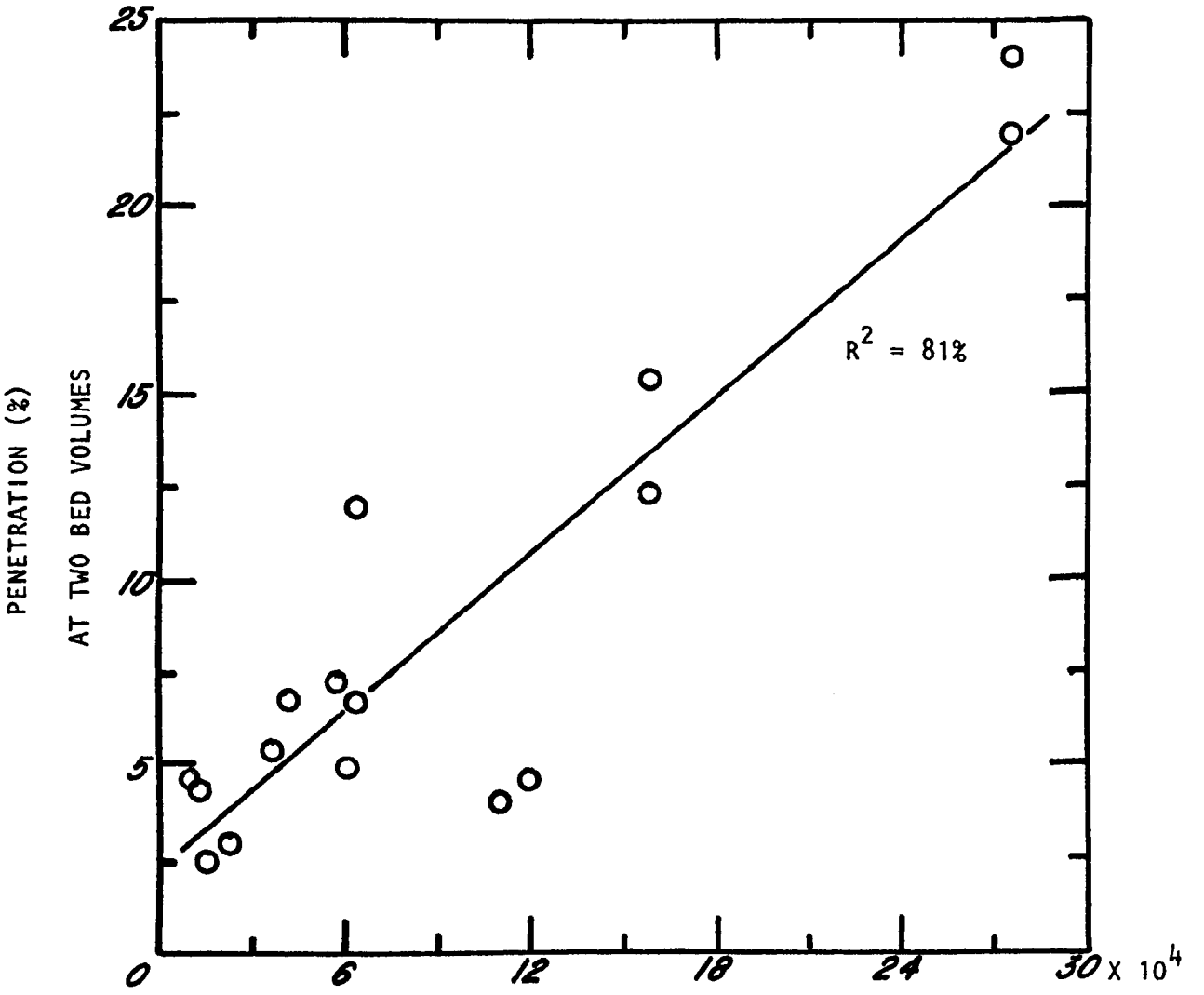

REGRESSION EQUATION: $PT\% = 2.42 + 0.69 \times 10^{-4} (KVB\ \%\text{-}mm^2/s)$

Figure 3 Penetration at two bed volumes regression equation.

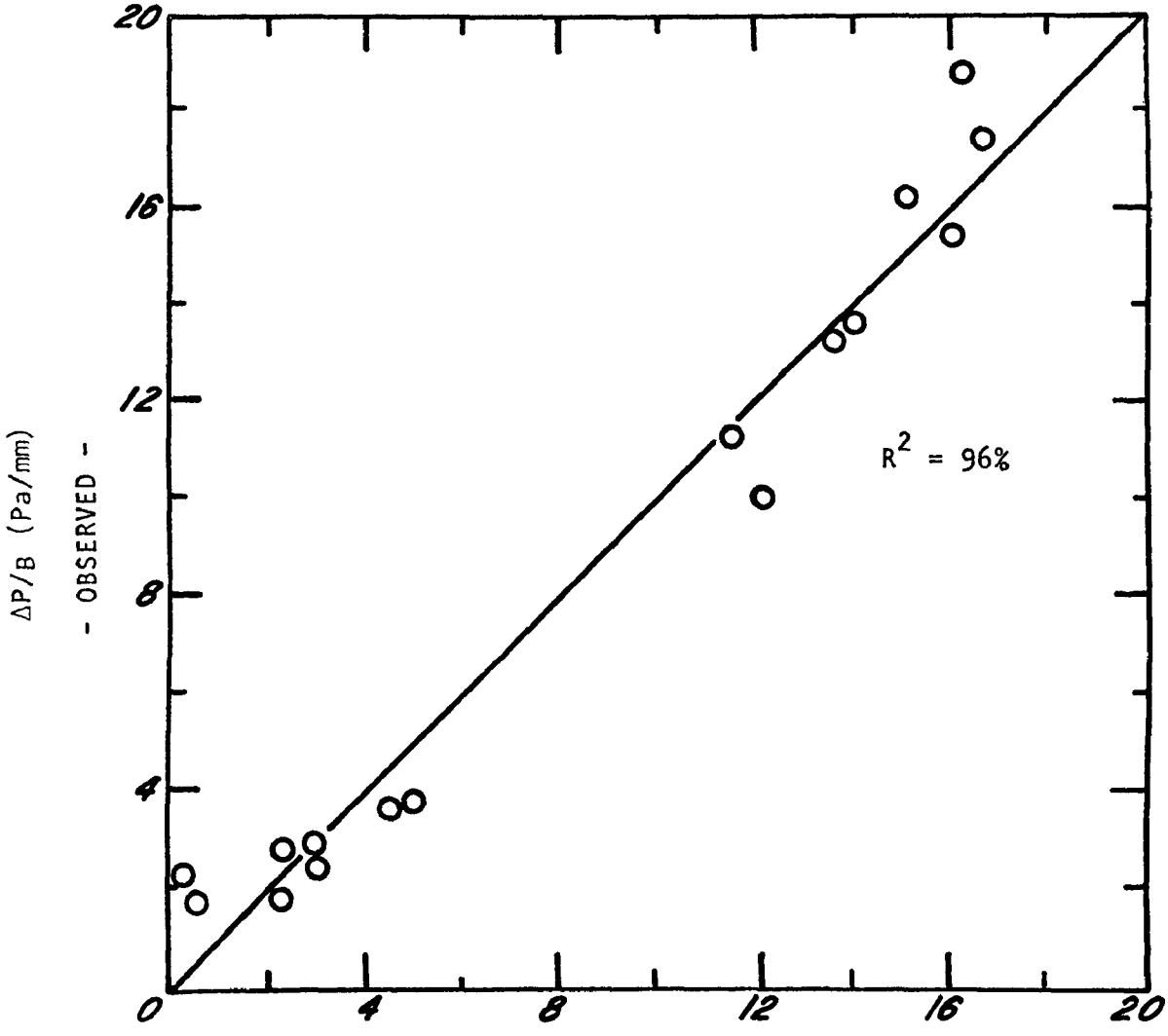

$$\Delta P/B \text{ (Pa/mm)} = 8.44 + 3.05(K\ \%) + 0.0099(V \text{ mm/s}) - 4.39(D \text{ mm})$$

Figure 4 Loaded bed pressure drop regression equation.

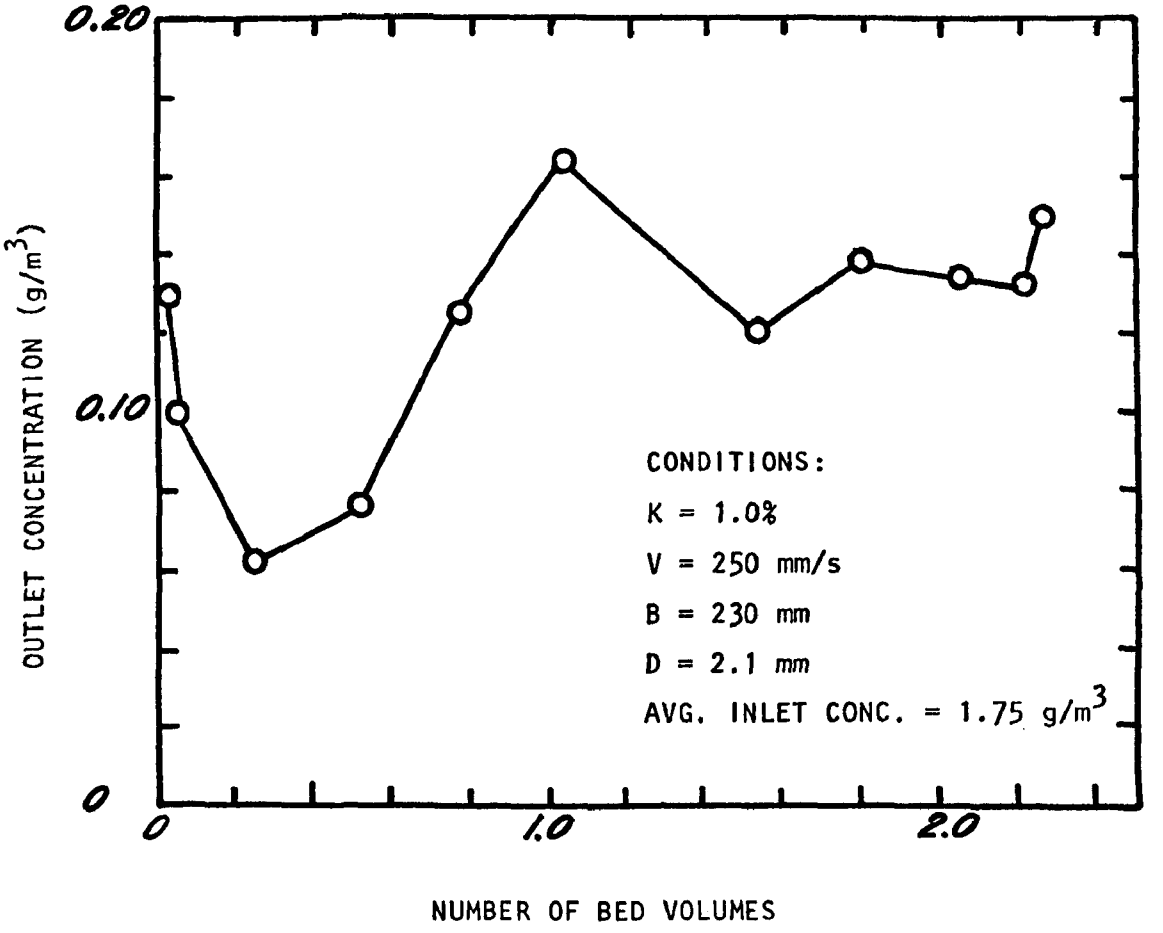

Figure 5 Outlet concentration versus number of bed volumes - run no. 4.

DEEP BED PARTICULATE FILTRATION

USING THE

PURITREAT(TM) PROCESS

By:

L. C. Hardison
Air Resources, Inc.
600 N. First Bank Drive
Palatine, IL 60067

for:

Presentation at the
Second Symposium on the
Transfer and Utilization of
Particulate Control Technology

University of Denver

July 23, 1979

DEEP BED PARTICULATE FILTRATION USING THE PURITREAT(TM) PROCESS

INTRODUCTION

Particulate control of tarry, semi-solid materials generated by industrial processes has presented a special problem because of the failure of conventional high efficiency equipment such as electrostalic precipitators and fabric collectors. Deep bed filtration with disposable media works well but replaces the air pollution emission problem with a solid waste disposal problem.

This paper describes a unique granular moving bed filter in which raw material for the process serves as the medium, and is "disposed" by introduction into the process. This approach was developed by Union Carbide Corporation and is offered for industrial use by Air Resources, Inc. for a variety of processes such as carbon calcination and ring furnaces, in which it is an energy efficient alternative to thermal incineration.

PROBLEM DESCRIPTION

The collection of particulate emissions from industrial processes is practiced to prevent air pollution and to recover raw materials or products which would otherwise be discharged into the atmosphere. A wide variety of techniques for emission control allows selection of equipment to fit the process and the properties of the particulate matter, and for many applications, the system designer has a choice of several alternatives. For example, utility power stations utilize wet scrubbers, electrostatic precipitators, and recently, fabric collectors for fly ash removal.

This is not generally true for processes which emit tarry organic fumes. The aerosol fumes produced by curing of carbon electrodes, which are composed of petroleum coke particles bound together with heavy petroleum tar or pitch, are difficult to collect because they are very small in particle size, and, more importantly, because they are sticky. Thus, the collection techniques most applicable to small particle size solid particulate collection are not workable because the collected material cannot be removed mechanically. This eliminates such conventional techniques as

(1) Mechanical (cyclonic) collectors

(2) Electrostatic precipitators

(3) Fabric filters

Wet collectors are a possibility but the small particle size limits the effectiveness and the wet tarry slurry tends to foul the internals and prevent good mechanical operation.

The remaining devices which can be used for mechanical collection of the fume materials are

(1) Disposable filters, such as the High Energy Air Filter (HEAF) developed by Johns Manville Corp.

(2) Disposable sand bed filters and, because the fumes are combustible organic materials:

(3) Thermal incineration.

Of these three, only thermal incineration has found any wide spread application for the abatement of pitch fumes, and there have also been some applications of wet electrostatic precipitation equipment.

In the production of carbon electrodes for use in metallurgical furnaces, prebake anodes for primary aluminum smelting, and other processes for making graphite products, petroleum coke and pitch are used as raw materials. The coke is ground to a relatively small particle size, generally on the order of 1/4" maximum, and blended with heated pitch to produce a semi-solid material. This paste is then formed into the desired shape in extrusion presses or molds. The formed product is heated to a temperature in excess of 1000°F in the presence of air to oxidize the pitch binder and solidify the mass. Subsequent high temperature treatment of the electrodes may be carried out at temperatures as high as 5500°F to bring about crystallization or graphitization of the carbon.

At each step in the process described, organic fumes are generated by vaporization of a fraction of the pitch binder. In particular, the initial heat treatment of the electrodes at temperatures over about 700°F gives rise to substantial emissions of tarry pitch fumes.

A prebake oven for curing the pitch binder in preformed electrodes might typically discharge 10,000 SCFM to 30,000 SCFM of flue gas, which is largely air containing a small amount of organic aerosol - in the range of a few pounds per hour - which generates a dense visible plume when discharged into the air. The fume material is typically a small particle size aerosol, with a maximum particle size of a few micrometers in diameter. The particles may vary in composition but are most frequently heavy, complex organics of high boiling point, which may contain such objectionable compounds as polycyclic organics (Benzo-a-Pyrene is a member of this group) and partial oxygenates formed by oxidative decomposition of the pitch.

Usually the particles form sticky or tarry semi-solid coatings on surfaces upon which the contaminated gas streams impinge.

SYSTEM DESCRIPTION

The Puritreat(TM) method for capturing these aerosol fumes at minimum cost involves the use of a bed of coke particles which forms, in effect, a deep bed particle filter. The fume laden air stream is passed downward through a layer of particles several inches deep, at velocities up to 1000 ft/min, which results in a pressure drop on the order of 30"W.C.

This results in collection of the aerosol particles at high efficiency by impingement of the droplets at high velocity on the larger particles making up the bed. This type of collection is well known, and "sand filters" or other granular beds have been subjects of a great deal of experimentation if not commercial application, for dry solids collection.

The novel approach utilized by UCCPD involved the use of a part of the granular carbon raw material for the electrode manufacturing process as the collection medium. Figure 1 illustrates the basic mechanism for collection and "disposal" of the fouled carbon by feeding it into the electrode manufacturing process.

Figure 2 indicates the further improvement of the system by use of an edge seal device which permits automatically advancing bed which is indexed forward as the pressure drop increases, indicating a significant reduction in the void volume available for retention of collected tars.

Figure 4 is a photograph of the feed hopper on a 30,000 cfm commercial unit operated on an electrode curing operation.

Figure 5 is a photograph taken from the opposite side of the unit. The coke hopper receives coke particles through a six-inch diameter screw conveyor. The preferred particle size range is obtained by screening the raw granular coke to between three and six mesh or about 1/4"

Figure 6 shows the blower and motor. Spent coke is raised to a spent coke hopper by a screw conveyor on the far side.

Figure 7 shows the coke bed and the typical yellow color of the collected pitch fumes.

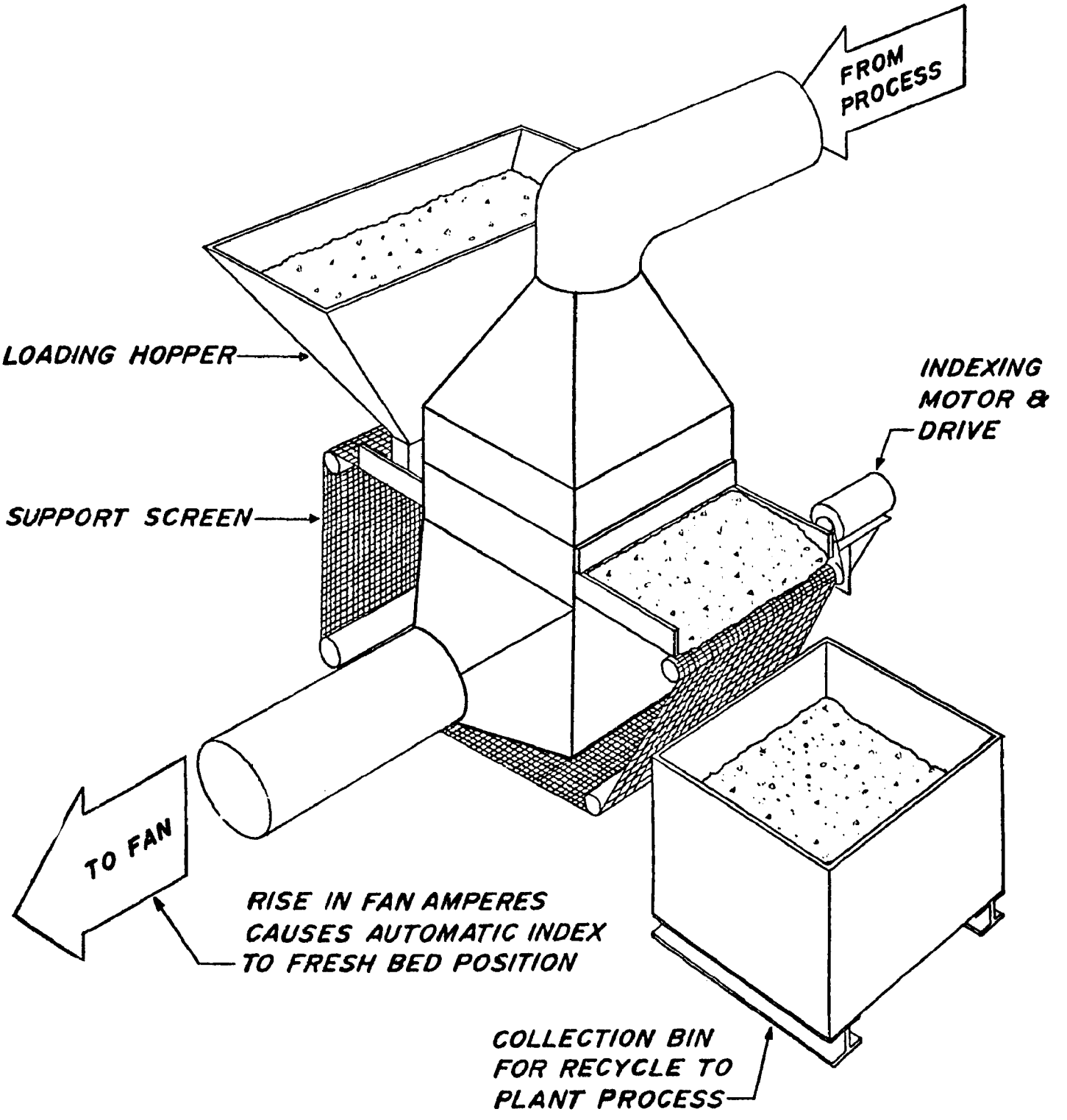

FIGURE 1

SCHEMATIC DIAGRAM FOR PURITREAT (TM) COKE BED FILTER

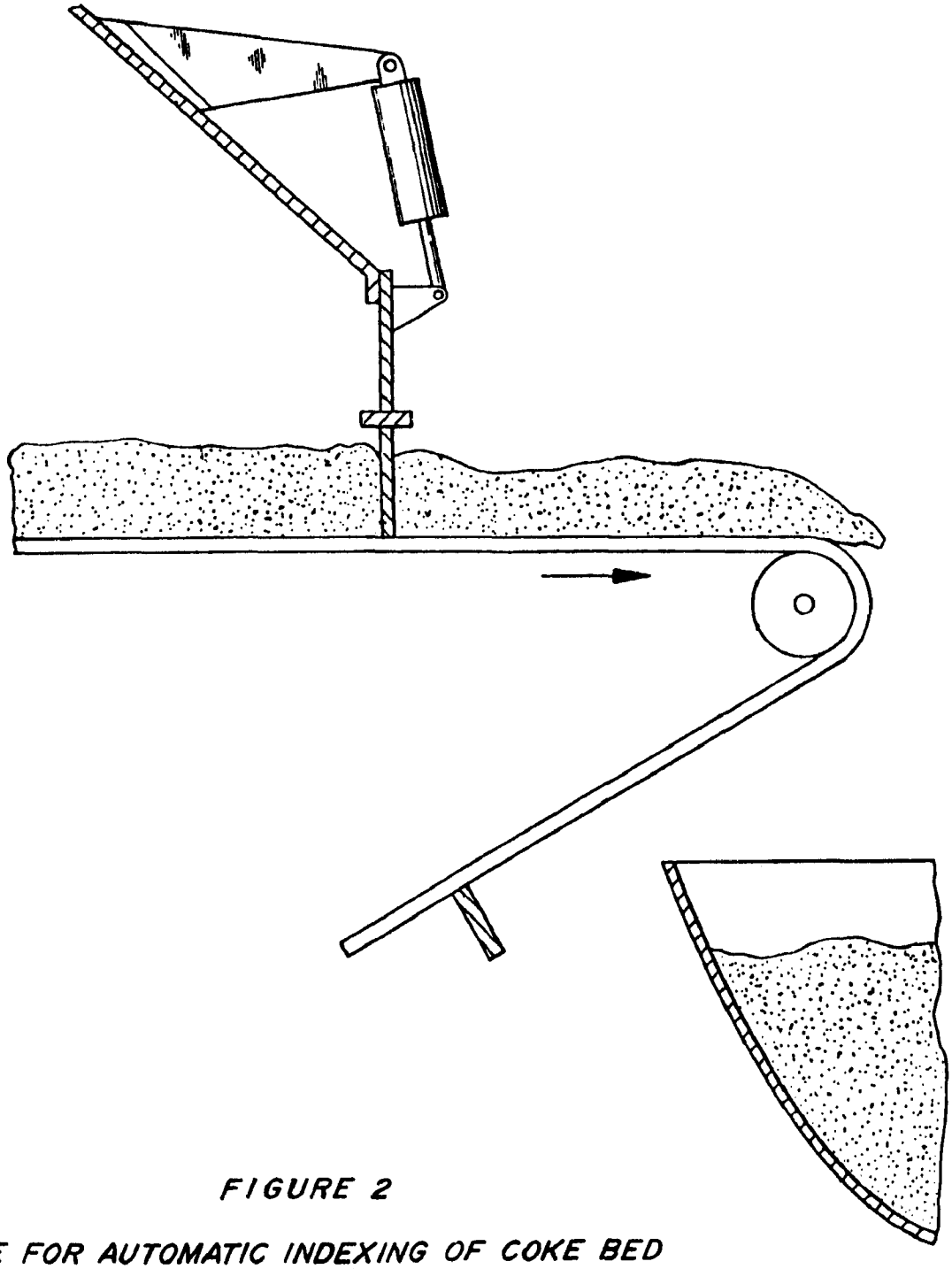

FIGURE 2

GATE FOR AUTOMATIC INDEXING OF COKE BED

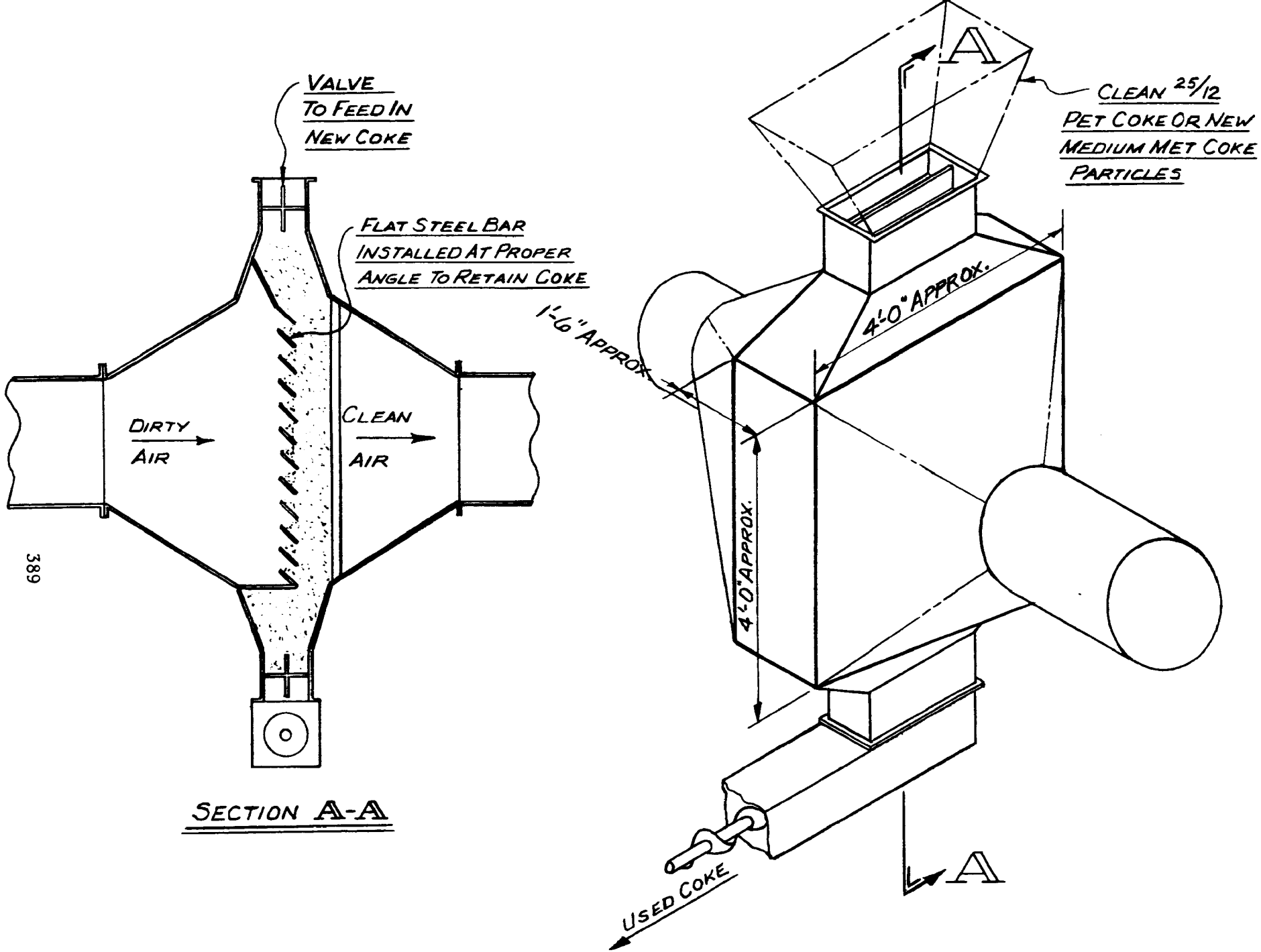

389

FIGURE 3

ALTERNATIVE BED CONFIGURATION

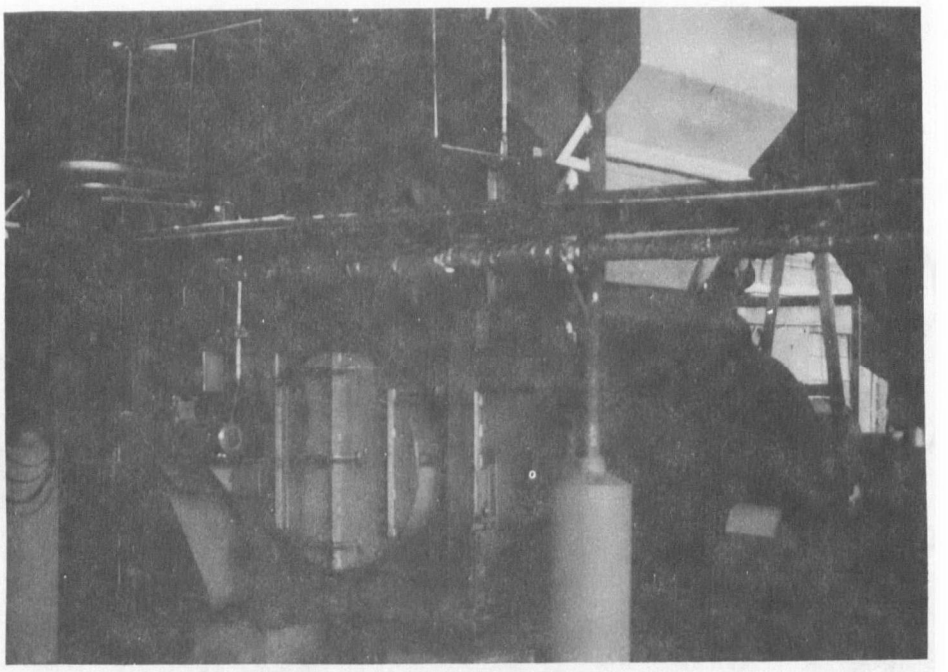

FIGURE 4

30,000 CFM Commercial Puritreat$_{TM}$ Unit

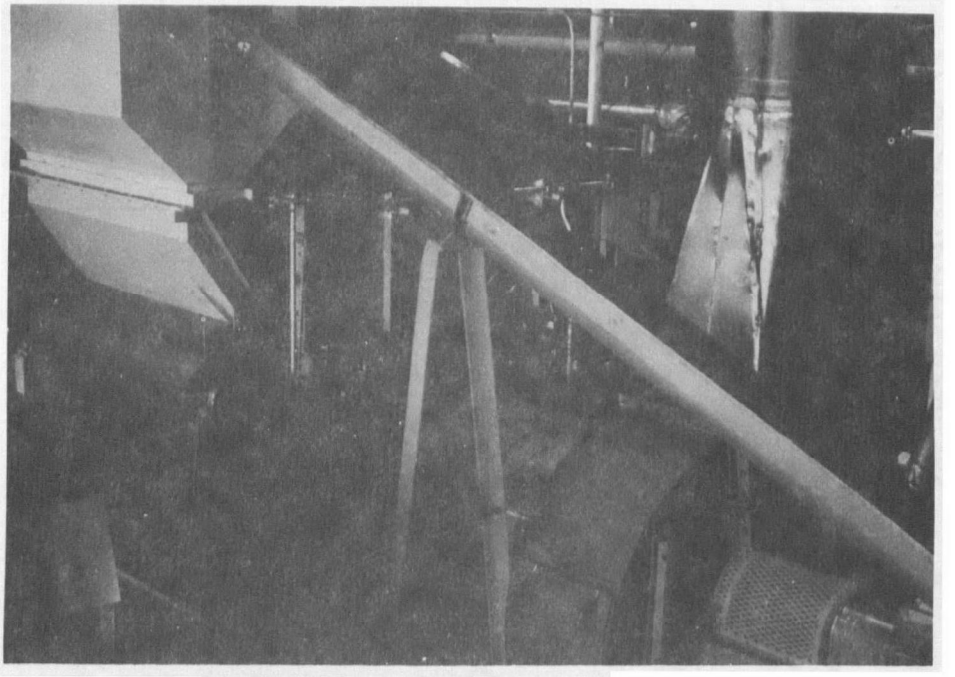

FIGURE 5

Coke Hopper and Screw Feeder

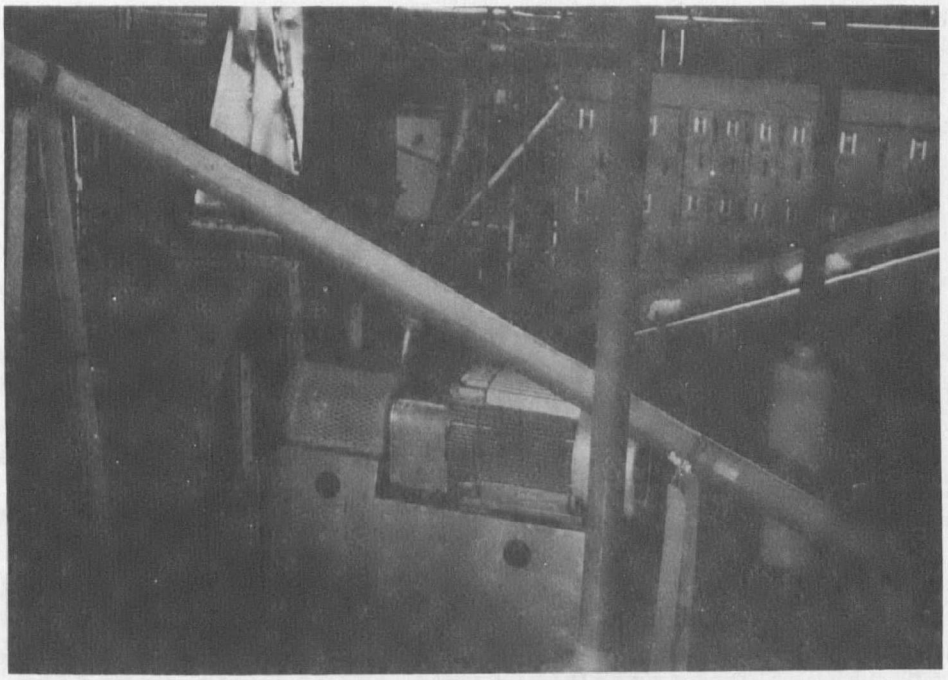

FIGURE 6

Blower and Spent Coke Conveyor

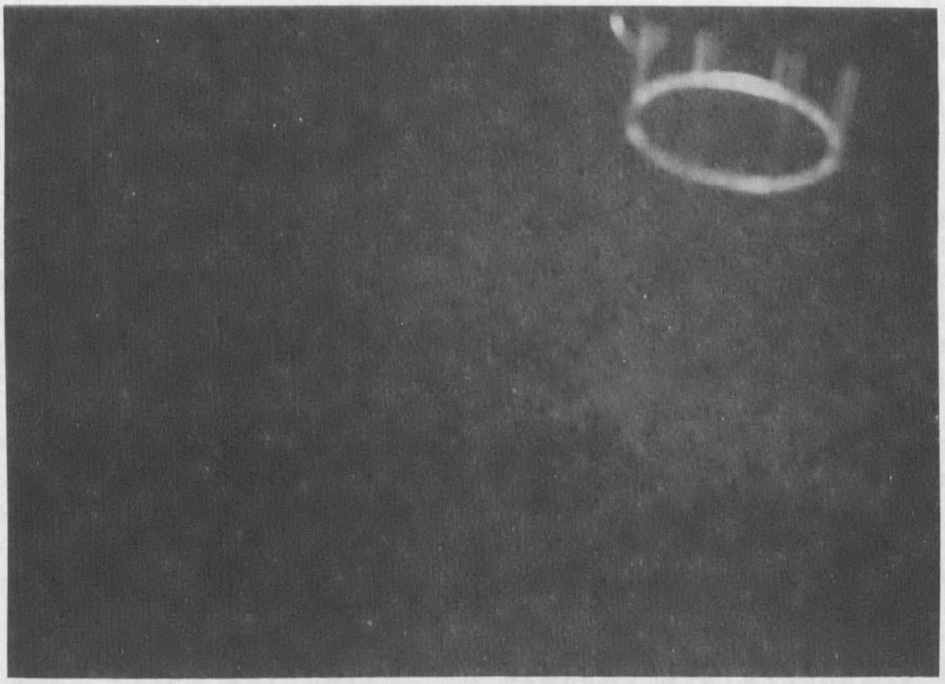

FIGURE 7

Coke Bed

ALTERNATIVE SOLUTIONS

Several alternatives are available for handling the abatement of tarry fumes. These are

a) Combustion

b) Physical removal

Because the tarry materials are almost entirely combustible organic materials, it is possible to remove them from the gas stream by incineration. Both catalytic and thermal incineration systems are capable of high removal efficiencies provided that the tarry materials are handled as vapors rather than condensed particulate matter.

Capital and operating costs for incineration are high, however, and are likely to involve operating costs of 25 to 50 times as high as the cost of operation of the Puritreat(TM) system. Heat recovery is difficult to practice on fume streams containing tarry materials because of the tendency of these materials to foul the heat exchange surface, and to cause fires. The capital and operating costs for both thermal incineration and Puritreat(TM) are compared in Figure 8. Catalytic incineration is capable of operating at about half the fuel cost, but has considerable uncertainty in many applications in carbon processing because of the high temperatures which may be required to assure that the organics are totally vaporized when they reach the catalyst. For this reason, the economic comparison with catalytic incineration was omitted.

High Energy filtration (HEAF) utilizing fixed filter elements composed of fiberglass or fixed granular beds is unworkable because the filter elements are rapidly fouled with tar and cease to function. HEAF filters with disposable, roll-type elements can be utilized, but have very high initial capital costs and high operating costs, as indicated in Figure 9.

For this comparison, two alternative processes with different fume loadings were checked because the fume loading greatly influences the cost of filter replacement. HEAF filters have a further disadvantage in that they generate large volumes of contaminated fiberglass filter elements which must be disposed of in an environmentally sound manner.

Wet scrubbers are capable of collecting tarry fume materials of relatively large particle size. The capital cost is relatively independent of the efficiency, and operating costs are comparable to the Puritreat(TM) unit. However, the efficiency of removal is low and the separation of the tarry slurry from the circulating water is extremely difficult.

OPERATIONAL DATA

Preliminary tests of the Puritreat(TM) system were carried out using a pilot unit configuration, as shown in Figure 10. The pilot unit data were then used to construct the commercial unit now in operation at the Union Carbide plant in Columbia, Tenn. The test data discussed in the following paragraphs was taken from a similar unit at Welland, Ontario.

Efficiency tests were carried out for total particulate collection and also for the removal of the specific polycyclic organics, benzo (a) pyrene (BaP) and benzo (k) fluoranthrene (BkF). Concentrations of total gaseous hydrocarbons were also measured at the bed inlet and outlet using a continuous total hydrocarbon analyzer.

Particulate loadings were measured by isokinetic sampling with a glass fiber filter, as shown in Table 1. The particulate collection efficiency ranged from 72.7% to 97.9% and averaged 83% over all of the tests. Operating conditions during the test period are given in Table 2.

The removal efficiencies of BaP and BkF are summarized in Table 3 and average overall average loadings during the test program are given in Table 4. Efficiencies for BaP and BkF tended to be slightly higher than for total particulate matter.

It should be emphasized that there are many variables involved in establishing the efficiency in a given situation. Many of these, such as particle size and density, are difficult to characterize except by on-site pilot test work. A pilot unit is available for on-site tests and should be used for characterizing existing applications.

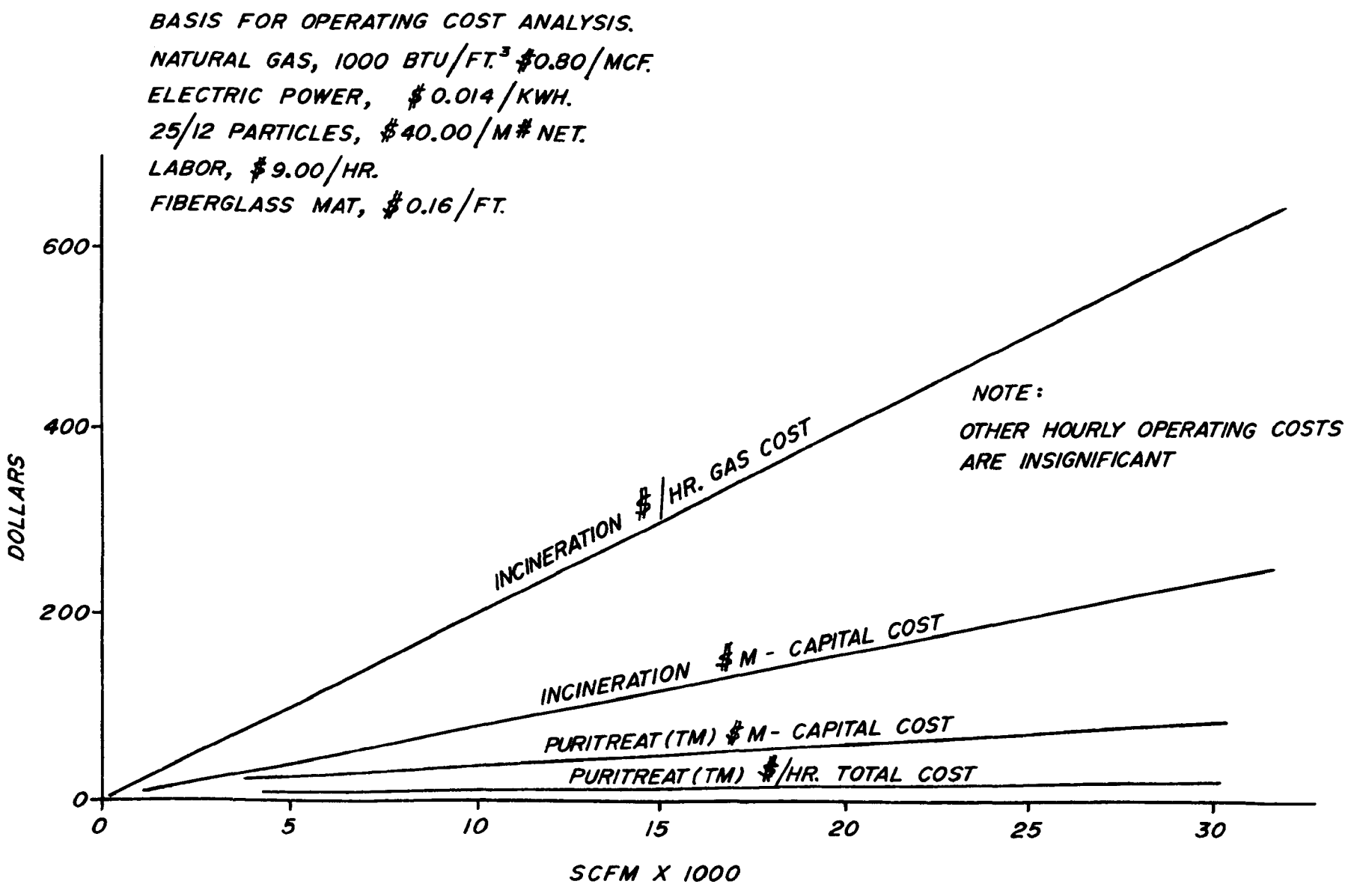

FIGURE 8

CAPITAL & GAS OPERATING COSTS FOR THERMAL INCINERATION
WITHOUT HEAT RECOVERY AND PURITREAT (TM)

FIGURE 9

CAPITAL & TOTAL OPERATING COSTS FOR H.E.A.F. & PURITREAT (TM)

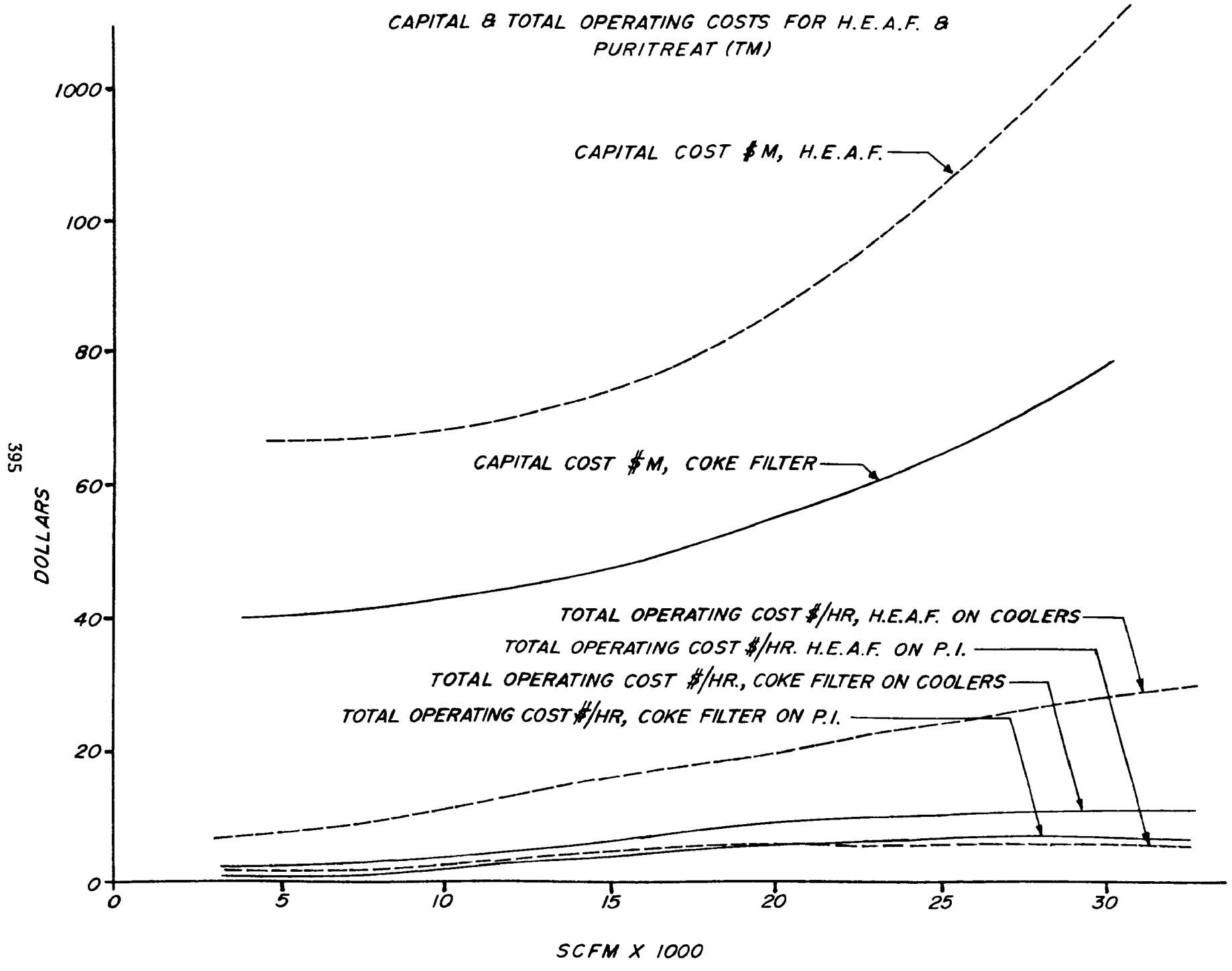

ADDITIONAL ADVANTAGES

The obvious advantages of the Puritreat(TM) system are mainly concerned with minimizing the capital and operating cost. Both of these are lower than for comparable systems such as thermal incineration, HEAF filtration with disposal of the filter medium, or wet scrubbing with disposal of the environmentally sound waste water and sludge.

Several less obvious advantages are also inherent in the Puritreat(TM) system.

(1) The recovered material recycles to the furnaces and is incorporated into the product, adding, if only a small amount, to the product yield, rather than to air pollution.

(2) There is no "byproduct" to dispose, as would be the case with either high energy filtration using disposable media. or with water scrubbing.

(3) Incineration - if it could be practiced in view of the very high fuel costs involved- would probably not effectively remove the heaviest polycyclic aromatic compounds and might, conceivably, add to the emission of benzo-pyrene and similar objectionable substances. The carbon bed is effective in removing such materials.

(4) Because the process is completely "dry" (even though the collected material may be liquid or semi-solid, it is handled as a dry solid in combination with the granular collection medium), the problems associated with wet systems such as corrosion and erosion are avoided. This contributes to increased reliability.

FIGURE 10

SKETCH OF PILOT UNIT

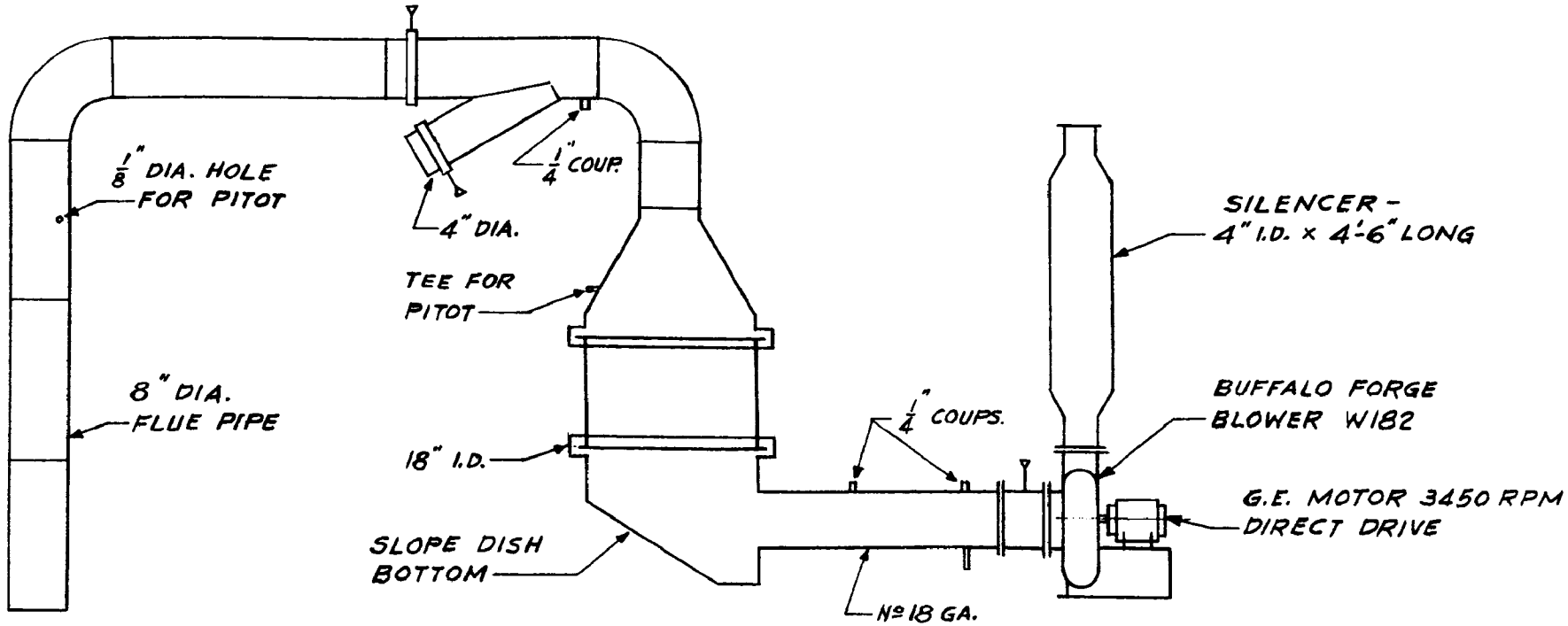

TABLE 1 TEST RESULTS FOR PARTICULATES

Test No.	Location	Weight of Particulate (mg)	Loading (grains/ft^3)	Particulate Emission Rate (g/sec)
1 *	Inlet	1067.8	0.104	1.03
1	Outlet	52.3	0.00041	0.0529
2	Inlet	1006.0	0.373	4.16
2	Outlet	20.1	0.0064	0.0875
3 *	Inlet	422.7	0.107	0.94
3	Outlet	9.9	0.00319	0.0241
4	Inlet	84.8	0.0287	0.302
4	Outlet	18.2	0.00646	0.0823
5	Inlet	89.0	0.0256	0.140
5	Outlet	16.8	0.00423	0.0301

*Glass fibre filter was contaminated by condensed oil running down the sampling probe in the vertical position.

TABLE 2 SUMMARY OF DUCT AND STACK CONDITIONS

Location	Average Flow Rate (scfm)	Average Stack Gas Temp. (°F)	Particulate Loading (grains/ft^3) *
Inlet	8,470	67.2	0.1424 (1)
Outlet	10,620	74.8	0.0047 (2)

* Dry gas at 70°

Moisture content was assumed to be approx. 2%

(1) Simple arithmetic average excluding contaminates samples 1 and 3

(2) Simple arithmetic average

TABLE 3 PURITREAT(TM) COLLECTION EFFICIENCY

Test	Particulate %	Benzo (a) Pyrene %	Benzo (k) Fluorathene %
1	(contaminated inlet filter)	-	-
2	97.9	86.0	79.3
3	(contaminated inlet filter)	-	-
4	72.7	94.9	89.4
5	78.5	98.3	99.2
AVERAGE	83.0	93.1	89.3

TABLE 4 AVERAGE TEST LOADING

Location	Average Particulate Loading (grains/ft^3)	Average Benzo (a) Pyrene Loading (grains/ft^3)	Average Benzo (k) Fluorathene Loading (grains/ft^3)
Inlet	0.142 (1)	7.2×10^{-5} (1)	1.2×10^{-4} (1)
Outlet	0.0047 (2)	3.6×10^{-6} (2)	7.6×10^{-6} (2)

(1) Simple arithmetic average excluding contaminated samples 1 and 3

(2) Simple arithmetic average

APPLICATION OF THE PURITREAT(TM) SYSTEM

The application of the Puritreat(TM) system to existing processes is relatively straightforward when on-site pilot studies can be used to characterize the variables. The following design parameters can be evaluated in the pilot unit and an optimum combination selected for the particular job.

1. Filter particle size, which is generated by screening the charge material to obtain a "cut" with good filter characteristics.

2. Bed depth is generally under 6" and can be varied considerably.

3. Filter velocity must be high enough to provide good collection efficiency without unnecessary fan power usage.

4. Temperature should be low enough to assure condensation of all of the heavy organics prior to the filter bed.

A reasonably complete test program can be carried out at an operating plant for a cost of several thousand dollars.

For new equipment, test data of this sort are unavailable, and it is necessary to design conservatively and estimate efficiencies on the basis of similar operations. The results given in Tables 1 through 5 are typical of a carbon electrode pitch impregnation process.

SUMMARY AND CONCLUSIONS

The Puritreat(TM) system can be used for abatement of tarry particulate emissions from industrial processes which use carbonaceous solids as raw materials at acceptable efficiency levels. In addition to the particulate reduction, the emission of objectionable polycyclic aromatic materials from pitch impregnation and similar processes is good.

Operating conditions should be selected or confirmed by pilot test work if possible, and conservative design parameters based on other similar applications used for new installations.

The Puritreat(TM) system offers an environmentally sound and economical alternative to incineration and fixed element filtration.

PILOT-SCALE FIELD TESTS OF HIGH GRADIENT MAGNETIC FILTRATION

by

C.H. Gooding and C.A. Pareja

Research Triangle Institute
P.O. Box 12194
Research Triangle Park, N.C. 27709

ABSTRACT

Bench-scale and lab pilot-scale experiments have indicated that high gradient magnetic filtration can be an efficient and economical method of controlling particulate emissions from selected sources in the iron and steel industry. A 5100 m^3/hr (3000 CFM) mobile pilot plant has been constructed, and tests are underway at a Pennsylvania sintering plant. The objective is to characterize the collection efficiency of the process with respect to gas throughput, applied magnetic field strength, collection media construction, and particle size. When the tests are completed, the data will be used to make economic projections of the application of magnetic filtration to sintering plants and other iron and steel processes. This paper describes the HGMF pilot plant and gives a status report of the field program.

PILOT-SCALE FIELD TESTS OF HIGH GRADIENT MAGNETIC FILTRATION

BACKGROUND

Since 1975 the Research Triangle Institute has been working under EPA sponsorship to investigate and develop high gradient magnetic filtration (HGMF) as a particulate control process. HGMF is a magnetically enhanced filtration process that has been proven commercially to be an effective and economical method of separating fine, weakly magnetic particles from non-magnetic solids and liquids (Oder, 1976).

The work at RTI began with a theoretical analysis of the particle collection mechanisms active in HGMF and a study to identify potential applications in particulate emission control. It quickly became evident that the most likely candidates for application were the iron and steel processes listed in Table 1. All of these processes produce large quantities of waste gas that contain significant concentrations of magnetic particulate. The first experimental work at RTI was conducted on a bench-scale HGMF unit with a flow capacity of 130 m^3/hr (75 CFM). Dust from a basic oxygen furnace (BOF) was dispersed in air and passed through the HGMF device. Variations were made in the superficial gas velocity, the applied magnetic field strength, and the density and depth of the steel wool filter. These experiments demonstrated that BOF dust could be collected with greater than 99 percent efficiency.

A 2550 m^3/hr (1500 CFM) pilot plant was subsequently designed and constructed at EPA's Particulate Aerodynamic Test Facility located in Research Triangle Park, N.C. Additional tests were conducted using BOF dust as well as dusts from an electric arc furnace (EAF) and a sintering machine. Once again the fractional collection efficiency was determined under a variety of operating conditions. The ranges of conditions tested are summarized in Table 2.

Figure 1 shows an experimentally determined magnetization curve for each of the dusts as a function of applied field. The BOF dust was particularly easy to collect because of its high magnetization. Satisfactory collection efficiencies were also obtained with the electric arc and sinter dusts although somewhat higher fields and more dense or deeper filters were required. Increasing the superficial gas velocity was observed to have a relatively weak but detrimental effect on collection efficiency with all dusts. Collection efficiency increased with particle size up to about 2 μm, above which the efficiency tapered off apparently due to reentrainment effects. As expected, temperature had no significant effect on particle collection within the range tested.

A preliminary economic evaluation showed that a full-scale application of HGMF to any of the three steel processes should require a capital investment in the range of \$1.8-3.6 per m^3/hr of gas flow (\$3-6/CFM) for uninstalled primary equipment; i.e., magnets and power supplies. The total energy requirement should be in the range of 3.2-4.8 kJ/m^3 (2-3 hp/1000 CFM) to power the magnets and the fans that would be required to move the waste gas through the filters.

Table 1. CANDIDATE PROCESSES FOR APPLICATION OF HGMF

Process	Dust Concentration g/m^3	Mass Median Diameter μm	Iron Composition % Total Fe	Noteworthy Gas Characteristics
Sinter Machine				
Windbox	1-2	10	25-50	5-15% H_2O, hydrocarbons, fluorides, SO_x, 120-180°C
Discharge End	5-12	10	25-50	120-180°C
Blast Furnace	10-25	20	35-50	20-40% CO, 2-6% H_2, 200-300°C
Basic Oxygen Furnace				
Open System	10-25	1	55-70	250-300°C
Closed System	40-70	2	55-70	70% CO, 250-300°C
Electric Arc Furnace	0.2-7	1	15-40	40-120°C
Open Hearth Furnace	4-7	5	55-70	7-15% H_2O, 250-350°C
Scarfing Machine	0.5-1	0.5	50-70	H_2O saturated, 50-60°C

Table 2. CONDITIONS TESTED IN PREVIOUS HGMF PILOT PLANT

Dust source:	Basic oxygen furnace Electric arc furnace Sintering machine windbox
Filter material:	AISI Type 430 stainless steel wool, medium grade (equivalent strand diameter $\cong$ 100 μm)
Filter depth:	0.075-0.30 m
Filter packing density:	0.0050-0.0100 volume fraction
Superficial gas velocity:	4.9-11.9 m/s
Applied magnetic field:	0.06 tesla
Gas temperature:	25 and 130°C
Filter pressure drop:	0.15-6 kPa (0.6-25 inches H_2O)

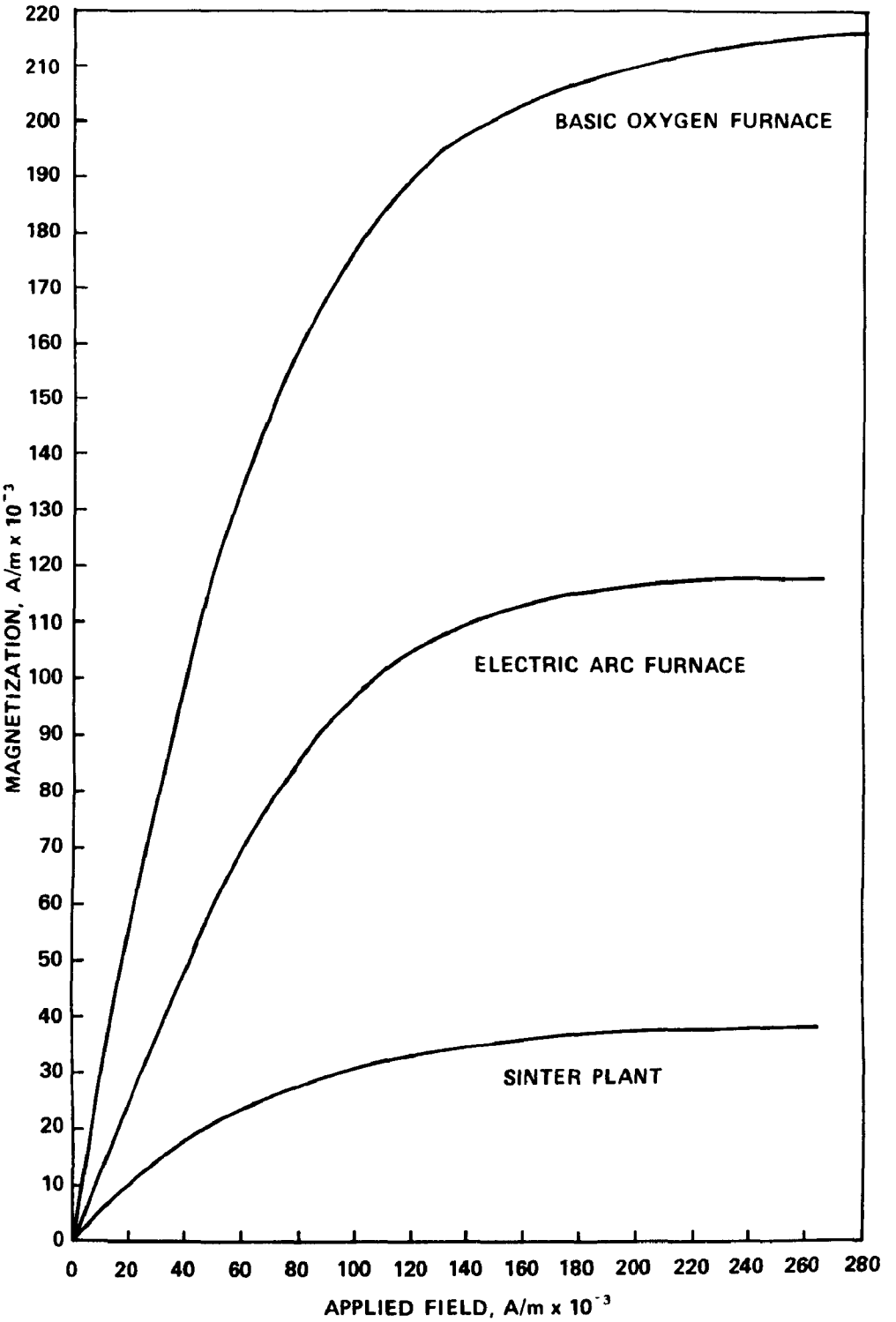

Figure 1. Magnetization curves of three steel industry dusts.

Additional details on theoretical aspects of the HGMF process and more complete results of the bench-scale and pilot-scale experiments are available in a series of published papers and reports (Gooding, et al., 1977; Gooding, et al., 1978; Gooding and Drehmel, 1979). The remainder of this paper describes the third stage of experimental development that is now being conducted by RTI.

OBJECTIVES AND SCOPE OF PILOT-SCALE FIELD TESTS

In August 1977 RTI received funding from EPA to design, construct, and field test a 5100 m^3/hr (3000 CFM) HGMF pilot plant. Backed by experimental data and economic projections derived from the previous work, RTI approached the American Iron and Steel Institute to cultivate their interest and support for the intended field program. In December, 1977 a presentation was made to the AISI Technical Committee on Environmental Quality Control. As a result of that presentation a member company of AISI expressed an interest in providing a sinter plant site for the field tests. Although sinter dust was not the obvious choice for a first evaluation of HGMF based on dust magnetization, it represents one of the more difficult environmental control problems presently facing the steel industry. Hence, selection of the field test site was influenced by the need of an alternative particulate control technique as well as by the potential for successful application of the HGMF process. Following a period of planning and negotiation, a Pennsylvania sintering plant was selected as the site for the field tests.

The overall objective of the field program is to develop sufficient information to compare the economics of a full scale HGMF application to the economics of competitive control technologies. To accomplish that objective, tests are first being conducted to verify data on the effects of important operating parameters of the HGMF process. We will then seek to demonstrate reliable and efficient operation of the HGMF pilot plant for up to 500 hours while the sinter plant is operated in a routine manner.

DESCRIPTION OF THE PILOT PLANT

The mobile pilot plant is housed in a 12.8 m (42 ft) freight van. It has a nominal flow capacity of 5100 m^3/hr (3000 CFM) based on the previous experimental work although the ultimate practical capacity will be determined from the field data. Figure 2 is a flow schematic of the portion of the system that is inside the trailer.

The dirty gas enters the trailer via a 0.317 m ID, 316 stainless pipe (12", Schedule 5) and passes by test ports through which samples can be drawn to determine the size distribution and concentration of the dust. The gas is then directed to one of two functionally identical HGMF devices. Two filtration paths are provided so that one can be cleaned while the other is in operation. Magnet A was constructed by Magnetic Corporation of America (MCA), Waltham, MA, and Magnet B was originally constructed by Sala Magnetics, Inc., Cambridge, MA for use in the earlier pilot plant. Magnet B was later modified by the addition of new pole pieces, stand, and DC power supply purchased from MCA. Each of the magnets now consists of an iron-bound solenoid surrounding a canister that measures 0.432 m (17") ID by 0.305 m (12") long. The filters

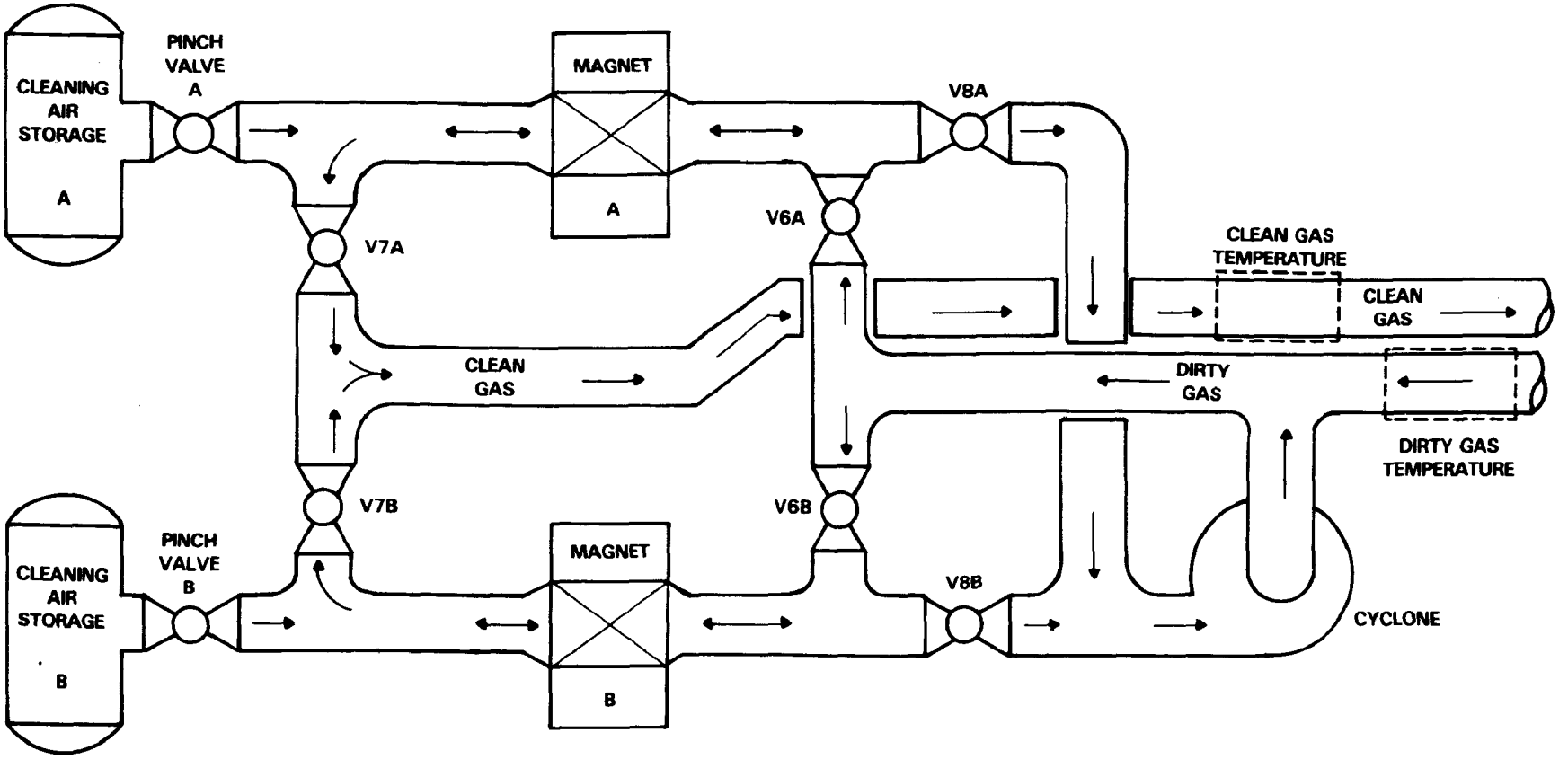

Figure 2. Flow schematic of HGMF pilot plant.

contained in the canisters are made of medium grade AISI Type 430 stainless steel wool. The equivalent cylindrical diameter of the irregular fibers is approximately 100 μm. Each of the magnets is capable of producing an applied field of up to 0.5 tesla throughout the canister volume.

After passing through the filter, the cleaned gas travels past another set of test ports and exits the trailer. It passes through an orifice and an induced draft blower and is then exhausted to the atmosphere through a 10.7 m (35 ft) high stack. An additional set of test ports is provided in the stack to give sufficient access for Method 5 testing.

The filters are cleaned by backflushing with a pulse of compressed air. The volume of the air tank associated with each filter is approximately 0.28 m^3 (10 ft^3). The compressed air is released through an 8" hypalon-lined, Galigher Delta™ valve (Galigher Company, Salt Lake City, UT), which is a pneumatically activated pinch valve with a throat diameter of approximately 20 cm. The agglomerated dust that is blown off the filter is removed from the pulse air by a cyclone. Any carryover is routed back into the dirty gas stream.

The blower that moves the gas through the pilot plant is a Centrifan Model RB50-2 (Centrifan Company, Greenville, SC). The blower will exhaust the required 5100 m^3/hr (3000 ACFM) at a suction pressure of -18.7 kPa (-75 inches H_2O) and a temperature of 150°C (300°F). With the exception of the Galigher valves, pneumatically or manually actuated Norris butterfly valves (Dover Corporation/Norris Division, Tulsa, OK) are used throughout the system. The entire system is designed so as to allow continuous operation at up to 205°C (400°F).

The front quarter of the trailer contains an enclosed, air-conditioned laboratory and control room. Two automated devices are incorporated to simplify operation of the pilot plant. A Xanadu Model UPT100-10-10 solid state programmable timer (Xanadu Controls, Springfield, NJ) sequences the operation of the butterfly valves, the pinch valves, and the magnets as the system cycles from one flow path to the other. The total cycle duration and the sequence of events may be easily changed in a few seconds by inserting a pencil-coded computer card and adjusting a thumbwheel switch. A Robertshaw DCM-1000 controller (Robertshaw Controls Company, Anaheim, CA) maintains constant gas flow through the pilot plant. The controller receives its signal from an orifice located in the clean gas pipe via a differential pressure transmitter and adjusts a butterfly valve located on the blower exhaust. The orifice pressure drop and the pressure drop across the magnetic filters are displayed on two strip chart recorders.

The laboratory/control room also contains bench space, a wet sink, a lab oven, a solvent sink and a lab hood. MRI Model 1502 cascade impactors (Meteorology Research, Inc., Altadena, CA) are used to determine the particle size distribution and concentration. A Perkin-Elmer Model AD-2Z microbalance (Perkin-Elmer Corp., Norwalk, CT) is used to weigh the impactor substrates. A Climet Model 208A particle size analyzer (Climet Instruments Co., Redlands, CA) is also available to monitor transient conditions in the particle size distribution and concentration on the clean side of the magnetic filters.

Figures 3 through 6 show several views of the pilot plant as it is presently installed at the sintering plant.

STARTUP AND PRELIMINARY RESULTS

The pilot plant arrived at the sintering plant on June 18, 1979. Over the next several days, the exterior piping and insulation were installed, and the water and electrical connections were made. Initial checkout and debugging of the system then began. The major components of the system operate off 480 VAC, which was not available at the fabrication site, so most of the equipment had not been operated prior to the field startup. A number of minor problems were identified and corrected. The 3600 rpm blower created a severe noise problem in the work area, but this was solved by installing a silencer on the stack and an insulated enclosure around the blower.

The first fully integrated operation of the pilot plant was accomplished on July 23. A factorial test was begun to evaluate the effects of superficial velocity, applied magnetic field, filter density, and filter depth on particle collection. Preliminary results from the first few tests show the outlet dust loading from the pilot plant to be approximately 0.11-0.18 g/Nm^3 (0.05-0.08 gr/DSCF), which is not low enough to meet applicable emission regulations. These runs were made with a relatively porous filter, however, so the results should improve as the tests proceed. The filter cleaning system appears to be working quite well with a pulse air pressure of 170 kPa (25 psig) and a total cycle duration of 15 minutes. The filter pressure drop increases linearly with time during the 7 1/2 minute filtration time and returns to its original value when the filter is cleaned and returned to service. Additional tests are planned to study the transient effects of loading on dust penetration using the Climet particle analyzer. The transient pressure drop and penetration characteristics will provide valuable data to select the optimum cycle duration for long-term operation. The results of the factorial tests will also be used to select appropriate levels of the operating parameters for the long-term, continuous operation that will be conducted later in the field program. The field work will be completed by November 1979, and a full report giving the results and conclusions from the tests will be submitted to EPA in December.

ACKNOWLEDGEMENTS

The authors are grateful to Doug VanOsdell, John Sauerbier, and Daryl Smith of Research Triangle Institute for their contributions to the design, construction, and initial operation of the pilot plant.

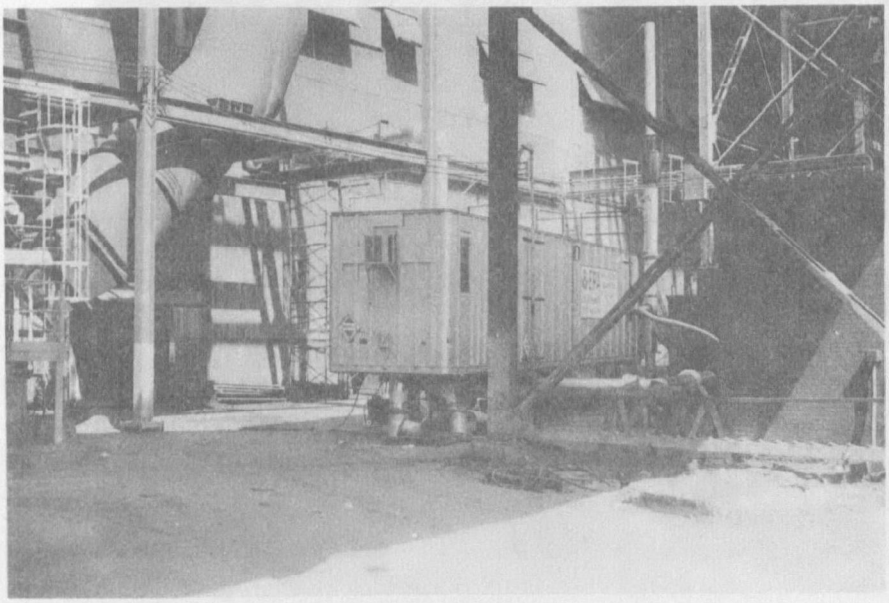

Figure 3. HGMF mobile pilot plant setup at the sintering plant.

Figure 4. Side entrance to pilot plant; gas from plant enters via pipe that passes under steps.

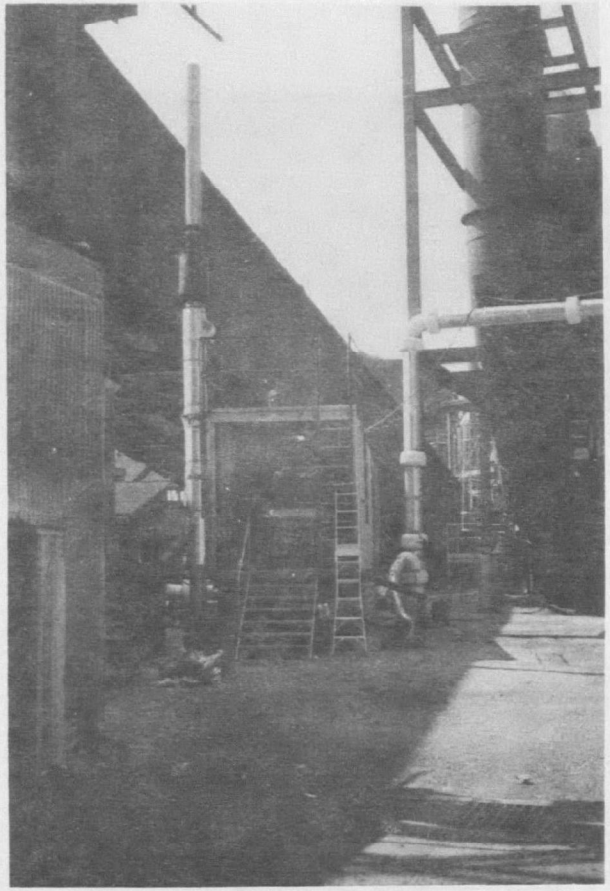

Figure 5. Rear view of pilot plant; gas enters from plant at right and exits through stack at left.

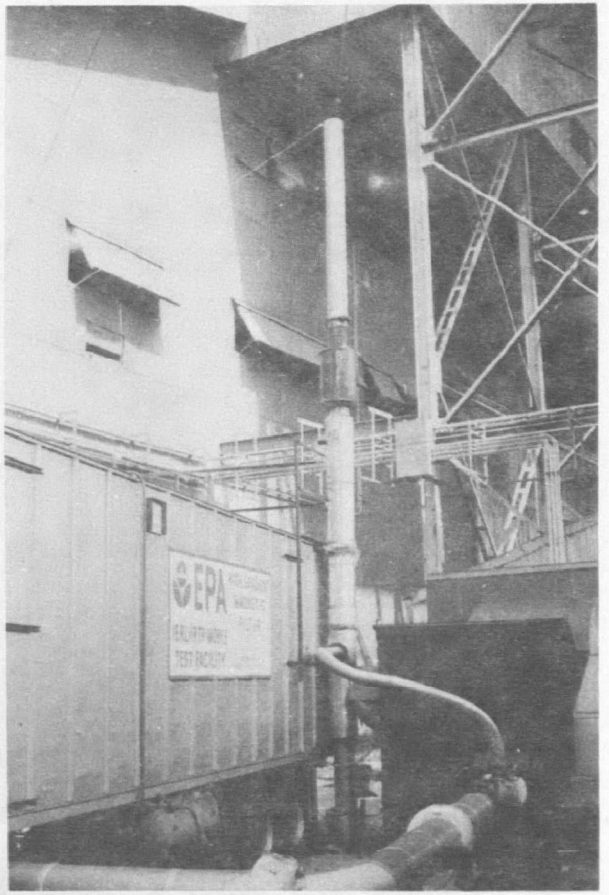

Figure 6. Clean gas piping, blower enclosure and stack with silencer.

REFERENCES

Oder, R. R. High Gradient Magnetic Separation Theory and Applications. IEEE Trans. Magn. Mag-12: 428-435, September 1976.

Gooding, C. H., T. W. Sigmon, and L. K. Monteith. Application of High-Gradient Magnetic Separation to Fine Particle Control. EPA-600/2-77-230. NTIS No. PB 276663/AS, November 1977.

Gooding, C. H., T. W. Sigmon, L. K. Monteith, and D. C. Drehmel. Application and Modeling of High Gradient Magnetic Filtration in a Particulate/Gas System. IEEE Trans. Magn. Mag-14: 407-409, September 1978.

Gooding, C. H., and D. C. Drehmel. Application of High Gradient Magnetic Separation to Fine Particle Control. JAPCA. 29: 534-538. May 1979.

EXPERIENCES WITH CONTROL SYSTEMS USING A UNIQUE PATENTED STRUCTURE.

By:

George C. Pedersen, P.E.
KIMRE, INC.

This paper will present practical design and operating experiences using Kimre's patented structure for particulate removal. The wide range of sizes allows unique capabilities: effectiveness to one-half micron or below can be achieved, as can unexcelled pluggage resistance and cleanability.

EXPERIENCES WITH CONTROL SYSTEMS USING A UNIQUE PATENTED STRUCTURE.

I. SUMMARY

The unique structure used by Kimre, Inc. is described and its uses explained. Kimre's history, position, and approach is described. Then a summary listing our experience is provided with an indication of the of uses. The major part of the paper is consideration of four case histories:

siliceous particulate,
fluoride,
urea, and
"smoke."

This structure as used in the patented B-GON™ mist eliminator and KON-TANE™ Tower Packing products, has been proven effective in an extremely wide range of problems.

II. INTRODUCTION AND BACKGROUND

The patented structure is totally unique in the industry. It is based on two sets of monofilament fibers interlacing perpendicularly in a ladder like arrangement, with specific three dimensional orientation between the fibers. This structure provides a number of novel features compared to other materials:

(a) Any type of monofilament materials can be used, including metals. However, only thermoplastics are routinely offered commercially.

(b) The fibers lie perpendicular to the gas flow for maximum effectiveness.

(c) The interlacings involve a very small fraction of the fiber but yeild a high compressive strength and high void fraction material.

(d) A very wide range of fiber diameters is easily produced providing the great design flexibility to handle a variety of circumstances.

(e) The media is made in large sections; each over 1830 mm (6') wide by many feet long.

(f) Since the individual fibers are straight, or nearly straight each in its own direction, the media has extreme dimensional stability and is very strong. This allows the large pieces to be installed with out difficulty and minimal support.

(g) Build up of foreign materials, or corrosion products does not cause "Mechanical shrinkage,"

as has occurred with knitted mesh materials particularly for metals.

(h) The structure is easily, and always, heat stabilized to well over the recommended operating temperature providing a substantial safety margin.

(i) Although strong, and resilient, thermoplastic materials are compressible, flexible and almost impossible to damage mechanically. They can be rolled up, twisted, compressed, jumped on, and in fact be driven over.

(j) Flexibility and compressibility is particularly interesting since it seems to be this feature that makes the material uniquely cleanable.

Since this paper deals with some specific details I must familiarize you with the standard nomenclature.

1. Our standard style designation splits fiber diameters and void fractions by a slash with fiber diameters (in mils) on the left and the void fraction (percentage) on the right. Thus Style 4/96 is made of 4 mil material and has a nominal 96% void fraction.

2. The material of construction is shown separately. Polypropylene, Kynar™, Teflon™ and Tefzel™ are common materials of construction (Kynar is the trademark of Pennwalt Corporation for their polyvinylidene fluoride, Teflon and Tefzel are trademarks for the DuPont Corporation for some of their fluoro-polymer resins.)

Kimre, Inc. was formed in 1973 and became active in 1974. It is a small privately held Florida Corporation with Headquarters and Manufacturing facilities in Perrine, Florida (a Miami suburb).

Kimre's position is unusual, possibly even unique. Primarily manufacturers, suppliers of our media (and technical expertise in their use), this company also supplies consulting services, conceptual design, and accessories such as support grids. Detailed engineering designs have been supplied although our preference is to work through, and in conjunction with, original equipment accounts and engineering companies.

We do not make scrubbers, absorbers, or any type of vessels.

Since 1974 we have grown at a gratifying rate, this has been done by boot strapping, without any goverment assistance or outside financing; in fact, the only real support has come from the Pennwalt Corporation. As a consequence Kimre operates on a very careful financial balance without any excess discretionary funds being available. I mention this, not to impress you with our

"Great American Initiative" but rather to lead into the consequences of our position which have a bearing on our market posture and the type of results that we will report:

> We cannot spend much money on testing, test facilities, pilot plants, or any thing else not having a significant dollar return in a reasonably short period.
>
> We cannot commit resources on large high risk project areas even if we have the best available technology.

When the Company originally started, as you might imagine, we got projects for which there were severe problems: usually an emergency where our GLS™ priority service allowed delivery before anyone else, or correcting a problem for which there seemed no other viable solution. Our product range, expertise, and acceptance have increased substantially. Many scrubber manufacturers now use our products regularly for routine as well as for especially difficult operations.

Scientists may be shocked at our approach and we anticipate criticism at the lack of specific information. Most of our customers are not willing (or at least not anxious) to authorize publication of company identification much less specific test information. Of course Kimre is not staffed to carry through on details to obtain approvals.

Our approach is frequently crude, and is always results oriented over 99% of our thousands of installations have been successful. Specific case histories are given below and are discussed in some detail. A partial summarization of our experience in air pollution control and chemical processing follows:

(a) Pulp and Paper for:

Smelt dissolving tank vents
scrubbers on recovery boilers
Chlorine absorbers
Chlorine dioxide absorbers
Chlorine scrubbers
Hydrogen recovery
starch or clay dust

(b) Sulfuric Acid for:

intake filters of sulfur burners
drying towers
inter-pass absorbers
final absorbers
Sulfuric acid concentrators
by product acid plant
Oleum vaporization

(c) Phosphorous Processing for:

wood process phosphoric acid fluoride scrubbers
Mono-ammonium phosphate
Di-ammonium phosphate
GTSP
storage building dust scrubbing
rock dryers
electric furnace
food grade phosphoric acid production

(d) Chloro-Alkali for:

Chlorine drying
Hydrogen purification
brine filtration

(e) Others including:

HCl scrubbing from a variety of sources
Hydrazine
oil mist removal
odor and dust from foundries
odor from sewage treatment plants
odor from animal by-products
fumes such as from brazing lines
organic vapor absorption into liquid
cooling towers
pickling
plating
fiberglass insulation
secondary smelters
desalination evaporators
etc. etc.

(f) One other interesting application area is incinerators, we have had particular success on chemical waste incinerator application.

Our experienced areas include: high vacuum to high pressure, cryogenic service to over 200°C, rates from one cubic m^3/hr to 860,000 m^3/hr (½ CFM to 500,000 CFM), particulate and mist removal from submicron to rocks or rain drops, efficiencies from minimal effects to sub ppb.

III. CASE HISTORIES

A. Phosphorous Furnance Application
B. Phosphoric Acid Fluoride Scrubbing
C. Urea
D. "Smoke" Scrubber

A. Phosphorous Furnace Application (Prefilter for a candle-type unit.)

In 1976 our engineering firm clients approached us to help with the design of a pollution control system for an electric arc-phosphorous furnace. It was necessary to control water soluble P_2O_5 and water insoluble siliceous materials. The materials ranged from over 10 microns in diameters to much less than half a micron. It was a nasty and fairly difficult job. Size distribution of the components is shown in Table I.

A high-efficiency candle-type mist eliminator would remove the emissions but would plug up from the insoluble materials. The approach taken was to use the Kimre materials to remove the bulk of the solids down to approximately one-half micron. Removal of the coarser particles would protect the candles from pluggage.

A small, 400 mm (16") diam pilot plant was installed with a two-page configuration. The details of the configuration and design parameters are shown in Table II. The pilot plant operated as predicted, except that pressure drop was slightly high. The reason for the high pressure drop was never determined although no pluggage occurred. Possibly high irrigation rate or higher than design velocities were responsible. Our pressure drop estimations are usually quite reliable or even a little high.

This story has, for us, a sad ending. Our joint venture technology was not accepted and the job went to another company. There may, however, be a silver lining: the unit selected has never worked well and our same concept is now being considered for a new installation by the same client. We have also learned that the original pilot plant was considerably over-designed and a much lower pressure drop unit would have been quite acceptable.

Table I.

Droplet Diameter	>14μ	14-9μ	9-6μ	6-4.2μ	4.2-2.7μ	2.7-1.4μ	1.4-.85μ	.85-.56μ	<.56μ
% of P_2O_5	10.7	.16	.20	.23	.59	17.1	18.1	26.1	28.5
% Insolubles	40	2	2	2	4	20	10	10	10
Design Penetration of Insolubles[1] in %	←----------Insignificant----------→						.1	2	98

[1]The insolubles are primarily siliceous in nature.

Table II.

PAD A

3 Layers Style 32/94, 3 layers Style 16/96, 2 layers Style 8/96, 5 layers Style 4/96, 1 layer Style 8/96, 1 layer Style 32/94.

PAD B

18 layers Style 2/96, 1 layer Style 8/96, 1 layer Style 32/94.

This design option for a 16" diam, 600 fpm, pressure drop of 8.5" yields an estimated effectiveness of 96% overall on all insulubles with 98% of remaining particulates less than .56 microns (μ). Note that the solubles were not a factor in the design.

B. Phosphoric Acid Fluoride Scrubber

This is a central Florida phosphate processing complex using a conventional crossflow scrubber design. This unit had never operated satisfactorily and work has been in progress since 1972. A great many steps were taken to improve the performance. Yet, despite this ongoing program with many changes and tests made, the unit was never capable of operating consistently below 0.045 Kg fluoride/ton P_2O_5 (0.1 lb fluoride/ton P_2O_5). One of their consultants had indicated that mist carryover was a problem, and a high-efficiency chevron-type mist eliminator (imported from Germany) was being utilized.

As a result of other work in the same complex we became aware of this problem in late 1976 and in early 1977. However, we were not called in to help solve the problem until July, 1978. At that time a review of the test data made it very clear that the conventional "approach-to-equilibrium" situation was probably not the major problem. We recommended a test sequence to the plant personnel. These tests were selected to define the "form" of the fluoride being emitted. Without getting into the technical details of the tests run we determined that emissions from the unit were a combustion of gaseous fluorides as well as fluorides in non-gaseous form. An appreciable percentage of the emitted fluorides were in non-gaseous form. We determined further that the non-gaseous fluorides were in a physical form that was not effectively collected by the equipment being used. A significant portion of the fluorides (present as non-gaseous fluoride) was in the size of 1-5 microns. This size is substantially below the size that is effectively collected in either the chevron-type mist eliminator or in the dumped packing.

In order to achieve the desired results we suggested a change in the scrubbing section of the unit to include the addition of a small amount of our media. Specifically we suggested the addition of two layers of Style 37/97, followed by two layers of Style 37/94 in polypropylene with a total thickness of 90 mm (3.6"). To install the media it was necessary to relocate some spray headers. Kimre KON-TANE™ media was installed directly ahead of the existing retaining frame and attached directly to it. Thus, there were no structural changes on the inside of the unit. In front of the existing chevron-type mist eliminator we suggested a high-efficiency B-GON™ Mist Eliminator* be installed. We suggested that this be comprised of two layers of Style 37/94 and three layers of Style 16/96, plus three layers of Style 8/96 in an irrigated mode of use. The mist eliminator was supplied as two pieces 2390 mm x 1830 mm (94" x 72") and two pieces 1780 mm x 610 mm (70" x 24") to conform to the superficial area of the chevron-type mist eliminator. These 76 mm (3.0") thick units were installed directly in front of, and attached to, the chevron-type mist eliminators.

The units were installed in October 1978, during one of the plants regular down days. Several problems occurred. First of all we had bypassing. It was necessary to put in a sealing piece around the edges, for which we have standard procedures. After this they found that the test results (although 50% better than the previous results) were not those anticipated. A check of the unit showed that the Style 8/96 material had sealed up with siliceous deposits as is a commonly problem with these operations. The Style 8/96 was removed.

Subsequent to this change the unit has consistently achieved the objective of 0.0091 Kg fluoride/ton P_2O_5 (0.02 lb fluoride/ton P_2O_5). It has been necessary to clean the media periodically as is easily determined by pressure drop of only a few inches WG.

Replacement of the original type of packing with KON-TANE™ Tower Packing is planned.

C. Urea

This was a retrofit on existing prilling towers, with details of the installation accomplished on the basis of pilot plant testing performed by customer's personnel. The pilot plant test included electrostatic precipitators, charged droplet scrubbers, and venturis. The venturi required seven times the pressure drop of the KON-TANE™ Tower Packing and B-GON™ Mist Eliminator materials to achieve the same collection. The plant has a capacity of 450 tons/day and an initial emission rate of 35 kg/hr (77 lbs/hr). Size distribution given as: 90% minus two microns, 85% minus one micron, 30% minus 0.5 microns, and a median diameter of 0.75 microns.

The scrubbing section is comprised of a total of 17 layers of materials, using our Styles 37/94, 16/97, and 8/96. The mist eliminator section uses the same materials. However, it has only 11 layers and is a different composite. The scrubbing modules are installed on top of the stacks. They are set up so that the flow comes up vertically in the internal of the unit, turns and moves radially, and horizontally, out through the scrubbing section, the mist eliminator section and then out to the discharge. Each of the six units handles 85,000 m^3/hr (50,000 CFM). The scrubbing sections operate at 2.3-2.45 m/sec (7½-8 fps) while the mist eliminator section operates at 1.5 m/sec (5 fps).

It was found that the liquid rate control is critical, having a requirement of approximately .43 l/m^3 (4 gal/1000 ft^3). Emissions as low as 11 mg/m^3 (0.0048 g/ft^3) were obtained). Pressure drops of only 90-100 mm WG (3½-4") are experienced in operation. All the units have been in service since Fall of 1977. There is no indication of anything to suggest any difficulties with the units which will limit their service life.

These units were unique in that the scrubbers were designed to fit on top of the existing stacks and caused a very low pressure drop. This obviated the necessity for massive reinforcing, or replacement, of the existing stacks; or the need to duct the entire gas flow down to ground level for treatment and then issue through a new stack. Installation in this manner obviously saved a lot of money and down time.

We think it interesting that the measured performance far exceeds projected theoretical performance. Actually when we were first approached on this there was a serious question in our mind whether or not we could achieve suitable results. Similar things have been observed, prior to this installation, and subsequent to it. The reasons for this delightful discrepancy are not known but are possibly due to the multitude of many venturis (up to 62 million/m^3 in Style 2/96) or the interaction of von Kármán eddies from one set of filaments which intersect the next set of filaments at right angles. Whatever the reason the effect is dramatic and always occurs to extend the useful range of collection.

D. "Smoke" Scrubber

In November of 1976 one of our original equipment manufacturer accounts (who supplies a variety of wet scrubber types) came to us with a "smoke" problem where they had installed a conventional crossflow packed-bed scrubber with 50 mm (2") packing. This was a 6800 m^3/hr (4000 CFM) scrubber with 2515 mm (8'3") of irrigated packing and a single mist eliminator stage which we had provided.

The "smoke" was originating from a plastic extrusion operation where nylon was being extruded and chopped into pellets. When the hot plastic contacted the cool room air significant quantities of "smoke" were given off; and as a result, everything in the area was coated with an oily coating. This "smoke" is a composite of many different things, a combination of caprolactam and oligomers, forming what seemed to be a mixture of mist, solid and gelled particles. The original installation was essentially of no effectiveness in removal of this "smoke." No mass emission figures were provided. Some preliminary tests indicated that our material, Style 4/96 in polypropylene, would definitely remove the "smoke." However, provision had to be made to handle gels and solids. A three-stage system was eventually installed in the shell left after removal of the conventional dumped packing.

The final stage, Pad C, is a simple mist eliminator operating at around 2.5 m/sec (500 fpm).

Pad B, the intermediate stage, is irrigated with fresh water at a very low rate. This section operates at around 4.3 m/sec (14 ft/sec) and utilizes 100 micron fiber, present in our Style 4/96, as the primary scrubbing material. This stage, the actual functioning stage on the unit to remove the "smoke", is less than 50 mm (2½") thick.

The initial stage, Pad A, is irrigated with recycled solution from a holding tank. This pad is comprised of a variety of materials designed to give a high degree of pluggage resistance while removing coarse materials and dirt present in the system from room air. It operates at 2.5 m/sec (500 fpm).

The intake to the actual scrubber is maintained at 50 mm (2") pressure with a manifold arrangement. The unit is set up so that if any of the extruders is operating it automatically switches into the manifold which causes an adjustment in the supplementary air, to maintain a constant total flow through the scrubbing system. This control system is necessary as Stage B is sensitive to velocity variations. Since its installation over a year ago the entire unit has been operating at the anticipated 180 mm (7") pressure differential without difficulty or pluggage. The measured efficiency has not been released to us. However, it operates at an emission level that is judged to be satisfactory. Prior to the installation of our material, the plume was essentially 100% opaque emitting from a 380 mm (15") stack with even one extrusion line in operation. With our materials in service it is barely possible to see that anything is being emitted. In addition

to that, the high speed blower operated completely dry and erosion of the blades, a previous operating problem, has ceased.

As a bonus they recover the monomer.

The only other device plant personnel considered proven effective was a "candle" type mist eliminator. That type of unit:

1. is much larger,
2. is much more expensive,
3. has higher pressure drop and
4. gets plugged up.

IV. CONCLUSION

The structure has a wide range of useful applications. The complete application area has not been defined. Current limitations are:

for sub micron particulates and mist,
temperature over 260°C, and
application using very high liquid and gas rates for counter current absorption.

ELECTROSTATIC EFFECTS IN VORTICAL FLOWS

P.W. Dietz
General Electric Company
Corporate Research and Development
Schenectady, New York 12301

ABSTRACT

Electrostatic forces have been shown to significantly enhance the collection efficiency of cyclones.* In this paper, an analytic model will be developed for the effect of an applied electric field on charged particle trajectories within a laminar, two-dimensional vortical flow. Boundary conditions for particle injection are developed and collection efficiencies are predicted.

*W.B. Giles, "Electrostatic Separation in Cyclones"
Symposium on the Transfer and Utilization of Particulate Control Technology, Denver (1978)

ELECTROSTATIC EFFECTS IN VORTICAL FLOWS

INTRODUCTION

In a conventional reverse-flow cyclone (see Figure 1), particle-laden gas is introduced tangentially to produce a vortical flow. Within this accelerating flow, the particles experience a radial force which tends to propel them to the cyclone wall. However, the radial motion of the particle is resisted by the combined action of turbulent mixing and fluid drag resulting from the inward gas flow. The separative performance of cyclones is thus determined by the competition between these forces (Leith and Licht 1972 and Dietz 1979).

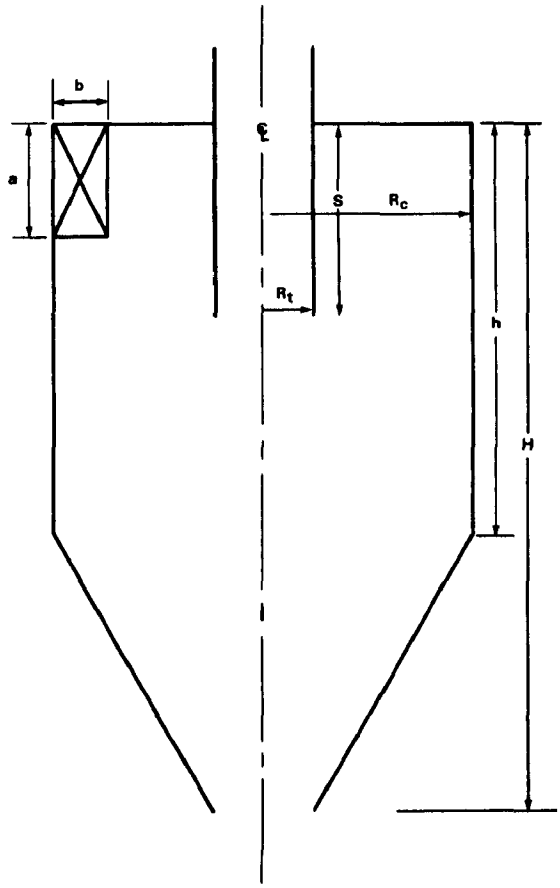

Figure 1. Conventional Cyclone Geometry

Since electrostatic forces are recognized as having a paramount effect in determining the particle trajectories in gas-solids flows (Soo 1971), it would seem obvious to attempt to augment cyclone performance through the application of electrostatic techniques and, indeed, several early investigators pursued this approach (Petroll and Langhammer 1962 and Molyneux 1963). However, in spite of demonstrated improvements in performance, this technique has not been pursued.

Soo (1973) has formulated equations for electrostatic effects in cyclones and has suggested that they may be important - especially in larger cyclones. However, his equations require numerical integration and have not been solved.

Recent experimental work by Giles (1978) has confirmed that electrostatic effects are significant in cyclones and, indeed, can dominate their performance. By varying the electrical charge carried by the dust entering the cyclone, Giles was able to demonstrate large changes in cyclone performance. Unfortunately, the level of charging was not characterized in these experiments and, thus, information on the fundamental process resulting in the electrostatically-enhanced performance is not available.

To address the fundamental issues of collection mechanisms and cyclone scaling, a program was initiated at General Electric Company's Corporate Research and Development Center. What is reported in this article is a model for collection in a two-dimensional, electrostatically-enhanced cyclone (termed "electrocyclone"). Based on this simple model, hydrodynamic and electrostatic cut-sizes are computed and the implications of the results for scaling to large cyclones are investigated.

THEORY

The study of charged-particle motions is inherently quite complex due to the coupled nature of the equations. The motion of the particle is governed by the flow pattern and the electric field. However, both the flow and field can be modified by the presence of particles. Thus, to analytically examine the effects of electrostatic forces on cyclone performance, certain simplifying assumptions are introduced:

1) the flow is two-dimensional (see Figure 2);

2) the dust loadings are low enough that the particles do not affect the gas flow;

3) the tangential velocity of the particle is the same as that of the gas;

4) the tangential velocity of the gas is given by the equation for a modified free vortex (Alexander 1949),

$$\frac{U_t}{U_{to}} = \left(\frac{R_c}{r}\right)^m , \qquad (1)$$

where R_c is the cyclone radius, U_{to} is the tangential inlet velocity and $0.5 \leq m \leq 1.0$ (note: for a free vortex in an inviscid flow, $m = 1$);

5) the drag on the particle is given by Stokes' Law;

6) the electric field is imposed (thus, space charge effects are negligible);

7) the cyclone is operating in the steady-state (no transients).

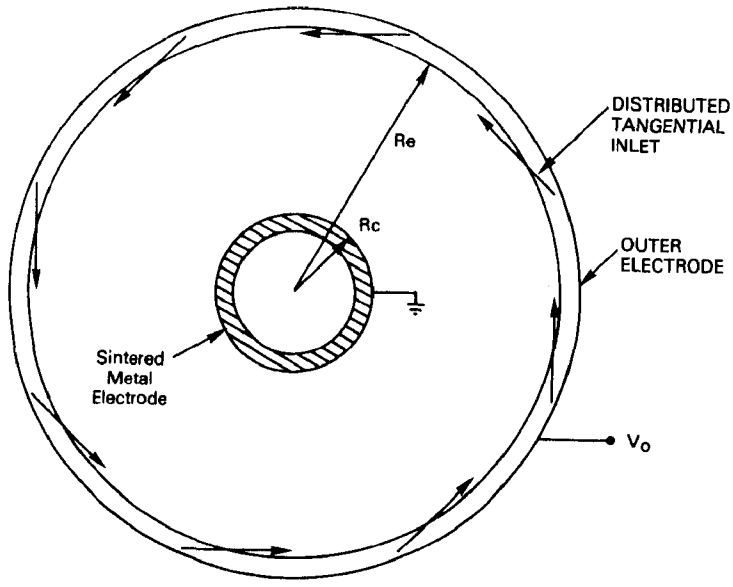

Figure 2. Two-dimensional Cyclone Geometry with Distributed Tangential Inlets and Axial Outlet

With these assumptions, a set of simple, tractable equations can be written describing the motion of the particles. First, conservation of particles gives

$$\frac{1}{r}\frac{d}{dr}\left[r\,\Gamma\right] = 0 \quad , \tag{2}$$

where Γ is the net radial flux of particles

$$\Gamma = n\,U_{pr} \quad , \tag{3}$$

where n is the number density of the particles and U_{pr} is their radial velocity at position r. A simple force balance on a particle yields

$$U_{pr} = bE_r + U_r + \beta\,\frac{1}{r}\,U_t^2 \quad , \tag{4}$$

where U_r is the radial gas velocity, b is the mobility of the particle in the radial electric field E_r,

$$b = \frac{q}{3\pi\mu\,d_p} \quad , \tag{5}$$

and

$$\beta = \frac{d_p^2 \rho_p}{18\mu}, \tag{6}$$

where d_p is the diameter of the particle of mass density ρ_p and μ is the gas viscosity.

Since the radial velocity and electric field are not affected by the presence of the particles, they are given by

$$U_r = -U_o\left(\frac{R_c}{r}\right) , \tag{7}$$

and

$$E_r = -E_o\left(\frac{R_c}{r}\right) , \tag{8}$$

where

$$E_o \equiv \frac{V_o}{R_c \ln (R_c/R_o)} \tag{9}$$

and V_o is the applied voltage.

Introduction of eqns. (1 and 3-9) into eqn. (2) and integration yields

$$\Gamma_o R_c \left(\frac{1}{R_c n_o} - \frac{1}{rn}\right) = \frac{2m\ \beta U_{to}^2}{(2m+1)R_c}\left[\left(\frac{R_c}{r}\right)^{2m+1} - 1\right] \tag{10}$$

where Γ_o and n_o are the particle flux and number density at the outer wall.

Because of the non-linear nature of the centrifugal force, stable orbits are possible. Particles which enter the cyclone can be "trapped" at a radial position at which all of the forces on the particle balance. This possibility is responsible for the singular behavior of eqn. (10). These particles are assumed to be collected (in practice, they would drop from the system under the influence of gravity). Thus, all particles above a certain critical diameter - termed the "cut-size" - are collected. The cut size is determined by the solution to the equation

$$bE_o + \frac{\beta U_{to}^2}{R_i}\left(\frac{R_c}{R_i}\right)^{2m-1} = U_o , \tag{11}$$

where it is important to recognize that both b and β are functions of the particle size! This abrupt transition from no collection to complete collection is shown in Figure 3.

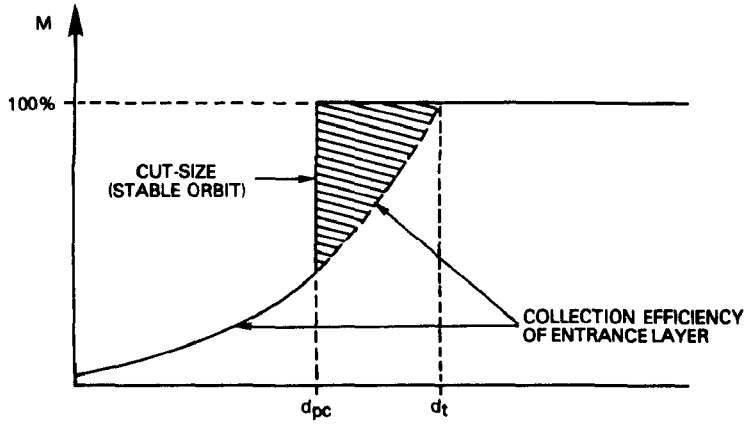

Figure 3. Efficiency of Cyclone Including Both Cut Size and Entrance Layer Effects

To complete the solution to the problem, it is necessary to specify the inlet conditions. At first glance, it would seem appropriate to set the inlet particle flux equal to the volume flow rate through the cyclone times the inlet number density. However, since particle flux conserved, this would imply that all entering particles pass through the cyclone uncollected (except for those trapped into stable orbits). In actual fact, the boundary condition at the outer wall needs careful examination. Because the flow is introduced over a finite thickness (see Figure 4), the radial velocity of the gas at the outer wall goes to zero. Consequently, even extremely fine particles can be thrown against the outer wall and collected.

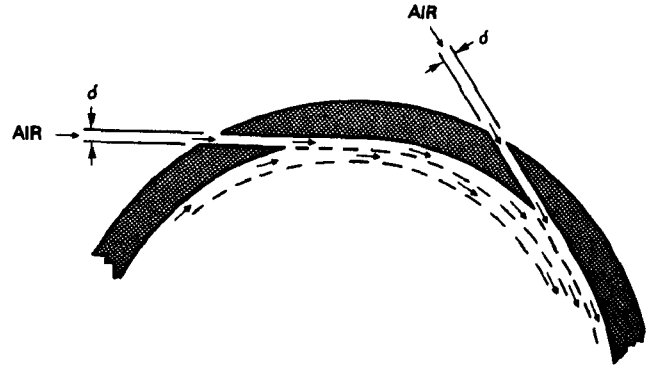

Figure 4. Close-up View of Distributed Inlets

Direct integration of the governing equations (eqns. 1-9) over this thin layer results in

$$\Gamma_o = n_o \left[U_o - \frac{\beta U_{to}^2}{R_c} - bE_o \right] . \tag{12}$$

Since the total rate at which particles enter the cyclone is given by

$$\Gamma_{in} = n_o U_o , \tag{13}$$

the efficiency of the outer entrance layer of the cyclone becomes

$$\eta_1 = \frac{\Gamma_{in} - \Gamma_o}{\Gamma_{in}} = \frac{\beta U_{to}^2 + bE_o}{U_o} \tag{14}$$

This result is shown in Figure 3. Note that all particles above a critical diameter, d_t, are collected in the entrance layer and do not participate in the main vortical flow. Thus, only those particles in the shaded region of Figure 3 are trapped into stable orbits.

DISCUSSION

The efficiency of a cyclone can be characterized by its cut-size. The general equation for the cut size of an electrocyclone is given by eqn. (11). In the absence of electrical effects, the inertial cut size, d_{pi}, is

$$d_{pi} = \sqrt{\frac{18\mu U_o R_i}{\rho_p U_{to}^2} \left(\frac{R_i}{R_c} \right)^{2m-1}} . \tag{15}$$

This result is the classic hydrodynamic cut size for a cyclone (Bhatia and Cheremisinoff 1977).

A similar cut size can be computed for electrostatic effects once the mechanism responsible for the particle charge is identified. In many electrostatic particle removal devices, the charge is imparted by a corona charger. For these systems, the saturation charge obtained by a conducting particle in a corona charger is given by

$$q \approx 3\pi\varepsilon_o d_p^2 E_c , \tag{16}$$

where ε_o is the permittivity of free space ($\varepsilon_o = 8.854 \times 10^{-12}$ F/m) and E_c is the electric field in the charging zone.

Thus, for a particulate suspension which has received its electrical charge from a corona source, the electrostatic cut-size, d_{pe}, can be computed from eqn. (11) in the limit of zero inertial effects

$$d_{pe} = \frac{\mu U_o}{\varepsilon_o E_o E_c}. \tag{17}$$

To compare the electrostatic cut size to the hydrodynamic cut size, it is necessary to specify a particular cyclone configuration. However, it is possible to make several general statements about the manner in which these cut sizes scale.

For example, varying the flow through a given cyclone will alter both cut sizes. With increasing flow rate, the electrostatic cut size increases while the hydrodynamic cut size decreases (see Figure 5). This result agrees with the increase in efficiency observed by Giles[7] at low flow rates.

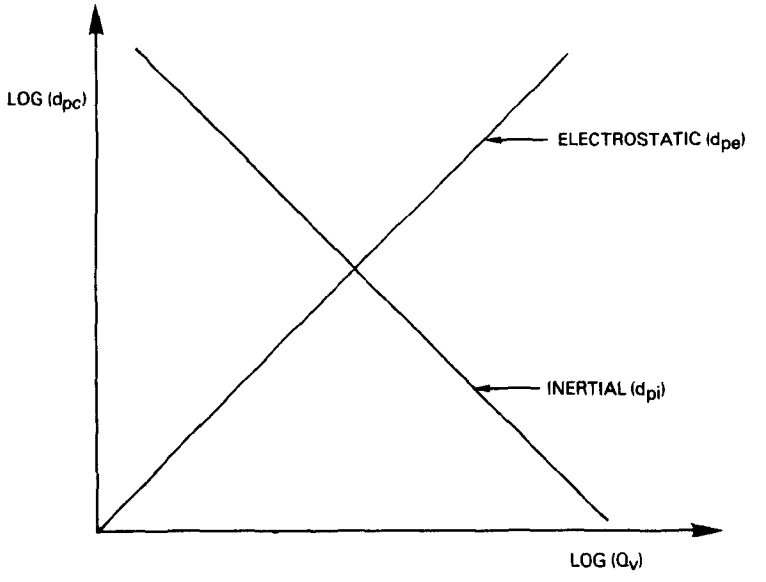

Figure 5. Qualitative Comparison of the Effect of Volume Flow Rate on Both the Electrostatic and Hydrodynamic Cut-size of a Specific Cyclone

As the size of conventional cyclones is increased, the efficiency decreases (cut-size increases). This decrease is a consequence of the erosion/saltation phenomena which limit the inlet velocity to approximately 30 to 40 m/sec. Since the tangential inlet velocity remains constant as the size of the device increases, the radial velocity also remains constant for geometrically similar cyclones. Thus, the cut size increases as the square-root of the cyclone size.

In contrast, the electrostatic cut size is unaffected by increases in size (at fixed inlet tangential velocity).

A comparison is made in Figure 6 between the effect of size on the electrostatic and hydrodynamic cut sizes.

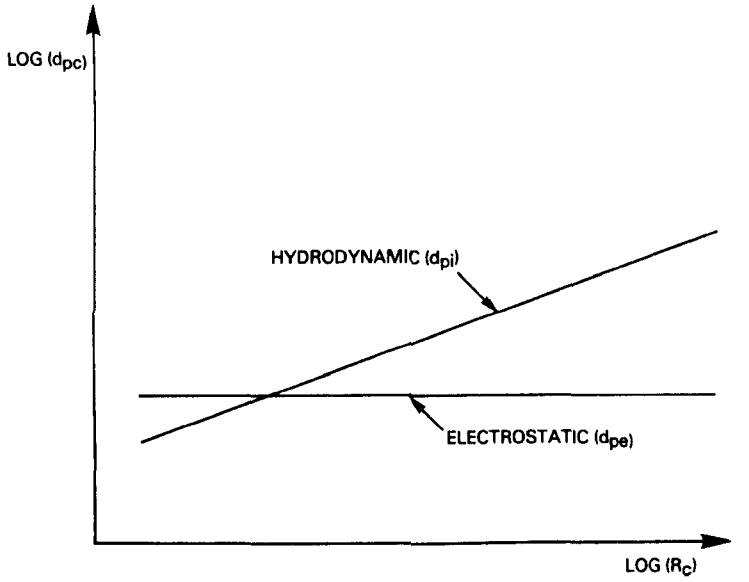

Figure 6. Qualitative Comparison of the Effect of Cyclone Size on Both the Electrostatic and Hydrodynamic Cut Size

CONCLUSION

A simple model has been developed for the collection efficiency of an electrostatically enhanced cyclone. The electrostatic forces are shown to augment the inertial forces in these electrocyclones resulting in improved performance.

Equations for the hydrodynamic and electrostatic cut sizes are presented and these results are used to investigate the scaling of electrocyclones with size and flow rate.

ACKNOWLEDGEMENT

This work was performed under DOE Contract No. EX-76-C-01-2357 to the General Electric Energy Systems Program Department by Corporate Research and Development.

REFERENCES

R. McK. Alexander, "Fundamentals of Cyclone Design and Operation", Proc. Aust. Inst. Mining and Met, 152-153, 203 (1949).

M.V. Bhatia and P.N. Cheremisinoff, "Cyclones" Chapter 10 in Air Pollution Control and Design Handbook, P.N. Cheremisinoff and R.A. Young, editors, Marcel Dekker, New York (1977).

P.W. Dietz, "Collection Efficiency of Cyclone Separators", submitted J.A.P.C.A. (1979).

W.B. Giles, "Electrostatic Separation in Cyclones", Symposium on the Transfer and Utilization of Particulate Control Technology, Vol. 3, EPA-600/7-79-044c, 291 (1979).

D. Leith and W. Licht, "The Collection Efficiency of Cyclone Type Particle Collectors - A New Theoretical Approach" AIChE Symp. Series Vol. 126, 68, 196 (1972).

F. Molyneux, "Electrostatic Cyclone Separator", Chem and Process Eng, 517 (1963).

J. Petroll and K. Langhammer, "Vergleichsversuche an Zyklonabscheidern" Freiberger Forschunsheft A-220, 175 (1962).

S.L. Soo, "Dynamics of Charged Suspensions", International Reviews in Aerosol Physics and Chemistry Vol. 2, G.M. Hidy and J. Brock, Ed., Pergamon Press (1971).

S.L. Soo, "Some Basic Aspects of Cyclone Separators", Proceedings of the First International Conference in Particle Technology, 9 (1973).

CONDENSATIONAL ENLARGEMENT AS A SUPPLEMENT TO PARTICLE CONTROL TECHNOLOGIES *

By:

James T. Brown, Jr.
Department of Physics
Colorado School of Mines
Golden, Colorado 80401

ABSTRACT

An experimental study has been undertaken at the Colorado School of Mines to evaluate the feasibility of using condensational enlargement to enhance the collection efficiency of existing dust control technologies for sub-micron particulates. Although the study was begun to consider the problem of respirable dust control in the underground coal mine environment, this enhancement technique shows promise for a more general class of applications.

In the experiments to be reported on, particulates are injected into a continuous flow thermal diffusion chamber and subjected to varying environmental conditions; saturation ratio (rel. humidity), temperature, and residence time were the parameters. The results show that condensation on a dust nucleus (~0.1 micron) can bring it to a size of several microns in a sufficiently short period of time as to indicate engineering applicability of the concept.

* This project was supported by Grant No. ROI OH 00565-02 awarded by the National Institute of Occupational Safety and Health.

INTRODUCTION

An experimental study of the properties of respirable particulates was undertaken at the Colorado School of Mines in 1975. The object of this study was to consider methods by which the control of respirable coal dust in underground mines might be enhanced. It was felt that particle enlargement via condensation of water vapor showed substantial promise for dust control enhancement and therefore, knowledge of the interaction of water vapor with respirable particulates became very important. The experimental results of our studies are the substance of this report.

A number of industrial situations exist wherein conventional dust scrubber technology cannot be applied because of constraints imposed by space, noise, safety or other environmental considerations. Such a situation exists in underground coal mines. Space in the working area near the face is very limited and therefore dust collecting devices must operate in close proximity to the miners. Hence noise is a factor. In addition, the mine atmosphere often contains a mixture of methane with the coal dust which could build up to explosive concentrations inside a collector. This, plus the overall mine ventillation requirements place lower limits on the air flow through the collector.

Inertial separators, besides losing efficiency for sizes below about five microns, generate considerable noise when operating at the volumes required in a typical coal mine operation. Nevertheless, inertial separators such as cyclones and wet venturis, some combined with filtering mechanisms, are being tried as machine-mounted scrubbers. Baghouses, which can be quite efficient even at smaller sizes, have not been employed to any great extent because of the ventillation requirements and heavy dust loading. Electrostatic precipitators, also efficient at small sizes, require operating voltages of 30 - 100 kV; the frequent arcing which occurs at these voltages presents a serious explosion hazard in the presence of methane and coal dust. The mainstay for dust control in almost all mining operations has been the water spray.

Water sprays and most inertial separators, unless operated at very high energy input levels, fall to near zero efficiency for particles smaller than five microns. It is only those particles smaller than five microns that have an appreciable probability of penetrating the upper respiratory track and only those smaller than about one micron are likely to be trapped in the alveoli. Those particles that are deposited in the alveoli give rise to coal workers' pneumoconiosis (black lung), silicosis, and other debilitating and sometimes fatal respiratory pathologies. Consequently, one concludes that although sprays and inertial devices reduce the mass loading of the air, little is done to reduce the respirable dust content. Since the efficiency of such commonly used control methods is strongly size-dependent (falling rapidly with decreasing particle size) particle enlargement if practical can improve their efficiency and decrease the health hazard of dusty environments.

Figure 1 hints at the difficulty in using water sprays for the control of small particulates; in order to attain optimal efficiency, the spray

droplet must be comparable in size to the dust particles, with the maximum occurring for a size ratio of about 0.7 (taken from Hocking, (1950)[1]). Figure 2 shows the same results but for larger droplets (taken from Mason, (1971)[2]).

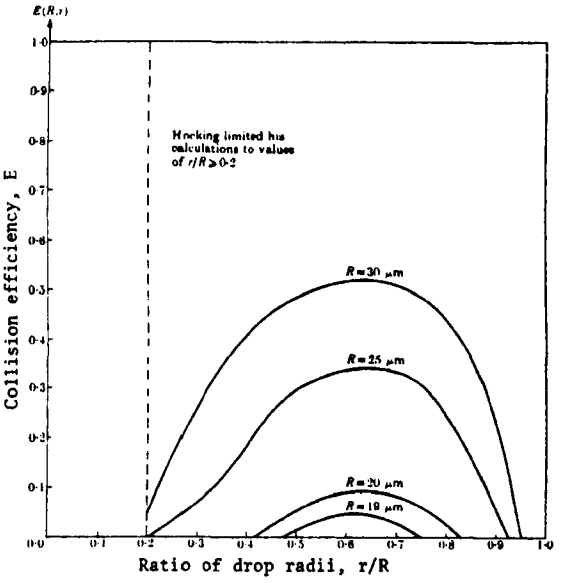

Figure 1. The collection efficiency of water droplets as a function of their size (R) relative to the size of the collected droplet (r). (from Hocking (1950)[1]).

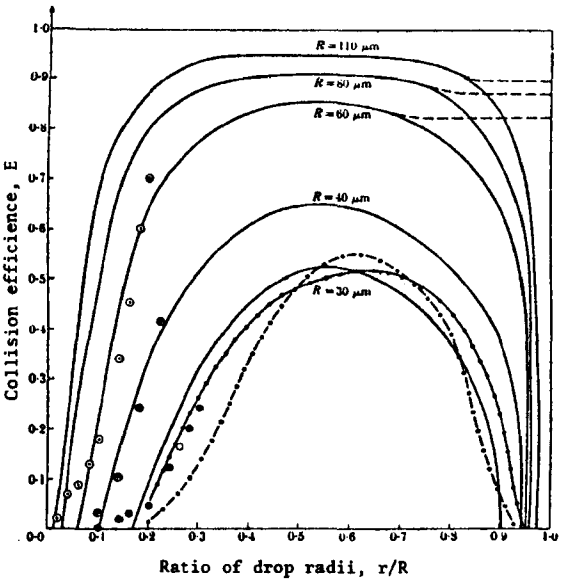

Figure 2. The collection efficiency of water droplets as in Figure 1. (from Mason (1971)[2]).

Studies of pre-conditioning by condensation enlargement in other scrubbing situations have been reported. The earliest appears to be that of Fanhoe et. al. (1951)[3] on radioactive aerosols. They report an increase from 40% to 90% for the efficiency of both cyclones and impingement scrubbers for particles of initial average diameter of 0.8 microns - enlarged to 2.0 microns or larger. Lapple and Kamack (1955)[4], Semrau, et. al. (1958)[5], and Rozen and Kostin (1967)[6], have studied condensation effects in specific types of scrubbers and all report marked increases in collection efficiency due to enlargement.

More basic studies aimed at elucidating condensation and phoretic mechanisms in particulate collection have been reported by Fuchs and Kirsch (1964)[7], Truitt and Davis (1971)[8], Semrau and Witham (1975)[9], and Yoshida et. al. (1976)[10]; Yoshida et. al. (1976)[10] present some quantitative data on the rate and extent of growth of sub-micron particles in supersaturated air produced by mixing hot saturated air with cold air.

BACKGROUND

In the experiments at the Colorado School of Mines Particulate Science Laboratory, particle enlargement by condensation of water vapor is being studied in a continuous flow, parallel plate thermal diffusion cloud chamber described later in this article. The supersaturated conditions necessary for particle growth are produced by the thermally-driven diffusion of water

vapor through air. In the work being presented, we have not included an analysis of the initiation of water droplet growth, i.e., heterogeneous nucleation, on the dust particles. However, a study of this phenomenon and the associated time lab is currently underway in our laboratory.

The classical model for droplet growth by condensation is due to Maxwell (of electricity and magnetism fame) and may be taken as a zeroth-order description for use here and is presented in detail by Mason (1971)[2]. A widely accepted generalization of the classical model has been presented by Fukuta and Walter (1970)[11] and should be used for a detailed description of condensational growth, particularly for small droplets (several microns). In the Maxwell model it is assumed that the diffusion and temperature fields are in a steady state, that the water vapor may be described as an ideal gas, and that the Clausius-Clapeyron equation gives the temperature dependence of the vapor pressure during the phase change. The resulting non-linear differential equation may be integrated to yield

$$r^2(t) = r_o^2 + 2(S - 1)t/(a + b) \quad (1)$$

a = diffusion related constant
b = conduction related constant
S = saturation ratio

In the Fukuta-Walter model the form of the equation remains the same but the constants a and b assume some implicit size dependence. When important, curvature and solution effects may be readily included into the model.

For the sake of the experiments under discussion, the second term in equation (1) is the important one, in particular the factor of (S - 1). When the ambient conditions are saturated, S = 1 and no growth occurs. If the relative humidity were 102%, then S = 1.02 and the growth rate would be twice as large as when the relative humidity is 101%. The growth rate could be increased dramatically by simply increasing the relative humidity from 101% to 110%. The conclusion is that the rate of growth is a very sensitive function of the relative humidity or saturation ratio. The results to be presented below correspond to values of S equal to 1.006, 1.011, 1.020, and 1.032.

EXPERIMENT

The experimental measurements of the condensational enlargement of submicron particulates were made in a continuous flow parallel plate thermal diffusion chamber. This chamber is a modification of one used earlier by Saxena and Fukuta (1974)[12] and has recently been thoroughly analyzed (Brown and Schowengerdt 1979[13]). Figure 3 is a schematic drawing of the diffusion cell of the chamber. Because of the continuous range of supersaturations produced, it is often referred to as a spectrometer. It consists of three functionally different parts; the inlet chamber, the thermal circuit or diffusion cell, and the exhaust chamber.

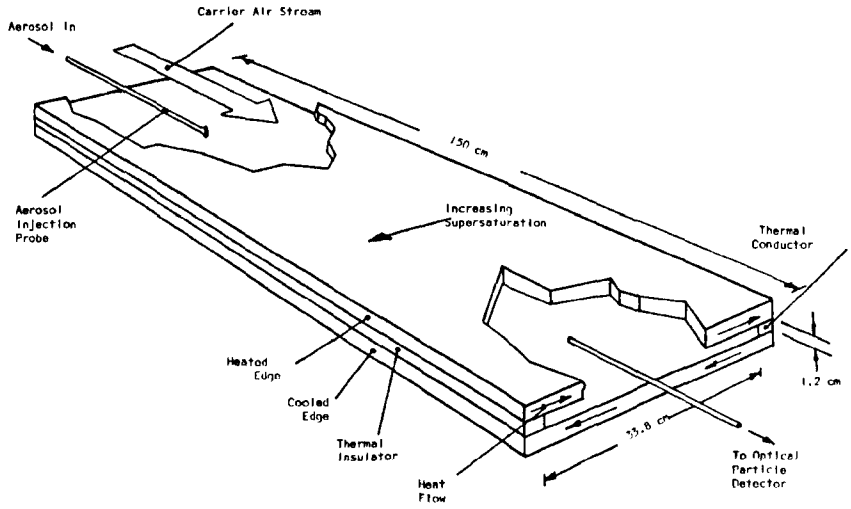

Figure 3. Continuous flow parallel plate thermal diffusion cell.

The inlet chamber (not shown) is designed to provide for the uniform distribution of pre-humidified carrier air over the cross section of the diffusion cell and for the alignment of the injection probe through which the dust nuclei and respirable particulates are injected into the air stream. It also insulates the inlet end of the diffusion cell from heat exchanges with the surroundings.

Similarly, the exhaust section is designed to maintain laminar flow at the exit, align the sampling probe of the particle counter with the inlet probe, and to insulate the outlet end of the cell from heat exchanges.

The supersaturated conditions ($S > 1$, see equation 1) necessary for droplet growth are produced in the diffusion cell. The heated and cooled junctions (Figure 3), which are separated by an insulating strip, establish an approximately linear thermal gradient along the metal top and bottom plates (the side opposite the heated and cooled junction is also conducting). This "folded" thermal circuit results in a continuously variable thermal gradient across the gap between the plates. The gradient has a maximum at the heated and cooled side and a minimum near zero on the opposite side next to the conducting junction. The inside surfaces of the chamber are covered with canvas which is periodically wetted in order to maintain saturated boundary conditions.

Figure 4 (taken from Wieland 1956[14]) shows qualitatively how the metastable supersaturated state results. At any point within the chamber the vapor density and temperature vary, to a high degree of accuracy, linearly from top to bottom. The Clausius-Clapeyron equation gives the saturated vapor pressure as a function of the temperature. The top line shows the actual vapor pressure which results from the diffusion of the water vapor from the saturated hot side to the saturated cold side where the vapor density is lower. As can be seen, the vapor pressure that results from the diffusion process is greater than the saturated pressure at the same

temperature. The ratio of the two is the saturation ratio:

$$(2) \qquad S = p(T)/p_{sat}(T)$$

The internal temperature of the chamber is monitored with an array of 60 thermocouples which extend through the metal plates and into the wetted canvas.

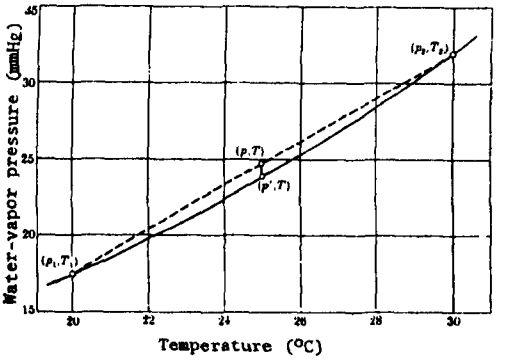

Figure 4. The saturation vapor pressure (solid line) and the vapor pressure resulting from the diffusion of water vapor between the plates of diffusion cell of Figure 3 (dashed line). (from Wieland (1956)[14]).

In making the droplet growth measurements the test aerosol is injected into the carrier air stream through the movable inlet probe shown in Figure 3. Care must be taken to insure that all transients in the velocity, temperature, and diffusion fields have disappeared before the injection of the test particulates (see Brown and Schowengerdt 1979[13]). The velocity of the carrier air is determined through a series of time-of-flight measurements. The residence time in the supersaturated environment is then inferred from the position of the inlet probe and the carrier air velocity.

An optical particle counter (Model 208, Climet Instruments, Redlands, California) is used to count and size the grown droplets. The output pulses from the white-light detector are processed and stored in a multichannel analyzer and droplet size data are obtained from it in the form of peak locations (modal diameters). The input particulates are the naturally occurring ones in the lab air and their size is monitored with a laser particle counter (ASAS, Particle Measuring Systems, Boulder, Colorado). Latex spheres are used for calibration.

RESULTS AND CONCLUSIONS

The results of the experiments are shown in Figures 5 - 8. The dashed curve is obtained from the application of the Fukuta-Walter model to conditions of the diffusion cell (see Brown and Schowengerdt 1979[15] for details of the analysis). The agreement with theory is good. There is, however, a clear indication of a small systematic disagreement in the slopes of the curves.

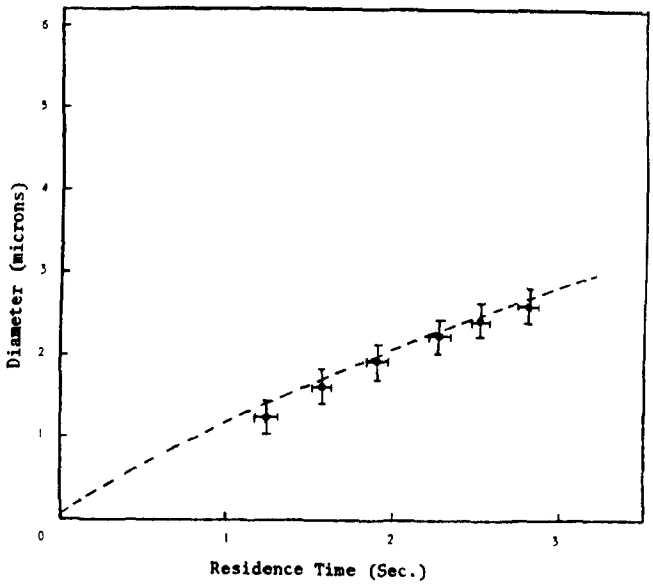

Figure 5. Experimental and theoretical growth curve for water droplets. S = 1.006, T = 28.3°C.

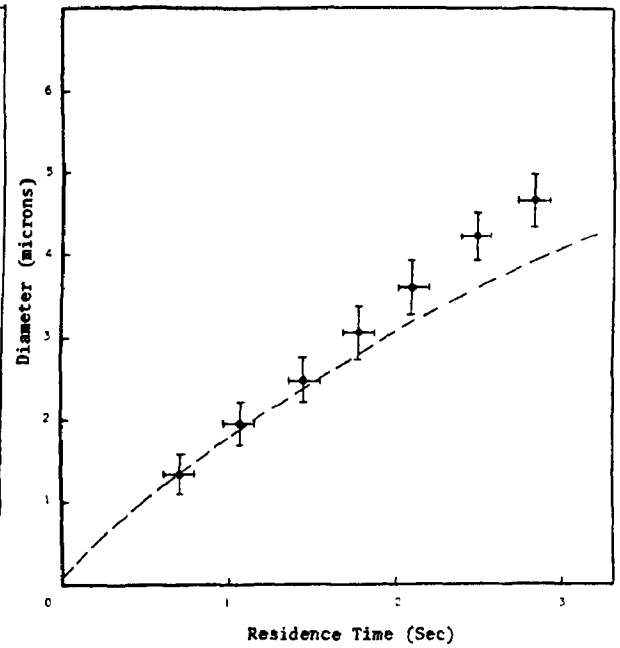

Figure 6. Experimental and theoretical growth curve for water droplets. S = 1.011, T = 27.5°C.

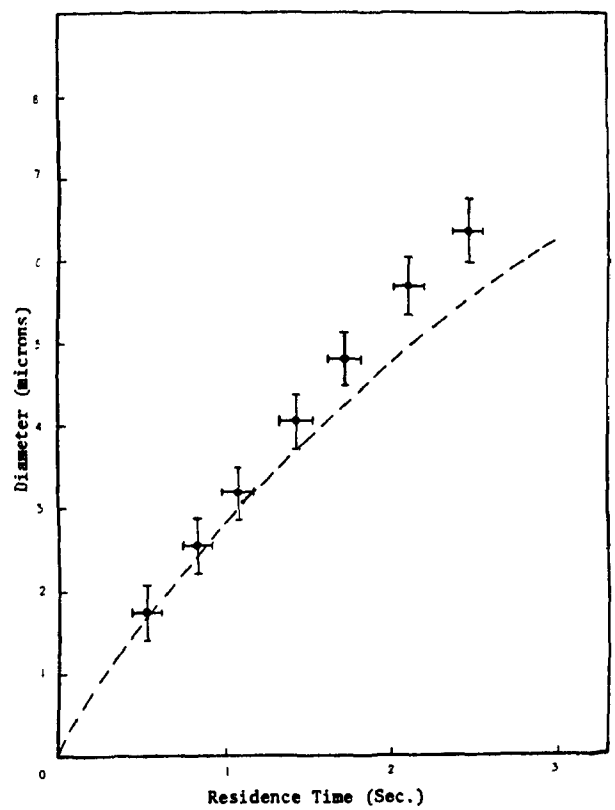

Figure 7. Experimental and theoretical growth curves for water droplets. S = 1.020, T = 27.5°C.

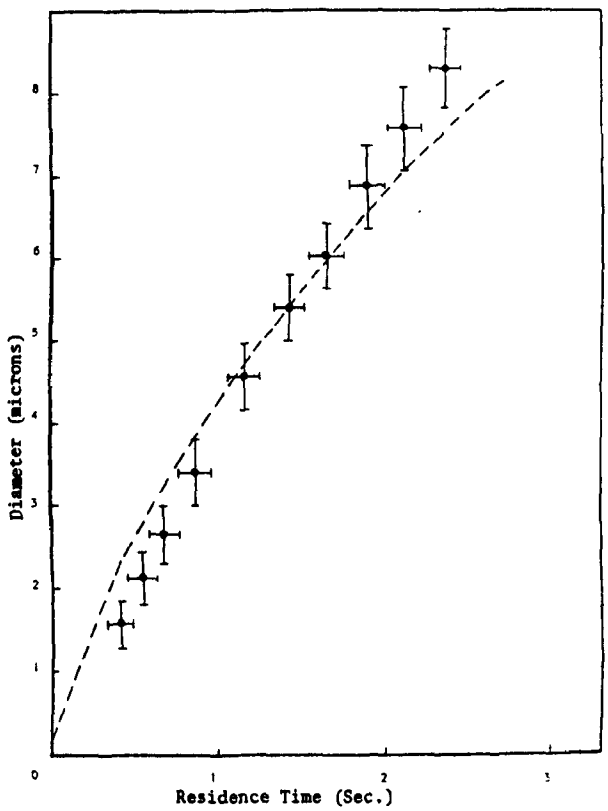

Figure 8. Experimental and theoretical growth curves for water droplets. S = 1.032, T = 28.2°C.

The conclusions to be drawn from these growth curves are as follows:

1. even for modest saturation ratios as in Figure 8, particles of initial size less than 0.2 microns can be enlarged to approximately 7 microns in about 2 seconds.

2. the growth rate is indeed a sensitive function of the saturation ratio and there is good reason to expect much more rapid growth to even larger sizes for increased saturation ratios.

The possibility of increasing the size of particles as small as 0.1 microns, which are far to small for most control devices to collect, to as large as 10 microns, offers the potential for enhancing the efficiency of several existing control methods. Since the particles in the 0.1 - 1.0 micron range constitute the major source of the degradation of meterologic visibility (Willeke and Brockman, 1977[16]) and are also largely responsible for respiratory disorders due to inhalable particulates, their efficient control is of profound importance.

REFERENCES

1. Hocking, L.M., Quart. J. Roy. Meteorol. Soc. 85, 44 (1950).

2. Mason, B.J., The Physics of Clouds, Clarendon Press, Oxford, 1971.

3. Fanhoe, R., Lindroos, A.E., and Ahelson, R.J., Ind. Eng. Chem. 43, 1336, (1951).

4. Lapple, C.E. and Kamack, H.J., Chem. Eng. Progr. 51, 110, (1955).

5. Semrau, K.T., Marymowski, C.W., Lunde, K.E., and Lapple, C.E., Ind. Eng. Chem. 50, 1615, (1958).

6. Rozen, A.M. and Kostin, V.M., Intl. Chem. Eng. 7, 464, (1967).

7. Fuchs, N. and Kirsch, A., Chem. Eng. Sci. 20, 181, (1965).

8. Truitt, J. and Davis, R.J., Am. Ind. Hyg. Assoc. J., p. 583, Sept. 1971.

9. Semrau, K.T. and Witham, C.L., APCA Proceedings, 68th Annual Meeting Paper #75-30.1.

10. Yoshida, T., Kousada, Y. and Okuyama, K., Ind. and Eng. Chem. Fund. 15, 37, (1976).

11. Fukuta, N. and Walter, N.A., J. Atmos. Sci. 27, 1160, (1970).

12. Saxena, V.K. and Fukuta, N., Denver Research Institute Report No. 2657, University of Denver (December 1974).

13. Brown, J.T. and Schowengerdt, F.D., J. Aerosol Sci. 10, 339, (1979a).

14. Wieland, W., Z. Angew. Math. Phys. 7. 428, (1956).

15. Brown, J.T. and Schowengerdt, F.D., J. Aerosol Sci., October 1979 (in press).

16. Willeke, K. and Brockman, J.E., Atmos. Environ. 11, 995, (1977).

WELDING FUME AND HEAT RECOVERY
THE PROBLEM, THE SOLUTION, THE BENEFITS

By:

Richard C. Larson
Technical Sales Manager
Torit Division, Donaldson Company, Inc.
St. Paul, Minnesota 55164

ABSTRACT

Welding is an important and constantly evolving technology enjoying a higher growth rate in the metalworking industries than the general industrial growth. Welding as with most industrial processes does have its inherent problems. One of the problems is the fumes and gases generated during the welding process. This paper presents a complete technical analysis of the problems associated with most of the more common types of industrial welding. In addition, alternative engineered solutions are investigated in detail which includes a descriptive analysis of several types of air cleaning devices. Finally, the control of the welding fume problem is analyzed based on actual test installations demonstrating the ability to achieve acceptable particulate and gas concentrations levels in the worker's environment, while achieving significant heat recovery (or conditioned air) by a unique approach to air recirculation.

WELDING - THE PROBLEM

The use of welding in joining metals has had a phenomenal use since about 1930; this growth has been faster than the general industrial growth. Most common everyday items are, in one way or another, dependent upon welding for their economical construction. Automobiles, electronic equipment, household appliances, kitchen utensils, bridges, ships, aircraft, buildings, farm machinery - all are made more economically in today's technology by using one or more methods for joining by welding. Welding continues to be a growing industry all over the world. In the last 28 years, the usage of welding has increased 900%.

Welding, as with most industrial processes, does have its inherent problems. One of those problems is the fume as gases generated during the welding process. The fumes and gases generated present real and distinct hazards not only to operational equipment, but especially to the health and well being of the personnel who undertake such tasks.

Historically, the approach to the fume and gas problem has been either to ignore it, or a mediocre attempt to ventilate this contaminated air by either general ventilating powered roof exhausters or localized fume exhausters in which in either case the air is exhausted outside. It is now apparent to most production companies, which utilize welding, that a good concerted effort must be made to handle the welding fume problem. This has, in large been brought about by the Occupational Safety and Health Act (OSHA) of 1970 and perhaps even to a greater degree by the energy conservation consciousness of most industrial plants. The impact of OSHA and rising fuel costs behooves companies which use welding processes to tackle the problem of welding fume more directly, to analyze the alternative solutions, and to justify the selected approach by any realized tangible and/or intangible benefits that may be gained.

ANALYZE THE PROBLEM

In the process of analyzing the welding fume problem, it is important not to lose sight of the final objectives, i.e. to control the fume to the point that it is not an industrial hazard while keeping constantly alerted to energy conservation.

Obviously, this will require a given air volume and an air moving device to remove this contaminated air from the working area and some sort of air cleaning device to hopefully clean the air to an acceptable level such that it would not have to be exhausted outside.

This problem analysis would include the type of welding, the metal being welded, the dimensions and layout of working areas, the number of welding stations or welders or both (gas and electric arc), the rate of welding, the presence or absence of air curtains or cross-drafts, the OSHA requirements, and the aspect of energy conservation.

The most common types of welding would include:

1. gas welding
2. torch brazing and soldering
3. shielded metal arc
4. gas shielded arc
5. plasma arc
6. submerged arc
7. flux cored arc
8. oxygen and arc cutting
9. thermal spraying
10. ultrasonic welding
11. laser welding
12. diffusion welding
13. explosive welding
14. resistance welding
15. friction welding

Analyzing the fume problem in light of the impact of OSHA, has only recently become rather obvious. There are, as briefly discussed earlier, many potential fume and gas hazards produced in most welding processes. A more complete list is tabulated in the Appendix (See Figure 1). OSHA has set Threshold Limit Values (TLV's) for all of these materials, and no worker is allowed to be exposed to concentrations above these levels (See Figure 2). These Threshold Limits are the maximum atmospheric concentrations, in milligrams per cubic meter of air, which is felt safe for the normal individual to breathe for eight hours a day, five days a week. Evaluation of a process involves all of the factors previously discussed and may include an air sampling program.

If there are existing air moving devices; fans, fume exhauster, etc., the problem should further be analyzed as to the amount of air and correspondingly the amount of heat which is presently exhausted outside.

Having analyzed all of the necessary aspects of the welding fume problem, the alternative solutions are investigated.

WELDING - THE SOLUTION

Ventilation for welding operations are dictated by all of the factors considered thus far; however, other factors such as weather, the amount of heat generated and the presence of volatile solvents also contribute to the need for a ventilation system. Welding screens, which shield nearby workers and onlookers from the ultraviolet light from the welding arc should not restrict ventilation. They should be mounted about 2' above the floor.

Depending on the welding process and the potential fumes and gases generated, the ventilation system could be one of three types: general ventilation; source ventilation; or a combination of source and general ventilation.

Ventilation for general welding and cutting, meaning for metals not specifically covered later is required when welding under any of the following conditions.

- In a space of less than 10,000 cubic feet per welder.
- In a room with a ceiling height less than 16'.
- In confined space or where the area contains partitions or other structures that significantly obstruct cross-ventilation.

SOURCE VENTILATION

Source ventilation, as we shall define it, consists of localized hoods interconnected with duct work hopefully with a high efficiency air cleaning device and a fan.

One of the more common type hoods used in welding fume control is the freely suspended hood. This type of hood is very similar to the articulating fume exhauster hood. The air volume required to control the fume is dependent on the distance 'x', which is the distance from the face of the hood to the point where the arc is struck. It is important to remember that it is not the volumetric air flow that you have in your hood that controls the fume. The control is achieved by the capture velocity at the point of fume generation. The capture velocity for welding fume is 100 feet per minute. If a variation of a source ventilation hood is used, remember you must achieve 100 feet per minute capture velocity. The American Welding Society has studied capture velocities for many types of welding under many types of conditions and has found that the required capture velocity can vary from 80 feet per minute to 200 feet per minute. (See Figure 3)

Another type of source collection hood that can be used in welding fume control is the cross-draft table. This type of hood is very adaptable to fixed position or fixture welding. The air volume is dependent on the length of the bench with a maximum bench width of 24 inches. Variations of this hood are frequently used. (See Figure 4)

Another type of hood that is sometimes used in fume control is the downdraft table. Note that in my opinion this type of hood is not recommended. Temperatures as high as 6,000 degrees centigrade exist at the arc zone and the fume will rise away very quickly for the first one to three feet. The thermal gradients that are created and the swift plume velocities make it difficult to pull the fume back down into the hood. In addition, if the weldment is a large piece and it covers most of the table, you have lost all air flow or capture velocity at the arc zone. (See Figure 5)

Once the proper source collection hoods have been designed, they are usually connected to a central duct system which must be designed for proper air balance. (See Figure 6)

An example of a source collection installation is at the Cornelius Company, which manufactures Vending Machines. The hoods that were used are slotted crossdraft hoods at about a 45 degree tilt. The slots are located all the way around the work piece at the critical weld areas. The complete absence of fume from the general plant air is easily viewed by looking down the length of this plant and noting there is no light scattering underneath the fluorescent light fixtures. If the exhaust system is turned off, the plant will fill up with fumes in a matter of 10 minutes. This system consists of the hoods and duct work mentioned earlier as well as a Torit TD-6120 cartridge collector and a fan which pulls approximately 15,000 cubic feet per minute of air. The cartridge collector has been tested to be 99.7% efficient on this welding fume which has an average particle size of 0.6

microns. All of the cleaned air from the TD is recirculated back into the plant during the heating season. The returned air has a particulate level of over 2,000 times below the OSHA Threshold Limit Value.

OSHA has established Ventilation Standards for General Welding and Cutting in Confined Spaces.

FEDERAL OSHA VENTILATION STANDARDS FOR GENERAL WELDING AND CUTTING IN CONFINED SPACES

- Adequate ventilation is required to prevent accumulation of toxic materials or oxygen deficiency for welders, helpers and other nearby personnel.
- All replacement air shall be clean and respirable.
- If it is impossible to provide ventilation, approved airline masks or hose masks are required.
- In areas that are immediately hazardous to life, approved hose masks with blower or self-contained breathing apparatus shall be used.
- If welders and helpers are provided with hose masks, hose masks with blower or self-contained breathing apparatus, a worker shall be stationed outside of the confined space to ensure the safety of those working within.
- Oxygen shall never be used for ventilation.

Operations involving specific toxic metals or other substances require source ventilation or approved respiratory protection without regard to workroom size and the other aforementioned conditions that govern whether ventilation is needed for general welding. The OSHA Standards that cover these materials are as follows:

- Operations involving fluorine (as a chemical compound, not a gas) in confined spaces require adequate ventilation to prevent the accumulation of toxic material or oxygen deficiency. The same standards as those for general welding in confined spaces apply. Outside of confined spaces the need for local exhaust ventilation or airline respirators depends on contaminant levels although "experience has shown such protection to be desirable for fixed-location production welding and for all production welding on stainless steels."
- Welding or cutting involving zinc in confined spaces must meet the same requirements as general welding in confined spaces. Indoors these operations require local exhaust booths or hoods meeting the standard of 100 feet per minute in the welding zone.
- Welding or cutting involving lead-base metals in confined spaces requires local exhaust ventilation. When these operations are conducted indoors, local ventilation or airline respirators are required. Outdoors approved respirators are needed. In all cases workers in the immediate vicinity of the operation shall be protected as necessary by local exhaust ventilation or airline respirators.

- Welding or cutting involving beryllium-containing base or filler metals whether conducted indoors, outdoors or in confined spaces requires local exhaust ventilation and airline respirators unless air sampling under the most adverse conditions shows that beryllium exposures are below acceptable OSHA limits. As with lead, nearby workers require protection by ventilation or airline respirators if needed.
- Welding or cutting involving cadmium-bearing or cadmium-coated base metals indoors or in confined spaces requires local exhaust ventilation or airline respirators unless air sampling under the most adverse conditions shows that worker exposures are within acceptable limits. Outdoors such operations require approved respiratory protection such as fume respirators.
- Welding or cutting indoors or in confined spaces involving metals coated with mercury-bearing materials including paint requires local exhaust ventilation or airline respirators unless air sampling under the most adverse conditions show that workers' exposures are within acceptable limits. Outdoors such operations require approved respiratory protection.
- Cutting of stainless steels with oxygen using either a chemical flux or iron powder, or using a gas-shielded arc, requires mechanical ventilation adequate to remove the fumes generated.
- Degreasing or other cleaning operations involving chlorinated hydrocarbons must be located so solvent vapors do not reach any welding operation. In addition, trichloroethylene and perchloroethylene should be kept out of atmospheres penetrated by the ultraviolet radiation of gas-shielded welding operations. This requirement is to avoid the decomposition of solvent vapors into toxic substances.

It is important to point out that air sampling of the welders breathing zone in a given plant is necessary to determine if one is in compliance with the OSHA Standards and/or the degree of ventilation that is required.

GENERAL VENTILATION

Natural ventilation is usually considered adequate to prevent the accumulation of excessive amounts of fumes when welding on mild steel with electrodes that do not contain fluorides in the covering, provided that room volume is not less than 10,000 cubic feet per welder, the ceiling height is at least 16' and cross-ventilation is not blocked by partitions, equipment, etc. In spaces that do not meet these requirements, general mechanical ventilation is required.

The air volume that is required for general ventilation could be computed by one or more of the following methods.

General Ventilation Air Volume Requirements

1. One air change every five (5) minutes.
2. 5 feet per minute updraft velocity per square foot of floor space.
3. 2000 cubic feet per minute per welder (OSHA recommendation).
4. American Conference of Governmental Industrial Hygienists recommendations.

General Ventilation, where local exhaust cannot be used:

Rod, diameter	CFM/welder*
5/32	1000
3/16	1500
1/4	3500
3/8	4500

OR

A. For open areas, where welding fume can rise away from the breathing zone: cubic feet per minute required = 800 X pounds per hour rod used.

B. For enclosed areas or positions where fume does not readily escape breathing zone: cubic feet per minute required = 1600 X pounds per hour rod used.

*For toxic materials higher air flows are necessary and operator may require respiratory protection equipment.

Each of the above methods must be thoroughly investigated since no one method is ideal; however, methods 3 and 4 are the most consistent direct methods since they deal with air volumes based on the amount of particulate that could be generated, i.e. the number of welders, the size of welding rod used and the amount of rod used per hour. Methods 1 and 2 are based on air volumes taking into account only the physical dimensions of the welding area without regard to the concentration of welders in this welding area.

In principle, general ventilation removes the fume-laden air usually at the roof level, or at intermediate levels above the welding areas. Since our objective is to not only control the welding fume, but also to conserve energy, our general ventilation system will include an air cleaning device and will return the cleaned respirable air back into the plant atmosphere. A typical layout for a general ventilation system is depicted in Figure 7. This is the general ventilation layout we have found to be the most successful. As is schematically illustrated, the warm fume-laden air is removed at or near the roof level. Since our objective is to not only control the welding fume but also to conserve energy, our system includes a high efficiency TD cartridge collector and we return the cleaned respirable air back into the plant. Note that the system includes a fan, a by-pass damper and low velocity exhaust grilles located at the floor level. Also note that the return air duct work is located up near the roof trusses so as to further take advantage of the elevated air temperatures by virtue of radiation convection heating. By removing the heated fume-laden air at the ceiling and reintroducing the cleaned recirculated air at the floor level combined with the thermal gradients that exist in all plants from the floor to the ceiling, our general ventilation system becomes a very efficient "push-pull" system. Note the inline centrifugal fan and the by-pass damper. This by-pass damper is normally used in the summer months to discharge the "super-heated" air to atmosphere. This causes induced natural ventilation creating a cooling effect within the plant. Additionally, this by-pass damper can be used for emergency by-pass if there should be an equipment failure.

The strategic locations of the exhaust hoods and TD units are based on the criteria mentioned earlier as well as the fact that the exhaust hoods and recirculation grilles must be located in a certain pattern to achieve an effective push-pull system.

One example of a General Ventilation system, based on this design, is located at the Bowen-McLaughlin-York Company in York, Pennsylvania. They manufacture military armored vehicles. The system consists of 27 Torit TD-6120 cartridge collectors. The system filters fume-laden air from the plant at the rate of 364,000 cubic feet of air per minute. At Bowen there are over 250 welders and this system collects more than 4,000 pounds of welding fume per month. This one million dollar air pollution control system will pay for itself in less than five years. An independent testing laboratory was unable to measure any particulate in the collector's return air grilles after 8 hours of sampling.

Occasionally, it may be necessary to design and use a combined general ventilation and source ventilation system. This may be necessary for several reasons, including a welder welding in an enclosed area or perhaps due to localized toxic fume and gas generation. For example a combined system could consist of our previously discussed general ventilation system and a separate hood and fan to remove the welding fume from an enclosed area. This fan blows the removed fume to the ceiling where the general ventilation system takes over and filters the air through the TD unit (See Figure 8). Another version of a combined system is to use a separate hood, fan and small TD collector to control fume generated in perhaps an isolated area within a plant. Note that this small TD unit also returns the clean air back into the plant working environement. (See Figure 9).

SELECTION OF AIR CLEANING EQUIPMENT

There are basically three types of air cleaning equipment that could be used to filter or clean the fume-laden air. This includes an electrostatic precipitator, or mechanically shaken baghouse and the Torit TD Cartridge Collector.

The principle of operation for a modular electrostatic precipitator is that the dust-laden air passes first through an ionizer section which charges the dust particles either positively or negatively depending on the design. These charged particles then pass through the collector plate section and are electrostatically attracted to these plates. Then the clean air (in theory) passes out of the collector plate section. (See Figure 10).

The mechanical shake baghouse uses filter tubes or bags of either natural or synthetic filter media. The contaminated air enters the unit through an inlet and then is filtered through the cloth bag from the inside to the outside. The cleaned air then passes out the outlet. Periodically a compartment is isolated or the unit is shut off and the material is removed from the bags by mechanically shaking them. (See Figure 11).

The Torit TD Cartridge Collector combines the technology of a continuous duty pulse jet baghouse with the technology of cartridge filtration. Each cartridge is 12-3/4" in diameter by 26" long and contains 300 square feet of filter media. The TD collectors we discussed earlier each contain 32 cartridges or the equivalent filter area of 9,600 square feet per unit. The contaminated air enters the inlet and the fume is removed from the air stream by passing through the cartridge from the outside to the inside. This ultra-

clean air is then recirculated back to the plant. As monitored on a pressure drop basis, the cartridges are cleaned automatically, on a "as required" frequency, by backflushing them with sonic velocity pulses of compressed air. The collected fume then falls into the storage hopper. (See Figure 12).

Capital expenditures are important, however, it should not be the base criteria for the selection of air cleaning equipment. A more meaningful criteria in the long term is to examine all of the advantages and disadvantages of each of the individual pieces of equipment, based on the operational characteristics and on a Life Cycle Analysis.

Electrostatic Precipitator (Modular)

Advantages	Disadvantages
Compact	High Maintenance
No complex duct work	Creates ozone and NO_x
Low power cost	Creates space charge
Continuous duty	Mechanical Rappers - moving parts or liquid wash system
Low pressure drop	Decreased efficiency overtime
	Able to handle only light loadings .004 grains per cubic foot or less

Mechanical Shake Baghouse

Advantages	Disadvantages
High efficiency	Intermittent duty
Low operating cost	Moving mechanical parts
	Large space required
	Normally requires precoating
	Requires external duct work

Torit TD Cartridge Collector

Advantages	Disadvantages
High efficiency	Requires compressed air
Low maintenance	Normally requires external duct work
No moving parts	
Compact - low headroom	
Continuous duty	
Low air-to-cloth ratios	

As a final step in the welding fume analysis, once the ventilation system has been designed and the fume collector and associated peripheral equipment has been selected, any and all benefits should be examined.

WELDING FUME - THE BENEFITS

The realized benefits resulting from a properly designed and installed welding fume ventilation system fall into two major categories. That being the benefits of a cleaner plant and the heat recovered from a properly applied air cleaning device. The benefits of a cleaner plant would include:

1. Fewer occupational hazards - respiratory, eyes, skin.
2. Improved worker efficiency and morale.
3. Longer machine life.
4. Lower plant maintenance.
5. Improved product quality.

Obviously, there will be some intangible benefits of a cleaner plant, which haven't been listed.

There are several ways of examining the energy conservation due to being able to recirculate this cleaned ventilation air. The most direct approach is to assume that the welding area were properly ventilated and that this contaminated air were simply exhausted to the outside atmosphere. If this were the case, make-up air would have to be supplied to the plant either by direct or indirect means. The dollar figures you see here represent the additional fuel burden per heating season if you exhausted 100,000 cubic feet per minute of air (See Figure 13). These dollar figures are based on the average industrial fuel costs in April of 1978. Escalating fuel costs will change these values dramatically.

The recovered heat from a general ventilation system, which recirculates the cleaned air, would be considerably higher in dollars per year than these figures. This is primarily due to the fact that in this unique general ventilation approach, the contaminated air is removed at the proximity of the roof level. Warm air rises and it has been measured that the temperature gradient from the floor level to the roof level can vary as much as 40 degrees Fahrenheit to 50 degrees Fahrenheit. The source of this heat can be from many sources such as the welding process itself, lights, operating equipment, motors, etc. After this super-heated air has been cleaned, we reintroduce it at the floor level primarily to facilitate the "push-pull" principle of the general ventilation system. This returned warm air is further heated due to the compression of air across the fan and to a greater degree by radiation-convection since the return air supply passes through the super-heated roof level air for the width of the welding area. The total heat recovery can be calculated knowing the air volume, the temperature gradients that exist within a building and the outside temperature. A good example of the considerable amount of heat that can be recovered is from the installation at Bowen - McLaughlin, which was discussed earlier, in which the entire plant heat load is maintained by the ventilation system, and the two newly purchased boilers were never installed.

Even though the welding process produces fumes and gases, it is possible to comply with current hygienic standards and recover enormous amounts of energy whether in the form of heated or cooled air. In order to do this one has to thoroughly analyze the problem and carefully investigate the alternative solutions which will enable compliance and energy conservation.

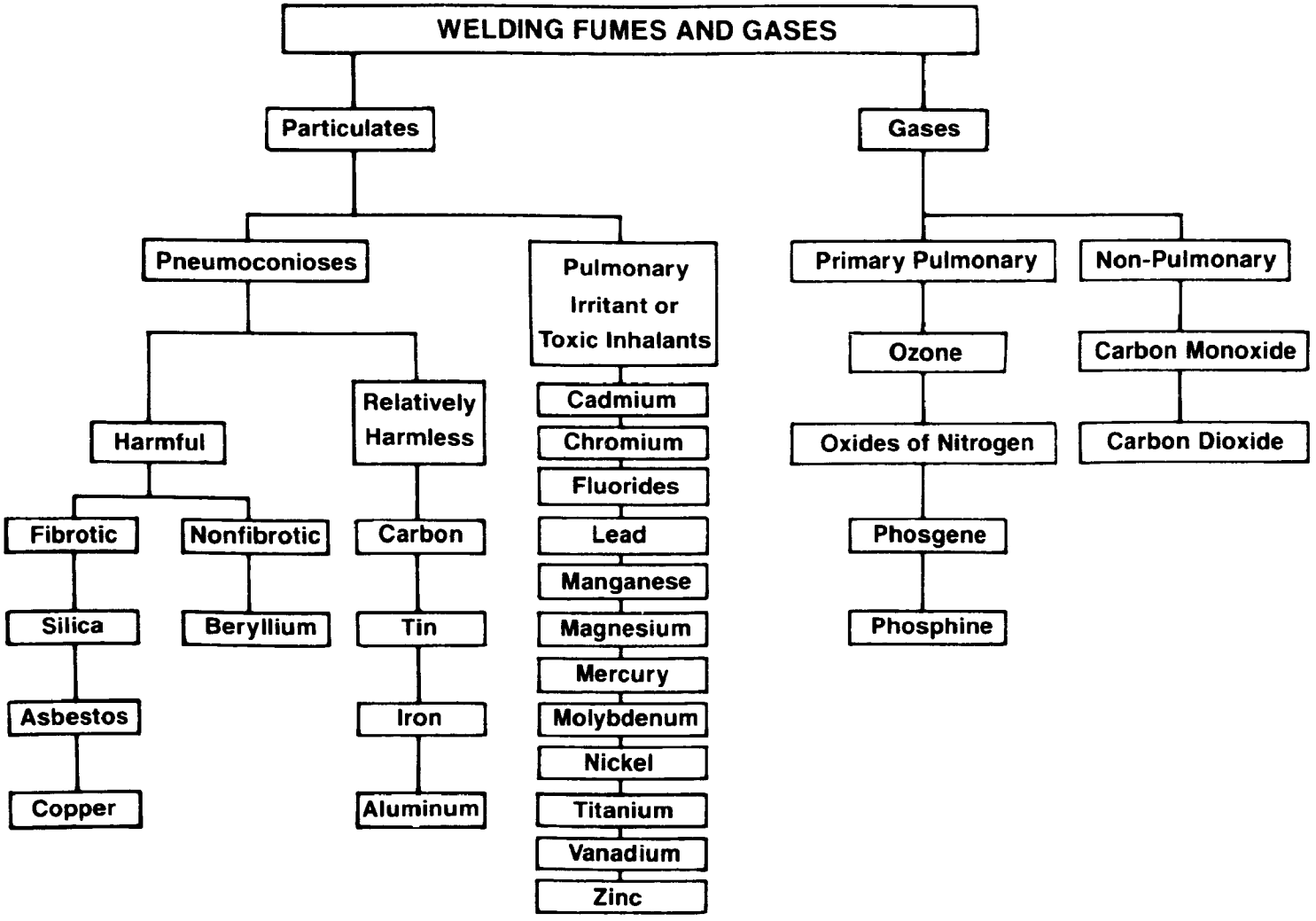

Figure 1 Welding fumes and gases.

Common materials that may be encountered in welding	Threshold Limit Values mg/m^3 (ACGIH)	Threshold Limit Values mg/m^3 (OSHA)
Antimony	0.5	0.5
Arsenic	0.5	0.5
Beryllium	0.002	0.002
Carbon dioxide	9,000.0	9,000.0
Carbon monoxide	55.0	55.0
Cadmium oxide fumes	0.05	0.1
Chromates (as CrO^3)	0.05	0.1
Chromium (metallic)	0.5	1.0
Cobalt	0.1	0.1
Copper Fumes	0.1	0.1
Fluoride	2.5	2.5
Hydrogen fluoride	2.0	2.0
Iron oxide fumes	5.0	10.0
Lead	0.15	0.2
Magnesium oxide fumes	10.0	15.0
Manganese	5.0	5.0
Mercury	0.05	0.1
Molybdenum	10.0	15.0
Nickel carbonyl	0.35	0.007
Nickel (metallic)	1.0	1.0
Nitrogen dioxide	9.0	9.0
Ozone	0.2	0.2
Phosgene	0.4	0.4
Selenium	0.2	0.2
Silver	0.01	0.01
Tellurium	0.1	0.1
Titanium dioxide	10.0	15.0
Uranium	0.20	0.25
Vandium fumes	0.05	0.1
Zinc oxide fumes	5.0	5.0
Zirconium	5.0	5.0

Figure 2 Threshold limit values for materials commonly encountered in welding and cutting.

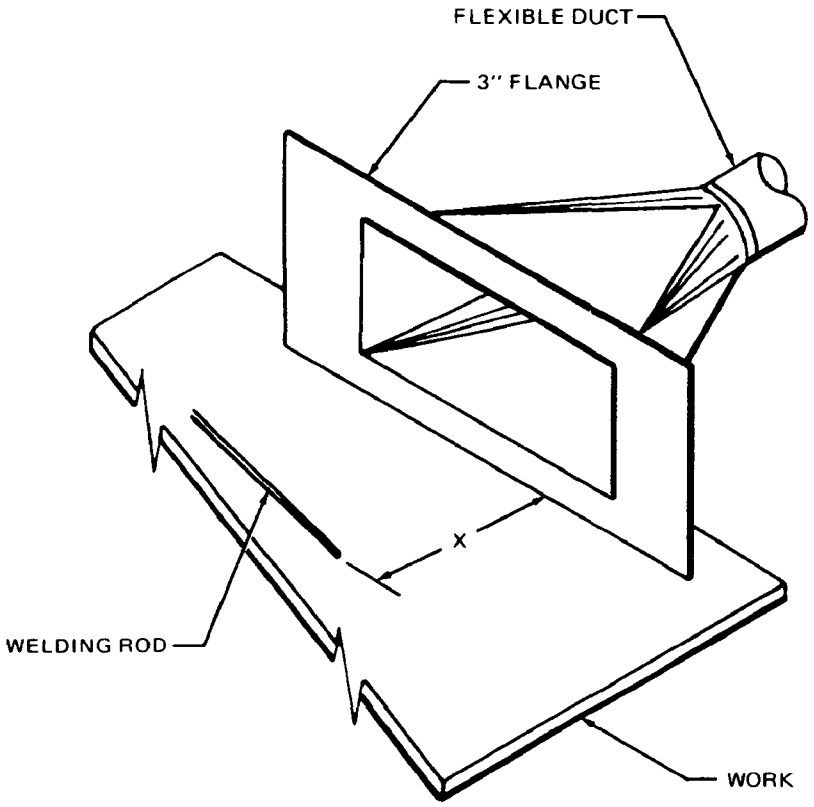

PORTABLE EXHAUST

X, INCHES	PLAIN DUCT CFM	FLANGE OR CONE CFM
UP TO 6	335	250
6 - 9	755	560
9 - 12	1335	1000

FACE VELOCITY = 1500 FPM
DUCT VELOCITY = 3000 FPM MINIMUM
ENTRY LOSS = 0.25 DUCT VP
ALSO SEE "GRANITE CUTTING" VS-909

Figure 3 Source collection (freely-suspended hood).

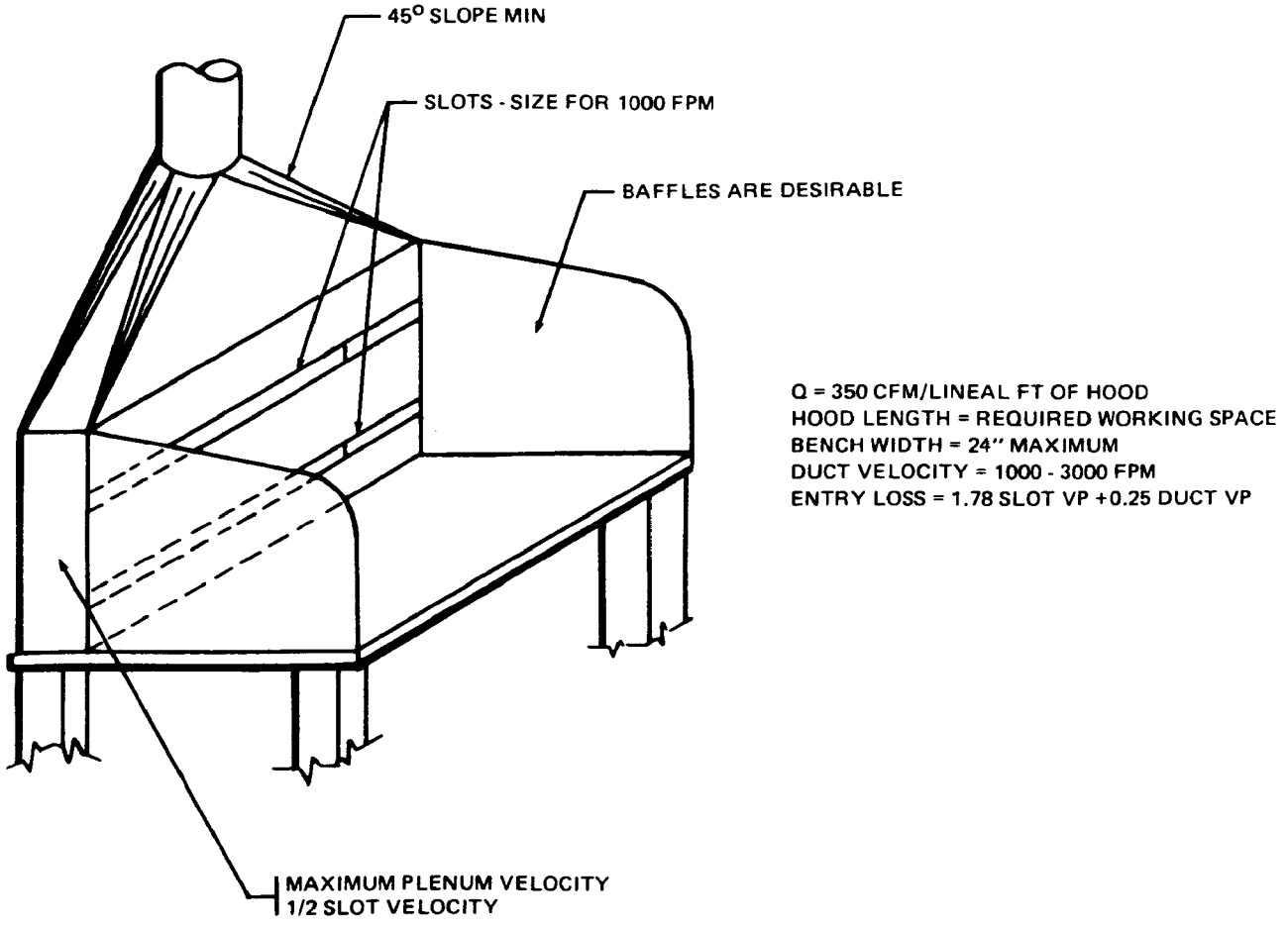

Figure 4 Source collection crossdraft table.

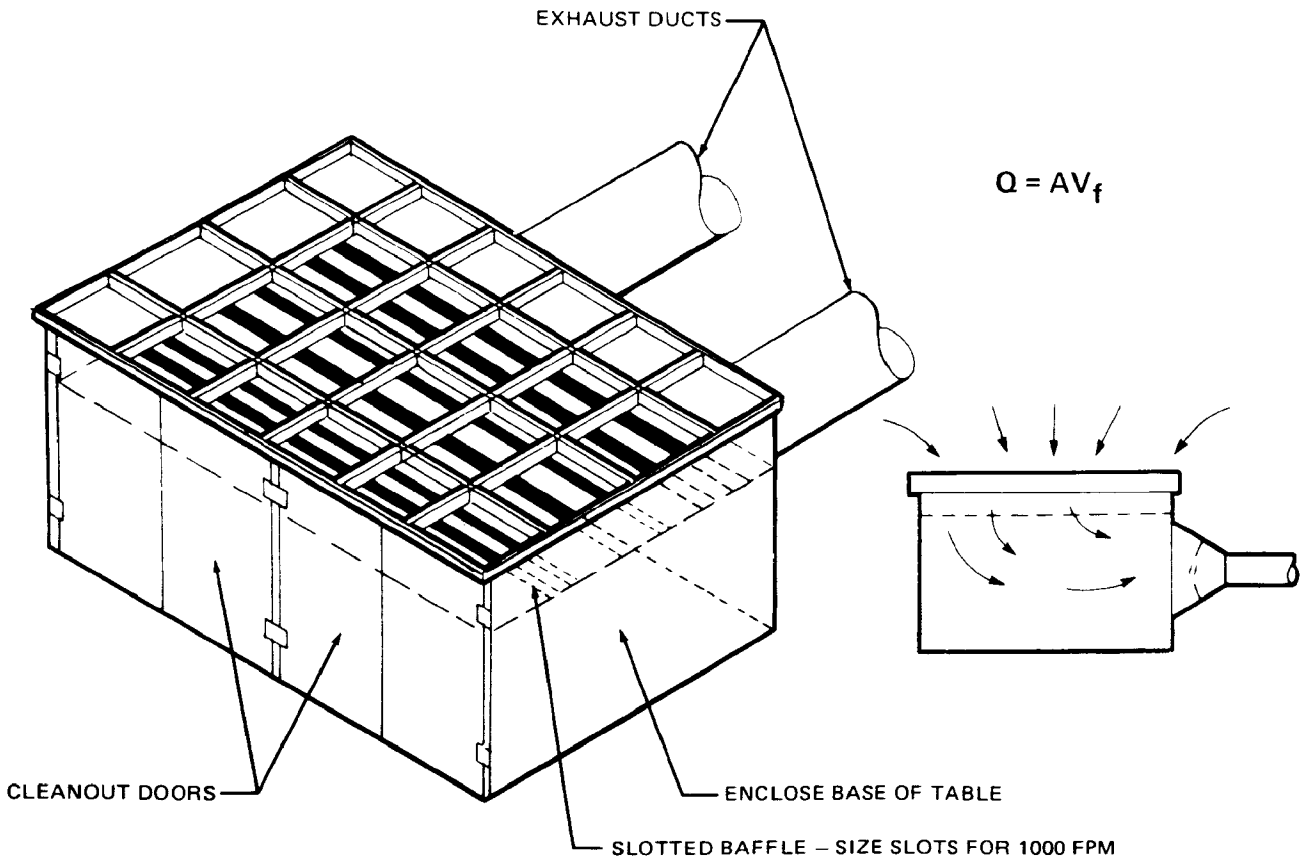

Figure 5 Source ventilation downdraft table (not recommended).

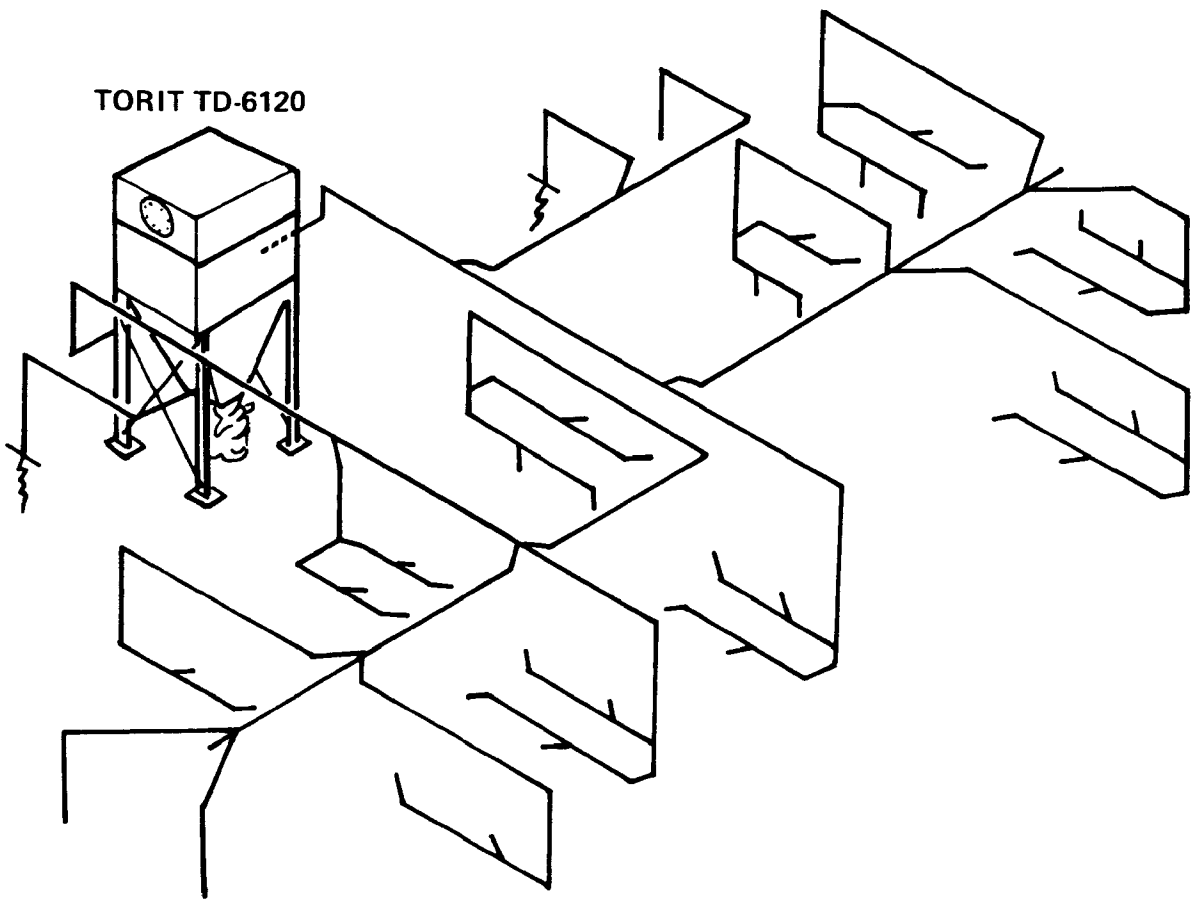

Figure 6 Source collection layout.

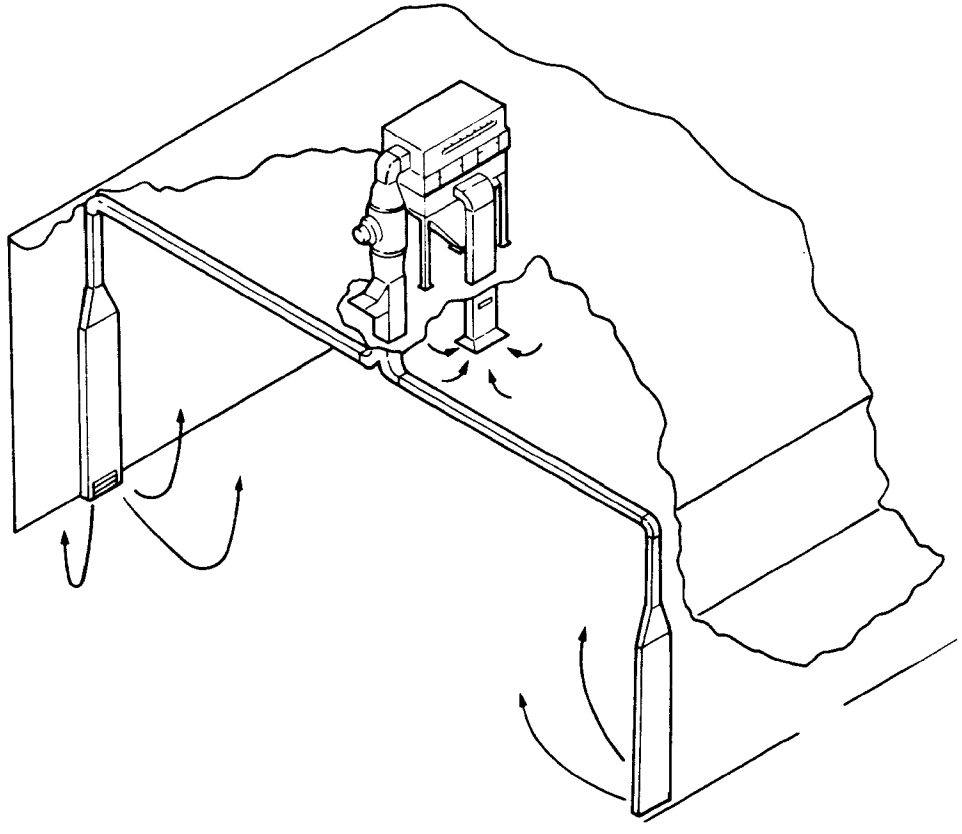

Figure 7 General ventilation layout.

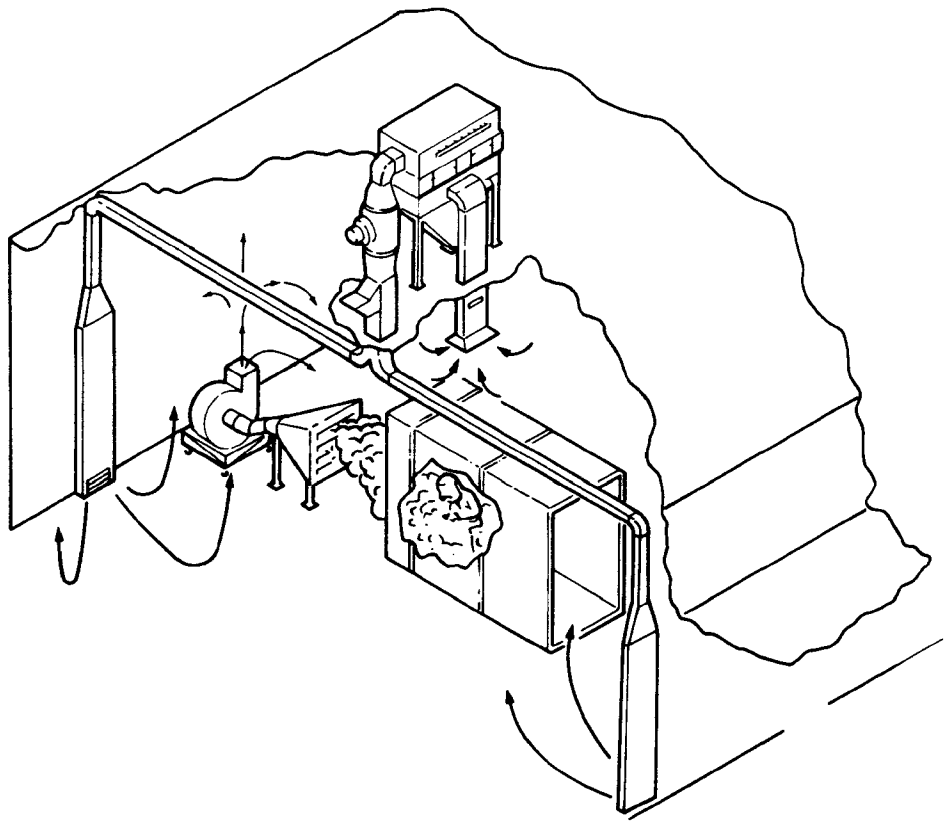

Figure 8 Combined general ventilation and source removal layout.

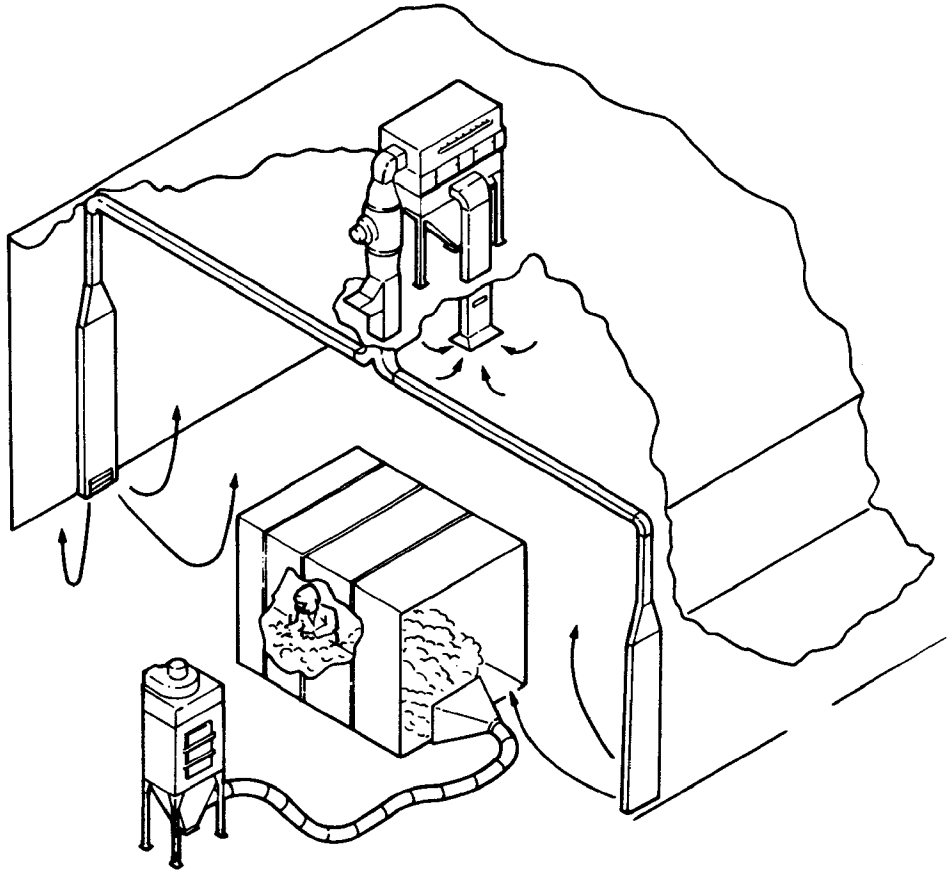

Figure 9 Combined general ventilation and source collector layout.

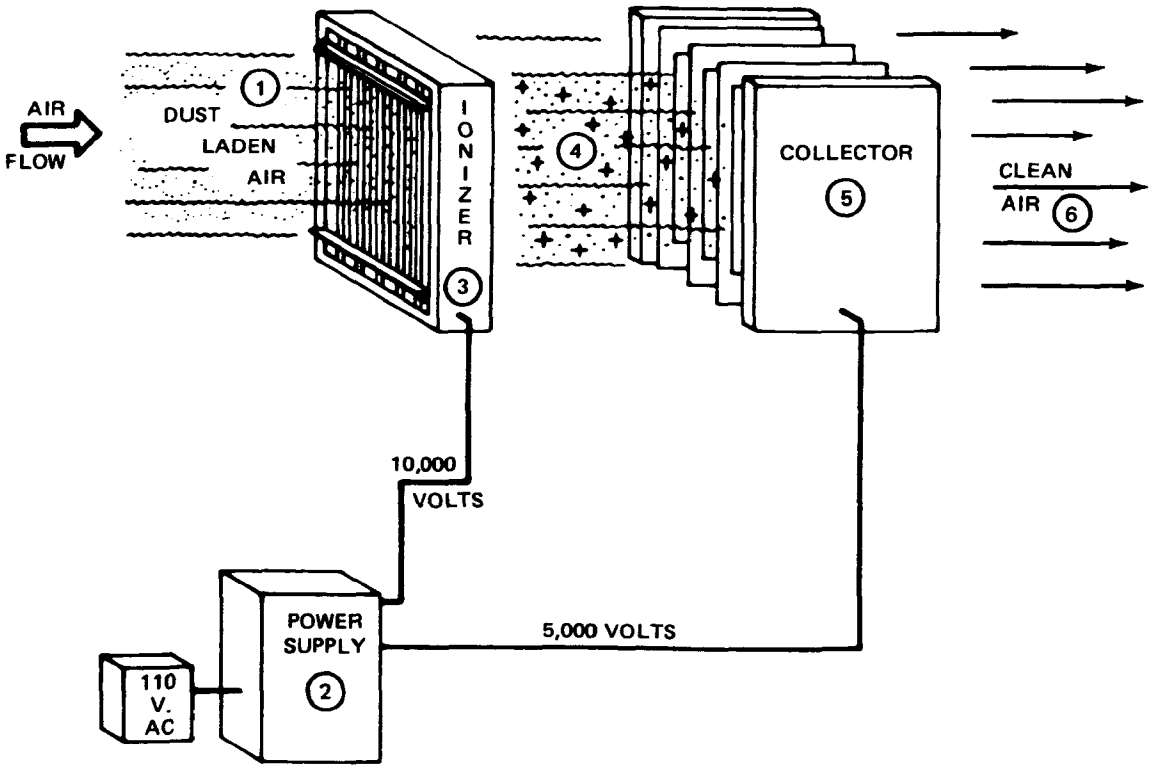

Figure 10 Electrostatic precipitators (modular).

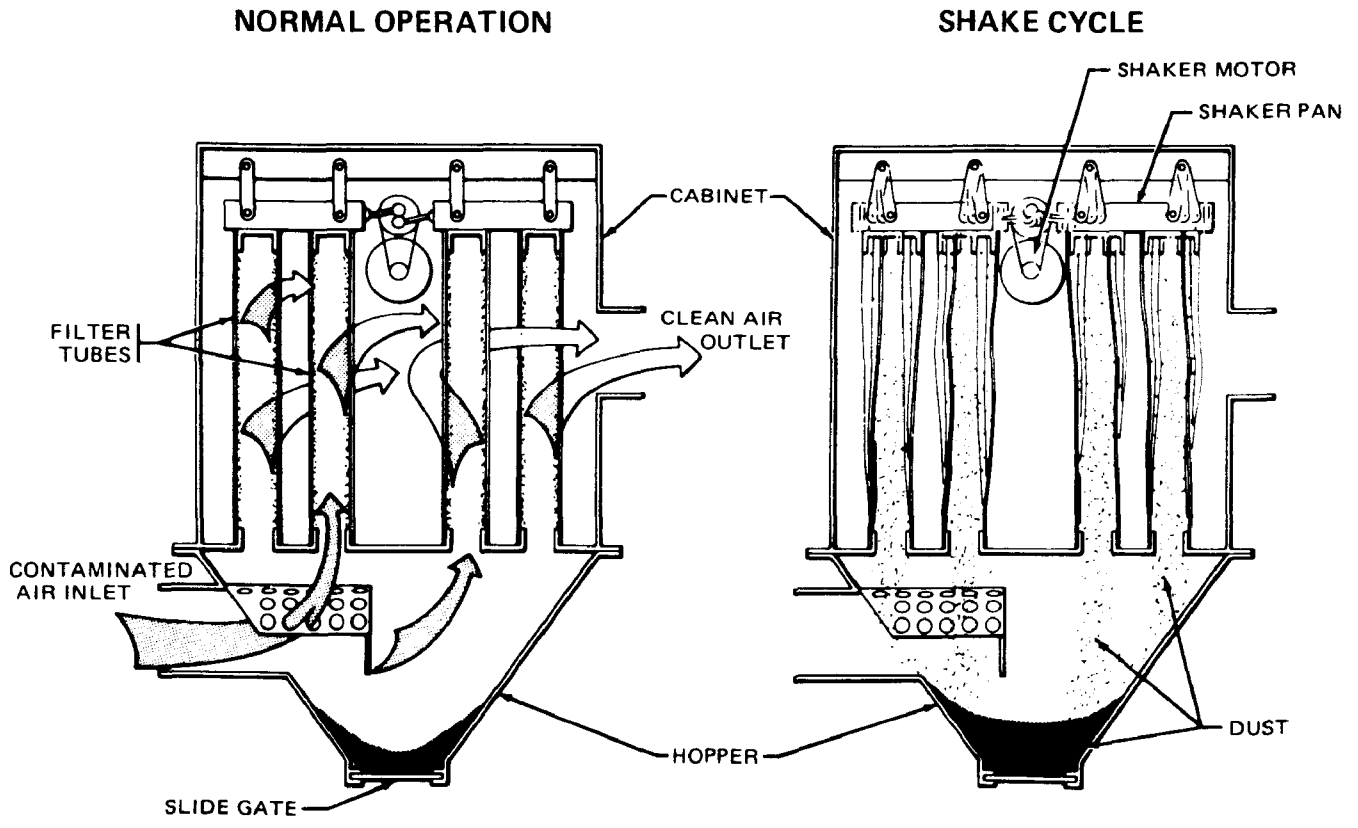

Figure 11 Mechanical shake baghouses.

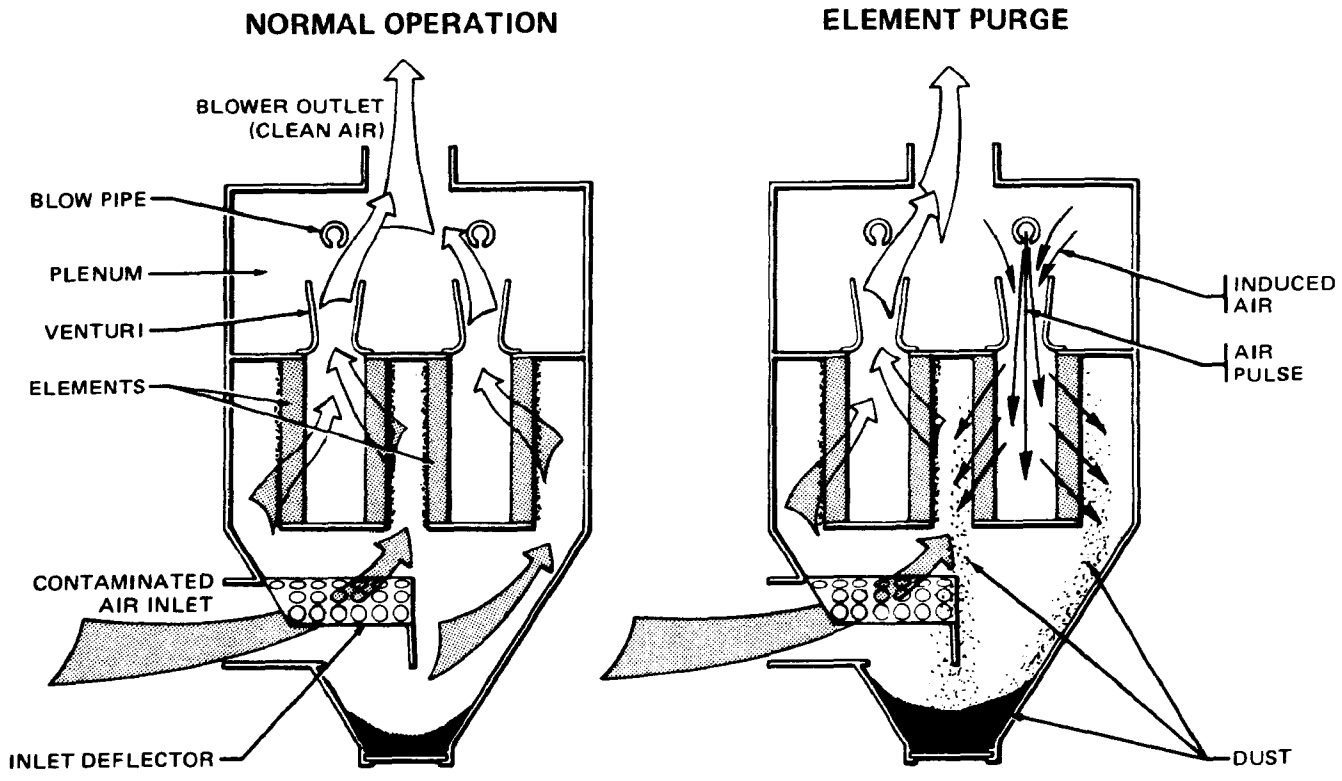

Figure 12 Torit TD cartridge collectors.

	NATURAL GAS	FUEL OIL (#2)	COAL
Atlanta, Georgia	$10,009	$12,201	$ 8,261
Boston, Massachusetts	18,179	22,161	15,005
Chicago, Illinois	21,012	25,615	17,343
Cleveland, Ohio	19,902	24,262	16,427
Dallas, Texas	7,406	9,028	6,113
Denver, Colorado	17,803	21,703	14,695
Detroit, Michigan	20,142	24,544	16,625
Honolulu, Hiwaii	0	0	0
Minneapolis, Minnesota	26,875	32,762	22,182
New York, New York	15,679	19,113	12,941
Nome, Alaska	46,328	56,476	38,239
Pittsburg, Pennsylvania	19,090	23,272	15,757
Richmond, Virginia	13,930	16,981	11,498
St. Louis, Missouri	14,508	17,686	11,795
Sacramento, California	9,194	11,208	7,589
Salt Lake City, Utah	19,350	23,589	15,972
Seattle, Washington	16,769	20,442	13,841
Wausau, Wisconsin	27,768	33,851	22,920

Figure 13 Benefits of energy conservation.

The cost of exhausting 100,000 cfm of air at current fuel prices (4/78) per heating season.

Addendum:

Recirculation of Filtered Air

In many cases, the economic and energy conservation factors are so important as to warrant the additional capital expense of safety when providing for recirculation.

In designing and using a recirculation system, the following items should be followed.

1. The air cleaning system should be capable of achieving a high enough efficiency to provide an exit concentration of at least one-half of the Threshold Limit Value.

2. Provisions should be made for a bypass of the recirculated air to the outdoors or shutdown of the process if there is an equipment failure. If a system is intended to conserve heat in the winter months and if adequate window and door openings permit sufficient "make-up" air when open, the system can discharge outdoors in warm weather.

3. It may be necessary to supply fresh makeup air in addition to the recirculated air to provide continuous dilution of any gases which may tend to otherwise accumulate.

4. The operation should be tested by a certified industrial hygienist after installed to insure compliance.

5. Routine testing, maintenance procedures and records should be maintained.

PARTICULATE REMOVAL CONSIDERATIONS IN SOLVENT EMISSION CONTROL INSTALLATIONS

A Case Study

By:

Eugene A. Brackbill
Peter A. Kalika
TRC - THE RESEARCH CORPORATION of New England
125 Silas Deane Highway
Wethersfield, Connecticut 06109

ABSTRACT

Organic emissions from surface coating processes are receiving increased regulatory attention. One of the commonly considered control techniques is activated carbon adsorption. This is very favorable when the emitted solvents have a cost saving reuse potential. However, the presence of condensed, submicron organic particulates and their impact upon the carbon is often overlooked.

This paper examines the case of a paper coating process utilizing a phenol-formaldehyde resin system. A pilot study revealed that the condensed organic particulate would greatly reduce the carbon's operating life. Two high efficiency particulate control devices were evaluated to determine their economic impact on the total system cost. The costs associated with both devices effectively eliminated the solvent recovery cost savings.

PARTICULATE REMOVAL CONSIDERATIONS IN SOLVENT EMISSION CONTROL INSTALLATIONS - A Case Study

INTRODUCTION

Recently, EPA has focused attention on the volatile organic compound (VOC) emissions from surface coating processes. Activated carbon adsorption has been defined as one of the reasonably available control technologies (RACT) for reduction of VOC emissions from many of these processes. Carbon adsorption is particularly attractive since it allows recovery of the collected solvent for reuse. The resulting process operation cost savings can offset the control system cost over a period of a few years. However, the solvent recovery potential often overshadows consideration of operational problems which severely limit the applicability of carbon adsorption.

The presence of condensible organic compounds in the process exhaust presents one of the most difficult problems. The condensation aerosols formed by these compounds are typically submicron and may form a polymeric coating which occludes the carbon pores. Such a coating usually cannot be removed by conventional on-line regeneration methods.

This paper examines the particulate problem as characteristic to specialty paper processes employing phenol-formaldehyde resins as binders and surface coatings.

PROCESS DESCRIPTION

The manufacture of some specialty papers includes the saturation or coating of the web with a resin system formulated to provide working strength to the paper. The basic unit operations comprising the process include web formation, wet saturation, and resin thermosetting.

The thermosetting process is typically accomplished in a recirculated flow, convection oven. The emissions from the oven are primarily alcohols and/or aromatic solvents. Additionally, small amounts of the resin components and partially polymerized materials may be emitted. It is these materials which exist in a transitional state in the exhaust stream and condense when mixed with ambient air, being evidenced by a visible plume.

IMPACT OF PARTICULATE ON ACTIVATED CARBON PERFORMANCE - PILOT STUDY

A 14 acmm (500 acfm) pilot scale carbon adsorption system was connected to a split stream from the curing oven exhaust. The purpose of the pilot study was to determine the activated carbon performance parameters relative to the carbon operating life. It had been predetermined that the solvent collection efficiency would be greater than 90 percent.

Although the initial measured performance was excellent, 99 percent solvent removal, the phenolic materials caused the carbon to plug and rapidly deteriorate in its ability to adsorb and retain the solvents. Carbon samples were extracted from the bed and laboratory tests performed to evaluate three important physical characteristics: activity, retentivity, and volatile matter content. Activity refers to the carbon's ability to adsorb organic vapors from a solvent laden airstream. After two weeks of operation the activity had decreased 39 percent and after one month the decrease was 52 percent. Retentivity, the ability to hold organic vapor after it has been adsorbed, likewise decreased by 51 percent and 84 percent following two weeks and one month on stream, respectively. The carbon volatile matter content after steam desorption showed an increase from the normal value of approximately 3 percent by weight to 11.5 percent after one month of operation. The deterioration trends of these parameters are depicted in Figure 1.

The rapid deterioration rate had not been anticipated even thcugh the presence of some particulate material in the oven exhaust was expected. Additionally, the pilot unit was preceded by a foam type filter which had been thought adequate for the trace particulate removal. In an effort to more accurately describe the problem, measurements for both filterable and condensible particulate material were performed downstream of the foam type prefilter using the EPA Method 5 sampling train. The sample train filter was maintained at approximately 110°C (230°F). The condensible fraction was collected in the impinger train with the outlet temperature from the last impinger maintained at approximately 21°C (70°F). Additionally, particle size determinations of the filter catch were performed by conventional optical microscopy techniques.

The results revealed an average total particulate loading of 16 g/hr (0.036 lb/hr). Although seemingly small, its impact becomes more apparent when viewed with respect to particle size. The particle size data, Table 1, indicated that the particulate were predominantly submicron. Therefore, it was realized that particle deposition would occur throughout the bed due to diffusional mechanisms. The volatile matter test had indicated this possibility since high residual levels were found in the carbon samples regardless of the location from which they had been extracted.

As a result of the pilot study, it was concluded that activated carbon adsorption was not a viable control technique unless the submicron particulate could be eliminated.

Figure 1. Activated carbon performance deterioration.

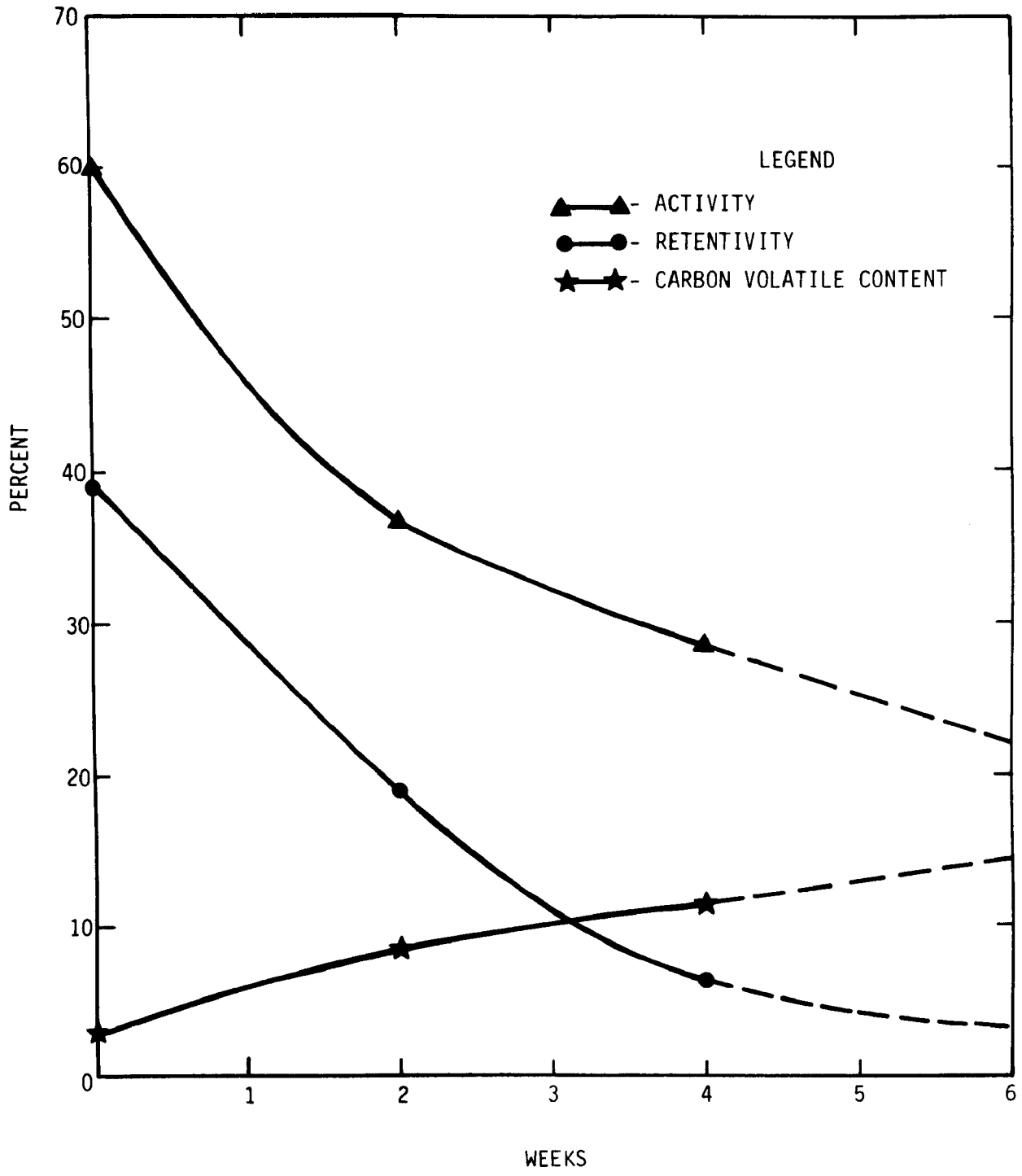

TABLE 1

PARTICLE SIZE DISTRIBUTION

Size Range, μm	Percent by Number
>3	3.3
1-3	31.2
<1	65.5

PARTICULATE CONTROL TECHNOLOGIES

Several control devices were considered but the particulate's submicron size and "tarry" characteristics eliminated the majority of obvious filtration and wet scrubbing choices. Electrostatic precipitation, both conventional and low voltage two-stage, was rejected because of the fire hazard potential and anticipated collected material removal problems.

Two control devices were eventually selected for economic evaluation. These were the Andersen HEAF (High Efficiency Air Filter), formerly marketed by Johns-Manville, and the Ceilcote IWS (Ionizing Wet Scrubber).

Andersen HEAF

This equipment has successfully been applied for control of phenol-formaldehyde emissions in several industries, most notably fiberglass impregnation. The unit employs a fiberglass medium for particle collection. The medium is a 25.4 mm (1 in.) thick mat which closely resembles home insulation in appearance. The contaminated gas stream is drawn through the mat at superficial velocities ranging from 400 to 550 meters/min (1,300 - 1,800 ft/min). Under these conditions the mat compresses to about 3.2 mm (0.125 in.) thick, increasing the volumetric fiber density. The particulates are removed by impaction and, to a lesser extent, diffusional mechanisms. Low viscosity liquid droplets agglomerate on the mat to form a nearly continuous liquid phase which migrates through the mat and is sheared by the airflow exiting the mat. The resulting larger droplets are removed by sedimentation, centrifugal fan separation, and mesh pad mist elimination. The more viscous compounds collected eventually blind the medium since they are retained rather than drained. When the airflow resistance reaches a predetermined level, the filter automatically advances to expose clean medium to the gas stream.

Ceilcote IWS

The ionizing wet scrubber combines the principles of electrostatic particle charging, image force attraction, inertial impaction, and gas absorption to collect submicron solid and liquid particles and gaseous contaminants simultaneously. A high voltage ionization section applies an electrostatic charge to the particles prior to their entering a conventional packed bed wet scrubber section where they are removed either by inertial impaction or attraction of the charged particles to the electrically neutral packing surface. The collected particles are flushed from the bed by the scrubbing liquid which, with the addition of chemical agents, also functions to absorb gaseous contaminants.

ECONOMIC EVALUATION

Cost estimates for the two control systems were prepared in terms of capital cost to purchase and install, and annualized cost. An estimate was also prepared for an activated carbon system. The process and economic parameters are presented in Table 2.

The overall accuracy of the estimates is expected to be in the range of ± 15 percent. In preparing the capital estimates, the equipment costs were based on manufacturer quotations. The installation, engineering, and contingency figures were calculated as a percentage of the equipment costs. Available space in and around the plant was limited. This was a major factor affecting the installation cost.

The annualized cost data were prepared employing standard procedures. The operating expenses included were plant overhead, maintenance, and utilities. Plant overhead is the cost associated with space utilization, administrative charges, insurance, and taxes. The equipment maintenance costs were difficult to assign since there are many design and operating factors which influence them. The estimated costs represent a best judgment but are likely generous. The electrical costs are essentially related to the fan motors. Additional costs characteristic to the devices are included and explained in the individual estimates which follow.

Activated Carbon

Table 3 describes the costs for the activated carbon control system. The operating expense includes the cost for a total bed replacement once each year. The carbon cost is based on 32 kg/acm (2 lb/acf) exhaust flow and $2.20/kg ($1/lb) carbon.

The solvent recovery reuse credit was calculated assuming that the adsorption efficiency would be 95 percent, desorption efficiency 90 percent, and the distillation efficiency 85 percent. Therefore, the overall recovery

TABLE 2

PROCESS AND ECONOMIC ESTIMATION BASES

Process

Nominal exhaust volume	1840 acmm (65,000 acfm)
Exhaust temperature	93°C (200°F)
Moisture content	5%, volume
Contaminant	50% isopropanol, 50% methanol
Concentration	1010 ppm
Estimated solvent evaporation rate	272l/hr (72 gal/hr)

Economic

Depreciation	12 year, straight line
Interest rate	10 percent
Electrical	$0.035/kw-hr
Steam	$3.30/1000 kg ($1.50/1000 lb)
Water	$0.004/1000 l ($0.15/1000 gal)
Recovered solvent value	$0.31/l ($1.18/gal)
Operation	6,240 hrs/yr

TABLE 3

ACTIVATED CARBON SYSTEM COST SUMMARY
(1840 acmm - 65,000 acfm)

CAPITAL COSTS	
Control device	$350,000
Ductwork	54,000
Fan	8,000
Evaporative cooler	30,000
Installation	98,000
Engineering	52,000
Contingency	58,000
TOTAL	$650,000
ANNUALIZED COSTS	
Depreciation	$54,000
Interest	33,000
Operating	
Overhead	6,000
Maintenance	11,000
Activated carbon	32,000
Steam	74,000
Water	26,000
Electrical	23,000
TOTAL	$259,000
SOLVENT RECOVERY	$383,000
NET ANNUAL COST	$124,000 credit

would be 73 percent. Applying this to the estimated solvent evaporation of 272 liters per hour (72 gal/hr), there would be a 198 liter per hour (52 gal/hr) recovery for reuse. At $0.31/liter recovery value, this equates to a savings of $383,000 per year.

The estimates reveal the carbon adsorption cost benefit. The difference between the annualized cost to own and operate and the recovered solvent value yields a cost savings of $123,950 per year. At this rate, the system capital cost would be recovered within 5.25 years (simple payback).

Particulate Control Equipment

The estimates for the HEAF and IWS, Table 4, were prepared in an identical manner as the carbon system. The IWS capital cost was based on two units in series. The filter cost associated with the HEAF operating cost was calculated from Andersen data on operating life and the price of replacement media.

Total System Estimates

The particulate control-activated carbon adsorption systems estimates are presented in Table 5. Obviously, the combined systems' capital costs became a significant concern. Of equal importance, the particulate control equipment contribution to the total annualized costs effectively eliminated the solvent recovery cost savings. Still, the annualized costs for both combination systems remained very reasonable, especially when compared with those had the solvent recovery credit not been available. In light of the increasing solvent cost and fluctuating supply situation, either control system remained economically attractive.

The combined systems approach presented another area of concern. The complexity of the control devices is such that maintenance and operation would become a labor intensive effort requiring specially trained personnel. That is, it was not anticipated that a simple planned maintenance schedule for the control system could be incorporated into the existing plant program.

In this case, it was decided to convert the process to a water-based resin system. Although process equipment changes would be required and some products eliminated, the overall economic impact on the plant would be less than that of controlling the solvent based process emissions.

TABLE 4

HEAF AND IWS COST SUMMARIES

CAPITAL COSTS

	Andersen HEAF	Ceilcote IWS
Control device	$110,000	$640,000
Ductwork	10,000	10,000
Fan	included	6,000
Pumps, piping, tanks	1,000	7,000
Installation	100,000	225,000
Engineering	25,000	25,000
Contingency	24,000	25,000
TOTAL	$270,000	$938,000

ANNUALIZED COSTS

Depreciation	$22,000	$78,000
Interest	14,000	47,000
Operating		
Overhead	3,000	5,000
Maintenance	2,000	7,000
Filter cost	25,000	
Electrical	98,000	37,000
TOTAL	$164,000	$174,000

TABLE 5

TOTAL SYSTEMS COST SUMMARIES

	Andersen HEAF	Ceilcote IWS
CAPITAL COSTS		
Activated carbon	$650,000	$650,000
Particulate control	270,000	938,000
TOTAL	$920,000	$1,588,000
ANNUALIZED COSTS		
Activated carbon	$259,000	$259,000
Particulate control	164,000	174,000
TOTAL	$423,000	$433,000
SOLVENT RECOVERY CREDIT	$383,000	$383,000
NET ANNUALIZED COST	$40,000	$50,000

CONCLUSIONS

The particulate emissions associated with some surface coating processes must be considered if activated carbon adsorption is selected to control organic solvent emissions. The capital and annualized costs attributable to particulate control equipment capable of high efficiency submicron particle removal can be a significant portion of the total system cost and offset the potential cost benefit of the solvent recovered for reuse by the carbon system.

ARSENIC EMISSIONS AND CONTROL TECHNOLOGY GOLD ROASTING OPERATIONS

John O. Burckle
Industrial Environmental Research Laboratory
Office of Research and Development
U.S. Environmental Protection Agency
Cincinnati, Ohio 45268

G. H. Marchant
Southern Research Institute
2000 Ninth Avenue South
Birmingham, Alabama 35205

Richard L. Meek
Southern Research Institute
2000 Ninth Avenue South
Birmingham, Alabama 35205

ABSTRACT

Since arsenic is a significant compound of ores processed in the nonferrous metals industries, it is of interest to characterize and evaluate control strategies which have demonstrated the potential for lowering the emission rates of arsenic and other hazardous effluents from smelter operations. The Campbell Red Lake Mines Gold Smelter at Balmerton, Ontario, Canada, has developed and implemented a successful control strategy for arsenic emissions from a nonferrous smelting operation. The control system was designed and installed by Hatch Associates, Toronto, Canada. The Red Lake smelter uses cyclones and a hot electrostatic precipitator to recover metal values from roaster dusts with subsequent air quenching to condense (or desublime) arsenic trioxide which is recovered in a low-temperature baghouse. This paper is a review of a test program conducted at Red Lake designed to characterize the control systems and to evaluate the potential for transferring the technology to smelting operations in the United States.

ARSENIC EMISSIONS AND CONTROL TECHNOLOGY GOLD ROASTING OPERATIONS

INTRODUCTION

The Campbell Red Lake Mines operation at Balmerton, Ontario, Canada has developed and implemented a successful control strategy for arsenic emissions from a nonferrous smelter. In the process, a gold-bearing arsenopyrite ore is roasted to eliminate arsenic and sulfur, the hot roaster calcines are recovered in cyclones and an electrostatic precipitator, and the hot gases from the precipitator are quenched with air to condense (or desublime) arsenic trioxide. The finely divided arsenic trioxide is then collected in cold bag filters. The overall collection efficiency of the system exceeds 99.9% for arsenic trioxide.

Since arsenic is a significant component of many ores processed in this country by the nonferrous metals industry, the characterization and evaluation of control strategies which have demonstrated capabilities for reducing the emission rates of arsenic and other hazardous emissions from smelters is of interest. The test program at Red Lake was conducted to evaluate the performance of their "hot ESP/cold bag" system and to assess the potential for transferring the technology to nonferrous smelting operations in the United States.

PROCESS DESCRIPTION

A simplified flowsheet of the overall operation of the Campbell Red Lake Mines Limited installation at Balmerton, Ontario, Canada, is shown in Figure 1. Ore from an underground mine is subjected to crushing, grinding, ball milling, flotation and tabling to obtain three cuts for further processing. The first cut (tabling overflow) is amalgamated directly for recovery of gold, the second (flotation tails and underflow) is relatively low in arsenic and sulfur and can be treated by cyanidation to liberate the gold, but the third cut (flotation and tabling overflow), which is high in arsenic and sulfur, requires roasting to eliminate arsenic, antimony, and sulfur before the gold can be economically extracted. Two-stage fluid-bed roasting effectively removes the arsenic, antimony and sulfur from the concentrate. The calcines from the roasters, cyclones, and hot electrostatic precipitator can then be treated by cyanidation to recover the gold. The hot gaseous effluent from the electrostatic precipitator is quenched with cold air to condense As_2O_3 which is recovered in a cold baghouse.

A more detailed flow diagram of the roasting, gas cleaning, and arsenic system at Campbell Red Lake Mines is shown in Figure 2. The concentrate (nominally 9% As, 18% S, 23% Fe) is fed to the first roaster as an 80% slurry

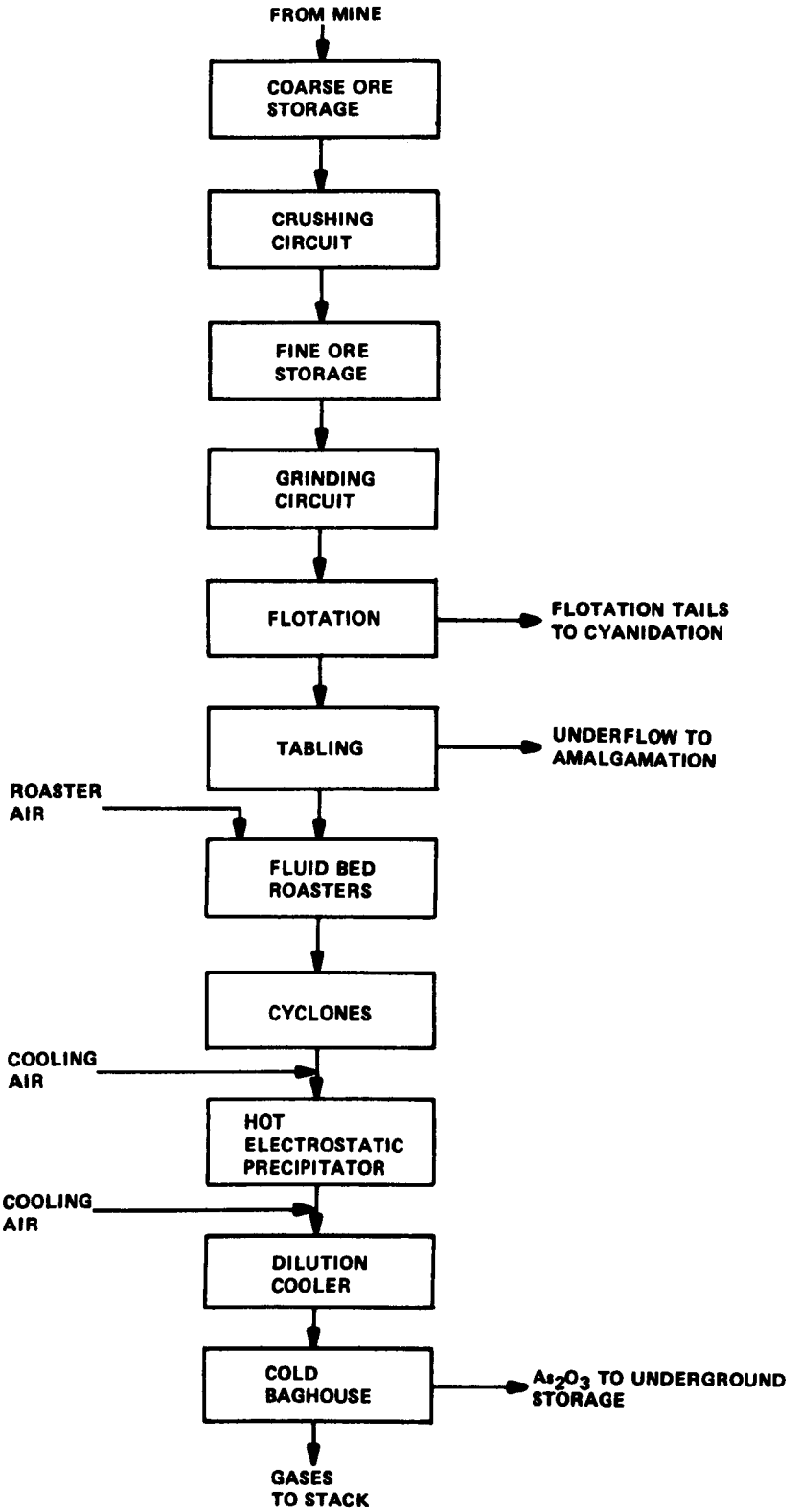

Figure 1. Simplified flow diagram.

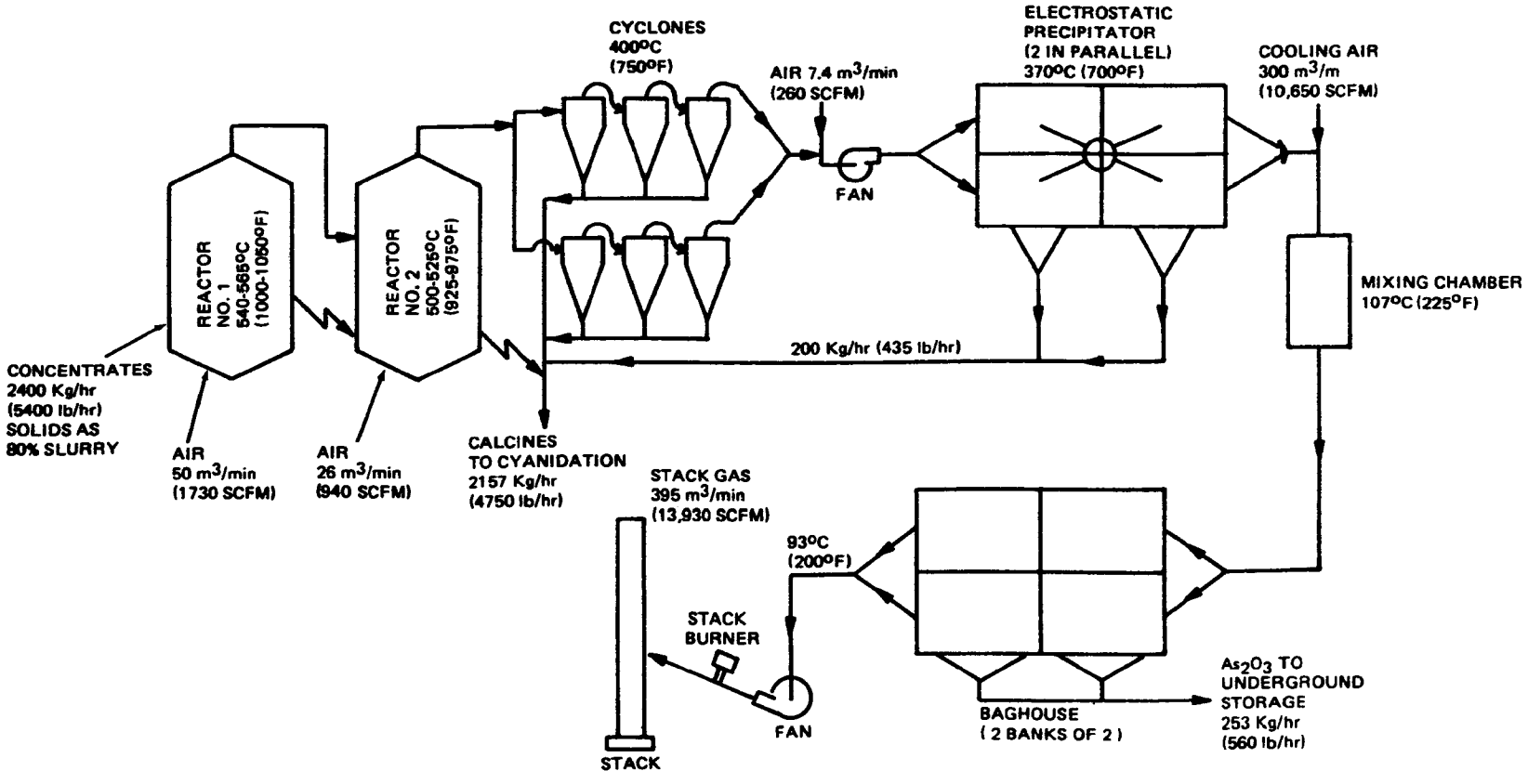

Figure 2. Roasting and Gas Cleaning Process (Design Flows).

at a design rate of 2500 Kg/hr (2.7 tons/hr) (dry basis). The first roaster is operated at about 540-565°C (1000-1050°F) where most of the As, Sb, and S are oxidized and volatilized. The overflow and underflow from the first roaster are further treated in the second roaster at about 500-525°C (925-975°F). The gases from the second roaster are fed through 2 parallel sets of 3-stage cyclones operated at about 400°C (750°F), and the calcine catch from the cyclones is combined with the roaster bed underflow for return to a cyanidation circuit for recovery of gold.

The gases from the two banks of cyclones are combined and diluted with air to reduce the gas temperature to 370°C (700°F) before being fed to the electrostatic precipitator which consists of 2 units in parallel with 2 chambers in each. As will be shown by the data, sublimed arsenic (primarily As_2O_3) is not condensed in the precipitator and only particulate arsenic (perhaps as As_2S_2 carry over, non-volatile oxides such as As_2O_5, or a combined complex) is removed with the other entrained particulate from the cyclones. The hoppers from the electrostatic precipitator are emptied periodically and the catch is combined with the roaster and cyclone calcines.

The hot precipitator off-gases are then mixed with ambient air to reduce the temperature to about 107°C (225°F) to condense the sublimed arsenic (As_2O_3). This particulate is caught in a 4-chamber baghouse before the gases are sent to a double-walled stack. The arsenic trioxide dust from the baghouse is removed periodically and conveyed to underground storage. The reheat stack burner shown in Figure 2 is not required in normal operation.

Descriptive parameters for the precipitator are given in Table 1. The precipitator is a double-walled unit, and electrically-heated air is circulated in the shell to maintain temperature and avoid wall condensation of arsenic. There are two chambers in each of the two parallel banks; however, one transformer rectifier powers all four chambers of the precipitator. During the test period, the roaster system was operated at around 90% of design capacity so the actual SCA during the test was about 60 $m^2/(m^3/sec)$ or about 300 $ft^2/1000$ acfm.

Parameters for the baghouse are shown in Table 2. The baghouse is insulated, and the stack is also a double-walled unit to avoid wall condensation.

A key feature of the Red Lake System is the mixing chamber used for cooling the hot gases from the precipitator to condense or desublime the As_2O_3. A simplified diagram of this mixer-cooler is shown in Figure 3. Ambient air is fed into the center of the mixer, and the hot gases from the precipitator are fed tangentially to create a swirling mixing action. Ideally, condensation (or desublimation) of As_2O_3 occurs only at the juncture of the hot and cold gas streams. Wall condensation is avoided by keeping the hot gases on the outer periphery and by heat tracing and insulating the walls.

SAMPLING PROGRAM

During the period of September 18-28, 1978, personnel from Southern Research Institute and Radian Corporation carried out a test program in the

TABLE 1. ELECTROSTATIC PRECIPITATOR DESCRIPTIVE PARAMETERS

Item	Metric	English
Collection electrode area (4 chambers-2 sets parallel)	187.3m^2	2016 ft^2
No. of fields per chamber	1	1
Collection electrode spacing	25.4 cm	10 in.
Collection electrode dimensions	1.83 x 1.83m	6 x 6 ft
Corona electrode dimensions (round wire)	0.268 cm	0.1055 in.
Wire spacing	22.86 cm	9 in.
Number of gas passages (per chamber)	7	7
Gas passage length	1.83 m	6 ft
Volume flow rate (design)	3.44 m^3/sec	7300 acfm
Design temperature	371°C	700°F
Design efficiency	98%	98%
Design specific collection area (SCA)	54.37 $m^2/(m^3/sec$	276.2 ft^2/ 1000 acfm
Measured efficiency (particulate)	98.3%	98.3%
Arsenic capture (total)	15%	15%

TABLE 2. BAGHOUSE DESCRIPTIVE PARAMETERS

No. of compartments	4
No. of bags (per compartment)	230 (10 rows of 23)
Bag material	Draylon T (acrylic)
Bag diameter	10.16 cm (4 in.)
Bag length	2.44 m (8 ft)
Air-to-cloth ratio (actual)	9.36 x 10^{-3} $(m^3/sec)/m^2$ (1.84 $ft^3/min/ft^2$)
Measured efficiency (particulate)	99.9+%
Arsenic capture (total)	99.8%

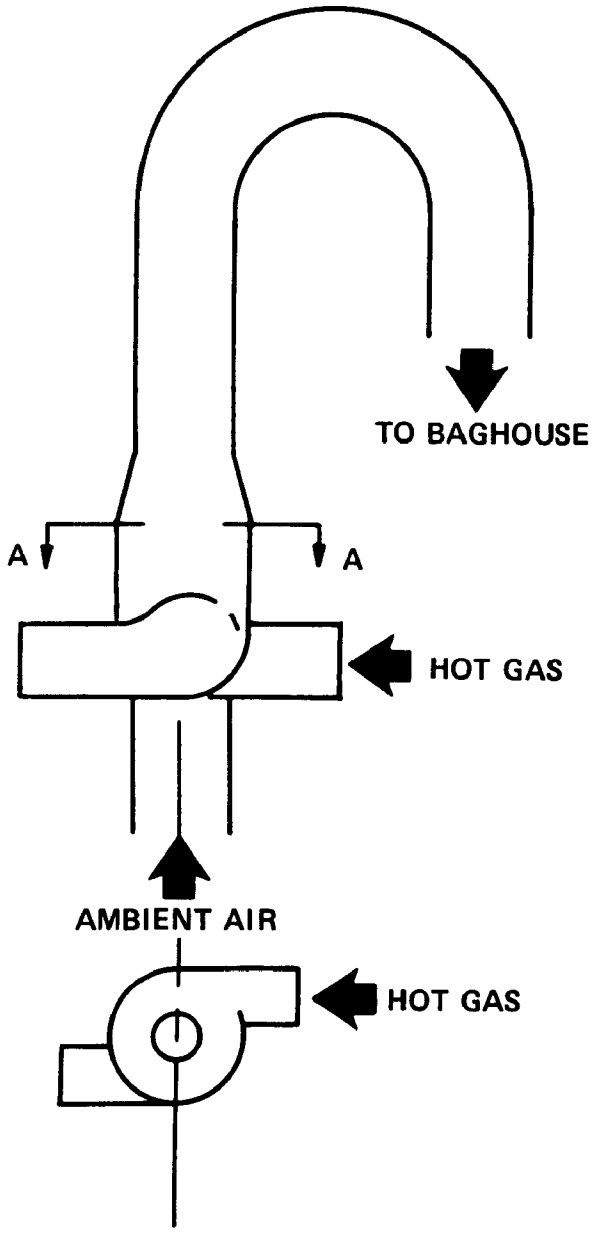

*Figure 3. Gas mixer-cooler.**

* U.S. Patent 4,126,425 and Can. Pat. 993,368 to Hatch Associates, Toronto, Canada.

Campbell Red Lake Mines Ltd. gold smelter at Balmerton, Ontario, Canada.

Radian Corporation personnel operated an integral sampling system designed to obtain samples for elemental analysis, and a gas sampling system for determining concentrations of sulfur oxides.

Southern Research Institute personnel operated cascade impactors for determination of the particle size distribution of the particulate in each gas stream, and a total particulate sampling system for determination of total particulate loading in each stream. SRI personnel also monitored the pressure drop across the baghouse, the operation of the roaster, and measured the in situ resistivity of the particulate entering the baghouse (for possible modeling of a precipitator which could replace the baghouse).

The primary purpose of the test program was to evaluate the performance of the gas treatment system which consists of a hot electrostatic precipitator for recovery of metal values, a mixer-cooler for condensation (desublimation) of As_2O_3 and Sb_2O_3, and a cold baghouse for removal of fine condensed particulate. A simplified sketch indicating sampling points is shown in Figure 4.

Sample Point 1 at the precipitator inlet was under positive pressure, and some difficulties were experienced in isokinetic sampling. The duct was vertical with an upward gas flow and an internal diameter of 0.43 m (17 in.).

Sample Point 2, which was on one leg of the precipitator outlet, was highly inaccessible and was not regarded as a satisfactory sampling point for several reasons: (1) Sampling of only one leg of the precipitator required an assumption that both sides in the parallel configuration were operating identically, (2) Possible dust accumulation in the bottom of the duct could affect flow measurements, and (3) The location was too close to converging and diverging ducts for uniform particulate sampling. In spite of these limitations, samples were taken from this 0.25 m (10 in.) square duct to provide an approximation of precipitator performance. Because the precipitator is closely connected to the mixer-cooler, this was the only sampling point possible for estimation of emissions at the precipitator outlet/ mixer-cooler inlet.

Sample Point 3 at the outlet of the mixer-cooler provided data for the baghouse inlet. Gas flow was vertically downward through the 0.71 m (28-in.) duct.

Sample Point 4 in the stack provided data for the baghouse outlet. The internal diameter of the stack was 0.76 m (30-in.).

Insofar as possible, all samples were taken isokinetically to assure that representative measurements were made.

There were some variations in operation during the test period that affected the sampling program; however, adequate data were obtained to evaluate the overall performance of the electrostatic precipitator and the baghouse.

A summary of plant operating data for the test period is shown in Table 3. These data show that the plant was in reasonably stable operation during

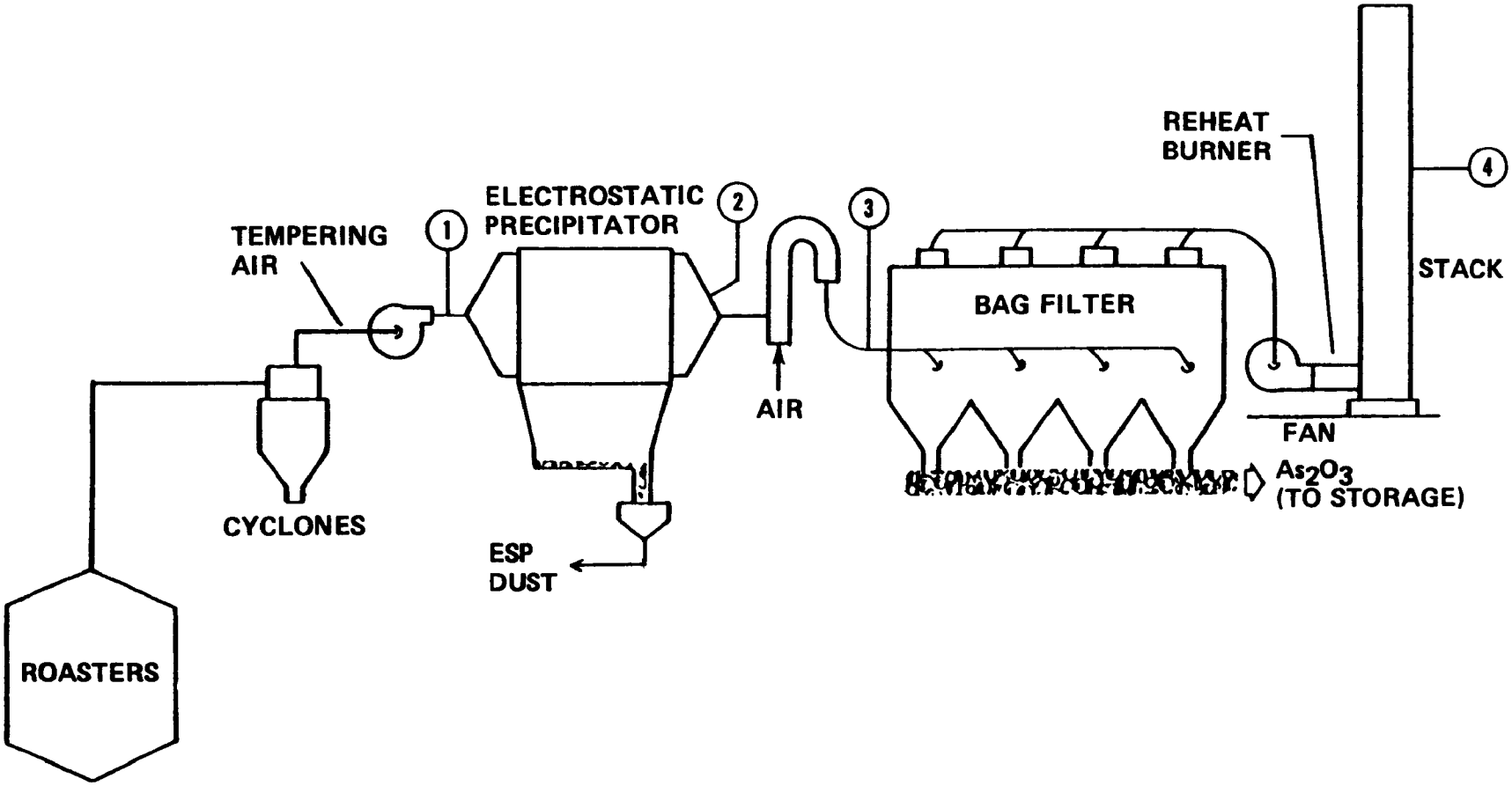

Figure 4. Sampling locations.

TABLE 3. PLANT OPERATING DATA

	Avg.	Range
Freeboard Temperatures		
Reactor No. 1, °F	1021	990-1037
°C	549	532-558
Reactor No. 2, °F	951	938-946
°C	511	503-508
Air Flow-to-Wind Box		
Reactor No. 1, cfm	1200	1190-1220
m /sec	34.0	33.7-34.6
Reactor No. 2, cfm	920	860-1000
m /sec	26.1	24.4-28.3
ESP and Baghouse Temperatures		
ESP Inlet, °F	737	713-768
°C	392	378-409
ESP Outlet, °F	586	531-620
°C	308	277-327
Baghouse Inlet, °F	245	229-250
°C	118	109-121
Baghouse Outlet, °F	232	228-236
°C	111	109-113
Stack, °F	216	212-219
°C	102	100-104
Precipitator*		
AC Amps	10.1	9.5-10.5
AC Volts	418	413-423
DC Milliamps	40	35-45
DC Volts x 1000	57.3	56.2-58.6

* Excluding data at end of test period.

the tests even though there was one operational shut-down during the test period, and the precipitator had an electrical malfunction near the end of the test period.

PARTICULATE MEASUREMENTS

Modified Brink cascade impactors were operated at the ESP inlet and baghouse inlet (Sample Points 1 and 3), while Andersen Mark III cascade impactors were operated at the precipitator outlet (Sample Point 2), and University of Washington Mark III (Pilat) cascade impactors were operated at the baghouse outlet (Sample Point 4). The collection substrates (glass fiber) used in the Brink and Andersen impactors were conditioned by acid washing in the laboratory to decrease the amount of substrates weight gain due to gas phase reactions. The collection substrates used in the University of Washington (Pilat) impactors were greased stainless steel substrates which were prepared in the laboratory prior to use in the field. All impactor data obtained at Red Lake were reduced using a computer program described in EPA Report Number 600/7-78-042, A Computer-based Cascade Impactor Data Reduction System, by J.W. Johnson, G.I. Clinard, L.G. Felix, and J.D. McCain, March 1978.

The impactor data collected at the ESP inlet sampling location are presented in Figure 5 as cumulative mass loading vs. particle size. Figure 6 presents the same data as cumulative percent vs. particle diameter. As can be seen from Figure 6, 50% of the particulate was less than 16 μm. A maximum particle diameter of 25 μm was used in the impactor data reduction program for each sampling location, since the size of the largest particle found in the cyclone catches of the Brink impactors operated at the ESP and baghouse inlets was 25 μm.

A limited number of impactor runs were made at the precipitator outlet to approximate the cumulative mass loading of particulate less than two microns in diameter which would be present at the outlet of the condenser in addition to particulate resulting from condensation (or desublimation). Figures 7 and 8 present data on the cumulative mass vs. particle size from the ESP outlet and baghouse inlet. Figure 7 shows that the mass loading of particulate below 2 microns diameter at the ESP outlet was less than 7×10^3 mg/ACM at a gas flow rate of 3888 dscm/hr (from Table 5). Figure 8 shows that the mass loading of particulate below 2 microns diameter at the baghouse inlet was about 7×10^4 mg/ACM at a gas flow rate of about 16,779 dscm/hr. The ratio of these numbers ($7 \times 10^3 \times 3888 \div 7 \times 10^4 \times 16{,}779$) indicates that less than five percent of the particulate entering the baghouse was particulate at the ESP outlet; therefore, greater than 95 percent of the particulate entering the baghouse resulted from condensation in the mixer-cooler. Figure 9 presents the baghouse inlet data as cumulative percent vs. particle diameter. From Figure 9, it can be seen that the mass median diameter of the particulate entering the baghouse (primarily as As_2O_3) was 1.2 μm, and 75% of the particulate mass was less than two microns.

Figure 10 presents the collection efficiency vs. particle diameter data for the baghouse and shows a minimum in collection efficiency at about 5 microns of approximately 99.8%. The bimodal distribution shown in Figure 10

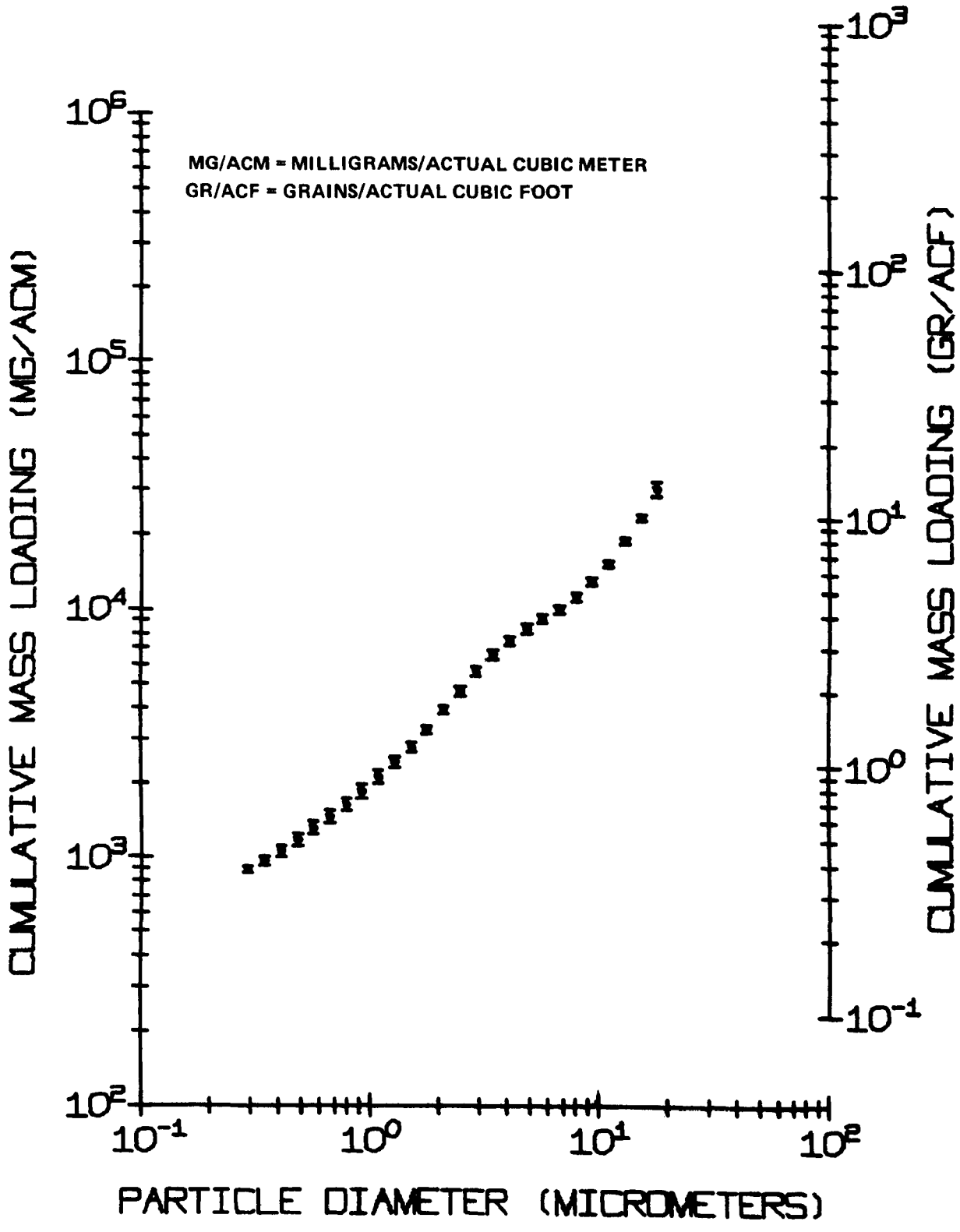

Figure 5. Average ESP inlet cumulative size distribution.

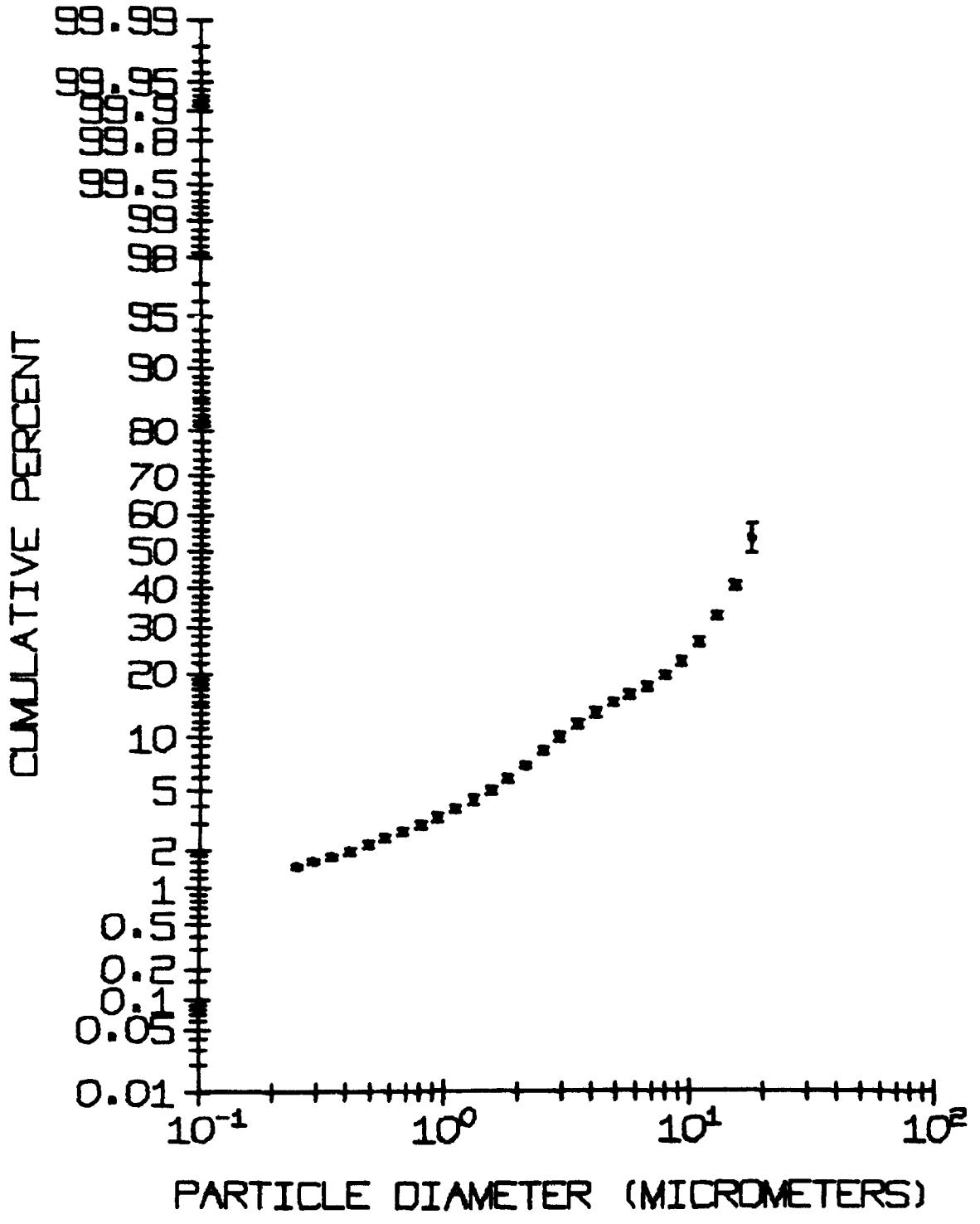

Figure 6. Average ESP inlet cumulative percent versus particle diameter.

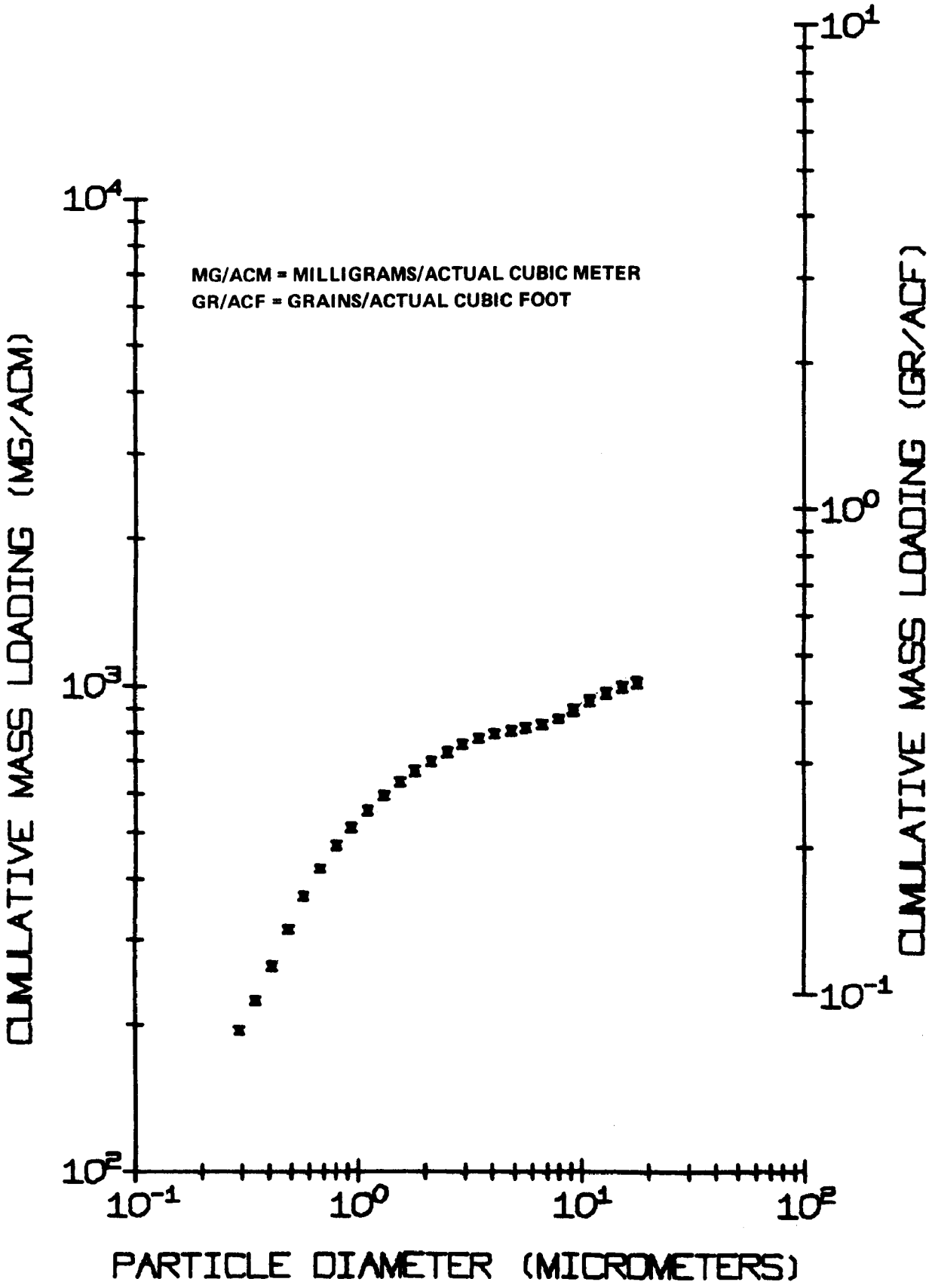

Figure 7. Average ESP outlet cumulative size distribution.

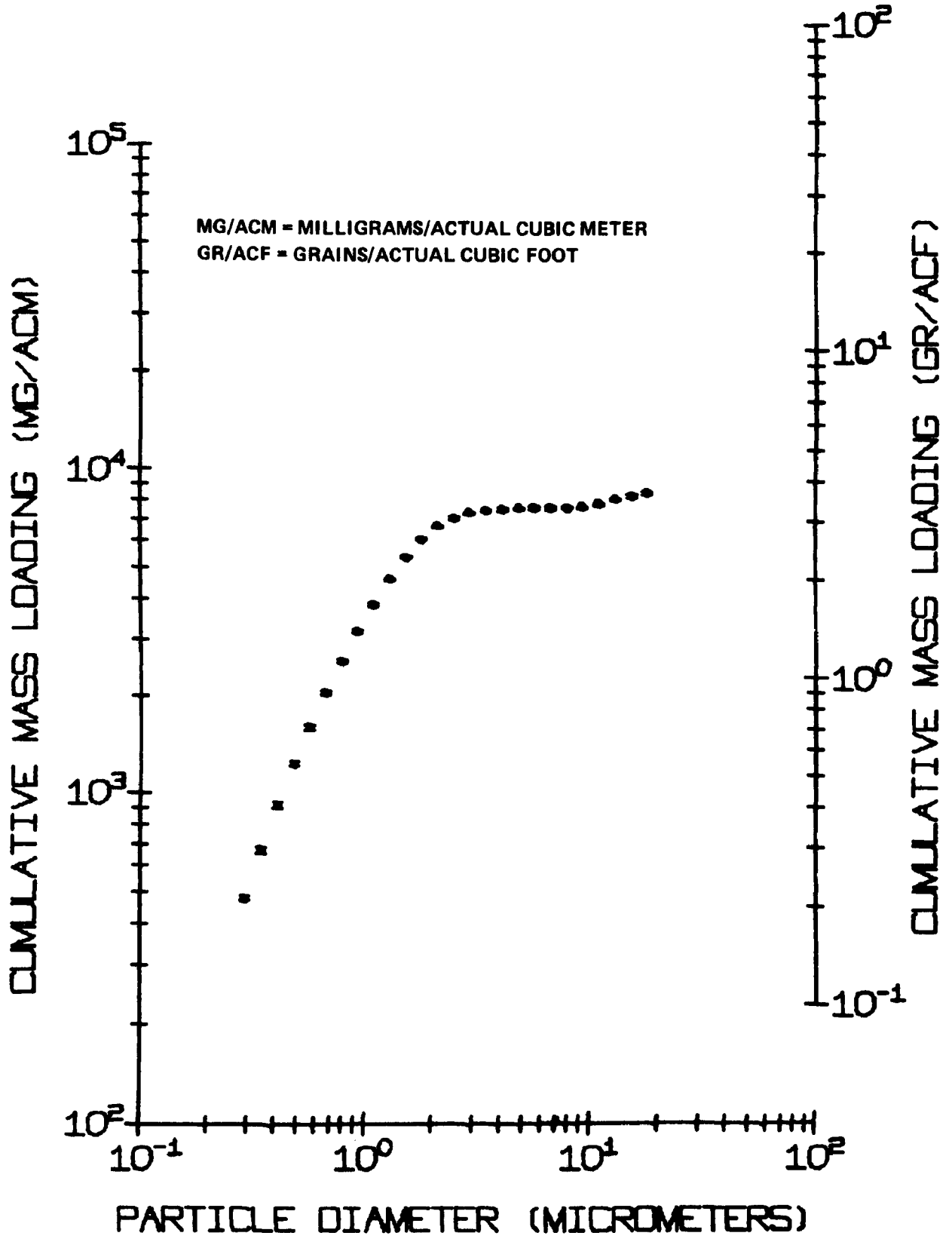

Figure 8. Average baghouse inlet cumulative size distribution.

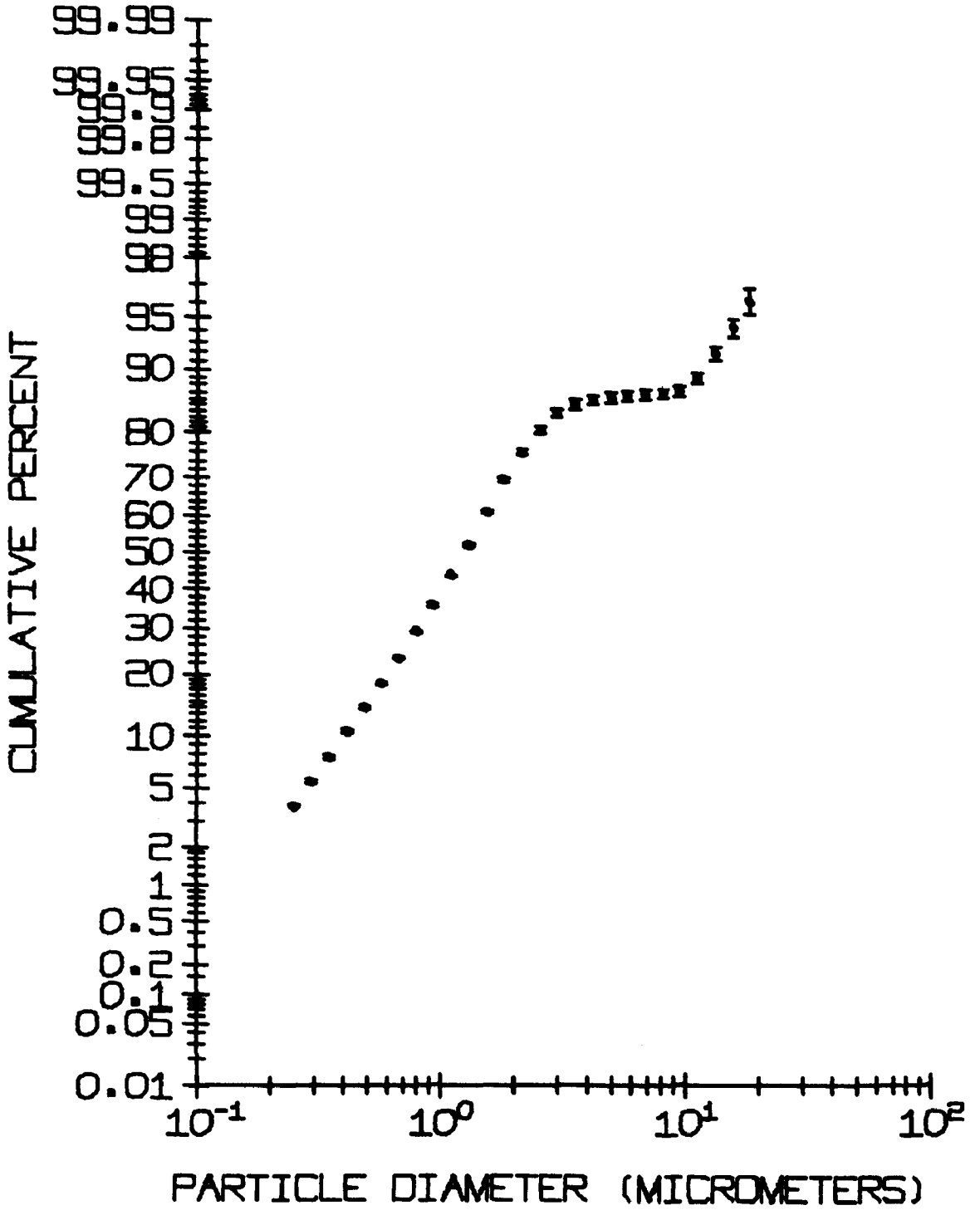

Figure 9. Average baghouse inlet cumulative percent versus particle diameter.

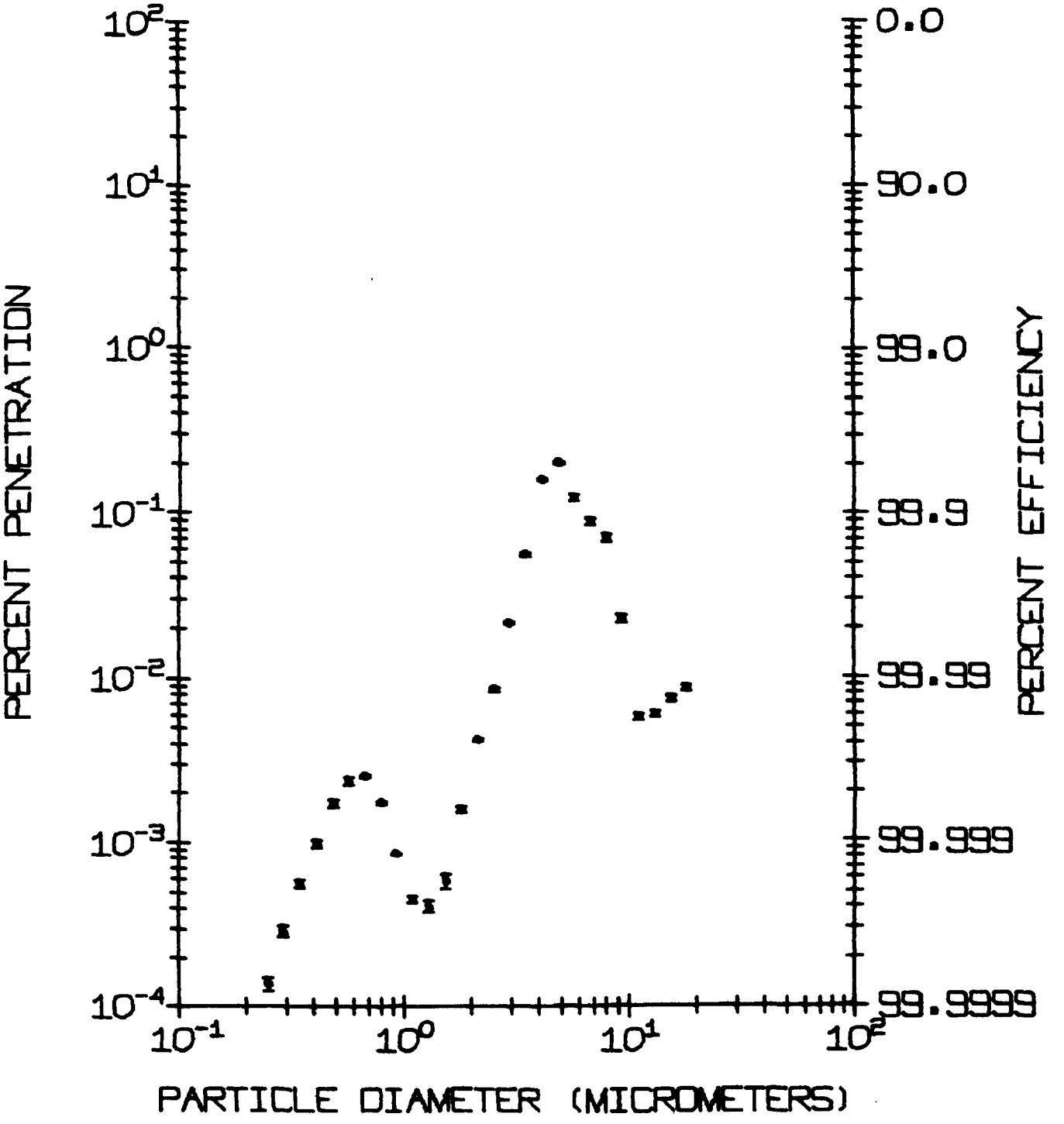

Figure 10. Baghouse particulate collection efficiency.

is not abnormal for baghouse performance. In other studies, the increased penetration around 0.5 μm has been attributed to the lack of inertial or diffusional collection mechanisms, and the increase around 5.0 μm has been attributed to seepage[1]. The mass loadings from all the impactor runs used in the data reduction programs are presented in Table 4. Based on these data, the average particulate collection efficiency of the baghouse exceeds 99.9%. Data from the mass sampling trains and the trace element trains also indicate an average efficiency above 99.9% for the baghouse.

Impactor data for the precipitator show a particulate collection efficiency of 98.3%. Trace element data (collected independently by Radian) show a somewhat lower precipitator efficiency of 97.1%. However, all data agree that the overall particulate collection efficiency of the "hot ESP/cold baghouse system" exceeds 99.9%.

GAS SAMPLING

Two types of modified EPA Method 5 sampling trains were used at each sampling site. These two trains differed from each other only in the number of impingers and the solutions in them. An illustrative gas sampling train is shown in Figure 11.

The trace element train absorbed basic and neutral species in the nitric acid impingers and acidic species in the sodium hydroxide impinger solutions. The gas was then scrubbed in 6% H_2O_2 and dried by silica gel.

The sulfur oxide train contained only five impingers. The first contained 80% isopropanol for absorption of SO_3. The second and third contained 6% H_2O_2 for absorbing SO_2, the fourth was empty, and the fifth contained silica gel.

Both trains contained in-stack and out-of-stack filters which were used to collect particulate (in-stack) and vaporous arsenic trioxide which condensed in the probe after removal of other particulate (out-of-stack).

After sampling, extensive cleaning of the sampling train was required to remove As_2O_3 which had condensed in the probe and glassware. The nozzle was rinsed with NaOH solution to dissolve As_2O_3. Since As_2O_3 is condensable and adheres to walls of sampling equipment, a rigid washing protocol was used to assure maximum recovery from the sampling trains.

Solid (particulate) and gaseous (volatile) components from the trace element sampling train were analyzed quantitatively for four elements: arsenic, antimony, lead, and selenium. A summary of the gas stream measurements and an overall distribution of the four trace elements are shown in Table 5.

The grain loading data in Table 5 show a particulate removal efficiency of about 97.1% for the ESP and 99.9% for the baghouse based on in-stack measurements. Lead and selenium analyses show only about a 90% overall removal, but the amounts present at the ESP inlet were very low. Antimony removed was about 99.5%, but the emission from the baghouse of 0.011 Kg/hr

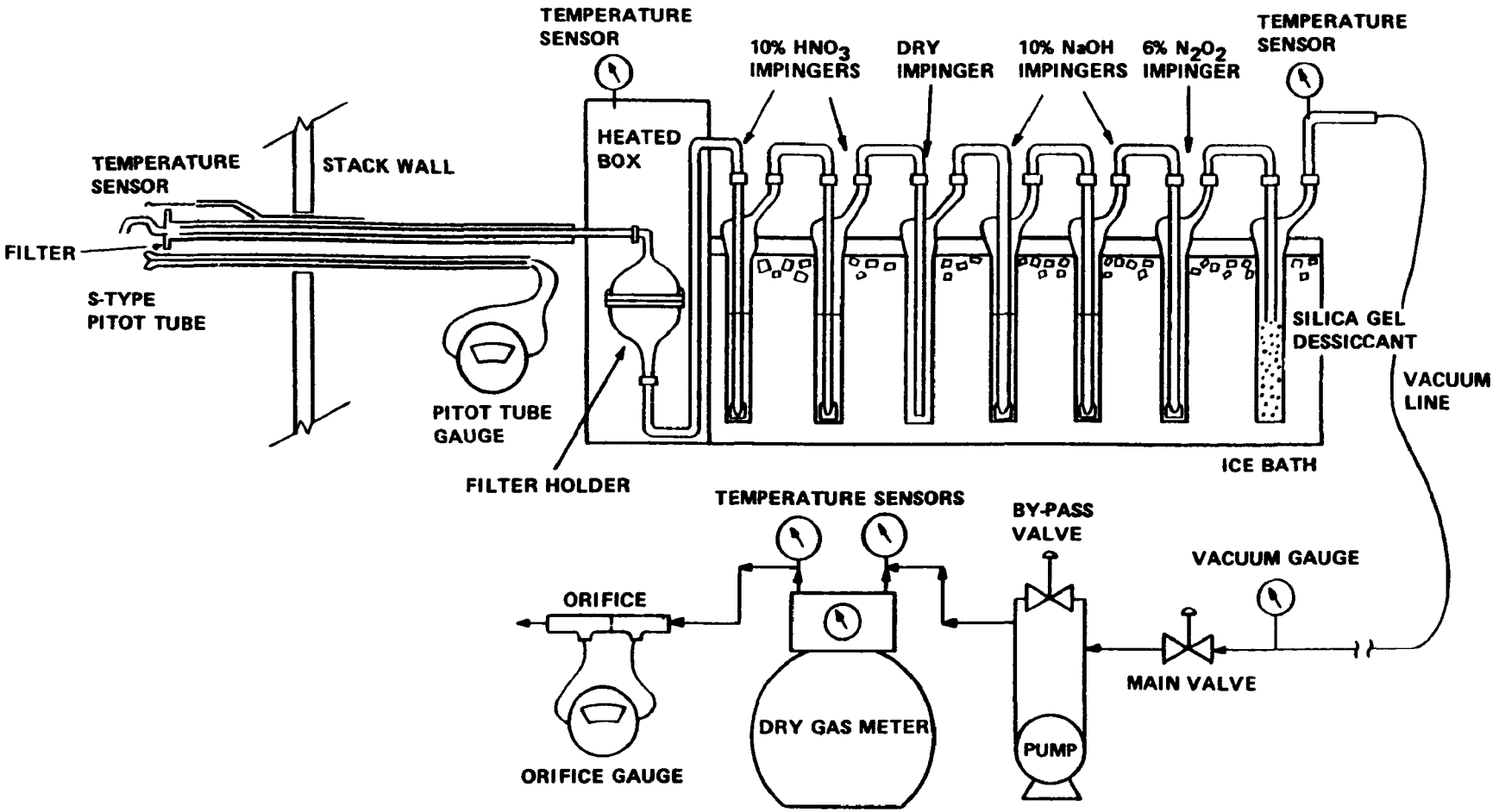

Figure 11. Trace element gas sampling train.

TABLE 4. IMPACTOR MASS LOADINGS

Location	Run#	Date	Sample Time, min	Impactor Temp. °F	°C	Mass Loading gr/SCF	mg/SCM
ESP Inlet	RLI-3	9/19/78	4	600	316	18.73	4.29×10^4
ESP Inlet	RLI-6	9/20/78	4	580	304	114.82	2.63×10^5
ESP Inlet	RLI-7	9/20/78	4	555	291	50.36	1.15×10^5
ESP Inlet	RLI-8	9/20/78	4	560	293	58.82	1.35×10^5
Bghs Inlet	RLI-12	9/21/78	4	244	118	5.25	1.20×10^4
Bghs Inlet	RLI-13	9/21/78	4	230	110	5.07	1.16×10^4
Bghs Inlet	RLI-14	9/21/78	4	225	107	5.34	1.22×10^4
Bghs Inlet	RLI-16	9/25/78	4	220	104	4.56	1.04×10^4
Bghs Inlet	RLI-17	9/25/78	4	220	104	5.04	1.15×10^4
Bghs Inlet	RLI-18	9/25/78	4	225	107	5.14	1.18×10^4
Bghs Inlet	RLI-19	9/25/78	4	230	110	5.80	1.33×10^4
Bghs Inlet	RLI-21	9/26/78	4	228	109	4.55	1.04×10^4
Bghs Inlet	RLI-22	9/26/78	4	243	117	5.19	1.19×10^4
Bghs Inlet	RLI-23	9/26/78	4	228	109	5.97	1.37×10^4
Bghs Inlet	RLI-24	9/26/78	4	243	117	6.70	1.53×10^4
Bghs Outlet	RLO-1	9/19/78	360	228	109	0.00024	0.550
Bghs Outlet	RLO-2	9/20-21/78	960	226	108	0.00029	0.657
Bghs Outlet	RLO-3	9/20-21/78	960	226	108	0.00028	0.642
Bghs Outlet	RLO-5	9/25/78	480	228	109	0.00027	0.621
Bghs Outlet	RLO-6	9/25/78	480	228	109	0.00029	0.667
ESP Outlet	RLO-8	9/26/78	4	575	302	1.017	2.33×10^3
ESP Outlet	RLO-9	9/26/78	4	575	302	1.079	2.47×10^3

Baghouse efficiency = 99.99+%
ESP efficiency = 98.3%

TABLE 5. GAS STREAM MEASUREMENTS AND TRACE ELEMENTS DISTRIBUTION

	ESP Inlet	ESP Outlet	Baghouse Inlet	Baghouse Outlet
Temperature				
°C	380	327	116	113
°F	716	621	240	236
Velocity				
m/sec	21.3	21.9	16.5	16.9
ft/sec	70.0	71.9	54.0	55.3
Grain Loading				
grams/dscm	35.2	1.01	11.40	0.00094
grains/dscf	15.4	0.442	4.98	0.00041
Flow Rate				
dscm/hr	3899	3888	16,779	19,817
dscf/hr	137,680	137,314	592,526	699,833
Trace Elements (total)				
As-Kg/hr	179	152*	105*	0.20
-lb/hr	393	334	232	0.44
Pb-Kg/hr	0.14	0.05	-	0.015
-lb/hr	0.32	0.11	-	0.034
Sb-Kg/hr	2.1	0.40	-	0.011
lb/hr	4.7	0.88	-	0.025
Se-Kg/hr	0.0045	0.0017	-	0.0004
-lb/hr	0.010	0.0037	-	0.0009

* Not measured simultaneously.

(0.025 lb/hr) is also very low. Overall arsenic removal for the ESP and baghouse combined was above 99.9%.

A more detailed analysis of the solid and vapor distribution for arsenic is shown in Table 6. This table shows that most of the arsenic entering the precipitator is in a volatile form and relatively little is caught by the ESP. However, most of the arsenic (as As_2O_3) entering the baghouse (after the gas stream has been quench-cooled) occurs as particulate and this is efficiently collected in the cold baghouse. Collection of particulate arsenic in the baghouse was greater than 99.95%; however, overall arsenic collection efficiency in the baghouse was only 99.8% due to passage of volatile As_2O_3. The total arsenic emissions from the system including both particulate and volatiles were less than 0.2 Kg/hr (0.5 lb/hr).

CONCLUSIONS

The test program conducted at Campbell Red Lake Mines confirmed that their system using a hot electrostatic precipitator, ambient air quenching to condense As_2O_3, and a cold baghouse is an effective technology for control of arsenic emissions from a nonferrous smelter. By comparison to most nonferrous smelters, the Red Lake installation is small. However, the control technology for arsenic has been shown to be highly efficient and would likely be applicable to other nonferrous installations. Major considerations would involve scale-up and sizing of the dilution mixer-cooler and an economic evaluation of the baghouse system for handling increased gas volumes.

ACKNOWLEDGMENTS

This test program was sponsored by the Metals and Inorganic Chemicals Branch of EPA's Industrial Environmental Research Laboratory, Cincinnati, Ohio, John O. Burckle, Project Officer. Assistance in arranging the test was provided by Environment Canada's Air Pollution Control Directorate, Ottawa, Ontario, W. A. Lemmon, Chief, Mining, Mineral and Metallurgical Division.

The gas sampling and analysis were conducted by Radian Corporation, Austin, Texas under the direction of Dr. John C. Terry.

We would like to give special thanks to Stewart Reid, General Manager, Ken Dickson, and Scott Roberts, Campbell Red Lake Mines Ltd., Balmerton, Ontario, Canada who were very cooperative in providing access to the plant and in making modifications required to conduct the test program.

REFERENCES

1. D.S. Ensor, R.G. Hooper, and R.W. Scheck, "Determination of the Fractional Efficiency, Opacity Characteristics, Engineering and Economic Aspects of a Fabric Filter Operating on a Utility Boiler," EPRI FP-297, November 1976.

2. Goodfellow, H. and Gellender, M., "Arsenic Poses Tricky Recovery Task," Canadian Chemical Processing, pp. 26-27, February 1978.

TABLE 6. SOLID AND VAPOR DISTRIBUTION OF As
(Trace element trains)

Phase	ESP Inlet	ESP Outlet	Baghouse Inlet	Baghouse Outlet
SOLID				
gm/dscm	1.21	2.68×10^{-2}	6.20	1.8×10^{-3}
lb/dscf	7.58×10^{-5}	1.67×10^{-6}	3.87×10^{-4}	1.1×10^{-7}
Kg/hr	4.7	0.10	104	0.02
lb/hr	10.4	0.23	229	0.07
VAPOR				
gm/dscm	44.6	39.0	7.82×10^{-2}	9.14×10^{-3}
lb/dscf	2.78×10^{-3}	2.43×10^{-3}	4.89×10^{-6}	5.71×10^{-7}
Kg/hr	174	152	1.31	1.81×10^{-1}
lb/hr	383	334	2.90	3.99×10^{-1}
TOTAL				
Kg/hr	179	152	105	0.20
lb/hr	393	334	232	0.44

3. Goodfellow, H. et al, "Arsenic Removal from Roaster Off-Gases," Fourth International Clean Air Congress (1978).

CONTROL OF SALT LADEN PARTICULATE EMISSIONS FROM HOGGED FUEL BOILERS

By:

Michael F. Szabo
Richard W. Gerstle
PEDCo Environmental, Inc.
11499 Chester Road
Cincinnati, Ohio 45246

and

Larry Sims
U.S. Environmental Protection Agency
Region X
1200 Sixth Avenue
Seattle, Washington 98101

ABSTRACT

This paper presents the results of an evaluation of excessive salt emissions from sixteen hogged fuel boilers in Washington, Oregon, and Alaska. Logs transported or stored in sea water, absorb substantial amounts of salt which is noncombustible, and is emitted as a fine particulate when the hogged fuel is burned, contributing to opacity and particulate emissions. Control measures considered are fuel pretreatment, combustion modifications, use of conventional particulate control devices (electrostatic precipitators, fabric filters, and wet scrubbers), and several novel particulate control devices. The best available control technology appears to be a mechanical collector - fabric filter combination; some electrostatic scrubber type devices have also shown excellent collection capability.

CONTROL OF SALT LADEN PARTICULATE EMISSIONS FROM HOGGED FUEL BOILERS

INTRODUCTION

In some areas of the country, principally the Pacific Northwest, wood fuel that is hogged,* and fired in industrial boilers, comes from logs that have been transported or stored in sea water, from which the bark may absorb substantial amounts of salt. There are 16 salt emitting installations in Washington, Oregon and Alaska, or about 4 percent of the total hogged fuel boiler population in these states, as shown in Table 1.

TABLE 1. HOGGED FUEL BOILERS WITH EXCESSIVE SALT EMISSIONS (1)

	Total no. of hogged fuel boilers	No. of boilers emitting salt	% of total	Approximate heat input of boilers emitting salt, 10^9 J/h (10^6 Btu/h)
Washington	98	10	10	1,051 (995)
Oregon	318	2	0.6	362 (343)
Alaska	10	4	40	786 (744)
Total	426	16	4	2,199 (2082)

Salt emission from hogged fuel boilers are a significant problem, principally because the salt portion of the particulate is primarily submicron in size. Particles larger than 5 μm are deposited in the nasal cavity or naso-pharnyx. The smaller particles, however, are deposited in the lungs, including over 50 percent of the particles from 0.01 to 0.1 μm diameter that penetrate the pulmonary compartment. The tendency of particulates to penetrate the respiratory systems and be captured is mainly a function of their geometry rather than their chemical properties.

Health effects of the captured fine particles depend largely on their chemical or toxic qualities, except for long fibrous material, whose physical qualities also provide potential for irritation of tissue. Because of the many unknown factors, it is unwise to generalize concerning health effects of fine salt particulates from hogged fuel boilers.

*A term derived from the machine that processes the mixture of wood and bark before it is burned, and is called a "hog" or "hogger".

The other important aspect of the problem is that salt-laden particulate emissions, after passing through a conventional mechanical collector, which is not efficient in collecting fine particulates, are usually in violation of both particulate emission and opacity regulations. A plume from these operations is often highly visible and aesthetically objectionable in the community.

Depending on the salt fraction of the fuel and the type of control device used, salt particles can constitute 30 to 90 percent of stack emissions from these boilers. Firing of auxiliary fuels such as No. 6 fuel oil, concurrently with the hogged fuel can also contribute to stack opacity. Although emissions from these boilers violate regulations set forth in the State Implementation Plans (SIP's) and local regulations, available ambient air data obtained near several of these plants have not shown violations of ambient air quality standards.

In responding to the salt emissions problem, some companies have cited potentially high costs and technical problems associated with control of these emissions with secondary control equipment. The smaller companies, particularly, regard control of salt emissions as a financial burden.

The purpose of this paper is to examine the salt emission problem, and define the technical problems, and compliance prospects of various control techniques.

CHARACTERISTICS OF SALT LADEN HOGGED FUEL

The properties of wood residues and bark fuels can vary so widely that no standard specification is possible.

Many species of wood can be used as fuel, but some are better than others. Wet cedar bark, for example, is stringy and difficult to reduce in size. By comparison, dry Douglas fir bark is considered a very desirable fuel.(1)

Other types of wood fuel are used to supplement the hogged fuel. Among these are sawdust, wood chips and shavings, wood waste material, and sanderdust. Sludges and spent liquors from wastewater treatment processes are burned occasionally, more as a means of disposal than for any advantageous fuel characteristics. At some installations where downtime of the hogged fuel boiler is critical to plant operations, the system incorporates provisions for the burning of an alternative fuel, such as No. 6 fuel oil.

The supplemental fuels are used in various quantities and combinations depending largely upon the function and design of the plant. Except for sludge and spent liquors, the supplemental fuels have more desirable burning characteristics (e.g., lower moisture content and higher heating value per equivalent mass) than does the hogged fuel. The supplies of hogged fuel, however, are usually more dependable; also, it is available in much larger quantities and at comparatively lower costs.

Salt Content of Hogged Fuel

In the northwest coastal areas of the United States, logs transported by water can be subjected to a salt or saline environment for long periods of time (sometimes weeks or months), especially if they are stored in saltwater. Such storage allows ample time for the deposition of the various salts and other chemicals present in seawater upon and in the bark of the logs.

Hogged fuel that is transported or stored in salt or saline waters and used in power boilers has been shown to contain anywhere from 0.09 to 2.2 weight percent salt (as sodium chloride, NaCl). The primary factors influencing salt content are length of time the logs remain in saltwater and concentration of salt in the water. These factors, in turn, are affected by plant location with respect to the wood source, log supply and demand, type of storage (i.e., dry or wet, fresh or salt water), and, in tidal estuaries or rivers, the amount of mixing of seawater with freshwater. MacLean and MacDonald (2) found that the average salt content of bark from hemlock after 6 months flotation was 1.44 to 3.13 percent, of which roughly half was absorbed in the first 3 weeks.

Since the concentrations and proportions of the various salt fractions in seawater vary greatly, it is difficult to predict the total emissions of particulate and salt from hogged fuel boilers.

The effect of mixing of fresh and salt waters is evident when comparing the salinity at high and low tides in a coastal river. Salinity at low tide would tend to be lower because there is a greater flow of fresh water past a given point as the tide moves out. At high tide, the reverse is true. Typical values are 9800 ppm NaCl at low tide and 13,000 ppm at high tide.

Salt Measurement Techniques

Salt content of wood fuel or flue gas can be expressed as a percentage of NaCl, of equivalent chloride, or of total sea salt. This can lead to confusion in interpretation of data, since no standard method is consistently applied to determinations of salt content and the method of analysis often is not given. The amounts of salt reported as NaCl, all chloride salts, and total sea salts can differ significantly.

In this regard the Council of Forest Industries of British Columbia has stated the following (3):

> "The salt content of particulate matter is commonly expressed as equivalent sodium chloride. This value is obtained by multiplying the chloride ion concentration by 1.58, the factor representing the weighted average of the ratios of chloride salt molecular weight to the chloride content of molecule. Actually, the value so obtained does not represent sodium chloride (which would be obtained by multiplying chloride by 1.66) but the total chloride salts. A further correction actually is required for accuracy because chloride salts represent about 90 percent of sea salts and so the factor to get total sea salts from chloride content is 1.76. This latter correction rarely has been made."

This statement emphasizes the importance of identifying the basis upon which salt concentrations are presented and the need for a standard reference method.

Particle Size Distribution of Salt Emissions

The size distribution of the salt particles strongly affects the removal efficiency of control equipment. Particulate emissions from boilers burning hogged fuel with no salt can be handled adequately by conventional control devices. With salt-laden hogged fuel, however, the size range of the particulate emissions is much smaller; and the size fractions below 1 μm typically are composed of more than 50 percent salt.

In an analysis of the effect of salt (NaCl) on overall mean particle size in emissions from hogged fuel boilers, the salt fraction reduced the overall mean particle size by a factor of approximately 10 (4) (see Figure 1). As this figure shows, the mean particle size of the nonsalt fraction is about 17.5 μm. The mean particle size of the salt fraction is about 0.23 μm. The overall mean particle size, about 2.15 μm, indicates the extent of size reduction caused by salt in the emissions. Some data show that the overall mean particle size of the salt-laden particulate can be as low as 0.2 μm.

Comparison of particle size data from the Weyerhauser North Bend plant with data from Crown Zellerbach's Port Townsend plant and data from British Columbia verifies the reduction in mean particle size due to salt particles. All of these impactor measurements were taken at the outlet of a multiclone or cinder collector. The reduction in the overall mean particle size can result in dust even finer than the composite shown in Figure 1, depending on the size distribution of the nonsalt fraction of the dust.

PREVENTIVE CONTROL TECHNOLOGY TO REDUCE SALT EMISSIONS

Handling and Pretreatment of Fuel

Among various preventive methods for reducing salt particulate emissions from hogged fuel boilers, the most obvious is not to transport the logs via saltwater; in most cases this is not possible. Transport by flat rafting rather than in bundles will reduce the salt content of hogged fuel, as will reducing the duration of storage in salt water (see Figure 2).

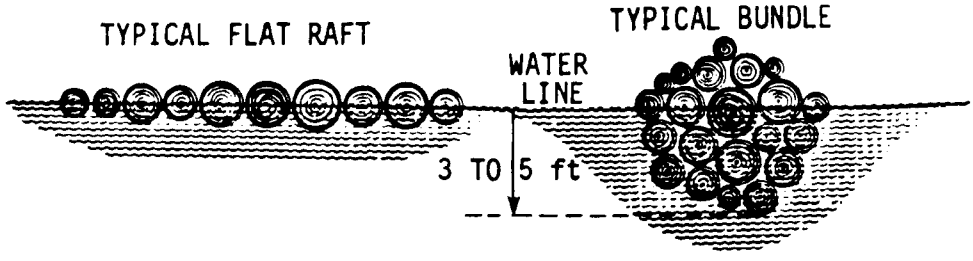

Figure 2. Storage of logs by flat raft and bundle.(5)

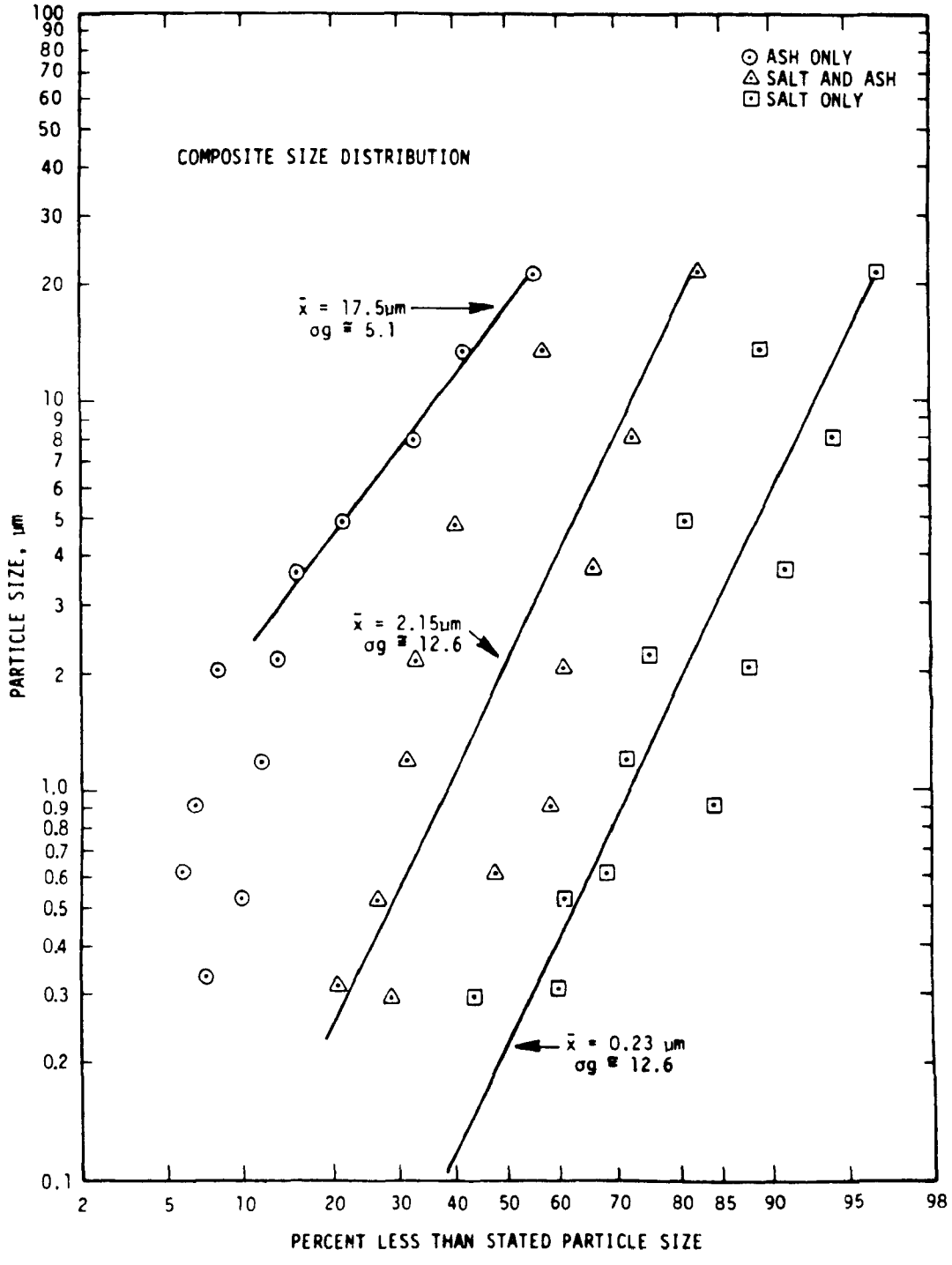

Figure 1. Particle size distribution at Weyerhauser Co., North Bend, Oregon, plant (composite from 11 tests).

About half of all salt absorbed in 6 months is absorbed in the first 2 or 3 weeks of contact with seawater.

Hydraulic deparking of logs with fresh water is reported to have reduced salt content in one instance but not in another (5).

Bark pressing can reduce moisture content by 50 percent and remove substantial quantities of salt in the process. This can result in lower opacity and particulate emissions because of increased boiler efficiency and fewer fine particles of salt. The disadvantage, however, is serious water pollution from the bark pressate wastewater.

Other methods of predrying fuel do not reduce the salt content, but do reduce combustible emissions by improving boiler efficiency.

Combustion Modifications

Combustion modifications can increase boiler efficiency and thereby reduce salt emissions because salt is not combustible.

About 65 to 85 percent of the salt in bark passes out of the chimney as particulate emissions; the remainder is retained in the boiler, on the grates, or on boiler surfaces, reducing efficiency of the boiler and disrupting uniform air flow through the fuel beds. Plant engineers therefore should try to reduce both the salt and moisture content of the bark at reasonable cost. The resulting improvement in fuel quality will reduce consumption of auxiliary fuel and boiler cleaning requirements. Additional research is needed into ways to slow the quenching effect on vaporized salt leaving the combustion zone in hogged fuel boilers. This would generate large particles of salt that would be more easily collected by a secondary control device. In most operations, however, additional control measures will be necessary to reduce salt-laden particulate emissions to acceptable levels.

SECONDARY CONTROL TECHNOLOGY TO REDUCE SALT EMISSIONS

Four types of conventional control devices are used to reduce particulate emissions from hogged fuel boilers: mechanical collectors, electrostatic precipitators (ESP's), wet scrubbers, and fabric filters. Only the latter three can remove submicron salt particles. Mechanical collectors, nonetheless, are used on salt-laden hogged fuel boilers and ESP's are not.

The following sections on each control device briefly summarize applicability for controlling salt emissions, performance on hogged fuel boilers (salt-free and salt-laden fuel), operation and maintenance problem, and disposal techniques for collecting salt/particulates. The best available method of collecting salt/particulates is also discussed.

Mechanical Collectors

Particulate emissions from hogged fuel boilers have traditionally been controlled by mechanical collectors. Although mechanical collectors generally do not meet applicable emission regulations when controlling salt-laden particulate, they are still important as part of a total system of particulate control. These collectors are usually designed for dust loadings of 2 to 11 g/m^3 (1 to 5 gr/scf) (6). Particle size distribution of ash from combustion of nonsalt bark is normally 30 to 40 percent less than 10 micrometers. Pressure drop across the mechanical collector ranges from 3.8 to 6.4 cm (1.5 to 2.5 in. water) for best collection efficiency.(6)

With ash from salt-free bark, mechanical collectors can sometimes achieve collection efficiencies of 85 to 90 percent with outlet loadings of 172 to 258 kg/J (0.4 to 0.6 $lb/10^6$ Btu). A collection efficiency of 30 to 70 percent is more realistic estimate. Even under optimum conditions opacity may be a problem, especially with stoker-fired boilers, which respond slowly to upset conditions. Opacity can be limited to 20 percent during normal operation, but may exceed 20 percent during boiler upsets.

With salt-laden particulate, the collection efficiency of the mechanical collector is considerably lower because of the fines of the salt particles; overall efficiencies of 30 to 50 percent would be expected. Test data from Weyerhauser's North Bend plant confirm this observation. (7)

Operation and maintenance problems associated with cyclone system removing particulates from flue gas of hogged fuel boilers are principally due to plugging, leakage of air into the system, and changes in gas flow to the cyclone.

Electrostatic Precipitators (ESP's)

Although ESP's are used widely in controlling particulate emissions from combustion sources, they are rarely used on boilers fired with hogged fuel. Several successful installations on boilers that burn salt-free wood have been put into operation in the last 5 or 6 years.

From the precipitation standpoint, ash from hogged fuel boilers poses two potential problems that must be accounted for in design:(1) 1) since it is carboneceous, the ash has a lower resistivity than coal ash and tends to lose its charge quickly, and 2) the ash is prone to reentrainment because of its low density, coupled with flake-like particle shape. When the ash is salt-laden, the submicron salt particles require a conservative design, i.e., a larger collecting surface.

Performance of ESP's on boilers burning salt-free hogged fuel has reportedly been excellent. Where an ESP was retrofitted downstream of a cyclone at a paper mill, the average outlet loading was 0.04 g/m^3 (0.018 gr/acf); guarantee was 0.06 g/m^3 (0.025 gr/acf).

The only reference to performance of an ESP on a boiler burning salt-laden hogged fuel comes from the Council of Forest Industries of British Columbia.(3) Test data from a pilot unit installed at the Victoria Sawmill Division of B.C. Forest Products, Ltd., showed that performance varied from excellent [0.05 g/m^3 (0.02 gr/dscf)] to poor [0.7 g/m^3 (0.3 gr/dscf)].(3) The program showed that the ESP could reduce salt fume to an acceptable level when it was maintained and operated within precise limits. When control of operation was not virtually perfect, however, the performance deteriorated markedly.

Expected operation and maintenance problems would be the possibility of fire from "char" build-up on precipitator walls, and especially in the hoppers. Reentrainment is also a problem with bark ash because of its low resistivity.

Pilot scale tests have reportedly been performed on a wet-ESP controlling salt laden particulate emissions from a hogged fuel boiler in Alaska, but data from this installation were not available for this paper.

Wet Scrubbers

Wet scrubbers are applied to a number of hogged fuel boilers to control particulate emissions. Most are installed downstream of a multiple cyclone collector. In salt-free applications under normal operating conditions the outlet loadings range from 0.05 to 0.14 g/m^3 (0.02 to 0.06 gr/scf) at pressure drops of 15 to 38 cm (6 to 15 in.) water.(8)

Only one boiler fired with salt-laden hogged fuel is currently equipped with a venturi scrubber, Crown Zellerbach, Port Townsend plant; this scrubber is installed downstream of a multiclone.(9) The reported outlet loadings are 0.16 to 41 g/m^3 (0.07 to 0.18 gr/scf), depending on the salt content of the fuel. A salt concentration greater than 1 percent will limit the performance of this venturi scrubber, which operates at a pressure drop of 38 to 51 cm (15 to 20 in.) water. The salt content of particulate emissions from the scrubber is reported to be 50 to 70 percent or more. Opacity of the stack effluent is estimated at 35 percent. This scrubber would require a pressure drop greater than 51 cm (20 in.) water to achieve the roughly 80 percent efficiency needed to meet the 0.23 g/m^3 (0.10 gr/dscf) particulate emission regulation, assuming a typical inlet concentration of 1.14 g/m^3 (0.50 gr/dscf), and greater than 1 percent salt in the fuel.

Using unpublished impactor data for this installation, an approximate fractional efficiency curve was prepared, and is shown in Figure 3. Overall mass efficiency from these data is approximately 68 percent. The characteristic sharp increase in penetration as particle size decreases, is evident in this curve.(10)

Common maintenance problems for venturi scrubbers include plugging of lines, nozzles, and pumps and erosion/corrosion and scaling of internal components.

Fabric Filters

Fabric filters are used on four hogged fuel boiler installations: Simpson Timber Co. in Shelton, Washington; Long Lake Lumber Co. in Spokane,

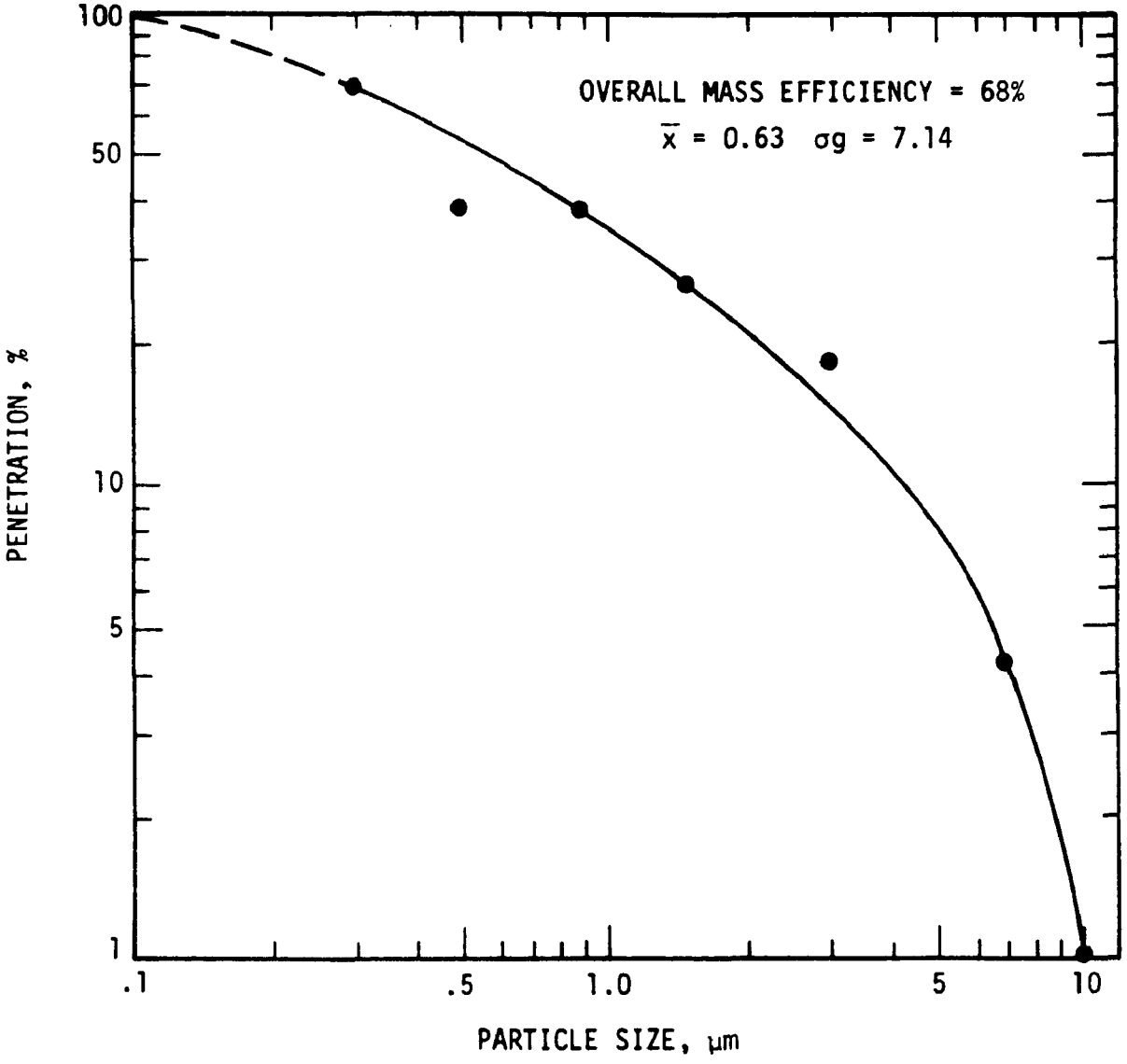

Figure 3. Approximate penetration as a function of particule size for a venturi scrubber operating on a salt-laden bark/oil fired boiler.(10)

Washington; Georgia Pacific Corp. in Bellingham, Washington; and the most recent installation, which started operation in the latter part of June 1979, at Scott Paper Co. in Everett, Washington. All of these installations except Long Lake Limber use logs that have been transported in sea water. Table 2 summarizes design parameters for these four installations.

Plant engineers estimate the overall mass efficiency of the Simpson Timber Co. baghouses at 90 to 95 percent, stating that a number of bags are always broken, due to improper installation, faulty construction, etc. Outlet mass loadings were tested at 0.03 g/sm^3 (0.01 gr/dscf), for the smaller unit and 0.092 g/sm^3 (0.09 gr/dscf) for the larger unit.(11) Opacity did not exceed 5 percent (mostly only heat waves were visible).

The Georgia Pacific Facility started up in February, 1979, and is reported to be operating well with no major problems. The plant was only recently tested for compliance, and plant officials unofficially estimate outlet loading to be approximately 0.05 g/m^3 (0.02 gr/dscf) with zero visible emissions. This is well within emission limitations.

Operating data are not available for the Scott Paper Co. facility since it only recently began operation.

The Long Lake facility reports an overall mass efficiency of 99 percent. However, operation at this facility has been marred by two fires.

Although no fractional efficiency data are available, the dramatic reduction in opacity with installation of the baghouses indicates that they are efficient collectors of submicron salt particles. Fractional efficiency data from tests of fabric filters in other industries support this view.

Disposal of Salt-Laden Ash

The disposal of salt-laden ash from secondary collectors is a problem sometimes overlooked in evaluating the salt emissions problem. Landfilling of the ash is complicated by the presence of salt, which presents a potential leachate problem. Return of a slurry containing salt and ash to a bay or ocean is unacceptable because of the ash content, and the ash cannot be sold for cement or asphalt production because of the salt.

Acceptable disposal practices include providing an impermeable liner for an ash pond or diluting the salt concentration by mixing the ash slurry with other plant wastewater streams or with municipal wastewater and processing the ash slurry by conventional wastewater treatment. Sometimes, the sludge is returned to the boiler. Wet treatment seems to be more effective in terms of efficiency and economy. Either method, however, increases capital and operating costs.

NOVEL FINE PARTICULATE CONTROL DEVICES

Experience at plants with salt particulate emissions shows that, except for fabric filters, the conventional control devices cannot consistently

TABLE 2. DESIGN PARAMETERS FOR BAGHOUSES ON HOGGED FUEL BOILERS

	Simpson Timber[a]	Long Lake Lumber	Georgia-Pacific[a]	Scott Paper[a]
Volume flowrate, acfm	130,000	25,000	180,000	260,000
Inlet gas temperature, °F	500	400(200)[b]	440	420
A/C ratio, acfm/ft^2	4.5	4.0	4.0	3.9
Bag cleaning method	Pulse jet	Pulse jet	Pulse jet	Pulse jet
Pressure drop, in. H_2O	9-9.5	5.8-6.8	not > 7	N.A.
Bag fabric	Teflon-coated fiberglass	Nomex	Teflon-coated fiberglass	Teflon-coated fiberglass
Precollector	Mechanical cinder collector	None	None	None
Material handling system	Screw conveyor	Screw conveyor	Screw conveyor	Water sluice

Metric conversions: acfm x 0.028 = m^3/min
acfm/ft^2 x 5.09 = m^3/s per m^2
(°F - 32)/1.8 = °C
in. H_2O x 2.54 = cm H_2O

[a]Salt-laden hogged fuel boilers.

[b]Operating temperature.

N.A. - not available.

reduce emissions enough for compliance with particulate and stack opacity regulations. Thus, there is a need for more effective control, especially in the submicron particle size range. This section evaluates some novel or promising particulate control devices now being tested for control of salt emissions from hogged fuel boilers.

Classification of Novel Control Devices

Three categories of wet scrubbing(12) are considered promising for control of the submicron salt particles from hogged fuel boiler emissions: foam scrubbing, flux force condensation, and electrostatic scrubbing. Of these, electrostatic scrubbing appears to offer the greatest potential for full-scale application to salt-laden hogged fuel boilers.

Dry scrubbers also are considered here as a novel device, since there have been two pilot tests and one full-scale test on three salt-laden hogged fuel boilers.

Electrostatic Scrubbing-This device embodies the principles of an electorstatic precipitator and a scrubber. The basic idea is to augment the collection processes associated with spray scrubbing and electrical collection forces. This involves the use of electrostatically charged water droplets or charged pollutant particles or both.(13,14) The scrubber may be of the spray or venturi type. Particulate collection efficiencies higher than 99 percent have been achieved with some devices.(14,15) The initial costs are somewhat higher than those associated with conventional methods, but lower than those of the foam and force-flux/condensation scrubbers. Operating costs are reported to be much lower than those of conventional methods.(16,17, 18) It appears that devices based on electrostatic scrubbing would provide good control over opacity of stack emissions and would be more effective than the other novel devices in controlling particulate emissions. Performance of the various types or electrostatic scrubbers indicates that these units should be tested further in full scale applications. Table 3 summarizes the various types of electrostatic scrubbers now available, and results of pilot and/or full scale tests on salt-laden hogged fuel boilers.

Dry Scrubbers-The dry scrubber is a recently developed system that uses a moving bed of granular material (media) instead of water droplets to capture particulates. The dirty media is shaken at the bottom of the unit, and particulates fall into a storage bin. The cleaned media is then conveyed back to the top of the unit. The following advantages are claimed for the unit:(1)

1. It requires no water supply.
2. The particulate is removed dry.
3. Because there is no corrosion potential, mild steel can be used.
4. The unit can be small and lightweight because of high-velocity throughput.

This device can be effective when temperature and natural collection are well controlled. Officials of the Simpson Timber plant at Shelton rejected the dry scrubber in favor of a baghouse because the scrubber would not eliminate

TABLE 3. NOVEL FINE PARTICULATE CONTROL DEVICES APPLIED TO BOILERS BURNING SALT-LADEN HOGGED FUEL[a]

Manufacturer/ unit	Commercially available	Base equipment	Particles charged	Water droplets charged	Results of outlet emission tests g/sdm^3 (gr/sdcf)
Ceilcote Co./ ionizing wet scrubber	Yes	Wet scrubber	Yes	No	0.005-0.042 (0.002-0.018)[b] <20% opacity
TRW Inc./ charged droplet scrubber	Yes	Wet scrubber	No	Yes	Data not available
Pollution Control Systems, Inc.,/ UW electrostatic scrubber	Yes	Wet scrubber	Yes	Yes	0.11 (0.05) 20% opacity
Union Carbide Bendix Division/ APS electrotube	Yes	Wetted-wall pipe precipitator	Yes	No	0.004-0.10 (0.002-0.04) near 0% opacity
Air Pollution Systems/electro-static scrubber	Yes	Venturi scrubber	Yes	No	Data not available

[a]All devices have undergone pilot-scale field tests on boilers burning salt-laden hogged fuel; information from some of the tests is sparse.

[b]After two stages of the collector.

the stack plume. A full-scale installation of a salt-laden hogged fuel boiler at Port Gamble, Washington, was shut down because of scrubber operating problems. These problems reportedly concerned cake build-up at the discharge of the moving bed and blinding of the screen that contains the moving bed.

On a more recent full-scale test on a salt installation in Canada, Combustion Power Company (CPC) has solved this problem by providing a steeper angle for the discharge cone. However, opacity limits are still being exceeded.

BEST AVAILABLE CONTROL TECHNOLOGY FOR CONTROLLING SALT EMISSIONS FROM HOGGED FUEL BOILERS

Operating data on boilers fired with salt-laden hogged fuel indicate that the best available conventional control system is a fabric filter preceded by a mechanical collector. A mechanical collector is needed to remove cinders that would increase the chance of fire in the fabric filter.

Simpson Timber Company's fabric filter installation at Shelton has operated successfully for over 2 years in compliance with both grain loading and opacity regulations. The dramatic decrease in opacity is evidence of the ability of the fabric filter to capture submicron particles of salt. This ability to maintain high levels of collection efficiency in the submicrometer particle size range has been demonstrated in fabric filter applications in other industries. Some maintenance problems were encountered but plant officials do not regard them as excessive. Likewise, operation at the Georgia Pacific facility has reportedly been excellent with low outlet levels, and no visible emissions.

Use of a venturi scrubber on the salt-laden hogged fuel boiler at Crownzellerbach's Port Townsend mill has been partially successful in that operations comply with the applicable emission regulation when the salt content of the fuel is below 1 percent. At higher salt levels the scrubber cannot remove enough of the additional fine salt particles to achieve compliance. More efficient removal of submicron salt particles would require additional pressure drop over the present maximum of 51 cm (20 in.) water. Opacity has not been measured but is estimated by plant officials at 35 percent. Plant engineers report that the Port Townsend scrubber has not required excessive maintenance although trouble areas may become apparent with more operating time.

Electrostatic precipitators have not been applied to boilers burning salt-laden hogged fuel, probably because ESP manufacturers will guarantee outlet grain loading but not visible opacity. For compliance with visible opacity regulations when the boiler fuel is salt-laden, an ESP may be too large to be economically competitive with a fabric filter or wet scrubber. Sizing of the ESP would have to accommodate the "worst case" in terms of salt content in the fuel.

In the novel device category the University of Washington (U of W) electrostatic scrubber, the Ceilcote ionizing wet scrubber (IWS), and the APS

electrotube show the best performance characteristics. A recent full scale test of the U of W scrubber on a salt-laden hogged fuel boilers showed outlet emission levels of 0.114 g/sdm^3 (0.05 gr/scf) and 20 percent opacity. Data from pilot tests of the Ceilcote IWS and the APS electrotube show outlet loadings of 0.09 g/dsm^3 (0.044 gr/dscf), and lower.

The dry scrubber marketed by Combustion Power Company (CPC), and recently redesigned with an electrostatic cage installed in the gravel bed of each scrubber, may be able to reduce opacity levels that have been one of the shortcomings of the dry scrubber, but further testing of this device is required.

CONCLUSIONS

Although the data base is small, test operations have demonstrated that salt-laden particulate emissions from hogged fuel boilers can be controlled to comply with stringent particulate and opacity regulations, using currently available control technology. The best available control technology is use of a fabric filter, preceded by a mechanical collector, to collect cinders and lessen the chance of fire. Pretreatment techniques such as hydraulic debarking, various drying systems or combustion modifications, do not reduce salt emissions significantly. Bark pressing can reduce moisture content by 50 percent and remove substantial quantities of salt as a result, but the bark pressate presents a serious water pollution control problem.

Electrostatic scrubbers, categorized as novel control devices, have shown the potential for effective collection of salt-laden particulate emissions from hogged fuel boilers, and additional full scale installations of these devices are likely in the future.

Acknowledgement

This paper is based on work done by PEDCo Environmental, Inc. (19) for U.S. EPA Region X, under Contract No. 68-01-4147, Task No. 51, Mr. Michael M. Johnston, Task Manager.

REFERENCES

1. Boubel, R.W. Control of Particulate Emissions from Wood-Fired Boilers. EPA 340/1-77-026. 1977.

2. MacLean, H., and B.F. MacDonald. Salt Distribution in Sea Water Transported Logs. State of Alaska, Information Report VP-X-45.

3. Council of the Forest Industries of British Columbia. The Basis for Requesting a Variance on Marine Salts as Polluting Particulates in Stack Gases from Hog Fuel Fired Boilers. Submitted to the Pollution Control Branch, Department of Lands, Forests, and Water Resources, Government of British Columbia, Victoria, B.C. September 1974.

4. Whyte, J.E. Hog Fuel Boiler Emissions - Particle Size Via Cascade Impactor Tests. Weyerhauser Co., North Bend, Oregon. Technical Report No. 046-4504. August 1976.

5. Leman, M.J. Special Environmental Problems Originated by Burning Bark from Saltwater-Borne Logs. Proceedings of a Conference on Wood and Bark Residues for Energy, Oregon State University. February 1975.

6. Horzella, T.E., and H.R. Newton. Controlling Air Pollution from Hogged Fuel Boilers. Pulp and Paper. February 1974. pp. 71-75.

7. Whitman, J.L., and H. Burkitt. Compliance Alternatives for Stack Emissions from the Hog Fuel Boilers at North Bend, Oregon. Prepared for Weyerhauser Company, Corporate Engineering. December 1977.

8. Mick, A.H. Wood Waste Fired Boilers: Wet Scrubber Technology. Georgia Pacific Corporation. Presented at the 69th Annual Meeting of the Air Pollution Control Association. Portland, Oregon. June 27-July 1, 1976.

9. Cupp, S.J. Operating Experience with a Boiler Firing Salt Water Borne Hogged Fuel. Crown Zellerbach Corporation. 1978.

10. Szabo, M.F. and R.W. Gerstle. Operation and Maintenance of Particulate Control Devices in Kraft and Pulp Mill and Crushed Stone Industries. PEDCo Environmental, Inc. EPA 600/2-78-210. October 1978.

11. CH_2M Hill, Inc. A Study of Particulate Emission Discharges from the Boiler Baghouse Installation. Prepared for Simpson Timber Co., Shelton, Washington. April 1976.

12. McIlvaine, R.W. Fine Particulate Scrubbing-New Problems and Solutions. EPA-600/2-77-193. September 1977.

13. University of Washington Electrostatic Droplet Scrubber. In Evaluation of Eight Novel Fine Particle Collection Devices. EPA-600/2-76-035. February 1978.

14. Pilat, M.J., G.A. Raemhild, and D.C. Harmon. Fine Particle Control with UW Electorstatic Scrubber. EPA 600/2-77-193. September 1977. pp. 308-318.

15. Keller, F.R. Fluidized Bed Combustion Systems for Energy Recovery from Forest Products Industry Wastes. Presented at Meeting of Forest Products Research Society, Denver, Colorado. September 1975.

16. Deardorff, D. Wet Wood Waste as a Viable Fuel Supply. Presented at meeting of Forest Products Research Society, Denver, Colorado. September 1975.

17. Jasper, M., and P. Koch. Suspension Burning of Green Bark to Direct-Fired High-Temperature Kilns for Southern Pine Lumber. Presented at meeting of Forest Products Research Society, Denver, Colorado. September 1975.

18. Guidon, M.W. Pilot Studies for Particulate Control of Hog Fuel Boilers Fired with Salt-Water Stored Logs. Georgia Pacific Corp., Bellingham, Washington. November 1977.

19. Szabo, M.F., S. Kothari, C. Doolittle, and R. Gerstle. Control of Salt-Laden Particulate Emissions From Hogged Fuel Boilers. PEDCo Environmental, Inc. Final Report. U.S. EPA contract No. 68-01-4147, Task No. 51. May 1979.

AUTHOR INDEX

AUTHOR NAME	PAGE
Ariman, T.	III-222
Bacchetti, J. A.	I-529
Bernstein, S.	II-125
Bibbo, P. P.	II-219
Bickelhaupt, R. E.	I-154
Blackwood, T. R.	IV-312
Bloomfield, D. P.	III-145
Brackbill, E. A.	III-472
Brines, H. G.	I-351
Brookman, E. T.	IV-274
Brown, J. T. (Jr.)	III-439
Buchanan, W. J.	II-168
Burckle, J. O.	III-484
Bush, J. R.	IV-154
Carlsson, B.	III-260
Carr, R. C.	I-35, III-270
Chang, C. M.	II-314
Chapman, R. A.	I-1
Chmielewski, R.	III-1
Cooper, D. W.	III-127
Cowen, S. J.	IV-424
Cowherd, C. (Jr.)	IV-240
Czuchra, P. A.	III-104
Darby, K.	I-15
Daugherty, D. P.	IV-182

AUTHOR NAME	PAGE
Dennis, R.	I-494
Dietz, P. W.	III-429
Donovan, R. P.	I-476
Drehmel, D. C.	IV-170
Durham, M. D.	IV-368
Dybdahl, A. W.	IV-443
Ellenbecker, M. J.	III-171, III-190
Engelbrecht, H. L.	II-279
Ensor, D.S.	III-39
Ernst, M.	IV-30, IV-42
Eschbach, E. J.	II-114
Evans, J. S.	IV-252
Fasiska, E. J.	IV-486
Faulkner, M. G.	IV-508
Fedarko, W.	IV-64
Ferrigan, J. J.	I-170
Finney, W. C.	II-391
Furlong, D. A.	I-425
Garrett, N. E.	IV-524
Gastler, J. H.	IV-291
Gavin, J. H.	III-81
Giles, W. B.	IV-387
Gooch, J. P.	I-132
Gooding, C. H.	III-404
Grace, D. S.	III-289
Guiffre, J. T.	I-80

AUTHOR NAME	PAGE
Hall, F. D.	III-25
Hardison, L. C.	III-382
Hoenig, S. A.	IV-201
Hudson, J. A.	I-263
Iinoya, K.	III-237
Isoda, T.	III-16
Jaasund, S. A.	II-452
Kalinowski, T. W.	III-363
Kallio, G. A.	III-344
Kearns, M. T.	III-61
Kelly, D. S.	I-100
Kinsey, J. S.	III-95
Kolber, A. R.	I-224
Ladd, K. L.	I-317
Lamb, G. E.R.	III-209
Lane, W. R.	I-410
Langan, W. T.	I-117, II-256
Larson, R. C.	III-448
Leonard, G.	II-146
Lipscomb, W. O.	I-453
Malani, S.	I-570
Marcotte, W. R.	I-372
Martin, J. R.	I-591
Masuda, S.	II-65, II-334, II-483
McCain, J. D.	IV-496
McDonald, J. R.	II-93

AUTHOR NAME	PAGE
Mitchell, D. A.	III-162
Modla, J. C.	II-399
Mosley, R. B.	II-45
Mycock, J. C.	I-432
Neundorfer, M.	II-189
Nixon, D.	I-513
Noll, C. G.	II-374
Nunn, M.	II-369
Ondov, J. M.	IV-454
Ostop, R. L.	I-342
Parker, R.	IV-1
Patch, R. W.	IV-136
Patterson, R. G.	IV-84
Pearson, G. L.	I-359
Pedersen, G. C.	III-416
Petersen, H. H.	II-352
Pilat, M. J.	I-561
Potter, E. C.	I-184
Ranade, M. B.	I-538
Raymond, R. K.	II-173
Rinard, G.	II-31, IV-127
Roehr, J. D.	II-208
Rolschau, D. W.	III-251
Ruth, D.	II-427, II-441
Samuel, E. A.	II-1
Schliesser, S. P.	I-56

AUTHOR NAME	PAGE
Self, S. A.	III-309
Severance, R. L.	IV-321
Shale, C. C.	I-390
Smit, W.	I-297
Smith, S. B.	II-502
Spafford, R. B.	I-202
Sparks, L. E.	II-417, IV-411
Stenby, E. W.	I-243
Stock, W. E.	IV-333
Surati, H.	II-469
Szabo, M. F.	III-508
Tendulkar, S. P.	IV-338
Tennyson, R. P.	III-117
Tsao, K. C.	IV-14
Umberger, J. H.	II-296
VanOsdell, D. W.	II-74
VanValkenburg, E. S.	IV-351
Wang, J. C.F.	IV-396
Weber, E.	IV-98
Wybenga, F. A.	II-242
Yung, S.	IV-217

TECHNICAL REPORT DATA
(Please read Instructions on the reverse before completing)

1. REPORT NO.	2.	3. RECIPIENT'S ACCESSION NO.
EPA-600/9-80-039c	IERL-RTP-1063	

4. TITLE AND SUBTITLE
Second Symposium on the Transfer and Utilization of Particulate Control Technology (Denver, July 1979)
Vol. III. Particulate Control Devices

5. REPORT DATE
Sept. 1980 Issuing Date.

6. PERFORMING ORGANIZATION CODE

7. AUTHOR(S)
F.P. Venditti, J.A. Armstrong, and Michael Durham

8. PERFORMING ORGANIZATION REPORT NO.

9. PERFORMING ORGANIZATION NAME AND ADDRESS
Denver Research Institute
P.O. Box 10127
Denver Colorado 80210

10. PROGRAM ELEMENT NO.
EHE624

11. CONTRACT/GRANT NO.
R805725

12. SPONSORING AGENCY NAME AND ADDRESS
Industrial Environmental Research Laboratory
Office of Research and Development
U.S. Environmental Protection Agency
Research Triangle Park, NC 27711

13. TYPE OF REPORT AND PERIOD COVERED
Proceedings; 6/79-6/80

14. SPONSORING AGENCY CODE
EPA/600/13

15. SUPPLEMENTARY NOTES
IERL-RTP project officer is Dennis C. Drehmel, MD-61, 919/541-2925. EPA-600/7-79-044a thru -044d are proceedings of the 1978 symposium.

16. ABSTRACT

The proceedings document the approximately 120 presentations at the EPA/IERL-RTP-sponsored symposium, attended by nearly 800 representatives of a wide variety of companies (including 17 utilities). The keynote speech for the 4-day meeting was by EPA's Frank Princiotta. The meeting included a plenary session on enforcement. Attendees were polled to determine interest areas: most (488) were interested in operation and maintenance, but electrostatic precipitators (ESPs) and fabric filters were a close second (422 and 418, respectively). Particulate scrubber interest appears to be waning (288). Major activities of attendees were: users, 158; manufacturers, 184; and R and D, 182. Technical presentations drawing great interest were the application of ESPs and baghouses to power plants and the development of novel ESPs. As important alternatives to ESPs, baghouses were shown to have had general success in controlling coal-fired power plant emissions. When operating properly, baghouses can limit emissions to < 5 mg/cu nm at pressure drops of < 2 kPa. Not all baghouse installations have been completely successful. Both high pressure drop and bag loss have occurred (at Harrington Station), but these problems appear to be solved.

17. KEY WORDS AND DOCUMENT ANALYSIS

a. DESCRIPTORS	b. IDENTIFIERS/OPEN ENDED TERMS	c. COSATI Field/Group
Pollution	Pollution Control	13B 07A
Dust	Stationary Sources	11G 21B
Aerosols	Particulate	07D
Electrostatic Precipitators	Baghouses	13I
Filters		14G
Fabrics		11E
Scrubbers		
Flue Gases		

18. DISTRIBUTION STATEMENT	19. SECURITY CLASS *(This Report)*	21. NO. OF PAGES
Release to Public	Unclassified	547
	20. SECURITY CLASS *(This page)*	22. PRICE
	Unclassified	

EPA Form 2220-1 (Rev. 4-77) PREVIOUS EDITION IS OBSOLETE ☆ U.S.GOVERNMENT PRINTING OFFICE: 1980--657-165/0159